Integrated Performance-based Design of Building-foundation Systems

A thesis submitted in partial fulfilment
of the requirements for the Degree of
Doctor of Philosphopy in Engineering
by

Maxim Millen

Supervisors: Professor Stefano Pampanin, Professor Misko Cubrinovski
Associate supervisor: Professor Athol Carr

Civil and Natural Resources Engineering
University of Canterbury
Christchurch, New Zealand

August 2015

Abstract

The effects of soil-foundation-structure interaction (SFSI) have been a topic of discussion amongst the structural and geotechnical community for many decades. The complexity of the mechanisms, as well as the need for inter-disciplinary knowledge of geotechnical and structural dynamics has plagued the advancement and the consequent inclusion of SFSI effects in design.

A rigorous performance-based design methodology should not just consider the performance of the superstructure but the supporting foundation system as well. Case studies throughout history (eg. Kobe 1995, Kocaeli 1999 and Christchurch earthquakes 2010-2011) have demonstrated that a poor performance at the foundation level can result in a full demolition of the structure and, in general terms, that the extent of damage to, and repairability of, the building system as a whole, is given by the combination of the damage to the soil, foundation and superstructure. The lack of consideration of the modifying factors of SFSI and an absence of intuitive performance levels for controlling foundation and soil behaviour under seismic loads has resulted in inadequate designs for buildings sited on soft soil. For engineers to be satisfied that their designs meet the given performance levels they must first, understand how SFSI affects the overall system performance and secondly have tools available to adequately account for it in their design/assessment.

This dissertation presents an integrated performance-based design procedure for building-foundation systems that considers all of the major mechanisms of SFSI. A new soil-foundation macro-element model was implemented into a nonlinear finite element software and validated against several experimental tests. The numerical model was used to provide insights in to the mechanisms of SFSI and statistical analysis on the results yielded simple expressions that allow the behaviour to be quantified. Particular attention was paid to the effects of shear force on the foundation response and the quantification of the rocking mode of response. The residual deformations of the superstructure and distribution of forces up the structure were also investigated.

All of the major SFSI mechanisms are discussed in detail and targeted numerical studies are used to explain and demonstrate concepts. The design procedure was validated through the design and assessment of a series of concrete buildings that were designed to account for the effects of SFSI.

Acknowledgements

First I would like to thank my supervisory team of Dr. Stefano Pampanin, Dr. Misko Cubrinovski and Dr. Athol Carr. This dissertation spans areas of geotechnical engineering, structural engineering, numerical modelling and dynamics, your expert knowledge in these areas has provided great insights into this research that I immensely grateful for. As well as your technical guidance you have provided a wisdom in other aspects of my personal and professional development that is invaluable. You are all fantastic entertainers and humble gentlemen.

I would like to acknowledge the financial support provided to me by the Natural Hazards Research Platform, The Todd Foundation, New Zealand Geotechnical Society and the University of Canterbury, which has allowed me to complete this dissertation.

I would like to make a shout out to all of those who have walked the hallowed hall of Level Three with me, especially my flatmate Harry Johnston and my office mates Asra Borzie, Robin Lee and Chris Watson, I am truly grateful to have shared in your experiences in the last three years. To the Grizzly Bairds and extended family, Tobias Smith, Francesco Sarti, Daniel Moroder, Andrew Baird, James O'Neill, Dennis Pau, Sam McHattie, Varun Joshi, Gareth Morris, Manya Deyanova, Jeff Tuck, Ethan Thomson, Royce Lui and Claudio Cappellaro. I am grateful for the on topic and off topic conversations we have shared. Thank you to my friends who made my Italian experiences ever richer, Matt Fox, Amaryllis Mou, Tessa Beetham, Ben Sporn, Gian Maria, Antonio Castiello, Vito Valotta, Claudia Zelaschi, Duncan Henderson and Anna Winkley.

To the staff of the University of Canterbury and especially Dr. Brendon Bradley and Elizabeth Ackermann, your understanding and clarity have made hard things easy.

To Dr. Misko Cubrinovski for mentoring me through my first experiences at lecturing at the University of Canterbury and along with Dr. Carlo Lai for providing me the teaching opportunity at the ROSE School.

To my flat mates, Paddy Neill, Brendon Gardner, Laura Ansell, Anna Johns, Harry Johnston, Becca Hasselman, Abby Shaw, Ben Parry,Ange Gray, Hamish Stace and Richard Hunter thank you for feeding me, supporting me and distracting me when necessary.

Finally I would like to acknowledge the support of my family. To my sister, Ramona, and my brother, Jules, thank you for your support and interest in my research. To my partner, Lucy Holland, I am grateful for your understanding, patience and creative views on life. To my mum, Renate, and papa, Paul, thank you for your support, energy, sound advice and holistic views, this dissertation is dedicated to you.

Contents

List of Figures

List of Tables

Chapter 1

Introduction

It is widely accepted that soil deformations modify the seismic response of a building, however, these modifications are not rigorously considered in the majority of design standards around the world. The lack of suitable consideration of the effects soil-foundation-structure interaction (SFSI) in the design of buildings has been plagued by the use of equivalent static loads to represent dynamic loading and a previously perceived view that SFSI effects are beneficial to the structural response. Unfortunately it is not easy to address the effects of SFSI as the entire building design philosophy is disjointed, with very little communication between the structural engineer designing the structure and the geotechnical engineering specifying the foundation requirements.

Recent events such as the Christchurch earthquake sequence have resulted in significant damage at the foundation level, highlighting the necessity to better understand the complexity of SFSI. Furthermore, there is a growing interest in a 'weak-foundation strong-superstructure' design philosophy, whereby the designer allows for nonlinear deformations in the foundation to limits the seismic energy entering the structure. The allowance for nonlinear deformations at the foundation level has prompted engineers to question what level of transient and permanent deformation is acceptable, as well as what are the ramifications to the structural response.

This dissertation attempts to unravel some of the mysteries of SFSI, addressing each of the major mechanisms individually and quantifying them using a series of simple expressions. An overarching building-foundation performance-based design framework is proposed and an integrated design procedure is developed which allows the designer to satisfy the limits imposed on the transient and residual deformations of the structure and foundation.

1.1 Research motivation

The lack of in-depth considerations for SFSI in seismic building design is the primary motivation for this dissertation. Not only are the interactions between the soil, the foundation

and the structure important but the performance of foundation needs to be considered with the same rigor as the superstructure. The current performance-based design philosophy provides suitable limits to structural performance but lacks specific requirements for foundation deformations.

The recent development of a weak foundation strong superstructure philosophy as a way to limit seismic forces entering the superstructure has shown promise with several massive structures being constructed, most notably the Rio-Antirion Bridge in Greece. While these structures demonstrate the potential advantages of the weak foundation concept, the implementation of such a design requires expert skills in structural and geotechnical engineering and complex numerical or experimental models to assess the influence of the yielding soil-foundation interface on the structural response and performance of the system as a whole. There are potentially large cost savings associated with such a design philosophy due the opportunity to specify considerably smaller foundations. To allow the wider engineering community to utilise such an economic design philosophy on less prominent buildings the effects of yield foundations need to be quantified without the requirement of expensive computer modeling.

While in many cases the effects of SFSI can be minimised in new design by specifying large foundation dimensions, this is not always an option due to limited space or money. In some cases the seismic excitation of the superstructure may result in excessive foundation loading. Conventional equivalent static assessment of the dynamic loads on the foundation may result in a factor of safety below 1.0 and would give no indication of the behaviour of the system, therefore making the design seem implausible. The more rational displacement-based approach can provide estimates of both the peak and residual deformations of the system and therefore allow a suitable design to be determined.

1.2 Objectives and tasks

The main objective of this dissertation was the development of a comprehensive performance-based design framework for building-foundation systems on soft soils. To achieve such an objective the effects of SFSI were first quantified to determined which mechanisms were the most important for performance. Given the limited number of experimental tests and the high number of potentially influential parameters, the effects of SFSI were quantified by first developing suitable numerical models of the building, foundation and soil systems. And to ascertain whether the building, foundation and soil models were suitable they were first validated against experimental test data.

Below is a list of all of the task in order of which they were completed during this study.

1. Implementation of a soil-foundation macro-element into the non-linear finite element

software Ruaumoko3D

1.1. Extensively validate the macro-element performance for pier-like structures using centrifuge test data

1.2. Validate the macro-element performance for frame structures with isolated footings using centrifuge test data

2. Understand the mechanisms of SFSI in relation to the following:

2.1. Develop a method to estimate peak foundation deformations, and validate its predictive capabilities for nonlinear concrete wall structures including P-delta effects.

2.2. Consider the effects of shear forces and shear deformations on the response of the foundation.

2.3. Develop and validate an expression to combine non-linear displacement modification factors for the prediction of the overall SFS system displacement.

2.4. Develop and validate a method to estimate settlement and foundation residual rotation, including the influence of SFSI and structural ductility.

2.5. Develop and validate a method to estimate residual superstructure deformations, and quantify the difference in behaviour between SDOFs and MDOFs and the influence of P-delta effects and SFSI effects.

2.6. Assess the effects of SFSI on multiple support systems.

3. Develop a performance-based design methodology for building-foundation systems that includes the major mechanisms of SFSI.

3.1. Develop a performance framework that includes foundation peak and residual deformations

1.3 Organisation

Chapter 2 provides a general overview of previous research in the study of SFSI. Chapter 3 covers more specific aspects related to performance-based design and design options to consider different mechanisms of SFSI. Chapters 4 and 5 are concerned with the development and validation of the macro-element model that is used for the remainder of the dissertation to help derive design expressions and validate assumptions. Chapters 6 through 10 are devoted to the development of particular design expressions that form an integral part of the proposed design procedure. Chapter 11 presents the full integrated performance-based design procedure. Chapter 12 presents the conclusions of the dissertation and there are four appendices which present further results from the validation of the macro-element and design examples for walls and frames.

Chapter 2 presents a study of the previous literature on the subject. The chapter is broken into the four facets of SFSI study, field studies, experimental studies, numerical/analytical studies and design methods.

Chapter 3 provides an overview of the key aspects of performance-based design and the major mechanisms of soil-foundation-structure interaction (SFSI). The conventional approach to seismic foundation design is first reviewed and then the various aspects of the proposed new design are discussed at a conceptual level to demonstrate how they were addressed in this dissertation.

Chapter 4 presents the implementation of the soil-foundation interface macro element model into the time history analysis software Ruaumoko3D (Carr, 2015). The element makes use of the foundation uplift formulation from Chatzigogos et al. (2011) and the plasticity formulation by Figini et al. (2012). The implementation of an advanced soil-foundation model into a well developed structural analysis software provides unprecedented opportunities for understanding the interaction between the soil, foundation and structure for more complex cases than the commonly considered single degree-of-freedom. The algorithms used in the model are explained in detail and some modeling examples and recommendations are given for single degree-of-freedom systems and frame structures with isolated footings.

Chapter 5 provides evidence of the accuracy and validity of the macro element model by comparing its performance against two well documented sets of experiments. The recommended calibration parameters from the Chatzigogos et al. (2011) and Figini et al. (2012) models are used to demonstrate that the parameters provide suitable estimates of the behaviour. The experimental validations showed that the model could accurately capture the transient behaviour of the footing deformations and the resulting level of settlement and foundation residual rotation.

Chapter 6 develops equations to estimate the level of peak foundation and superstructure deformation through the consideration of foundation rotation and soil-foundation shear deformations. The equations developed in this chapter present the first validation that the deformations of two nonlinear systems can be estimated through the combination of their nonlinear displacement modification factors. This assumption is a cornerstone for the displacement-based design of multiple deformation mechanism structures and allows the designer to control both the deformations in the superstructure and the foundation.

Chapter 7 develops equations to predict the level of SFSI-induced settlement and foundation residual rotation. The dependence of both the residual foundation deformation parameters on peak foundation rotation and foundation axial load is explained through simple concepts. Equations to predict the foundation residual deformations are developed from the statistical regression of data from two parametric studies on SDOF structures. The equations are an integral piece of the proposed performance-based design framework and allow the designer to control the expected level of SFSI-induced settlement and residual foundation rotation.

Chapter 8 investigates the prediction of superstructure residual deformations with special consideration for P-delta effects and foundation deformations. A series of fixed base concrete wall structures were designed and their SDOF equivalent structures were assessed through nonlinear time history analysis. The results highlighted the influence of the post yield stiffness ratio and P-delta effects on the ratio of residual to peak drift. A series of concrete wall structures were then designed using the proposed displacement-based design procedure and assessed to quantify the effects of foundation deformation on the ratio of residual to peak drift. Multi-linear regression analysis was performed on the two data sets to develop a unique expression to account for all of the major factors considered in the analyses.

Chapter 9 presents the effects of SFSI on multi-degree-of-freedom systems with vertically distributed mass. A series of fixed based concrete wall buildings were analysed as MDOF systems to demonstrate the ability of DDBD to predict inter-storey drifts, moment and shear distributions. The wall buildings were redesigned to consider SFSI and were analysed using the implemented macro-element from Chapter 4. The results demonstrated that the amplification of the base shear due to higher mode effects increases the plastic response of the soil.

Chapter 10 presents the effects of SFSI on multi-degree-of-freedom systems with multiple supports. A set of case study frame buildings were analysed to demonstrate the additional key mechanisms that can not be captured with a simple SDOF model. A small parametric study of a series of frame buildings were designed using the integrated design procedure and analysed to demonstrate how the additional mechanisms result in further deformations.

Chapter 11 presents the integrated building-foundation performance based design procedure. A performance framework is presented to include the building and foundation deformations. Each of the major mechanisms of SFSI are discussed and accounted for in the design procedure. The design procedure is based on a displacement-based design procedure presented by Paolucci et al. (2013).

Chapter 12 is a summary of the findings and conclusions made throughout the dissertation. It details them chapter by chapter and finishes with comments on further research that would benefit the integrated design procedure.

Chapter 2

Literature review

This chapter provides an overview of some of the more extensive studies into the issues surrounding soil-foundation-structure interaction (SFSI) both in terms of analysis and design. SFSI falls into the much larger category of soil-structure-interaction, which concerns many different structures such as retaining walls, tunnels and pipelines, however, in this dissertation SFSI is constrained to the effects involving buildings on shallow foundations. The additional effects of structure-soil-structure interaction, where adjacent buildings interact through the soil, is beyond the scope of this research, so too is liquefied soil, which represents an extreme case of SFSI involving additional complex mechanisms.

The effects of SFSI have been considered in engineering for over half a century and the understanding and quantification of the effects has been attempted using many different approaches. This chapter groups these approaches into four main areas, explaining the progress made in each and how it has contributed towards a better understanding of SFSI.

Different areas of SFSI:

- Field studies
- Experimental testing
- Numerical/Analytical modelling
- Design methods

While this chapter attempts to provide a coherent story about the developments in each of these areas, the finer details of experimental tests, numerical modelling techniques and design methods have been reserved for later chapters.

2.1 Field studies

Major seismic events such as Chilean earthquakes 1960, Northridge 1994, Kocaeli 1999 (Figure 2.1), Chi-Chi 1999 and Christchurch 2010-2011 have highlighted the importance of SFSI and provided useful case studies to help understand the complex phenomenon.

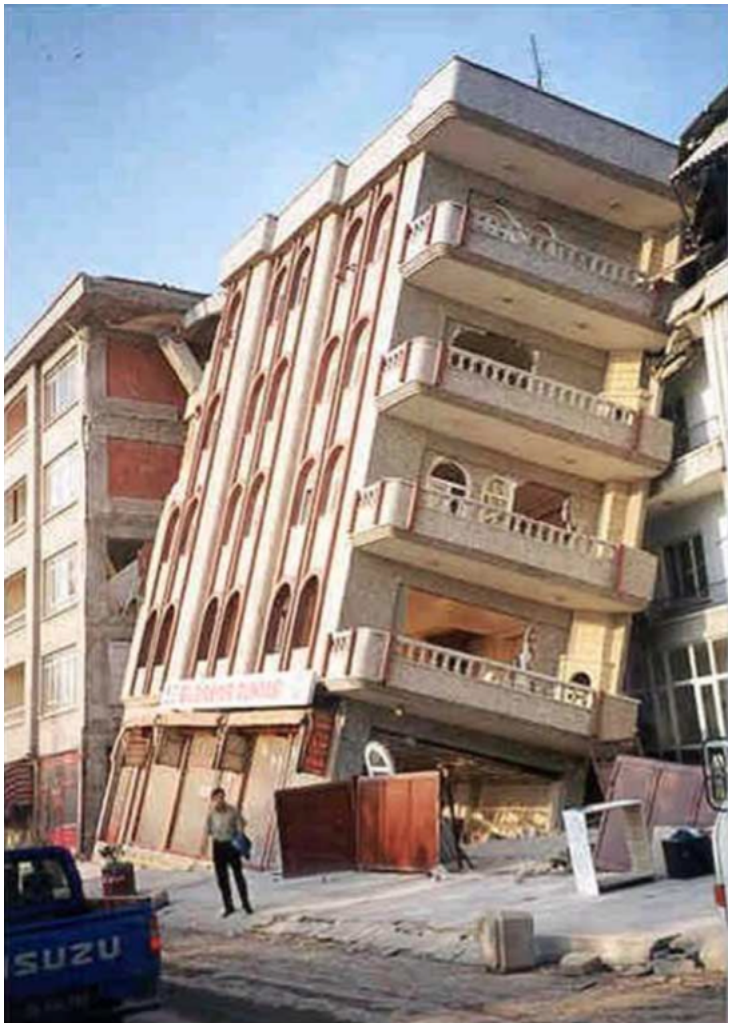

Figure 2.1: Tilted building in Adapazari, Turkey, after the 1999 Kocaeli earthquake, *Photo courtesy of the Earthquake Engineering Field Investigation Team (EEFIT)*

The advantage of field studies is that the results are 'real', meaning there are no modelling assumptions or design simplifications made, unlike those applied to the simple structures used in experimental tests and numerical studies that often miss some mechanisms and phenomenon that may occur in real structures. Unfortunately the effects of SFSI are implicit to the response of the structure and therefore it is difficult to isolate the effects of SFSI and prove that they ultimately lead to the failure of a building.

Issues such as induced stresses in buildings from differential settlements as seen in the Christchurch earthquake sequence (Cubrinovski and McCahon, 2012) highlight that a single degree-of-freedom model is inadequate for analysing multiple support structures. Figure 2.2 (b) shows an example of the differential settlement seen in Christchurch, where a mixed pile-raft foundation was used to account for variations in the soil stiffness, however, each foundation type behaved differently in seismic events and the building suffered both rigid body rotation (tilt) and some additional differential settlement. Figure 2.2 (a) shows another building located in Christchurch where a more rigid foundation was used, however, due to

varying soil conditions and lateral spreading the building suffered rigid body rotation.

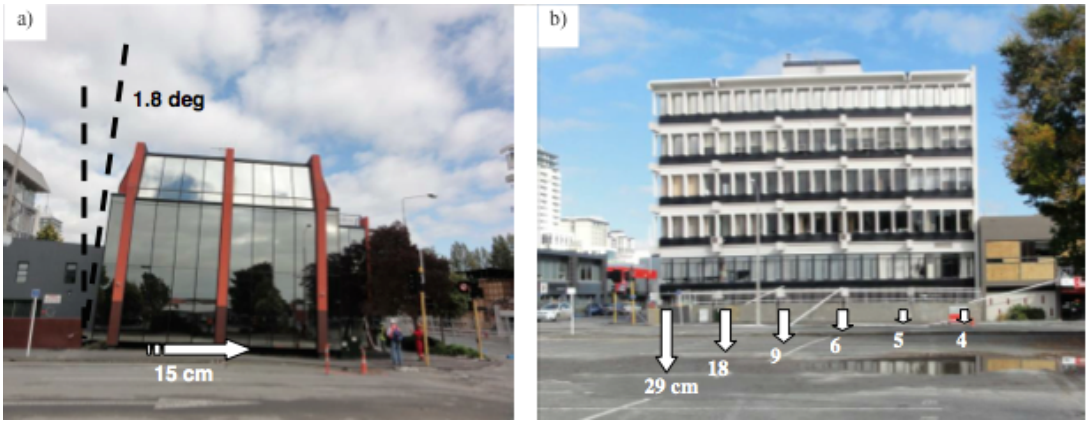

Figure 2.2: Differential settlement observed in Christchurch following the February 2011 Earthquakes, *Cubrinovski et al. (2011)*

Foundation failure was observed in many buildings following the Canterbury earthquake sequence. Although liquefaction was a large contributor, another contributor was superstructures having excessive strength capacity resulting in foundation loads exceeding their capacity (Smith and Devine, 2012). These sorts of design and construction issues need to be addressed and field studies of failed structures often highlight their significance.

Unfortunately field studies are often disadvantaged since the analysis is usually done post-event and thus significant assumptions are required in order to understand the complex behaviour, especially in regards to the transient behaviour of the structure. In some unique cases, buildings and surrounding free-field sites were instrumented with accelerometers prior to events, allowing for the quantification of seismic demands and measurements of the natural frequencies during the event (Çelebi and Safak, 1992; Safak and Çelebi, 1992; McHattie, 2013). These field studies have shown a significant contribution from the rocking mode of the foundation and also provide an opportunity to calibrate and validate state-of-the-art numerical tools to ensure they can adequately model real structures.

Bird et al. (2005, 2006) examined the deformation states of buildings in central Adapazari, due to ground deformations from the Kocaeli 1999 earthquake. Importantly it was noted that when isolated footings underwent differential settlement, the superstructure behaved as a rigid body and all deformation was taken in the ground floor columns and not the beams.

The influence of site-effects such as basin amplification and geometric amplification are often not captured in simple numerical and experimental tests, however studies by Mylonakis et al. (2000) into the Kobe 1995 earthquake have highlighted that site-effects and soil-structure interaction led to the collapse of expressway piers. The Mexico City earthquake of 1985 provided another example of ground motion amplification due to site effects, with spectral accelerations being amplified by eight times. Ground motion amplification is an important phenomenon to understand in the context of SFSI, as SFSI causes an elongation in the vibrational period of

the building that could coincide with the period of amplification from site effects.

2.2 Experimental data

Experimental testing has always been an essential part of the process for understanding the effects of SFSI. Two different approaches have been considered when constructing experimental prototypes of a soil-structure system. The first approach is full scale testing of a prototype structure, which is difficult due to the forces required to excite a full sized soil-structure system. The alternative is to scale the soil-structure system, which is difficult due to the stress dependence of soils and therefore enhanced gravitational conditions are often required to get meaningful results. Another issue with experimental testing is the consolidation time required to test on clay. Therefore the majority of SFSI tests to date have been on sands in a centrifuge to create enhanced gravitation conditions. Some of the pioneering tests are briefly discussed and Table 2.1 provides an overview of more recent tests that have been performed.

Early experimental tests at the University of Auckland (Taylor and Williams, 1979) involved rocking foundations under constant axial load on clay and sand. The findings showed that settlement was dependent on the number of cycles, with five cycles at 0.035 rad resulting in a settlement of 0.2% of the footing width. The bearing pressure at yield was strongly dependant on the breadth of contact area of the footing for sand and less so for clay soils. The hysteretic energy dissipation was reduced significantly after the first cycle and rounding at the edges under cyclic loading reduced the rotational stiffness. It was also recommended that footings should be designed with large factors of safety to prevent large settlements during rocking.

The Camus IV test (Combescure and Chaudat, 2000) used a one third scale five storey wall building resting on a 40cm deep sand layer and tested at normal gravity conditions on a shake table (Figure 2.3). The case where the foundation could uplift was compared to an early test where the building was fastened directly to the shake-table (fixed base conditions), and the foundation uplifting case had superior performance. The wall from the uplifting foundation suffered no damage up to the maximum horizontal shaking of 1.0g, while the fixed base wall failed at 0.71g. These tests demonstrated the advantages of uplifting foundations to dissipate and limit the amount of energy entering the superstructure.

Figure 2.3: Test setup and photo from Combescure and Chaudat (2000)

Gajan et al. (2005) conducted an extensive set of centrifuge tests with variation in footing size, embedment, loading type, soil type and vertical load. From these tests several different empirical and analytical expressions were developed and validated. Empirical relationships were developed for settlement based on the cyclic amplitude, number of cycles and vertical factor of safety. The moment capacity of the footing was derived as Equation 2.1 and was shown to be stable under cyclic loading. In Equation 2.1, N is the axial load, L_f is the footing length and FS_V is the vertical load factor of safety.

$$M_{c,footing} = \frac{NL_f}{2}(1 - \frac{1}{FS_V}) \tag{2.1}$$

Gajan et al. (2005) also plotted the results from the tests against bounding surfaces (in axial-shear-moment space) suggested by Cremer et al. (2001) and Houlsby and Cassidy (2002), demonstrating that the bounding surfaces show good agreement to experimental results. Finally an empirical relationship for the decrease in rotational stiffness was developed based purely on the amount of rotation (Equation 2.2); this differs from the one developed by Paolucci et al. (2009) (Equation 2.3) based on the large-scale cyclic tests on sand at the Joint

Research Centre at Ispra, Italy (Negro et al., 1999) and at the Public Works Research Institute, Japan (PWRI, 2005) where axial load was an important factor. In the equations below, θ_f is the foundation rotation and parameters a and m are constants that depend on the vertical factor of safety.

$$\frac{K_\theta}{K_{\theta,max}} = 0.003\theta_f^{-0.6} \tag{2.2}$$

$$\frac{K_\theta}{K_{\theta,max}} = 1.0/(1.0 + a\theta_f^m) \tag{2.3}$$

Centrifuge tests by Chang et al. (2006) looked at non-symmetric dual wall-frame systems on dry sand and conducted both dynamic and in a slow cyclic tests under enhanced 20g gravitational conditions. These tests showed that the outer footings have non-symmetric behaviour due to the changes in axial load and resulted in residual rotations, demonstrating a clear coupling between rotational stiffness, moment capacity and the axial load. The non-symmetric frame also had differential settlements between the different footings. It was noted that at small levels of excitation, footing energy dissipation accounted for about 90% of total energy dissipation and even at higher drifts this remained at about 65%.

1g experiments by Algie et al. (2010) tested parallel shear walls resting on clay (Figure 2.4). The tests were conducted in the field and therefore the soil stiffness and strength was determined using cone penetration tests, wave activated stiffness tests and shear vane tests. The theoretical moment capacity (Equation 2.1) determined using the field test data matched well with the experimental results. The elastic stiffness values suggested by Gazetas (1991) considerably overestimated those observed at the start of the tests. The settlements and rotation time histories showed that rocking foundations have consistent energy dissipation with minimal settlements.

Figure 2.4: Test frame and photo from Algie et al. (2010)

Centrifuge tests by Mason et al. (2010) and Trombetta et al. (2013) contained a one-storey and a three-storey frame building sitting on dry sand. The buildings were initially located apart as seen in Figure 5.3, where the one-storey frame (highlighted in red) provided one of the seta of experimental results for the validation of the numerical modelling used in this dissertation. The researchers main goal was to investigate structure-soil-structure interaction, however, this initial experiment provided a benchmark for the level of settlement and differential movement that could be expected between the footings.

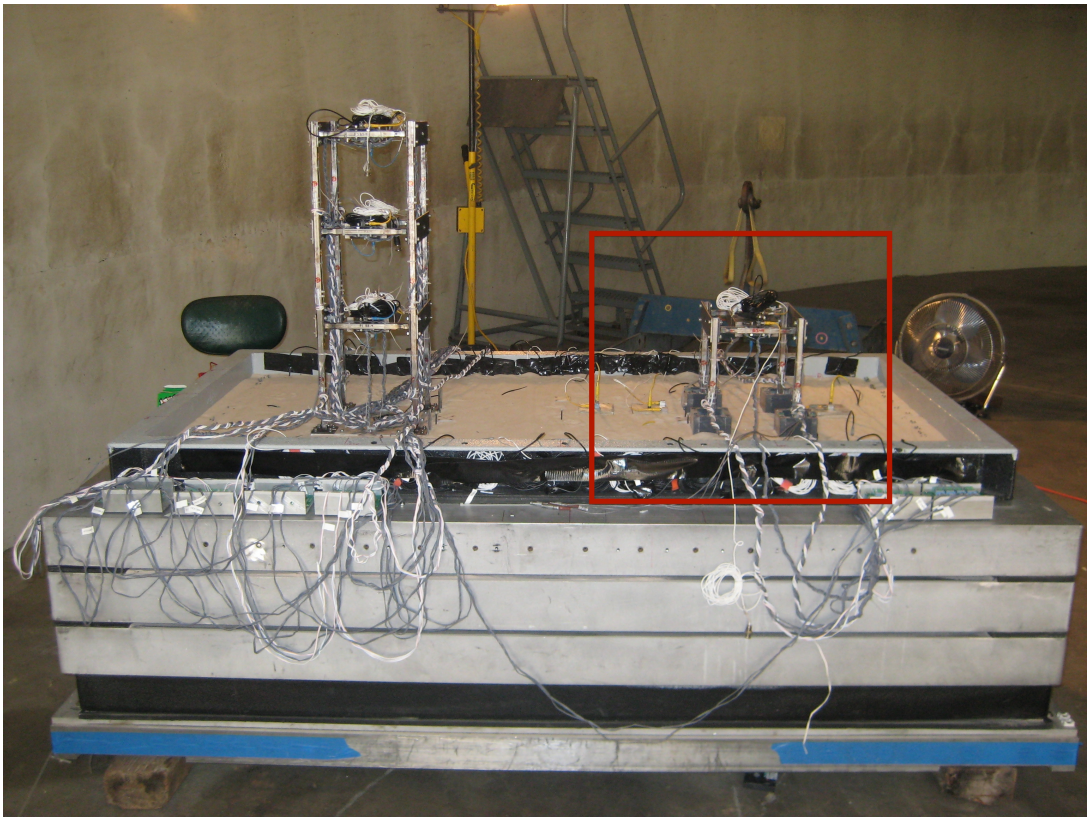

Figure 2.5: Test setup *after Mason et al. (2010)*

Research by Deng and Kutter (2012); Deng (2012); Deng et al. (2012) has addressed the preconception that bridge piers with hinging columns out-perform piers with rocking foundations. A series of centrifuge tests on single support and two-column bridge bents showed that the bents designed for rocking foundations reached higher peak displacements but their residual displacements were lower due to the re-centring nature of the rocking mechanism. One of the single support bridge bents from the fifth experiment (LJD03) (Figure 5.1) was used to validate the predictive capabilities of the numerical modelling technique used in this dissertation. The re-centring also contributed to the rocking foundation surviving higher intensity shaking than the hinging column counterpart and reduces ductility demand in the structure significantly. In the tests on the two column bridge bent it was noted that the bent designed for rocking footings dissipated 37% of its energy through hysteretic rocking while the conventionally designed bent still dissipated 12% through the footings. The foundation moment capacity suggested by Gajan et al. (2005) (Equation 2.1) and the initial stiffness estimate from Gazetas (1991) were in agreement with the experimental results with a slight underestimation of the stiffness for large footings. Furthermore the SFSI-induced settlement was determined as a function of the axial load ratio and the cumulative plastic rotation, providing a simpler approach to estimating settlements than that by Gajan and Kutter (2008). The settlement can be estimated based on the expression in Equation 2.4 between the cumulative plastic rotation (θ_{cum}) and settlement (S_{dyn}). If it is assumed that the foundation goes through two full cycles to the design rotation (θ_d), Equation 2.4 can be modified to give Equation 2.5, which can be

used as a design check.

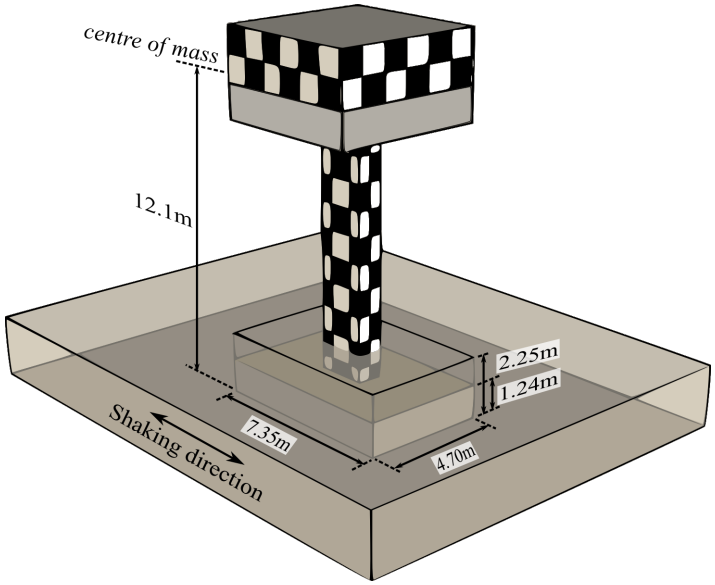

Figure 2.6: Experimental setup *after Deng and Kutter (2010)*

$$S_{dyn} = c_{sett} L_f \theta_{cum} \tag{2.4}$$

$$S_{dyn} = 4 c_{sett} L_f \theta_d \tag{2.5}$$

Where c_{sett} is a settlement coefficient based on the vertical factor of safety and L_f is the length of the footing.

Centrifuge studies by Liu et al. (2013) considered both SDOF and frame structures to determine the influence of SFSI on the yielding behaviour of structures. Frames that were designed to be dominated by foundation rocking and frames designed to have a balance of foundation rocking and structural yielding, were compared with the response of a frame that was design to have its dominant energy dissipation being structural yielding only. The results showed a marked decrease in residual displacements and ductility demand on the frame with the rocking foundations (FRD) compared to the fixed based frame (SHD) as seen below in Figure 2.7.

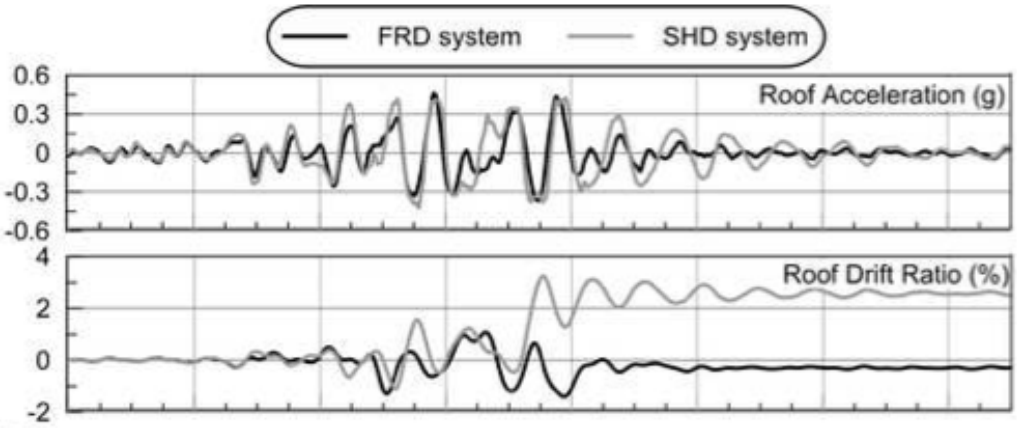

Figure 2.7: Comparison of the foundation rocking dominated (FRD) and structure yielding dominated (SHD) frame buildings *from Liu et al. (2013)*

In recent years there have been numerous experimental studies investigating various effects of SFSI with SDOF structures or more complex structures, using dynamic excitation or pseudo static loading, on different soil conditions with elastic and non-linear superstructures. These experimental tests provide excellent insight into the complexities of SFSI. Table 2.1 is by no means a comprehensive list of the experiments investigating SFSI but it provides a summary of some of the major tests in recent years.

Table 2.1: Summary of experimental tests investigating SFSI

Reference	Structure	Excitation	Scale	Laboratory	Soil
Negro et al. (1999)	Linear-elastic embedded bridge pier	Applied: ground motions and cyclic	1g		Saturated Ticino sand D_r= 45% & 85%
Combescure and Chaudat (2000)	Non-linear RC 1/3 scale 5.1m high parallel-walls	Shake table: 3 ground motions	1g	CEA, Saclay, France	40cm deep Dry sand D_r= 71%
Gajan et al. (2005)	Linear walls	Shake table: ground motions & static push	55g	UC, Davis, USA	Dry Nevada sand D_r= 60% & 80% and San Francisco Bay Mud LL= 90% and PL=38%
Chang et al. (2007)	Steel dual wall-frame	Shake table: Slow cyclic and 1 ground motion	20g	UC, Davis, USA	Medium dense dry Nevada sand
Shirato et al. (2008)	Linear-elastic bridge pier	Shake table: Cyclic and ground motions	1g	PWRI, Tsukuba, Japan	Dry sand D_r= 80%
Deng et al. (2012)	Non-linear bridge pier single and multiple supports	Shake table: ground motions and pulses	40g-49g	UC, Davis, USA	Dry Nevada sand D_r= 38-77%
Liu et al. (2013)	Non-linear 2-storey frame	Shake table: Ground motions	30g	UC, Davis, USA	Silty clay (Yolo Loam) LL = 29.1%, PL= 20.8% and PI = 8.3%
Massimino and Maugeri (2013)	Elastic Pier	Shake table: loaded centrically and eccentrically	1g	University of Bristol, UK	dry Leighton Buzzard sand, D_r= 50%
Drosos et al. (2012) Anastasopoulos et al. (2013)	Linear bridge pier	Static and Shake table: Cyclic and ground motions	1g	NTUA, Athens, Greece	Dry Longstone sand D_r= 85%
Trombetta et al. (2013)	Non-linear steel frame	Shake table: ground motions	55g	UC, Davis, USA	Dry Nevada sand D_r= 80%
Loli et al. (2014)	Non-linear concrete bridge pier	Shake table: Ricker wavelets and ground motions	50g	University of Dundee, Scotland	Dry Congleton silica sand, D_r = 60%
Storie et al. (2015)	Elastic pier	Shake table: ground motions and pulses	50g	University of Dundee, Scotland	Dry Congleton silica sand, D_r = 83%

2.3 Numerical/Analytical modelling

This section outlines the range of different approaches used to model SFSI, covering analytical expressions (replacement oscillators), lumped parameter approaches (macro-elements and Winkler beams) and direct approaches (finite elements). The lumped parameter approach will be discussed extensively with more weighting on the macro-element approach since this was the modelling technique utilised in the numerical studies of this dissertation. A brief discussion outlining the two phenomena: kinematic interaction and inertial interaction will preclude this to explain how these aspects are commonly dealt with in numerical modelling.

2.3.1 Kinematic and inertial interaction

In conventional SFSI analysis the interactions between the soil and the structure are decoupled into two separate phenomena; kinematic interaction and inertial interaction. The kinematic interaction is considered as the modification to the motion due to the difference in stiffness between the foundation and surrounding soil. The result is waves being reflected and interacting as they pass through to the structure. While the effects on non-embedded foundations are negligible for vertically propagating shear waves, embedded foundations can have additional overturning moments at certain frequencies as seen in Figure 2.8.

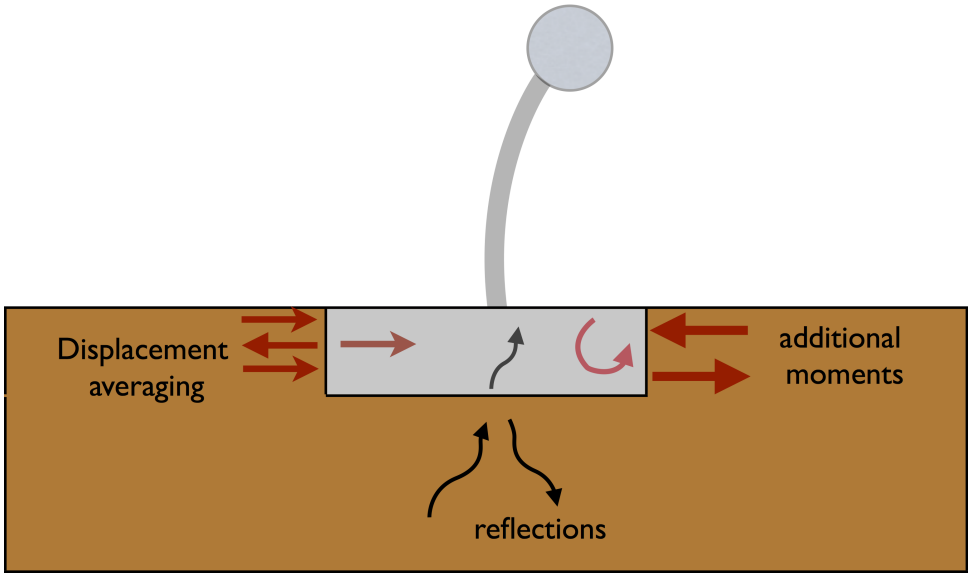

Figure 2.8: Kinematic interactions

These effects are highly frequency dependent and are difficult to rigorously quantify with many researchers Veletsos et al. (eg. 1997); Lin and Miranda (eg. 2007) showing their effects to be beneficial to the seismic response of the structure and therefore they are often omitted from design/analysis and do not feature in any formal design code with the exception of EC 8 Part 5 (2004). This dissertation makes no attempt to quantify kinematic effects and

therefore the remainder of the discussion will focus on the second phenomena, inertial interaction. Guidance on considering inclined shear waves and embedded footings can be found in NEHRP Consultants Joint Venture (2013).

Inertial interaction is the modification of the response due to consideration of the difference in inertia of the foundation and attached superstructure compared to the soil. The additional mass of the superstructure results in the structure lagging when soil pushes against it and as the superstructure moves it gets out of phase with the soil and subsequently pushes against the soil as well. These effects are modelled using impedance functions (springs and dashpots) attached to the base of the foundation with the ground motion applied at the other end. The springs and dashpots allow the structure to move relative to the ground and only be constrained by the stiffness and damping of the soil. This consideration often leads to increased damping and flexibility for a linear system, which often leads to a beneficial seismic response. The behaviour of a non-linear system is somewhat more difficult to determine and will be discussed in the following sections.

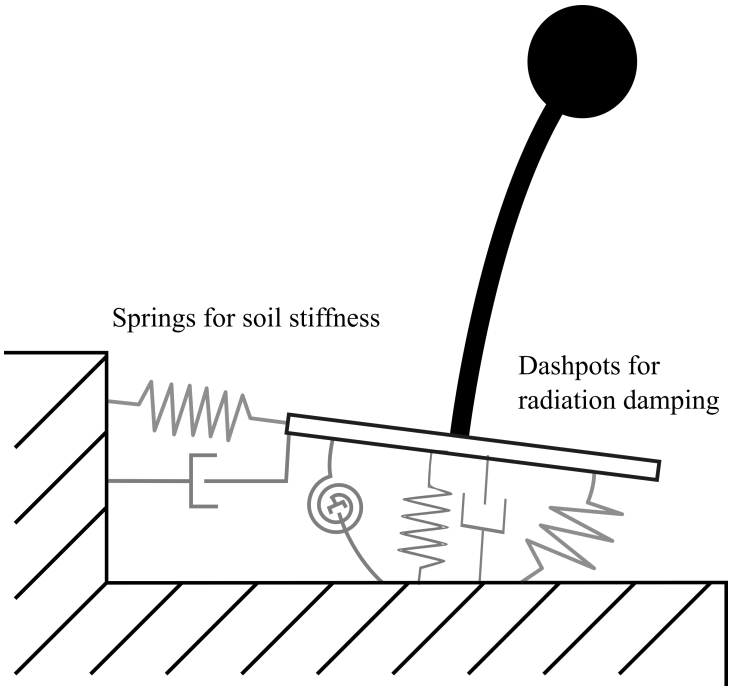

Figure 2.9: Modelling inertial interaction

The de-coupling of the two foundation compliance phenomenon (inertia and kinematic interaction) allows the engineer to determine where the modifications to the response comes from and through superposition can determine the overall system behaviour (Pecker, 2007). The de-coupling relies on the superposition of forces and deformations, which requires a linear system (Kramer, 1996), therefore application of this approach to non-linear systems would be incorrect, however it is often done in practice. Gazetas and Mylonakis (1998) discussed the issue of superposition of these two effects for moderately non-linear systems arguing that the solution is still appropriate, because inertial interaction dissipates in very short distances from

the foundation, while kinematic interaction is influenced by the soil surrounding the foundation, with the significant area of influence being a function of the wavelength. Therefore inertial interaction may affect small wavelength motions but these are often not influential to the overall behaviour since kinematic interaction essentially provides a high-pass filter.

2.3.2 Analytical expressions

Analytical expressions have been derived to account for the effects of SFSI using linear or equivalent viscoelastic linear impedance functions. These functions follow a replacement oscillator approach where the different modes of displacement are combined together to give a single mode. Figure 2.10 demonstrates the setup for the different modes of deformation. For full derivations of the following expressions (Equations 2.6 - 2.8) describing an equivalent replacement oscillator please refer to Wolf (1988). The following expressions determine the replacement oscillator with a natural frequency ($\tilde{\omega}$), damping ($\tilde{\xi}$) and input amplitude ($\tilde{u_g}$).

$$\frac{1}{\tilde{\omega}^2} = \frac{1}{\omega_s^2} + \frac{1}{\omega_h^2} + \frac{1}{\omega_\theta^2} \tag{2.6}$$

$$\tilde{\xi} = \frac{\tilde{\omega}^2}{{\omega_s}^2}\xi_s + \frac{\tilde{\omega}^2}{{\omega_h}^2}\xi_h + \frac{\tilde{\omega}^2}{{\omega_\theta}^2}\xi_\theta \tag{2.7}$$

$$\tilde{u_g} = \frac{\tilde{\omega}^2}{{\omega_s}^2}u_g \tag{2.8}$$

The frequencies terms, which represent fictitious frequencies of vibration for the structural mode (ω_s), foundation sliding mode (ω_h) and foundation rocking mode (ω_θ) are given by:

$$\omega_s = \sqrt{\frac{k}{m}} \tag{2.9}$$

$$\omega_h = \sqrt{\frac{k_h}{m}} \tag{2.10}$$

$$\omega_\theta = \sqrt{\frac{k_\theta}{h^2 m_\theta}} \tag{2.11}$$

Where the impedance terms (k_h and k_θ for foundation shear stiffness and foundation rotational stiffness) can be determined from a variety of textbooks. An excellent summary of the development of the impedance terms, which are a core component of the SFSI problem, can be found in Kausel (2010).

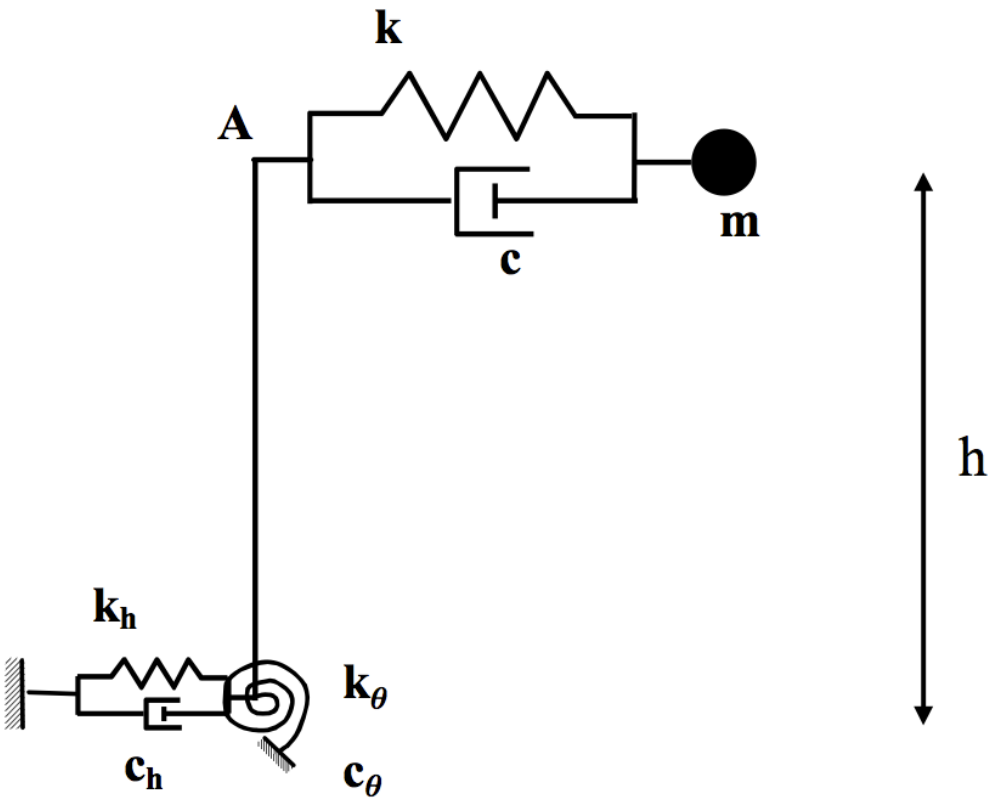

Figure 2.10: Setup of SFSI showing the impedance functions *from Pecker (2007)*

By using the following set of non-dimensional parameters and Equations 2.6-2.8 it can be concluded that SFSI decreases the frequency of vibration (Figure 2.11a), increases the damping ratio (Figure 2.11b) and decreases the amplitude of the input motion (Figure 2.11c). The mass ratio and stiffness ratio provide a convenient properties to show that the influence is most pronounced for heavy structures on soft soil, however, the overall influence is actually governed by the ratio of the different pseudo frequencies.

- Aspect ratio: $\tilde{h} = \frac{h}{r}$
- Stiffness ratio: $s = \omega_s h / V_s$
- Mass ratio: $= \tilde{m} = m / \rho r^3$

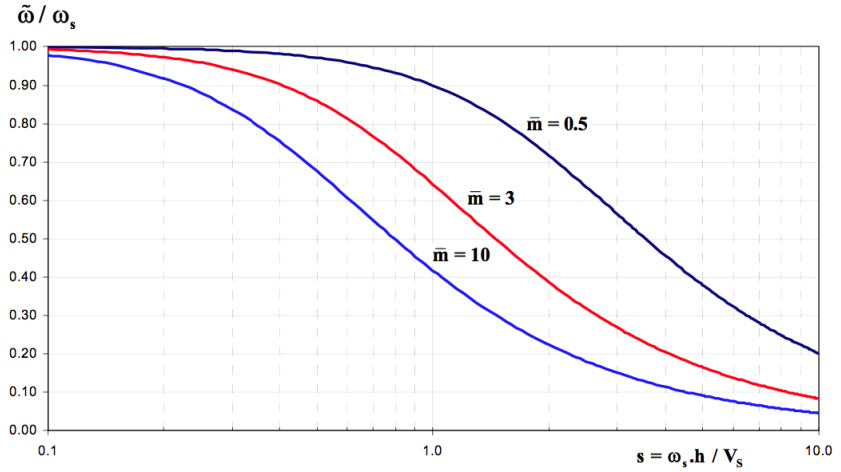

(a) System natural frequency

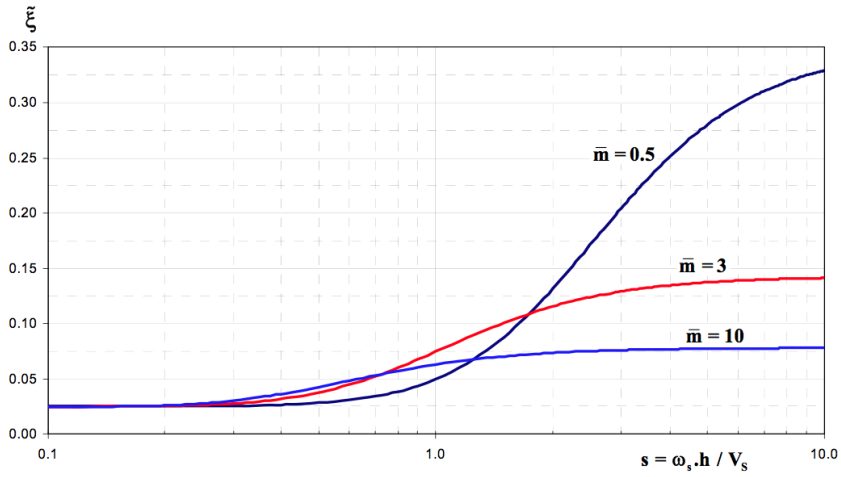

(b) System damping

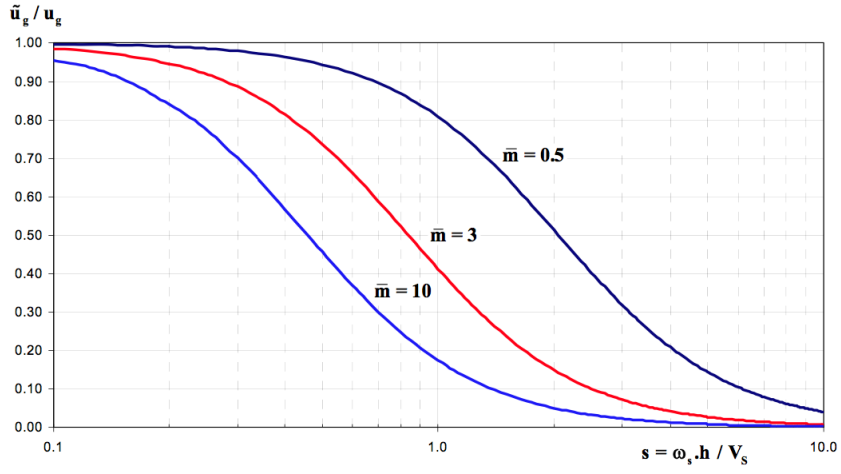

(c) System input motion

Figure 2.11: Modification to response using analytical expressions *from Pecker (2007)*

2.3.3 Lumped parameter approach

The lumped parameter approach uses a series of springs and dashpots to represent the soil-foundation interface, which improves on simple analytical techniques by allowing for direct consideration of non-linear effects through time history analysis. The lumped parameter approach also requires considerably less computing power and expertise than the direct finite-element approach and therefore uncertainty in the parameters can be accounted for through a parametric study.

The two predominant methods for a lumped-parameter approach are the macro-element (Figure 2.12a) and the Winkler-beam (2.12b). The macro-element considers only six degrees-of-freedom (three translational, three rotational) in the footing and accounts for their non-linear interactions through an applied hysteresis rule. The Winkler-beam approach models the soil along the footing with a series of translational springs. The rotational and vertical stiffnesses of the footing are modelled by the position and stiffness of the springs.

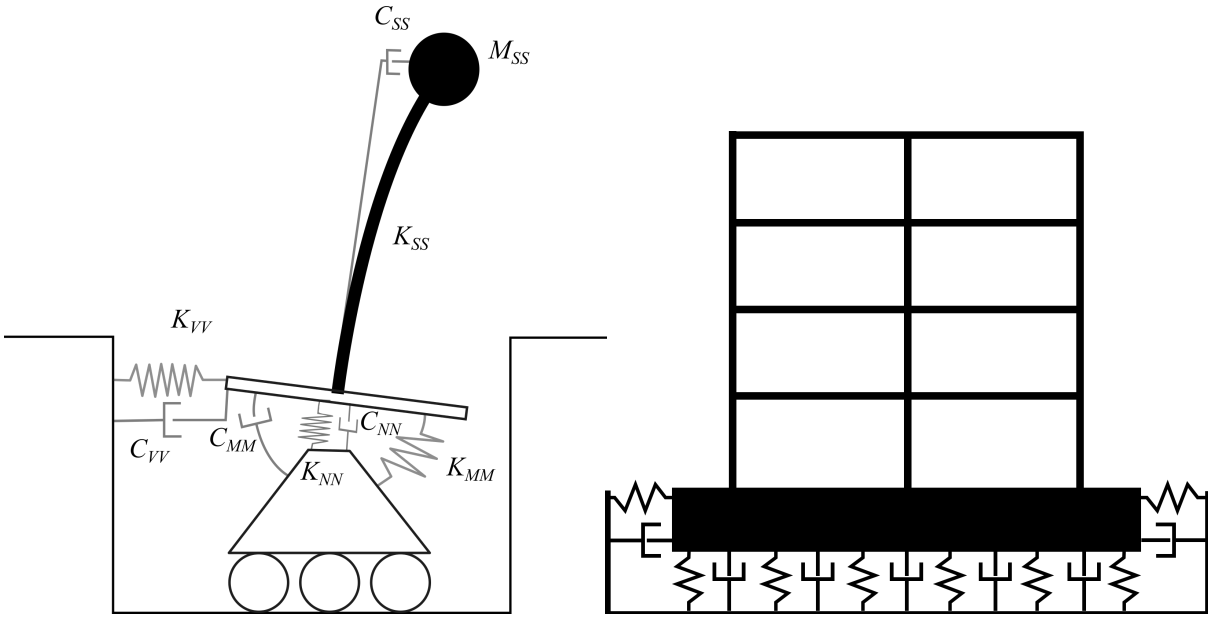

(a) Macro-element (b) Winkler-beam

Figure 2.12: Lumped parameters model for SFSI

Both approaches have been used extensively and for a linear analysis the two approaches give the same answer if the foundation is rigid, however, the Winkler-beam has the advantage of modelling a flexible foundation, while the macro-element often has less spring elements and therefore is more computationally efficient and easily interpretable. The differences in the two approaches are more noticeable when the soil-foundation interface is modelled to consider non-linear effects (see Sections 2.3.3 and 2.3.3). The following subsections cover, an explanation of the two models and their differences; an overview of the advancements made through linear modelling of SDOF structures, an explanation of some of the key findings

of non-linear SFSI and an outline of advancements numerical analysis of SFSI effects on multiple-degree-of-freedom (MDOF) structures.

Macro-element modelling

The simplicity of a macro-element model allows for a computationally efficient modelling method that directly includes the coupling of the degrees-of-freedom to capture non-linear behaviour such as: uplift, soil yielding, sliding and settlement. In recent years there have been many macro-elements proposed in literature (ie. Cremer et al., 2001; Wolf and Deeks, 2004; Chatzigogos et al., 2007, 2009; Grange et al., 2009a), many of these have been able to capture both the uplift of the foundation and yielding of the soil, which both significantly influence the design forces (Pecker and Chatzigogos, 2010).

Recent macro-element formulations have decoupled the uplift mechanism from the soil yielding mechanism. The uplift mechanism is considered as an elastic, geometrically non-linear mechanism based on the coupling of the moment and axial load. The soil yielding mechanism is based on the moment, shear and axial load, and utilises plasticity theory, using either a yield surface for elasto-plastic response or a bounding surface for continuous plastic response. The decoupled approach has allowed researchers to match the rotational behaviour both in terms of uplift and inelastic response with considerable accuracy but with little success in matching the settlement of footings (Paolucci et al., 2008).

The latest model by Figini et al. (2012) attempts to accurately capture the rotational behaviour and the settlement for single-support structures, and the model has been validated against several experimental tests (Negro et al. (1999), Combescure and Chaudat (2000) and Shirato et al. (2008)). Figure 2.13 demonstrates the basis of the plasticity algorithm, with the bounding surface being the combination of ultimate loads. The position of the current load state (blue dot) relative to the bounding surface defines the amount of plasticity and this is determined through either a radial mapping rule (blue line) or a vertical mapping rule (red line). The direction of plastic flow is governed by the plastic potential, which for associative plasticity is equivalent to the bounding surface. The entire formulation is normalised by the axial load capacity and length of the footing. A full explanation of the macro-element development and algorithms can be found in Chapter 4.

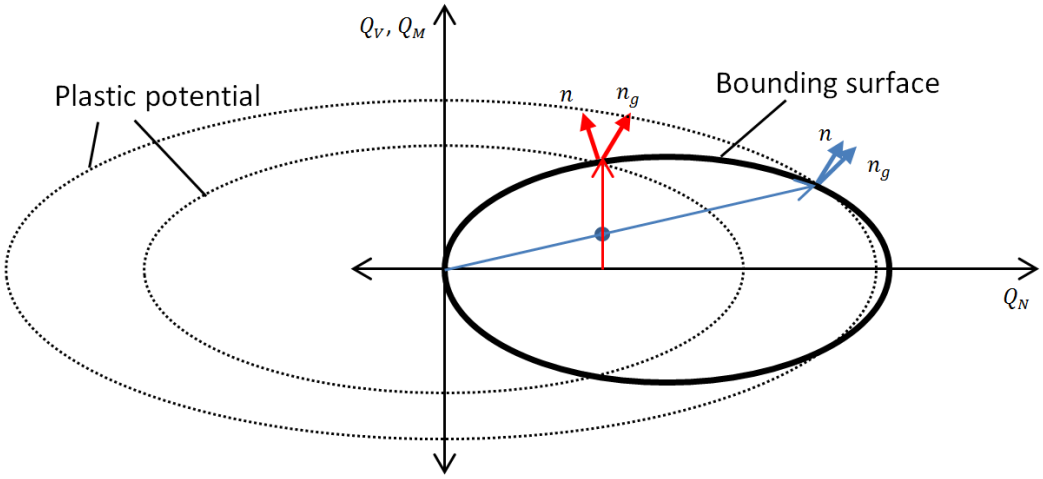

Figure 2.13: Coupling of forces in macro-element

Winkler-beam model

The Winkler-beam model uses a series of translation springs to model the vertical and horizontal stiffnesses of the footing. The number of springs and their stiffnesses are determined by ensuring the sum of the vertical spring stiffnesses matches the vertical stiffness from an impedance function from literature (eg. Gazetas, 1991). The position of the springs under the footing is determined by ensuring that the sum of each of the springs stiffness multiplied by its lever arm matches the rotational stiffness of the footing. While it is a relatively straightforward process for an elastic analysis, the calibration of these springs for non-linear behaviour is considerably more difficult. The footing uplift is modelled using zero-tension springs so that the spring detaches as compression on the tension edge reaches zero (see Figure 2.14). The accuracy to which the change in vertical and rotational stiffness is modelled is governed by the number of springs under the footing and their position, thus a calibrated Winkler-beam model must ensure that accuracy is not unduly limited as well as satisfying the above vertical and rotation stiffness requirements. The calibration is further complicated by the inclusion of soil yielding, where the choice of hysteresis for the spring modifies the rotational and vertical stiffnesses differently. An elasto-plastic rule results in a continuous plastic response for moment-axial load combinations however, under purely axial load the response is only elasto-plastic. Another shortfall of the Winkler beam model is that the soil-foundation shear springs are de-coupled from the vertical springs, so shear induced settlement and soil yielding under a combination of foundation shear force and moment can not be captured.

The choice of hysteresis rule, number of springs and spring spacings provide the user with options that should be calibrated against experimental tests. Many numerical studies have employed a non-linear Winkler-beam model and provide an excellent reference for implementation (eg. Wotherspoon, 2009; Harden and Hutchinson, 2009).

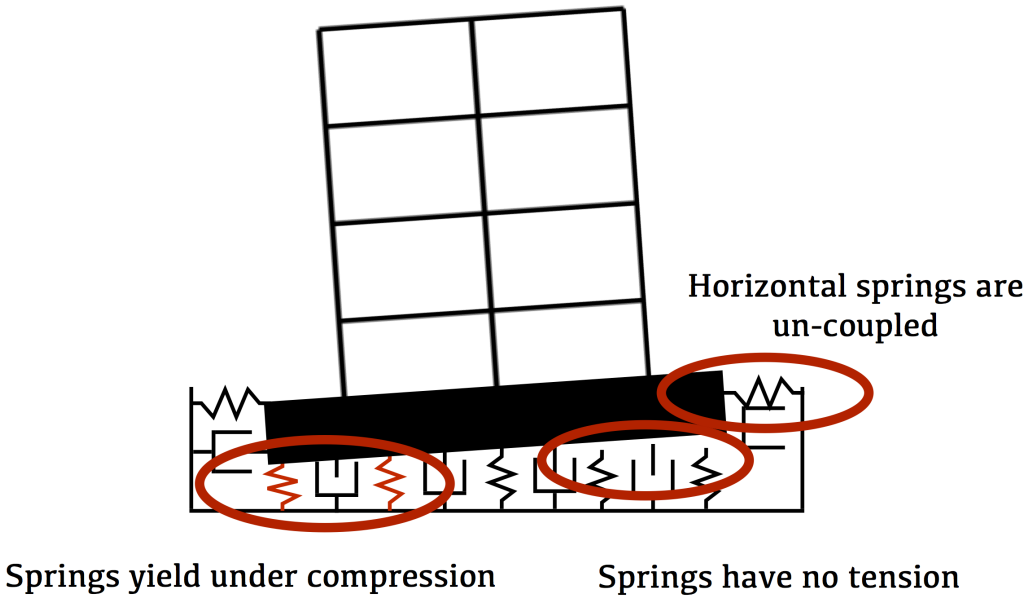

Figure 2.14: Non-linear response using a Winkler-beam model

2.3.4 Linear single-degree-of-freedom structure

The linear single-degree-of-freedom (SDOF) structure model includes the three foundation degrees-of-freedom and a single sway mode for the superstructure. There have been extensive frequency domain and time domain analyses using this model to demonstrate how the contributions of sliding and rocking of the foundation can modify the overall response (eg. Moghaddasi et al., 2011a). The main findings of the analyses are that the increased damping and increased flexibility of rocking and sliding result in a modification to behaviour with its overall effect being dictated the frequency content of the earthquake record. Figure 2.15 demonstrates this modification using a SDOF response spectra, where a fixed based structure (1) located at 1.3 seconds with 5% damping displaces 0.23m, while the equivalent SFSI structure with increased damping of 10% and a longer natural period of 1.7 seconds displaces only 0.2m. Looking at structure 2 the fixed-base period at 1.8 seconds moves to SFSI period of 2.2 seconds resulting in a considerable increase in displacements.

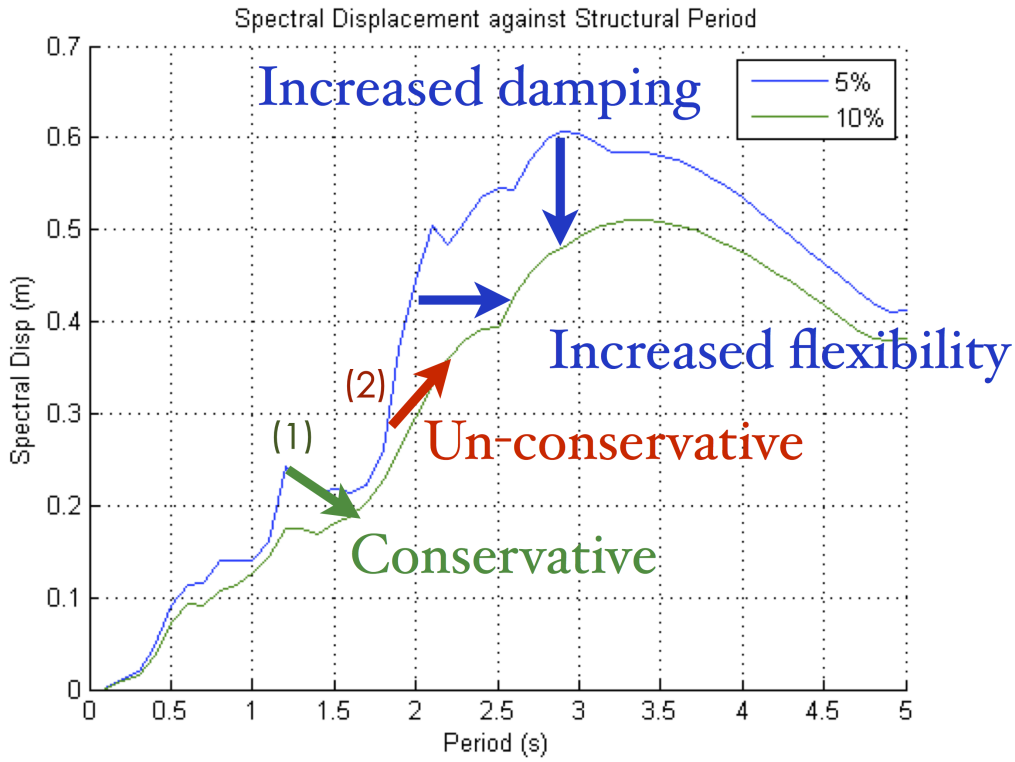

Figure 2.15: The effect of SSI on the spectral response

2.3.5 Non-linear superstructure, linear soil-foundation interface - single-degree-of-freedom

In most cases SFSI has less influence on yielding structures since a yielding structure softens and dissipates energy through hysteresis similar to the effects of SFSI (Veletsos and Verbic, 1974; Avilés and Pérez-Rocha, 2003). However, the influence of SFSI on the behaviour of yielding structures is more complex due to the potential reduction in structural ductility. Some of the major studies are summarised here:

- Ghannad and Jahankhah (2007) used a macro-element model to investigate the effect of SFSI on strength reduction factors, concluded that ignoring SFSI can be detrimental.
- Comartin et al. (2000) showed that ignoring SFSI can result in the wrong part of the structure being retro-fitted.
- Studies by Jeremic et al. (2004) concluded that the characteristics of the earthquake motion determined whether SFSI was beneficial or detrimental.
- Studies by Nakhaei and Ali Ghannad (2008) into the influence of SFSI on the expected damage to a building used the macro-element model (equivalent linear) proposed by Wolf (1994). The research showed that the SFSI structure will suffer more damage compared to the fixed based equivalent when the period is less than the predominant

period of the record and vice versa. The research assumed a rigid foundation and showed that the SFSI effects are more prominent for slender structures due to the larger elongation of period.

- Avilés and Pérez-Rocha (2011) showed that yielding structures suffered from detrimental effects of SFSI when the structural period was less than 65% of the dominant period of the record and had beneficial effects when greater than 75%. The study recognised three influential parameters: (1) relative stiffness of soil and foundation; (2) slenderness of the structure; (3) foundation embedment in the soil. These parameters had increased influence as the ductility and normalised base shear were decreased, with the relative stiffness being the most influential parameter and the embedment being the least.

2.3.6 Non-linear soil-foundation interface and superstructure - single-degree-of-freedom

The extension to include non-linear footing behaviour meant that the effects of uplift, sliding and soil yielding could be quantified. Simple numerical tools such as macro-elements and Winkler beam models offer intuitive and computationally efficient ways to satisfactorily capture the non-linear behaviour.

Research by Paolucci (1997) using a macro-element model with elasto-plastic properties and no uplift concluded that: (1) load eccentricity is the main factor that affects settlement, (2) the spectral acceleration is the best indicator for foundation damage, (3) the vertical accelerations may increase the settlement for near field earthquakes, otherwise they can be ignored.

Apostolou and Gazetas (2005) found that permanent rotations of a system depend strongly on A/A_c (sustained acceleration compared to pseudo static failure acceleration), N_{ult}/N (static factor of safety against bearing capacity failure) and the frequency, where records containing large portions of low frequency content were more destructive.

Extensive macro-element based parametric studies by Moghaddasi et al. (2010, 2011a,b, 2012) using a combination of linear and non linear SDOF structures and linear and non-linear soil-foundation interface models have drawn the following conclusions:

1. In the majority of cases the structural forces and deformations in the SFSI system were reduced when compared to the complementary fixed-based system
2. The drifts in the SFSI system were in some cases more than double their fixed-based counterparts
3. The effect of SFSI on the system was sometimes detrimental and sometimes beneficial
4. The ratio of SFSI system drift to the complementary fixed-based system had higher variation in the shorter periods

5. The variation in the ratios of drift between the structure-foundation-soil system and the fixed base model were amplified when the structure behaved inelastically
6. The inclusion of modelling geometric non-linearity (foundation uplift) resulted in residual drifts of up to 0.015 rad compared to 0.005
7. Modelling soil-nonlinearity can capture system failure, especially under intense shaking

The above findings will be elaborated upon here to explain their occurrence. First it should be noted that this research used SDOF systems for the structure, subject to a suite of natural earthquake records. From Figure 2.15, Observations 2, 3 and 4 can be explained due to the irregularity in the frequency content of a natural earthquake ground motion. The variation in results is clearly a function of whether the fixed-based period and corresponding SFSI period are in peaks or troughs of the elastic response spectra. Although this is not exact for a non-linear system, the elastic spectra does give an indication into the frequency content that the non-linear structure would be exposed to and therefore the above postulates will hold true in the majority of cases. The increased variation in short periods (Observation 4) is due to the characteristics of earthquake records, where short period motion is far more stochastic than long period motion.

When considering non-linear SFSI, it would be expected that the additional complexity of non-linear behaviour would result in additional variation between the behaviour of the structure-foundation-soil system and the fixed base system (Observation 5). An important consideration about this point is that when the structure behaves inelastically considerable energy is dissipated through in-elastic action, while the deformation in the foundation can cause a reduction in the level of ductility demand and therefore a reduction in the energy dissipation from the structure. Additionally observation 5 shows that when the system behaves in-elastically its response can change dramatically from the linear case.

The final two observations reflect the nature of the problem, where non-linear behaviour often leads to permanent deformations.

2.3.7 Multi-degree-of-freedom analysis

Current research into the effects of SFSI has largely been constrained to SDOF analysis, mostly to reduce computational effort. Previously, dynamic analysis of SFSI problems were predominantly assessed using time history analysis of meshed Finite-Element (FE) models with the need to use a small time step and fine mesh resolution, thus a simple structure model was preferred to reduce computational cost.

Early studies by Jennings and Bielak (1973) into the effects of SFSI on MDOFs showed that the effects of SFSI inertial interaction result in a significant decrease in the response of the first mode of a building and a slight decrease in all other modes. This effect is also seen in

fixed base structures where yielding occurs at the base. The effect was explained by Priestley (2003) demonstrating that the effect of yielding at the base only caps the energy entering the building from the first mode of response, while the higher modes have not formed a full mechanism.

Numerical studies by Bárcena and Esteva (2007) into the effects of SFSI on MDOFs concluded that SFSI reduced the ductility in the structure if the structural period (T_s) was shorter than the dominant ground motion period (T_a). SFSI also reduced ductility when T_s exceeded T_a while an increase in ductility was seen when $T_s \approx T_a$ for structural aspect ratios (building height over building width) of greater than 1.4 and a decrease for aspect ratios less than 1.4. The dependence on aspect ratio was due to radiation damping having a higher contribution for squat structures, resulting in less ductility.

Studies by Halabian and Erfani (2010) and Halabian and Kabiri (2011) using a sub-structure approach have shown that SFSI has little influence on the reduction factor used to account for a reduction in design loads due to yielding. These studies considered 2D frames with generic structural properties.

Tang and Zhang (2011) conducted a series of time history analyses modelling non-linear shear walls on non-linear foundations. In general the inter-storey drift decreased when the soil-foundation interface was modelled when compared to the fixed-based conditions, however, there were cases where an increase was seen.

Ganjavi and Hao (2011, 2012b) highlighted some shortfalls in the SDOF analysis when mapping them to a MDOF response. Studies on shear walls (5 storey, 10 storey, 15 storey) using an equivalent linear macro-element model investigated the difference in response when changing the distribution of strength and stiffness up the structure. These studies showed that the reduction in base shear due to SFSI was influenced by the distribution of strength by about 15%. The reduction in base shear demand from SFSI effects was more prominent in highly inelastic structures but was essentially negligible for low ductility structures. Very uncommon slender structures with a short period of vibration showed an increase in base shear demand for the SFSI case, which was more pronounced at high design ductilities. Ganjavi and Hao (2012a) used the coefficient of variation (COV) of the ductility demand up a shear wall building to determine the effects of SFSI and strength distribution on the building ductility demand. It was shown that SFSI increased the COV across all periods for three different design levels of ductility. Ganjavi and Hao (2012a) also highlighted that slender structures are more influenced by SFSI effects and that the distribution of ductility demand was influenced by SFSI effects. It was noted that no strength distribution method suggested in literature achieved an optimal uniform ductility demand up the structure. This study was carried out using an equivalent linear soil model, which was verified against a non-linear soil model proposed by Grange et al. (2009b) and the results were very similar up to a PGA of 0.5g.

All of the above studies have not looked at multi-support structures (eg. Frames on isolated

footings) or flexibility in the foundation which reduces the foundation stiffness and increases ductility demand in beams. Figure 2.16a demonstrates rocking behaviour for slender structures with a rigid foundation. While Figure 2.16b demonstrates flexibility in the foundation which is more common in squat structures where rocking occurs under each pad, resulting in a rotational demand in the beams. With the added complexity of foundation flexibility the use of a SDOF model may not be appropriate and that the current results for squat structures may be incorrect.

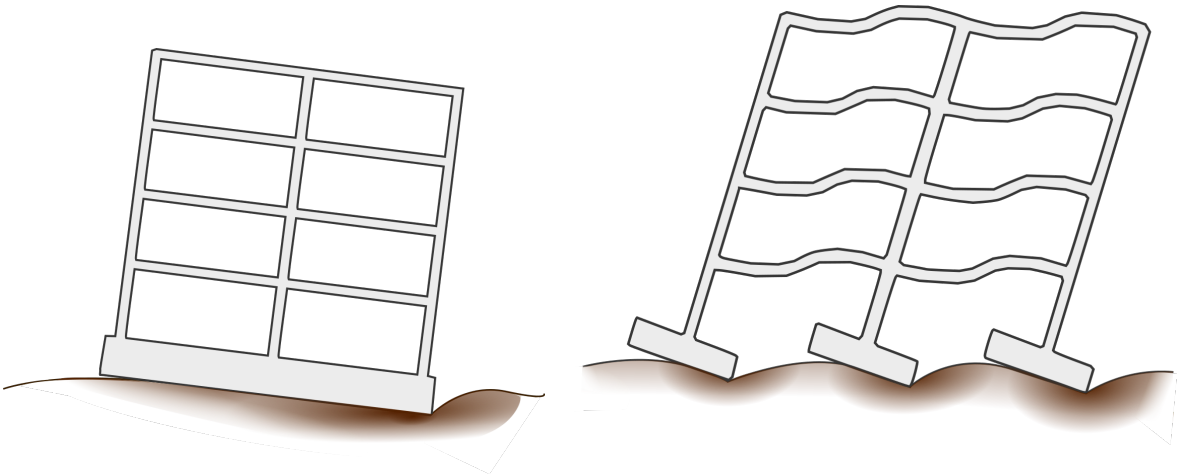

(a) Stiff foundation assumption

(b) Flexible foundation

2.3.8 Direct approach

Finite-element, finite difference and discrete particle methods can analyse the whole SFSI problem at once and can result in realistic approximations of behaviour. Unfortunately due to the large number of degrees-of-freedom, the computational time is too large to allow for a significant parametric study of important parameters. These models often give a deterministic view of the situation and can highlight important features that may need to be more closely looked at. These modelling techniques are extremely demanding on the user since they require a sufficient background in structural and geotechnical engineering as well as knowledge in SFSI and numerical modelling to be able to produce useful results and correctly interpret them.

2.4 Design methods

The focus of this section is how designers can make sense of the extensive research available about SFSI and what methods are available to design buildings to account for these effects. Numerical and experimental studies supporting the beneficial and sometimes unavoidable effects of SFSI where the soil acts as a fuse to limit the forces entering the building include (but are not limited to) Gerolymos et al. (2009), Gajan and Kutter (2008), Gajan et al. (2010), Pecker

and Chatzigogos (2010), Giorgini et al. (2012), Deng et al. (2012) and Sáez et al. (2013). While papers citing the detrimental effects of SFSI causing increased displacements, and structural demands include but are not limited to Mylonakis et al. (2000), Moghaddasi et al. (2011b) and Pecker et al. (2012). Other authors (eg. Anastasopoulos, 2009; Sullivan et al., 2010; Deng, 2012; Gazetas et al., 2013; Paolucci et al., 2013) have suggested that instead of relying on the perceived beneficial effect of SFSI the designer should directly account for it in their design and in doing so, come up with suitable designs that may be both cheaper and have better seismic performance than conventional designs. Successful implementation of such a design philosophy has already been achieved for the Rion-Antirion Bridge (Pecker and Pender, 2000) where the footings were designed to slide along the ground surface and therefore reduced lateral forces entering the structure. The design procedure has also shown good merit in experimental tests where buildings designed to rock on their foundations out performed the equivalent building with over-sized foundations (eg. Deng et al., 2012; Liu et al., 2013).

This section is structured such that conventional design approaches are first discussed followed by state-of-the-art approaches.

2.4.1 Foundation design in New Zealand

The current practice for foundation design in New Zealand is based around the guidelines of Verification method 4 (VM4) from the New Zealand Building Code (Dep. Building & Housing, 2011). These guidelines follow conventional static analysis (Terzaghi, 1943) to determine the ultimate capacity of a foundation, with strength reduction factors applied to ensure the strength of the soil is adequate to support the loads imposed by the superstructure (see Figure 2.16). The superstructure loads are usually determined based on an analysis of the structure under lateral earthquake loads with either no consideration for the modification due to SFSI or using analytical expressions (Section 2.3.2) or spectra modification factors (Section 2.4.3). Equation 2.12 is the soil capacity equation given in VM4, with N_c, N_q and N_γ being the standard capacity coefficient based on the cohesion and friction of the soil and overburden pressure (Terzaghi, 1943), and the remaining terms modifying the strength due to foundation shape, foundation depth, inclination of load and ground slope.

$$q_u = c\prime\lambda_{cs}\lambda_{cd}\lambda_{ci}\lambda_{cg}N_c + q\prime\lambda_{qs}\lambda_{qd}\lambda_{qi}\lambda_{qg}N_q + 1/2\gamma\prime B\lambda_{\gamma S}\lambda_{\gamma d}\lambda_{\gamma i}\lambda_{\gamma g}N_\gamma \tag{2.12}$$

Strength reductions factors for earthquake load should be in the range of 0.8-0.9. In the case of moment loading, suitable footing sizes should be used to prevent the vertical reaction force acting more than $B/6$ from the edge, to prevent uplift of the edge of the footing, with B being the foundation length. The foundation is also sized to prevent excessive settlement under static loading conditions.

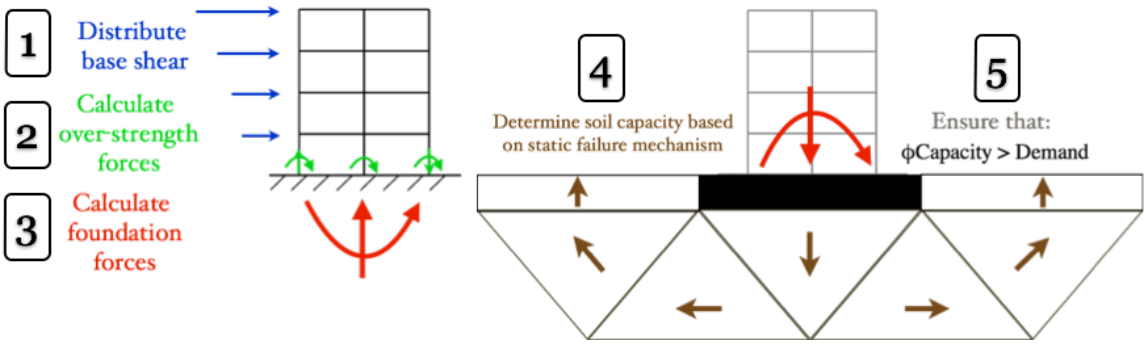

Figure 2.16: Design sequence following NZ design code

The allowance for rocking structures (or uplift of the edge of the foundation) was made in the old loadings code NZS 4203:1992, where for frames, uplift of one quarter of the footings was permitted.

NZS 4203:1992:

> *'Where dissipation of energy is primarily through rocking of foundations, the structure shall be subject to a special study, provided that this need not apply if the structural ductility factor is equal to or less than 2.0."*

The clause means that provided the structure does not exceed a ductility demand of 2.0, no special (time-history) analysis would be required. This clause was based largely on research by Priestley et al. (1978) and Taylor and Williams (1979), which demonstrated that rocking could be a suitable energy dissipation mechanism provided that the axial load capacity is far greater than the demand, to control settlements. In fact the South Rangitikei Rail Bridge (Beck and Skinner, 1972), an industrial chimney at Christchurch Airport (Sharpe and Skinner, 1983) and the Deadman's Point Bridge at Cromwell, Central Otago (Sharpe and Binney, 1984) were all designed to take advantage of rocking footings. The clause has been removed in the newer New Zealand loadings code NZS 1170.5:2004 (2004), where structures that dissipate energy by rocking require a special case study (ie. time-history analysis).

Following the Christchurch earthquake sequence of 2010-2012, McManus argued in the Royal Commission of Enquiry court hearings and supporting report (McManus, 2012) that the lack of a standard foundation design code for New Zealand is of significant concern and the poor communication between geotechnical and structural engineers in the area of foundation design may have led to serious miscalculation of design factors of safety. Furthermore, in practice factors of safety as low as 1.1 are permitted which may result in significant and unpredictable deformations at the foundation level.

Currently more robust design of foundations is met with reluctance from practitioners due to the complexity of the issues and lack of codification of practice as well as the potential of additional upfront costs.

2.4.2 Foundation design around the world

The general procedure for the design of foundations around the world is similar to that in New Zealand. Either using an assumption of a rigid base or a de-coupled approach the over-strength forces are determined in the superstructure and these are used as the demand on the foundation. Equation 2.13 given below is that available in Appendix F of the Eurocode 8 part 5 (EC 8 Part 5, 2004).

$$\frac{(1-eF\prime)(\beta * V\prime)^{c_T}}{(N\prime)^a[(1-mF\prime^k)^{k\prime}-N\prime]^b} + \frac{(1-fF\prime)^{c\prime_M}}{(N\prime)^c[(1-m*F\prime^k)^{k\prime}-N\prime]^d} - 1 \leq 0 \tag{2.13}$$

Where $N' = \frac{\gamma_{RD} N_{sd}}{N_{max}}$, $V' = \frac{\gamma_{RD} V_{sd}}{N_{max}}$ and $M' = \frac{\gamma_{RD} M_{sd}}{B * N_{max}}$ are the normalised corrected axial load, shear and moment on the foundation respectively. The factor γ_{RD} (which is 1.2-1.5 in a static loading case) accounts for uncertainties due to the simplifications made in the design model. In a seismic loading case this factor can be as low as 1.0, which allows for small deformations in the soil, provided the designer can demonstrate that these deformations will not result in collapse. The allowance for small deformations during seismic events is based on the recognition that seismic loads are transient and therefore the strength capacity may be exceeded temporarily but this does not result in collapse, rather in small permanent deformations (Pecker, 1996).

2.4.3 Spectra modification factors

The prediction of seismic forces and displacements for design, is often made through the use of the elastic response spectra modified by some factor to account for non-linear behaviour. The modification factor is commonly based on the expected level of ductility in the structure. Early reduction factors were based on Newmark and Hall's 'equal displacement' theory and 'equal energy' theory and fail to capture significant factors such as the hysteretic behaviour of the structure. Many authors (e.g., Newmark and Hall, 1969; Riddell et al., 1989) have criticised the lack of rigour on which these reduction factors are based, and produced new reduction factor models; however, many design codes/standards including New Zealand's loading standard (NZS 1170.5:2004, 2011) still make use of these early reduction factors. An alternative approach to the prediction of seismic loads is to directly use inelastic response spectra (e.g., Pal et al., 1987; Bozorgnia et al., 2010), where the displacements can be directly obtained from the inelastic spectra and can be combined with the backbone curve of the structure to obtain the design forces. While these modified reduction factors consider the hysteretic nature of the yielding structure, they do not incorporate any consideration for modifications to the hysteresis due to SFSI effects.

The analytical expressions from Section 2.3.2 provide spectra modification factors but are strictly limited to elastic systems and therefore combining the expressions with non-linear

modification factors would be a misguided.

Many authors have demonstrated through case histories (Section 2.1), experimental tests (Section 2.2) and numerical analyses (Section 2.3) that SFSI can reduce the structural ductility as well as dissipate significant energy at the foundation level. An attempt to quantify the reduction in hysteretic energy dissipation in the superstructure and the increase at the foundation level due to SFSI has been made in the displacement-based design framework (see Section 2.4.5), with equations relating energy dissipation to structural drift and foundation rotation. The modification to the vibrational period of the structure is also accounted for. A similar attempt to quantify these SFSI effects in a force-based spectral modification procedure is lacking. A conventional consideration of SFSI would simply result in an increased vibrational period and damping of the system, regardless of the structural behaviour.

2.4.4 Non-linear foundation design

A rethink of foundation design in recent years has led to the proposed methodology of using yielding at the foundation level as a fuse to limit forces in the structure. The benefits of such a design have been highlighted in Gerolymos et al. (2009), Pecker and Chatzigogos (2010) and Gazetas (2013) as well as other authors; notably the following points were emphasised:

- The requirement for elastic design may result in over-sized and uneconomical foundations
- The retrofitting of a foundation for elastic behaviour can be practically impossible
- Earthquakes can exceed the design spectrum level and therefore soil yielding can be unavoidable
- The allowance for yielding can provide a fuse at the base of the structure to reduce seismic forces in the structure
- Post-earthquake inspection of foundations (including piles) is often feasible using inclinometers, borehole cameras, shock testing and excavations, an example of such is the inspections following the Kobe 2005 earthquake

This sort of design process has been implemented successfully in experimental setups such as Deng et al. (2012) and Anastasopoulos et al. (2014) and in practice with the Rion-Antirion Bridge (Combault et al., 2000) being one such example. However, in the case of the experiments, the soil behaviour was well understood using a controlled laboratory environment and for the Rion-Antirion Bridge the soil was strengthened against deep-seated failure using inclusions and a uniform gravel was used at the footing interface to give a predictable sliding resistance. The implementation of a yielding foundation design on other real structures may be more difficult when ground improvement techniques would be uneconomical and there is greater uncertainty in the soil behaviour. Research by Deng (2012) supporting such a design

methodology has addressed several issues, demonstrating that rocking foundations are have predictable moment capacities and stiffnesses, and the structural drift can be predicted using the same methods as used for conventional structures.

While results from SDOF numerical analyses with non-linear SFSI (Section 2.3.6) have shown a beneficial design can be achieved by allowing yielding at the foundation base, a multiple support structure has to deal with additional issues. Multiple-support structures such as frames have changes in axial loading due to seismic forces, which make their behaviour less predictable and can result in non-uniform settlements. Further issues arise when considering non-symmetrical frames where there are different column sizes and bay lengths resulting in different moments, shear forces and axial loads acting on each pad footing. These loads may result in differential movements and cause residual forces and settlement. Further differential movements can be a result of heterogeneous soils or mixed foundation systems. For a non-linear foundation design to be accepted in practice it will have to address all these issues.

2.4.5 Displacement-based design including SFSI

The framework for displacement-based design has been used by several researchers to incorporate the effects of non-linear SFSI into design (Sullivan et al., 2010; Calvi, 2012; Deng, 2012; Paolucci et al., 2013). The displacement-based design framework directly accounts for hysteretic damping from different sources as well as considering the reduction in stiffness due to non-linearity by basing the design on the secant stiffness at peak response. Design curves relating foundation hysteretic damping and foundation rotational stiffness to foundation rotation have been suggested by Paolucci et al. (2009), Adamidis et al. (2013) and Gazetas et al. (2013).

Sullivan et al. (2010), Calvi (2012) and Paolucci et al. (2013) incorporated the foundation design curves and quantify the reduction in structural ductility in a displacement-based design procedure for walls and bridge piers.

The procedure set out in Calvi (2012) is outlined below:

1. Set drift limit (θ_{lim}) - dependant on material strain limits or code drift limits
2. Set a foundation rotation ($\theta_{foundation}$) - governs the distribution of ductility between the superstructure and foundation
3. Set an axial load ratio ($N_{capacity}/N_{demand}$) - controls moment-rotation relationship (also effects amount of settlement)
4. Determine design displacement profile - accounting for foundation rotation
5. Convert to equivalent SDOF system
6. Calculate superstructure yield rotation

7. Determine superstructure ductility
8. Determine equivalent viscous damping from the superstructure - based on ductility
9. Determine equivalent viscous damping from the foundation - based on foundation rotation
10. Determine the system damping based on a displacement weighted average of the superstructure and foundation damping.
11. Determine the effective stiffness from the displacement spectra
12. Determine the base shear
13. Distribute the base shear up the structure
14. Calculate the moment and axial load at the foundation
15. Set foundation aspect ratio ($length/width$), to fulfil the rotation requirement using moment-rotation curves
16. Set the foundation size to satisfy the $N_{capacity}/N_{demand}$
17. Check that both $\theta_{foundation}$ and $N_{capacity}/N_{demand}$ are satisfied - otherwise chose new values and iterate from 2.
18. Design ductile elements and perform capacity design on remaining elements

Although this procedure appears lengthy, many of the steps are almost trivial due to the availability of simple formulas in the model code for Direct Displacement-based Design (Sullivan et al., 2012). This procedure provides a rigorous method to account for foundation rotation but as yet does not account for settlements directly. Although the designer has the ability to control settlement using the $N_{capacity}/N_{demand}$ ratio, there is no clear guidance on how to do so. This method also requires that designers have curves that relate the damping and stiffness of the soil to the foundation rotation, similar to those proposed by Paolucci et al. (2009).

Deng (2012) developed an independent displacement-based design procedure for SFSI. The development of a DDBD procedure for bridge piers based on the regression of experimental data has led to some useful equations, notably Equation 2.14.

$$Rd = \frac{FS_v}{2.565 + 1.016FS_v} \tag{2.14}$$

Where Rd is the displacement recentring ratio and FS_v is the vertical factor of safety. This allows the design to control the amount of residual drift.

Chapter 3

Requirements for the proposed building-foundation design procedure

3.1 Summary

This chapter provides an overview of the key aspects of performance-based design and the major mechanisms of soil-foundation-structure interaction (SFSI). The conventional approach to seismic foundation design is first reviewed and then the various aspects of the proposed new design are discussed at a conceptual level to demonstrate how they were addressed in this dissertation.

3.2 Introduction

The effects of SFSI have been a topic of discussion amongst the structural and geotechnical community for many decades. The complexity of the mechanisms in SFSI as well as the need for inter-disciplinary knowledge of geotechnical and structural dynamics has plagued the advancement and the consequent inclusion of SFSI effects in design. It is well established that SFSI modifies the seismic response of a building. This modification is often considered 'beneficial' and thus in design practice the building is designed assuming that the soil and foundation provide a rigid base with no deformation. The assumption of a rigid base for the structure is reinforced by following the capacity-based design process to avoid foundation and soil yielding, often resulting in very large foundations. Recent events (eg. Christchurch earthquake sequence 2011-2012) and research (eg. Mylonakis and Gazetas, 2000) has provided evidence to the contrary of this beneficial effect. Studies by Nakhaei and Ali Ghannad (2008) showed that by modelling SFSI the structure would generally suffer more damage compared to a fixed based equivalent when the superstructure period was less than the predominant period of the record and vice-versa. It was noted in a study by Moghaddasi et al. (2012) that structures appropriately design for fixed-base conditions may be susceptible to failure at the foundation level due to soil yielding or foundation toppling when exposed to design level ground motions.

Amongst the discussion over the detrimental or beneficial effects of SFSI, the concept of purposefully designing yielding foundations to limit forces entering the superstructure has shown considerable promise (Housner, 1963; Priestley et al., 1978; Gazetas, 2014). Deliberately designing to harness the effects of non-linear SFSI has been successfully demonstrated in laboratory experiments (eg. Chen et al., 2006; Liu et al., 2013; Deng, 2012; Anastasopoulos et al., 2014; Loli et al., 2014) as well as in massive structures such as the South Rangitikei Rail Bridge, New Zealand (Beck and Skinner, 1972) and The Rion-Antirion Bridge, Greece (Pecker, 2011). Unfortunately, often in design, buildings and their foundations are decoupled and considered separately. By decoupling the building and foundation it becomes difficult to determine the effects of SFSI and to implement a design philosophy that is dependent on both the building and the foundation dynamic behaviour.

Several authors have recently suggested integrated design procedures for the superstructure and foundation employing the Direct Displacement-based Design (DDBD) (eg. Sullivan et al., 2010; Algie, 2011; Paolucci et al., 2013). The integrated approach allows the effects of increased flexibility, shared ductility and modified mode shapes to be considered directly in the design of both the superstructure and foundation. Currently available procedures focus on achieving a particular design drift for mainly single-degree-of-freedom (SDOF) structures and have little guidance on controlling foundation deformations, understanding the influence of SFSI on higher mode effects and the change in foundation behaviour due to frame-action. The earthquake engineering profession is moving towards low damage building designs, however, an investigation into the performance of buildings during the Christchurch earthquakes by Giorgini et al. (2014) has shown that buildings were deemed irreparable due to superstructure damage, foundation damage or a combination of both. To maintain consistency in the design of buildings, the foundation performance levels need to be considered with the same rigour as that of the structure.

3.2.1 Conventional design approach

In a conventional design of a building and foundation, the building and foundation are designed separately (Figure 3.1). The superstructure loads are determined by considering the dynamic behaviour of the superstructure as if the foundation and soil are rigid (Step 1). The superstructure is designed based on the internal actions from the superstructure loads (Step 2). The foundation loads are determined by considering how the internal forces of the superstructure will act on the foundation when considering the superstructure to behave with some additional over-strength (Step 3). The foundation loads are considered as pseudo static forces acting on the foundation and the foundation is then sized and designed to avoid static and dynamic bearing capacity failure, foundation uplift, excess static settlement and foundation in-elastic behaviour (Step 4).

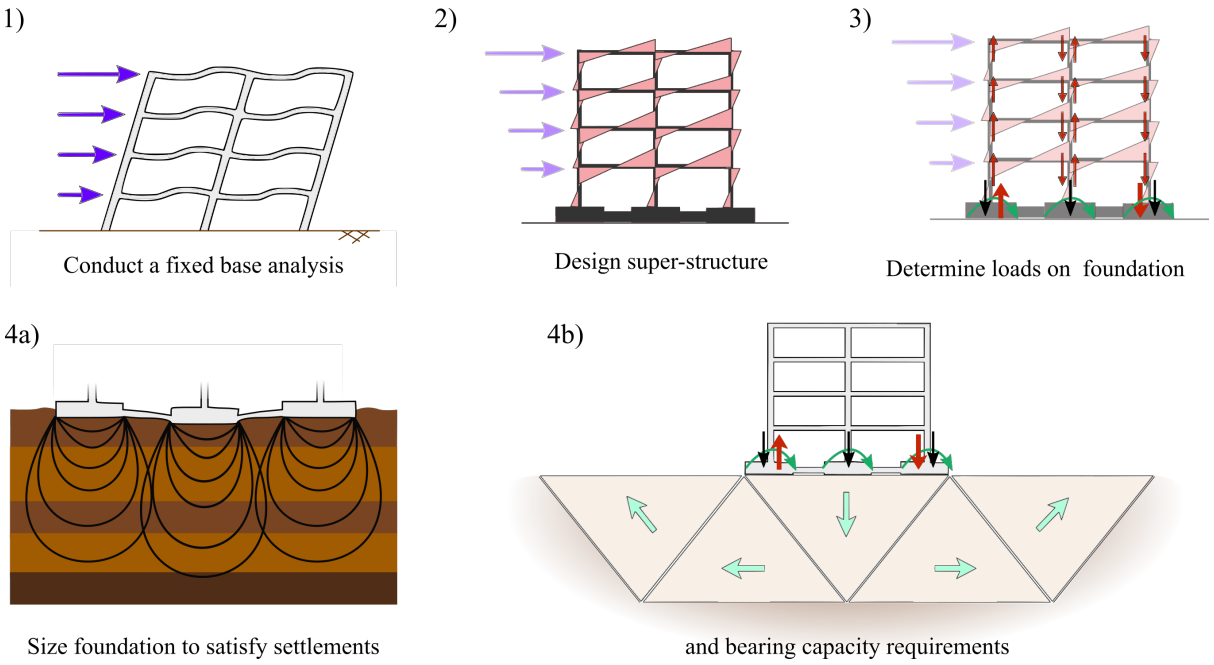

Figure 3.1: Conventional design of building and foundation

There is an inconsistency with the conventional design approach, essentially the superstructure is designed assuming zero foundation deformation (eg. angular distortion and settlement), while the foundation design has minimal consideration for minimising foundation deformation. The pseudo-static procedure for considering seismic demands fails to capture key mechanisms of cyclic dynamic loading. By not accounting for the dynamic effects of SFSI or attempting to control SFSI-induced residual deformations the foundation design can be irrationally over or under designed and the designer does not have the procedures available to optimise it.

3.3 Aspects of an integrated performance-based building-foundation design

3.3.1 Deformation mechanisms

The proposed design procedure attempts to consider all the major deformation mechanisms and forces in the soil, foundation and superstructure. In this section these mechanisms are systematically assessed demonstrating their importance to the seismic response, and how they can be accounted for in the design procedure.

Fixed base deformations

To determine the major mechanisms of deformation we can first consider only deformations in the superstructure and consider the soil and foundation as rigid (Figure 3.2).

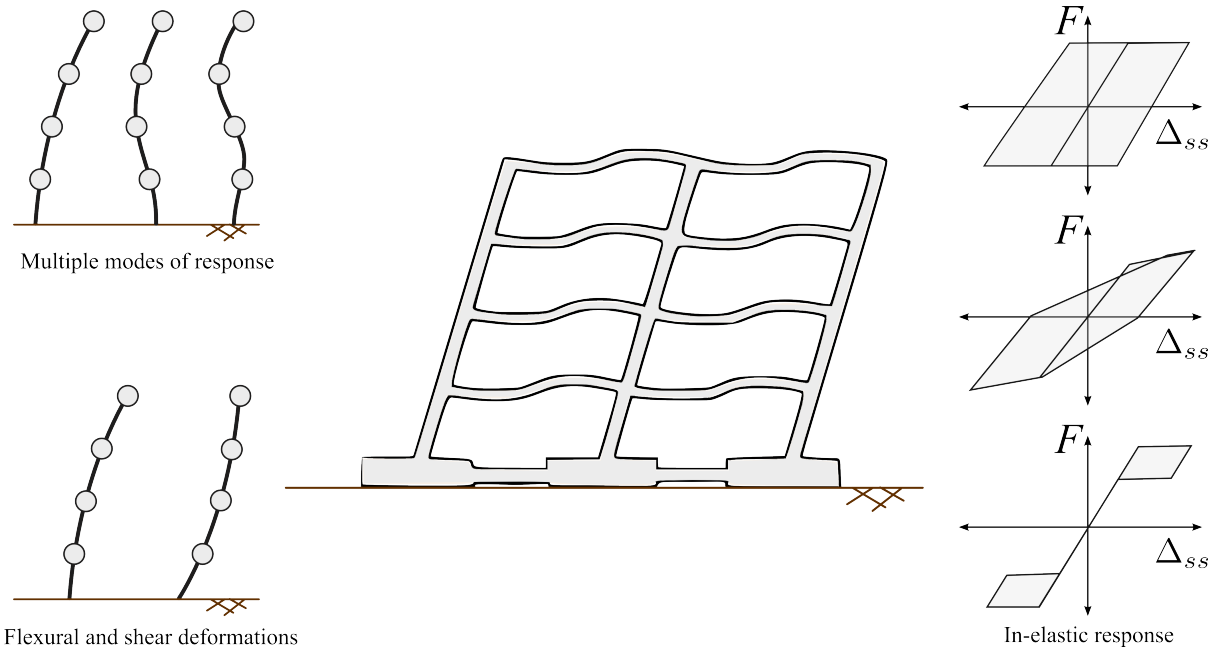

Figure 3.2: Superstructure deformation considerations

This basic model of the system demonstrates several complex mechanisms, including: inelastic structural response, multiple modes of response, and shear and flexural deformations.

The inelastic structural response of the superstructure is often allowed for in a design as the yielding of the structure can be used to limit the forces and accelerations in the structure. The inelastic response of the structure modifies the flexibility, energy dissipation and displacements.

The key performance parameters for superstructure deformations are the peak and residual inter-storey drifts. The prediction of peak deformations has been studied by numerous researchers and there are several equivalent linear methods as well as more complex methods involving non-linear time history analysis. In this dissertation the DDBD from Priestley et al. (2007) along with the displacement modification factors from Pennucci et al. (2011a) were used to estimate the peak inter-storey drift. The estimated peak inter-storey drift can then be used to estimate the residual deformations as the level of residual deformation is highly dependent on the level of non-linear displacement and the hysteretic properties of the structure.

While DDBD is a first mode design procedure, it recognises that higher modes can amplify the forces and displacements up the structure. The multiple modes of response are due to the distributed mass of the superstructure often considered as lumped at the floor levels. The

distribution of mass, stiffness and strength up the structure affects the amount of participating mass in each mode, which changes as the structure deforms inelastically. The factors suggested by Priestley et al. (2007) were used in this dissertation to modify the displacements, the shear and moment up the structure due to high mode effects.

Deformable structure and soil, rigid foundation mechanisms

By releasing the constraint on the soil, rigid-body mechanisms can contribute to the seismic response of the system (Figure 3.3).

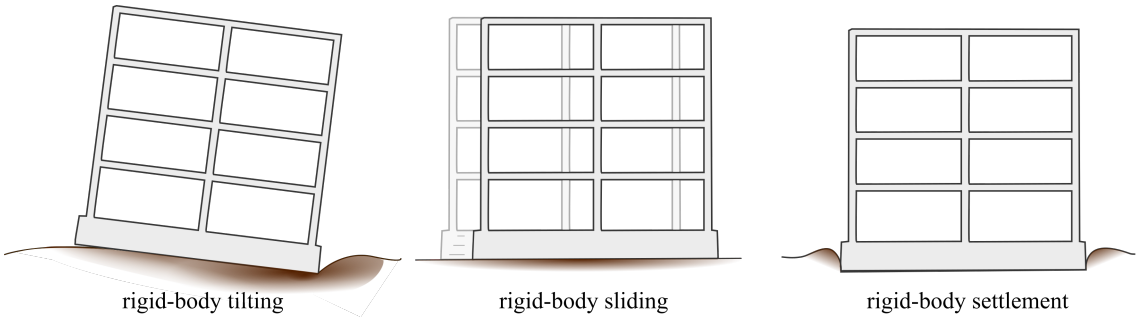

Figure 3.3: Flexible soil (rigid-foundation) deformations

The foundation rotation and soil-foundation shear deformation provide additional flexibility to the translational mode of vibration, thus modifying the seismic response of the building. When structures are tall with small foundations the foundation rotation can provide considerable modification to the dynamic properties of the system.

The additional mechanisms allow for deformation in the system that can limit the forces in the structure, however, the additional flexibility tends to result in increased displacements. The foundation rotation and shear deformation are non-linear and therefore the choice of soil-foundation stiffness and level of energy dissipation must be quantified for use in design and to allow accurate predictions of the transient displacements of the soil-foundation-structure system.

Foundation rotation

Three separate mechanisms can contribute to foundation rotation (Figure 7.1):

- Elastic rotation is a linear elastic mechanism, where the rotation is fully recoverable and the elastic stiffness comes from the footing dimensions, initial shear modulus and Poisson's ratio of the soil.
- Uplift is a non-linear elastic mechanism, whereby the deformation is fully recoverable but the rotational stiffness reduces as uplift occurs due to a geometric non-linearity.

- Soil yielding (plastic rotation) is a non-linear inelastic mechanism, whereby the rotation is not recoverable and the stiffness changes as the soil yields.

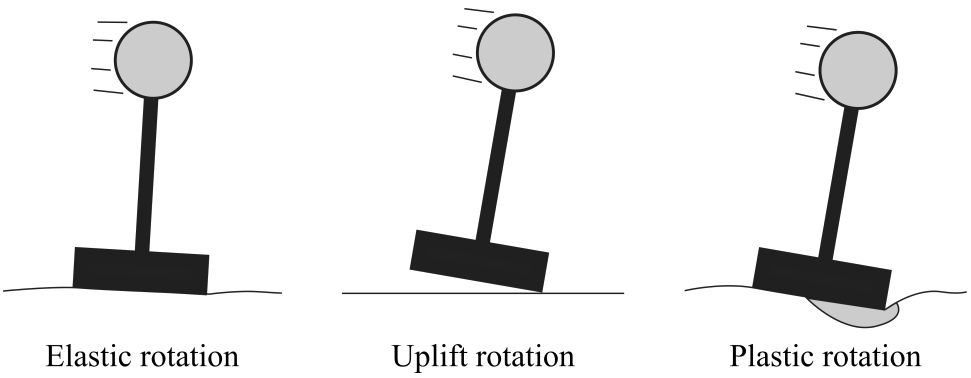

Figure 3.4: Mechanisms of foundation rotation

Each of these mechanisms contributes different amounts of rotation depending on the level of axial load, strains in the soil and amount of rotation. The elastic rotation tends to be dominant for small levels of rotation, while for large rotations the heavily loaded footings have mainly soil yielding and the lightly loaded footings have mainly uplift, as conceptually shown in Figure 3.5. The predictions of peak rotation and residual rotation are highly dependent on the non-linear deformation and whether it is inelastic (irrecoverable) deformation or not. The level of peak and residual deformation is also influenced by the non-linear behaviour of the structure where eccentric P-delta loads from residual superstructure deformations may cause a ratcheting effect on the foundation deformations.

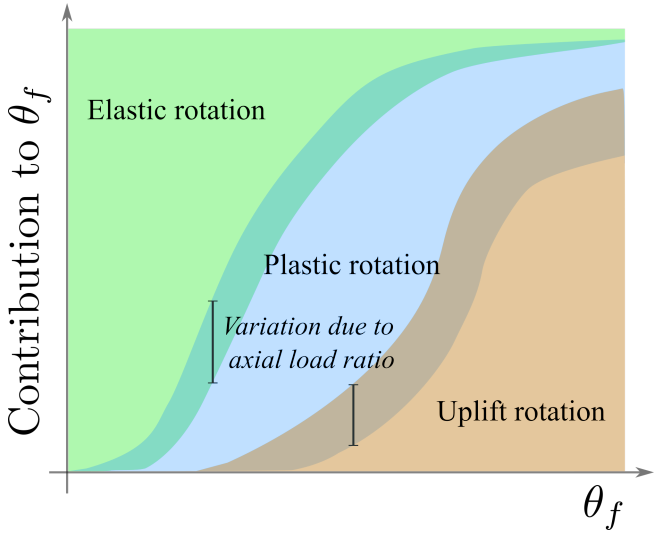

Figure 3.5: Contributions from rotation mechanisms

Foundation settlement

A mechanism approach can also be applied to the settlement. Two mechanisms contribute to settlement, static settlement and SFSI-induced settlement. The static component can be

considered as the settlement from the compressibility of the soil under the applied gravity loads and many methods already exist to estimate the magnitude (eg. Schmertmann, 1999), thus it will not be discussed further here. The SFSI-induced settlement occurs due to a shakedown of the foundation into the soil through subsequent cycles of irrecoverable soil yielding through rotation (Figure 7.4).

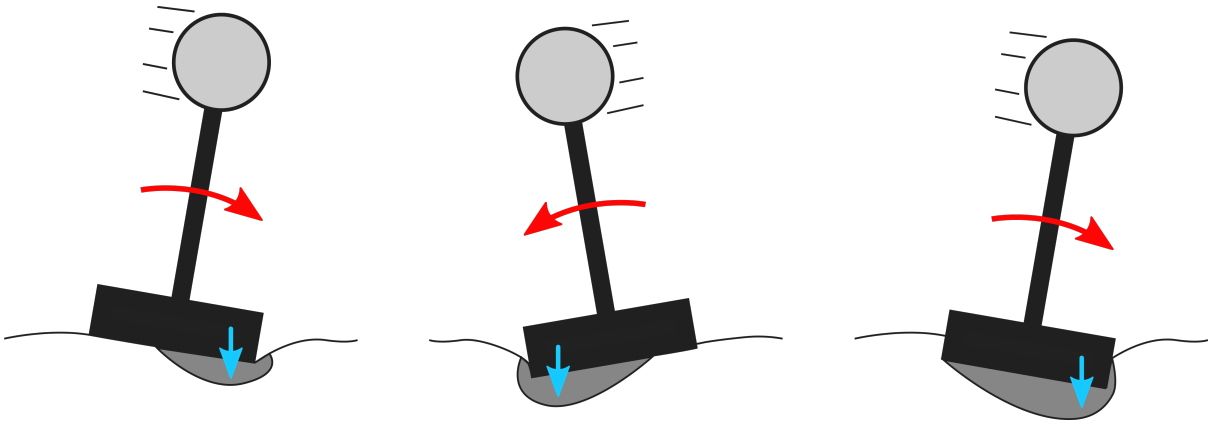

Figure 3.6: Dynamically induced foundation settlement

The level of settlement induced in a single cycle has been investigated by Gajan et al. (2005) through an extensive set of cyclic loading tests of footing under centrifugal conditions. Gajan et al. (2005) findings demonstrated a strong influence from the axial load, the level of rotation and the relative density of the soil. Further research by Deng and Kutter (2012) investigated the link between settlement and 'cumulative plastic rotation', where the axial load was also recognised as an important parameter.

The prediction of settlement is important for the design of buildings to avoid excessive settlements that would render the building unusable. Settlement occurs due to shear forces yielding the soil and therefore the influence of foundation shear forces and higher mode shear forces is of interest in the prediction of SFSI-induced settlements, as well as the quantification of effects of axial load, peak rotation and other influential parameters.

The effects of SFSI on the superstructure behaviour

Also of interest in for an integrated building-foundation design is how SFSI influences the superstructure behaviour in terms of peak and residual deformations. SFSI results in a softening of the system at the base of the structure, thus less force is potentially entering the structure so potentially less yielding of the superstructure. The reduction in yielding and change of vibration period of the structure may reduce the level of residual deformation, although counter to this is the influence of eccentric P-delta forces from foundation residual deformations that may cause a ratcheting effect which increases superstructure deformations.

The softening at the base of the structure may also influence how the high modes contribute to the displacement of the system. The deformation at the foundation level immediately

shifts the first mode period and can even cap the magnitude of the forces in the first mode by providing a non-linear mechanism at the base of the structure. A mechanism at the base hardly influences higher modes at all, resulting in a greater proportional increase in the influence of higher modes, thus design procedures that are based on the first mode response, such as DDBD should recognise this. To demonstrate this effect a cantilever column with distributed mass along its length can be considered in Figure 3.7. The first three modes are all shown for both the fully elastic cantilever and for the non-linear case, where the cantilever forms a perfect hinge at the base. Notice how the first mode period tends to infinity while the second and third mode periods are only shifted by 33% and 20% respectively.

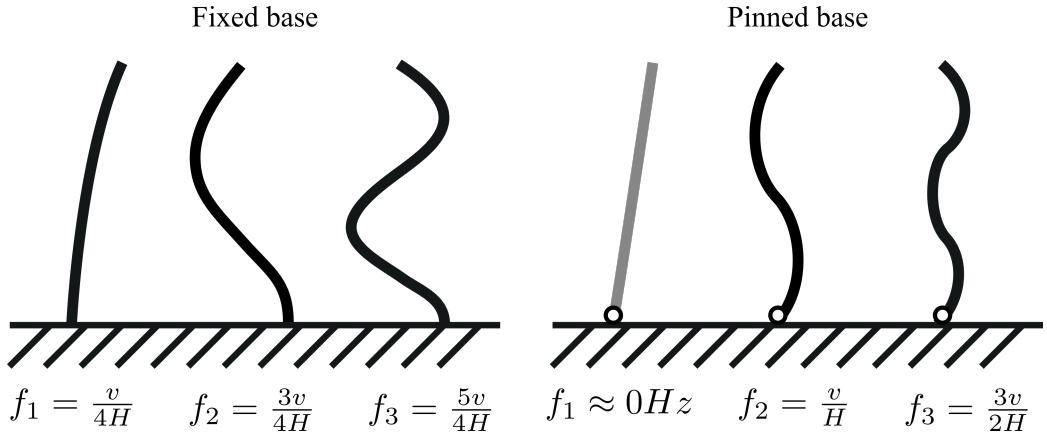

Figure 3.7: Influence on vibration modes due to a nonlinear mechanism at the base for a distributed mass model

Deformable structure, soil and foundation mechanisms

Finally the deformations in the foundation can be considered (Figure 3.8). The major mechanisms being the localised rotations and vertical non-uniform deformations that can occur in the footings of the foundation. The relative horizontal displacements of footings are not very common unless the soil suffers from lateral spreading and if so, then large deformations can cause large ground floor column curvatures.

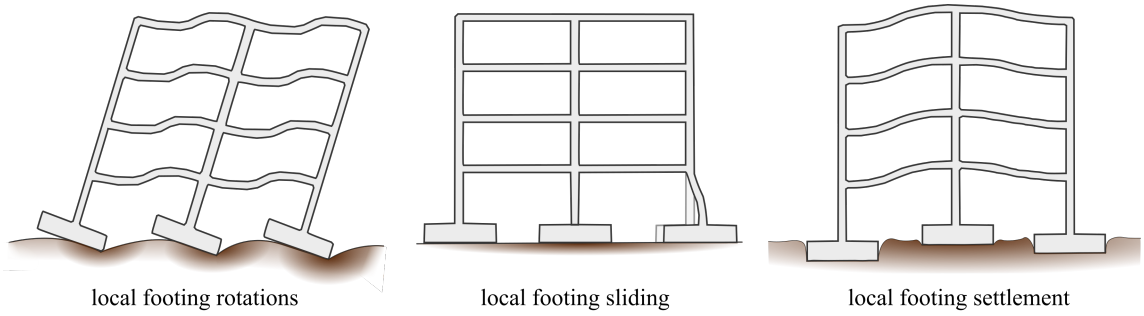

Figure 3.8: Flexible foundation deformations

The level of deformation from each mechanism is governed by the geometry of the structure

and its footings. Figure 3.9 considers two hypothetical frames to demonstrate this. The left frame has short wide footings, which have relatively low rotational stiffness and high vertical stiffness; the right frame has long thin footings, which have high rotational stiffness but a comparatively low vertical stiffness. The two buildings have the same superstructure but under earthquake loading the internal moments that develop are noticeably different. The low rotational stiffness in the left frame means that the moment demand is largely distributed to the beams; while the relatively low vertical stiffness in the right frame limits the shear and moment demand that can be generated in the beams.

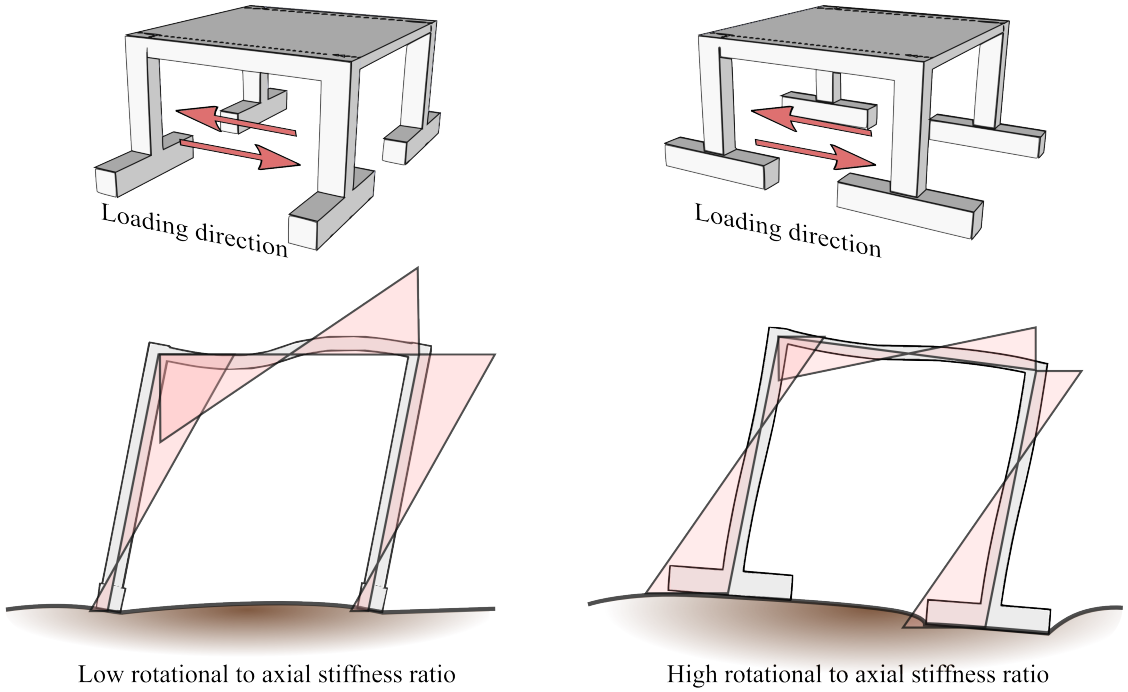

Figure 3.9: Variations in foundation rotational and vertial stiffness and corresponding displaced shape and moment demand

The effect of frame action must also be considered on the behaviour of the individual footings, where the additional cyclic axial load creates a further mechanism for settlement and asymmetric rotational stiffness and strength. As the axial load reduces the footing is more likely to uplift as illustrated in Figure 3.10. The asymmetric behaviour may result in additional permanent deformations.

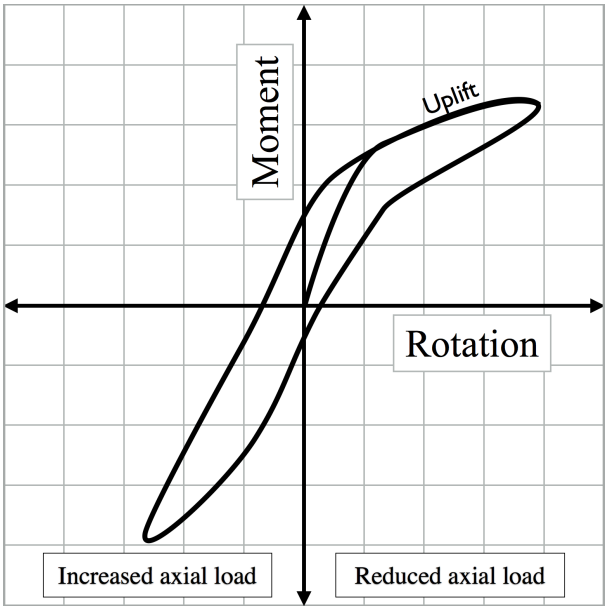

Figure 3.10: Frame action causing assymetric foundation rotational stiffness and strength

3.3.2 Performance based design

A performance-based design framework means that the building-foundation system must satisfy a series of performance criteria for several different levels of seismic hazard, thus rationally managing the risk by designing according to the level of acceptable risk and the level of exposure to the hazard.

Most modern design standards are based on a performance-based design framework to some extent, however, in some design standards the definitions of individual performance levels are ambiguous and limited to just two performance levels. The values presented in Priestley et al. (2007) (Table 3.1) provide clear requirements on the performance for various levels of building importance and different likelihoods of occurrence, thus effectively managing the risk.

Where the level of performance is dependent on the hazard and the importance of the structure (see Figure 3.11).

The design levels specified in Table 3.1, correspond to:

- Level 1: Immediate occupancy and functionality
- Level 2: Repairability
- Level 3: Collapse prevention

The importance classes are from EC 8 (2004):

- Importance level 1: Buildings of minor importance for public safety

- Importance level 2: Ordinary buildings, not belonging in the other categories
- Importance level 3: Buildings whose seismic resistance is of importance in view of the consequences associated with a collapse
- Importance level 4: Buildings whose integrity during earthquakes is of vital importance for civil protection

Table 3.1: The probability of exceedance for a performance level in relation to importance of structure (Priestley et al., 2007)

Importance Class	Level 1	Level 2	Level 3
I	Not required	50% in 50 years	10% in 50 years
II	50% in 50 years	10% in 50 years	2% in 50 years
III	20% in 50 years	4% in 50 years	1% in 50 years
IV	10% in 50 years	2% in 50 years	1% in 50 years

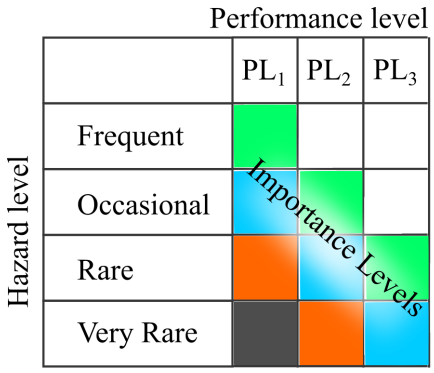

Figure 3.11: Variation in performance and return period based on importance level

3.3.3 Suitable combination of limit states

The performance of a building is measured through a series of performance parameters which have limits set at each performance level. To provide satisfactory building performance the designer must understand how various performance parameters from the foundation and superstructure can be combined to form an overall system performance.

Commonly the superstructure and the foundation are designed separate and therefore the performance criteria set for each are separate as well. Unfortunately, the recent Christchurch earthquake sequence resulted in structurally repairable buildings being demolished due to extensive foundation damage (Cubrinovski and McCahon, 2012), while the reverse was also evident, with extensively damaged superstructures sited on almost unscathed foundations. This discrepancy between performances can be unnecessarily wasteful and a more holistic design approach whereby the performance of the foundation and superstructure are consider in combination may reduce this mismatch.

The combination of the foundation and superstructure performance levels requires weighting factors which represent the relative importance of the performance criteria in relation to the overall system performance as conceptually displayed in Figure 3.12.

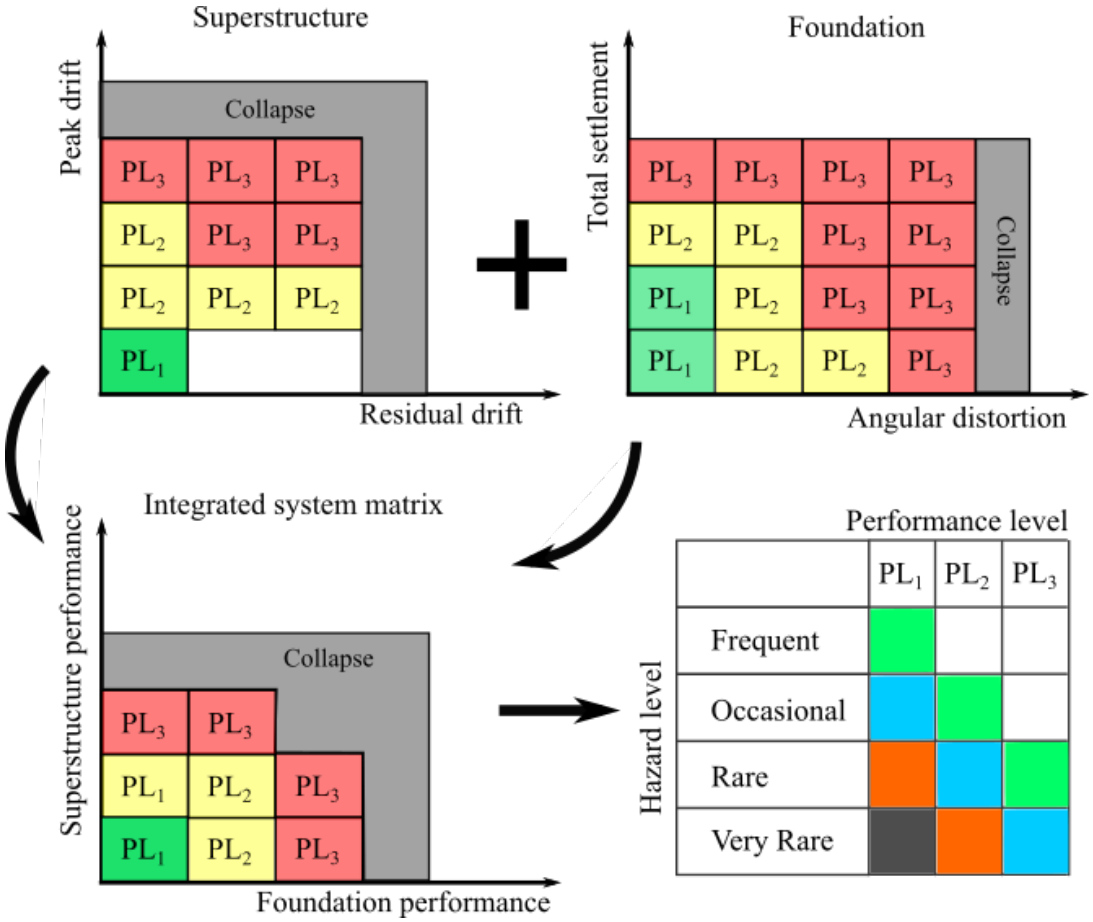

Figure 3.12: Method to establish performance matrix

In Figure 3.12 it can be seen that the superstructure peak drift and residual drift are combined to give a superstructure performance level (from Christopoulos and Pampanin (2004)) and the same is carried out for the foundation. These two performance levels are combined in the integrated system matrix and the system performance level is assessed against the performance matrix for a given hazard level to determine whether it meets the design objectives. This approach allows the designer to chose the level of performance at both the foundation and the superstructure and assess whether this would result in suitable performance of the system.

Foundation performance levels

Previous attempts to provide foundation performance criteria for DDBD can be found in (Sullivan et al., 2012), which limit the reduction of equivalent (secant) soil shear stiffness. The equivalent soil shear stiffness can provide an indication to the level of inelastic response but

does not provide an indication to the level of residual deformations that can be expected. Further issues with the equivalent soil shear stiffness as a parameter is that it is not unique and requires considerable interpretation, as well as the current curves used in the DDBD procedure do not directly consider soil stiffness and only consider foundation rotational stiffness (Paolucci et al., 2013). The foundation rotational stiffness is based on three separate mechanisms, the first being elastic deformation, the second being soil yielding and the third being foundation uplift. Imposing severe limits on the level of foundation stiffness degradation when the degradation is predominantly due to the elastic uplift mechanism may be misguided.

Alternatively, imposing direct limits on deformations (Figure 3.13), such as foundation residual rotation, settlement and peak foundation rotation, provide intuitive and measurable limitations to the performance.

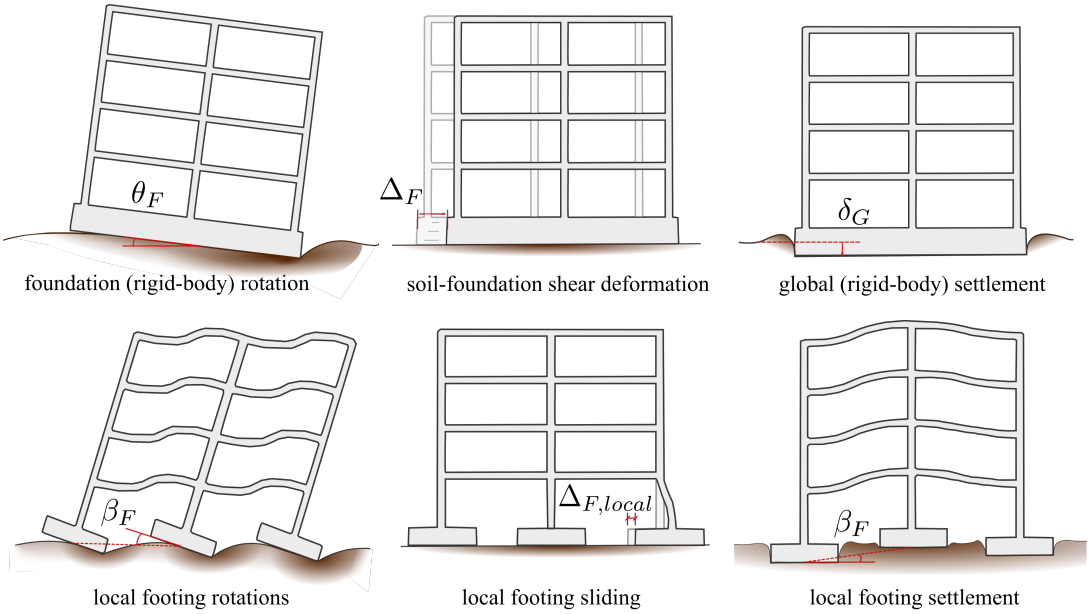

Figure 3.13: Foundation deformation mechanisms

Superstructure performance levels

The limitations on superstructure peak drift are governed by material strains, non structural elements drift limits, pounding against adjacent structures and toppling. Different design standards specify different requirements on each of these parameters depending on the material and perceived level of risk. Design limits will continue to shift as new design methodologies can allow for greater displacements with less damage while other performance parameters such as floor accelerations may be recognised as more important as designers look to further protect the buildings contents.

Global performance levels

The foundation and superstructure limit states provide useful limits on the deformations. However, an investigation into the performance of buildings during the Christchurch earthquakes by Giorgini et al. (2014) has shown that buildings were deemed irreparable due to superstructure damage, foundation damage or a combination of both. Global performance criteria such as limiting the total (superstructure plus foundation deformations) peak and residual drift could be used to reduce the mismatch between the superstructure performance and the foundation performance, and to ensure that the overall performance is satisfactory.

Controlling the performance during design

The performance-based assessment framework outlines acceptable levels for performance parameters at a global level (toppling, pounding, residual drifts, settlements), element level (beam curvatures, column curvatures, foundation curvatures, non-structural elements displacement demands) and material level (concrete strains, rebar strains) for certain levels of earthquake loading. The performance parameters intrinsically satisfy a series of response limit parameters relating to life safety, usability and economic loss. A performance-based design procedure must allow the designer to satisfy all of the performance parameter conditions through carefully chosen design parameters. Figure 3.14 demonstrates how the two parameters, peak superstructure drift and peak foundation rotation, can be used to satisfy all the considered performance criteria. By developing analytical or empirical relationships between the chosen design parameters and all of the other design parameters, the design parameters can be restricted in their deformations and thus satisfy the performance objectives and implicitly satisfy the response limit parameters.

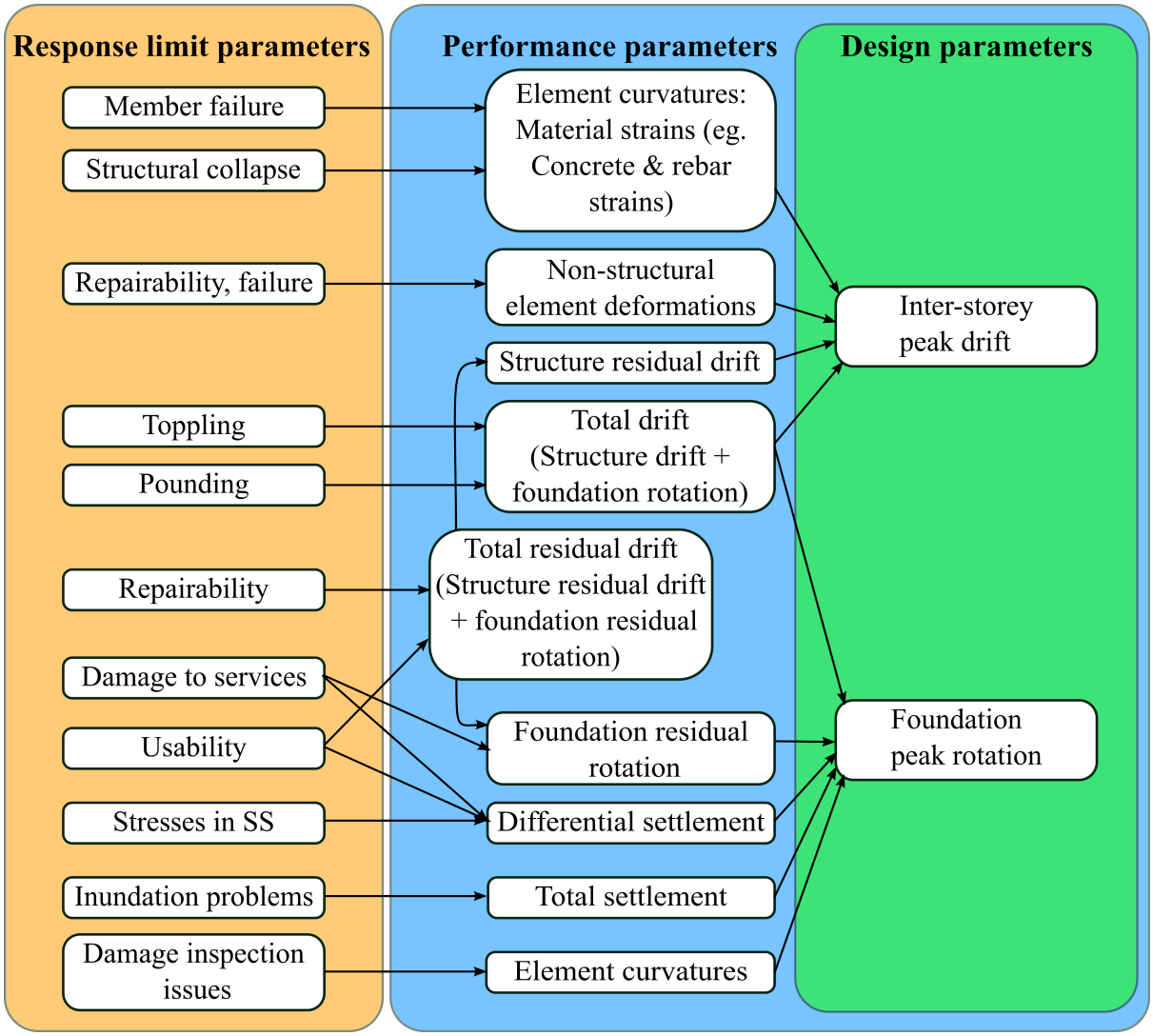

Figure 3.14: Controlling performance limits using two design parameters

3.3.4 SFSI considerations in Direct Displacement-based Design

The fundamental steps from Paolucci et al. (2013) for a DDBD considering dynamic non-linear soil-foundation-structure interaction are presented conceptually in Figure 3.15, where the design loads for a non-linear, multiple degree-of-freedom structure are determined based on an equivalent linear SDOF. The first step uses an assumed displaced shape (Δ_i) based on the first mode response at peak design response, which accounts for the displacement contribution from foundation deformations. The displaced shape and an assumed mass distribution (m_i) are used to determine an equivalent SDOF mass (m_e), effective height (H_e) and equivalent displacement (Δ_e). The non-linear behaviour is converted to an equivalent linear behaviour in steps two and three. The secant-to-peak stiffness is used as the effective stiffness (K_{eff}) and the equivalent viscous damping is determined based on the displacement contributions from the foundation (Δ_f) and superstructure (Δ_{ss}) and their corresponding hysteretic behaviour. The effective period (T_e) is determined based on the interception of the design displacement

with the reduced spectral displacement, where the spectral displacement is reduced based on the EVD. The final step is to compute the base shear (V_{base}) from the effective stiffness and the design displacement.

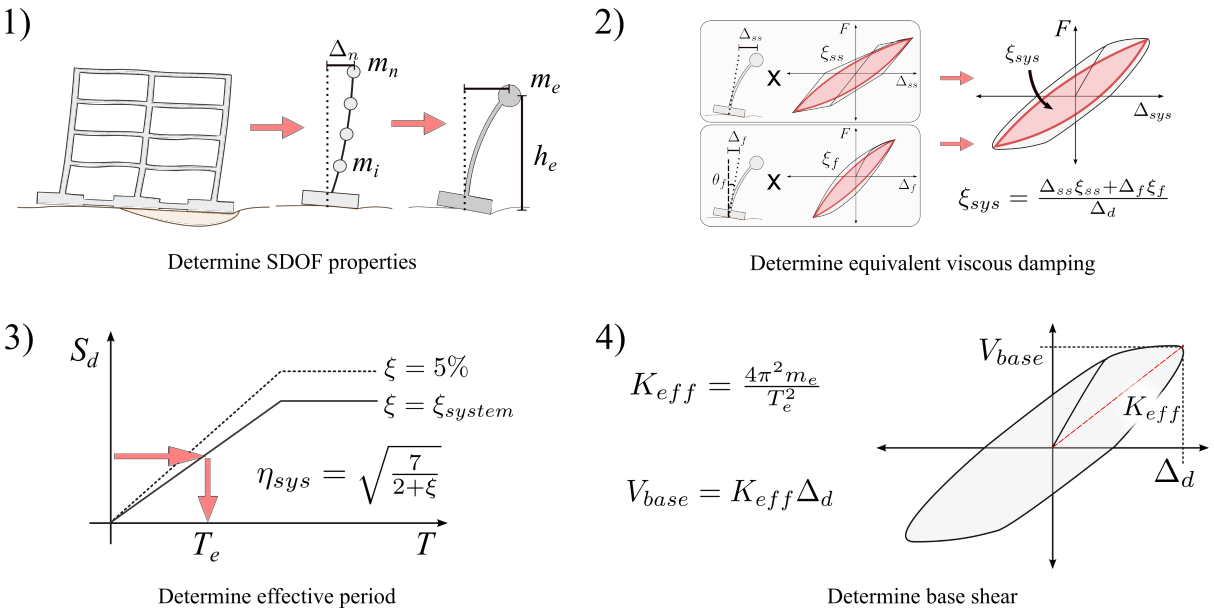

Figure 3.15: Direct displacement based design procedure considering non-linear SFSI *after Paolucci et al. (2013)*

This procedure presents a rational approach to the design of buildings considering dynamic soil-structure interaction as it directly accounts for the change in the dynamic properties of the system due for foundation rotation. The change in the first mode shape is recognised through the consideration of foundation rotation in the displaced shape. The energy dissipation from the foundation is recognised through equivalent viscous damping and the change in superstructure ductility is recognised through the contribution of the foundation to the overall displacement.

However, the procedure proposed by Paolucci et al. (2013) has not been experimental validated and only a single set of numerical tests were presented as validation where the results showed a poor match between expected and numerically obtained displacements. The discrepancy between the displacements was mainly attributed to the difference between the design foundation stiffness and foundation equivalent viscous damping estimates compared to those obtained from the numerical model. The procedure is also limited in that it ignores other soil-foundation deformation mechanisms, such as foundation shear deformation. Finally the procedure uses equivalent viscous damping as a parameter to reduce the spectral displacement, which has been recognised by Pennucci et al. (2011a) as being sensitive to the frequency content of ground motions. The issue of equivalent viscous damping is compounded when combined with the unfounded use of equivalent viscous damping expressions that are defined based on the equal hysteretic to viscous energy dissipation assumption.

Many of the fundamental steps of the above procedure can provide the basis for a design procedure that can be validated through numerical modeling and that reasonable includes the additional SFSI mechanisms and calibrated displacement reduction factors instead of equivalent viscous damping.

3.4 Conclusion

This chapter provides an overview of the various aspects of SFSI and performance-based design to explain the requirements and motivation for the proposed design procedure. The shortfalls of the conventional pseudo-static design approach for buildings and foundation were discussed. The deformations of the soil-foundation-structure system were discussed through individual mechanisms by first looking at only structural deformations and incrementally including further into soil and foundation deformations. The expected interactions between different mechanisms were discussed to provide a basis for the development of numerically calibrated expressions in later chapters. Finally the advantages and limitations of the current procedure for including soil-foundation deformations into a DDBD procedure were discussed.

Chapter 4

Implementation of a soil-foundation macro-element for non-linear time-history analysis

4.1 Introduction

The consideration of soil deformations and soil-foundation-structure interaction in design and analysis is becoming common place for structural engineers. This is largely motivated the need to understand and quantify the complex dynamic behaviour of SFS systems to check loads and transient displacements, or to evaluate the effects of soil and foundation flexibility on permanent deformations.

The practicing engineering community is often constrained to considering the soil-foundation interface through a series of linear un-coupled springs and dashpots, which can miss some of the most beneficial effects of SFSI (Pecker and Chatzigogos, 2010) as well as the potentially detrimental consequences (Moghaddasi et al., 2012). While direct mesh finite-element modeling of the soil and structure can capture the non-linear effects, it requires a vast knowledge of soil and structural mechanics as well as experience in finite element modeling. The calculation intensive approach of directly modeling the soil, foundation and structure in a full finite element mesh is not a practical option for many non-critical structures due to the time and expertise required. The need for a simple, reliable and sufficiently accurate numerical tool to predict the non-linear soil-foundation interface has prompted considerable development in lumped parameter approaches to consider soil-foundation-structure-interaction (SFSI).

Two different numerical approaches dominate this type of analysis, the conventional Winkler-beam (Figure 4.1a) and the macro-element (Figure 4.1b). The Winkler-beam uses a series of independent translational springs that can yield and detach (eg. El Ganainy and El Naggar, 2009; Harden and Hutchinson, 2009). The combination of the springs provides the rotational and vertical stiffness of the footing, while an additional uncoupled translational spring models horizontal stiffness. The macro-element models the rotational, horizontal and vertical

stiffness of the foundation directly using coupled translational and rotational springs. The condensation down to only one spring for each degree-of-freedom or mode of deformation (axial, shear and moment) is provided for by assuming that the footing itself acts as a rigid body. The non-linear effects, such as uplifting and soil yielding, are captured by considering the coupling of the forces through a coupled hysteretic model. Dashpot elements can be added in parallel to the macro-element to model the radiation damping in each degree-of-freedom. The macro-element formulation allows for greater control of the coupling between the different loadings, which is one of the shortfalls of the Winkler-beam model. The macro-element is the model used in this dissertation to capture the behaviour at the soil-foundation interface.

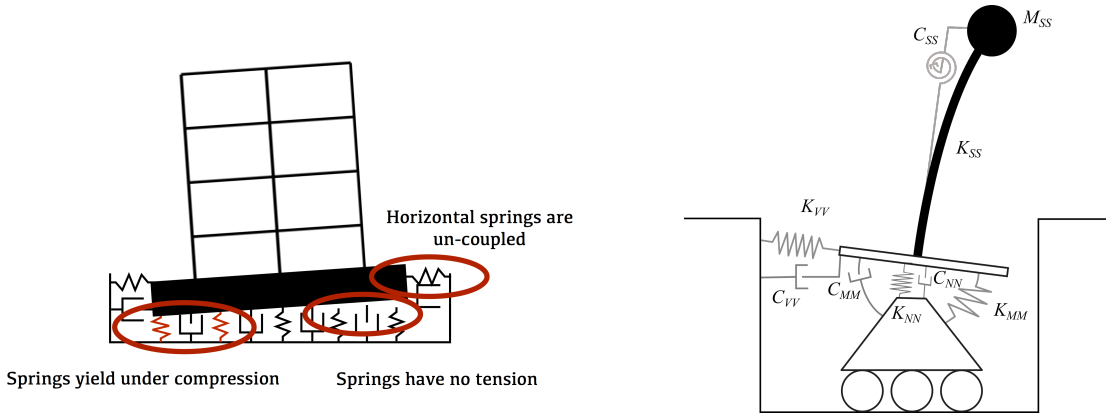

(a) Winkler-beam (b) Macro-element

Figure 4.1: Lumped plasticity models for SFSI analysis

The first macro-element for modeling soil behaviour was suggested as early as Roscoe and Schofield (1957), while the full development of a plasticity framework for monotonic loading was achieved by Nova and Montrasio (1991) with a non-associative flow rule for a foundation on sand. Additional developments of this model include (eg. Houlsby and Martin, 1999; di Prisco et al., 2003; Bienen et al., 2006). Paolucci (1997) was the first to implement a macro-element into dynamic seismic analysis using an elastic-perfectly plastic formulation. Cremer et al. (2001, 2002) included a distinct uplift mechanism which was combined with the plasticity model to give the overall response for strip footings on cohesive soils. The Paolucci et al. (2008) model introduced a degradation factor to account for softening of the response due to the rounding of the soil contact surface from irrecoverable deformations. Chatzigogos et al. (2009) developed a model with coupled plasticity and uplift mechanisms for undrained soil conditions. Chatzigogos et al. (2011) extended the Chatzigogos et al. (2009) model to capture frictional soils and frictional sliding with a non-associative flow rule. Figini et al. (2012) used the bounding surface suggested by the failure envelope from Nova and Montrasio (1991) to model foundations on sand and used a vertical mapping rule to define the image point resulting in reduced levels of settlement under small cycles. Figini et al. (2012) adopted the degradation model used by Paolucci et al. (2008) and the uplift formulation was based

on works by Wolf (1988). The experimentally validated macro-element model developed by Figini et al. (2012) gives good approximations to base moment, base shear, rotation, translation and settlement, with validations against experimental tests from Negro et al. (1999), Combescure and Chaudat (2000) and Shirato et al. (2008).

4.2 Aspects of the macro-element

The model presented here is based on the uplift model from Chatzigogos et al. (2009, 2011) and the plasticity formulation from Figini et al. (2012). The combined model has been implemented into the non-linear time history analysis program Ruaumoko3D (Carr, 2015). Ruaumoko3D solves the equations of motion in force, distance and time space, while the macro-element formulation is presented and implemented using normalised displacements and forces (Equations 4.1 - 4.3). At every time step an algorithm converts the global forces from the structure into the normalised form to run the macro-element algorithms to compute the normalised stiffness. The normalised stiffness is then converted back to the global values to be input into the global stiffness matrix.

The forces (N - axial load, V - shear load, M - moment load) and normalised forces (Q) are shown in Equation 4.1, which have been normalised by the static ultimate axial capacity of the footing (N_{max}) and the footing length (L) respectively.

$$Q = [Q_N, Q_V, Q_M] \qquad = [\frac{N}{N_{max}}, \frac{V}{N_{max}}, \frac{M}{N_{max}L}] \tag{4.1}$$

The displacements (δ_N - axial displacement, δ_V - shear displacement, θ_M - rotation) and normalised displacements (q) are shown in Equation 4.2.

$$q = [q_N, q_V, q_M] \qquad = [\frac{\delta_N}{L}, \frac{\delta_V}{L}, \theta_M] \tag{4.2}$$

The stiffness matrix (K_{glob}) and normalised stiffness matrix (κ) are shown in Equation 4.3

$$\kappa = \begin{bmatrix} \kappa_{NN} & \kappa_{VN} & \kappa_{MN} \\ \kappa_{NV} & \kappa_{VV} & \kappa_{MV} \\ \kappa_{NM} & \kappa_{VM} & \kappa_{MM} \end{bmatrix} \qquad = \frac{K_{glob}}{N_{max}} \begin{bmatrix} L & L & 1 \\ L & L & 1 \\ 1 & 1 & 1/L \end{bmatrix} \tag{4.3}$$

The stiffness matrix is composed of two components connected in series, the elastic stiffness and the plastic stiffness, which result in elastic and plastic displacements (Equations 4.4 - 4.5). The elastic stiffness accounts for the elastic impedance of the soil based on the foundation geometry and fitted over a frequency range of interest (eg. Gazetas, 1991), as well as capturing

the geometric non-linearity associated with uplift behaviour. The 'plastic' stiffness captures the plastic deformation associated with the yielding of the soil.

$$\frac{1}{\kappa} = \frac{1}{\kappa^{elastic}} + \frac{1}{\kappa^{plastic}} \tag{4.4}$$

$$q = q^{elastic} + q^{plastic} \tag{4.5}$$

4.2.1 Elastic stiffness

For the purely elastic case with minimal embedment, the off diagonal stiffness terms are negligible, therefore the elastic stiffness matrix consists of only the following impedance terms.

$$\kappa_{elastic} = \begin{bmatrix} \kappa_{NN} & 0 & 0 \\ 0 & \kappa_{VV} & 0 \\ 0 & 0 & \kappa_{MM} \end{bmatrix} \tag{4.6}$$

The diagonal terms can be approximated based on the foundation impedances derived based on early works on machine vibrations. A variety of textbooks and software packages are available to determine these values for different shaped footings and soil profiles (eg. Mylonakis et al. (2006)). Table 4.1 displays the closed form elastic foundation stiffness and radiation damping terms for circular footings, where the vertical term can be attributed to Boussinesq (1883), the horizontal term to Mindlin (1949) and the rotational term to Borowicka (1943). Table 4.2 displays the approximate solutions to arbitrarily shaped footings from Gazetas (1991), with no embedment on a homogeneous half space. The circular footings are in terms of the footing radius (R), Poisson's ratio (v) and the initial small-strain soil shear modulus (G). For the rectangular footings, l and b are the half length and width of the footing respectively and I_y is the area moment of inertia of soil-foundation contact (Figure 4.2). The k terms are the frequency dependent dynamic stiffness coefficients.

Table 4.1: Impedances for circular foundations

Mode	Stiffness
Vertical	$K_{NN} = \frac{4GR}{1-v}$
Horizontal	$K_{VV} = \frac{8GR}{2-v}$
Rotational	$K_{MM} = \frac{8GR^3}{3(1-v)}$

Table 4.2: Stiffness terms for rectangular foundations

Mode	Stiffness
Vertical	$K_{NN} = \frac{2Gl}{(1-v)}\left[0.73 + 1.54(\frac{b}{l})^{0.75}\right] k_n$
Transverse shear	$K_y = \frac{2Gl}{(2-v)}\left[2 + 2.5(\frac{b}{l})^{0.85}\right] k_y$
Longitudinal shear	$K_{VV} = K_y - \frac{0.2Gl}{(0.75-v)}\left[1 - \frac{b}{l}\right] k_v$
In-plane rotation	$K_{MM} = \frac{G}{(1-v)} I_y^{0.75}\left[3(\frac{l}{b})^{0.15}\right] k_m$
Out-of-plane rotation	$K_{xx} = \frac{G}{(1-v)} I_x^{0.75}(\frac{l}{b})^{0.15}\left[2.4 + \frac{b}{l}\right] k_m$

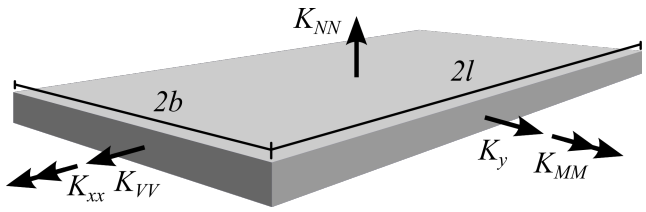

Figure 4.2: Notation for foundation stiffness terms

4.2.2 Uplift modeling

The uplift of the foundation results in a reduction of the contact area and elastic stiffness due to a geometric non-linearity. As the foundation uplifts, the contact area reduces with the resisting moment coming from the remaining surface contact and a force couple from the axial load as shown in the schematic in Figure 4.3.

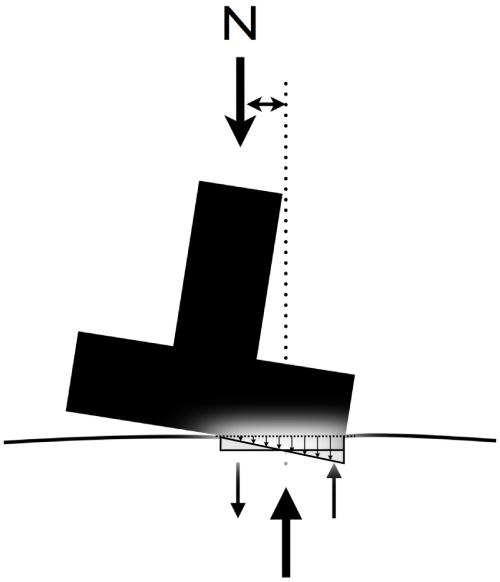

Figure 4.3: Overturning moment at uplift

The macro-element formulation requires that the displacements of the entire footing are represented as a single point and while the footing may behave as a rigid body, the displacements at each location on the footing are not the same. The macro-element formulation presented in this chapter uses the uplift model from Chatzigogos et al. (2009), which captures the displacements at the centre of the footing. This has the advantage of being a common location for joining columns and piers. An alternative formulation proposed by Wolf (1988) was implement by Figini et al. (2012) which captures the displacements at the centre of the compliant part of the footing, therefore requiring a geometric conversion to capture the displacements at joining members.

The uplift model proposed in Chatzigogos et al. (2009) constructs a tangent stiffness matrix by first assuming that the horizontal (shear) stiffness remains unaffected during uplift and therefore $\kappa_{VV} = \kappa_{VV}$ and the shear coupling terms are all equal to zero ($\kappa_{NV} = \kappa_{VN} = \kappa_{MV} = \kappa_{VM} = 0$). Uplift initiation is determined based on the moment exceeding some threshold level ($Q_{M,0}$) (Equation 4.7), where α is the factor controlling the uplift moment, based on the stress distribution under the soil. The uplift limit in the formulation is given as a pseudo uplift angle ($q^{el}_{m,uplift}$) (Equation 4.8), where the normalised uplift moment is divided by the normalised elastic stiffness (κ_{MM}) and uplift occurs when the elastic component of rotation exceeds the pseudo uplift angle. For a purely elastic case, the rotation at which uplift would occur would be equal to the pseudo uplift rotation, however when soil plasticity is considered the actual rotation would be greater due to the reduction in rotational stiffness

due to plasticity.

$$Q_{M,0} = \pm \frac{Q_N}{\alpha} \tag{4.7}$$

$$q^{el}_{m,uplift} = \frac{Q_{M,0}}{\kappa_{MM}} \tag{4.8}$$

The element's vertical and rotational stiffnesses are governed by Equations 4.9 - 4.11, where the form and values for the numerical parameters are based on finite element simulations from Wolf (1988) and Wolf and Song (2002) for circular footings and Cremer et al. (2001, 2002) for strip footings. Table 4.3 provides values for the uplift parameters to be consistent with the suggested values of Chatzigogos et al. (2011). The formulation was based on constant axial load, thus loadings with large changes in axial load may not be accurately captured. For more information on the derivation of these equations see Chatzigogos et al. (2009).

$$\kappa_{MN} = \kappa_{NN} * \epsilon(1 - \frac{q_{m,uplift}}{q^{elastic}_m}) \tag{4.9}$$

$$\kappa_{NM} = \kappa_{MN} \tag{4.10}$$

$$\kappa_{MM} = \kappa_{MM}\gamma\delta \left(\frac{q_{m,uplift}}{q^{elastic}_m}\right)^{(\delta+1)} + \kappa_{NN}\epsilon^2 \left(1 - \frac{q_{m,uplift}}{q^{elastic}_m}\right)^2 \tag{4.11}$$

Table 4.3: Default values for strip and circular footings

	α	ϵ	δ	γ
Strip	4.0	0.5	1.0	$1/\delta$
Circular	6.0	0.75	1.0	$1/\delta$

4.2.3 Plasticity formulation

The plasticity formulation adopted here is based on the macro-element proposed by Figini et al. (2012). This model employs a rugby ball shaped bounding surface with a vertical mapping rule. A bounding surface approach allows for continuous plastic response, with the shape based on the experimentally determined ultimate loads surface from Nova and Montrasio (1991) and almost identical to the experimentally determined surface of moment and axial load determined by Gajan et al. (2005). The rugby ball shape attempts to capture the reduction in the soil-footing contact area during uplift, which results in an increased load over the contact area and hence an additional yield deformation. This is in contrast to the elliptic bounding surface centred around the origin as used in Chatzigogos et al. (2009), which is based on a fully compliant footing and only the uplift model captures the reduction

in compliant area. The vertical mapping rule was justified by Figini et al. (2012) due to most footings having loads paths mainly in the $Q_M - Q_V$ plane and therefore the projection to the bounding surface should follow the load increments. This assumption is certainly true for wall and bridge pier structures, however, frame structures can experience considerable variations in axial load, which may invalidate such an assumption. For further discussion on the use of a vertical mapping rule, please refer to the paper by Figini et al. (2012).

The shape of the plasticity bounding surface is shown in light blue in Figure 4.4 and is constructed through Equation 4.12. The shape is governed through the parameters $Q_{V,max}$ and $Q_{M,max}$, which Figini et al. (2012) suggest $Q_{V,max} = 3/4 \tan\phi$, ϕ being the soil friction angle and $Q_{M,max} = \Psi$. Ψ can be defined according to the ultimate capacity of the footing under eccentric loading, eg. 0.48 from Vesic (1975). The other parameter, ξ is often taken as 0.95 to follow the bounding surface formulation by Nova and Montrasio (1991) with the advantage of having a vertical tangent at $Q_N = 1.0$, while a value of 1.0 for ξ would be in line with works by Georgiadis and Butterfield (1988).

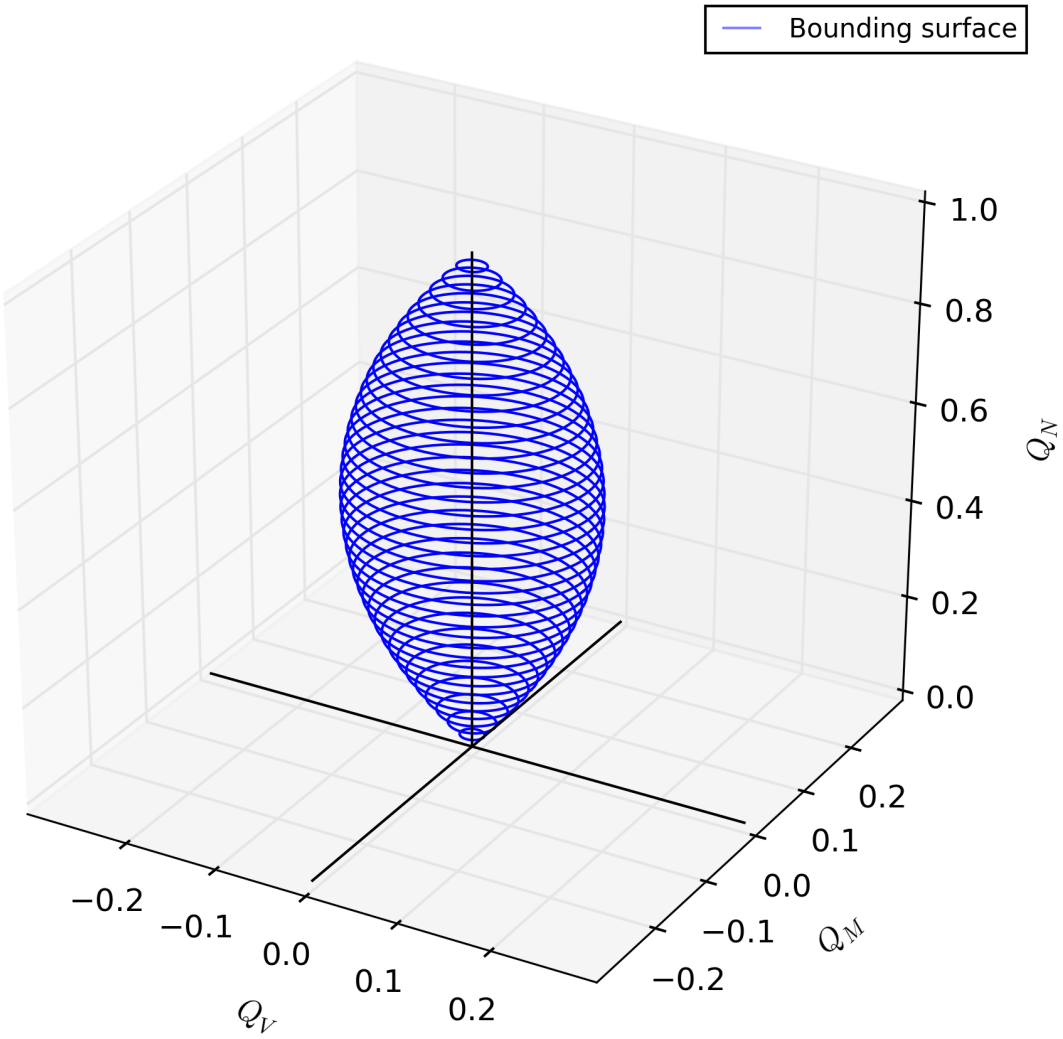

Figure 4.4: Foundation bounding surface

$$f_{BS}(Q) = \left(\frac{Q_V}{Q_{V,max}}\right)^2 + \left(\frac{Q_M}{Q_{M,max}}\right)^2 - Q_N^2(1 - Q_N)^{2\xi} \tag{4.12}$$

It is widely accepted that a frictional soil has non-associative plastic behaviour and the macro modeling of a foundation on such a soil should be no different. The plastic potential surface (G_{PS}) defines the direction of plastic flow and the shape of this surface is from Figini et al. (2012), as expressed in Equation 4.13. The shape takes the form of an ellipse centred on the origin in $Q_N - Q_V - Q_M$ space and the parameters λ and χ are introduced to control the radii.

$$G_{PS} = \lambda^2 \left(\frac{Q_V}{Q_{V,max}}\right)^2 + \chi^2 \left(\frac{Q_M}{Q_{M,max}}\right)^2 + Q_N^2 - 1 = 0 \tag{4.13}$$

Values of λ=2.5 and $\chi = 3.0$ were recommended by Figini (2010) as default values for predictive testing, however, these should be calibrated against experimental tests or finite element analysis results.

To compute the inverse plastic stiffness matrix (Γ^{-1}), the tensor product of the normal to the plastic potential surface and the bounding surface must be computed as in Equation 4.14. In this equation n_g is the normal to the bounding surface and n is normal to the plastic potential surface at the vertically mapped image point (Figure 4.5).

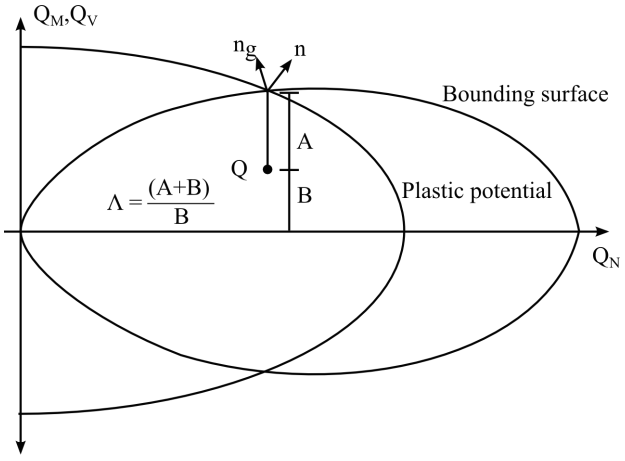

Figure 4.5: Plasticity formulation with vertical mapping rule

$$\Gamma^{-1} = \frac{1}{h} n_g \otimes n \tag{4.14}$$

The parameter h defines the magnitude of plastic modulus and is determined through Equa-

tion 4.15. The fitting parameter h_0 is a numerical constant in this formulation taken as some ratio (p_1) of κ_{NN} as in Equation 4.16. The second parameter, Λ is the ratio of the distance to vertically mapped image point on the bounding surface over the current load state (Q), taken from the Q_N axis as seen in Figure 4.5 and given by Equation 4.17.

$$h = h_0 \ln \Lambda \tag{4.15}$$

$$h_0 = p_1 \kappa_{NN} \tag{4.16}$$

$$\Lambda = \sqrt{\frac{Q_N^2 (1 - Q_N)^{2\xi}}{(\frac{Q_M}{Q_{M,max}})^2 + \frac{Q_V}{Q_{V,max}})^2}} \tag{4.17}$$

To determine whether the element is loading (plastic response) or unloading/neutral loading (elastic only), the force increment (Q_{inc}) is projected onto n, a positive projection results in loading behaviour (Figure 4.6).

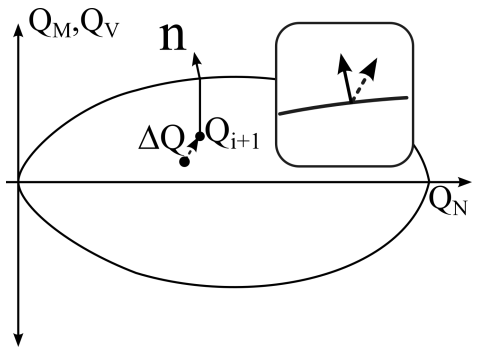

Figure 4.6: Determine the loading direction

$$\begin{aligned} Q_{inc} \cdot n > 0 \quad & \text{loading} \\ Q_{inc} \cdot n = 0 \quad & \text{neutral loading} \\ Q_{inc} \cdot n < 0 \quad & \text{unloading} \end{aligned}$$

The response is less plastic during reloading than during virgin loading. This increase in stiffness can be accounted for by replacing Equation 4.15 with Equation 4.18, where the parameter Λ_{min} is the lowest value of Λ obtained during the loading history to date and the parameter p_2 controls the increase in stiffness. For virgin loading $\Lambda = \Lambda_{min}$, which returns the same answer as Equation 4.15. Figini et al. (2012) suggests calibrating the parameter p_2 by fitting to the reloading stiffness of an experimental test but suggests $p_2 = 1.0$ for predictive testing.

$$h = h_0 \ln \left(\frac{\lambda^{p_2+1}}{\lambda_{min}^{p_2}} \right) \tag{4.18}$$

4.2.4 Coupling of uplift and plasticity

Based on work by Cremer et al. (2001, 2002), the point of uplift initiation is not constant when the soil behaves non-linearly. Cremer suggests Equation 4.19 to define the uplift moment, replacing Equation 4.7 with:

$$Q_{M,0} = \pm \frac{Q_N}{\alpha} e^{-\zeta Q_N} \tag{4.19}$$

The parameter ζ varies according to the plasticity of the soil and Cremer et al. (2001, 2002), suggests a value between 1.5 and 2.5.

4.2.5 Foundation radiation damping

Wave reflections at the soil-foundation interface result in large amounts of energy dissipating into the soil, which is referred to as geometric or radiation damping. It is essential to capture this energy loss in the numerical formulation and the current setup requires dashpot elements connected in parallel to the macro-element model in each degree-of-freedom. The damping coefficients for the dashpots can be determined using the expressions given in Table 4.4 from Gazetas (1991).

Table 4.4: Foundation dashpot coefficients for radiation damping

Mode	Damping (C)
Vertical (NN)	$\rho(V_{La} A_b).c_n$
Horizontal (VV)	$(\rho V_s A_b).c_v$
Rotational (MM)	$(\rho V_{La} I_{by}).c_m$

Where ρ is the soil density, A_b is the area of the base of the foundation, V_s is the soil shear wave velocity, $V_{La} = \frac{3.4}{\pi(1-v)} V_s$ is Lysmer's analog wave velocity. Where v is the Piosson's ratio. The c terms are the frequency dependent dynamic damping coefficients.

4.3 Implementation in Ruaumoko3D

The proposed macro-element model has been implemented into the finite-element software Ruaumoko3D. To provide a numerically efficient and stable algorithm further modifications were required. The first being a state correction algorithm to ensure that the predicted level of force increment during a time step was inside the bounding surface, creating a realistic loading. The second modification was to convert the non-symmetric stiffness matrix from the plasticity formulation into a symmetric form that could be used in the global stiffness matrix allowing for a more efficient matrix solving algorithm and global damping models to be used.

4.3.1 State correction algorithm

The cutting-plane algorithm is used when a force increment causes the force state to exceed the bounding surface. This scenario provides unrealistic behaviour as the bounding surface represents the ultimate load that can be mobilised on the footing. The realistic behaviour should show a large reduction in stiffness associated with respective footing displacements without a large increase in forces. The state correction algorithm therefore takes the previous force state (which is inside the bounding surface) and scales back the force increment (by a 100th of the force increment) until it finds a force state that does not exceed the bounding surface (Figure 4.7), the stiffness is then updated using the new force state. The new stiffness is very low because the force state is near failure and therefore the displacement increment does not result in a large force increment.

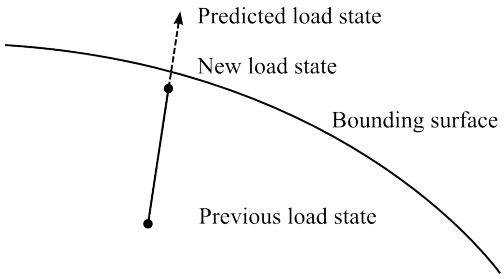

Figure 4.7: New load state iterates until inside the bounding surface

4.3.2 Dealing with a non-symmetric stiffness matrix

The non-associative behaviour in the plasticity formulation results in a non-symmetric stiffness matrix. The non-symmetric stiffness matrix means that matrix solving algorithms and damping models that require a symmetric stiffness matrix are unusable. To make use of these algorithms the macro-element stiffness matrix can be converted into a symmetric form to be solved in the global stiffness matrix and the difference in forces due to the conversion can be calculated and passed to the next time step. The symmetric matrix is formed by the average

of the original matrix and its transpose (Equation 4.20). The difference in forces is simply the difference in stiffness matrices multiplied by the displacement vector (Equation 4.21).

$$K_{sym} = \frac{K_{nonsym} + K_{nonsym}^{T}}{2} \tag{4.20}$$

$$F_{diff} = K_{nonsym}\Delta - K_{sym}\Delta \tag{4.21}$$

4.3.3 Iteration scheme

The algorithm to implement each of the different components of the macro-element is summarised in the flowchart shown in Figure 4.8.

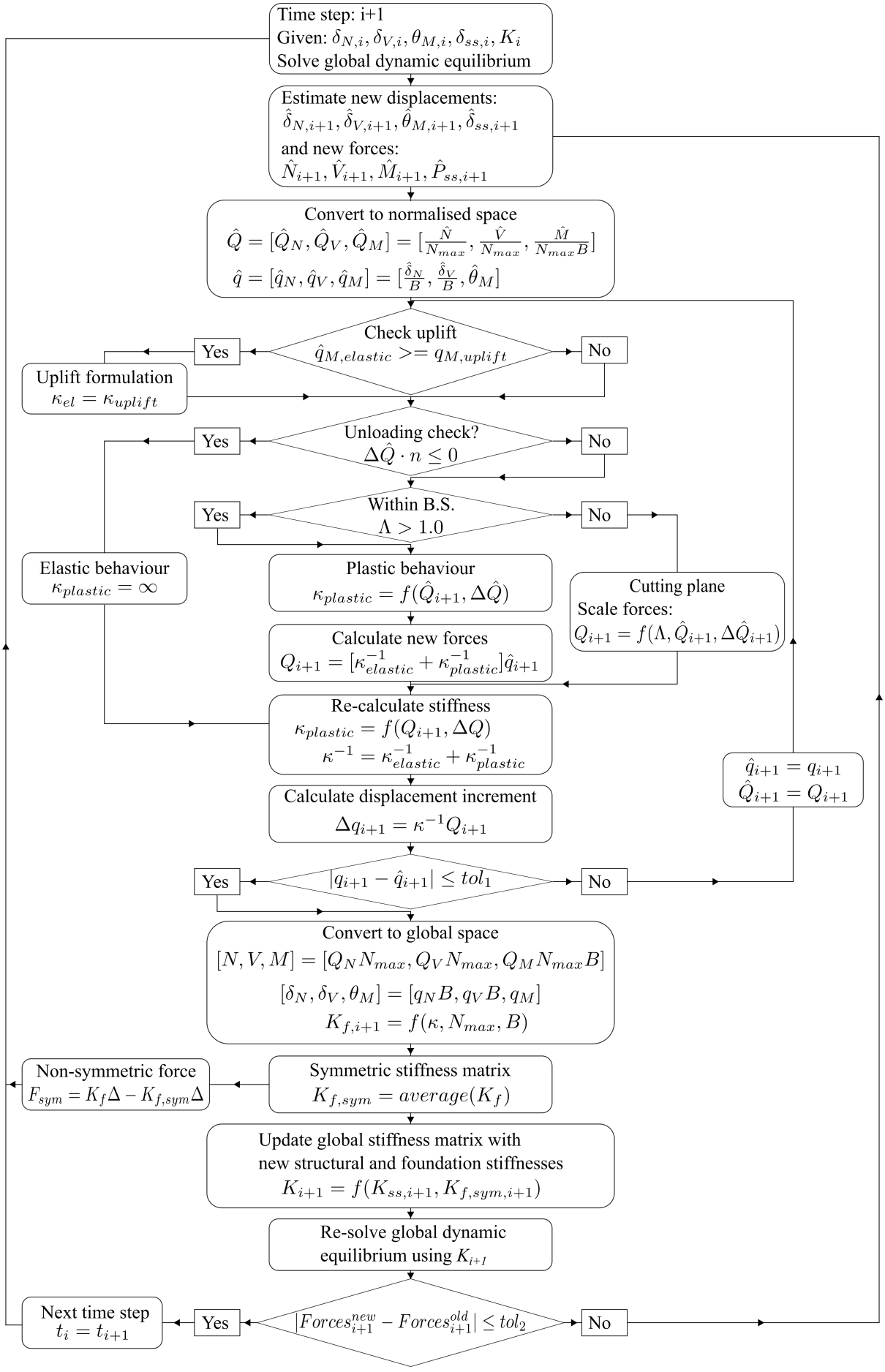

Figure 4.8: Macro-element implementation in Ruaumoko3D

4.3.4 User defined inputs

The following section outlines the user defined inputs required by the macro-element algorithm. Ruaumoko3D reads from an input file in Fortran free-format, where each input line provides a set of data to the program. The first line for the macro-element provides the basic information.

IPLAS	ISL	DIAM	QQMAX	KNN	KVV	KMM	PSI	KSI	PL_P1	PL_P2	WGT

Parameter	Description	Recommended
IPLAS	= 0 - Member remains elastic = 1 - Member non-linear	
ISL	= 0 - Macro-element located at first node = 1 - Macro-element located at second node	
DIAM	Length of footing (B)	-
QQMAX	The ultimate bearing capacity of the footing under axial load only (N_{max})	Salgado (2008)
KNN	Elastic vertical stiffness of footing (K_{NN})	Gazetas (1991)
KVV	Elastic horizontal stiffness of footing (K_{VV})	Gazetas (1991)
KMM	Elastic rotational stiffness of footing (K_{MM})	Gazetas (1991)
PSI	Bounding surface parameter for horizontal forces ($Q_{V,max}$)	$3/4 \tan\phi$
KSI	Bounding surface parameter for moment forces ($Q_{M,max}$)	0.48 (Vesic, 1975)
PL_P1	Plastic stiffness virgin loading parameter (p_1)	0.2 (Figini et al., 2012)
PL_P2	Plastic stiffness reloading parameter (p_2)	1.0 (Figini et al., 2012)
WGT	Weight of footing	-

The second line provides the uplift control parameters and additional switches for different macro-element formulations.

UP_ALPHA	UP_BETA	UP_GAMMA	UP_DELTA	UP_EPSIL	UP_ZETA	NON-ASS
TOPL	MIN_LAM	TENS	FRIC	MAPP		

Parameter	Description	Recommended
UP_ALPHA	Uplift parameter (α)	= 4 (Table **??** - strip)
UP_BETA	Not used	-

UP_GAMMA	Uplift parameter (γ)	= $1.0/\delta$
UP_DELTA	Uplift parameter (δ)	= 1.0 (Table 4.3 - strip)
UP_EPSIL	Uplift parameter (ϵ)	= 0.5 (Table 4.3 - strip)
UP_ZETA	Uplift-plasticity coupling parameter (ζ)	= 1.5 (Cremer et al., 2002)
NON-ASS	Must be set to one	1
TOPL	Limit on ratio of moment to uplift moment	= 100 (to remove effect)
MIN_LAM	The initial value of Λ_{min}	= 1e6 (no over consolidation)
TENS	= YES - h_0 is matrix $h_0 = p_1 K$	NO
	= NO - h_0 is a singular $h_0 = p_1 K_{NN}$	
FRIC	YES - Rugby-ball shaped bounding surface (Equation 4.12)	YES
	NO - Elliptic bounding surface centred at the origin	
MAPP	YES - Vertical mapping rule (Equation 4.17)	YES
	NO - Radial mapping rule	

The last line provides further plasticity formulation parameters.

K_ALFA K_BETA G_LAM G_CHI G_XI

Parameter	Description	Recommended
K_ALFA	Parameter to change h_0	1.0
K_BETA	Parameter to change h_0	1.0
G_LAM	Plastic potential shear parameter (λ)	2.5 (Figini et al., 2012)
G_CHI	Plastic potential moment parameter (χ)	3.0 (Figini et al., 2012)
G_XI	Bounding potential shape factor (ξ)	0.95 (Figini et al., 2012)

4.4 Numerical models

4.4.1 Single-degree-of-freedom models

One of the most common ways to analyse structures considering SFSI is a single-degree-of-freedom (SDOF) analysis, whereby the mass of the entire system can be lumped into a single

point and considered to only displace laterally. This conversion of a building to a SDOF is often made based on the first mode of response of the system. The SDOF analysis not only provides a very simple and efficient way to approximate the dynamic behaviour of the building but also allows for a direct comparison to the elastic response spectra. For this reason the SDOF model is of particular importance in determining how SFSI affects the behaviour of a structure. However to consider the uplift response more correctly the vertical inertia and vertical damping are of interest and the rocking response is most easily considered by modeling the 'true' geometry of the SDOF and therefore the foundation rotational degree-of-freedom is also of interest. The SDOF analyses used in this dissertation are consequently not true SDOF analyses but consider a single lumped mass with horizontal and vertical components and with horizontal, vertical and rotational degrees of freedom. The rotational inertia of the mass is not modeled as it is difficult to quantify for buildings and the level arm of the SDOF to the lateral mass provides the majority of the rotational inertia around the point of foundation rotation. To maintain the geometry of the SDOF, the numerical model can be modeled in Ruaumoko3D using a Beam element with length being the effective height of the SDOF. The Beam element should have zero shear deformation to simplify the response and allow for a simple damping model. The beam stiffness (EI) can be determined from the superstructure stiffness (K_{SS}) and the SDOF effective height (H_{eff}) using Equation 4.22. Figure 4.9 shows the numerical model with the mass of the system lumped at one end and the macro-element attached at the other. The other end of the macro-element is connected to the fixed node where the ground motion input is applied.

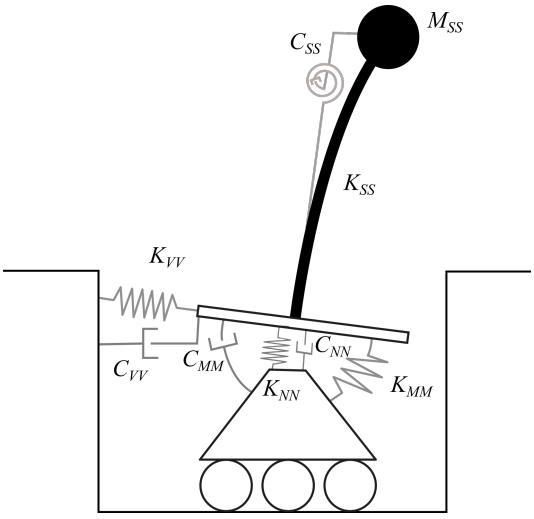

Figure 4.9: Schematic of SDOF analysis

$$EI = \frac{K_{SS} L^3}{3} \tag{4.22}$$

The modeling of 'viscous damping' in the superstructure is of considerable interest, the damp-

ing represents the additional energy dissipated in the structure that is not captured through the hysteretic model. This additional damping for the superstructure is often set as 5% of critical damping of the superstructure displacement mode, and in this numerical model it is captured through a rotational Dashpot element between the superstructure node and the foundation node. The translational damping coefficient (C_x) is given by Equation 4.23 and the equivalent rotational damping coefficient (C_r) (Equation 4.24) can be determined based on the relationship between cantilever displacement and rotation (Equation 4.25).

$$C_x = \frac{2\xi_{ss} K_{ss}}{\omega_{ss}} \tag{4.23}$$

$$C_r = \left(\frac{2H}{3}\right)^2 C_x \tag{4.24}$$

$$\Delta = \frac{2H}{3}\theta \tag{4.25}$$

$$\tag{4.26}$$

Where ξ_{ss} is the superstructure damping ratio and ω_{ss} is the angular frequency. There are two advantages of using a rotational dashpot as opposed to a translational dashpot. First, the displacement of the superstructure is isolated using the difference in rotational displacement, while using a translational dashpot the displacement from foundation rotation would contribute to the difference in translational displacements. Second, when the structure enters the non-linear range of response the damping forces of a translational dashpot may increase considerably, whereas for a rotational dashpot the forces would be lower due to the change in the relationship between displacement and rotation of the cantilever. The relationship between rotation and displacement changes from $\theta = 3\Delta/2H$ for a linear cantilever to close to $\theta = \Delta/H$ post yielding, resulting in close to a 33% reduction in the damping force.

Superstructure damping is a widely debated subject, with disagreements about what are realistic levels of damping, what it represents and how it should be considered in design and analysis. In displacement-based design, 5% is often set as the amount of superstructure damping for the system displacement mode, while in geotechnical textbooks (eg. Pecker, 2007) the damping of the superstructure is set for over just the superstructure displacement mode and is therefore reduced when considered over the system displacement mode. In this dissertation the damping is set to act over the superstructure mode for analysis but for design purposes it is assumed to act over the system displacement mode. The discrepancy is minimal but most noticeable for linear systems where the superstructure and foundation contribute evenly to the displacement. For example, a SDOF building-foundation system with a superstructure displacement mode period of 1s and foundation displacement mode period of 1s would result in a system period of 1.4s. The damping from the foundation displacement mode over the system displacement mode ($\xi_{f,sys}$) can be conveniently set to 5% for purposes

of this example. The damping from the superstructure mode for the superstructure displacement mode ($\xi_{ss,ss}$) can be considered as 5% and therefore over the system displacement mode ($\xi_{ss,sys}$) equals 3.6% from Equations 4.27 to 4.29.

$$C_{ss} = \frac{2\xi_{ss,ss}K_{ss}}{\omega_{ss}} = \frac{2 \times 0.05 \times K_{ss}}{2\pi} \tag{4.27}$$

$$\xi_{ss,sys} = \frac{\omega_{sys}c_{ss}}{2K_{ss}} = \frac{\frac{2\pi}{1.4} \times \frac{2 \times 0.05 \times K_{ss}}{2\pi}}{2K_{ss}} \tag{4.28}$$

$$= \frac{0.05}{1.4} = 3.6\% \tag{4.29}$$

$$\xi_{sys} = \frac{\Delta_{ss}\xi_{ss,sys} + \Delta_f\xi_{f,sys}}{\Delta_{sys}} = \frac{0.5 \times 3.6\% + 0.5 \times 5\%}{1} = 4.3\% \tag{4.30}$$

Where Δ_{ss} is the displacement of the SDOF due to superstructure deformation, Δ_f is the displacement of the SDOF due to foundation soil-foundation deformation and Δ_{sys} is the total displacement of the SDOF. The difference in response would be minor, however, for lower levels of damping or when the superstructure damping is considerably larger than the foundation damping, the effect is more significant.

The numerical damping model also differs slightly from the theory (Equation 4.30) due to an attempt to better capture reality and limitations of the numerical model. In conventional theory the damping forces from the superstructure are considered to dissipate into the air and not be transferred to the foundation; however, if the damping is representing the energy lost through in-elastic action and interaction of non-structural elements and is not a true viscous energy loss due to the superstructure moving through the air, the damping forces could arguably be transferred to foundation. Therefore in the numerical model the forces from the rotational dashpot element are transferred into the foundation element, making minimal difference for low levels of damping but is an important consideration for equivalent linear analyses (see Section 4.4.2).

The damping at the foundation level can be modeled by setting dashpot elements in the vertical, horizontal and rotational directions based on the terms given in Table 4.4. The dashpot elements connect in parallel to the macro-element and the forces absorbed through these elements are passed to the fixed node. The issue with the dashpots connected in parallel is that the uplift model is based on the felt vertical forces. As the foundation travels upwards during uplift the forces on the soil-foundation interface would be expected to reduce as the foundation moves away from the soil and as it returns the forces should increase. Unfortunately the opposite occurs as the dashpot forces are not passed to the soil-foundation interface, although the dashpot still correctly dissipates the energy. The effect is only significant during large velocities when it would generate a large change in axial force and therefore to minimise the influence, the vertical dashpot forces can be limited to 20% of the static load.

4.4.2 Validation of SDOF model

The SDOF model can be compared to the response of a true linear SDOF whereby the damping is based on conventional damping formulas in order to validate the model. Table 4.5 shows the inputs used for the numerical model implemented as suggested in this chapter. The inputs were not chosen to represent a realistic structure but to provide a structure where the foundation deformations contribute an equivalent amount of displacement to the structural deformations. Issues with the combination of damping are most prevalent when the displacement contributions are balanced.

Table 4.5: Numerical model inputs for SDOF model

Parameter	Value
Height (H)	12 m
Mass (M)	509 T
Fixed base period (T_{SS})	1.2 s
Structure stiffness (K_{SS})	14.2 MN/m
Fixed base damping (ξ_{SS})	5%
Footing Length (L)	4 m
Footing Breadth (B)	4 m
Footing embedment (D)	0 m
Soil shear modulus (G)	55 MPa
Soil shear wave velocity (V_s)	180 m/s
Soil mass density (ρ)	1.7 T/m^3
Soil friction angle (ϕ)	40
Soil Poisson's ratio (v)	0.25
Bearing capacity (N_{cap})	25.4 MN
Footing vertical stiffness (K_{NN})	714 MN/m
Footing horizontal stiffness (K_{VV})	583 MN/m
Footing rotation stiffness (K_{MM})	2343 MNm
Footing vertical damping (C_{NN})	7.57 MNs/m
Footing horizontal damping (C_{VV})	4.90 MNs/m
Footing rotation damping (C_{MM})	5.05 MNs/rad
System elastic period ($T_{initial}$)	1.7 s
System viscous damping (ξ_t)	2.1%

The model was first considered as only linear elastic with the superstructure damping set at 5% of critical. The comparisons shown here are for the behaviour during the unscaled ground motion NGA_0175_1 from the NGA ground motion database Chiou et al. (2008), which is a recording of the magnitude 6.5 Imperial Valley 1979 earthquake at the El Centro Array #12 station at a distance of 32 km with a peak ground acceleration of 0.14g.

The comparison between velocities of the SDOF due to the different components (foundation shear, superstructure deformation and foundation rotation) in Figure 4.10 demonstrates the even contribution from the foundation and superstructure.

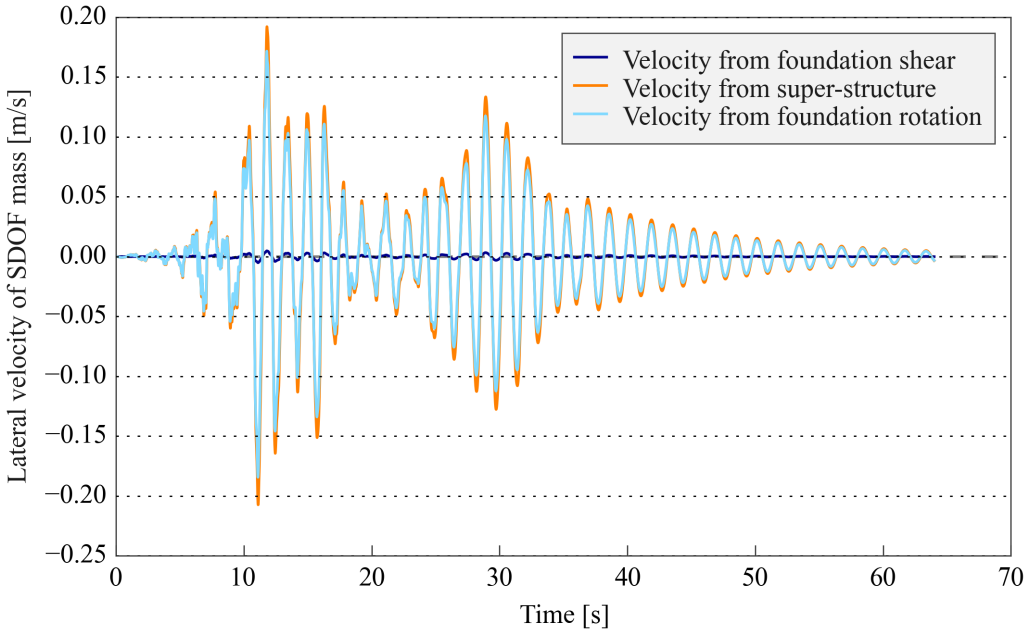

Figure 4.10: Contributions to velocity from different mechanisms for linear SDOF analysis ($\xi_{ss} = 5\%$)

The model was compared against the response of a true SDOF solved with Duhamel's integral and $\xi = 2.1\%$ in Figure 4.11. The behaviour was essentially identical. For larger levels of superstructure damping (xi_{SS} = 30%) (Figure 4.12) a small difference can be observed, with the numerical model exhibiting a less damped behaviour than its theoretical equivalent. This is due to the damping forces from the superstructure getting passed to the foundation. This difference is an important consideration for analyses that use equivalent linear properties for the structure, where the large damping forces should be transferred through to the foundation to some extent.

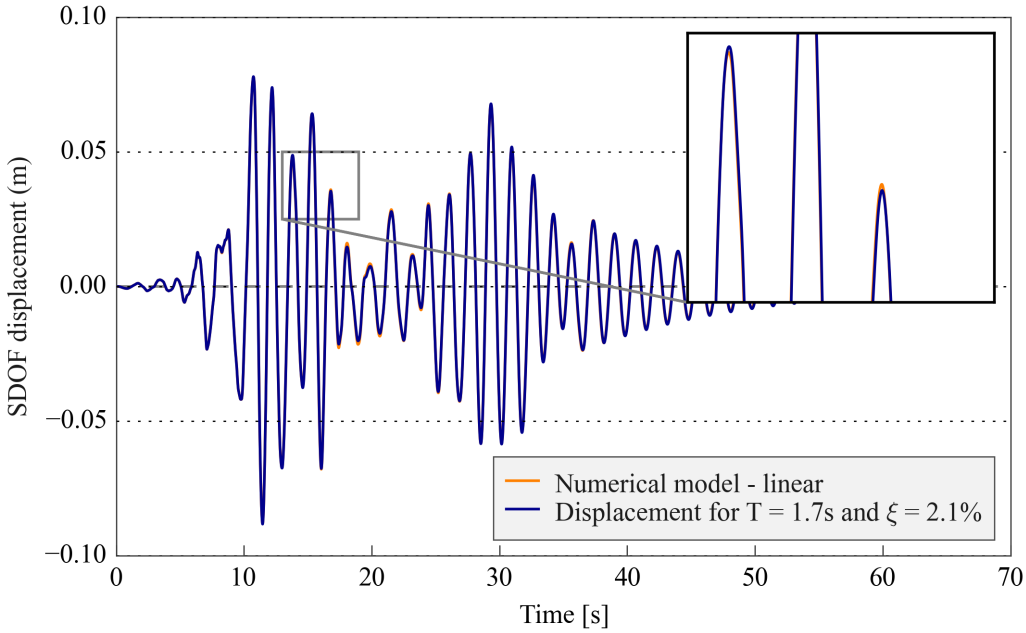

Figure 4.11: Comparison of linear elastic SDOF analysis with $\xi_{ss} = 5\%$

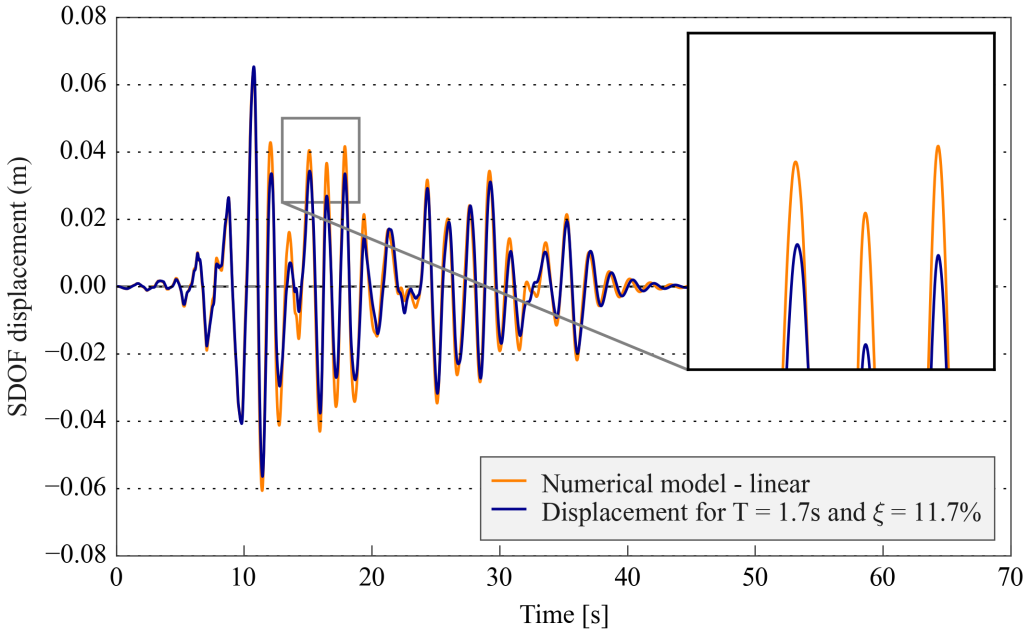

Figure 4.12: Comparison of linear elastic SDOF analysis with $\xi_{ss} = 30\%$

The non-linear model was subjected to the same ground motion, however, Figure 4.13 shows that the behaviour was considerably different to the linear elastic model with some residual deformation at the end of the time history. Figure 4.14 shows the uplift behaviour that is evident in the moment-rotation plot of the foundation and the slight degradation in stiffness due to soil plasticity.

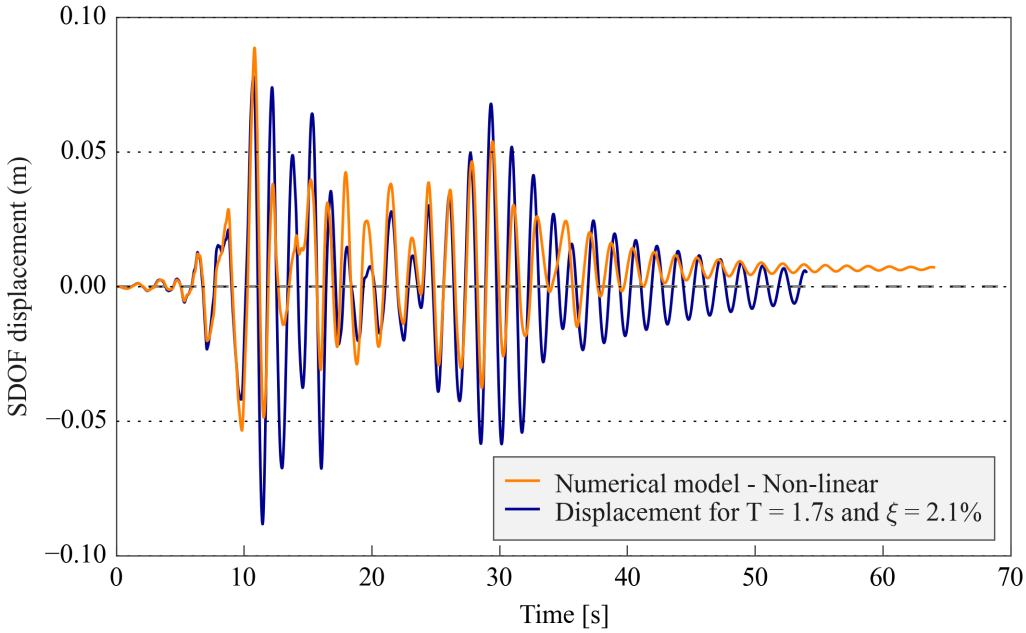

Figure 4.13: SDOF model with non-linear soil-foundation interface ($\xi_{ss} = 5\%$)

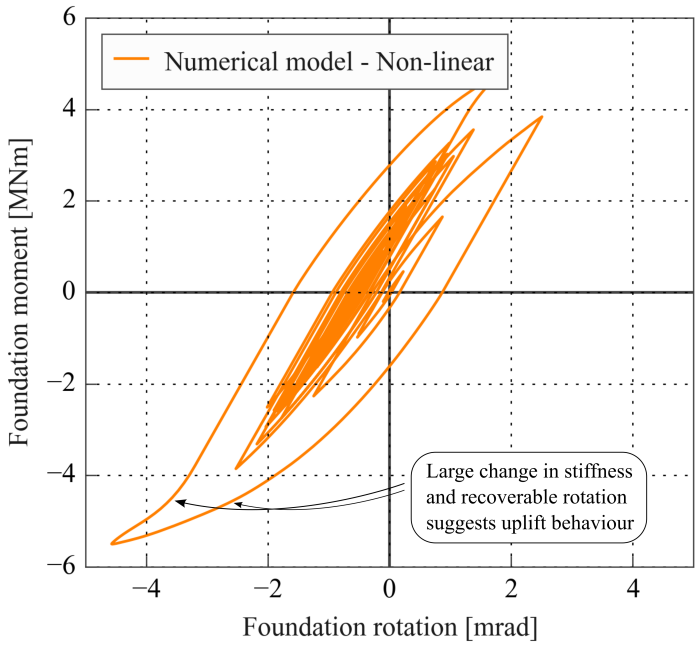

Figure 4.14: Foundation moment-rotation behaviour al mass ($\xi_{ss} = 5\%$)

4.4.3 Multi-degree-of-freedom models

The modeling of full structures such as frames is also of interest as it does not require the assumptions to convert to an equivalent SDOF, as well as providing the loads/displacements of each of the structural elements. Simple lumped mass and lumped plasticity models were used for the modeling of frames and walls in this dissertation, as they are easily understood

and computationally efficient.

It is considerably more difficult to define appropriate dashpot elements for structures with many degrees-of-freedom therefore a global damping matrix can be defined using the mass and stiffness matrices. The damping model used for this dissertation was the Wilson-Penzien damping model with constant damping over all modes. This means that the damping matrix is constant over the analysis and as the structure softens due to yielding the effective damping increases. The foundation radiation damping was still modeled using additional dashpots based on the equations in Table 4.4 and the additional damping from the global damping matrix made little difference to the damping in each mode of foundation deformation.

4.4.4 Validation of the frame model

An example of a frame numerical model is provided here to demonstrate the abilities of the numerical model to capture key aspects of SFSI on frame structures. Figure 4.15 shows a schematic rendering of the numerical model implemented as suggested in this chapter and the inputs are summarised in Table 4.6.

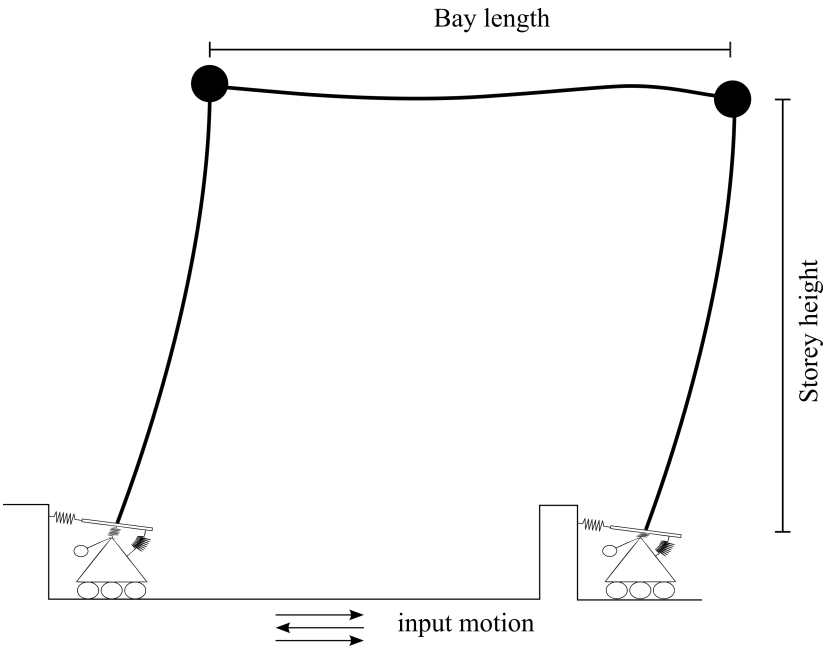

Figure 4.15: Simple numerical model of frame structure on soil

Table 4.6: Numerical model inputs for frame

Parameter	Value
Height (H)	8 m
Bay length	4 m
Total mass (M)	140 T
Fixed base period (T_{SS})	1.5 s
Structure stiffness (K_{SS})	2.46 MN/m
Fixed base damping (ξ_{SS})	3%
Footing Length (L)	2 m
Footing Breadth (B)	2 m
Footing embedment (D)	0.4 m
Soil shear modulus (G)	40 MPa
Soil shear wave velocity (V_s)	150 m/s
Soil mass density (ρ)	1.8 T/m^3
Soil friction angle (ϕ)	38
Soil Poisson's ratio (v)	0.3
Bearing capacity (N_{cap})	5.05 MN
Footing vertical stiffness (K_{NN})	259 MN/m
Footing horizontal stiffness (K_{VV})	212 MN/m
Footing rotation stiffness (K_{MM})	218 MNm
Footing vertical damping (C_{NN})	1.67 MNs/m
Footing horizontal damping (C_{VV})	1.08 MNs/m
Footing rotation damping (C_{MM})	0.195 MNs/rad
System elastic period ($T_{initial}$)	1.6 s

The numerical model was subjected to the same Imperial Valley ground motion as the SDOF model. The frame footings exhibited different behaviour to the simple SDOF foundation as they had a variation in axial load due to frame action. Figure 4.16 shows the asymmetric behaviour of the left footing due to the variation in axial load. During negative moment loading the axial load decreased and caused the footing to slightly uplift at a moment close to 200 kNm. In the positive moment direction the behaviour was almost linear even at moments above 300 kNm as the additional axial load provided additional moment capacity to the footing. The settlement behaviour also demonstrated an asymmetric behaviour, whereby the variation in axial load caused an up-down motion while the footing shakes into the ground.

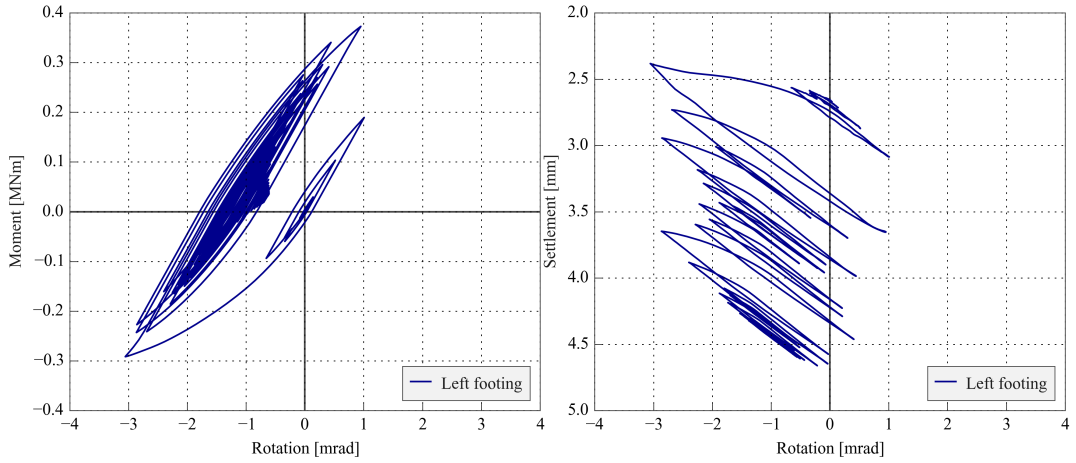

Figure 4.16: Left footing moment-rotation (left) and Rotation settlement (right) for frame

4.5 Model limitations

The macro-element model presented here offers a suitable tool to incorporate and even estimate the deformations of the soil and foundation for both SDOF and more complex structures. Unfortunately the model is not without limitations, and an understanding of these limitations is important when interpreting results.

4.5.1 Plasticity formulation

The model uses a vertical mapping rule and therefore cannot predict plastic behaviour under purely axial conditions. While this is not often an issue for piers and non-coupled walls as there is very little variation in axial load, it can be an issue for moment resisting frames or coupled walls where the dynamic change in axial load from frame action is significant. The model still captures an increased level of plastic behaviour due to increased axial load if there is some moment or shear loading but completely misses the mechanism under purely axial loading conditions. Also the more trivial case of purely axial load to failure does not predict any plasticity until it hits the failure surface at $N = N_{max}$.

Another issue with a purely axial load mapping rule is that the initial rotational stiffness is independent of the axial load. Under large axial load it could be expected that the initial rotational stiffness would be less than for lighter conditions, since the soil is already under considerable shear stress. With the vertical mapping rule the initial stiffness is alway the stiffness determined using the small strain shear modulus of the soil.

The use of an ellipsoidal shape provides a convenient mathematical expression for the bounding surface and plastic potential surface; however research by Gourvenec (2007) has shown dependence on whether the moment and shear are acting in the same direction which would

result in a skewed ellipsoidal shape. This is due to the increased shear stress when loads are in the same direction, however, the magnitude of the effect does not warrant the additional complexity. The slightly different bounding surfaces that are obtained for different shaped footings based on work by Gottardi et al. (1999), Gourvenec (2007) and Bransby and Randolph (1998) are also not accounted for.

The elliptic shaped bounding surface accounts for the footing uplift/sliding at failure and hence it has zero moment and shear capacity at the origin. However, the plastic response when the foundation has not uplifted should be based on the fully compliant section with full moment capacity at the origin. Therefore the plasticity bounding should not be constant and should depend on the level of uplift, where after uplift the bounding surface should reduce from a full compliant surface down to the given failure surface. The plastic response may therefore be over-predicted during loadings less than uplift.

Figini (2010) suggests that the model can be used for quantitative prediction for rotations up 0.01 rads, however it can still qualitatively capture the behaviour at rotations of 0.2rad.

4.5.2 Damping

The current formulation uses dashpot elements that are connected in parallel to the macro-element to model the radiation of energy into the soil. The felt force by the macro-element is therefore the applied forces minus the dashpot forces, while the uplift and plasticity models are based on the applied forces. The difference is only significant during large uplift and could be accounted for by including the dashpot elements into the macro-element formulation. However, the development of a viscous macro-element is not trivial given that the uplift and plasticity models are based on static behaviour and therefore the modification to soil properties during dynamic loading should also be accounted for. The large damping forces that can be generated during uplift may not be realistic either as during uplift the footing is not releasing large amounts of energy into the ground; however, this is somewhat balanced by the impact loading when the footing returns to the surface which can dissipate considerable energy. A modification to the vertical dashpot element to limit the damping force to 20% of the applied axial load provides a simple approximation to the complex dynamic behaviour and energy dissipation during footing uplift.

4.5.3 Further issues

- The current model is for surface foundations and could be considered suitable for an embedded foundation with no contact along the side walls. The frictional forces and earth pressures from sidewalls are not accounted for and these can be significant for deep foundations.

- The current macro-element model only accounts for soil stiffness degradation through shear induced by the structure, however, the soil under the structure undergoes additional shear deformation and potentially a reduction in stiffness due to ground shaking.
- The macro-element cannot capture the build up of pore pressures and associated degradation of stiffness including liquefaction effects.

To address some of the above limitations the macro-element was validated against two experimental data sets in order to demonstrate its predictive capabilities (Chapter 5).

4.6 Conclusions

This chapter presents a macro-element formulation for predictive assessment of the effects of SFSI on simple SDOF structures and full frame and wall structures. The model captures the major non-linear aspects of SFSI through two interacting constitutive models. The plasticity model captures the effects of soil yielding, while the uplift model captures the geometric non-linearity's during footing uplift. The macro-element was implemented in the time history analysis software Ruaumoko3D. Two numerical models were presented to demonstrate the macro-element behaviour for simple SDOF analyses and for frame structures.

Chapter 5

Validation of soil-foundation macro-element against centrifuge experiments

5.1 Introduction

The predictive capabilities of every new soil-foundation macro-element formulation must be validated and calibrated against simple, accurately measured experimental tests. In the past, macro-element validations have focused on experiments with simple support structures generally under low levels of rotation (eg. Chatzigogos et al., 2011; Figini et al., 2012). With a growing interest in using foundation rocking and sliding as an energy dissipation mechanism (Pecker and Pender, 2000; Gazetas et al., 2014), there is a need to use these simple models when extended to large levels of foundation rotation. The use of such models in the assessment of more complex superstructures, such as frame structures or coupled wall systems, is also desirable. In these structures there can be large changes in axial load, therefore the axial-moment interaction must be assessed.

In the past 15 years several research programmes have conducted experiments that subject simple structures to large levels of rotation and other experiments have been been performed using frames with isolated footings beneath the columns. The focus of this chapter is the validation and calibration of the macro-element, introduced in Chapter 4, under large levels of rotation and in frames with isolated footings (multiple supports). The validation was performed using two separate sets of test results:

- The fifth experiment (LJD03) from the NEES project: "Innovative Economical Foundations with Improved Performance that is Less Sensitive to Site Conditions" (Deng and Kutter, 2010), was used for evaluation of the model under large levels of foundation rotation where the foundation was close to toppling.
- The first experiment (HBM02) from the Network for Earthquake Engineering Simulation (NEES) project: "Seismic performance assessments in dense urban environments" (Mason et al., 2010), was used for evaluation of the performance of the model for isolated footings in frame structures.

The numerical simulations used default values for model calibration parameters together with soil and structural properties that were suggested in the testing reports and recorded free-field ground motions as input motions to demonstrate the model's ability as a predictive tool.

5.2 Experimental test data

The validation of the non-linear macro-element model required accurate characterisation of the input parameters as well as accurate measurement of the response of the experimental tests to compare against. Unfortunately many physical parameters of soil are difficult to accurately determine, are anisotropic, vary spatially and vary during earthquake excita-

tion. Structural parameters tend to be more easily characterised but enhanced gravitational conditions and large scale factors can modify the behaviour and mechanisms of structural elements. Time history data can also be difficult to capture as high centrifuge accelerations and frequencies can push recording devices to their limits and unintended vibrations and permanent displacements in reference frames can make transient displacement measurements uninterpretable. This section outlines the experimental models and the processes used to determine various input and output motions.

5.2.1 Scale factors

The experimental models were scaled using centrifugal conditions resulting in enhanced gravity (Bridge pier: $N = 49$, Frame: $N = 55$) and therefore the scale factors in Table 5.1 apply when converting from prototype to model scale. Note that all inputs and results presented here are given in prototype scale unless explicitly stated.

Table 5.1: Scale factors to convert from prototype to model scale

Parameter	Scale factor
Time	$1/N$
Acceleration	N
Frequency	N
Period	$1/N$
Length	$1/N$
Density	1
Mass	$1/N^3$
Strain	1
Stress	1

5.2.2 Bridge pier experiment

Test setup

The fifth experiment (LJD03) from the NEES project: "Innovative Economical Foundations with Improved Performance that is Less Sensitive to Site Conditions" contained models of four bridge pier structures sitting on 183mm (model scale) of dry sand (Deng and Kutter, 2010). The subject of this experimental validation was the single-support pier structure with a small footing designed to rock (Figure 5.1 - dimensions in prototype scale). The test model was subject to enhanced gravitational conditions of 49g using a centrifuge.

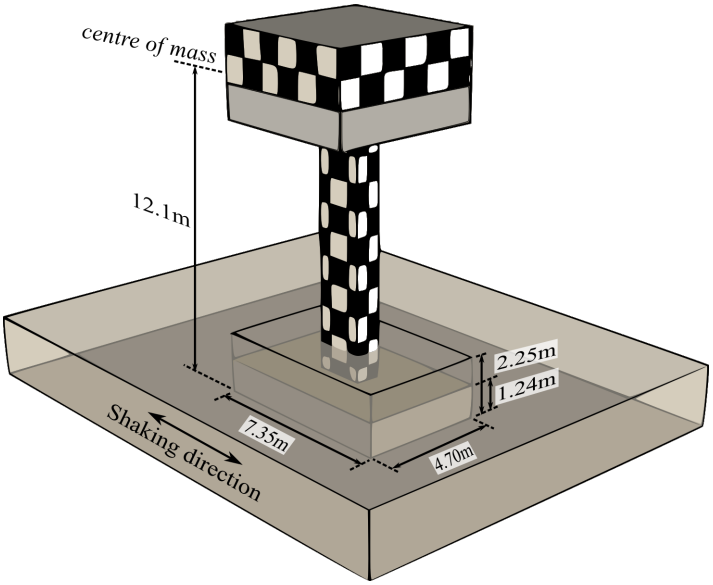

Figure 5.1: View of centrifuge model in prototype scale *after Deng and Kutter (2010)*

Soil properties

The soil properties from the experimental test shown in Table 5.2 were all were taken from the test report (Deng and Kutter, 2010), with the exception of the soil shear modulus which was determined based on the confining stress and void ratio as shown below. The sand was pluviated into the container to build a uniform sand deposit.

Table 5.2: Soil properties for pier test

Property	Value
Name	Nevada Sand
Classification	Uniform, fine sand
Specific gravity	2.67
Mean grain size, D_{50}	0.17mm
Coefficient of uniformity, C_u	2.0
Maximum void ratio, e_{max}	0.887
Minimum void ratio, e_{min}	0.511
Dry unit weight, γ_d	16.4 kN/m$^(3)$
Relative density, D_r	38%
Friction angle, ϕ	32^o
Shear modulus, G	23.5 MPa

The confining stress to approximate the soil shear modulus under the foundation was determined using Equation 5.1 from Perkins and Madson (2000). Where L is the foundation length, B the foundation width and N the applied static load on the foundation.

$$\sigma_{mp} = \frac{1}{6}\left(0.52 - 0.04\frac{L}{B}\right)\frac{N}{L \times B} \quad = \frac{1}{6}\left(0.52 - 0.04\frac{7.35m}{4.7m}\right)\frac{6193kN}{7.35m \times 4.7m} \quad = 13.7kPa \quad (5.1)$$

The soil shear modulus was then approximated using Equation 5.2 from Hardin (1978) with the additional correction factor, CF, from Arulmoli et al. (1992), where the correction factor was based on available resonant column tests on Nevada Sand. The other factor is the void ratio of the soil ($e = 0.654$).

$$G = \frac{625CF\sqrt{100kPa \times \sigma_{mp}}}{0.3 + 0.7e} \qquad = \frac{625(0.77)\sqrt{100kPa \times 13.7}}{0.3 + 0.7e} \qquad = 23.5MPa \qquad (5.2)$$

Pier ground motions

The input motions adopted in the analyses were taken as the measured surface acceleration from the free field accelerometers (average of BEH and BWH accelerometer). It is expected that the actual motion close to the footings may have differed from the chosen accelerometer motions due to the presence of the building modifying the soil response and through kinematic interactions of the foundation. This variation in the ground motions may have caused differences between the results of the experiments and the simulations.

The bridge pier was subjected to 20 ground motions over four different centrifuge spins. The ground motions were a mixture of impulse motions and recorded earthquake ground motions. The first eight motions were of very low amplitude to test recording equipment and the data from these tests was not useable. The record indexing starts at the sixth motion (consistent with the raw data), the data from motion ten (ID 5) was also not available so is missing in the validation process. The remaining eleven motions consisted of six earthquake ground motions (motion IDs: 4, 6, 7, 8, 9 and 15) and five pulse motions (motion IDs: 10, 11, 12, 13 and 14) consisting of four pulses each. The goal of the experimental investigation was to experimentally investigate the toppling behaviour of rocking foundations and therefore the motions had very high velocities and resulted in large footing rotations greater than 0.02 rad. Table 5.3 summarises the ground motions used in the experimental tests, with the peak ground acceleration (PGA) and peak ground velocity (PGV) being the recorded values from the accelerometers on the ground surface. Figure 5.2 shows the spectra of the input ground motions for the numerical model.

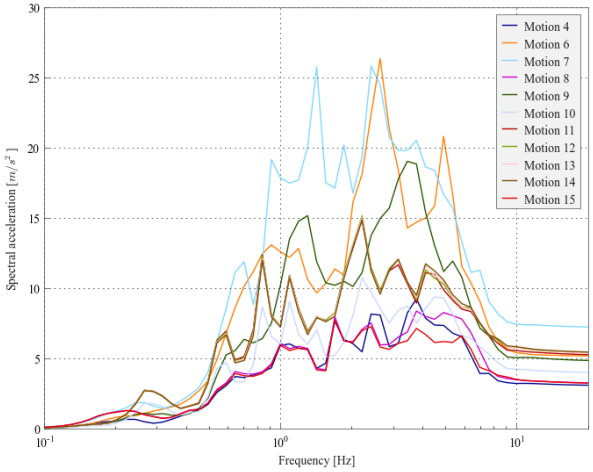

(a) 5% Acceleration response spectra

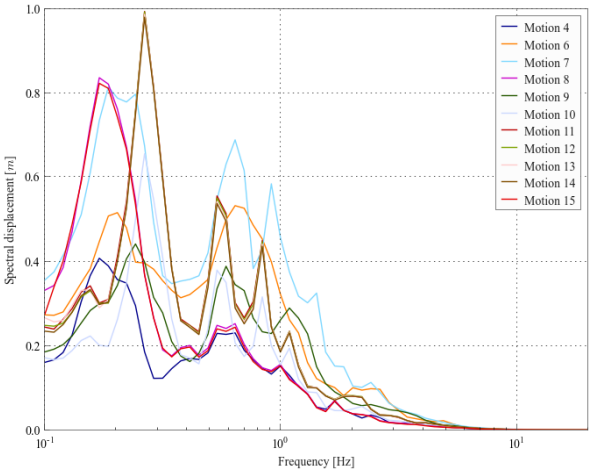

(b) 5% Displacement response spectra

Figure 5.2: Pier input motions

Table 5.3: Ground motions used in Pier test

ID	Spin	PGA (g)	PGV (m/s)	Earthquake
4	2	0.31	0.34	1999 Chi-Chi earthquake (Filtered at 10Hz)
6	3	0.53	0.76	1971 San Fernando earthquake
7	3	0.73	0.83	1976 Gazli earthquake
8	4	0.33	0.43	1999 Chi-Chi earthquake
9	4	0.49	0.54	1984 Morgan Hill earthquake
10	4	0.41	0.59	Four velocity pulses
11	4	0.53	0.76	Four velocity pulses
12	4	0.55	0.75	Four velocity pulses
13	4	0.54	0.74	Four velocity pulses
14	4	0.55	0.75	Four velocity pulses
15	4	0.33	0.39	1999 Chi-Chi earthquake

5.2.3 Frame structure experiment

Test setup

The first experiment (HBM02) from the NEES project: "Seismic performance assessments in dense urban environments" contained two model frame buildings sitting on 536mm (model scale) of dry sand as seen in Figure 5.3 (Mason et al., 2010). The centrifuge model was subject to enhanced gravitational conditions of 55g using a centrifuge. The one-storey and three-storey model buildings were located 0.62 m apart (34 m metres in prototype scale) essentially making the soil-structure-interaction effects isolated, without any cross interaction between the buildings. The one-storey building was a one bay frame sitting on isolated footings (Figure 5.3 - inset) and its seismic performance was numerical modeled using the proposed macro-element model.

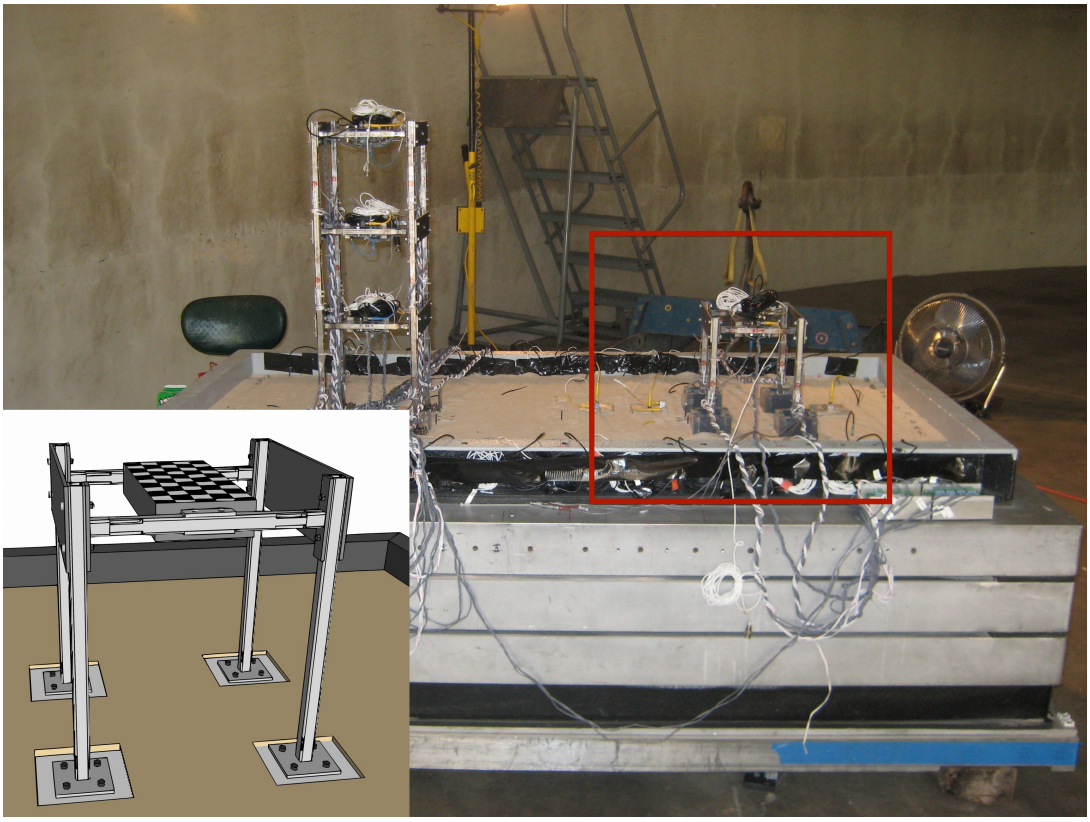

Figure 5.3: Test setup *after Mason et al. (2010)*

Soil properties

The soil properties from the experimental test shown in Table 5.4 were all were taken from the test report (Mason et al., 2010), with the exception of the soil shear modulus which was determined based on bender element tests conducted on a subsequent experiment (Test 3) at a depth of 4.4m (prototype scale)(Trombetta, 2013). This is exactly the same shear stiffness

($G = 43.6MPa$) that would be obtained using the formula from Hardin (1978) (Equation 5.2) assuming $CF = 1.0$, but with the correction factor $CF = 0.77$ from Arulmoli et al. (1992) would give $G = 33.5MPa$. The sand was pluviated into the container to build a uniform sand deposit.

Table 5.4: Soil properties for frame test

Property	Value
Name	Nevada Sand
Classification	Uniform, fine sand
Specific gravity	2.67
Mean grain size, D_{50}	0.17mm
Coefficient of uniformity, C_u	2.0
Maximum void ratio, e_{max}	0.748
Minimum void ratio, e_{min}	0.510
Dry unit weight, γ_d	16.4 kN/m$^(3)$
Relative density, D_r	80%
Friction angle, ϕ	40^o
Shear modulus, G	43.6 MPa

Frame ground motions

The input motion was taken as the measured surface acceleration from the free field accelerometer (HA14 accelerometer). Just like for the pier experiment it can be expected that the actual motion close to the footings may have differed from the chosen motion, in fact, there were accelerometers closer to the frame, which may have accounted for these effects. However, these motions also suffered from tilting and disturbance from soil deformation, thus the ground motion recordings were not useable for some tests, so all input motions used the free field accelerometer recordings.

The frame structure was subjected to 17 recorded ground motions over four centrifuge spins. The ground motions were applied in increasing levels of amplitude within each spin up and between each spin up, and several ground motions were repeated between spin ups. Table 5.5 summarises the ground motions, with the peak ground acceleration (PGA) and peak ground velocity (PGV) being the recorded values from the accelerometers on the model ground surface. For more information on the input motions please refer to page 67 in Trombetta (2013). The spin number refers to which centrifuge spin the test was conducted on. Figure 5.4 shows the spectra of the input ground motions.

Table 5.5: Ground motions used in Frame test

ID	Spin	PGA (g)	PGV (m/s)	Earthquake
JOS_L_1	1	0.14	0.16	1992 Landers
TCU_L	1	0.23	0.21	1999 Chi Chi
RRS	1	0.38	0.52	1994 Northridge
PTS	2	0.19	0.25	1987 Sup. Hills
SCS_L_1	2	0.31	0.32	1994 Northridge
LCN	2	0.34	0.52	1992 Landers
JOS_L_2	3	0.17	0.16	1992 Landers
SCS_L_2	3	0.32	0.32	1994 Northridge
WVC_L	3	0.40	0.51	1989 Loma Prieta
SCS_H	3	0.61	0.77	1994 Northridge
JOS_H	3	0.47	0.49	1992 Landers
WPI_L	3	0.39	0.56	1994 Northridge
JOS_L_3	4	0.16	0.16	1992 Landers
WPI_H	4	0.46	0.66	1994 Northridge
PRI	4	0.71	0.75	1995 Kobe
TCU_H	4	0.46	0.35	1989 Chi Chi
WVC_H	4	0.44	0.68	1989 Loma Prieta

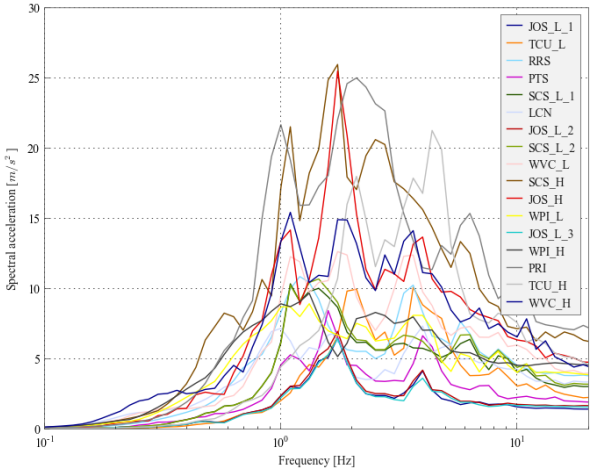

(a) 5% Acceleration response spectra

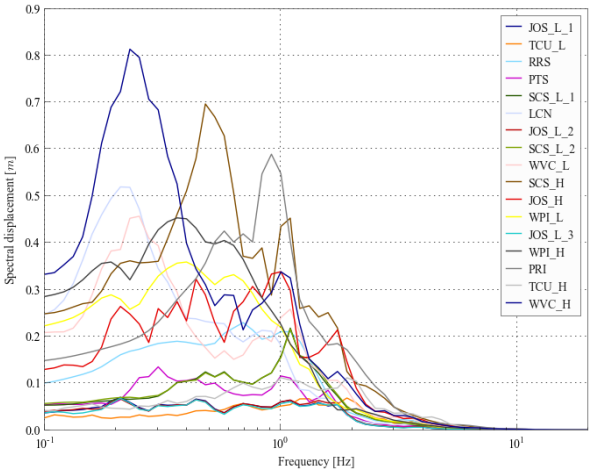

(b) 5% Displacement response spectra

Figure 5.4: Frame input motions

5.2.4 Signal processing

The majority of the instruments from both experiments suffered from tilting during excitation and contained some high frequency background noise, thus their data required correction. All accelerograms were first baseline corrected by removing the average acceleration of the record and then filtered. The accelerograms used for the input in the time history analysis and validation of the roof/deck accelerations were filtered using a 4th order band pass Butterworth filter between 0.2Hz and 30Hz.

The displacement transducers from both experiments were not fixed to the deck/roof or foundation, and the reference frame for the displacement transducers used to capture footing rotations, sliding and settlements, was not rigid and deflected and shook during excitation (Mason et al., 2010), thus they did not reliably capture the high frequency movements. The long period and residual deformations were still captured by the displacement transducers and could be extracted from the transducer output using a running average and combined

with the high frequency component of the accelerometer displacements. To combine the two motions the accelerometer displacements were used for frequencies above a set change frequency and the displacement transducers were used for the lower frequency displacements. For the pier test the change frequency for the settlement time histories was 0.15 Hz, for the deck and foundation rotation it was 0.17 Hz and for the deck lateral displacement it was 0.09Hz. The change frequencies were chosen to be consistent with the recommendations in the experimental report by Deng and Kutter (2010) and represent the limit of the displacement transducers before their behaviour is no longer mimicked by the accelerometer. For the frame the change frequency was set at 0.37 Hz for all transducers, as at higher frequencies the displacement transducer (Pot) showed large amplification in the response, unmatched by the accelerometer (Figure 5.5).

The accelerometers displacements were determined by first filtering the acceleration signal using a 4th order lowpass Butterworth filter at 30Hz then integrated twice to obtain the displacement time series. The low frequency displacements were determined using a running average through the displacement transducer time series. The running average window width for the displacement transducer was equal to the change frequency (eg. frame averaging window = 2.7 seconds). The low frequency displacement transducer records were combined with high frequency accelerometer displacements by using 6th order Butterworth low and high pass filters to combine the motions at the change frequency. The filtering steps are shown in the frequency domain in Figure 5.5 and in the time domain in Figure 5.6.

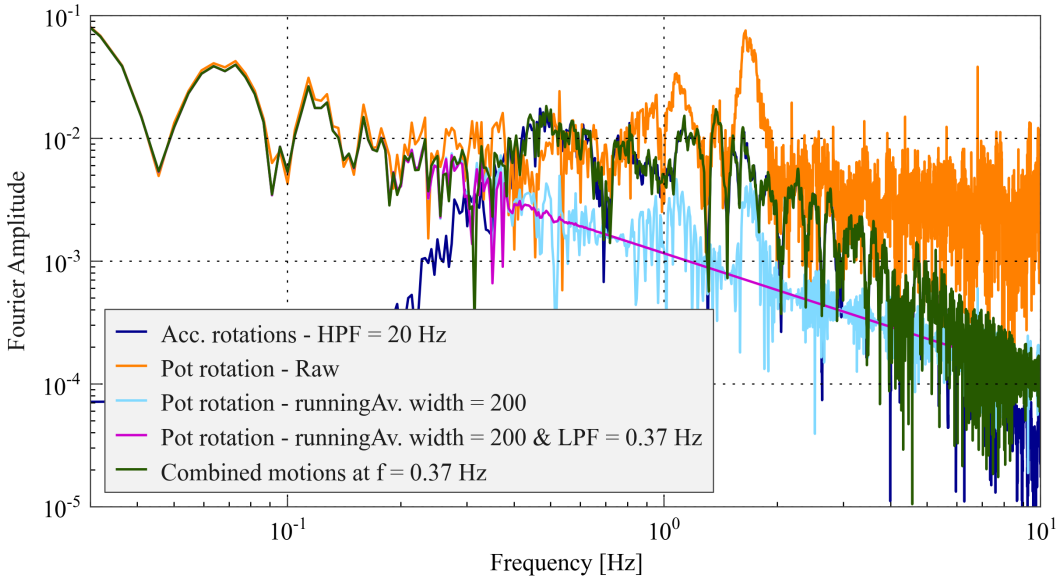

Figure 5.5: Fourier amplitudes during filtering of frame left footing rotation for SCS-L-2 motion

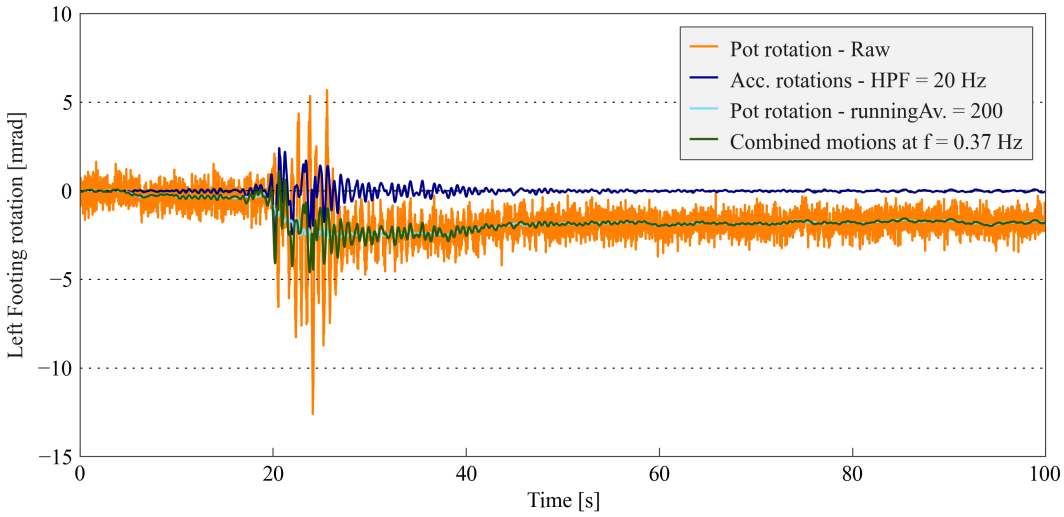

Figure 5.6: Combined high frequency and low frequency motions for frame left footing rotation for SCS-L-2 motion

For the bridge pier the footing base moment was approximated based on the measured translational and rotational accelerations multiplied by the deck mass and mass moment of inertia respectively. The moment was adjusted for P-Delta effects using the deck displacement time history. There were no vertical displacement transducers located on the bridge pier footing, therefore the settlements were assumed to be equal to the vertical displacements of the deck minus the free-field settlements. The pier footing rotation was determined using the two vertical accelerometers located on the footing to capture the high frequency component, while the low frequency motion was assumed to be equal to the deck rotation minus the calculated rotation of the pier due to the felt moment divided by the moment rotational inertia of the pier.

Strain gauges were used to determine the strains in the frame structure and these were filtered using a 4th order low pass Butterworth filter at 5Hz.

5.3 Numerical model

The numerical models were developed in Ruaumoko3D using a lumped mass and lumped plasticity model for the superstructure and the macro-element for the soil-footing interface, and were modeled only in the plane of shaking.

The geometry of the structure and footings along with the structure and soil mechanical properties were all provided in the the test reports (Bridge pier - Deng and Kutter (2010), Frame structure - Mason et al. (2010)) and were used directly in the numerical models, along with the recommended control parameters for the uplift model from Chatzigogos et al. (2011) and control parameters for the plasticity model from Figini et al. (2012). Better estimates of the

behaviour can be obtained by fitting the mechanical properties of both the soil and structure for both tests, however, by using the provided properties the models could be assessed for a 'Class C' type prediction.

The foundation stiffness and damping terms for both models were based on the impedance equations in Table 5.6 from Gazetas (1991). Where G is the soil shear modulus, v is the the soil Poissons ratio, b and l are the half-length and half-width of the footing (see Figure 5.7), and I_y is the second moment of area of soil-foundation contact. The additional k terms are the dynamic stiffness factors which were taken as 1.0 in all cases. The damping expressions use the soil mass density (ρ), shear wave velocity V_s, area of soil-foundation contact (A_b) and the Lysmer's analog wave velocity,$V_{La} = \frac{3.4}{\pi(1-v)} V_s$. The additional dynamics terms were taken as $c_n = c_v = 1.0$ and $c_m = 0.35$ from charts by Gazetas (1991).

Table 5.6: Foundation stiffnesses and radiation damping

Mode	Stiffness (K)	Damping (C)
Vertical (NN)	$\frac{2Gl}{(1-v)}\left[0.73 + 1.54(\frac{b}{l})^{0.75}\right] k_n$	$\rho(V_{La}A_b)c_n$
Transverse horizontal (K_y)	$\frac{2Gl}{(2-v)}\left[2 + 2.5(\frac{b}{l})^{0.85}\right] k_y$	
Horizontal (VV)	$K_y - \frac{0.2Gl}{(0.75-v)}\left[1 - \frac{b}{l}\right] k_v$	$(\rho V_s A_b)c_v$
Rotational (MM)	$\frac{G}{(1-v)} I_y^{0.75}\left[3(\frac{l}{b})^{0.15}\right] k_m$	$(\rho V_{La} I_{by}).c_m$

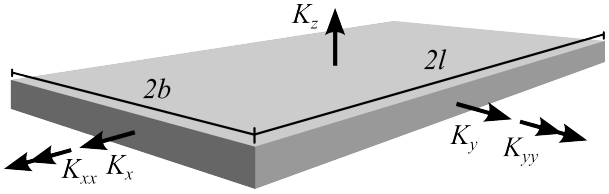

Figure 5.7: Notation for impedance functions

5.3.1 Input parameters for the bridge pier

The numerical model used in this study consisted of a lumped mass superstructure (M_{SS}) attached to a soil-foundation interface element (Figure 5.8). The pier and deck were modeled linear-elastically as there were no reports of damage on the pier during testing. The superstructure damping was modeled with a rotational linear dashpot (C_{SS}) set to provide 5% of critical damping for relative lateral displacement between the foundation and the superstructure. The vertical displacement from the superstructure was slaved to the foundation node providing an axially perfectly rigid superstructure. The foundation mass (M_f) was modelled with horizontal and vertical masses. The foundation radiation damping was modelled with vertical (C_{NN}), horizontal (C_{VV}) and rotational (C_{MM}), dashpots between the foundation

and surrounding soil based on the radiation damping equations from Table 5.6. All of the dashpots had a linear relationship between force and velocity, except for the vertical dashpot, which was limited to 1400 kN to avoid excessive damping forces that could make the macro-element unstable.

The initial stiffnesses (K_{NN}, K_{VV}, K_{MM}) for the macro soil-foundation element were determined from the equations in Table 5.6, where the correction for embedded foundations was not used as it was assumed that the contact area of the sidewalls was zero, as the numerical model was developed for shallow foundations on the surface. The foundation capacity (N_{cap}) was chosen to match that reported in Deng and Kutter (2012) which was determined based on the shallow foundation bearing capacity equations from Salgado (2008). The masses and geometry of the deck and footing were based on values reported in the testing report (Deng and Kutter, 2010). The pier stiffness (K_{SS}) was determined to match the reported natural frequency of the fixed base system of 0.84 Hz. Large displacement P-delta effects were considered in the analysis.

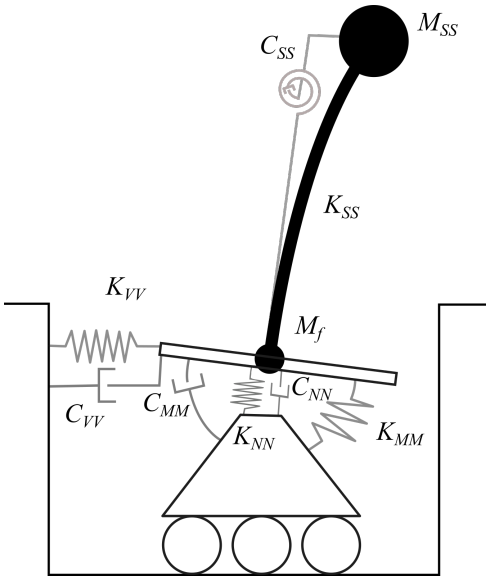

Figure 5.8: Numerical model for bridge pier

5.3.2 Input parameters for the frame structure

The numerical model used in this study consisted of a two dimensional frame with lumped plasticity beam and columns elements attached to two soil-foundation interface elements (Figure 5.9). The roof mass (M_{SS}) was lumped at the beam centre and at the beam ends and the foundation masses (M_f) were lumped at the foundation level. The columns consisted of four sections (from bottom to top): elastic member - plastic hinge - elastic member - column end block. The beam consisted of seven sections: rigid end block - elastic member - plastic hinge - elastic member - plastic hinge - elastic member - rigid end block. The non-linear behaviour in the hinges was assumed to be elasto-plastic in flexure and shear, with no flexure-

shear-axial load interaction considered in the beams or column hinges. The column end blocks had some flexural stiffness to account for joint deformation which was taken as 4 times the stiffness of the full section flexibility.

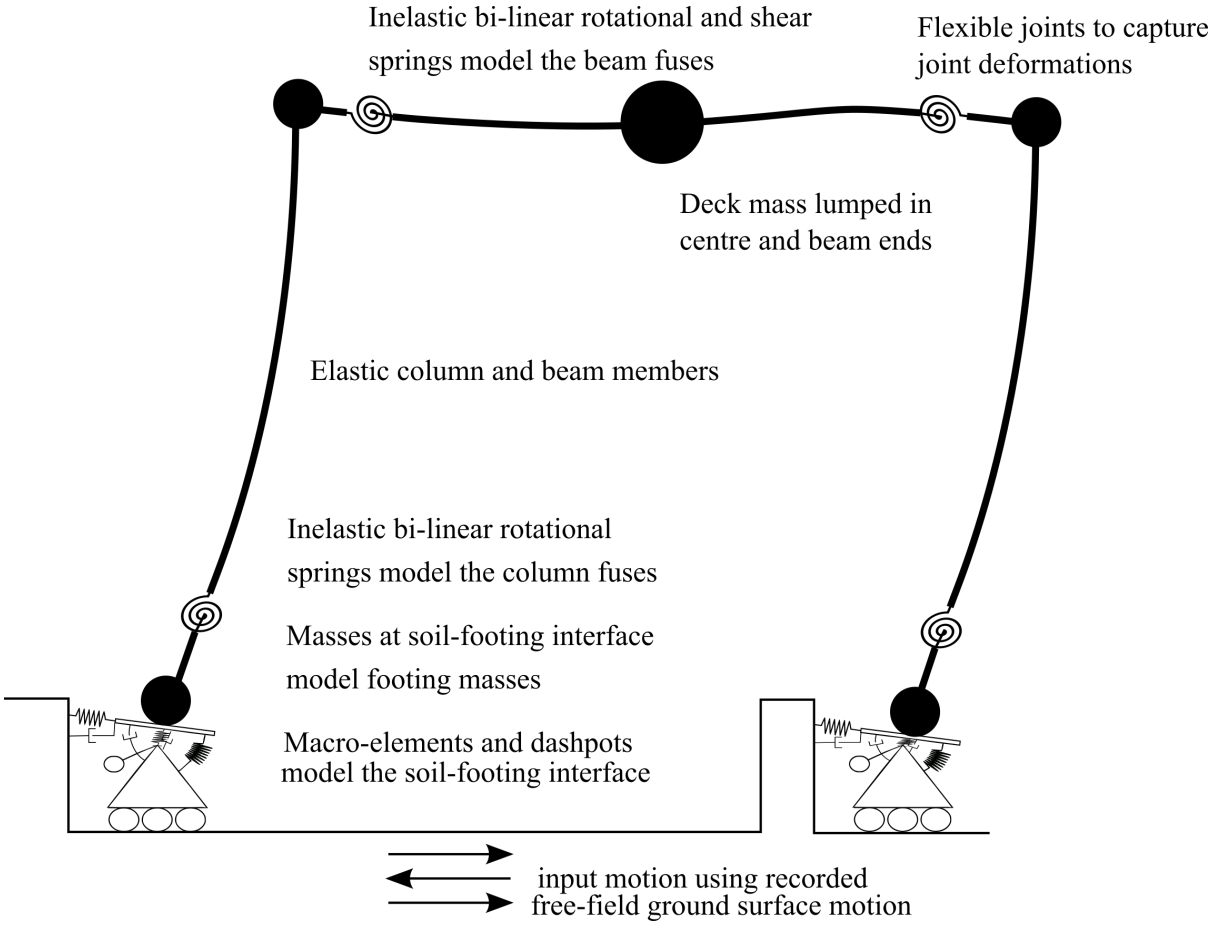

Figure 5.9: Numerical models of soil and structure system

In the tests, the hinge sections were deliberately reduced to provide localised plastic rotation, the cross-sections can be seen in Figure 5.10. The first and second set of tests (1-3 and 4-6) were conducted using Beam I beams. During testing the beams suffered from considerable shear deformation and the experimental team decided that the beams would be replaced and the roof mass would be reduced by 25% after the sixth motion. The third set of motions (7-12) were also conducted with the Beam I beams and further shear deformation was observed, this was undesirable so the experimental team replaced the beams with type II beams for the remaining tests.

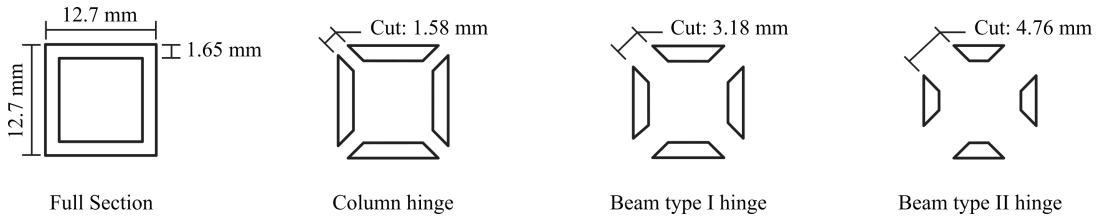

Figure 5.10: Prototype scale member cross-sections

The moment-rotation relationships of the hinges were extracted from simple moment-rotation tests performed by the experimental team (Figure 5.11). The shear and axial capacities and stiffness properties were determined from gross cross-section areas and the material moduli (Young's modulii E = 200 GPa, shear modulus G = 80 GPa). The mechanical and geometric properties of the sections are summarised in Table 5.7.

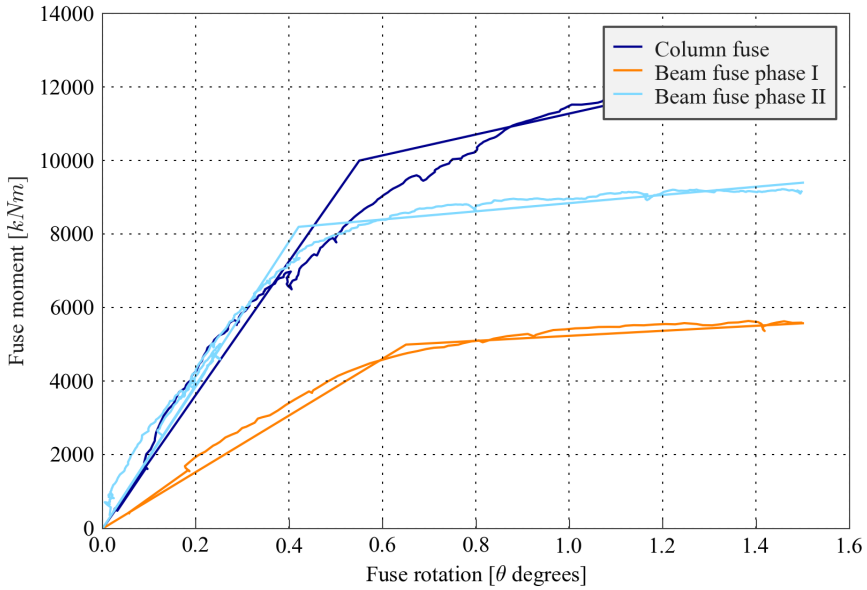

Figure 5.11: Fuse moment-rotation behaviour computed based on experimental data from Mason et al. (2010)

Table 5.7: Parameters used in numerical model

Member	Column	Beam I	Beam II	Full
Initial rotational stiffness [MNm^2]	750	617	783	2780
Yield moment [MNm]	10.0	5.0	8.2	-
Post yield rotational stiffness ratio	0.16	0.09	0.06	-
Initial shear stiffness (G $\times$ A) [MN]	14,700	5,500	10,600	17,500
Yield shear force [MN]	17.5	3.5	9.7	-
Post yield shear stiffness ratio	0.01	0.01	0.01	-
Axial stiffness (E $\times$ A)[MN]	36,700	13,800	26,500	44,000
Hinge length [m]	0.72	1.4	0.7	-
Hinge Area (A) [m^2]	0.18	0.13	0.15	0.22

The foundation impedances were determined using the expressions from Table 5.6. The damping from the superstructure was model using the Wilson-Penzien modal damping set to 2% over all modes. The use of global damping meant that additional damping forces occurred at the foundation-soil interface, however, the increased damping from the global damping only increased the foundation damping by 1.5% in the vertical mode, less than 2.0% in the shear and rotational modes.

5.3.3 Summary of input parameters for the numerical models

Table 5.8 summarises the inputs used for the numerical models. The two values listed in the frame column are for the first sequence of ground motions and the final sequence of ground motions after the mass was reduced and the beam I beams were replaced with the type II beams.

Table 5.8: Parameters used in numerical model

Parameter	Pier	Frame
Pier/Column height	12.1 m	12.8 m
Beam length	NA	9.96 m
Superstructure mass (M_{SS})	553 T	443 T, 368 T (per frame)
Fixed base period (T_{SS})	1.2 s	1.0 s, 0.88 s
Superstructure damping	5 %	2 %
Non-linear superstructure	None	see Section 5.3.2
Footing length	7.35 m	4.37 m
Footing width	4.70 m	4.37 m
Footing depth	1.24 m	0.87 m
Footing embedment	2.24 m	1.16 m
Footing mass (M_f)	79 T	522 T
Soil initial stiffness (G_{max})	23.5 MPa	43.6 MPa
Poisson's ratio (v)	0.3	0.3
Soil density (ρ)	1539 kg/m^3	1700 kg/m^3
Friction angle (ϕ)	32.7	40.0
Relative density (D_r)	38.0 %	80.0%
Footing axial load capacity (N_{cap})	68.0MN	58.0MN
Vertical stiffness (K_{NN})	603 MN/m	617 MN/m
Horizontal stiffness (K_{VV})	447 MN/m	504 MN/m
Rotational stiffness (K_{MM})	6330 MNm	2414 MNm
Vertical radiation damping (C_{NN})	12.8 MNs/m	8.03 MNs/m
Horizontal radiation damping (C_{VV})	7.43 MNs/m	5.20 MNs/m
Rotational radiation damping (C_{MM})	18.9 MNms/rad	4.47 MNms/rad
Uplift limit factor (α)	4.0	4.0
Uplift stiffness factor (ϵ)	0.5	0.5
Uplift stiffness factor (δ)	1.0	1.0
Uplift stiffness factor (γ)	1.0	1.0
Uplift plasticity factor (ζ)	1.5	1.5
Bounding surface shear parameter (μ)	0.469	0.565
Bounding surface moment parameter (ψ)	0.48	0.48
Bounding surface shape parameter (ξ)	0.95	0.95
Plasticity modulus factor (p_1)	0.2	0.2
Reload stiffness factor (p_2)	1.0	1.0
Plastic potential shear parameter (λ)	2.5	2.5
Plastic potential moment parameter (χ)	3.0	3.0

5.4 Comparison of numerical results and experimental data

5.4.1 Bridge pier

The numerical prediction of the bridge pier response was compared against the measured experimental deck acceleration, deck rotation, footing moment, footing rotation and footing

settlement. Both the deck rotation and the footing rotation were computed as in several cases the sensors on the footing had some interference, so the reader can assess the accuracy of the footing rotation by checking its congruency with the deck rotation. To provide a range of earlier and later tests the time series of the fourth, seventh, tenth and fifteenth motions for both the numerical and experimental behaviour can be seen Figures 5.12 to 5.15 respectively.

The numerical model captured the general behaviour of the moment, rotations and settlement throughout the time series and even gave reasonable estimates of the residual behaviour. The level of uplift was sightly under estimated according to the presented experimental time series. The exact peaks from the experiment were difficult to capture and the large temporary drops in the measured settlement time series suggest that the amplitudes of the high frequency part of the signal were not accurate, however there was good agreement with the timing of the peaks due to uplift and the general trend of the settlement. The only exception with the match on the settlement time series is motion seven, where the experimental time series shows some unrealistic uplift under almost no excitation, this uplift was produced by the free-field sensor recording an unusual settlement before returning back to its original level.

The deck acceleration was not captured very well as there was a large discrepancy in the high frequency content. The additional high frequency content in the numerical time series made very little difference to the displacements as the deck rotation time series have good agreement. A similar level of comparison was obtained for all the tests (comparisons for all time series can be found in Appendix A - Experimental test validation - Pier).

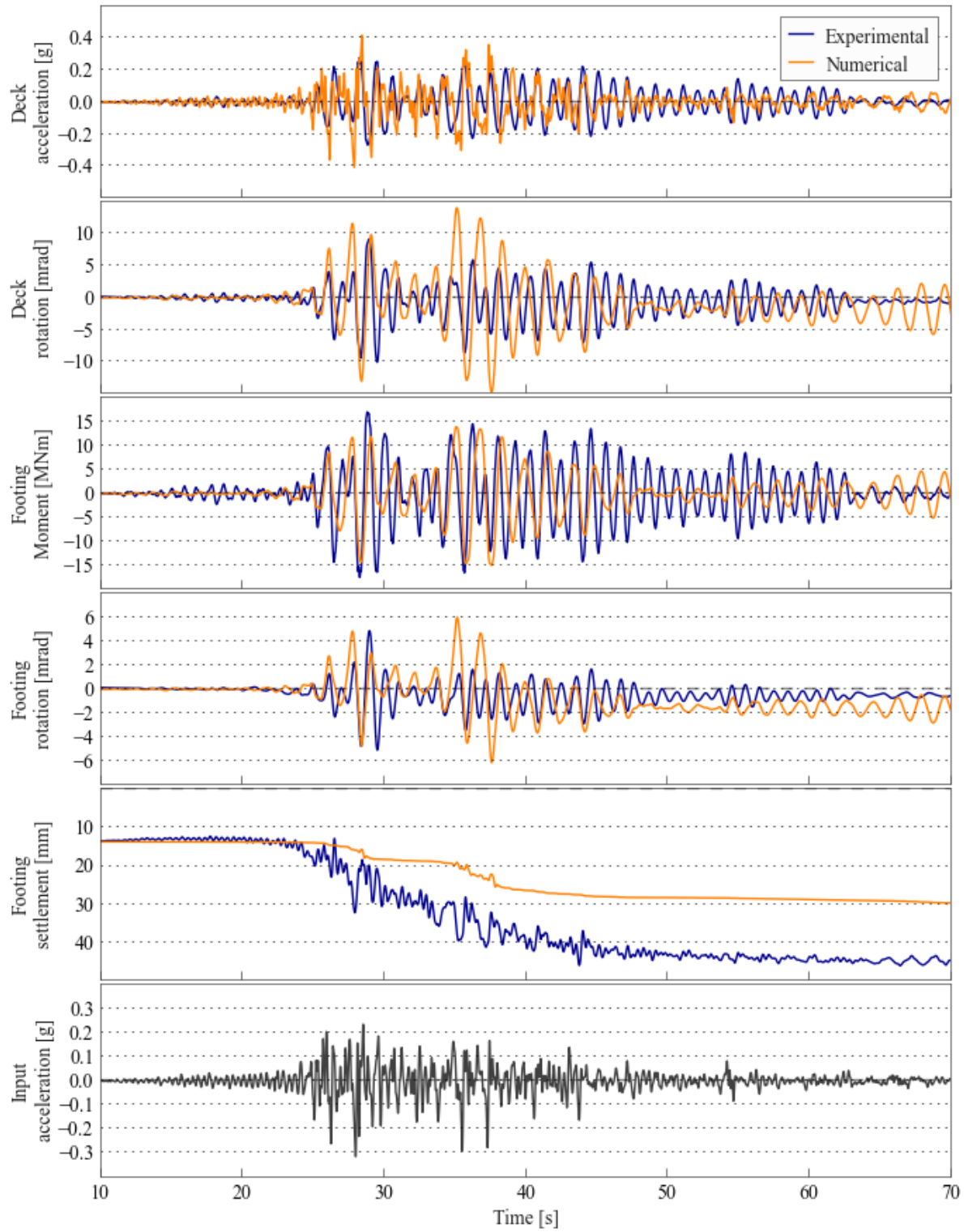

Figure 5.12: Comparision of numerical and experimental behaviour of pier test - motion four

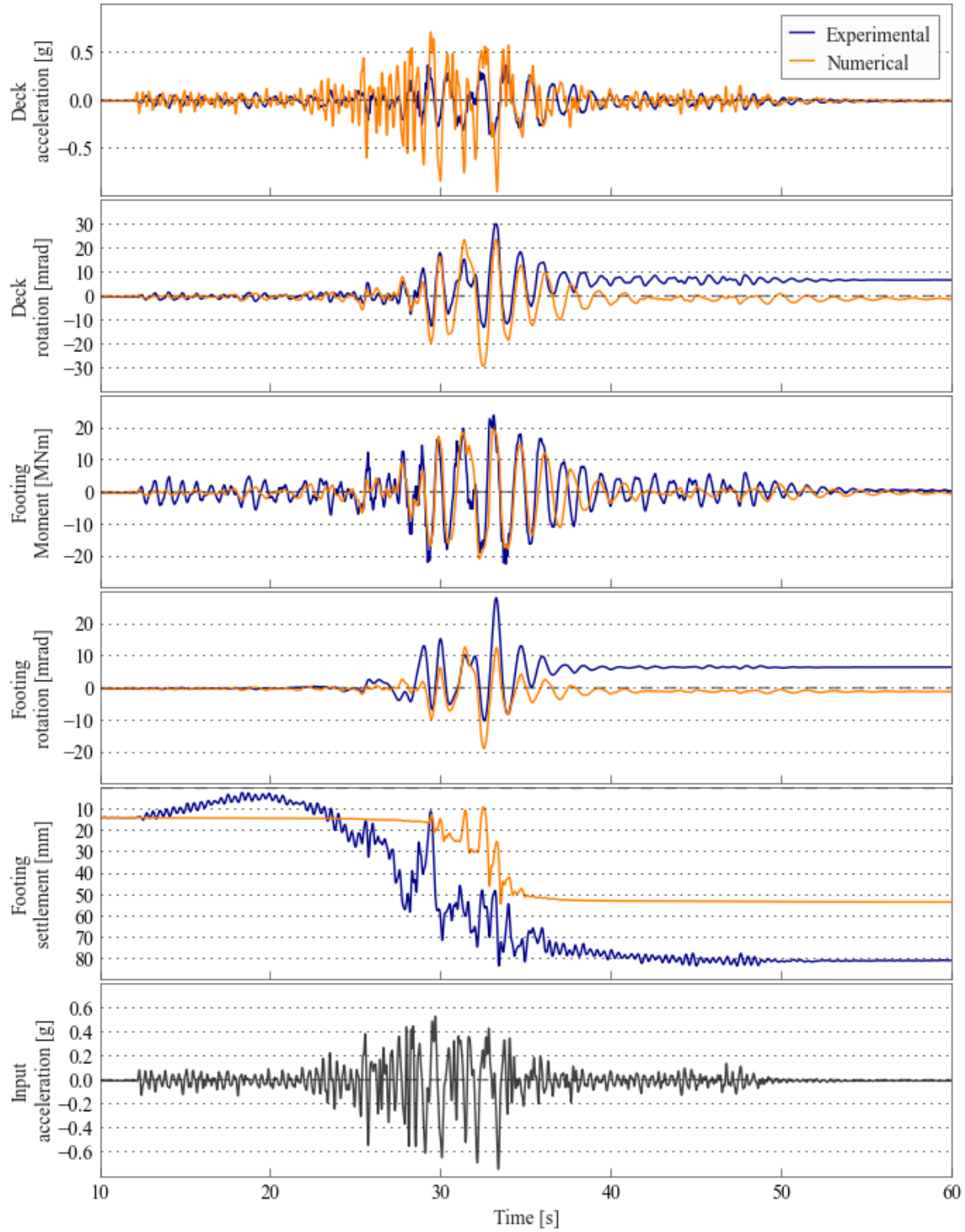

Figure 5.13: Comparision of numerical and experimental behaviour of pier test - motion seven

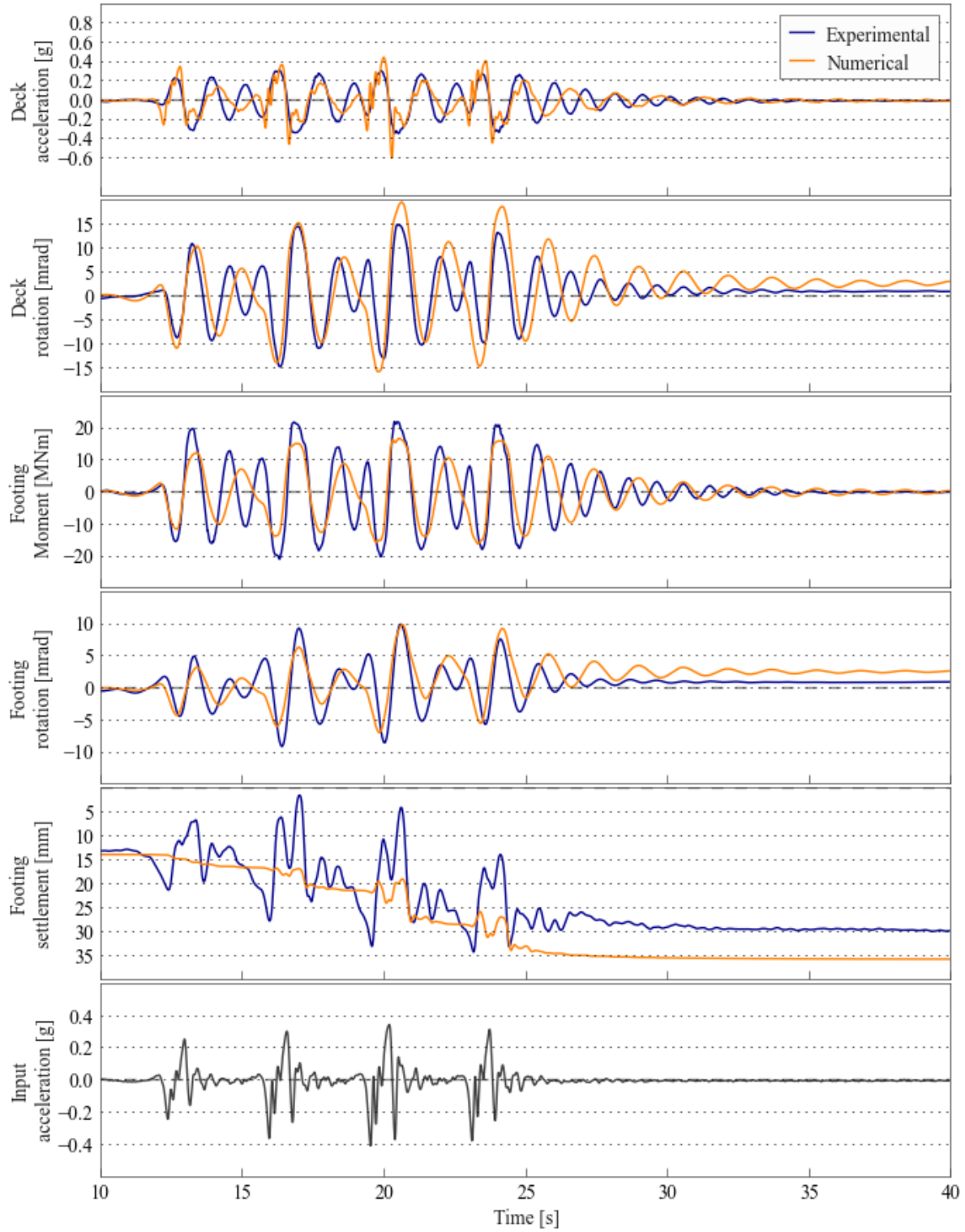

Figure 5.14: Comparision of numerical and experimental behaviour of pier test - motion ten

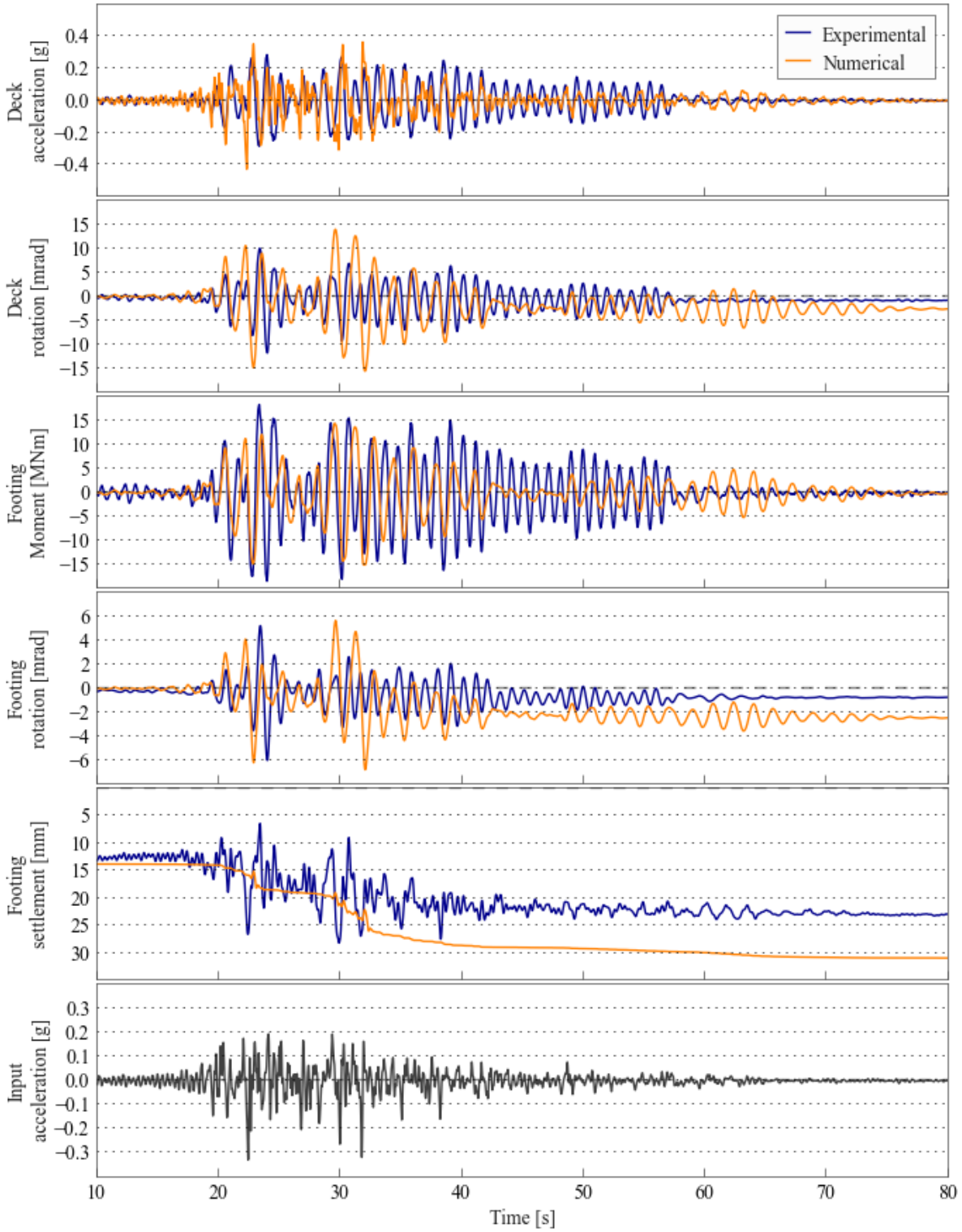

Figure 5.15: Comparision of numerical and experimental behaviour of pier test - motion fifteen

The roof acceleration was investigated further and Figures 5.16a - 5.16b show the roof acceleration in the frequency domain for motions 7 and 10 respectively. The numerical and experimental results were very similar in the frequency domain up to about 2 Hz, after which

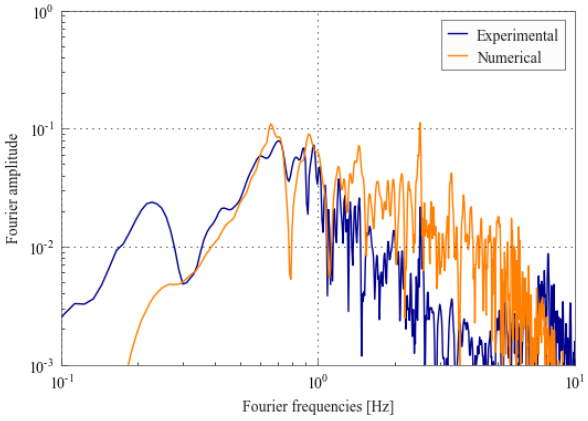

(a) Motion seven

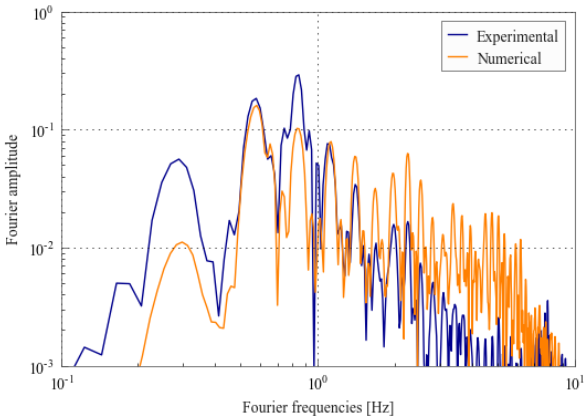

(b) Motion ten

Figure 5.16: Comparison of roof frequency content

the numerical model had larger amplitudes, suggesting that some additional filtering of the ground input motion occurred when it passed into the structure. Since kinematic interaction was not accounted for in the numerical model, all the high frequency content was passed from the free field motion to the near-field motion and may explain some of the discrepancy between the amplitudes at high frequency levels.

Figures 5.17a - 5.17b show the moment rotation behaviour from the seventh motion and tenth motions. The experimental hysteresis plot is irregular, as would be expected with the complexities involved in capturing data under enhanced gravitational conditions. The hysteresis from the numerical model shows a similar trend to the experimental behaviour for motion seven, with the peak behaviour well predicted. The trend of moment-rotation of the tenth motion was very consistent, with the initial stiffness being approximately the same and the change in stiffness (most likely due to uplift) also occurring at similar levels of moment demand. The peak moment was under-predicted and this discrepancy may be due to the sidewalls contributing to the moment capacity in the experimental tests, as well as the settlement that occurred during previous motions causing additional bearing and moment capacity.

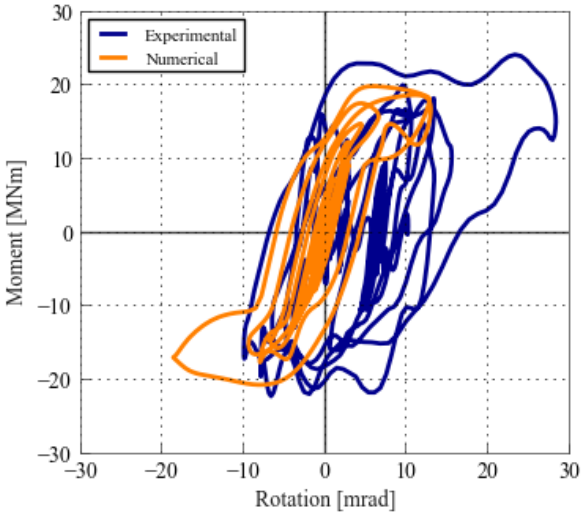

(a) Motion seven

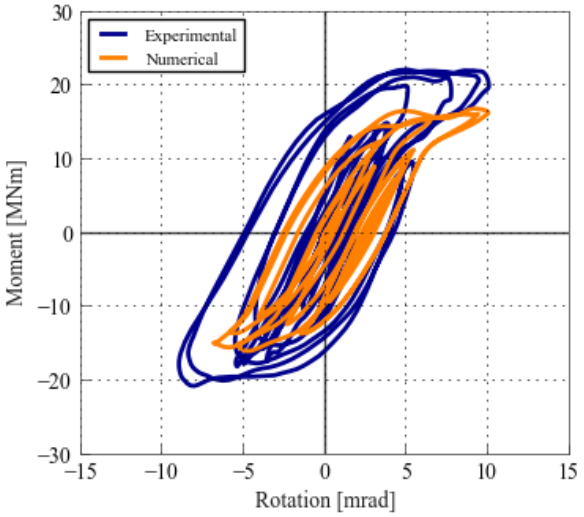

(b) Motion ten

Figure 5.17: Comparison of moment versus rotation behaviour of footing

The rotation versus settlement plots for the seventh and tenth motions can be seen in Figures 5.18a and 5.18b respectively. The experimental behaviour in motion seven was highly irregular as the peak values of the vertical displacement signal appeared to be inconsistent. Motion ten showed a more consistent trend, with both the experimental and numerical plots showing the characteristic shake-down behaviour as the foundation shakes itself into the ground with each subsequent cycle. The footing uplift was also captured at the peak of the footing rotation (seen in Figure 5.18b where the settlement of the footing centre point momentarily decreases).

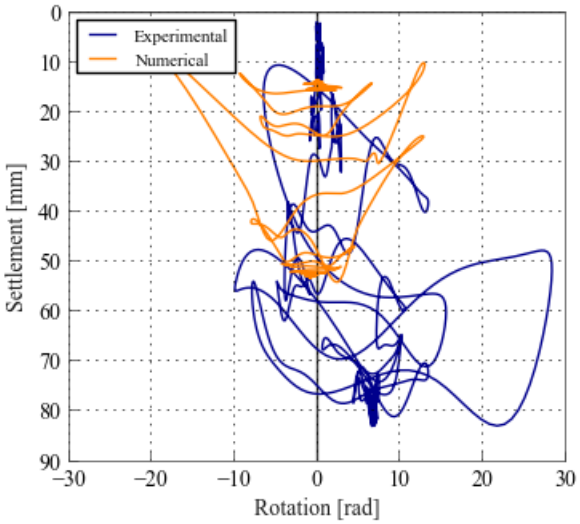

(a) Motion seven

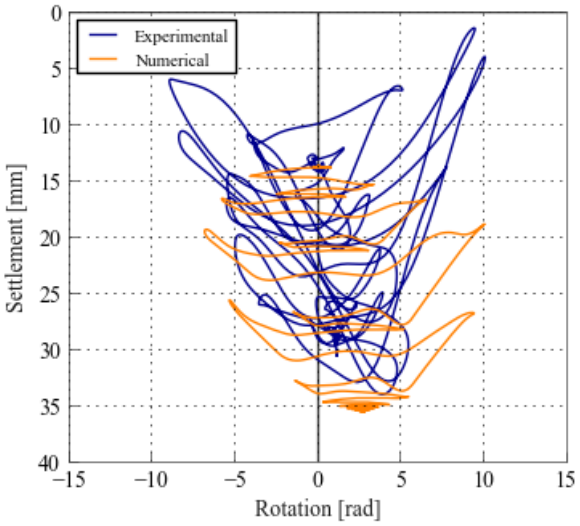

(b) Motion ten

Figure 5.18: Comparison of settlement versus rotation behaviour

All motions

The peak foundation rotation from the experimental and the numerical model are compared in Figure 5.19, with the percentage difference between the two values given in reference to the experimental value. The behaviour was generally very well predicted with most numerical values being within 20%. The largest difference occurred in motion 7, where the peak rotation was under predicted by 34%. Looking at the foundation rotation in motion 7 in Figure 5.13 the general behaviour was well modelled, however, at a time of 34 seconds the numerical model predicts a greater rotation than the experimental model and on the subsequent reverse cycle the numerical model under predicts the rotation. The peak-to-peak rotation amplitude during this cycle was still approximately equal, suggesting the dynamic behaviour was modelled

well. Given that the residual rotations for motion 7 were quite different, the issue was most likely caused by a slightly larger inelastic deformation in the numerical model.

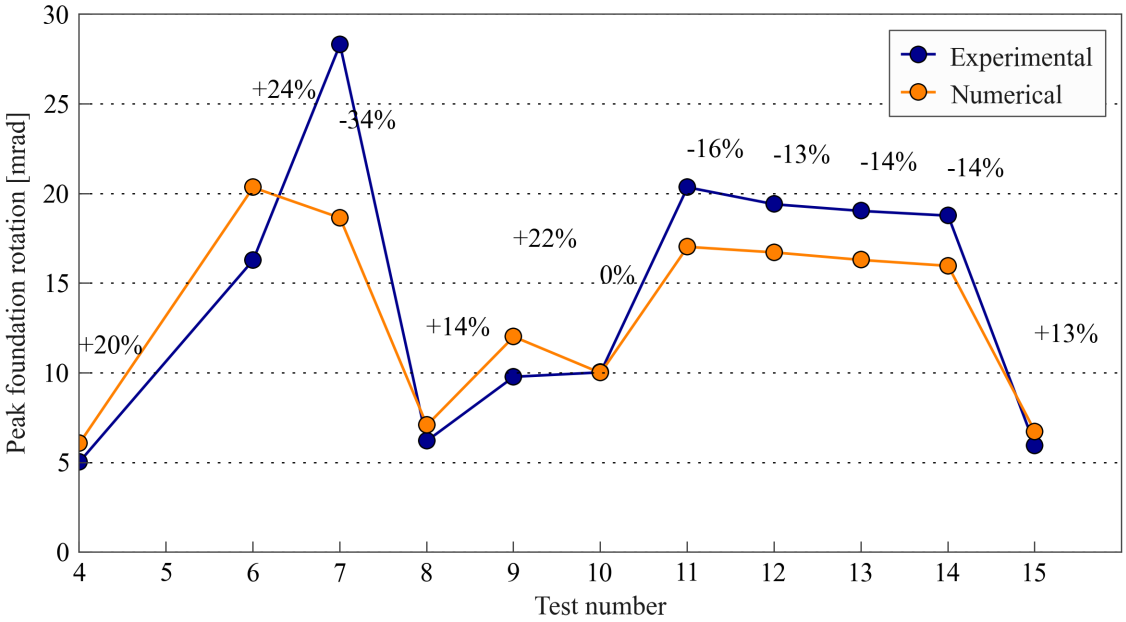

Figure 5.19: Comparison of peak rotation verse test number

The modelling of the SFSI-induced settlement can be seen in Figure 5.20, where the numerical predictions are compared against the experimental results. During the initial motions, the numerical model slightly underestimated the level of settlement, possibly because the soil density was very low. Interestingly, the input motions for motion 4 and 15 were nearly identical but the experimental settlement was 30 mm and 10 mm while the numerical model consistently predicted 17 mm. As the soil densified the experimentally measured settlement reduced, which was not accounted for in the numerical model. The behaviour can clearly be seen in Figure 5.20 where the initial motions show the settlement behaviour was under-predicted by the model, while the later motions show an over prediction. The behaviour is most clear when looking at the behaviour of the pulse type motions, where the peak rotation is nearly identical for all motions (Figure 5.19) and the numerical model predicts very similar settlements for motions 11-14, however, the experiments show a decreasing trend in settlement.

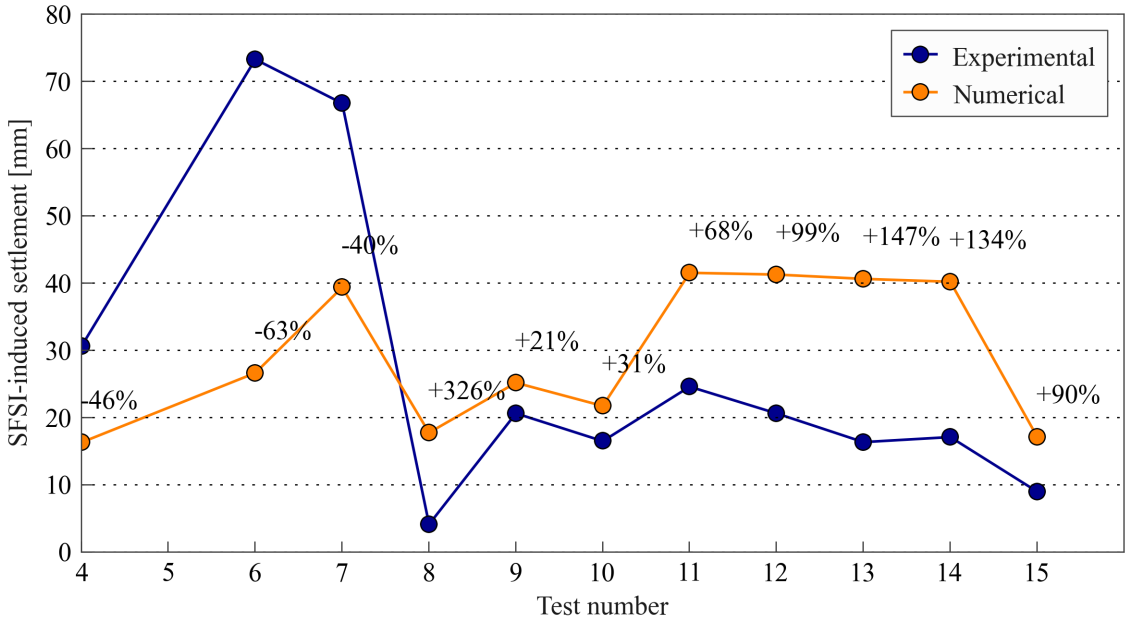

Figure 5.20: Comparison of settlement verse test number

Unfortunately the model did not capture the change in bearing capacity of the footing due to settlement nor the change in the mechanical properties of the soil due to densification. Although the soil started out at a relative density of 38% the large amount of shaking only caused 220mm of free-field settlement (prototype scale), resulting in a relative density of 48%(Figure 5.21). This suggests that the mechanical properties of the soil directly under the foundation after long periods of shaking may be considerably different to the free-field, and this localised change caused a reduction in the tendency to settle.

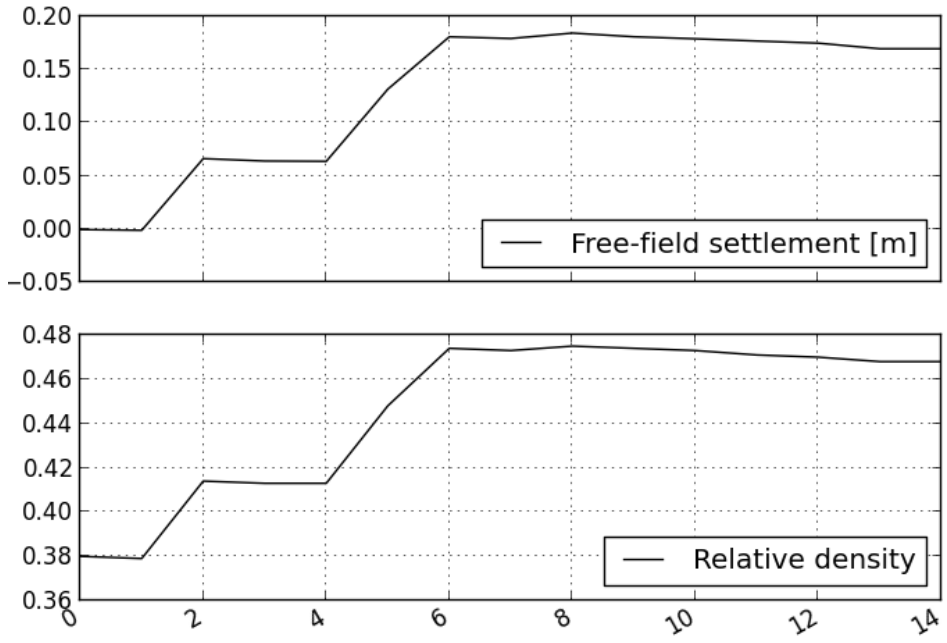

Figure 5.21: Free-field settlement and relative density verse test number

It was seen in the time series plots that the trend of residual rotation was well predicted, however, the predicted final values were in some cases quite different to the experimental measurements. The comparison of the experimental and numerical residual rotations for all motions can be seen in Figure 5.22. The direction of residual rotation was correctly predicted for most tests with the most notable exception being motion 6, where the rotation was well predicted except for the behaviour at 37-40 seconds (Figure 5.23).

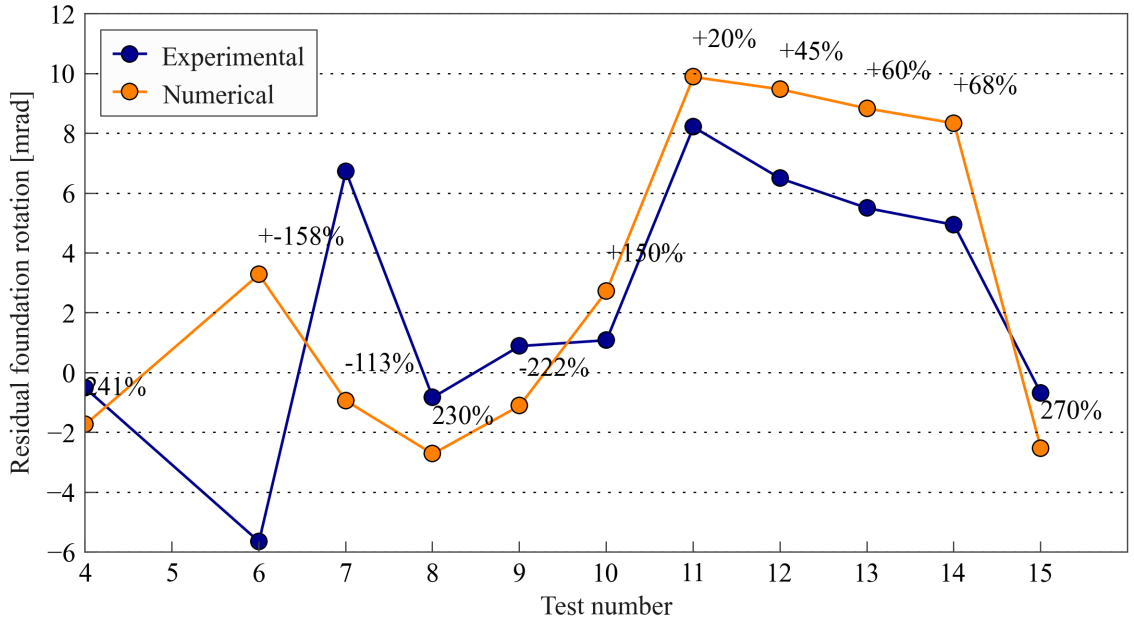

Figure 5.22: Comparison of residual rotation verse test number

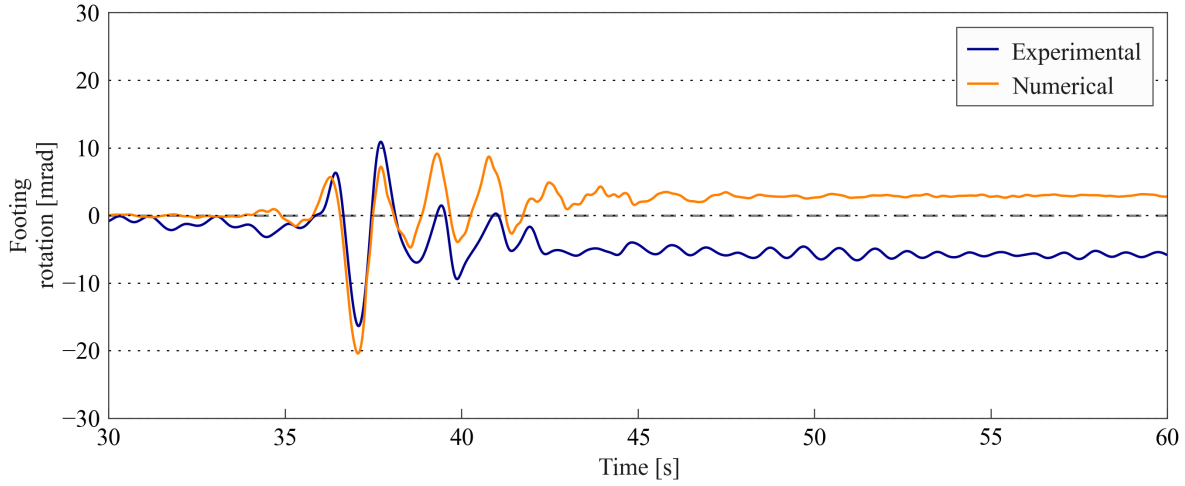

Figure 5.23: Comparision of numerical and experimental pier foundation rotation - motion six

5.4.2 Frame structure

The behaviour of the more complex frame structure was well predicted by the numerical model with Figures 5.24 - 5.27 showing the time series behaviour from the LCN, WVC_L, WPI_H and TCU_H motions. The LCN motion was a low amplitude motion from the second spin up using the full mass and the type I beams. The WVC_L motion was a low amplitude motion from the third spin up using the reduced mass and the type I beams. The WPI_H and TCU_H motions were high amplitude motions from the last spin up using the reduced mass and the type II beams.

The roof acceleration for all motions was well estimated except for the additional high frequency content in the experimental model not seen in the experimental record. This behaviour was the reverse to what was observed in the pier test and may be due to the experimental model activating a second mode that was not accurately modeled numerically. The discrepancy in the high frequency content made very little difference to the roof displacement which was well predicted in most motions.

The footing rotations were difficult to extract from the experimental data and in some motions contained additional high frequency content that was not observed in any of the other recording devices. The general trend of the rotational behaviour was captured, however, the residual behaviour was not well predicted in all cases. The residual behaviour was most inconsistent for very small levels of shaking where the static moment in the footing from the superstructure mass caused the footings to creep and dissipate the moment. While the creep may occur in reality to an extent, the numerical model was reset after every ground motion and therefore the dissipation of the footing moment from previous excitations was not accounted for. The footing settlement was well predicted in the earlier motions, however due to the numerical model not accounting for the soil densification, the reduction in settlements that was seen in the experimental tests through repeating motions, was not observed in the numerical behaviour. The rising up of the footing due to a reduction in axial load through frame action was captured by the numerical model and was consistent with the experimental time series. A similar level of comparison was obtained for all the tests except for cases when a sensor did not capture the response data (comparisons for all time series can be found in Appendix B - Experimental test validation - Frame).

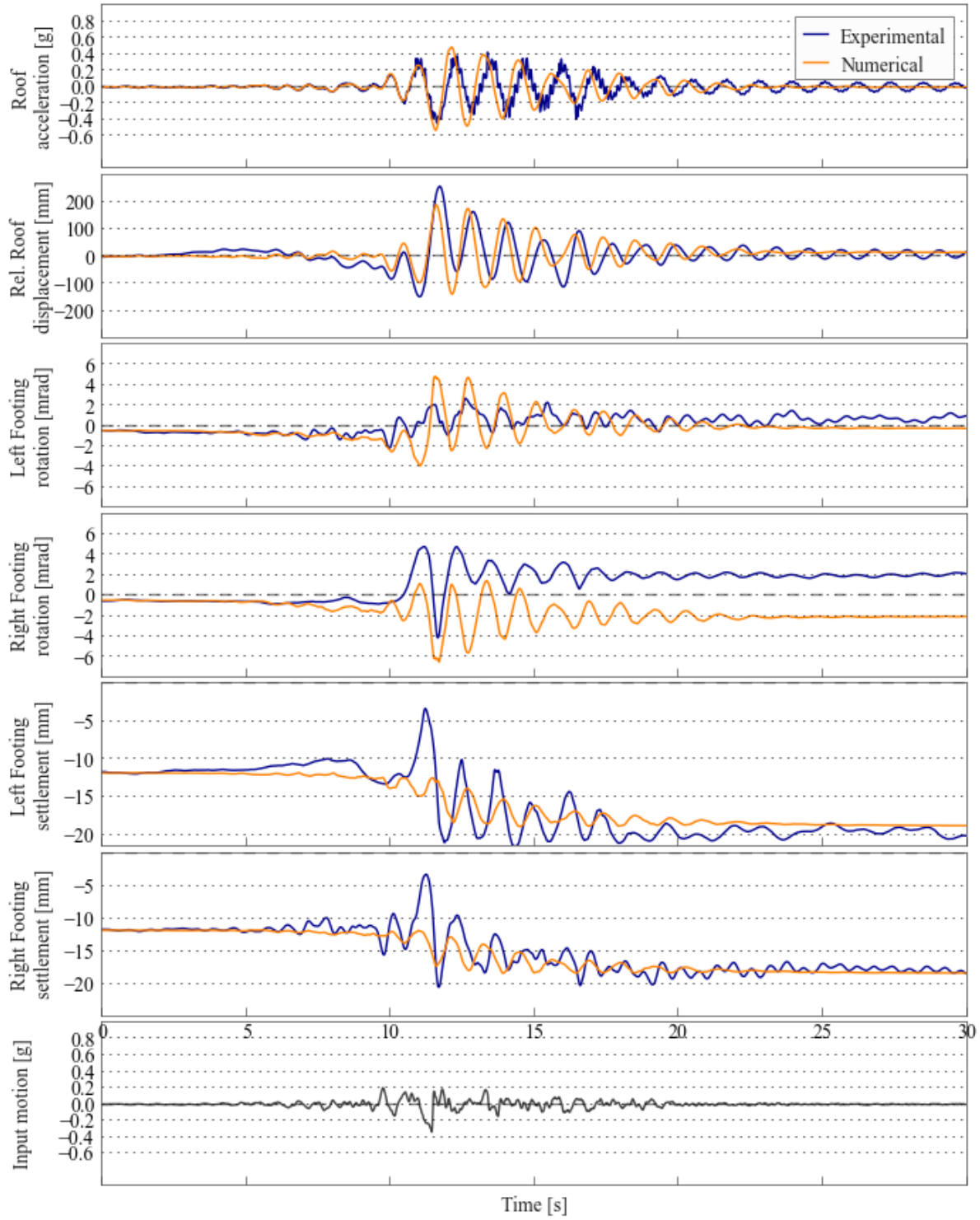

Figure 5.24: Comparision of numerical and experimental behaviour of frame test - motion LCN

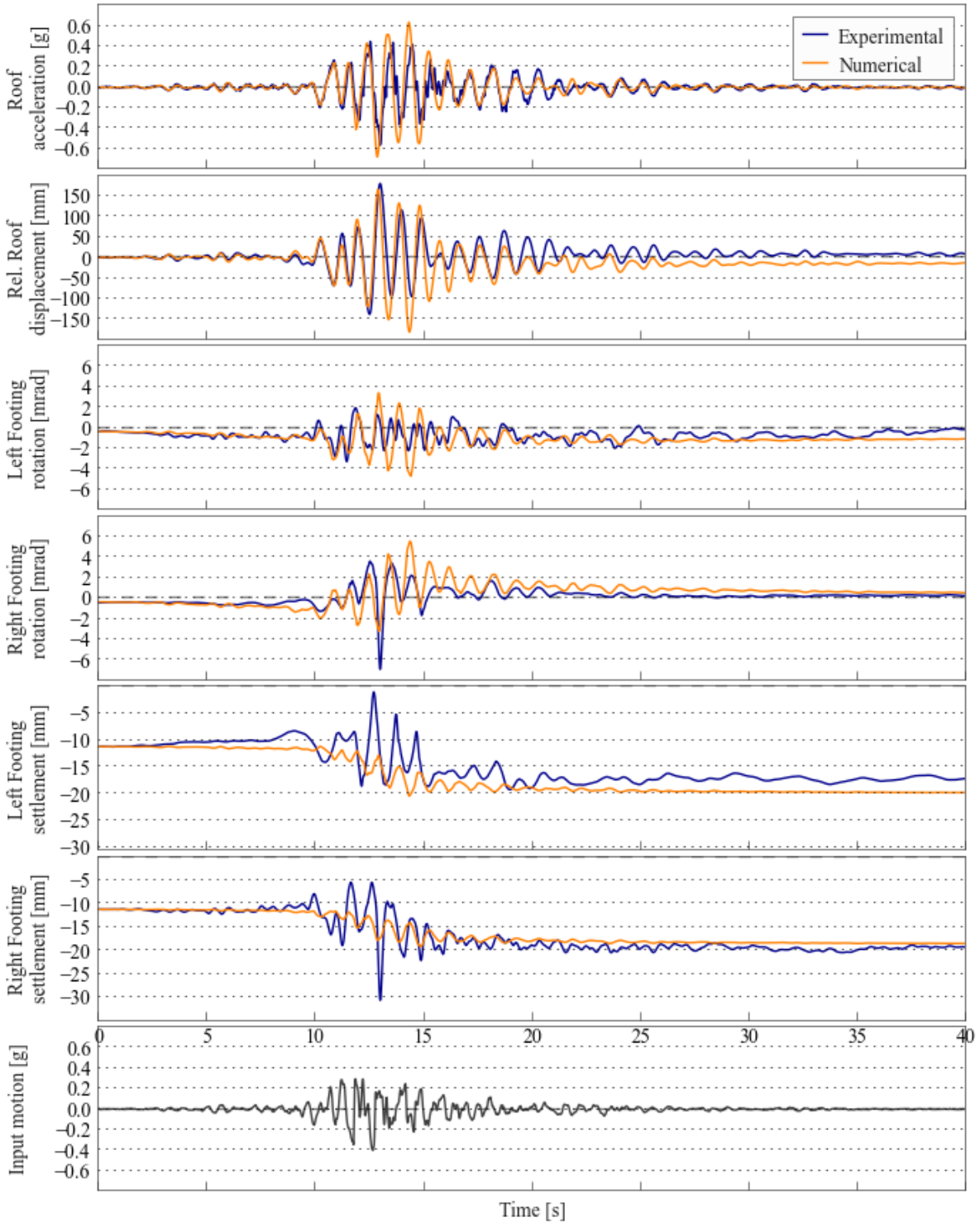

Figure 5.25: Comparision of numerical and experimental behaviour of frame test - motion WVC_L

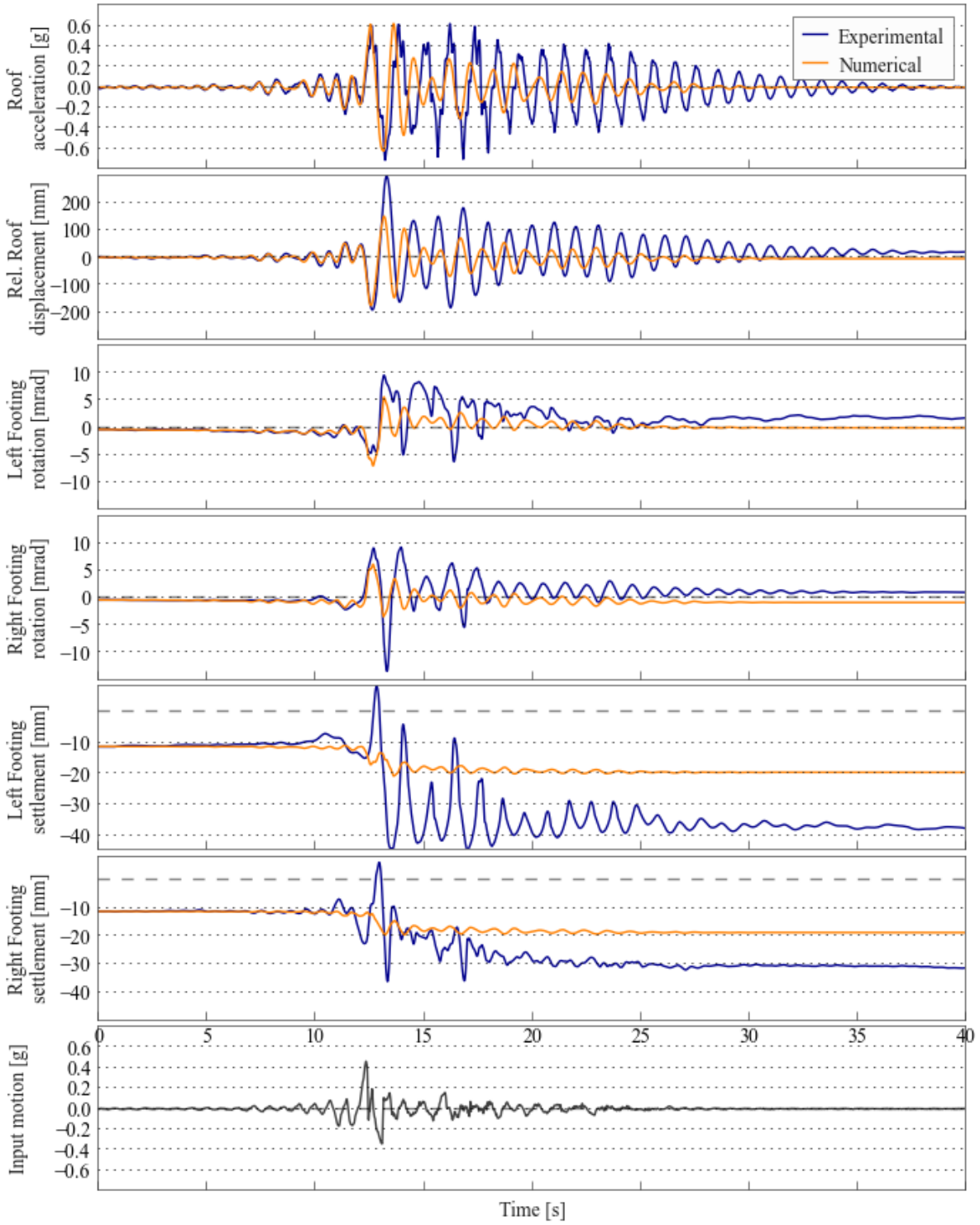

Figure 5.26: Comparision of numerical and experimental behaviour of frame test - motion WPI_H

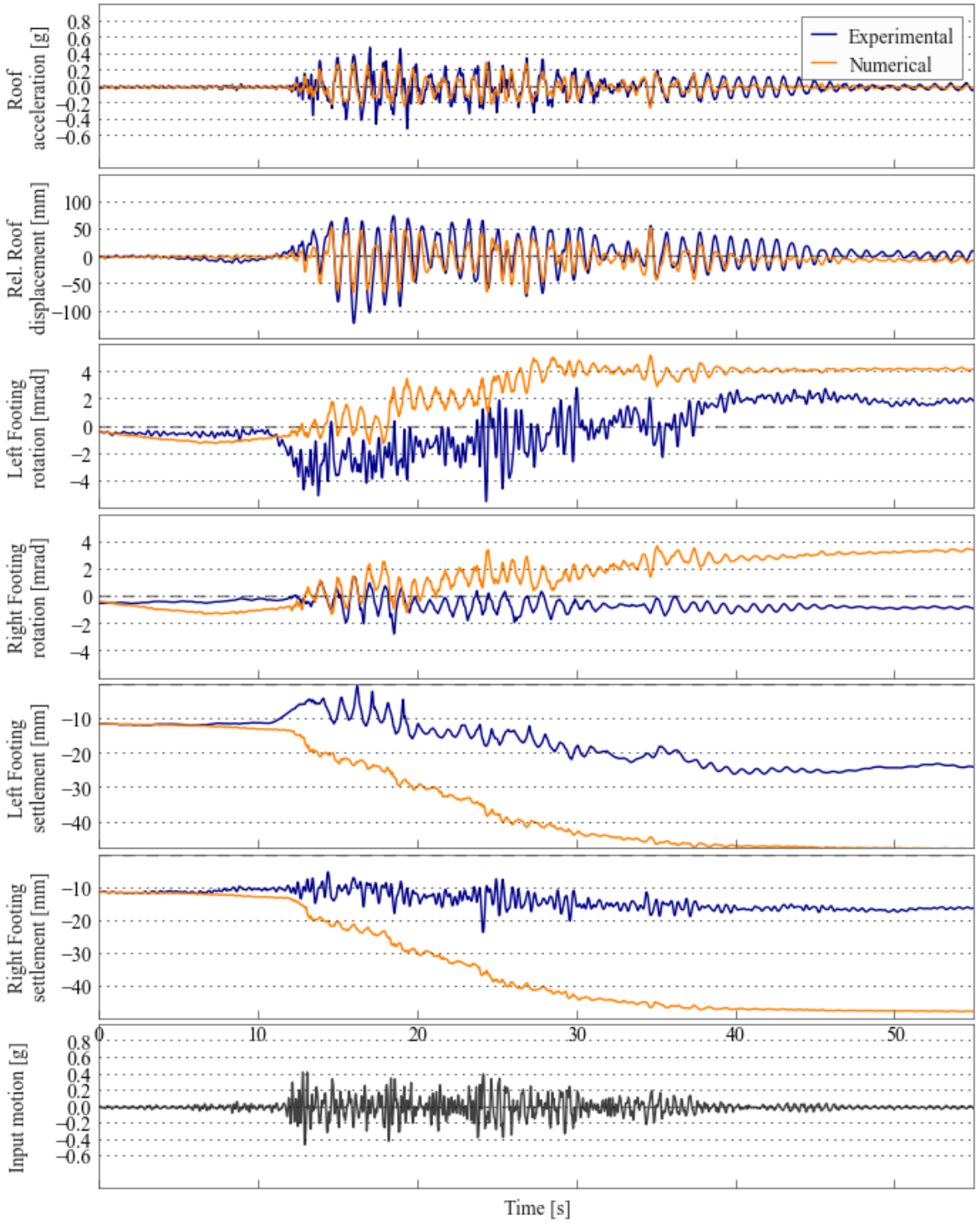

Figure 5.27: Comparision of numerical and experimental behaviour of frame test - motion TCU_H

The roof frequency content in Figures 5.28a and 5.28b for the LCN and WPI_H were well matched up to two hertz, at which point the experimental motion showed increased amplitude unmatched by the numerical model, most likely attributed to white noise. Another explanation may be due to a second mode in the experimental model since the experimental

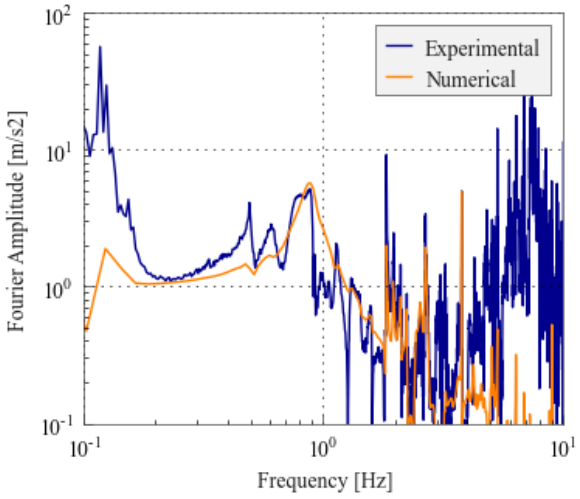

(a) Motion LCN

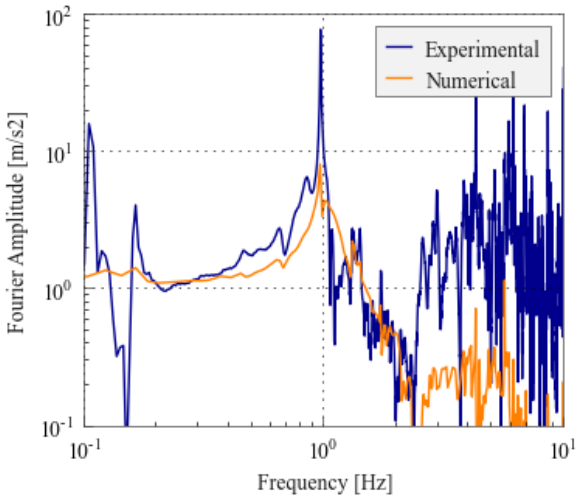

(b) Motion WPI_H

Figure 5.28: Comparision of roof frequency content

team noted that the one-storey frame model exhibited a torsional response as well as the lateral displacement of the roof (Mason et al., 2010). The second mode is certainly not clear in the Fourier amplitude plots as there was no clear second peak in the amplitude.

The rotation-settlement response of the footings exhibited a different behaviour to the simple pier structure. The variation in axial load due to frame action meant that two mechanisms contribute to the settlement, shake-down due to plastic rotation and cyclic axial loading. The settlement-rotation behaviour shows an asymmetric behaviour, which is most clearly seen in the numerical plots in Figures 5.29 and 5.30. The asymmetric behaviour can also be seen in the experimental plots, with the exception of the left footing in Figure 5.30 where the odd rotational signal results in unusual observed behaviour. The numerical model captures the shake-down and the cyclic axial loading trends, although the numerical and experimental plots look quite different.

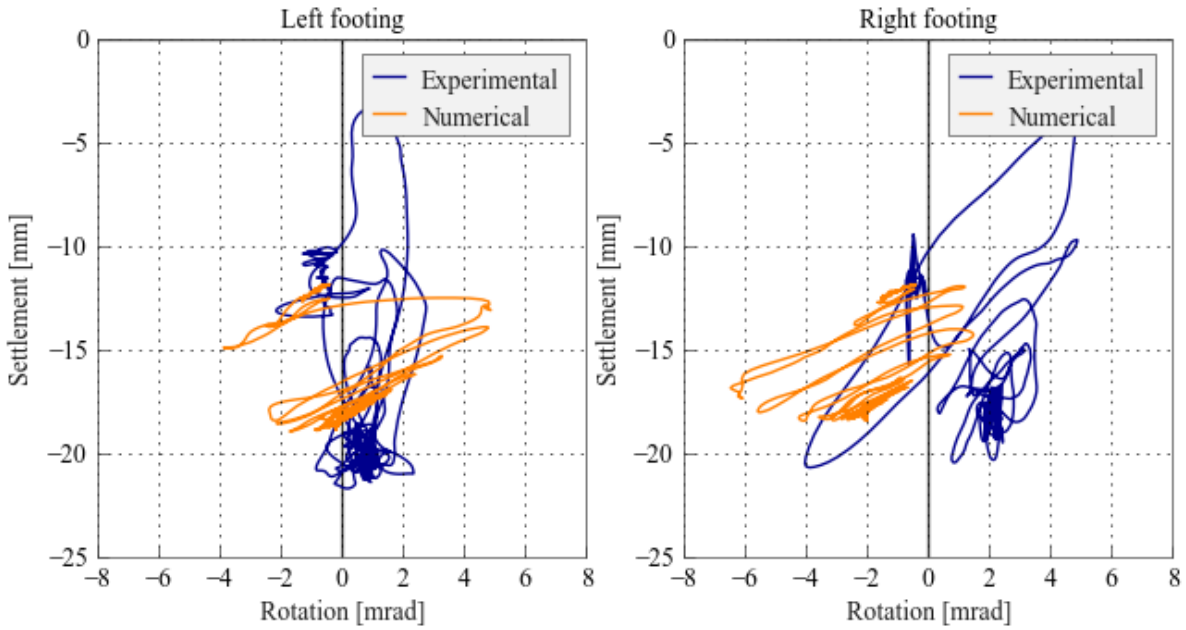

Figure 5.29: Comparision of rotation-settlement behaviour - motion LCN

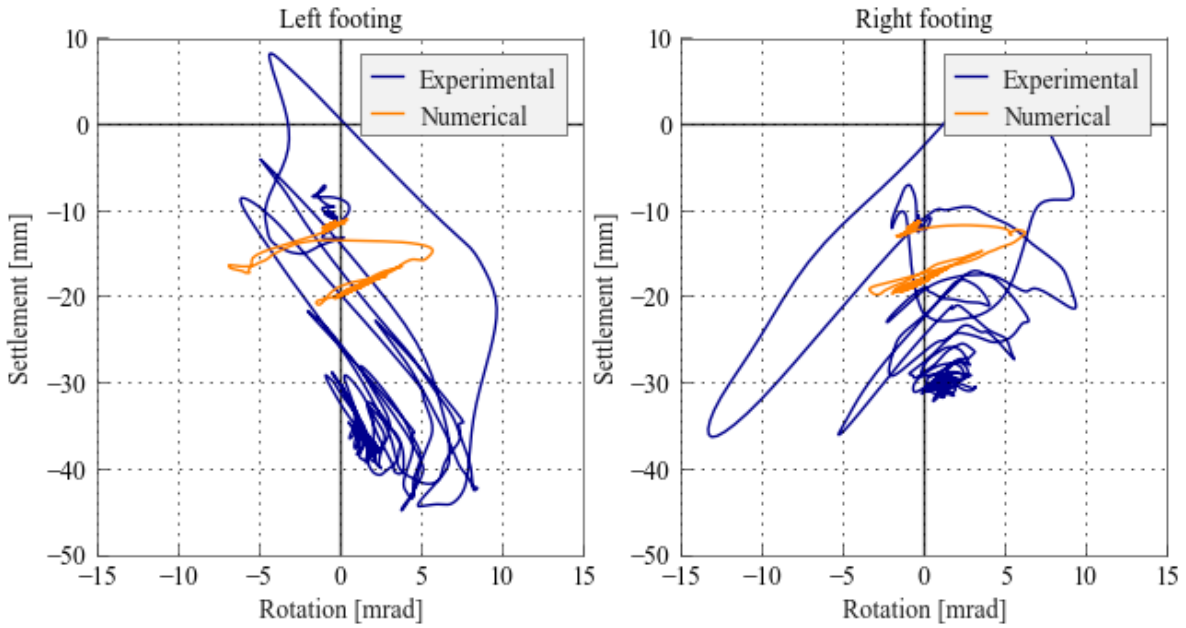

Figure 5.30: Comparision of rotation-settlement behaviour - motion WPI_H

The moments in the beam and column ends were extracted by multiplying the curvature (obtained through two strain gauges) by the rotational stiffness. Unfortunately the column moments were very low as the strain gauges did not accurately measure the strain in the column hinges, as the hinges experienced some highly local deformations, making the assumption of uniform strain in the strain gauges less plausible. The footing moments were extrapolated through equilibrium from the moments and shear forces in the columns. The poor measures of the column moments meant that the experimental moment forces were ap-

proximately a factor of five less than the corresponding numerical values and therefore have been scaled up by five in Figures 5.31 and 5.32 for comparison purposes to show the general behaviour of the footing and the non-symmetric rotational stiffness. The change in stiffness can be seen in the plots and is more predominant in the positive moment direction for the left footing and negative direction for the right, as this corresponds to a reduction in axial load due to frame action, most likely causing the footing to uplift.

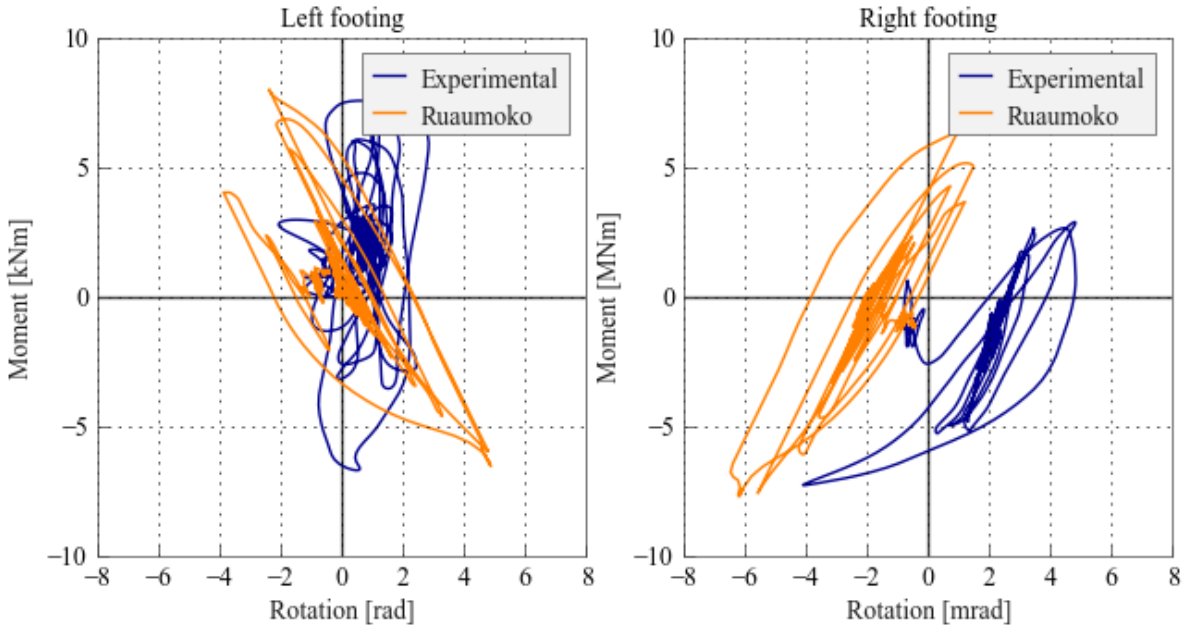

Figure 5.31: Comparision of moment-rotation behaviour - motion LCN

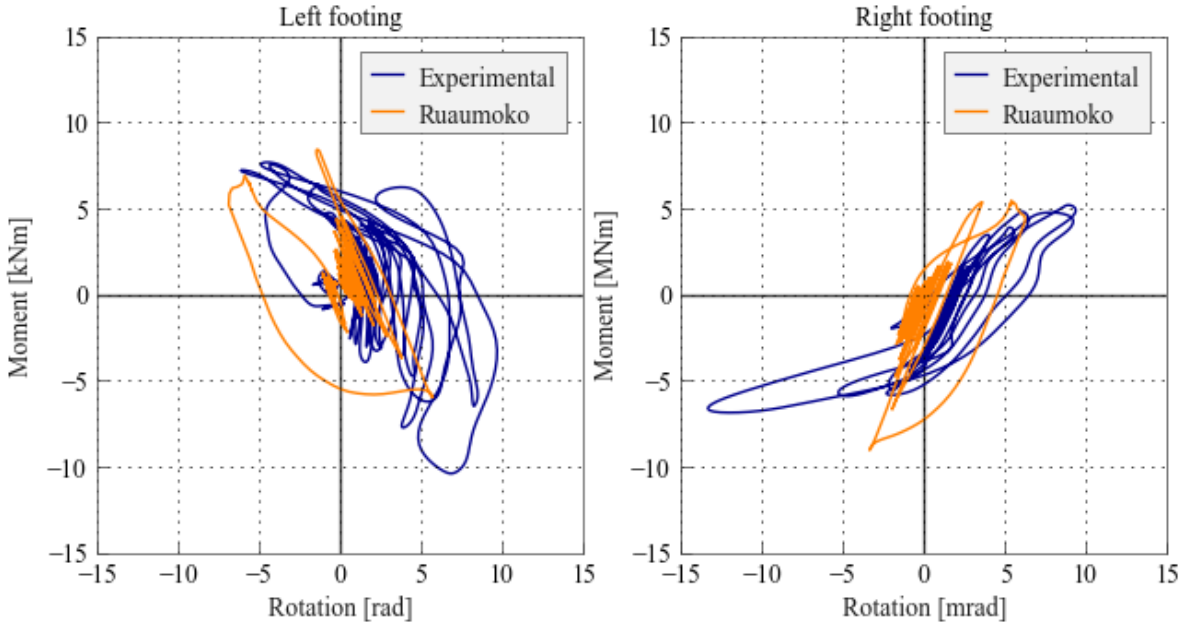

Figure 5.32: Comparision of moment-rotation behaviour - motion WPI_H

All motions

The comparison between the experimental and numerical peak rotation values can be seen in Figure 5.33, with percentage difference between the two values given in reference to the experimental value. All motions except for the motions in sequence one and the last motion WVC_H are shown, as in these motions the high frequency content of the footing was not recorded. The behaviour was generally very well predicted although not as well as the pier peak rotation, and the percentage differences at low levels of peak rotation being quite high. The comparative different between the numerical and experimental values was fairly consistent through the entire set of tests with the worst difference in absolute terms occurring during the strong SCS_H motion.

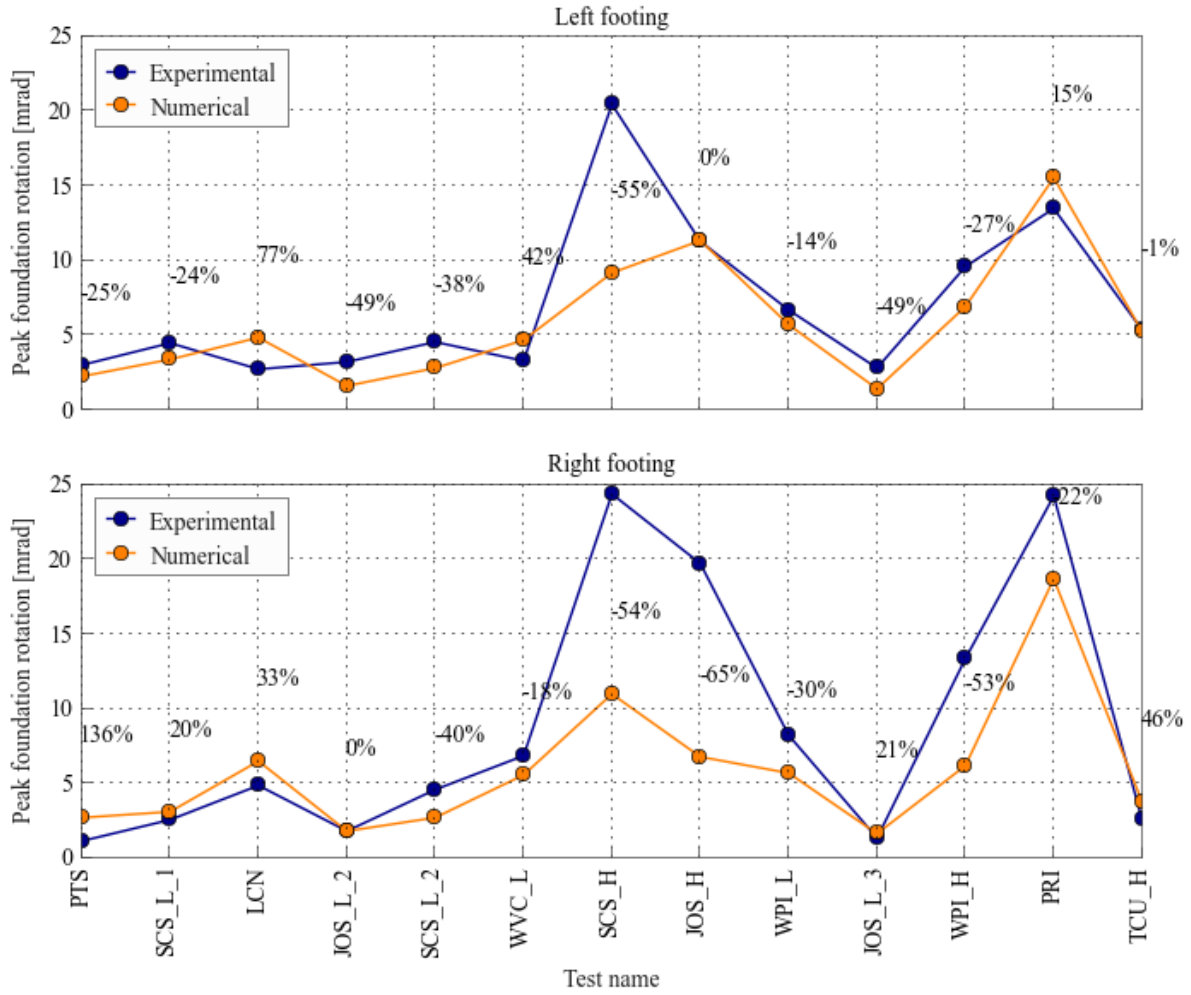

Figure 5.33: Comparision of rotation-settlement behaviour - all motions

The SFSI-settlement can be assessed for all motions for both the experimental and numerical plots in Figure 5.34. The numerical settlement was reasonably consistent with the experimental values and just like in the pier test, the settlement was under estimated in the earlier motions and over estimated in the later motions. The magnitude of the settlement was similar

to the level observed in the Pier tests with largest being 91mm and the average being 15mm from all of the motions. As expected the larger settlement values (motions SCS_H, JOS_H and PRI) all correspond to large peak rotation values as seen in Figure 5.33.

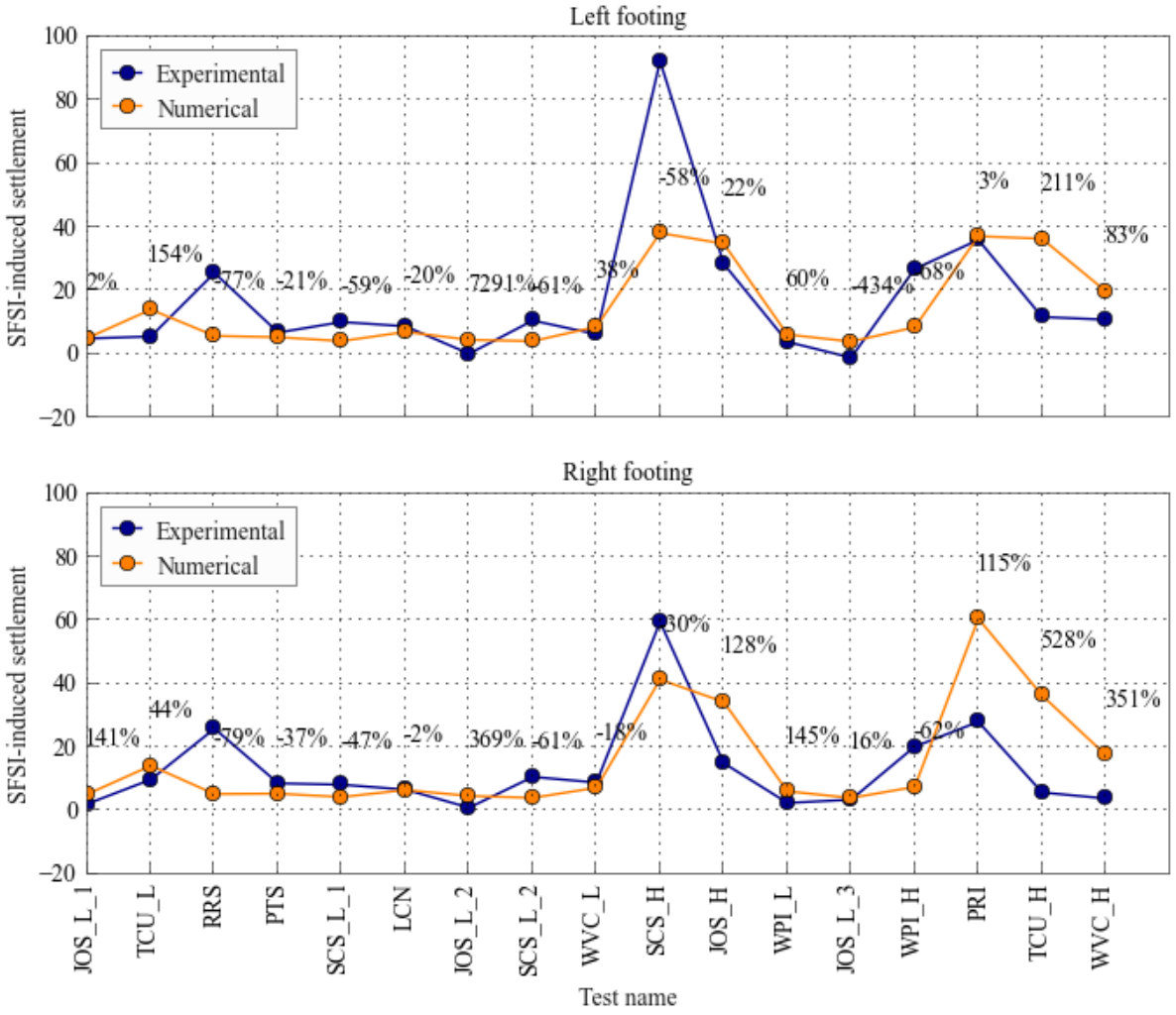

Figure 5.34: Comparision of rotation-settlement behaviour - all motions

In Figure 5.35 the numerical residual rotation can be compared to the experimental values for all of the ground motions. The numerical model did not capture the residual rotation of the experiment very well. IThe signed residual rotation is shown to demonstrate that the numerical model sometimes predicted a residual rotation in the opposite direction to the experimentally measured value. The residual rotation is more difficult to capture as it is more dependant on the plastic response of a single cycle, while the settlement is a cumulative measure of plastic response. Further issues with the prediction of residual deformations arose due to the dissipation of the static footing moment that occurred in each of the numerical model simulations that may not have occurred for each experimental test due to the tests being run in a sequence. This dissipation of moment was accompanied by a permanent rotation of the footing.

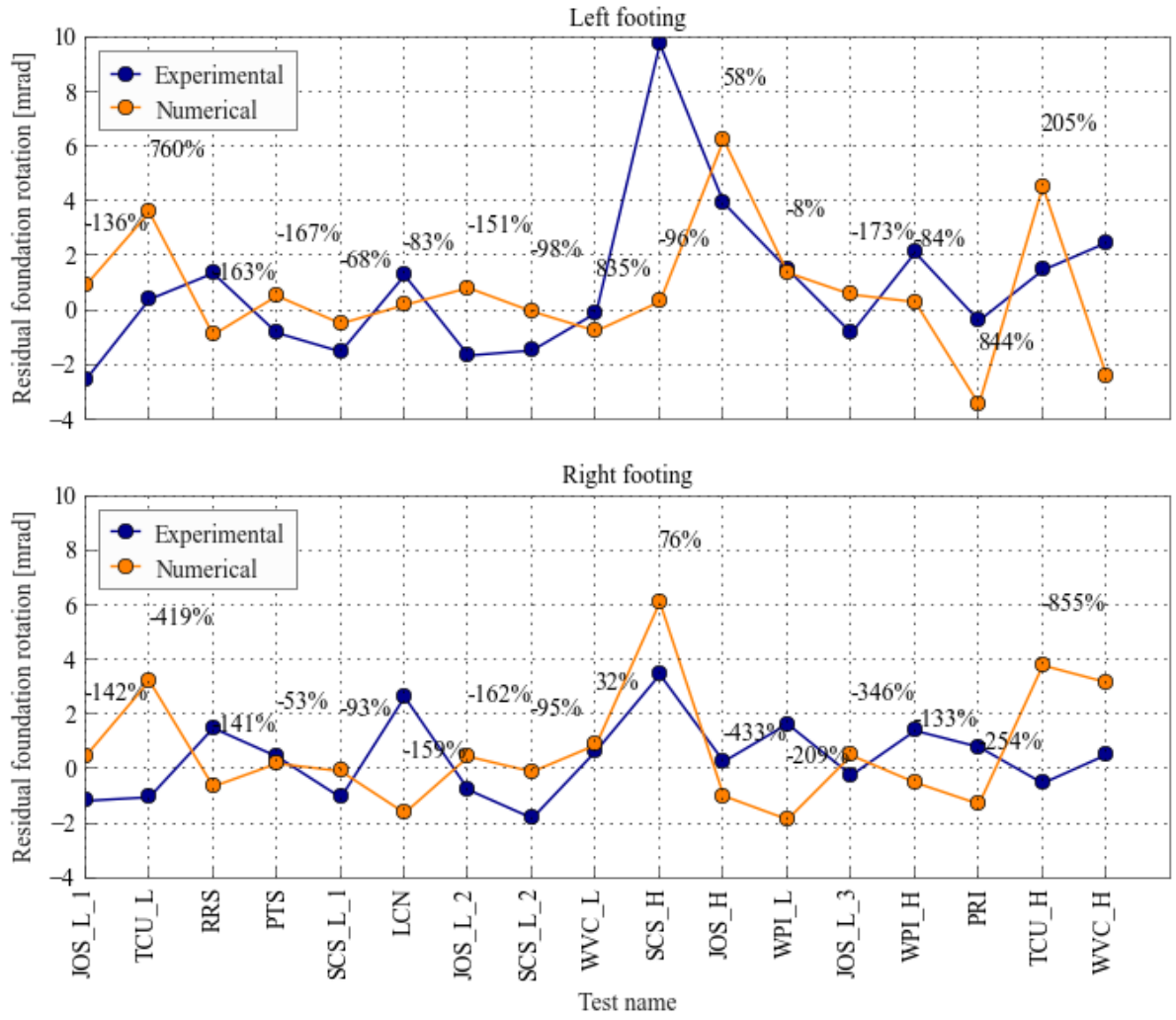

Figure 5.35: Comparision of computed peak rotation and residual rotation with respective measured values for all motions

5.5 Conclusions

This chapter presented the validation of a newly developed macro soil-foundation interface element against two experimental tests. In the first experiment a pier structure was shaken to levels close to toppling using both recorded and pulse type ground motions. The second experiment was a complex single storey frame structure with a non-linear superstructure and isolated footings, exposed to recorded ground motions at varying levels of intensity. The experimental tests and the processing of the experimental data is discussed in detail. The numerical model provided generally good estimates of the performance in a number of important areas for both tests.

The majority of the simulations from the pier test predicted peak foundation rotations, SFSI-induced settlement and residual rotation values within 20%, 10mm, 60% respectively. The examination of the time series of several pier simulations showed that the transient behaviour

throughout the excitation was also well modelled, including the forces and deformations in the superstructure. The settlement-versus rotation plots of the pier motions demonstrated the shakedown of the footing due to plastic rotation and the uplift of the centre of the footing due to the tension edge of the foundation detaching under large rotations. The numerical model also under predicted the SFSI-induced settlement and residual deformation in the earlier motions and over predicted them in later motions, suggesting that the behaviour of the experimental model was modified due to exposure to numerous ground motions, which was not captured by the numerical model.

The simulations of the frame structure were reasonably well modelled, with the majority of the peak foundation rotation, SFSI-induced settlement and residual rotation values within 30%, 10mm, and 100%. The assessment of the time histories showed reasonably consistent behaviour between the experiment and numerical simulation, with congruent foundation and roof deformations. The major exception to this was the simulation of the foundation rotation at the beginning of many ground motions, where the applied moment on the footings due to gravity load would be dissipated under small cycles and result in permanent foundation rotation.

The settlement versus footing rotation was examined and demonstrated that the additional axial load due to frame action resulted in considerable cyclic vertical displacement. The footing moment versus footing rotation plots showed that the cyclic axial load from frame action also caused asymmetric footing rotational stiffness and strength as the reduction in axial load increased the tendency for the footing to uplift.

The proposed tests were both on Nevada sand, however, the calibration parameters for the model were taken from experiments conducted on other sand including Fontainebleau sand, Toyoura sand and Ticino sand, providing confidence that the model can be adapted for other sands. The applicability of the model for clayey soils has not been validated as there are only a limited number of experimental tests using clayey soils.

Most importantly, since the input values for the macro-element used values suggested in literature, the physical and geometric properties of the numerical model were all taken from the test reports and the input ground motions were the recorded free field motions, the presented results can be assessed as class C predictions.

5.6 Acknowledgements

I would like to thank the members of the both research teams working at UC Davis, who conducted the experimental research and provided the experimental data for this chapter.

Chapter 6

Prediction of peak transient displacements considering foundation deformations

Summary

It is a requirement of performance-based design to provide an estimate of the expected level of deformation of the structure. For many years this estimation has ignored the influence of soil-foundation-structure interaction (SFSI), however, it is widely accepted that SFSI modifies the response and displacements of the structure. Advanced tools exist to model the soil, foundation and structure using non-linear time-history analysis that can provide reasonable estimates of the deformations throughout the system. Unfortunately, these numerical tools require considerable knowledge of soil and structural dynamics and results are strongly impacted by the characteristics of the employed input ground motion time history. The alternative approach of determining the inelastic displacements based on the response of an equivalent linear structure is still the most widely adopted approach and forms the basis of many seismic design codes.

Design procedures that adopt equivalent linear properties require the engineer to quantify both the effective response period and a displacement modification factor, often considered as an equivalent viscous damping. The two properties are interdependent and by no means intrinsic to the building. Equivalent viscous damping requires calibration based on the assumptions of the effective response period to match some behavioural aspects of the non-linear system. Currently, expressions exist that quantify the foundation hysteretic energy dissipation in terms of an equivalent viscous damping, based on pseudo static cyclic loading of foundations; these expressions however, use an equal viscous-to-hysteretic energy dissipation assumption, based on cyclic loading to peak displacement and do not attempt to account for the erratic dynamic loading from earthquakes.

This chapter provides an overview of the displacement-based design of buildings considering soil-foundation-structure interaction with emphasis on the assumptions around period shift and equivalent viscous damping. The equivalent foundation rotational stiffness is calibrated using a series of pushover analyses and the influence of the level of shear force on the foundation is uniquely accounted for in the development of a simple general expression for equivalent foundation rotational stiffness on sand. New foundation displacement modification factors are proposed based on non-linear time history analysis results, using an elastic single-degree-of-freedom structure with a non-linear macro soil-foundation interface element. The proposed stiffness and displacement modification expressions are combined with displacement modification factors for inelastic modified Takeda hysteretic behaviour to design a series of wall buildings using Direct Displacement-based Design. The buildings are then assessed with further non-linear time history analysis to validate the accuracy of the developed expressions for design considering both inelastic superstructure and inelastic soil-foundation behaviour.

6.1 Introduction

It is widely accepted that foundation deformations or "soil-foundation-structure interactions" (SFSI) modify the displacements of the structure. The quantification of this modification has been attempted by many researchers (eg. Veletsos and Verbic, 1974; Bárcena and Esteva, 2007; Nakhaei and Ali Ghannad, 2008; Moghaddasi et al., 2011b). The wealth of existing literature has highlighted a series of important parameters that influence the level of modification, namely structure-to-soil stiffness ratio, structure height-to-foundation length ratio and building period-to-ground motion predominant period; however, these studies provide no design orientated expressions to estimate displacements.

A performance-based design methodology, as adopted in many seismic codes around the world, imposes limits on deformations and displacements; therefore, there is a need to quantify the modification of displacements due to SFSI in the context of design. The prediction of the inelastic displacements of a structure can employ a full non-linear model of the structure and soil system, or the more pragmatic approach, where the system is converted to an equivalent linear single-degree-of-freedom (SDOF) system and the linear response spectrum can be utilised. While the full modeling of the structure and soil provides a robust and rational approach to the prediction of displacements, it is hindered by the requirement that the design must be complete to formulate the numerical model, thus resulting in an expensive iterative process. The full modeling is further hampered by several non-trivial decisions, such as ground motion selection, level of model complexity and material physical properties. Simple equivalent linearisation techniques therefore remain a cornerstone in inelastic design, even in the face of ever growing computational power.

The linearisation of a non-linear system requires an estimate of an effective vibration period and an estimate of a displacement modification factor often provided as an equivalent viscous damping. The modification to the vibration period accounts for the increased flexibility of the system after yielding, while equivalent viscous damping (EVD) has been used to account for hysteretic energy dissipation. Many linearisation procedures rely on a conversion from hysteretic energy dissipation to viscous energy dissipation. Equivalent linear site response analysis tools use EVD and a degraded stiffness to model the hysteretic behaviour of the soil. For site response analysis the EVD is based on an equal hysteretic-to-viscous energy dissipation assumption, assuming equivalent linear strain corresponding to 65% of the peak response with a period based on the secant stiffness to 65% of peak shear strain response.

The equivalent linearisation of structures uses a similar approach. Jacobsen (1960) pioneered the development of an equivalent structure concept, whereby a non-linear structure could be approximated by a linear structure with additional damping. Jacobsen's equivalent structure used the initial stiffness and matched the viscous energy dissipation to that of the hysteretic energy dissipation, with the requirement that the structure would be at steady-state

resonance. This procedure gives a good approximation to the displacements for structural periods equal or greater than the excitation period (Dwairi et al., 2007), however, the additional requirement of steady-state resonance, makes it inappropriate for earthquake loadings. Considerable research exists on equivalent linearisation techniques for structures using the initial period for predicting structural deformation during earthquake excitation (eg. Miranda and Bertero, 1994; Miranda, 2000; Ruiz-García and Miranda, 2003). Alternatively, the Direct Displacement-based Design (DDBD) procedure uses a period shift based on the secant-to-peak stiffness and puts considerable emphasis on quantifying hysteretic energy dissipation as an equivalent viscous damping to match displacements (Grant et al., 2005; Priestley et al., 2007; Dwairi et al., 2007; Pennucci et al., 2011a).

Miranda and Ruiz-García (2002) reviewed six different methods of estimating the displacement of a non-linear system using an equivalent linear structure. Two methods used an equivalent stiffness equal to the initial stiffness, two used a stiffness equal to the secant-to-peak response and two used a calibrated stiffness, all the methods could provide suitable estimates of the peak displacement, through different modifications to the elastic displacement using equivalent viscous damping or some other displacement modification factor.

It is important to understand the differences and implications of different linearisation techniques and the variation in the level of displacement modification or EVD. It is clear that EVD is inherently linked to the assumption of the period shift and the parameter which the equivalent model attempts to match. In design, it is imperative to use the correct EVD for the assumed period shift and the match parameter (see Jennings (1968)). Figure 6.1 demonstrates three different period shift assumptions and the values of damping that would be obtained if the equivalent linear response matched the non-linear displacement response. However, the figure also illustrates that the application of these damping levels and equivalent periods would result in poor estimates of accelerations. An inconsistent combination of period-shift and EVD assumptions would also lead to poor displacement estimates.

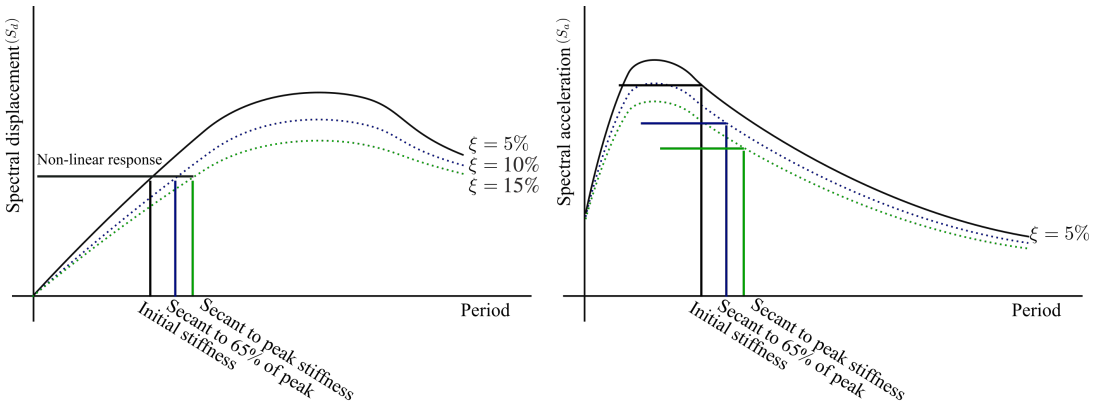

Figure 6.1: Dependence of period shift on equivalent viscous damping

Recent developments in DDBD have bypassed the step of estimating the EVD, due to the

imperfect correlation with area-based hysteretic energy and the variation of sensitivity of spectral displacement to viscous damping between ground motions (Pennucci et al., 2011a). Pennucci et al. (2011a) presents Displacement Reduction Factors (DRF) for different hysteresis models and demonstrates the agreement with earlier EVD estimates. Importantly by removing the need for estimating the reduction in spectral displacement due to viscous damping (spectral reduction factor), Pennucci et al. (2011a) demonstrates that conflicting results from Priestley and Grant (2005) and Dwairi et al. (2007) that used different spectral reduction formulations and ground motions, result in indistinguishable DRFs. Pennucci et al. (2011a) concludes that while the EVD is dependent on the damping sensitivity of the ground motions, the DRF is not.

The use of DRFs further alleviates the issue when calibrating EVD expressions, of whether to average the response displacements (Dwairi et al., 2007) of a series of ground motion records or average the EVD values (Priestley and Grant, 2005), which are co-related through a non-linear expression.

Equal energy/equivalent area based viscous damping equations exist for foundation rotation based on experimental data from cyclic loading tests (Paolucci et al., 2009) and from finite element cyclic loading analyses (Adamidis et al., 2013), which provide a useful point of reference to gauge the level of displacement modification from hysteretic behaviour. Both studies also recognised the axial load ratio ($\tilde{N}$), defined as the ratio of the axial load to cause bearing capacity failure divided by the applied axial load, as an important parameter in the variation of energy dissipation. To make a more rational estimate of the displacements of a non-linear system there is a need for DRFs that are calibrated against a series of non-linear time-history results for a given period shift.

6.2 Displacement modification considerations in Direct Displacement-based Design

The individual steps from Paolucci et al. (2013) for a DDBD considering dynamic non-linear soil-foundation-structure interaction are shown in Figure 6.2. The first step is setting the building geometry, then conducting a fixed base analysis to get an estimate of the seismic loads. The foundations are sized to satisfy bearing capacity requirements and settlement under gravity (static) conditions. Using the estimated distributed seismic loads (F_i) the overturning moment can be computed using Equation 6.1. The foundation rotation can be predicted using Equation 6.2 by estimating the elastic rotational stiffness ($K_{f,0}$) from expressions such as those found in Gazetas (1991) and using the computed overturning moment.

$$M_f = \sum_{i=1}^{n} F_i(h_i + h_f) \tag{6.1}$$

$$\theta_f = \frac{M_f}{K_{f,0}} \tag{6.2}$$

The rotational stiffness reduces as rotation increases due to soil yielding and foundation uplift and this is accounted for using stiffness degradation curves, such as those available in Paolucci et al. (2009) or Gazetas et al. (2013). The foundation rotation is recomputed using Equation 6.2 to get a better estimate of the rotation using the degraded rotational stiffness (K_f) instead of the elastic rotational stiffness.

The next step is to estimate the design displaced shape (Δ_i) based on the first mode at the peak design response, which accounts for the displacement contribution from foundation rotation. The displaced shape and an assumed mass distribution (m_i) are used to determine an equivalent SDOF mass (m_e), effective height (H_e) and equivalent displacement (Δ_e) using Equations (6.3 - 6.5).

$$\Delta_d = \frac{\sum_{i=1}^{n} m_i \Delta_i^2}{\sum_{i=1}^{n} (m_i \Delta_i)} \tag{6.3}$$

$$m_e = \frac{\sum_{i=1}^{n} (m_i \Delta_i)}{\Delta_d} \tag{6.4}$$

$$h_e = \frac{\sum_{i=1}^{n} (m_i \Delta_i h_i)}{\sum_{i=1}^{n} (m_i \Delta_i)} \tag{6.5}$$

The displacement contributions from the foundation (Δ_f) and superstructure (Δ_{ss}) are computed at the effective height. The EVD from both the foundation can be computed using equal viscous to hysteretic energy dissipation expressions from Paolucci et al. (2009) and the superstructure EVD can be determined from appropriate expressions in Priestley et al. (2007) depending on the building typology. The system EVD is determined using a simple displacement-weighted expression (Equation 6.6).

$$\xi_{sys} = \frac{(\Delta_s \xi_s + \Delta_f \xi_f)}{\Delta_d} \tag{6.6}$$

$$\tag{6.7}$$

The system EVD is then converted to a displacement reduction factor to reduce the 5% damped design spectrum (Equation 6.8). The effective period is determined based on the interception of the design displacement with the reduced spectral displacement and effective

stiffness is taken as that corresponding to the effective period (Equation 6.9).

$$\eta = \sqrt{\frac{7}{2 + \xi_{sys}}} \tag{6.8}$$

$$K_{eff} = \frac{4\pi^2 m_{eff}}{T_{eff}^2} \tag{6.9}$$

$$\tag{6.10}$$

The base shear is then computed from the effective stiffness and the design displacement (Equation 6.11) and distributed up the structure according to Equation 6.12. The overturning moment is then computed

$$V_{base} = K_{eff}\Delta_d \tag{6.11}$$

$$F_i = \begin{cases} kV_{base}\dfrac{(m_i\Delta_i)}{\sum_{i=1}^{n}(m_i\Delta_i)} & \text{Floors 1 to n-1} \\ (1-k)V_{base} + kV_{base}\dfrac{(m_i\Delta_i)}{\sum_{i=1}^{n}(m_i\Delta_i)} & \text{Roof (Floor n)} \end{cases} \tag{6.12}$$

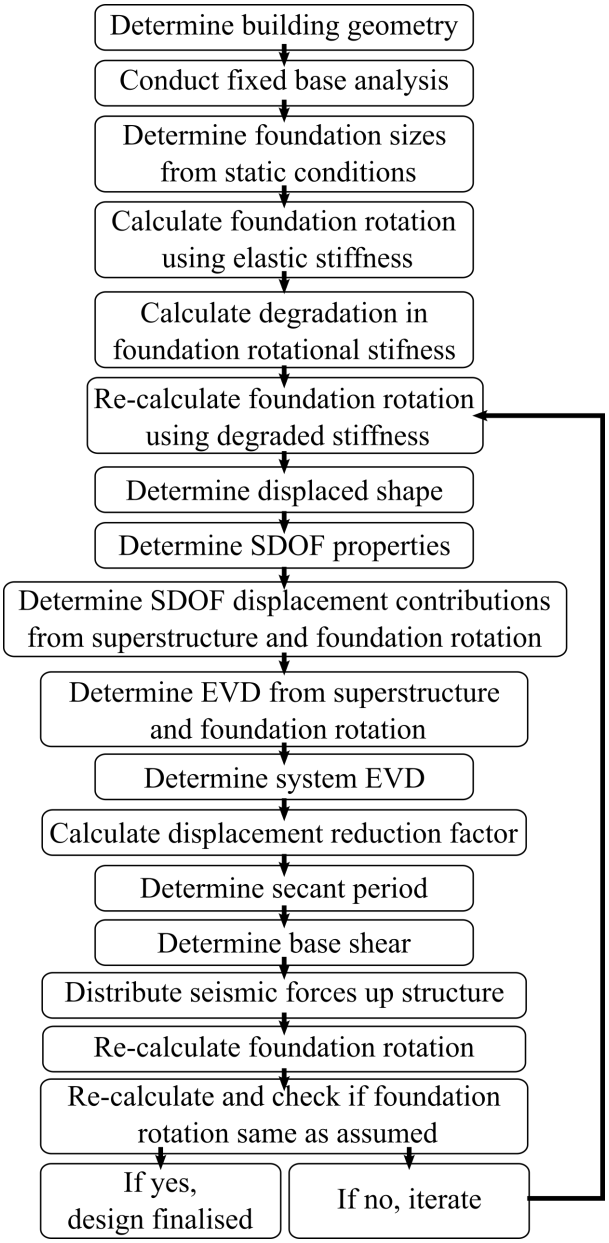

Figure 6.2: Direct displacement based design procedure considering non-linear SFSI *after Paolucci et al. (2013)*

6.3 Foundation displacement mechanisms

Conventional SFSI analysis considers the soil to be deformable and the foundation to be rigid, thus two additional displacement mechanism can be captured, foundation rotation and soil-foundation shearing (Figure 6.3). Additional mechanisms exist when the foundation is deformable, which are addressed later in Chapter 10. The displacements from the two mechanisms considered here can be quantified by determining their stiffnesses and their energy dissipation through respective stiffness degradation factors and DRFs.

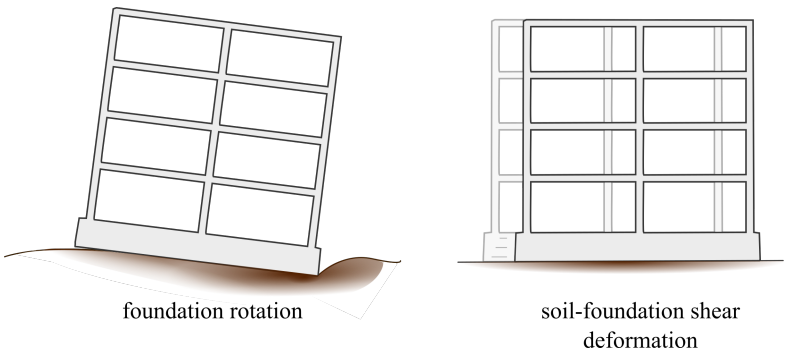

Figure 6.3: Foundation displacement mechanisms

By considering multiple foundation mechanisms, Equation 6.19 must be replaced with Equation 6.13, where the subscripts $_{f,rot.}$ and $_{f,shear}$ correspond to the rotational and shear deformation respectively.

$$\eta_{sys} = \frac{\Delta_{ss}\eta_{ss} + \Delta_{f,rot.}\eta_{f,rot.} + \Delta_{f,shear}\eta_{f,shear}}{\Delta_{sys}} \tag{6.13}$$

Although this increases the design complexity, if the designer can demonstrate that the shear deformation is negligible, then $\Delta_f = \Delta_{f,rot.}$ and Equation 6.19 is returned. Figure 6.4 demonstrates the disaggregation of the displacement into the three mechanisms for a set of 20 soil-foundation-structure systems during push-over simulations, where SFSI deformations were significant (see Table 6.3 in Section 6.5.3 for a summary of the inputs of models used in these analyses). The buildings were extreme cases where foundation deformations were large and the results show that the soil-foundation shear mechanism only contributes at most 30% at very large displacements.

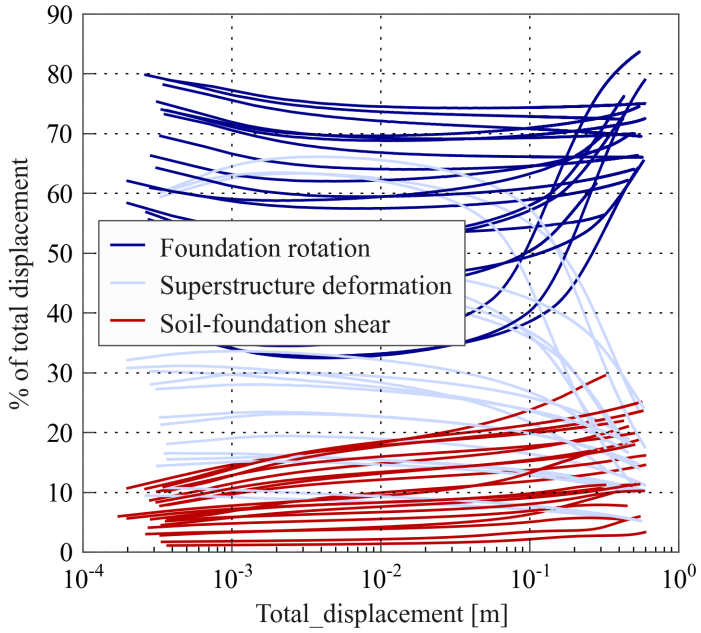

Figure 6.4: Disaggregation of displacements for systems on soft soil with linear superstructures

It is difficult to isolate each mechanism to quantify its displacement reduction effect, especially since they are interdependent to some extent. Not only does the shear deformation behave in a non-linear manner with reduced stiffness and dissipation of energy, but increased shear force results in a more plastic moment-rotation response.

To estimate the approximate contributions from each mechanism the ratio of foundation length to building effective height can be used as a proxy to estimate the ratio of foundation rotation to soil-foundation shear deformation. The contribution from each mechanism is highly dependent on the ratio of foundation length to effective height, where a small ratio leads to a high ratio of moment to shear applied to the foundation and thus a foundation rotation dominant behaviour.

While buildings exist with large foundation length to height ratios, the shear mechanism is often very stiff and therefore the contribution to displacement is quite small, thus, the foundation rotation mechanism is the main focus of this chapter. Since the rotation mechanism was the main focus, all the analyses were constrained to buildings where the ratio of foundation length to building effective height is equal to or less than one.

To account for the soil-foundation shear deformation the shear stiffness can be assumed as being half of the elastic shear stiffness and the DRF can be determined by assuming the radiation damping dominates the energy dissipation in this mode. In this study the soil-foundation shear deformation was taken as 0.76 based on assuming an average radiation damping value of 10% and using Equation 6.14 Priestley et al. (2007) identical to Equation 6.8.

$$\eta_{f,shear} = \sqrt{\frac{7}{2+\xi_{f,shear}}} = \sqrt{\frac{7}{2+10}} = 0.76 \tag{6.14}$$

(6.15)

These are broad assumptions but given that the shear deformation tends to contribute very little to the overall displacement, any error in the stiffness and DRF make little difference to the expected system behaviour.

The effect of the shear load on the rotational stiffness can be accounted for as described in the next section.

6.4 Foundation rotational stiffness degradation factor

The estimate of the effective stiffness is often made based on the back-bone hysteretic behaviour, such as DDBD using the secant-to-peak stiffness from the assumed back-bone non-linear behaviour. The back-bone curve for foundation moment-rotation behaviour is complex due to the multiple mechanisms that contribute to the non-linear rotational behaviour. To quantify the backbone curve as a simple expression given as a stiffness reduction curve, the mechanisms must be accounted for. Figure 6.5 shows the footing rotational secant stiffness versus rotation for 65 SDOF structures randomly selected from the database in Table 6.1 during pushover analyses, where the soil-foundation interface was modelled using a macro-element in Ruaumoko3D (Carr, 2015). Although the behaviour looks similar, there is considerably variation in the stiffness-rotation relationships.

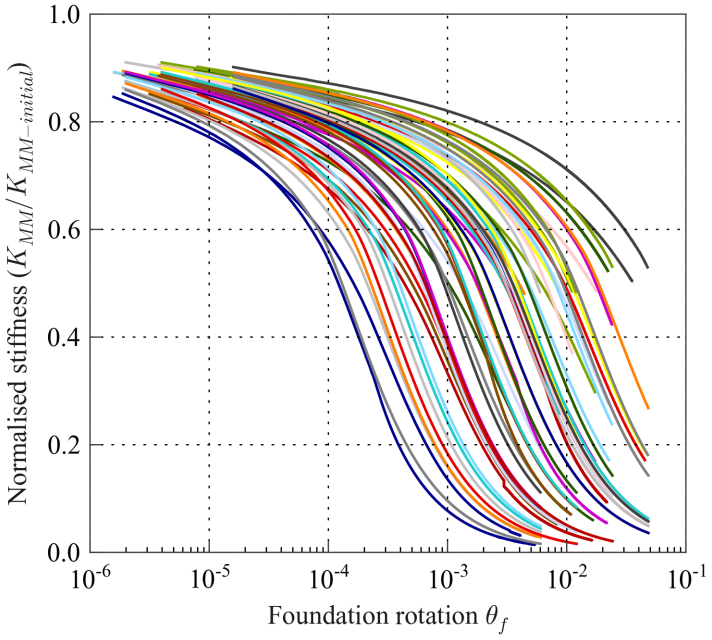

Figure 6.5: Push-over rotational behaviour of foundations

Previous researchers have attempted to compute foundation rotational stiffness reduction curves before. Paolucci et al. (2009) used results from large-scale experimental cyclic loading tests on dense and medium-dense sands, carried out at the Joint Research Center in Ispra, Italy (TRISEE Project (Faccioli et al., 1998; Negro et al., 1999)) and at the Public Works Research Institute (PWRI) in Tsukuba, Japan (PWRI, 2005), supplemented with numerical results using the macro-element model from di Prisco et al. (2003). In their research, the axial load ratio was recognised as an important parameter as well as the soil relative density; unfortunately, due to the limited number of results, other influential parameters were not identified.

Algie (2011) computed stiffness reduction curves from large-scale snap-back tests of walls on clay soil. The axial load was identified as a key parameter.

Gazetas et al. (2013) used finite-element results from pseudo-static push over analyses on clay applying only moment loading to the foundation. Their research identified the axial load ratio as an important parameter and the foundation shape; however, through normalisation of the foundation rotation by a characteristic angle parameter and normalising the stiffness by the initial stiffness, the curves were modelled by a single expression.

6.4.1 Calibration of stiffness reduction curve

The rotational stiffness degradation curves presented here are specifically for foundations on sand and were determined based on results from push over analyses using the macro-element model in Ruaumoko3D, which was calibrated against two sets of experimental shake table tests under centrifugal conditions on Nevada Sand. Details of the macro-element model are

provided in Chapter 4 and the experimental validation results can be found in Chapter 5. The curves are limited by the ability of the macro-element to simulate the actual behaviour of the foundation and therefore do not encompass the same levels of rotation under such large axial loads as previous studies, but represent levels commonly seen in design.

The curves were developed from simple push-over analyses, where a load was applied to a rigid element at a height (H) above the foundation macro-element. Table 6.1 shows the parameters that were varied to produce the 256 push over curves. The range on each parameter does not attempt to capture theoretical asymptotes, where values would be unrealistic and the macro-element may not capture the behaviour, instead the limits were set to give a realistic range where SFSI would be considered in design.

Table 6.1: Input parameters to determine stiffness reduction curves

Parameter	Values
Axial load ratio	2, 3, 5, 10
Foundation length (m)	4, 8
Height to foundation length	1, 2, 5, 10
Foundation width to length	0.5, 2
Soil friction angle	30, 40
Soil shear modulus (MPa)	40, 120

The foundation static bearing capacity was determined using equations from Salgado (2008), where the foundation was considered to have no embedment. The foundation stiffness terms were determined from expressions in Gazetas (1991), where the soil Poisson's ratio was taken as 0.3.

Since the macro-element uses a vertical mapping rule, the initial rotational stiffness was independent of the axial load ratio and therefore the stiffness could simply be normalised by the elastic rotational stiffness. The rotation was normalised by the pseudo uplift angle (θ_{uplift}) (Equation 6.16) which is defined as the moment required for uplift from Cremer et al. (2001, 2002), divided by the elastic rotational stiffness ($K_{MM,elastic}$). The pseudo uplift angle provides a convenient expression accounting for the elastic stiffness, the foundation axial capacity (N_{cap}) and the applied axial load (N). The $\alpha = 4$ parameter accounts for the stress distribution at the point of uplift for elastic soil and the $\zeta = 1.5$ parameter provides a correction to the uplift moment for inelastic soil behaviour.

$$\theta_{uplift} = \frac{N \times L}{\alpha K_{MM,elastic}} e^{-\zeta N / N_{cap}} \tag{6.16}$$

Figure 6.6 shows the normalisation of the curves using the pseudo uplift angle, where the curves fall in a narrow band with a distinct variation due to the foundation length to structure

height ratio (L/H). The variation is most noticeable for high ratios of L/H, while at L/H equal to 0.2 or less, there is no noticeable change in behaviour. The variation due to L/H is due to a proportional increase in the shear load applied to the soil-foundation interface which in turn increases the overall plastic behaviour. This means that the foundation has rotated further before uplift, and consequently has a lower effective rotational stiffness.

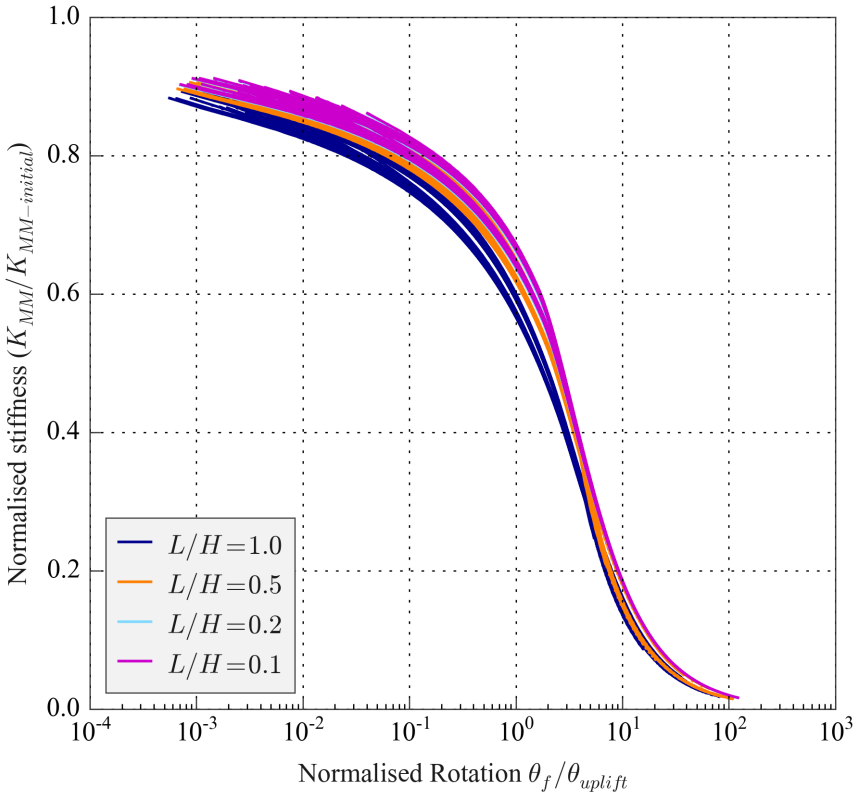

Figure 6.6: Stiffness reduction curves using normalised rotation

The foundation length to height aspect ratio provides a proxy for the shear to moment ratio. For high values of L/H the effect can be corrected using the corrected normalised rotation (Φ), which can be obtained through Equation 6.17. At low levels of L/H the correction can be ignored and at $L/H = 0$ the corrected normalised rotation is equal to the normalised rotation.

$$\Phi = \left(\frac{\theta_f}{\theta_{uplift}}\right)^{1-0.2(L/H)} 10^{0.25(L/H)} \tag{6.17}$$

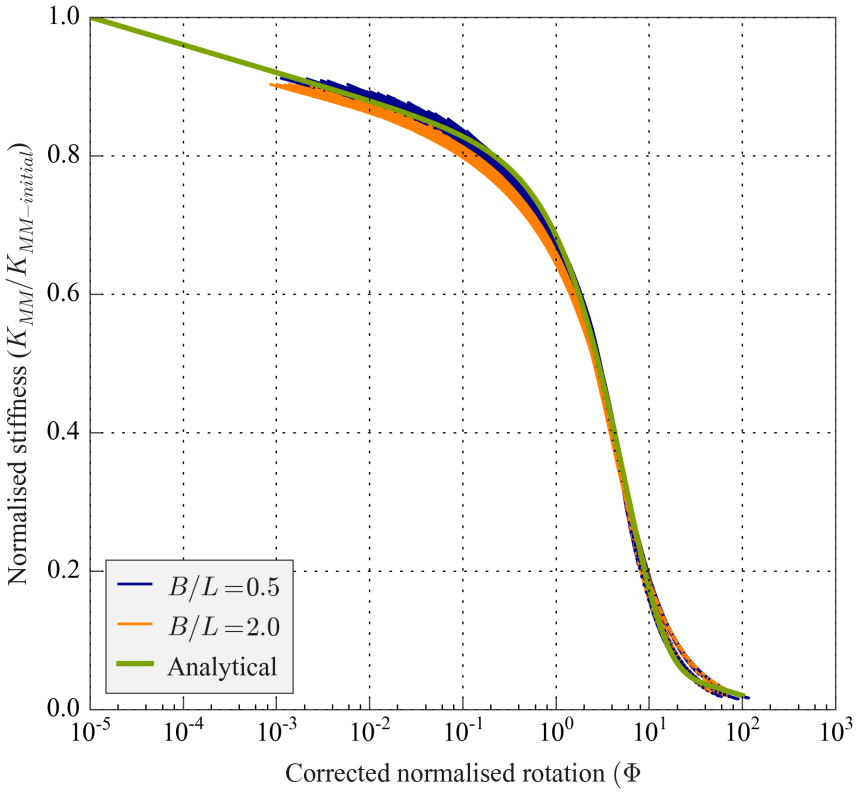

Figure 6.7: Stiffness reduction curves using corrected normalised rotation

The corrected normalised curves in Figure 6.7 fall into a very narrow band, where the only distinguishable difference is due to the foundation width to length. This variation is due to the way the plastic stiffness modulus is defined in the macro-element model and although the behaviour may be represented accurately, the difference is not worth the added complexity. The design equation (Figure 6.7 - green) for the back-bone curve can be determined using Equation 6.18, where the design curve was extrapolated to small rotations to give full elastic stiffness at $\Phi = 1e^{-5}$.

$$\frac{K_f}{K_{f,0}} = 0.8 - 0.04\log(\Phi) - 0.7(1 - \exp^{-0.18\Phi}) \tag{6.18}$$

6.5 Foundation displacement reduction factor

As an alternative to using EVD to compute the DRF, the above procedure from Paolucci et al. (2013) can be modified to directly use DRFs as suggested Pennucci et al. (2011a) and the DRF from the structure (η_{ss}) and the foundation (η_f) could be combined using a simple displacement-weighted expression such as Equation 6.19.

$$\eta_{sys} = \frac{\Delta_{ss}\eta_{ss} + \Delta_f \eta_f}{\Delta_{sys}} \tag{6.19}$$

In this section, simple expressions are developed for foundation DRFs for use in the modified design procedure.

6.5.1 Calibration procedure

The majority of EVD and DRF equations proposed for use in the DDBD procedure have been calibrated against time history analysis results. To maintain consistency with other works, a similar calibration process to that used by Pennucci et al. (2011a) was adopted in this study.

The DRF factor was related to the corrected normalised foundation rotation (Equation 6.17), which can be considered as a proxy for ductility in the foundation. The DRF relationship was empirically derived based on parametric numerical analysis results using an experimentally validated modeling technique (see Chapter 4) to mimic 280 different structure-foundation-soil systems. Each system was subject to 40 ground motions scaled to four different levels, thus providing a considerable range of input parameters and extent of foundation deformation.

The system non-linear DRF (η_{sys}) for each building was determined by the ratio of the average non-linear displacement of the 40 records and the average of the 5% damped spectral displacement at the secant-to-peak period ($\overline{Sd_{\xi=5\%,T_{secant}}}$) (Equation 6.20).

$$\eta_{sys} = \frac{\overline{\Delta_{NL}}}{\overline{Sd_{\xi=5\%,T_{secant}}}} \tag{6.20}$$

It was essential to model the superstructure as a flexible linear elastic system, since the flexibility of the superstructure contributes significantly to the dynamic response of the system and would therefore apply more realistic loading to the foundation. Having both a superstructure displacement component and a foundation displacement component creates a further complication to determining EVD or DRF expressions for DDBD, compared to previous studies. While the total displacement of the system should match the equivalent linear SDOF, only the displacements from the foundation experience the hysteretic behaviour. To simplify the back calculation of the foundation DRF (η_f) from Equation 6.13 the superstructure was modeled as a linear beam element. The superstructure damping was modeled with a dashpot set at 5% damping so that the superstructure displacement factor (η_{ss}) could be taken as 1.0. While $\eta_{ss} = 1.0$ is not strictly correct, as the dashpot element contributes less as the system vibration period increases due to foundation deformation, the error is small and the assumption is convenient for design (see Chapter 4 for further details on this aspect). Given that the error

exists in both the back-calculation and the design, the DRF relationship developed here is consistent with the accuracy of the design procedure.

Another mechanism that contributes to the displacement is the foundation shear. Foundation shear deformation tends to be quite small and therefore makes very little difference to the system DRF. Thus, to simplify the expression for use in design the shear stiffness can be taken as half of the elastic stiffness and a DRF of 0.76 corresponding to an EVD value of 10% according to Equation 6.8. The foundation rotation DRF then absorbs the errors from the simplifying assumption of the superstructure DRF equal to one and the simplification of the foundation shear DRF equal to 0.76 and effective foundation shear stiffness equal to half of the elastic value. The back-calculation of $\eta_{f,rot.}$ is given in Equation 6.21 whereas Figure 6.8 summarises the calibration process.

$$\eta_{f,rot.} = \frac{\Delta_{sys}\eta_{sys} - \Delta_{ss}\eta_{ss} - \Delta_{f,shear}\eta_{f,shear}}{\Delta_{f,rot.}} \tag{6.21}$$

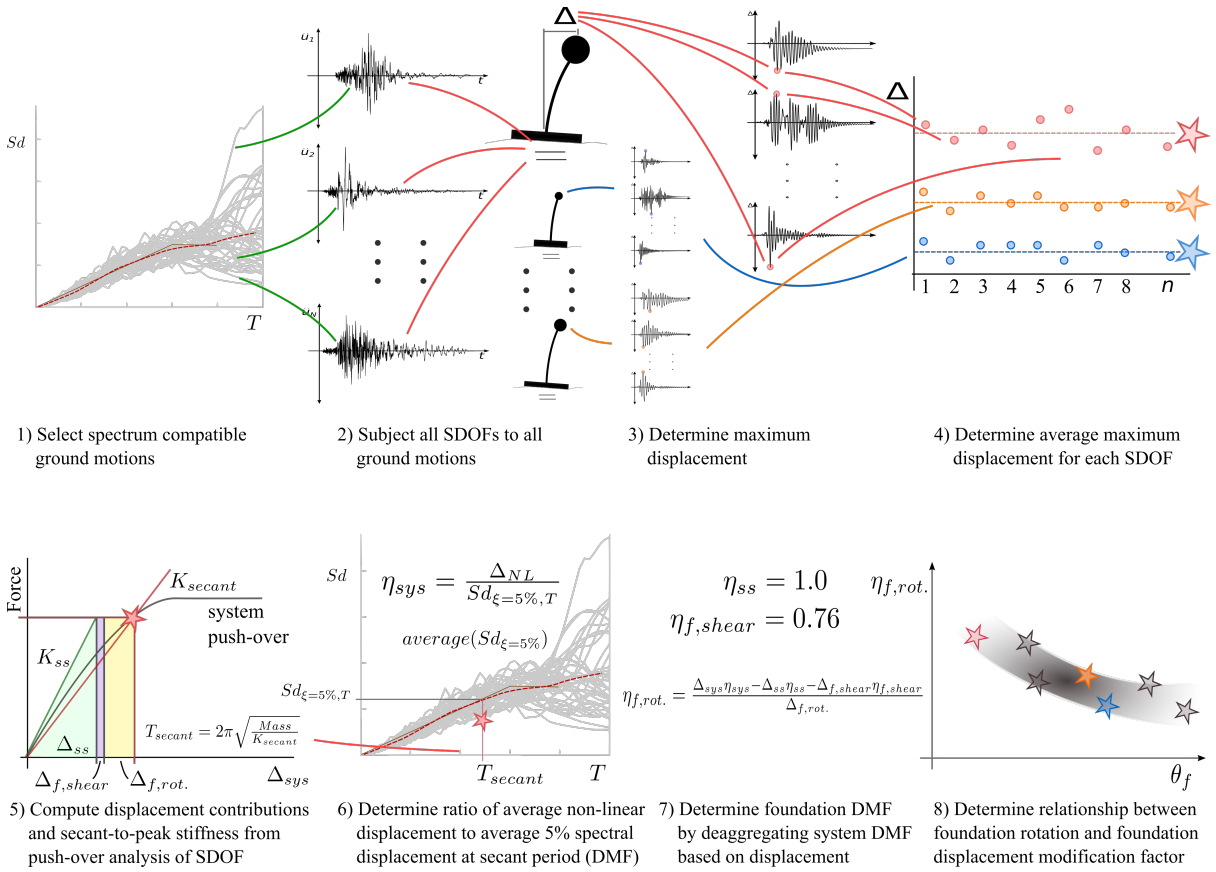

Figure 6.8: Procedure to calibrate foundation rotation displacement reduction factor

6.5.2 Numerical model

The numerical model used in this study consisted of a lumped mass superstructure (M_{SS}) attached to a macro soil-foundation interface element (Figure 6.9). The superstructure was modelled as a linear elastic member with a linear rotational dashpot (C_{SS}) set at 5% of critical damping between the foundation and the superstructure. A rotational dashpot was used as opposed to a translational dashpot, as it isolated the velocity to only that from the superstructure deformation. The other advantage of a rotational dashpot is that it reduces its effect as the structure behaves non-linearly, due to the change in the relationship between displacement and rotation of a cantilever. The decrease in the effective damping coefficient is similar to the decrease in tangent stiffness proportional damping, but not to the same extent.

The vertical displacement from the superstructure was slaved to the foundation node providing a perfectly rigid superstructure axial stiffness. The foundation mass was not modelled since the displacement was based on the **single** degree-of-freedom response spectra. The foundation radiation damping was modelled with horizontal (C_{VV}), vertical (C_{NN}) and rotational (C_{MM}), linear dashpots connected in parallel to the macro-element, based on the radiation damping equations from Gazetas (1991). The vertical dashpot was limited to a maximum force equal to 20% of the applied vertical load on the foundation. The initial stiffnesses (K_{NN}, K_{VV}, K_{MM}) for the soil-foundation macro-element were based on the stiffnesses suggested in Gazetas (1991), where for embedded foundations the contact area of the sidewalls was assumed to be zero as the numerical model was developed for shallow foundations on the surface.

The modification to the stiffnesses due to uplift was captured using the uplift formulation from Chatzigogos et al. (2011). The uplift model has the advantage of capturing the vertical displacement of the centre of the footing, allowing for the vertical inertia and damping to contribute to the behaviour. The soil yielding was modelled using the plasticity model and model parameters from Figini et al. (2012). The plasticity model uses a bounding surface and vertical mapping rule and it has been experimentally validated to reasonably accurately capture the rotational and settlement behaviour (Figini et al., 2012; Millen et al., 2015). The foundation capacity (N_{cap}) was determined based on the shallow foundation bearing capacity equations from Salgado (2008). The input parameters for the uplift and plasticity models and other inputs are summarised in Table 6.3.

P-delta effects were not considered in the analyses, since P-delta effects are considered separately in design and the influence of P-delta forces depends on structural geometry which can not be captured in the simple displacement reduction factors suggested here. All analyses were carried out using the non-linear time history analysis software Ruaumoko3D (Carr, 2015).

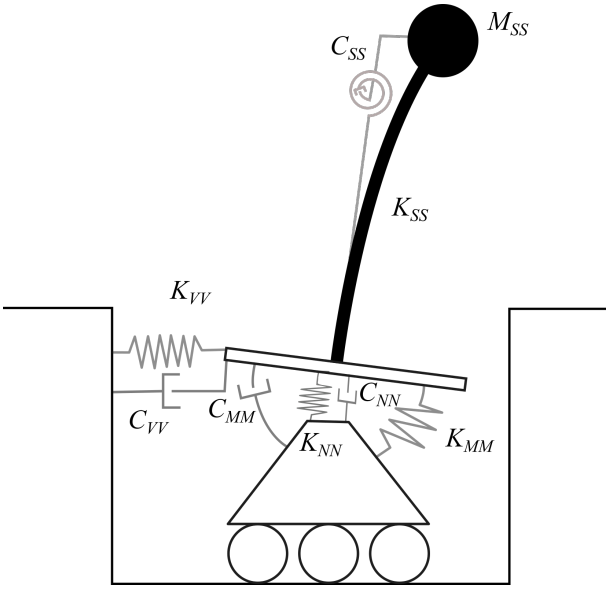

Figure 6.9: Numerical model setup

Table 6.2: Plasticity model and uplift model parameter values

Parameter	Value
Uplift limit factor (α)	4
Uplift stiffness factor (ϵ)	0.5
Uplift stiffness factor (δ)	1.0
Uplift stiffness factor (γ)	1.0
Uplift stiffness factor (ζ)	1.5
Bounding surface shear factor (μ_{BS})	$\tan(\phi)$
Bounding surface moment factor (ψ_{BS})	0.48
Bounding surface shape factor (ξ_{BS})	0.95
Plasticity modulus factor (p_1)	0.2
Reload stiffness factor (p_2)	1.0
Plastic potential shear factor (λ_{BS})	2.5
Plastic potential moment factor (χ_{BS})	3.0
Foundation stiffness terms (K)	Gazetas (1991)
Foundation damping terms (C)	Gazetas (1991)
Foundation axial capacity (N_{cap})	Salgado (2008)

6.5.3 Inputs for parametric study

The parametric study used input parameters for the SDOF system that reflected the range of realistic building/soil types where SFSI may be of interest. Table 6.3 summarises the range and limitations on the parameters. A limit was imposed on the length of foundation perpendicular to the axis of foundation rotation (L) using Equation 6.22 based on the expected over-turning moment, foundation shear and the foundation capacity from work by Nova and Montrasio (1991). The foundations were sized so that the expected moment demand would be slightly less than the moment capacity, while the ($\pm$0.4) term provides a random variation

to the foundation length in an attempt to remove any bias on the results from the imposed limitation.

$$L = \frac{2S_a(T)H_{eff}}{\sqrt{1-(1/\tilde{N})^2-\left(\frac{3S_a(T)}{8\tan\phi}\right)^2}} \times (1 \pm 0.4) \tag{6.22}$$

Table 6.3: Plasticity model and uplift model parameter values

Parameter	Range
Soil shear wave velocity (V_s)	$100 \leq V_s \leq 360$ m/s
Soil mass density (ρ_s)	$1.6 \leq \rho_s \leq 1.9$ t/m^3
Poisson's ratio (v)	$[0.2, 0.3]$
Soil internal friction angle (ϕ)	$30 \leq \phi \leq 40$
Structural period (T_{SS})	$0.6 \leq T_{SS} \leq 1.8$
Effective height (H)	$\max(2, 9.1T_{SS}^{1.33}) \leq H \leq \min(20, 26.8T_{SS}^{1.33})$ m
Design hazard factor (Z)	$Z = 0.3$ for use in NZS 1170.5:2004
Spectral acceleration (S_a)	$S_a = f(T_{SS}, Z, N = 1, R = 1)$ from NZS 1170.5:2004
Axial load ratio ($\tilde{N}$)	$\tilde{N} = [2, 3, 5, 10]$
Length of foundation perpendicular to the axis of rotation (L)	$\max(3, H/3) \leq L = Eq.1 \leq H$ m
Length of foundation parallel to the axis of rotation (W)	$L/2 \leq W \leq 2L$
Embedment of foundation (D)	$D = [0, 0.2L]$
Axial load capacity (N_{max})	$N_{max} = f(\phi, L, W, D)$ Salgado (2008)
Vertical weight (N)	$N = N_{max}/\tilde{N}$
Seismic mass (M_{SS})	$M_{SS} = N/g$
Structural stiffness (K_{SS})	$K_{SS} = 4\pi^2 M_{SS}/T_{SS}^2$

Figure 6.10 shows the distribution of the structure-foundation-soil systems used in the analysis in terms of three important parameters, the height to foundation length aspect ratio ($\frac{H}{L}$), the structural stiffness to soil stiffness ($\frac{\omega_{ss}h}{V_s}$) and the initial period of the structure ($T_{initial}$).

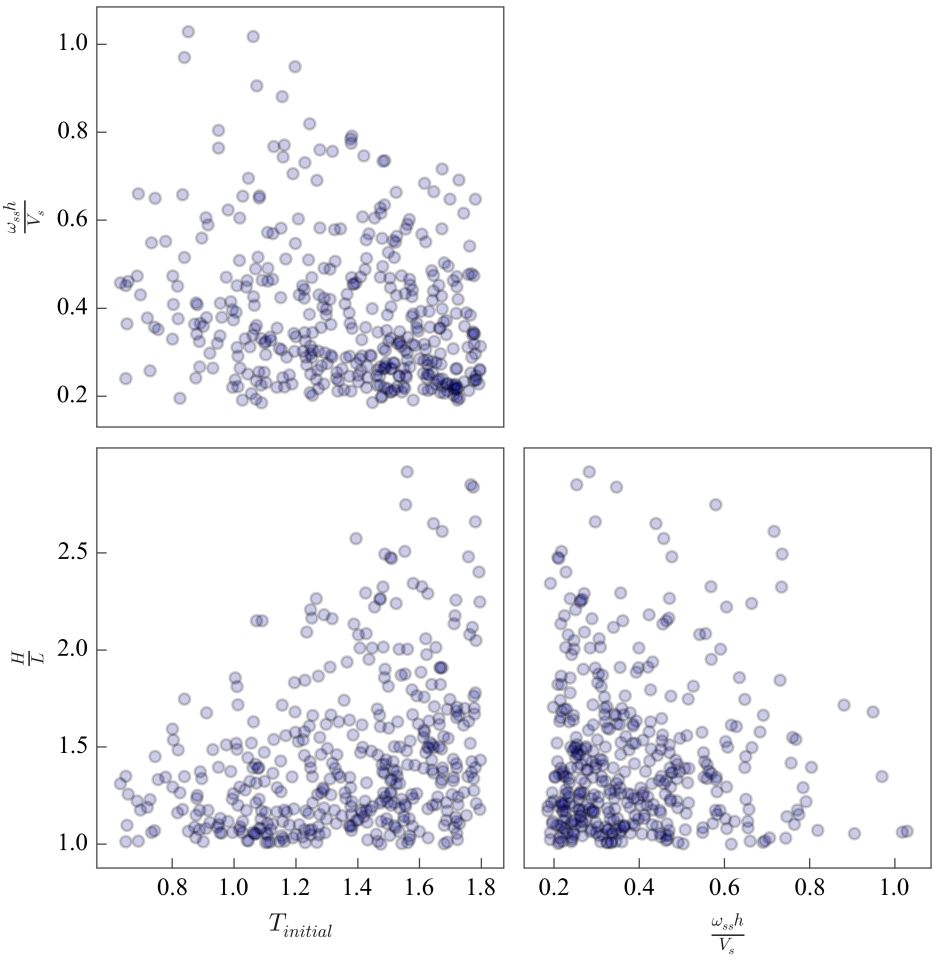

Figure 6.10: Distribution of input parameters

6.5.4 Ground motion selection

The presented procedure used 40 carefully selected earthquake records from the NGA-West ground motion database (Chiou et al., 2008); all ground motions were recorded on deposits with Vs30 values of 100 - 360 m/s and at least 20 km from the epicentre. The records were scaled and selected to give the smallest normalised least squared variation from the design spectrum between periods of 0.4 s and 4.0 s for the NZS 1170.5:2004 (2004) site class C. The normalisation of variation between the ground motion spectra and the design spectrum meant that at large design values the match in absolute values was not very good, but this meant that the relative variation was consistent weighted along the spectrum. The motions were initially scaled to match the spectra for a Z factor of 0.3, noted as 100% of the design level. The ground motions were also scaled to 50%, 30% and 10%, to provide a range of foundation rotation values without having to redesign the building or select new ground motions.

Table 6.4 summarises the selected ground motions and Figure 6.11 displays the acceleration and displacement response spectra.

Table 6.4: Input ground motions

ID	Record	E. dist [km]	Mw	Scale	Vs30 [m/s]	Arias I [m/s]	PGA [g]	Earthquake	Year	Station
1	NGA0176_1	36.0	6.53	2.56	250	0.26	0.12	Imperial Valley-06	1979	El Centro Array #13
2	NGA0985_1	28.2	6.69	1.76	297	0.67	0.24	Northridge-01	1994	LA - Baldwin Hills
3	NGA0457_1	38.2	6.19	2.72	350	0.34	0.19	Morgan Hill	1984	Gilroy Array #3
4	NGA3276_1	69.5	6.3	1.9	212	0.32	0.15	Chi-Chi, Taiwan-06	1999	CHY037
5	NGA0161_2	43.2	6.53	1.46	209	0.44	0.22	Imperial Valley-06	1979	Brawley Airport
6	NGA0183_1	28.1	6.53	0.74	206	1.59	0.60	Imperial Valley-06	1979	El Centro Array #8
7	NGA0175_1	32.0	6.53	1.76	197	0.38	0.14	Imperial Valley-06	1979	El Centro Array #12
8	NGA3266_1	61.5	6.3	2.86	226	0.11	0.12	Chi-Chi, Taiwan-06	1999	CHY026
9	NGA0174_1	29.4	6.53	0.92	196	1.95	0.36	Imperial Valley-06	1979	El Centro Array #11
10	NGA0180_1	27.8	6.53	0.7	206	1.65	0.52	Imperial Valley-06	1979	El Centro Array #5
11	NGA0175_2	32.0	6.53	2.12	197	0.33	0.12	Imperial Valley-06	1979	El Centro Array #12
12	NGA1484_1	78.4	7.62	1.14	273	1.14	0.25	Chi-Chi, Taiwan	1999	TCU042
13	NGA0172_1	35.2	6.53	2.68	237	0.27	0.14	Imperial Valley-06	1979	El Centro Array #1
14	NGA0172_2	35.2	6.53	3.8	237	0.21	0.13	Imperial Valley-06	1979	El Centro Array #1
15	NGA1495_1	35.9	7.62	0.94	273	1.70	0.24	Chi-Chi, Taiwan	1999	TCU055
16	NGA0178_1	28.7	6.53	0.84	163	1.13	0.27	Imperial Valley-06	1979	El Centro Array #3
17	NGA0186_1	68.9	6.53	3.34	208	0.18	0.11	Imperial Valley-06	1979	Niland Fire Station
18	NGA1153_1	171.4	7.51	3.68	275	0.10	0.10	Kocaeli, Turkey	1999	Botas
19	NGA1000_1	31.7	6.69	2.72	270	0.19	0.10	Northridge-01	1994	LA - Pico & Sentous
20	NGA0176_2	36.0	6.53	2.92	250	0.26	0.14	Imperial Valley-06	1979	El Centro Array #13
21	NGA3275_1	61.5	6.3	2.2	233	0.28	0.14	Chi-Chi, Taiwan-06	1999	CHY036
22	NGA0767_2	31.4	6.93	0.84	350	1.35	0.37	Loma Prieta	1989	Gilroy Array #3
23	NGA1762_2	48.0	7.13	1.58	271	0.68	0.15	Hector Mine	1999	Amboy
24	NGA1236_1	68.8	7.62	1.72	273	0.70	0.14	Chi-Chi, Taiwan	1999	CHY088
25	NGA0882_1	32.3	7.28	2.32	345	0.64	0.14	Landers	1992	North Palm Springs
26	NGA0970_1	50.8	6.69	2.5	309	0.23	0.12	Northridge-01	1994	El Monte, Fv. Av
27	NGA3275_2	61.5	6.3	1.32	233	0.51	0.20	Chi-Chi, Taiwan-06	1999	CHY036
28	NGA2715_1	39.9	6.2	2.48	273	0.24	0.14	Chi-Chi, Taiwan-04	1999	CHY047
29	NGA0832_2	75.2	7.28	1.56	271	0.75	0.15	Landers	1992	Amboy
30	NGA1636_2	84.0	7.37	2.36	275	0.42	0.13	Manjil, Iran	1990	Qazvin
31	NGA0726_1	26.5	6.54	3.4	191	0.18	0.12	Superstition Hills2	1987	SSWR
32	NGA0836_1	123.9	7.28	3.58	271	0.24	0.11	Landers	1992	Baker Fire Station
33	NGA0138_1	74.7	7.35	2.56	339	0.28	0.11	Tabas, Iran	1978	Boshrooyeh
34	NGA1481_2	73.1	7.62	1.32	273	1.03	0.17	Chi-Chi, Taiwan	1999	TCU038
35	NGA2694_2	50.4	6.2	2.64	229	0.15	0.10	Chi-Chi, Taiwan-04	1999	CHY015
36	NGA0169_2	33.7	6.53	0.88	275	3.28	0.35	Imperial Valley-06	1979	Delta
37	NGA0719_1	29.9	6.54	3.26	209	0.22	0.16	Superstition Hills2	1987	Brawley Airport
38	NGA1491_1	38.5	7.62	1.12	273	1.24	0.19	Chi-Chi, Taiwan	1999	TCU051
39	NGA1528_2	45.1	7.62	1.04	273	0.99	0.25	Chi-Chi, Taiwan	1999	TCU101
40	NGA0187_2	48.6	6.53	2.34	349	0.22	0.20	Imperial Valley-06	1979	Parachute Test Site

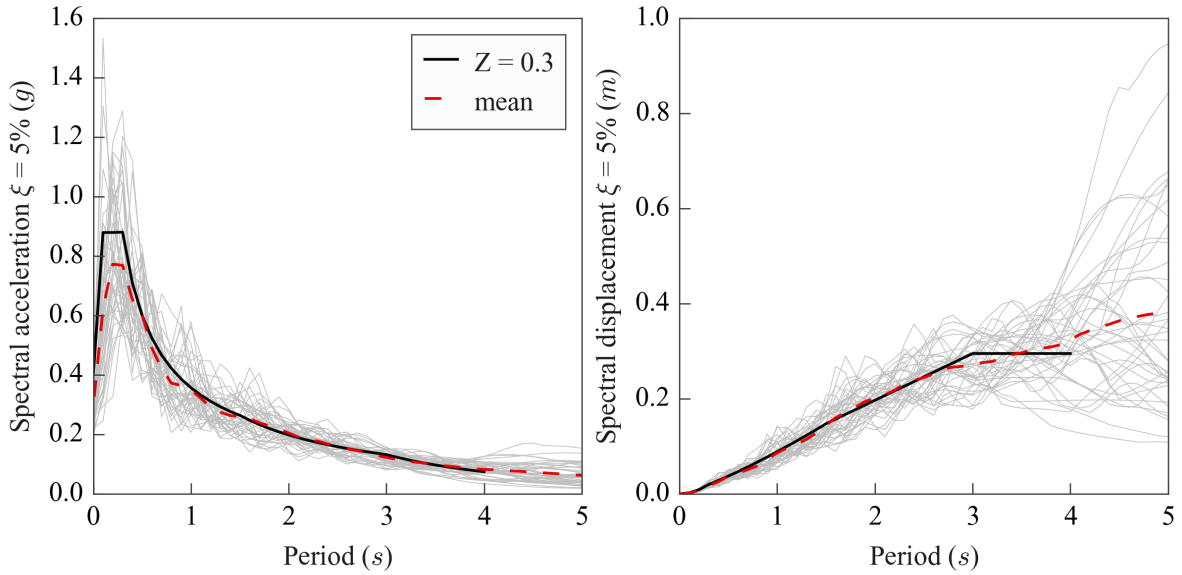

Figure 6.11: Ground motion response spectra

6.5.5 Design curves

The back-calculated DRF values are shown in Figure 6.12 as a function of the corrected normalised foundation rotation over a range of approximately $\Phi = 0.001 - 20$. The DRF for foundation rotation showed no major trend with axial load ratio, when plotted against the corrected normalised foundation rotation. This is consistent with work by Adamidis et al. (2013), where a single expression captured the EVD for different axial load ratios when the results were normalised by the characteristic angle. This suggests that the period shift and post-yield stiffness are the most important parameters in the prediction of displacements, of which both are carefully accounted for using the corrected normalised rotation.

A design DRF expression was fitted to the data for each level of axial load. Two constraints were applied to the curve fitting, the first being that at very low levels of Φ, the DRF was set to 1.0, while it could be expected that the DRF goes slightly above 1.0, given that purely elastic rotational behaviour has radiation damping values of about 2 - 4%. This simple constraint is of little importance for most structures as at these small levels of rotation the foundation energy dissipation makes very little difference to the system response. The second constraint was set at very large levels of rotation where the DRF tended towards 0.41, corresponding to an EVD value of 40%, similar to the limit imposed by Paolucci et al. (2009) for dense sand of 37%. The final constraint was that only displacements where the foundation deformation contributed 50% or greater to the overall response were used, as this reduced the sensitivity of the extracted foundation rotation DRF factor when the rotation was very small. The fitted expressions for all four axial load ratios resulted in nearly identical expressions and therefore the design expression was fitted over all of the data, resulting in Equation 6.23.

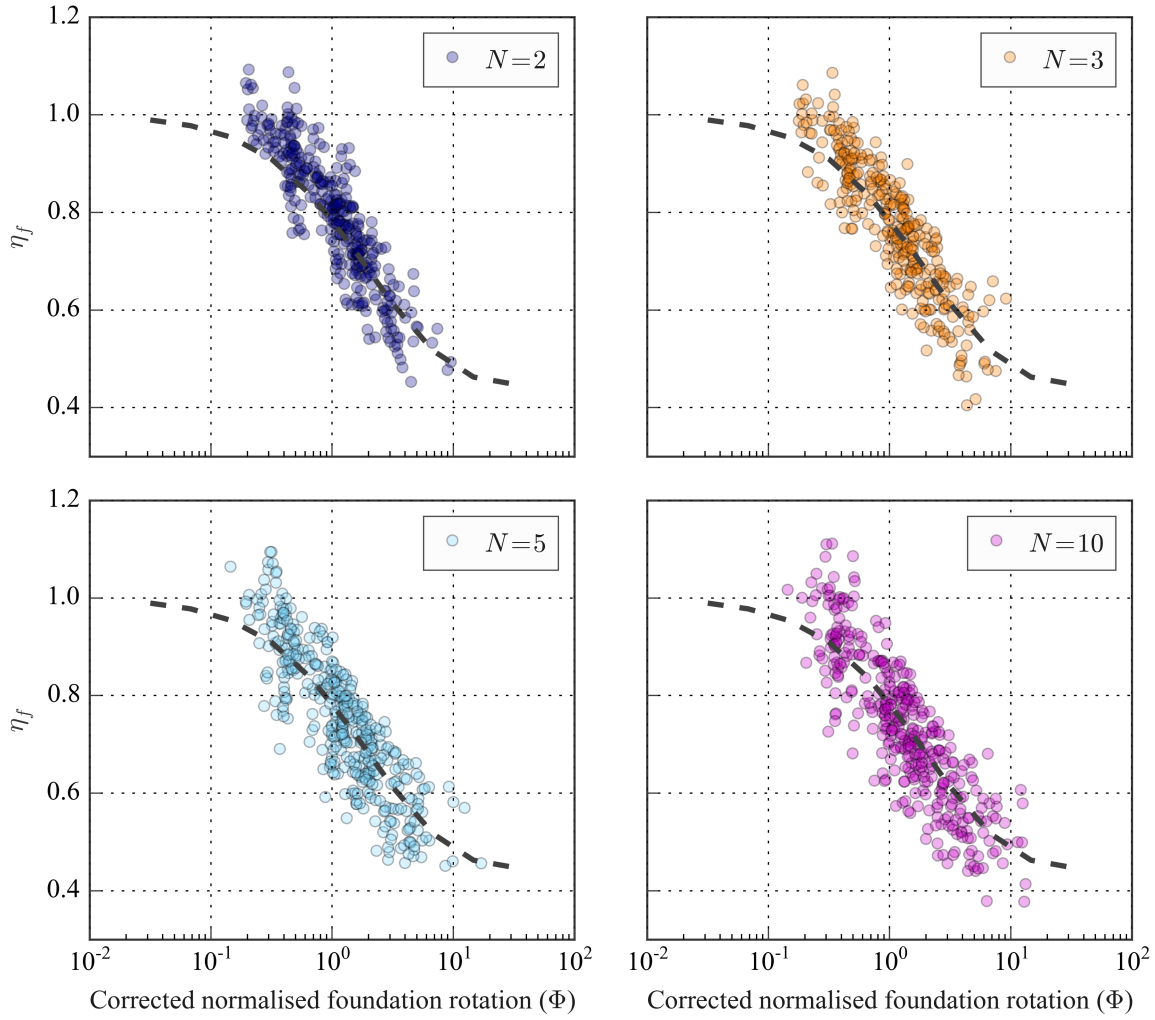

Figure 6.12: Results

$$\eta_{f,rot.} = \sqrt{\frac{1.0}{1.0 + 5.0(1 - e^{-0.15\Phi})}} \tag{6.23}$$

The simple expression makes it easy for use in design; however, the distribution of the DRF should be investigated in terms of other potentially influential parameters. Figure 6.13 shows the DRF error (DRF calculated from analysis - DRF from design) for each analysis along with the mean error and standard deviation. For most parameters there was no bias and the error showed homoscedasticity (an even variation of the error). There was a small bias for the corrected normalised rotation (Φ) as the expression used to fit the data was forced to tend to 1.0 as Φ approached zero (Figure 6.13 a). The DRF error exhibited a bias for initial period (b), with an over-estimate of displacement for short period systems (This sort of behaviour was also noticed by Dwairi et al. (2007) for period independent expressions of EVD for superstructures) and there was an under-estimate of displacements at periods around 3.5s

and greater. This behaviour was also noted by Pennucci et al. (2011a) when the average of the ground motion spectra has a distinct corner period, as was the case in this parametric study. The bias on the initial period was also seen in the period of the superstructure (Figure 6.13 d), which is closely related to the initial period. Another small bias was seen with the foundation length to structure height ratio (L/H) (Figure 6.13 g), where at small values of L/H the displacements were slightly under predicted, which may be due to the simple expression used to account for the shear stiffness and shear DMF. The only other significant bias was seen in Figure 6.13 (k) for the soil friction angle (ϕ), where the DRF was conservative for low values of ϕ and goes above 1.0 for at values greater than 35.

While there are some clear but small trends seen in the distribution of the residuals, these trends were not accounted for in the final expression as the input parameters for the analyses came from a structured sampling process. The structure in the sampling process may have introduced these trends rather than some physical phenomenon.

Most interesting is the lack of a trend for the foundation length multiplier (*L multiplier*), suggesting that the change in demand to capacity ratio on the foundation was correctly accounted for in the expression. The variation in the error does increase with increased hazard demand, as expected as there would be more non-linear behaviour, but there was no strong trend to suggest that a scaling of the demand would influence the expression.

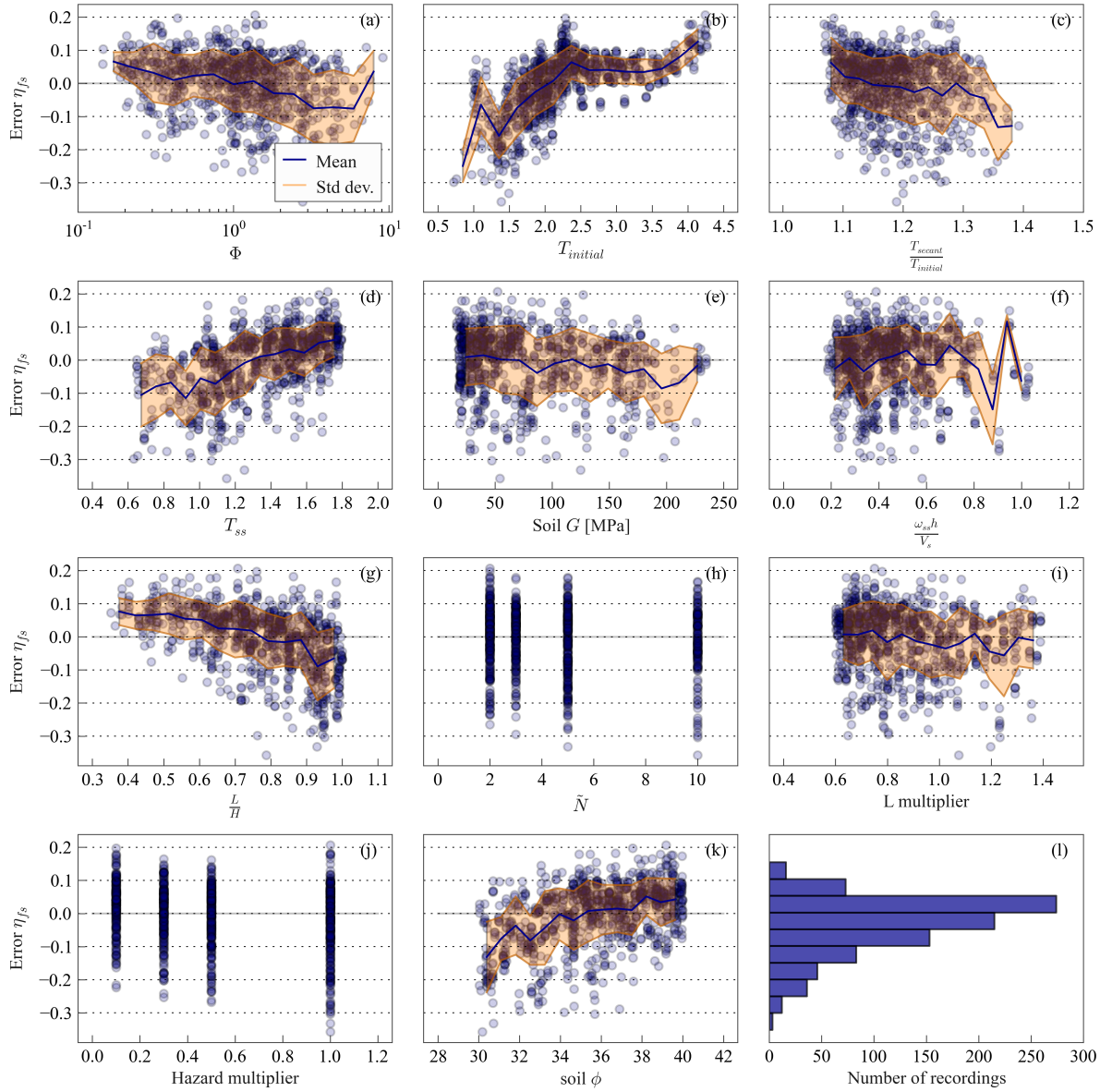

Figure 6.13: Results

While the design procedure presented in Figure 6.2 uses a generic design spectra and the displacement modification factors are calibrated based on the average response spectra of the 40 ground motions, it is of interest to know the influence of particular ground motions on the level of non-linear response.

For each ground motion the displacement for each building ($\Delta_{b,i}$) was divided by the expected design level of displacement for the building ($\Delta_{b,exp}$) from Equation 6.13 to determine the ground motion influence. The average of the ground motion influence from all the buildings was determined for each ground motion using results from analyses where the ground motions were scaled to 100%, and the ratio $\frac{\Delta_{b,i}}{\Delta_{b,exp}}$ was plotted against several ground motion characteristics in Figure 6.14. What is obvious is that the majority of the ground motions produced an average response within 10% of the expected design response while two mo-

tions had an average response of 20% or higher than expected. Although the ground motion scaling method in Section 6.5.4 may not provide the most uniform non-linear response, it attempts to be consistent with the DDBD method. The influence of ground motions on the non-linear response of structures is a complex phenomenon (Gazetas, 2012). However, the important thing is that there appears to be no major trends or bias with the chosen ground motion parameters. Given that 40 ground motions were used, it can be expected that the average response provides a suitable measure for the expected response for a hazard defined by generic design response spectra.

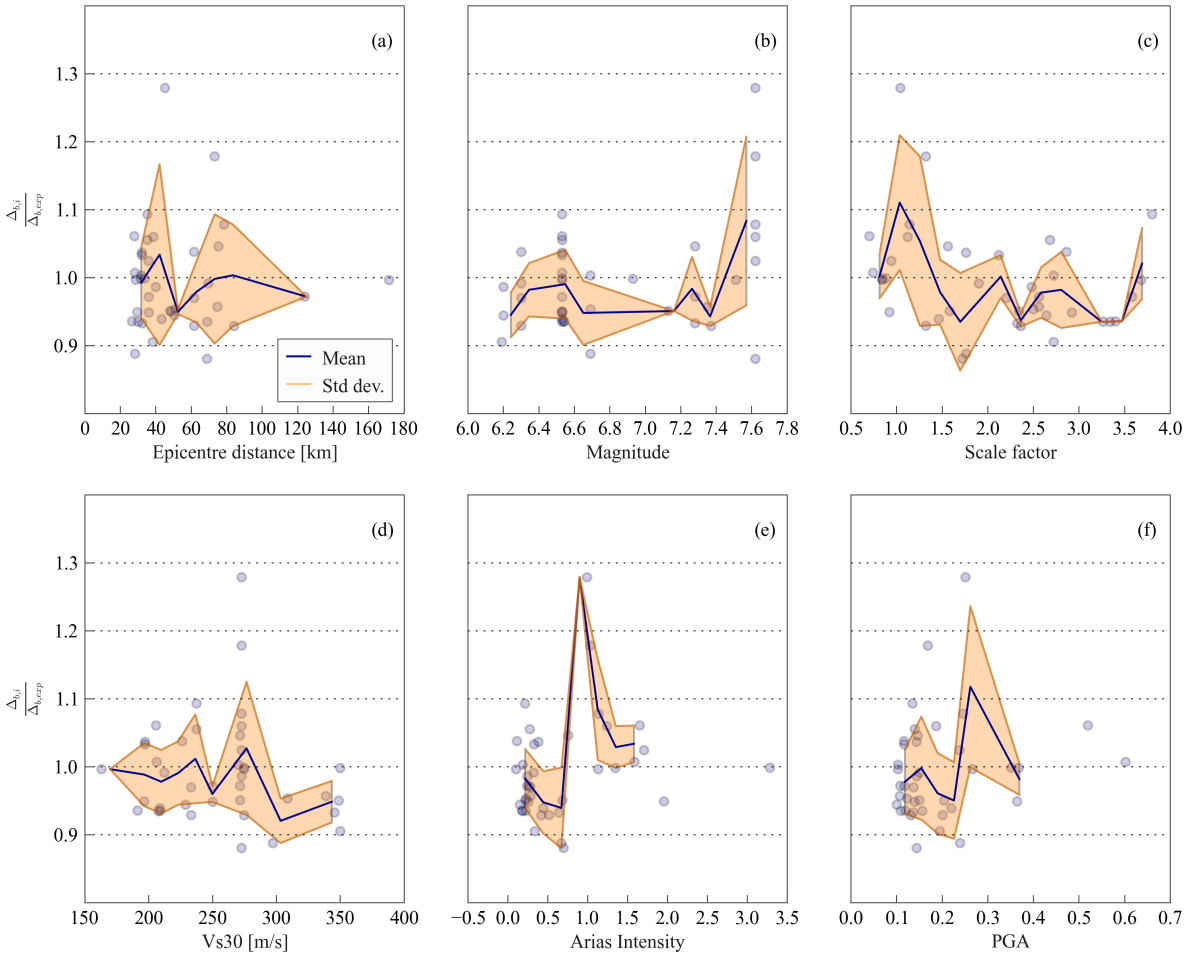

Figure 6.14: Displacement modification factor versus ground motion parameters

6.6 Validation of displacement prediction expressions

The newly developed expressions and assumptions for the procedure to predict displacements with consideration of SFSI effects was validated for wall buildings designed using the DDBD procedure. The following validation procedure was adopted, design 96 structure-foundation-soil systems using the procedure outlined in Section 6.2 in Figure 6.2 and the modifications to include assumptions for foundation shear stiffness, foundation shear DRF

(Equation 6.14), the foundation rotational stiffness reduction factor from Section 6.4, the foundation rotation DRF from Section 6.5, DRF factors for wall buildings from Pennucci et al. (2011a) (Equation 6.24) and the DRF system expression (Equation 6.13). The effects of P-delta were also included in the design by increasing the design base shear using the recommended DDBD approach (Equation 6.25), with the factor C taken as 0.5 due to the natural recentring behaviour of rocking foundations (see Priestley et al. (2007)). The expected behaviour of the SDOF models from the design process was compared to the maximum displacement, foundation rotation and ductility obtained from time history analysis. A full design example can be found in Appendix C.

$$\eta_{ss} = \sqrt{\frac{\pi\mu}{8.94\mu - 5.8}} \tag{6.24}$$

$$V_{base} = K\Delta + C\frac{P\Delta_d}{H_{eff}} \tag{6.25}$$

6.6.1 Input parameters for validation study

The input parameters for the numerical SDOF model were based on the non-linear SDOF that was obtained during the design procedure. To provide a reasonable range of SDOF models a range of wall buildings were designed with the design inputs summarised in Table 6.5. The foundations were first sized for static conditions and were then resized if the level of foundation deformation was too extreme to meet the total drift requirement. The target factor of safety was for the factored gravity load conditions (see Dep. Building & Housing (2011)) and does not represent the axial load ratio during earthquake excitation. The choice of factor of safety values was 2.0, 3,5 and 7.0, representing industrial buildings, standard buildings and settlement controlled design buildings. The buildings were designed to restrict the system drift to 2.5% and the superstructure drift to 2.0%, to demonstrate how different performance requirements for superstructure drift and total drift can be achieved.

Table 6.5: Wall design inputs

Parameter	Range
Number of storeys	$[4, 6, 8, 10]$
Wall width	0.3 m
Storey heights	3.4 m
Wall height to depth ratio	$[4, 6]$
Number of walls	4
Building length	20 m
Building width	12 m
Footing height	$1.2 + height_{wall}/60$ m
Footing length to width ratio	2.5
Footing depth to breadth ratio	0.0
Target static bearing factor of safety	[2.0, 3.5, 7.0]
Soil type	C
Design hazard level	0.3
Live load on floor	3 kPa
Dead load on floor	6 kPa
Total peak drift (θ_t)	0.025
Superstructure inter-story drift (θ_{ss})	0.02
Soil shear modulus (G)	$[50, 120]$ MPa
Soil friction angle (ϕ)	$[30.0^o, 36.0^o]$
Soil unit weight (γ_s)	18.0 kN/m^3
Concrete compression strength (f_c)	30 MPa
Rebar strength (f_y)	300 MPa

The building designs resulted in a structured distribution of SDOF model inputs as can be seen by the inputs plot shown in Figure 6.15. This shows a more realistic range of building typologies.

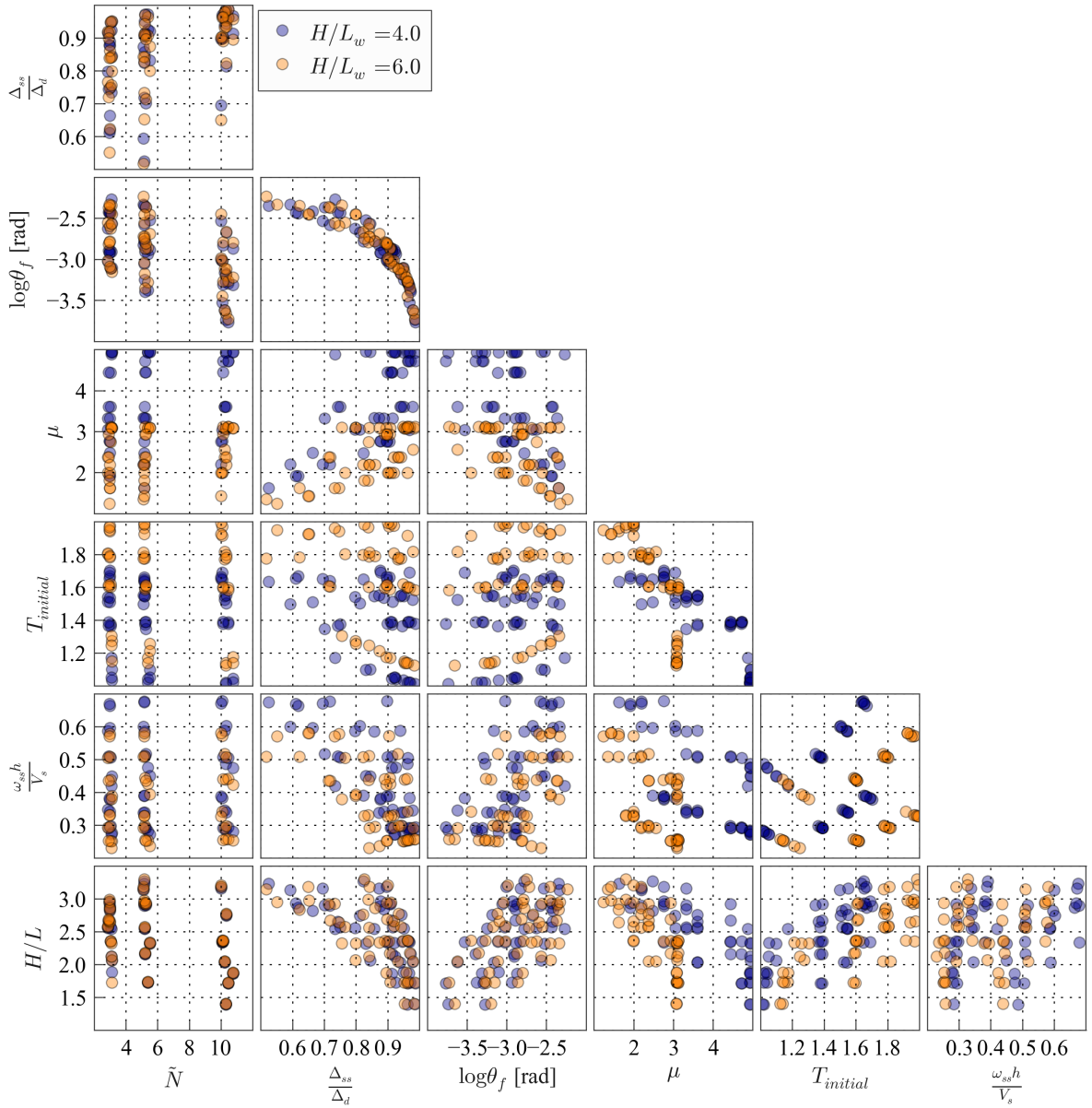

Figure 6.15: SDOF parameters for validation

6.6.2 Numerical model

The numerical model was identical to that in Section 6.5.2, except that in this model the horizontal and vertical masses were based on the effective mass, while to keep foundation behaviour consistent, the vertical load was based on the design axial load on the foundation. To have P-delta behaviour consistent with the design assumptions, the vertical load lumped at the superstructure was equal to the effective mass and the remaining vertical load was located at the foundation node. The other essential difference was that the beam behaved inelastically with a hinge at the base of the beam element set at 5% of the beam length. The hinge post-yield stiffness was calibrated to give a post-yield translational stiffness for the structure of 5% of the initial stiffness (see the derivation of the hinge post-yield stiffness

ratio below). The superstructure hysteretic behaviour was modelled using the Ruaumoko3D Modified Takeda rule with 'Takeda thin' properties ($\alpha = 0.5$, $\beta = 0.0$, NF = 1.0, KKK = 2). The initial superstructure stiffness was determined through Equation 6.27 where $K_{ss,eff}$ is the secant superstructure stiffness (Equation 6.26), V the base shear and r is the post-yield stiffness ratio taken as 0.05 as suggested in Priestley et al. (2007). The yield displacement was taken from Equation 6.28.

$$K_{ss,eff} = \frac{V}{\Delta_{ss}} \tag{6.26}$$

$$K_{ss} = \frac{\mu K_{ss,eff}}{1 + r(\mu - 1)} \qquad \mu \geq 1.0 \tag{6.27}$$

$$\Delta_y = \frac{\Delta_{ss}}{\mu} \tag{6.28}$$

Derivation of the hinge post-yield stiffness ratio

The majority of the displacement reduction factor equations for DDBD were calibrated based on SDOF systems that have a post-yield stiffness ratio of 5%. To maintain consistency with the design procedure, the hinge PYSR was calibrated to provide a PYSR to the system of 5% through the linear and nonlinear relationships between beam curvature and end displacement. The derivation of the calibration is shown in Equations 6.29 to 6.39, where the following notation was used:

r_e	Post yield stiffness ratio for lateral behaviour at beam end
r_h	Post yield stiffness ratio of beam hinge
K_t	Tangent stiffness for lateral behaviour at beam end
K_i	Initial stiffness for lateral behaviour at beam end
EI	Beam element rotational stiffness
H	Beam length
$\Delta_{NL,e}$	Lateral displacement of beam end for non-linear behaviour
P	Lateral force applied at beam end
θ_p	Plastic rotation of the hinge
ϕ_h	Curvature in hinge
ϕ_y	Yield curvature of hinge
P_y	Lateral force applied at beam end to cause yield in hinge

The lateral post-yield stiffness is defined by the nonlinear tangent stiffness divided by the initial stiffness:

$$r_e = \frac{K_t}{K_i} \tag{6.29}$$

The initial stiffness can be defined as the lateral cantilever stiffness:

$$K_i = \frac{3EI}{H^3} \tag{6.30}$$

The nonlinear tangent stiffness is more difficult to define as it must account for the elastic displacement and the nonlinear rotation of the hinge. The nonlinear displacement can be defined as follows, assuming the rotation occurs at the centre of the hinge.

$$\Delta_{NL,e} = \frac{PH^3}{3EI} + \theta_p H(1 - \frac{y}{2}) \tag{6.31}$$

Where:

$$y = \frac{L_p}{H} \tag{6.32}$$

$$\theta_p = (\phi_h - \phi_y)yH \tag{6.33}$$

for $P > P_y$:

$$\theta_p = \frac{(P - P_y)H(1 - y/2)}{r_h EI} yH \tag{6.34}$$

$$\Delta_{NL,e} = \frac{H^3}{EI}\left(\frac{P}{3} + \frac{(P - P_y)(1 - y/2)^2 y}{r_h}\right) \tag{6.35}$$

Thus the tangent stiffness can be defined as an increment change in lateral force divided by the incremental change in lateral displacement:

$$K_t = \frac{\delta P}{\delta \Delta_{NL,e}} \tag{6.36}$$

$$K_t = \frac{EI}{H^3(\frac{1}{3} + \frac{(1-y/2)^2 y}{r_h})} \tag{6.37}$$

The lateral post-yield stiffness ratio can be rearranged to determine the hinge post-yield stiffness ratio:

$$r_e = \frac{r_h}{r_h + 3(1 - y/2)^2 y} \tag{6.38}$$

$$r_h = \frac{3r_e(1 - y/2)^2 y}{(1 - r_e)} \tag{6.39}$$

6.6.3 Ground motions

The buildings were subjected to a completely different set of 40 ground motions selected from the NGA-West2 database (Ancheta et al., 2013) to demonstrate that the equations are applicable to a generic set of ground motions. The ground motions were selected and scaled based on the same principles as in Section 6.5.4 but this time scaled just to a Z value of 0.4 (See Table 6.6). Using a Z value of 0.4, instead of 0.3 from the calibration tests, meant that larger demands could be imposed on the structure and foundation. At low hazard levels the the wall design ends up being elastic as the elastic wall deformation is a constant and therefore the structure may never be excited into the non-linear range. Given that there was no observable trend with the scale of the hazard during the calibration tests, this modification to the hazard should be insignificant.

Table 6.6: Input ground motions

ID	Record	E. dist [km]	Mw	Scale	Vs30 [m/s]	Arias I [m/s]	PGA [g]	Earthquake	Year	Station
1	RSN3271_1	80.1	6.3	3.3	193	0.15	0.10	Chi-Chi, Taiwan-06	1999	CHY032
2	RSN3317_2	50.0	6.3	2.2	259	0.30	0.15	Chi-Chi, Taiwan-06	1999	CHY101
3	RSN3512_1	55.7	6.3	4.0	223	0.24	0.15	Chi-Chi, Taiwan-06	1999	TCU141
4	RSN3663_1	76.3	7.3	1.5	309	0.67	0.15	Taiwan S1(45)	1986	SMART1 I02
5	RSN3670_1	76.3	7.3	1.9	309	0.44	0.11	Taiwan S1(45)	1986	SMART1 I11
6	RSN3671_1	76.4	7.3	1.7	276	0.54	0.12	Taiwan S1(45)	1986	SMART1 I12
7	RSN3675_1	75.5	7.3	1.7	306	0.62	0.13	Taiwan S1(45)	1986	SMART1 M05
8	RSN3675_2	75.5	7.3	1.6	306	0.62	0.15	Taiwan S1(45)	1986	SMART1 M05
9	RSN3676_1	75.2	7.3	1.7	308	0.66	0.13	Taiwan S1(45)	1986	SMART1 M06
10	RSN3682_2	75.7	7.3	1.9	329	0.31	0.11	Taiwan S1(45)	1986	SMART1 O09
11	RSN3679_1	77.0	7.3	1.7	300	0.46	0.11	Taiwan S1(45)	1986	SMART1 M11
12	RSN3758_1	42.8	7.28	2.4	334	0.47	0.10	Landers	1992	Thousand Palms PO
13	RSN3758_2	42.8	7.28	2.7	334	0.48	0.12	Landers	1992	Thousand Palms PO
14	RSN3863_1	63.1	6.3	2.3	235	0.30	0.21	Chi-Chi (as 5)	1999	CHY002
15	RSN3934_2	33.2	6.61	2.7	139	0.42	0.15	Tottori, Japan	2000	SMN002
16	RSN3937_1	55.5	6.61	3.7	182	0.22	0.13	Tottori, Japan	2000	SMN005
17	RSN4204_2	38.6	6.63	2.3	128	0.59	0.12	Niigata, Japan	2004	NIG014
18	RSN4840_1	55.1	6.8	2.3	334	0.41	0.18	Chuetsu-oki	2007	Joetsu Kita
19	RSN4855_2	32.1	6.8	2.1	245	0.62	0.13	Chuetsu-oki	2007	Sanjo
20	RSN4860_1	27.7	6.8	1.9	278	1.08	0.26	Chuetsu-oki	2007	Sanjo Shinbori
21	RSN4883_1	34.4	6.8	3.1	255	0.41	0.16	Chuetsu-oki	2007	Niigata Nishi Kaba
22	RSN5259_1	34.3	6.8	3.6	175	0.36	0.11	Chuetsu-oki	2007	NIG013
23	RSN5260_2	32.0	6.8	2.1	128	0.59	0.11	Chuetsu-oki	2007	NIG014
24	RSN5619_1	27.1	6.9	2.1	279	0.96	0.22	Iwate	2008	IWT011
25	RSN5805_1	48.3	6.9	2.5	253	0.30	0.11	Iwate	2008	Yokote City - Nobita
26	RSN582_1	74.8	7.3	2.1	357	0.43	0.14	Taiwan SMART1(45)	1986	SMART1 O08
27	RSN5838_1	55.3	7.2	2.0	186	0.96	0.19	El Mayor-Cucapah	2010	El Centro - Meloland
28	RSN5859_2	88.5	7.2	2.5	194	0.70	0.16	El Mayor-Cucapah	2010	Westmorland Fire Sta
29	RSN5829_1	32.4	7.2	1.1	242	3.98	0.40	El Mayor-Cucapah	2010	RIITO
30	RSN5990_1	62.9	7.2	2.1	211	1.38	0.24	El Mayor-Cucapah	2010	El Centro Array #7
31	RSN6890_1	46.7	7.1	1.1	204	1.10	0.23	Darfield, NZ	2010	Chch Cashmere HS
32	RSN6923_1	56.2	7	1.4	255	1.49	0.36	Darfield, NZ	2010	Kaiapoi North School
33	RSN6965_1	27.2	7.1	3.7	263	0.61	0.15	Darfield, NZ	2010	SBRC
34	RSN721_1	35.8	6.54	1.4	192	1.10	0.36	S. Hills-02	1987	El Centro Imp. Co.
35	RSN760_1	65.7	6.93	2.3	126	0.29	0.11	Loma Prieta	1989	FC Menhaden Court
36	RSN776_2	48.2	6.93	1.6	282	0.79	0.18	Loma Prieta	1989	Hollister - S & P
37	RSN778_1	45.1	6.93	1.3	216	0.81	0.27	Loma Prieta	1989	Hollister Diff. Array
38	RSN800_2	46.4	6.93	3.3	280	0.24	0.11	Loma Prieta	1989	Salinas - John & Work
39	RSN803_1	27.1	6.93	1.2	348	1.09	0.26	Loma Prieta	1989	Saratoga - W V Coll.
40	RSN8161_2	58.0	7.2	1.1	197	2.78	0.33	El Mayor-Cucapah	2010	El Centro Array #12

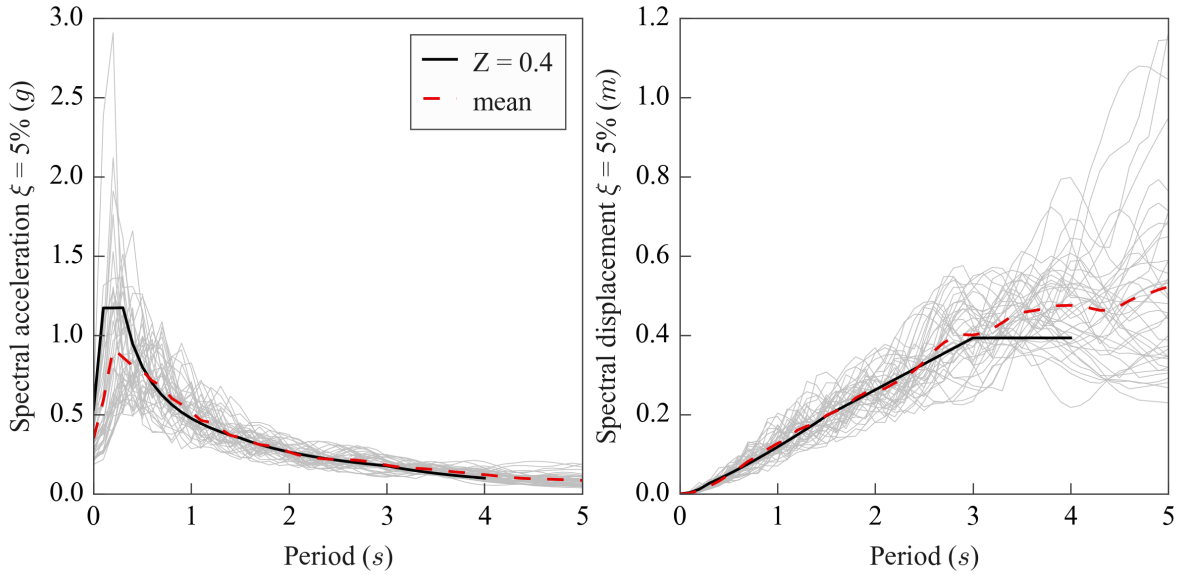

Figure 6.16: Response spectra of validation set of ground motions

6.6.4 Validation results

Figure 6.17 shows the expected behaviour of the SDOF models from the design process, compared to the maximum displacement, foundation rotation and ductility obtained from time history analysis. The small triangles represent individual time history results, while the large circles are the average of the 40 records for a single building. The final plot in Figure 6.17 demonstrates the level of non-linearity in the foundation by plotting the average secant rotational stiffness divided by the elastic rotational stiffness against the level of corrected normalised foundation rotation.

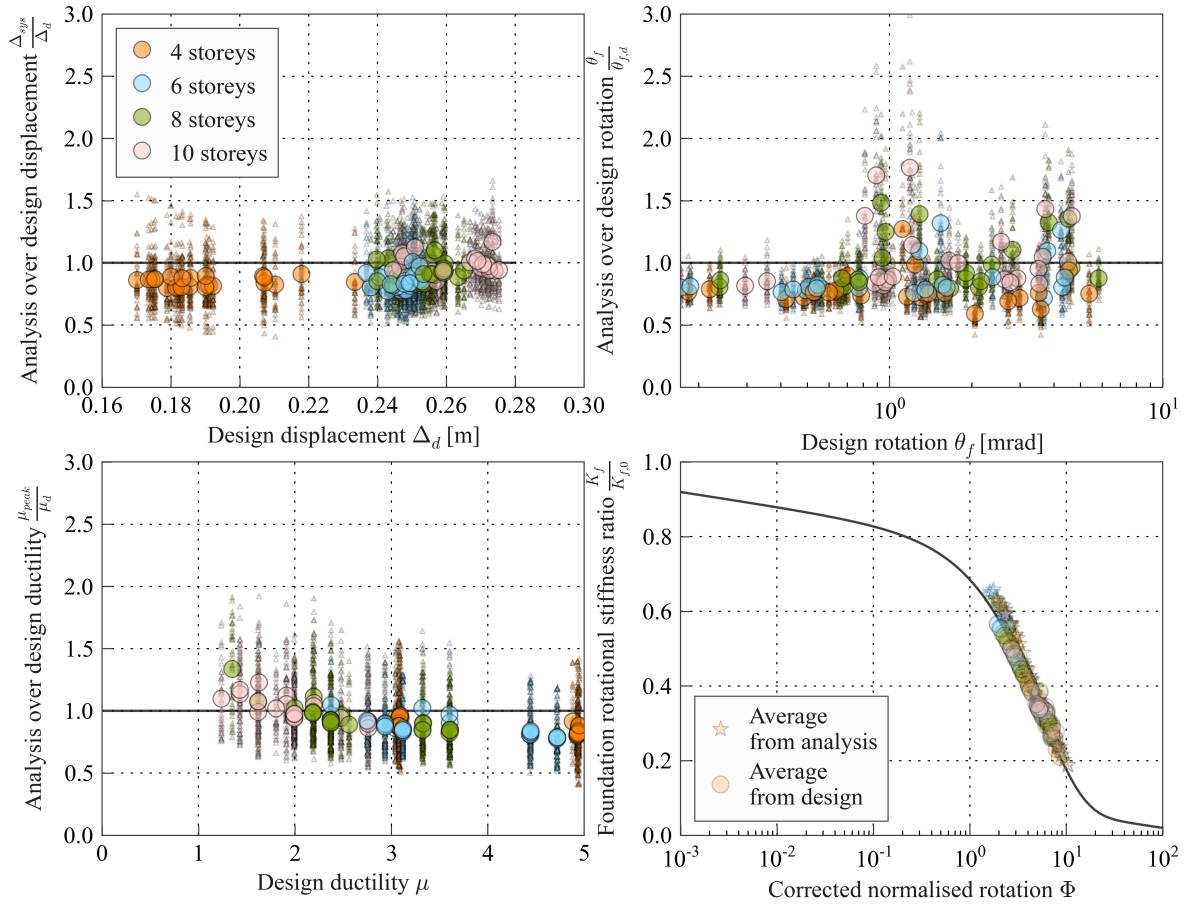

Figure 6.17: Validation of displacement prediction equations

The average peak displacement from the analyses was very closely correlated with the displacement prediction from the design, however, there was considerable record-to-record variability, as expected from using recorded ground motions.

The foundation rotation also showed good correlation with a small under prediction of the rotation, with the median ratio being 0.84 and the 85th percentile 1.14, considering all the ground motions individually. The most noticeable exceptions are the three ratios that are around or exceed 1.5; interestingly, these values all have a secant period of 3.0 seconds, equal to the design spectrum corner period. The ratios of the average analysis displacement and the expected displacement from design are investigated in Figure 6.20 and it can clearly be seen that designs restricted by the corner period were not as accurate as those where the secant period was less than 3.0 seconds. The level of scatter for the foundation rotation was similar to the level observed during the calibration process, which is promising given the analyses involved the added complexities of a non-linear superstructure and P-delta effects.

The analysis ductility showed excellent correlation to the expected ductility calculated during design, however, there was an obvious bias where at higher levels of ductility the analysis ductility was less than the design ductility. The bias was due to the way the superstructure

was modelled, most likely due to the considerations of damping, when compared to the tangent stiffness proportional damping model used by Pennucci et al. (2011a). The damping in this model used a rotational dashpot element over the cantilever beam member, calibrated to give 5% damping to the horizontal mass for linear conditions. The calibration was based on the relationship between the end rotation and end displacement of the cantilever. As the hinge becomes non-linear, the relationship between rotation and displacement changes from $\theta = 3\Delta/2H$ for a linear cantilever to close to $\theta = \Delta/H$ for post yielding, thus providing a reduction to two-thirds for the effective damping coefficient C. For Rayleigh tangent stiffness proportional damping the decrease is much greater, the damping co-efficient reduces to the square root of the post-yield stiffness so $\sqrt{0.05} = 22\%$.

Similar bias was observed with the prediction of ductility at high levels of ductility when assessing fixed based SDOF representations of concrete wall buildings. The concrete wall buildings were designed and analysed using the same procedure, with the exception that no P-delta effects and no foundation deformations were included in the design and analysis. The results of the fixed base study can be seen in Figure 6.18, the trend with ductility seen here confirms that the issue is related to the superstructure model. This level of bias was also observed by Pennucci et al. (2011a) when investigating multiple degree-of-freedom wall structures where the first mode damping is almost entirely mass proportional and therefore the damping forces are larger than intended.

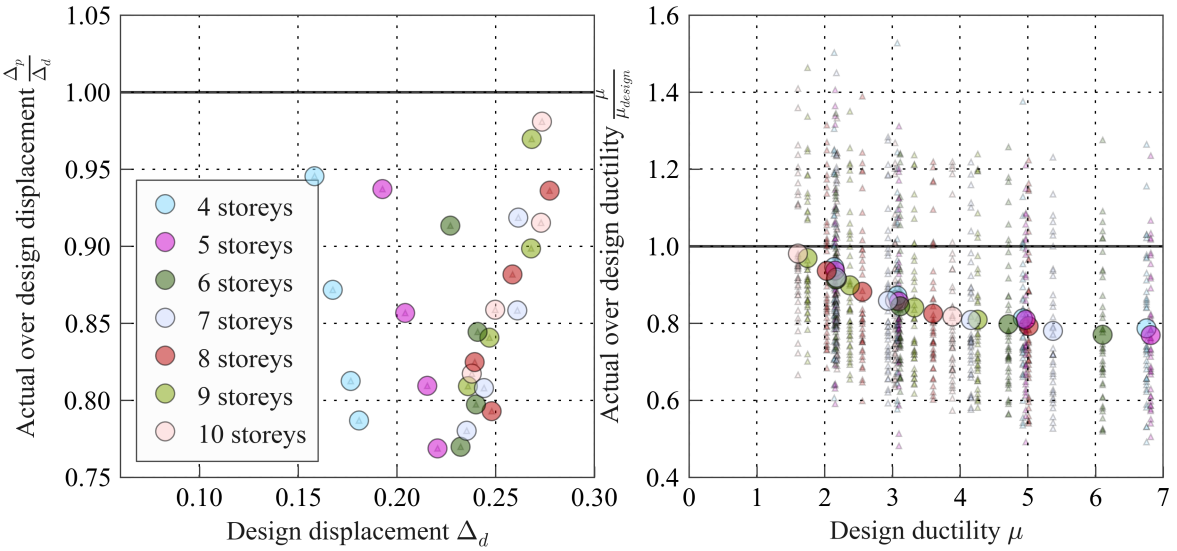

Figure 6.18: Bias in ductility observed for fixed base analyses

The predicted displacement was examined against other important parameters in Figure 6.19. There was a clear trend between the ductility (a) which can be expected as at large levels of ductility the damping forces were larger than for tangent stiffness proportional damping. The dependance on the ductility was very strong due to the large contribution from the superstructure to the overall displacement. Unlike in the calibration study, where the foundation

deformation contributed most of the overall displacement, in Figure 6.19 (c) it can be seen that in most cases the superstructure contributed over 60% of the displacement, as can be expected from a typical concrete wall design. The under prediction of superstructure deformation was also reflected in the trend with building height to foundation length (H/L) (d). The H/L ratio strongly affects the distribution of displacement between the foundation and the superstructure, where at low levels of H/L the deformation is nearly completely from the superstructure and therefore the disparity between predicted and obtained structural deformation is directly reflected in the total displacement. The trend with the initial period ($T_{initial}$) that was observed in the calibration study was also noticeable in plot (g). There were minor trends with the stiffness ratio (e) and soil friction angle (h), however, given that all of the buildings were designed using the same design process, the fitting of additional parameters to the displacement prediction equations would potentially make them unusable outside of the proposed design procedure.

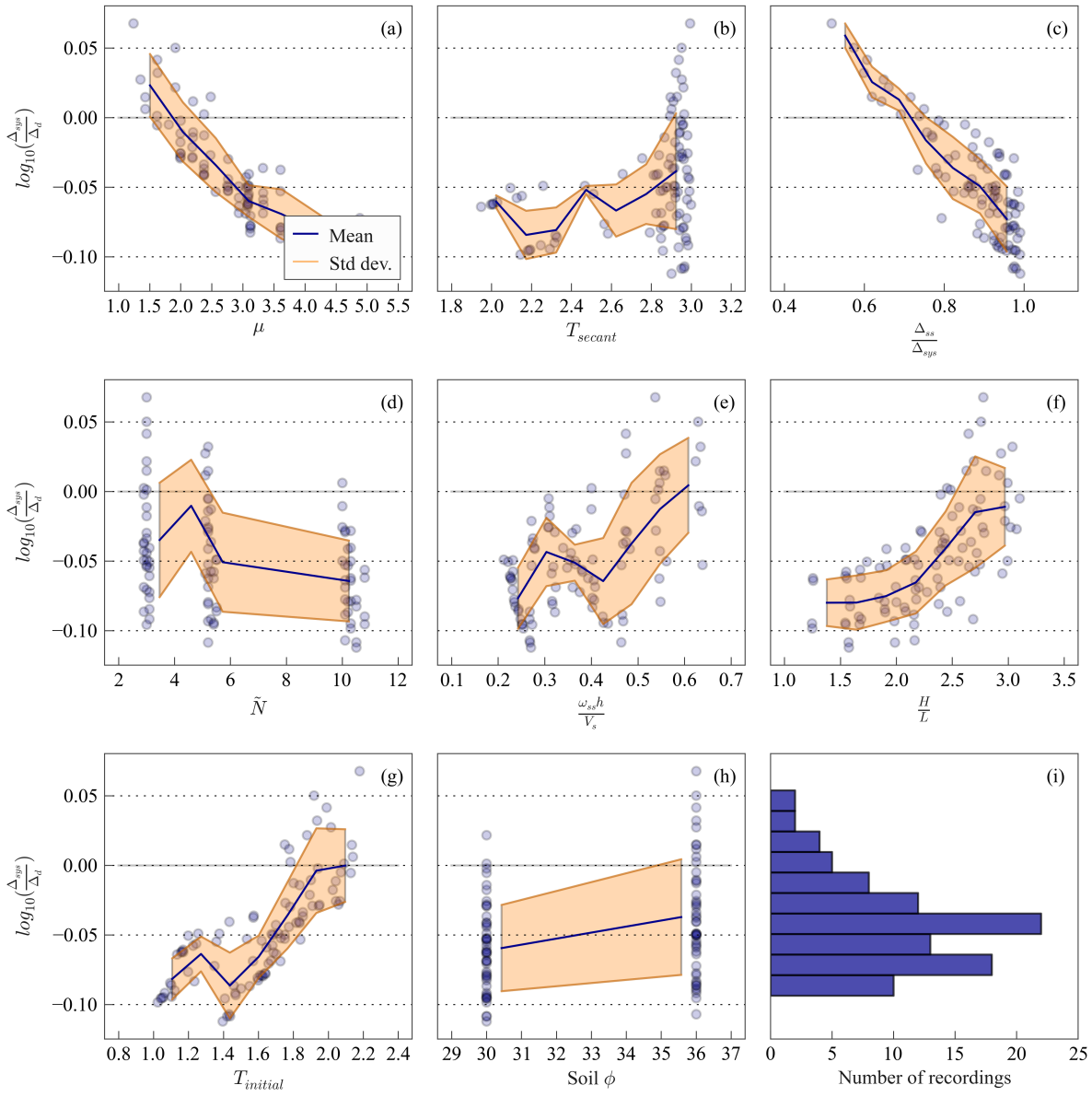

Figure 6.19: Residuals for the prediction of displacement

The predicted rotation was examined against other important parameters in Figure 6.20. The ductility had an almost negligible trend with the prediction of foundation rotation, while the estimated rotation did approach the prediction at low levels of ductility, as expected. The design secant period showed that many of the designs were constrained by the displacement plateau and it was these buildings that resulted in some poor estimates of the peak rotation. There was a small under prediction of rotation for analyses where the superstructure displacement contribution was large. The scatter in the prediction of rotation was greater for foundations with low axial load ratio. The same trends with the height to foundation length and with the initial period that were seen in the displacement prediction were also observed for the prediction of rotation, suggesting that the correction for this trend in the rotation would result in an improvement to the prediction of displacement.

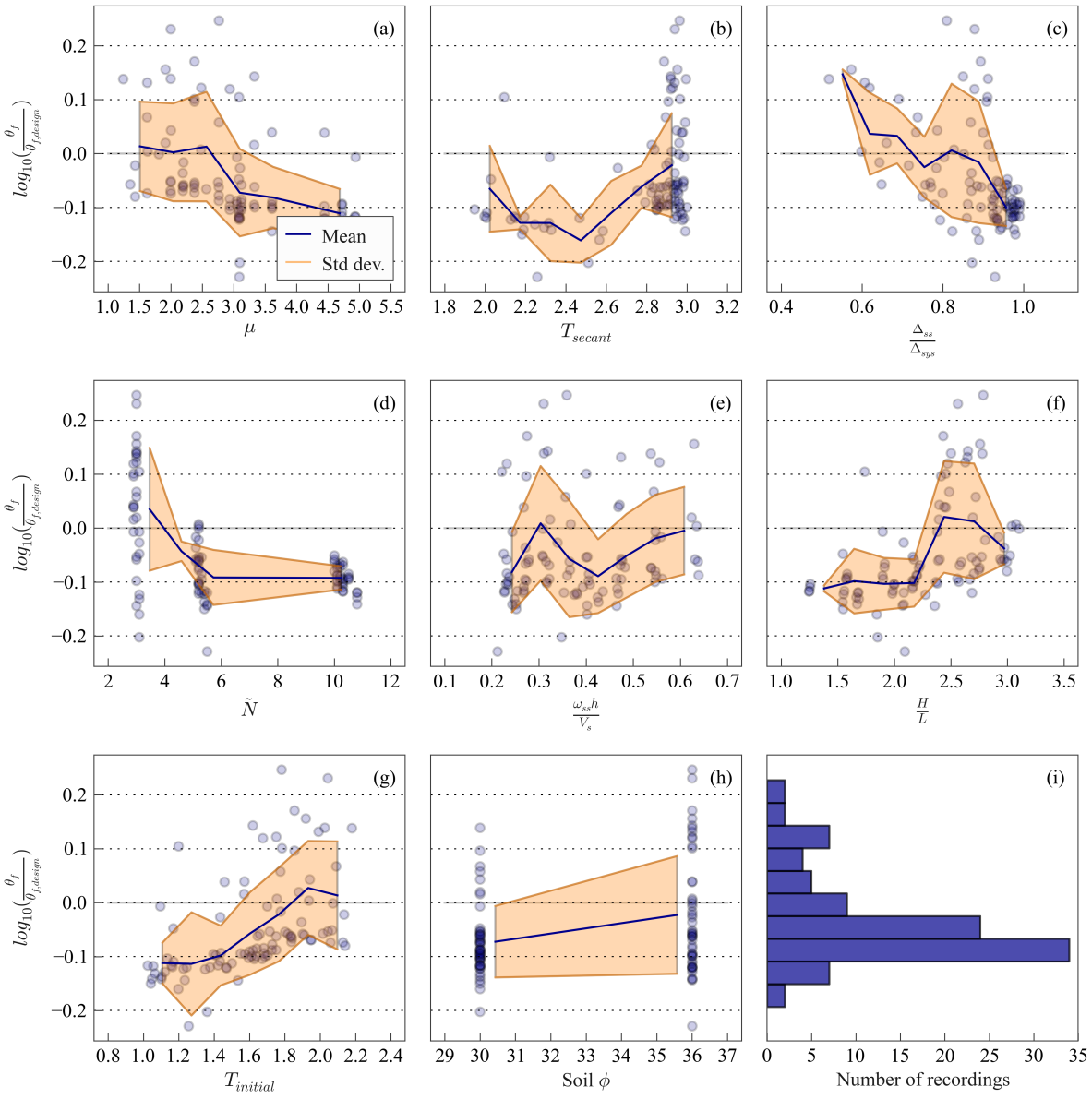

Figure 6.20: Residuals for the prediction of rotation

This set of tests validated the use of the newly proposed DRF expressions and foundation reduction factors for use in DDBD, using a different suite of ground motion records, with the additional complexity of P-delta effects. The system DRF equation was also validated, confirming that the modification factor for a non-linear superstructure and modification factors for non-linear foundation deformation can be combined to estimate the effects of the non-linear deformations on the system behaviour; to the best of the authors knowledge, this is the first published validation of such a combination, making it hugely important in the context of design.

6.7 Updates to design procedure

This section briefly explains the updates to the design procedure due to the findings in this chapter, the flowchart presented in Figure 6.2 in section 6.2 can be used as a reference to view the updates in Figure 6.21, which are shown in bold.

The major updates include:

- Foundation stiffness degradation expression that includes the effects of shear force
- The inclusion of soil-foundation shear deformation in the design procedure
- Removal of the EVD to instead directly use DRFs
- New expressions to calculate the foundation rotation and soil-foundation shear DRFs
- A new expression to combine the superstructure, foundation rotation and soil-foundation shear DRFs to calculate the system DRF

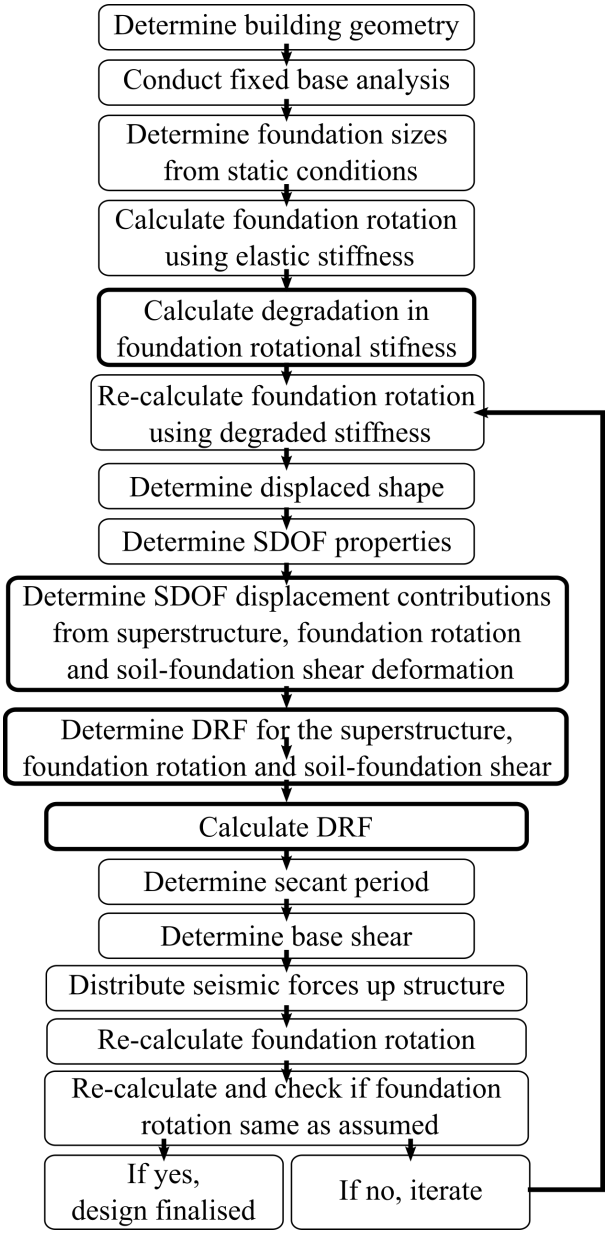

Figure 6.21: Modified direct displacement based design procedure considering non-linear SFSI

The other major update to the design procedure was that it was validated using time history analysis for a series of buildings designed using the new design procedure, demonstrating that it can provide accurate predictions of superstructure and foundation deformations.

6.8 Conclusions

This chapter provides an overview of the displacement-based design procedure presented by Paolucci et al. (2013) that includes the influence of foundation rotation on the dynamic behaviour. The design procedure provides the reference for the work presented in chap-

ter where improvements are made to several expressions and the procedure is extended to include foundation shear forces and shear deformations.

A foundation rotational stiffness degradation expression was developed based on a series of numerical push-over analyses of SDOF systems with rigid superstructures that were connected to a soil-foundation macro-element. A foundation rotation displacement reduction factor (DRF) expression was developed based on a series of numerical non-linear time history analyses, where SDOF systems with linear elastic superstructures were attached to a soil-foundation macro-element. The calibration of the foundation rotation DRF expression made use of a proposed displacement-weighted expression to combine different DRFs from the superstructure, foundation shear and foundation rotation. The calibration also required an assumption for the soil-foundation shear stiffness degradation which was taken as half of the elastic stiffness an assumption for the soil-foundation shear deformation DRF, which was taken as 0.76.

An updated design procedure was presented that made use of the new DRF expressions instead of the equivalent viscous damping expressions presented in Paolucci et al. (2013). The updated design procedure also included shear deformations, making use of the proposed assumptions for soil-foundation shear stiffness degradation and soil-foundation DRF, and made use of the new foundation rotational stiffness degradation expression.

A series of concrete wall buildings were designed using the updated design procedure and the equivalent SDOF soil-foundation-structure system developed during the design was submitted to 40 ground motions using non-linear time history analysis. The equivalent SDOF model consisted of a non-linear superstructure, modeled as a linear member with a non-linear hinge at the base, which was connected to a soil-foundation macro-element. The total displacement, superstructure ductility and foundation rotation from the analyses were all compared to the expected deformations from design procedure and the comparison showed generally good agreement. There was some bias at large structural ductility were the damping model implemented in the time history analyses was different to the damping model used to calibrate the superstructure DRF expression and therefore superstructure ductility levels from the analyses were approximately 20% less at a ductility level of 5.0. The comparison between the deformations predicted in the design procedure and those obtained from the time history analyses provided some validation that the updated design procedure could provide suitable predictions of the peak deformations of the soil-foundation-structure system, which is an important component of a performance-based design.

Chapter 7

Prediction of foundation residual rotation and settlement

7.1 Introduction

A performance-based design methodology requires designers to control the level of deformations in the structure for a given set of design loads. The peak transient deformations have been the major focus of performance-based design, since they are important in controlling collapse and damage to non-structural elements; however, according to Priestley (2003) '. . . It is at least arguable that residual displacements are ultimately more important than maximum displacements, given the difficulty of straightening a bent building after an earthquake.' Residual deformations indicate the possibility of repairing the structure and can result in partial or total loss of a building if static incipient collapse is reached, if the structure appears unsafe to occupants or if the response of the system to a subsequent earthquake is impaired by the new at rest position of the structure. Christopoulos et al. (2003) provide a framework to explicitly consider residual superstructure deformations in performance-based design, through weighting factors between peak and residual drift to give a building performance factor. It is somewhat of a curiosity that the residual foundation deformations are not considered in performance-based design given the wide scale foundation damage seen in recent earthquakes such as Kocaeli 1999, Chi Chi 1999 and Christchurch 2011, resulting in many buildings deemed economically irreparable.

There exists a considerable body of research on the prediction of the peak displacement of structures with no foundation deformation (eg. Chopra and Goel, 2001; Miranda and Ruiz-García, 2002; Priestley and Grant, 2005; Dwairi et al., 2007; Pennucci et al., 2011a). There are several empirical equations available for predicting the residual drift of the superstructure (eg. MacRae and Kawashima, 1997; Kawashima et al., 1998; Christopoulos and Pampanin, 2004; Ruiz-García and Miranda, 2006b). There are design orientated expressions for predicting the peak foundation rotation (eg. Paolucci et al., 2009; Adamidis et al., 2013; Paolucci et al., 2013) (Chapter 4). To have a comprehensive performance-based design the same attention and

predictive capacity is needed for the foundation residual deformations.

Early experimental tests by Taylor and Williams (1979) involved rocking foundations under constant axial load on clay and sand. The findings showed that settlement was dependent on the number of cycles, with five cycles at 0.035rad resulting in a settlement of 0.2% of the footing width. It was recommended that footings should be designed with large factors of safety to prevent large settlements during rocking.

The level of settlement induced in a single cycle has been investigated by Gajan et al. (2005) through an extensive set of cyclic loading tests of footing under centrifugal conditions. In their work the axial load ratio ($\tilde{N}$, defined as the ultimate vertical capacity over the applied vertical load), the peak footing rotation and the relative density were all recognised as important parameters relating to settlement. Further research by Gajan and Kutter (2009) investigated the influence of moment to shear ratio on the level of settlement and showed that the influence of shear to moment was accounted for by using the ratio of foundation contact area to the critical contact area that would result in loss of bearing capacity.

Deng et al. (2012) developed relationships between the settlement and the cumulative plastic rotation (defined as the sum of all the rotations that exceed an arbitrary threshold) based on slow cyclic and dynamic centrifuge tests. Their research also recognised the axial load as an important parameter. In fact many previous experimental researchers have shown the importance of axial load on the settlement (eg. Taylor and Williams, 1979; Ugalde et al., 2007a; Anastasopoulos, 2012).

Numerous experimental research campaigns have shown very low levels of foundation residual rotation, especially for footings with low axial load (eg. Combescure and Chaudat, 2000; Ugalde et al., 2007b; PWRI, 2005). Deng (2012) developed an equation for the recentring ratio of the foundation (Rd) based on regression of experimental data (Equation 7.1). Where FS_v is the vertical factor of safety for static loads.

$$Rd = \frac{FS_v}{2.565 + 1.016FS_v} \tag{7.1}$$

For engineers to be able to control the residual deformations in the design, results and equations from previous research need to be adapted to allow for prediction of residual deformations based on easily attainable engineering demand parameters.

There is a growing interest in a 'weak foundation, strong super-structure' design philosophy, where the designer deliberately allows for large foundation deformations to limit the seismic forces entering the superstructure (Pecker, 2011; Gazetas, 2014). This has prompted engineers to question what level of foundation deformations is acceptable. Should we prevent foundation uplift as suggested in many codes around the world (eg. Dep. Building & Housing,

2011)? If we allow for large transient deformations in the foundation, will this result in large residual settlements and residual rotations? Can we control the level of residual foundation deformation in a rational manner? This chapter addresses these questions, not to advocate for a 'weak foundation, strong super-structure' design approach, but to provide engineers with a tool so that they can estimate the residual deformations of the foundations, regardless of their design philosophy.

7.2 Mechanisms of rotation

Foundation rotation can be considered as consisting of three separate mechanisms (Figure 7.1):

- Elastic rotation, which is a linear elastic mechanism. The rotation is fully recoverable upon removal of the load and the elastic stiffness comes from the footing dimensions (L and B), initial shear modulus (G) and Poisson's ratio (v) of the soil as calculated using the expression in in Table 7.1. The additional term, I_y, is the second moment area of the foundation in contact with the soil and the k terms are the dynamic stiffness terms (see Gazetas (1991) for more information).
- Foundation uplift is a non-linear elastic mechanism, whereby the deformation is fully recoverable, but the rotational stiffness reduces as uplift occurs due to a geometric non-linearity.
- Soil yielding is a non-linear inelastic mechanism, whereby the rotation is not recoverable and the stiffness changes as the soil yields.

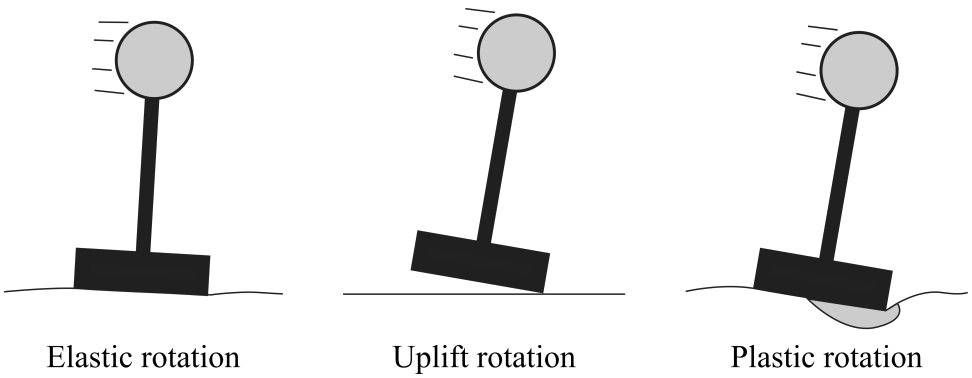

Figure 7.1: Mechanisms of foundation rotation

Table 7.1: Stiffness terms for rectangular foundations

Mode	Stiffness
Vertical	$K_z = \frac{2Gl}{(1-v)}\left[0.73 + 1.54(\frac{b}{l})^{0.75}\right].k_n$
Transverse shear	$K_y = \frac{2Gl}{(2-v)}\left[2 + 2.5(\frac{b}{l})^{0.85}\right].k_y$
Longitudinal shear	$K_x = K_y - \frac{0.2Gl}{(0.75-v)}\left[1 - \frac{b}{l}\right].k_x$
In-plane rotation	$K_{yy} = \frac{G}{(1-v)} I_y^{0.75}\left[3(\frac{l}{b})^{0.15}\right].k_m$
Out-of-plane rotation	$K_{xx} = \frac{G}{(1-v)} I_x^{0.75}(\frac{l}{b})^{0.15}\left[2.4 + \frac{b}{l}\right].k_m$

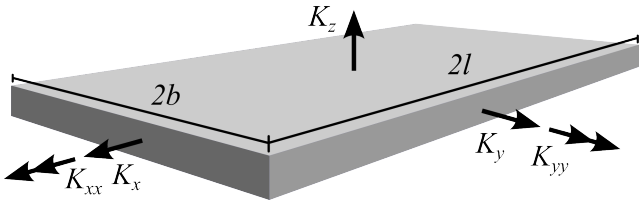

Figure 7.2: Notation for foundation stiffness terms

Each of these mechanisms contributes different amounts of rotation depending on the level of axial load and amount of rotation (Figure 7.3). The elastic rotation is the biggest contributor at small levels of rotation, while for large rotations, heavily loaded footings are dominated by soil yielding and lightly loaded footings are mainly affected by uplift. Although each mechanism affects the other, this systematically illustrates why the level of residual rotation would be dependent on both the level of rotation and the axial load.

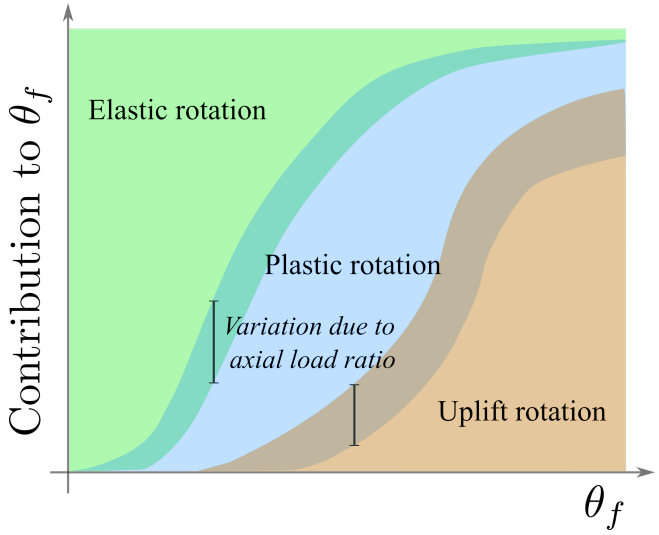

Figure 7.3: Contributions from rotation mechanisms

A common measure to estimate the level of non-linear foundation rotation is the peak foundation rotation normalised by the pseudo uplift angle (θ_{uplift}) (See Chapter 6). The pseudo uplift angle provides a convenient expression accounting for the elastic rotational stiffness (K_{MM}), the foundation axial capacity (N_{cap}) and the applied axial load (N). The $\alpha = 4$ parameter accounts for the stress distribution at the point of uplift for elastic soil and the $\zeta = 1.5$ parameter from work by Cremer et al. (2001), provides a correction to the uplift moment for inelastic soil behaviour.

$$\theta_{uplift} = \frac{N \times L}{\alpha K_{MM,elastic}} e^{-\zeta N / N_{cap}} \tag{7.2}$$

7.3 Mechanisms of settlement

A mechanism approach can also be applied to the prediction of settlement. Two mechanisms contribute to settlement, static settlement and SFSI-induced settlement. The static component can be considered as the settlement from the compressibility of the soil under the applied gravity loads and many methods already exist to estimate the magnitude of gravity-induced settlement under static loads (eg. Schmertmann, 1999), thus it will not be discussed further here. The SFSI-induced settlement occurs due to a shakedown of the foundation into the soil through subsequent cycles of irrecoverable soil deformation (yielding) through rotation (Figure 7.4). The amount of settlement that occurs under a single loading cycle depends on the plasticity of the soil, the peak amplitude of the rotation and the amount of axial load on the foundation.

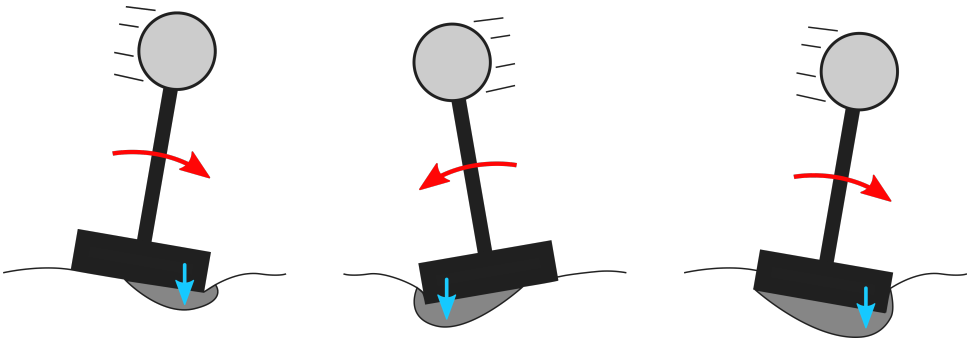

Figure 7.4: SFSI-induced foundation settlement

7.4 Foundation deformation performance limits

The emergence of a 'weak foundation, strong super-structure' design philosophy has prompted engineers to consider what levels of foundation deformation are acceptable. Sullivan et al. (2012) attempts to implicitly control the level of residual deformation by limiting the level

of design effective soil shear stiffness (Table 7.2). Where the effective stiffness is the secant stiffness at the peak design response. This criterion attempts to limit the level of inelastic response, but provides no indication to the level of residual deformations that can be expected, and imposes limits on the effective soil shear stiffness, which is non-unique and requires considerable interpretation. A further difficulty being that current foundation effective rotational stiffness curves used in the DDBD procedure do not directly consider soil stiffness and only consider foundation rotational stiffness (Paolucci et al., 2013). The foundation rotational stiffness is based on the three separate mechanisms (elastic rotation, soil yielding and foundation uplift) and hence imposing severe limits on the foundation stiffness degradation when the degradation is predominantly due to the elastic uplift mechanism may be misguided.

Table 7.2: Soil stiffness degradation limits

Type	Level 1	Level 2	Level 3
Soil stiffness	$G/G_{max} \geq 0.8$	$G/G_{max} \geq 0.3$	$G/G_{max} \geq 0.2$

Alternatively, imposing direct limits on deformations (Figure 7.5), such as foundation residual rotation or angular distortion and settlement, provide intuitive and measurable limitations to the performance. The limits on foundation performance summarised in Table 7.3 were interpreted from several documents.

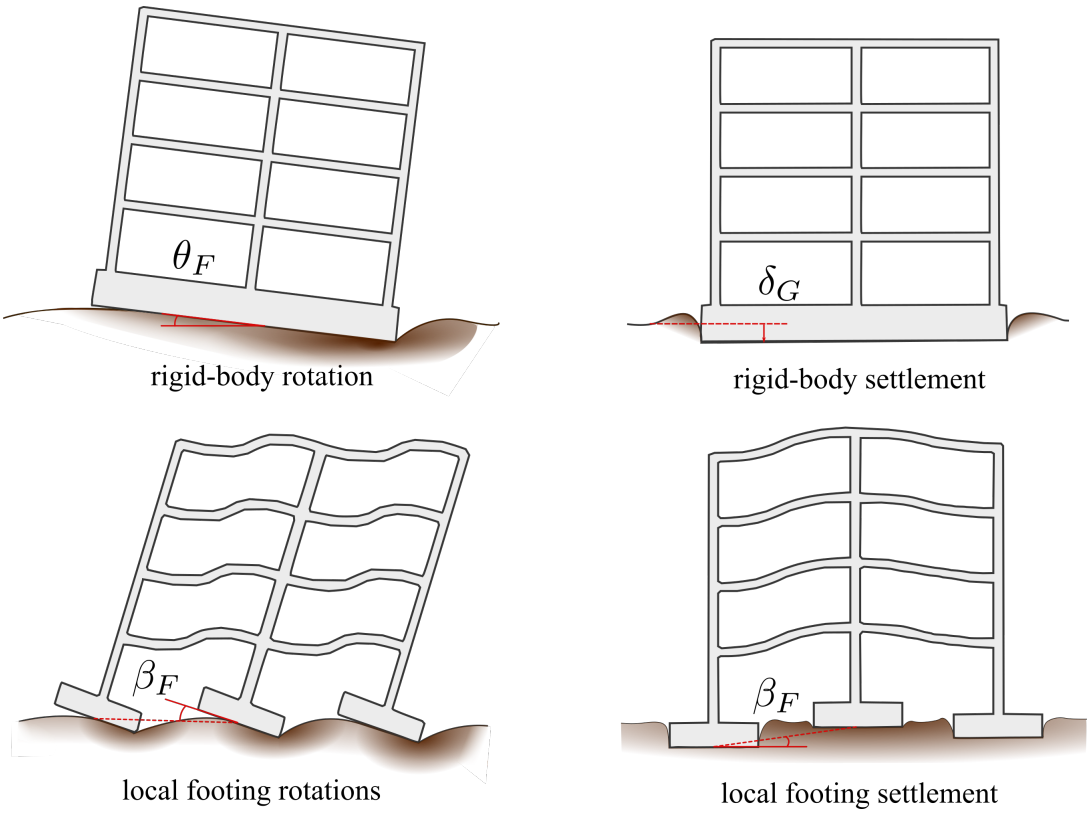

Figure 7.5: Foundation deformation mechanisms

Table 7.3: Foundation performance limits

Type	Level 1 - No damage	Level 2 - Repairable	Level 3 - No Collapse
Peak rigid-body tilt ($\theta_{F,P}$)	0.6%*	1.2%*	2.0%*
Residual rigid-body tilt ($\theta_{F,R}$)	0.33%†	0.67%†	P-delta limits
Rigid-body settlement (m) (δ_G)	0.025‡	0.050†	-
Peak angular distortion ($\beta_{F,P}$)	0.6%*	1.2%*	2.0%*
Residual angular distortion ($\beta_{F,R}$)	0.33%†	0.67%†	2.0%*

† Skempton and H (1956)

‡ Eurocode 1 (1994)

∗ Task Force Report (2007) (Interpreted)

While the limits on foundation deformation are debatable for many reasons and require considerable engineering judgment, their use as a measure for performance based design is widely supported by the engineering community (Pender, 2014). The limits on SFSI deformations should consider the level of static deformations that have occurred prior to the seismic event. Furthermore, the deformation limits should reflect their consequences, which are highly dependent on the structural typology and building use. Foundation deformation limits are discussed in many foundation engineering textbooks and articles (eg. Burland et al., 1977; Ricceri and Soranzo, 1985; Boscardin and Cording, 1989) for various building typologies and uses.

7.5 Existing experimental results

Experimental tests provide evidence of correlation between residual rotation and peak rotation including the effects of axial load, and for dynamically-induced settlement. Unfortunately, there are a limited number of experimental test results that can clearly demonstrate these relationships. Many tests use synthetic earthquake records or have recorded data that has unintended noise or deformations that make the measurements difficult to interpret. Figure 7.6 shows the residual settlement and residual rotation in relation to the peak rotation and axial load ratio ($\tilde{N}$), extracted from various experimental testing programs.

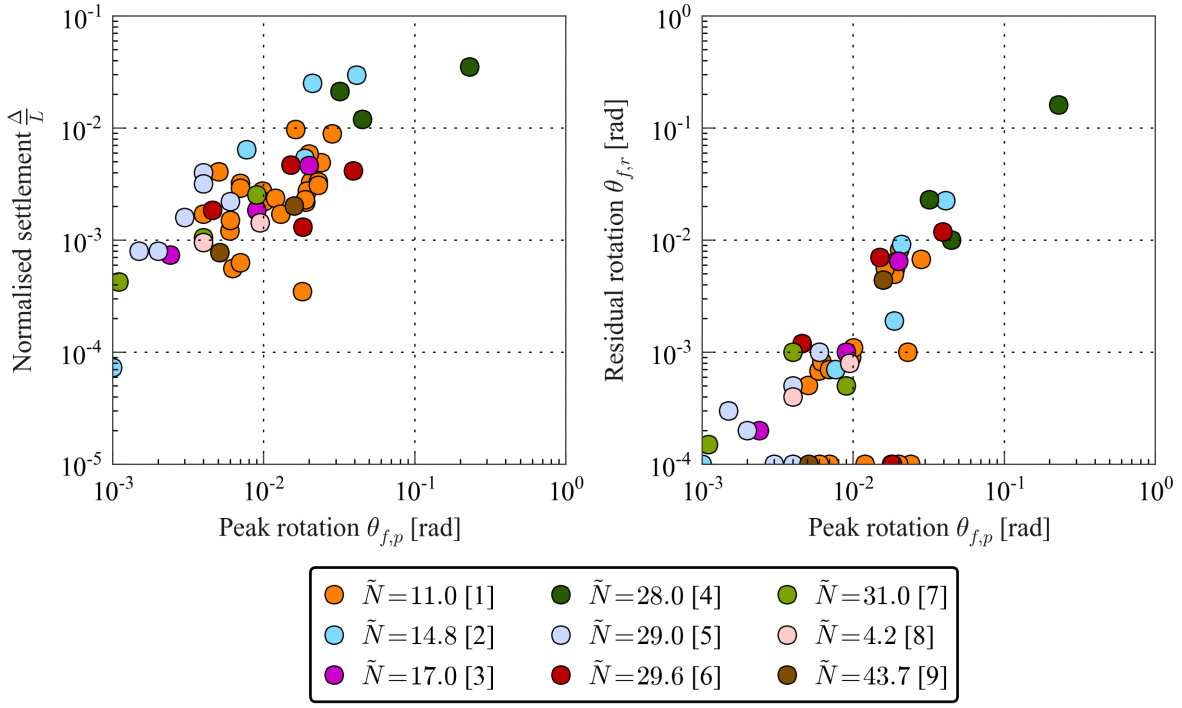

Figure 7.6: Correlation between residual deformation and peak rotation

1	(Test LJD03) Deng et al. (2012)	2	(Test LJD01) Deng et al. (2012)
3	Ugalde et al. (2010)	4	PWRI (2005)
5	(Test LJD02) Deng et al. (2012)	6	(Test LJD01) Deng et al. (2012)
7	Ugalde et al. (2010)	8	Combescure and Chaudat (2000)
9	(Test LJD01) Deng et al. (2012)		

Although the data set shows that in general a larger peak rotation will result in both larger settlements and larger residual rotations, the data set is not significant enough to deduce the influence of axial load or any other bias. Also there are a series of residual rotation points at 10^{-4}, which were from recordings were the residual rotation was to small to accurately determine.

To supplement this data set, a series of time-history analyses were conducted using a SDOF structural model attached to a soil-foundation macro-element, to simulate simple structures on soil.

7.6 Development of residual deformations curves

This section derives expressions for predicting foundation residual deformations from the results of the numerical parametric study presented in Chapter 6, Section 6.5. The study consisted of 345 randomly generated soil-foundation-structure systems, where the superstructure was a linear SDOF and the soil-foundation interface was modelled with a non-linear macro

element (Figure 7.7). Each system was subjected to 40 ground motions and the resulting average peak and residual deformations were used to determine design expressions through multi-linear regression analysis.

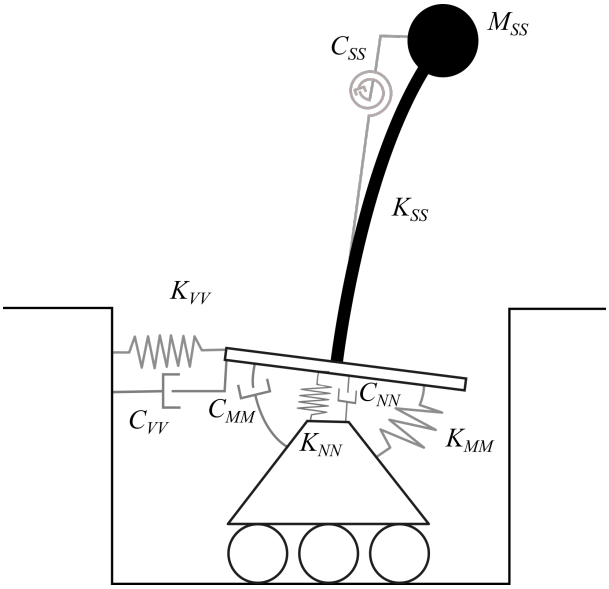

Figure 7.7: Numerical model setup

Figure 7.8 shows the foundation deformations for a 18.3 m tall SDOF with a foundation length of 10.0 m and an axial load ratio of 5.0 during the Imperial Valley 1979 ground motion recorded at El Centro Array #3 station (NGA0175_1, (Chiou et al., 2008)). The peak foundation rotation was taken as the largest rotation measured in the positive or negative direction. The residual foundation rotation was taken as the rotation after the building had returned to rest. The dynamically induced settlement (of the centre of the foundation) was taken as the peak value of settlement minus the initial static settlement; the peak settlement was used as in some cases the residual rotation of the foundation caused the centre point of the foundation to uplift and therefore give a vertical displacement value that was not representative of the settlement of the foundation.

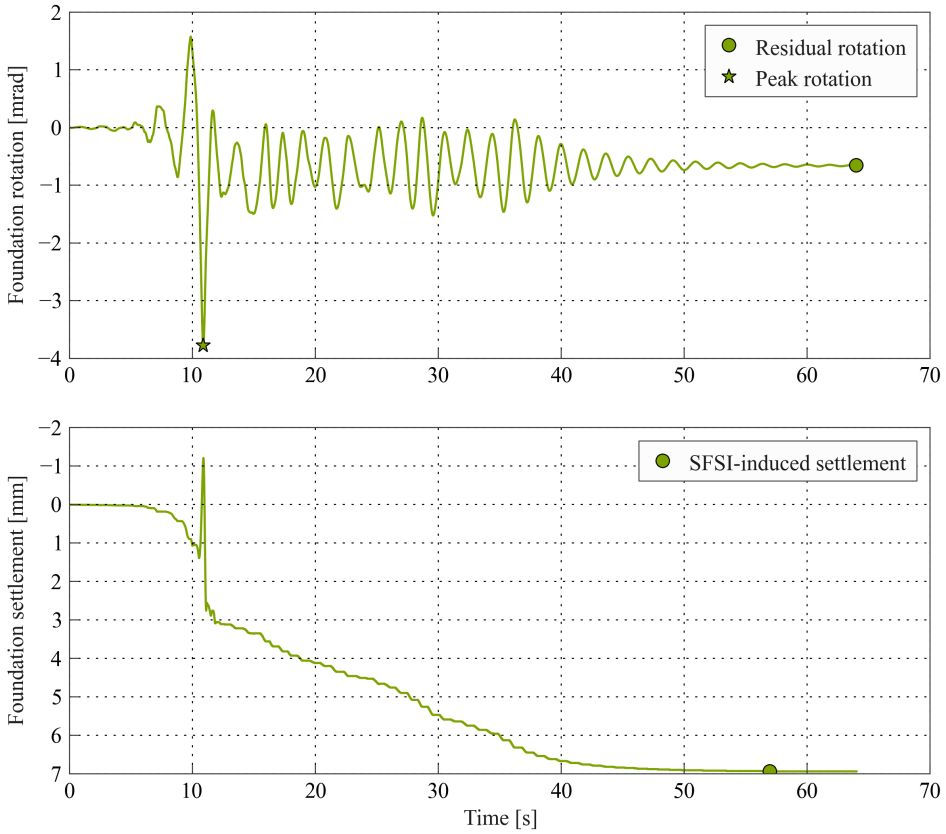

Figure 7.8: Foundation deformations from a SDOF structure subject to the Imperial Valley 1979 ground motion

7.6.1 Results

The time history results from the parametric study were examined to determine relationships between the peak foundation rotation and the two residual deformation parameters. The SFSI-induced settlement was first normalised by the foundation length and foundation peak rotation based on the clear geometric relationship between these parameters and supported by previous studies (eg. Taylor and Williams, 1979; Gajan et al., 2005)). The residual rotation was also normalised by the peak rotation, as residual drifts are often given as a ratio of the peak drift. Forward selection multiple linear regression was conducted using the statsmodels package in Python 2.7, based on minimising the Bayesian Information Criterion (BIC) considering the following parameters:

- $(\frac{\delta}{L\theta_{f,p}})$: The average SFSI-induced settlement divided by the foundation length and normalised by the peak foundation rotation
- $\frac{\theta_{f,r}}{\theta_{f,p}}$: The average residual foundation rotation divided by the average peak rotation
- $\theta_{f,p}$: The average peak foundation rotation during an earthquake
- $\tilde{N}$: The ratio of vertical load required to cause bearing capacity failure under static

conditions over the applied foundation vertical load

- $T_{initial}$: The elastic vibrational period of the building and soil system
- $\theta_{f,uplift}$: The pseudo uplift angle (Equation 7.2)
- $\frac{\omega_{ss}h}{V_s}$: The ratio of building stiffness to the soil shear stiffness
- $\frac{H}{L}$: The ratio of the building height to the foundation length
- T_{SS}: The vibrational period of the building
- FL_{multi}: The scale factor applied to the foundation length

While the BIC provides a strict parameter selection tool for statistical purposes, the results from the forward selection resulted in every parameter showing some significant improvement to the fitted model. Given that the expressions are intended for design purposes and that the results are based on SDOF models that were created using a structured sampling process, an expression with so many terms may be considered over-fitted making it difficult to implement in design and have considerable bias toward the structured sampling process used for creating the SDOF models. The forward selection process was useful for determining the most relevant parameters and allowed developing simpler design oriented expressions with less parameters.

Design expression for SFSI-induced settlement

For the normalised foundation settlement, the most important parameter was the axial load ratio. The peak rotation showed an additional trend, resulting in a settlement expression with a non-linear dependence on the peak rotation. The first peak rotation term explains the geometric relationship between the SFSI-induced settlement and rotation, while the second term uses the log of the peak rotation and represents the plastic component of the deformation, where larger rotations induce greater plastic response and therefore greater settlement. The $T_{initial}$ parameter was important, as this can be considered as a proxy for the number of cycles of rotation, with longer initial period systems going through less cycles than shorter period systems (see how the foundation goes through several oscillations, each inducing settlement in Figure 7.8). It should be noted that the duration of the earthquake influences the number of cycles and should be considered if the expected earthquake duration is very long. The other parameters showed only a small reduction in the BIC value and these trends are more likely to be subject to bias due to the structured sampling process of the SDOF models, so were removed from the final expression (Equation 7.3).

$$\frac{\delta}{L\theta_f} = (0.0337 + \frac{0.218}{\tilde{N}})log_{10}(\theta_f) + \frac{1.33}{\tilde{N}} + 0.556 - 0.136T_{initial} \tag{7.3}$$

Figure 7.9 shows the parametric results after they have been normalised to an initial period of 1.0s and shows the regression trends through the data.

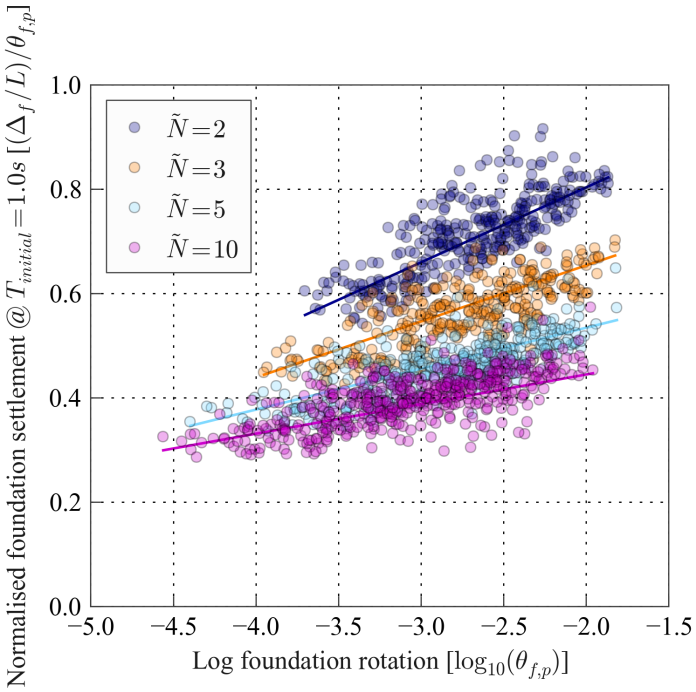

Figure 7.9: SFSI-induced settlement versus peak foundation rotation

Interestingly when the foundation peak rotation was normalised by the pseudo uplift angle a clear non-linear expression was obtained (Figure 7.10). The normalisation of the rotation using the pseudo uplift angle demonstrates the change in the dominant mechanism, where at rotation values just larger than the pseudo uplift angle the uplift mechanism starts to dominate the rotational behaviour and the geometric relationship between the settlement and rotation no longer holds true.

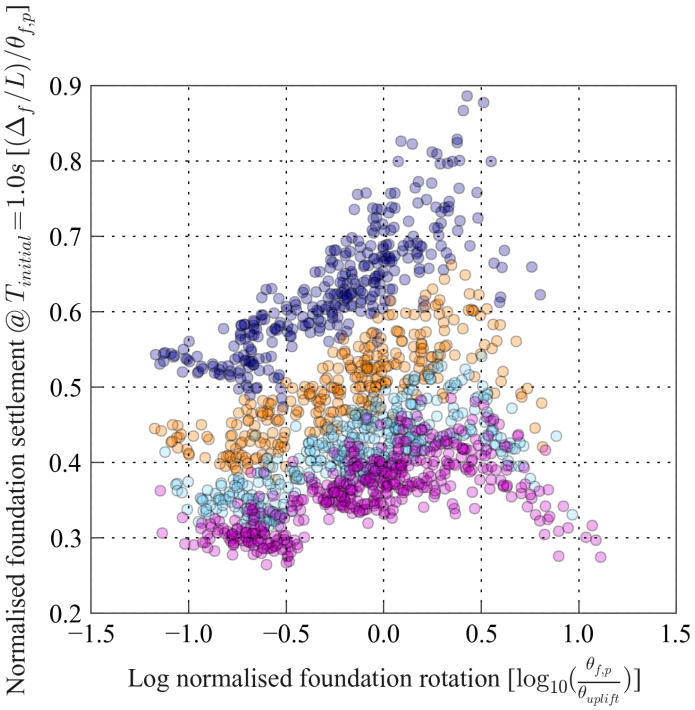

Figure 7.10: SFSI-induced settlement versus normalised peak foundation rotation

The residual errors for SFSI-induced settlement were examined to assess whether any further structure existed in the data (Figure 7.11). It can be seen that there are no major trends in the errors and that the trends with stiffness ratio and aspect ratio are insignificant compared to the scatter in the results.

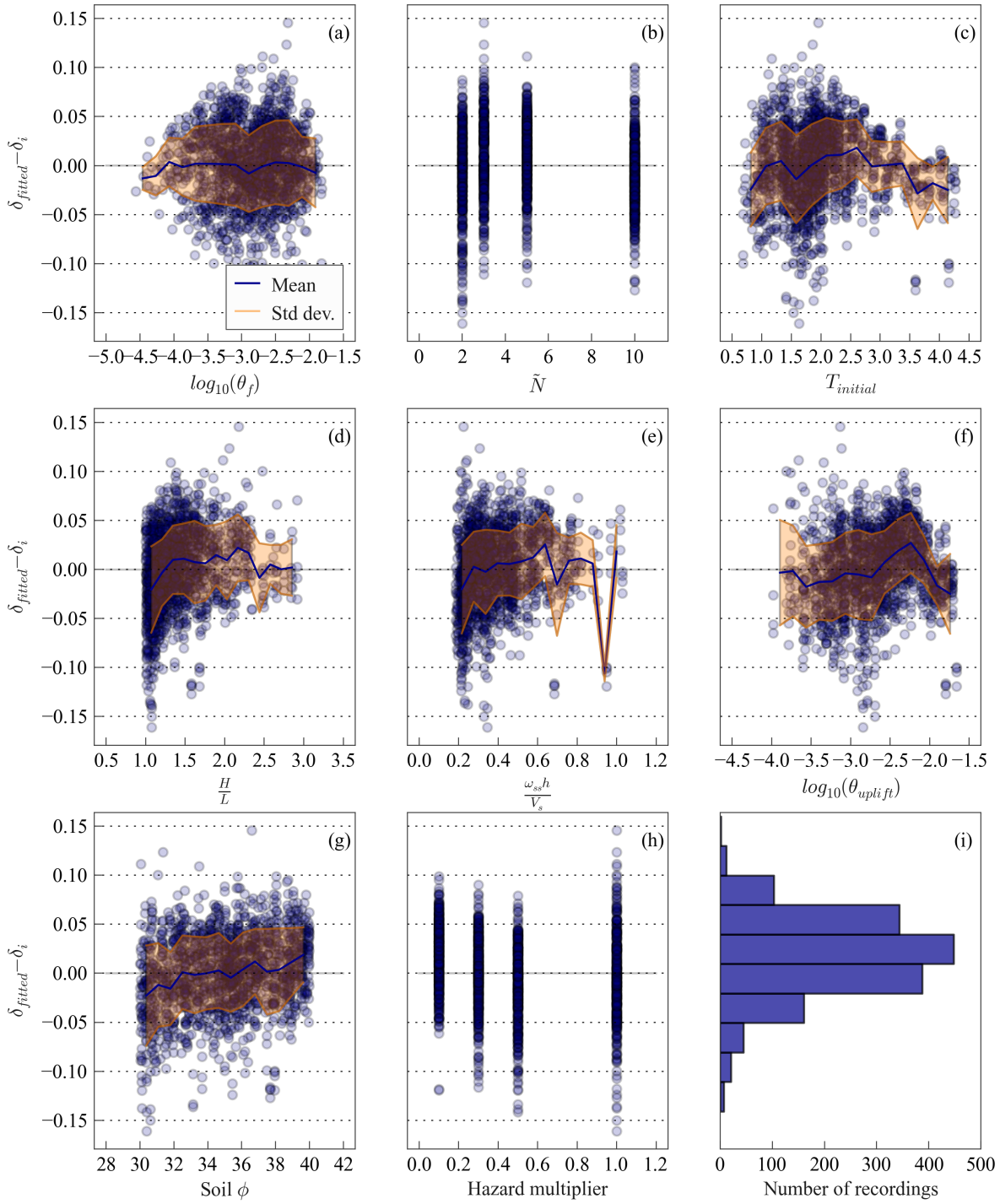

Figure 7.11: Residual errors for SFSI-induced settlement versus peak foundation rotation

Design expression for residual foundation rotation

For the residual rotation the peak foundation rotation was the most important parameter. No other parameters that were investigated contributed significantly to the residual expression and the expression determined from regression analysis is given in Equation 7.4

$$\frac{\theta_{f,r}}{\theta_{f,p}} = 0.0094 \log_{10}(\theta_{f,p}) + 0.0489 \tag{7.4}$$

The lack of a trend between residual rotation and axial load was surprise and may be due to the macro-element formulation. In Section 4.5 in Chapter 4 the limitations of the macro-element were discussed and it was noted that at levels of rotation less than foundation uplift the level of plasticity may be artificially large due to the plasticity bounding surface using the foundation ultimate loads surface. The other major limitation to the above residual rotation expression is that no P-delta (second order geometric effects) were considered in numerical analyses. P-delta effects may cause ratcheting effect that amplifies the residual rotation, so the presented trend may be considerable lower than in reality.

The error in the residual rotation expression was examined against a series of potentially influential parameters in Figure 7.12. The average residual rotations from the analyses were divided by the expression in Equation 7.4 and the log of the results is plotted to demonstrate that the results were skewed. In theory the residual rotation can vary anywhere between the peak rotation minus the elastic rebound rotation and zero, given that no P-delta effects were included in the analyses a permanent rotation in one direction is just as likely to be cancelled out in the next cycle as it to increase.

Figure 7.12 also demonstrates that there were no other strongly influential parameters. The log of the uplift rotation showed a small decrease residual rotation with increasing uplift rotation in plot (f).

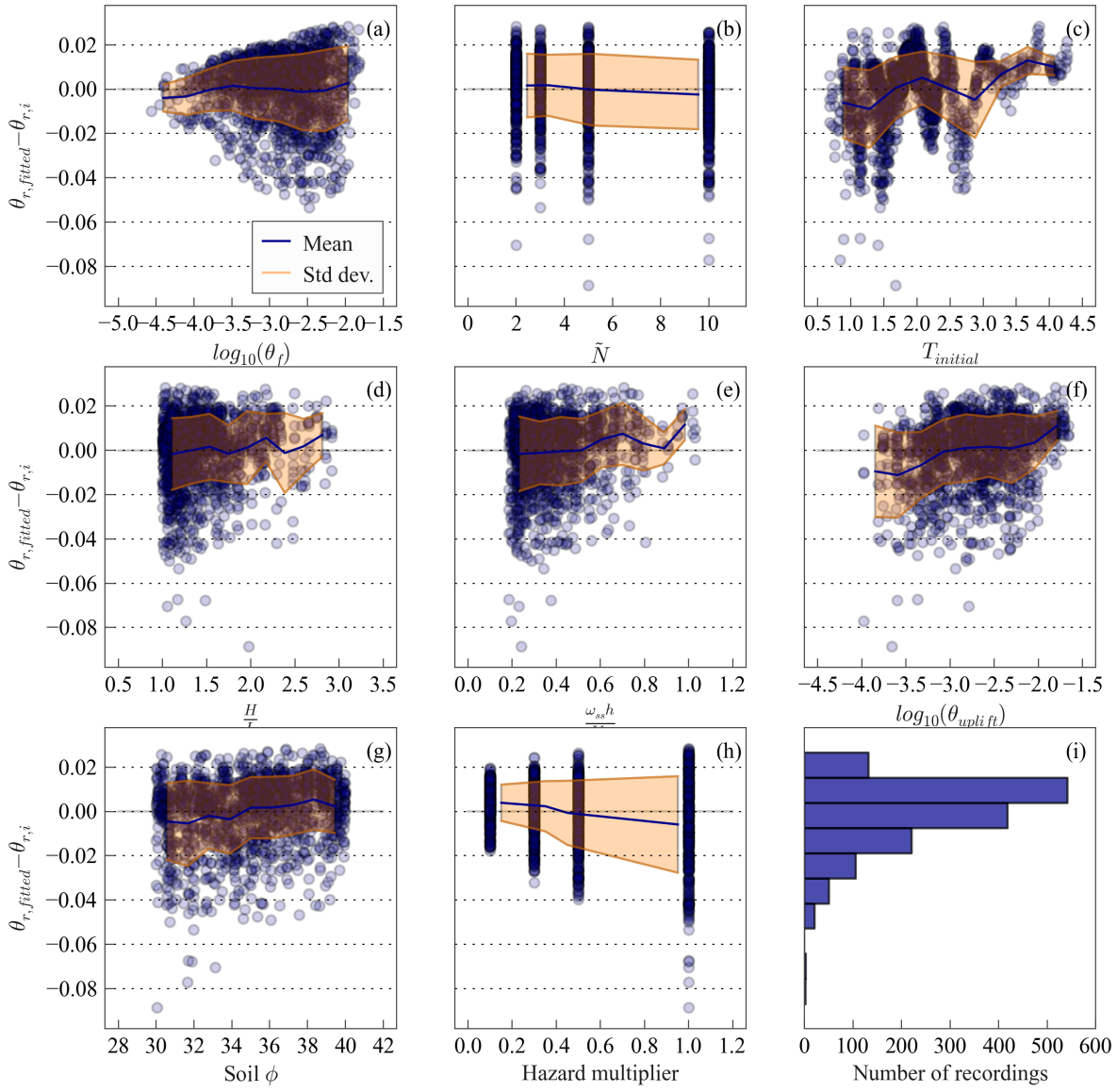

Figure 7.12: Error in the residual foundation rotation expression versus other parameters

7.7 Validation of the prediction of residual deformations

The above expressions were validated against a series of building-foundation-soil systems that were designed using the Direct Displacement-based Design procedure outlined in Chapter 6. The design and numerical study were presented in Chapter 6 Section 6.6 and will not be repeated here, however, a full design example can be found in Appendix C.

The designs were not only more realistic than the randomly generated buildings in Section 7.6 but the design provided a prediction of the peak rotation which was used to predict the residual deformations during the design phase. The predicted residual deformations were compared to the average residual deformation that was obtained from the numerical analyses to validate the use of the proposed equations. The design and numerical modelling

also allowed for the inclusion of non-linear superstructure deformations and the inclusion of P-delta effects, which could then be assessed for their influence on the prediction of residual foundation deformation.

7.7.1 Results

Figures 7.13 (a) and (b) show the predicted foundation settlement (Equation 7.3) and residual rotation (Equation 7.4) versus the average from the numerical analyses, where there is a clear over prediction of the settlement and under prediction of the residual rotation. The peak foundation rotation is shown in Figure 7.13 (c), where the rotation was slightly under predicted especially for low levels of rotation. The last plot, Figure 7.13 (d) shows the level of non-linear foundation behaviour to give an indication of the level of non-linear behaviour.

What is immediately clear from the plot in Figure 7.13 is that the level of foundation deformation is quite small, which is promising from a design point-of-view, as there were no direct limits imposed on the level of foundation rotation. The maximum settlement and residual rotation were approximately 20mm and 1.4mrad respectively. While the design rotations for the buildings were all well less than 1%; it would be expected that for bridge pier structures and other buildings with very stiff superstructures, the foundation peak rotation would be much larger and therefore the residual deformation levels may reach unacceptable levels. Also if the design hazard spectrum did not have such a low displacement plateau then larger drifts would have been reached.

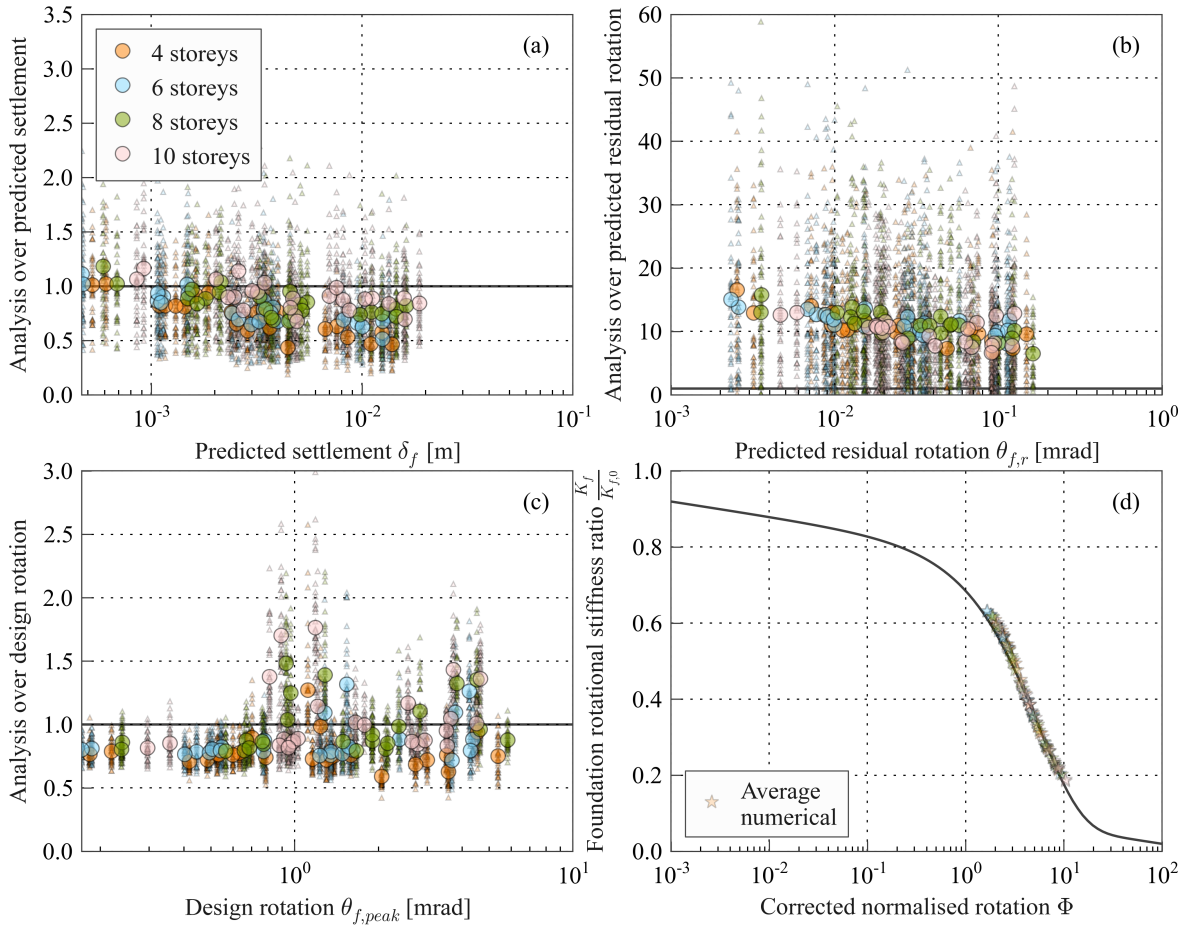

Figure 7.13: Predicted versus numerical residual foundation deformations

Predictor residuals for SFSI-induced settlement

Figure 7.14 illustrates the trends in the data for the ratio of average to predicted SFSI-induced settlement. There are several interesting trends, and just as important, there are several parameters showing no trend. The peak rotation (a), initial period (c) and ductility (h) showed strong trends, while the normalised height (d), normalised stiffness (e) and pseudo uplift angle (f) all showed no trend. The trend with peak rotation indicated that at low levels of rotation the settlement is slightly under estimated while at large rotations it is over estimated, the change in settlement behaviour for the non-linear structure may be due different small cycle behaviour or some change in behaviour due to residual deformations. Given that the under estimation only occurs at for very low levels of settlement the predicted settlement expression was not adjusted to account for this effect.

The trends with the initial period and ductility, indicated that for shorter period buildings and large ductility buildings there was a greater under prediction of settlement; unfortunately the DDBD procedure results in co-linearity between the initial period and the level of ductility, where tall buildings result in longer periods of vibration and lower design ductilities. Due to

this co-linearity it is difficult to determine the causative relationship from the data, however, given that the initial vibrational period was already accounted for in the prediction relationship, the cause is most likely due to the ductile behaviour and not some additional trend with the initial period. In fact, as the ductility approaches 1.0 the ratio of estimated displacement to predicted displacement approaches 1.0. It could be expected that the non-linear behaviour of the superstructure causes an elongation of the natural period of vibration and more importantly absorbing more energy during each cycle so reducing the amount of free vibration oscillations, which in turn results in less settlement.

The normalised parameter $\frac{PH}{K_{MM}}$ in plot (g) was as a gauge of the influence of P-delta forces, where the parameter represents the change in effective stiffness due to P-delta forces divided by the lateral SDOF stiffness from foundation rotation. The P-delta forces showed almost no trend with the SFSI-induced settlement.

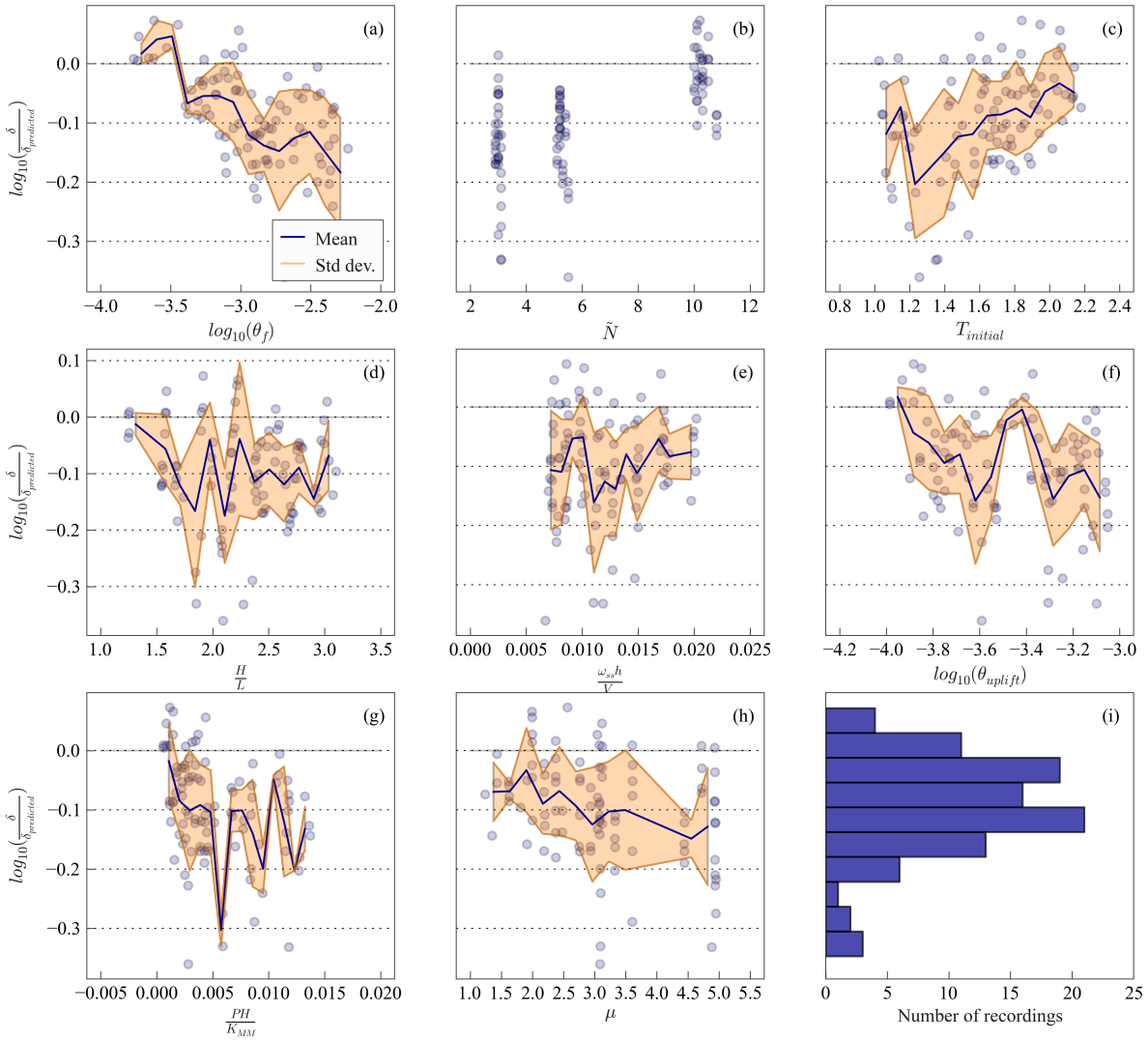

Figure 7.14: Predictor residuals for SFSI-induced settlement

Given that nearly all of the average settlement values were less than the predicted value, it in-

dicated that the worst case scenario for foundation settlement occurs when the superstructure remains elastic; thus the design expression (Equation 7.3) developed in Section 7.6.1 provides a suitable estimate to the level of settlement.

Foundation residual rotation

Given that the residual rotation was severely under predicted by approximately a factor of ten, the previous expression was proven to be a poor choice. The major difference between the two sets of analyses is the consideration of P-delta effects, which causes a ratcheting of the foundation rotation once permanent rotation has occurred in one direction. This major discrepancy in results between the two analyses highlights the importance of making sure the numerical model can capture all of the important loading and deformation mechanisms.

A new expression was fitted to the results and is given in Equation 7.5.

$$\frac{\theta_{f,r}}{\theta_{f,d}} = 0.025 log_{10}(\theta_{f,d}) + 0.30 \tag{7.5}$$

The error between the analysis results and the new expression can be seen in Figure 7.15. The results are less skewed then for the first set of analyses as the P-delta effects meant that small permanent rotations were more likely to amplify than cancel out. There is considerable scatter in the results with a standard deviation of normalised residual rotation calculated as 0.031. The largest errors in the residual rotation occurred for the most heavily loaded footings (plot b), the trend is insignificant but demonstrates that heavily loaded footings have a greater tendency for residual rotations. The other interesting trend can be seen in plot (h) where at low levels of ductility the residual rotation was less than calculated from the expression. This may be due to an amplification in residual deformations when structures behaviour non-linearly and have a residual drift that causes further residual rotation in the foundation. The trend was not strong enough to capture but suggests that the above expression may be different for other structures that have a greater propensity for residual drift.

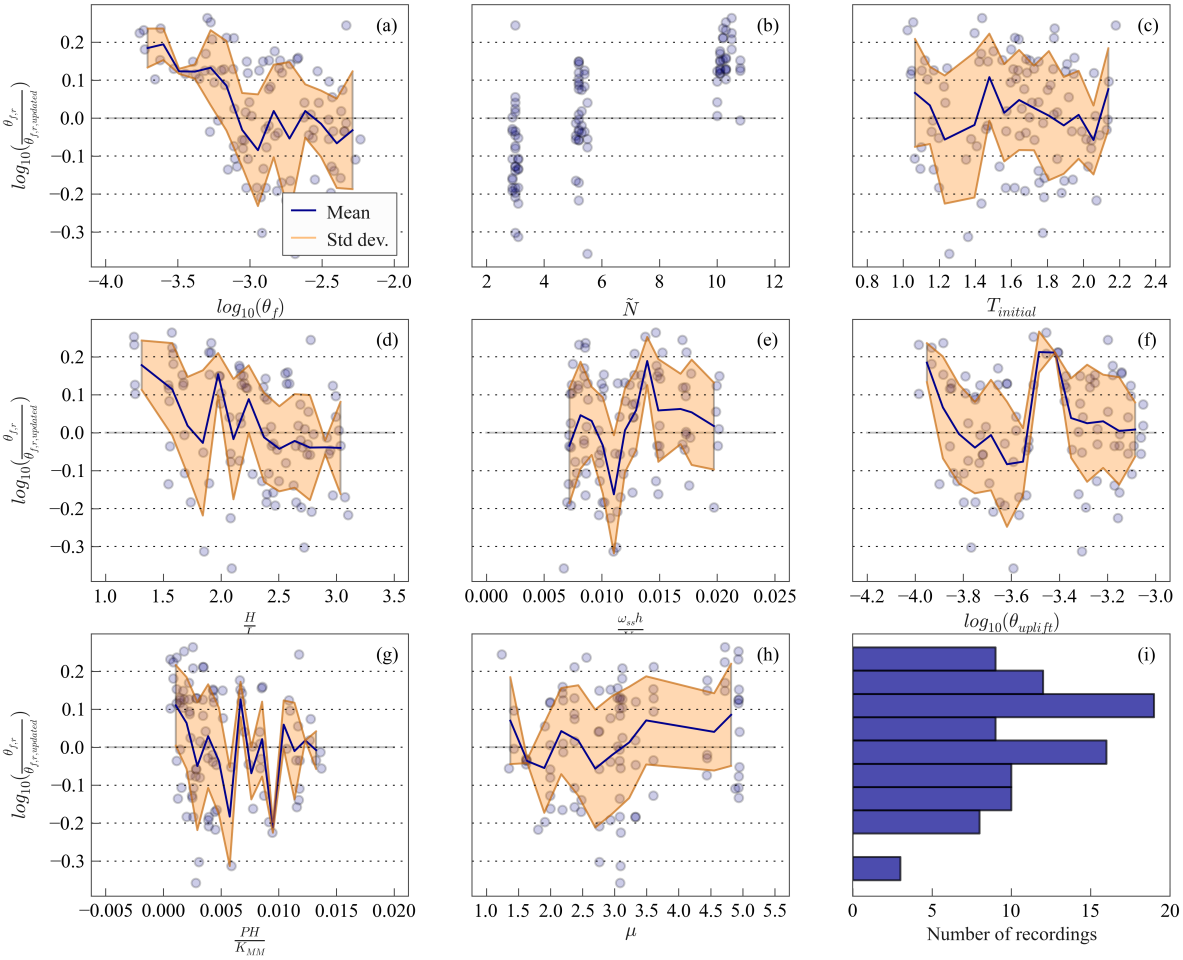

Figure 7.15: Predictor residuals for new residual rotation expression

7.8 Limitations of the results

The expressions developed in this chapter account for the major influences on the level of SFSI-induced settlement and residual rotation, however, there are several limitations to the expressions. The expressions were based on results from a numerical modelling technique that was calibrated against only a few experimental tests (see Chapter 5), it could be expected that different soils and improvements to the modelling techniques could lead to different predictor constants for the derived relationships. The one of the most important parameters that is missing in the expressions is the relative density, which was recognised in experimental tests as influential (Gajan et al., 2005). The limited number of experimental tests that were used to calibrate the macro-element model meant that the relative density was not considering as parameter to modify the behaviour. The other parameter that needs further investigation is the duration of the ground motion, it is expected that the longer duration earthquakes would lead to more residual deformations since there would be more cycles of foundation rotation. The expressions were also only for simple supported structures and validated for concrete

wall buildings. The behaviour may be different for different foundation and structural typologies.

The main purpose of this chapter is to provide expressions for the prediction of a soil-foundation interface that behaves the same as the macro-element model. By understanding the key parameters influencing the residual rotation and SFSI-settlement, more refined experimental tests and advanced numerical modelling studies can be conducted that focus on these influential parameters. These expressions can be considered preliminary and provide a guide to the engineer, however, given their limitations it would be wise to use a significant margin of safety in a design considering these expressions.

To better understand the accuracy of these expressions they can be compared to experimental values from literature. Figure 7.16 shows the experimentally measure SFSI-induced settlement versus the value that would be obtained using Equation 7.3 and assuming $T_{initial} = 1.0s$ and $log_{10}(\theta_f) = -2.0$ to provide a simple comparison.

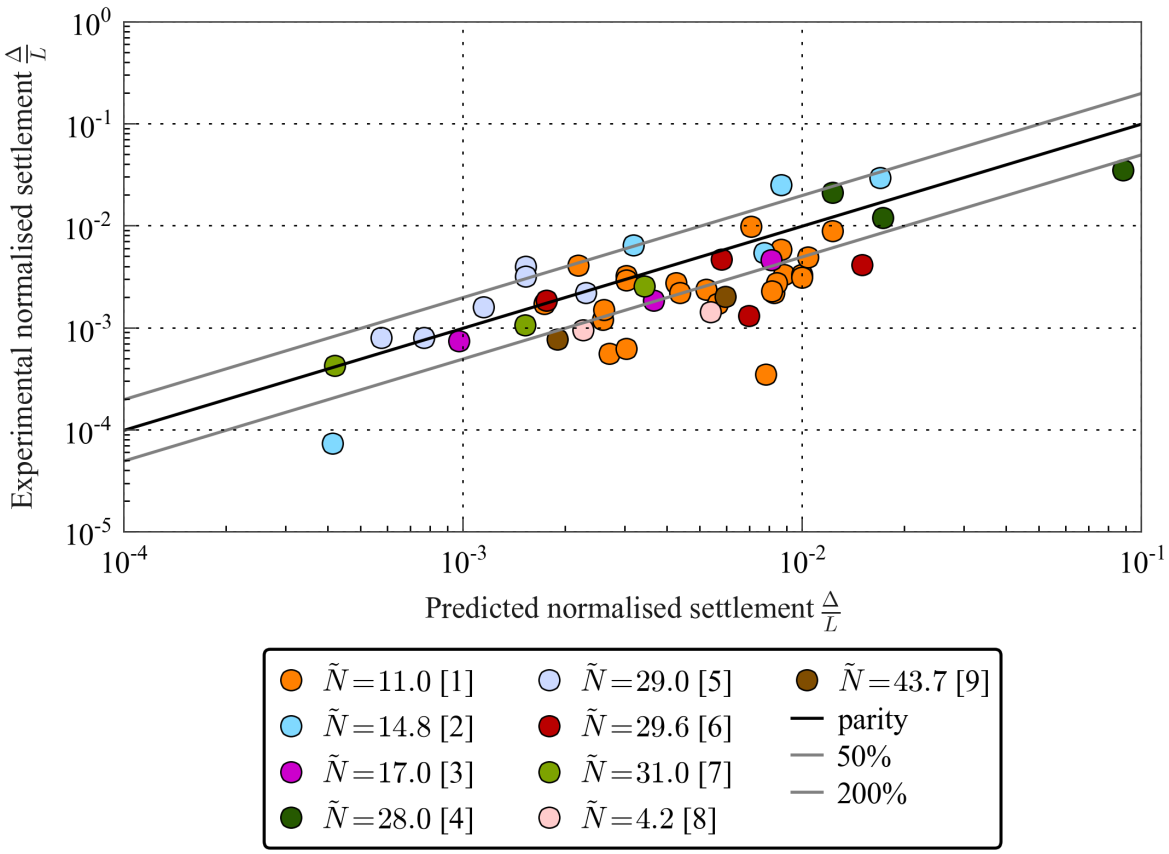

Figure 7.16: Assessment of the SFSI-induced settlement expression

The expression provides a reasonable estimate to experimental values with the majority of the experimental data points falling within half and double of the calculated value.

The exp For SFSI-induced settlement the equation from Gajan et al. (2005) can be used when

assuming the foundation goes through two complete cycles to peak. The equation from Deng (2012) can also be used to predict settlement, where the cumulative plastic rotation can also be considered as equal to two full cycles to peak (as recommended on page 182 in Deng (2012)). The results are compared in Table 7.4 against the newly developed expression (Equation 7.3), where the initial period of the system was taken as 1.5s and the peak rotation was taken as 1%. From the tabulated results it can be seen that all three expressions are reasonably consistent. The new settlement equation provides a means of calculating the settlement based on the vibrational period of the building and does not require the assumptions of two full cycles to peak rotation. The new equation also has the advantage of encompassing the effects of peak foundation rotation and different axial load ratios in a single expression, without the need to look up and interpolate between coefficients. Finally, the equation was derived through a rigorous statistical procedure demonstrating that other potentially influential factors such as structural ductility and P-delta effects did not results in increased levels of settlement.

Table 7.4: Comparison of SFSI-induced settlement divided by foundation length expression to existing literature

Axial load ratio	Equation 7.3 mm	Gajan et al. (2005) mm	Deng (2012) mm
2	0.009	0.015	0.016
3	0.007	0.01	0.016
5	0.005	0.005	0.011
10	0.004	0.001	0.005

The new residual rotation ratio (Equation 7.5) was compared to the recentring ratio from Deng (2012) (Equation 7.1) in Figure 7.17 and experimental residual rotation and peak rotation values. The expression by Deng (2012) gives considerably higher values of residual rotation ratio than the new expression, especially for heavily loaded foundations. For design purposes it would be prudent to use the more conservative estimates from Deng (2012), but the new residual rotation expression will be used throughout this thesis to maintain consistency with the numerical model, which allows further influences to be identified.

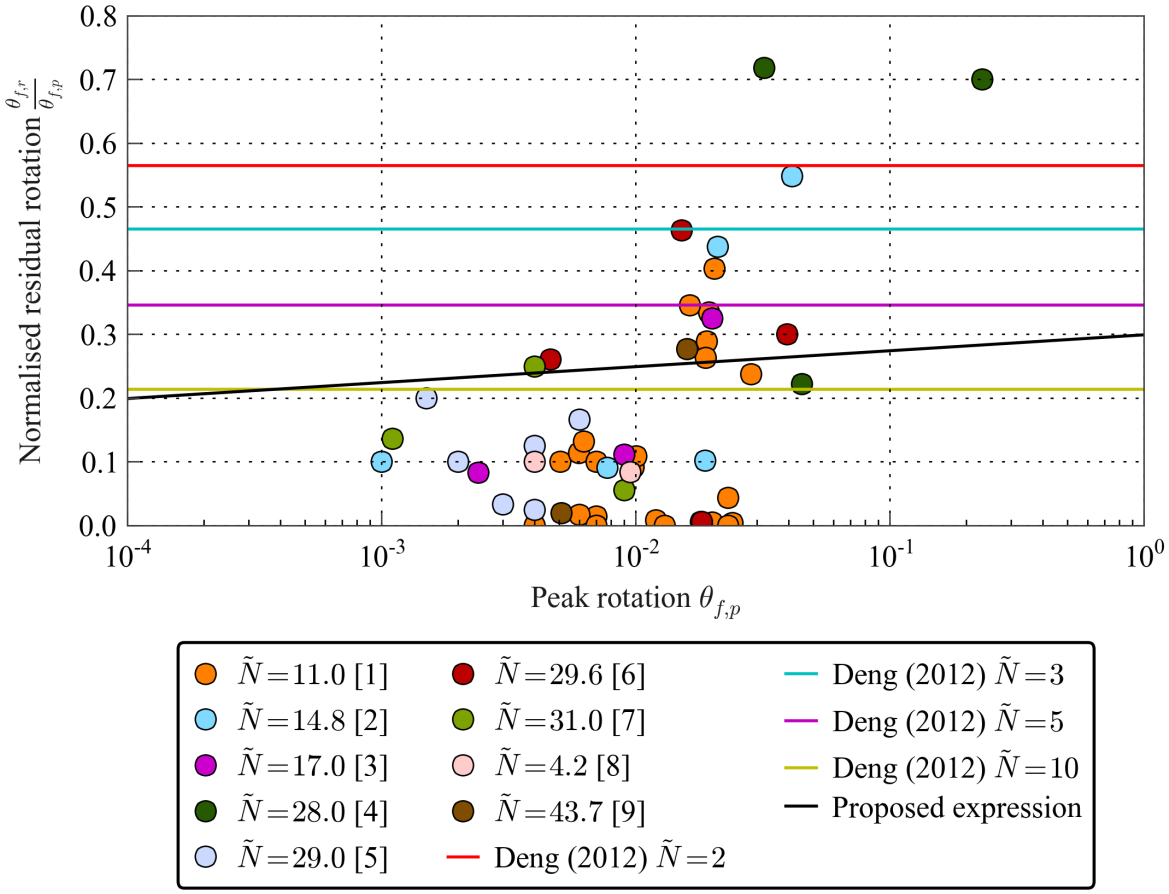

Figure 7.17: Assessment of the residual foundation rotation expression

7.9 Updates to design procedure

This section briefly explains the updates to the design procedure due to the findings in this chapter, the flowchart presented in Chapter 6 Figure 6.21 can be used as a reference to view the updates in Figure 7.18, which are shown in bold.

The major updates include:

- Considerations for foundation performance levels
- Expressions to calculate SFSI-induced settlement and foundation residual rotation

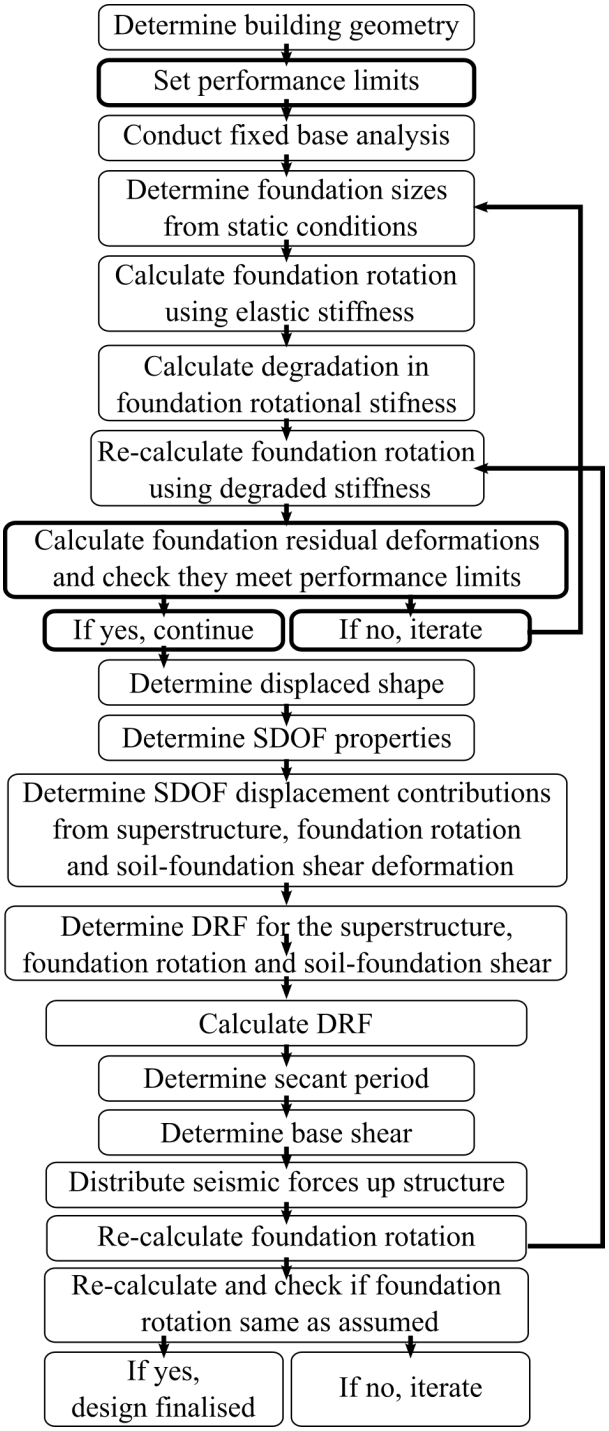

Figure 7.18: Modified direct displacement based design procedure considering non-linear SFSI

7.10 Conclusion

This chapter develops relationships between the peak foundation rotation and residual foundation deformations to allow the prediction and even control the level of foundation residual deformations in design. A mechanism approach was utilised to understand what the driv-

ing factors are behind the occurrence of SFSI-induced settlement and residual rotation. The findings from previous research helped guide a multiple parameter regression analysis on an extensive set of numerical results from simple SDOF analyses. The regression analysis led to simple expressions for both of the residual deformation parameters.

The predictive capabilities of the expressions were examined against a set of numerical results where the input SDOF models were based on a DDBD procedure that directly included SFSI and P-delta effects. The non-linear response of the superstructure, resulted in reduced SFSI-induced settlement and demonstrated that the developed settlement expression was suitable from the design of concrete wall buildings. Conversely the P-delta effects and non-linear response in the superstructure resulted in increased residual rotation, highlighting the importance of having a model that can capture all of the force and deformation mechanisms. A new expression was developed based on the improved numerical model results.

The developed expressions were compared against experimental results and other expressions in literature. The settlement expression provided a very good approximation to the majority of available data, while the residual rotation expression provided a good estimate to some of the experimental data but provide lower levels of residual deformation then the expression from Deng (2012) when the footing was heavily loaded.

Using the provided expressions and suitable limits on foundation residual deformations, engineers can be better informed about what level of foundation deformation is acceptable and not be constrained to unfounded criteria such as limiting foundation rotational stiffness degradation or preventing foundation uplift.

Chapter 8

Prediction of super-structure residual drift

8.1 Introduction

The most pertinent goal of the structural engineer is to prevent collapse of the structure. This overarching goal has served the engineering community well, however, recent events such as the Christchurch earthquake sequence (2010-2012) resulted in major economic losses due to buildings with large residual deformations being demolished after the events.

The commonly adopted 'ductile design' philosophy offers a suitable methodology for the prevention of collapse and can result in considerable cost savings during construction, due to designing for lower than elastic design loads; however, it ignores the fact that inelastic action can result in residual deformations. If the residual deformations are excessive, such that the building is close to incipient collapse, the cost of repair is too large, or if functionality of the building is affected, then the building may need to be demolished. Even moderate post event residual deformations are undesirable, as research has shown that occupants living in houses with a tilt larger that 1/100 rad are significantly more likely to suffer from insomnia (Keino and Kohiyama, 2012).

In many cases it would be unreasonable to design the structure to remain elastic; however, there are many ways of controlling the residual deformations of inelastic systems, including the use of rocking foundations (Liu et al., 2013), ductile jointed connections (Pampanin, 2005) and additional elastic structural systems (Pettinga et al., 2007). If engineers continue to focus on collapse prevention and limiting peak drifts, the economic loss seen in Christchurch is doomed to be repeated.

With the promotion of residual deformations as a performance measure (JRA, 1996; Kawashima et al., 1998; Christopoulos and Pampanin, 2004), there have been several attempts to predict the level of residual deformations. Studies by MacRae and Kawashima (1997) highlighted the influence of the post-yield stiffness ratio (PYSR) (ratio of post-yield stiffness to initial elastic stiffness) of bilinear SDOF systems, on the amplitude of residual displacements. The PYSR can be strongly influenced by P-delta effects, and can result in a negative post-yield stiffness, leading to large residual deformations.

Christopoulos et al. (2003) investigated different hysteretic behaviours and recognised that the residual displacements were highly sensitive to the unloading stiffness.

Ruiz-García and Miranda (2006a) investigated residual drifts in multi-storey steel frames. . The results were given as a ratio of the residual inter-storey drift to the peak inter-storey drift and increased with more storeys and with greater flexibility of the structure. Ruiz-García and Miranda (2006b) also recognised the post-yield stiffness and the unloading stiffness as important parameters in the estimation of residual deformations, while parameters such as earthquake magnitude and distance to source were not strongly influential.

Pampanin et al. (2002), Pampanin et al. (2003) and Christopoulos and Pampanin (2004) in-

vestigated four framed building models having 4, 8, 12, and 20 stories when subjected to two suites of 20 earthquake ground motions, and suggested a preliminary multi-degree-of-freedom (MDOF) multiplier to apply to single degree-of-freedom (SDOF) residual deformations to account for additional complexities, with residual drifts being magnified up to three times for MDOF frame systems.

Although not comprehensive, Figure 8.1 presents the results from previous studies that have been extracted either directly from published charts or published equations to provide a indication of the general trend of the behaviour between peak displacement, ductility and residual displacement.

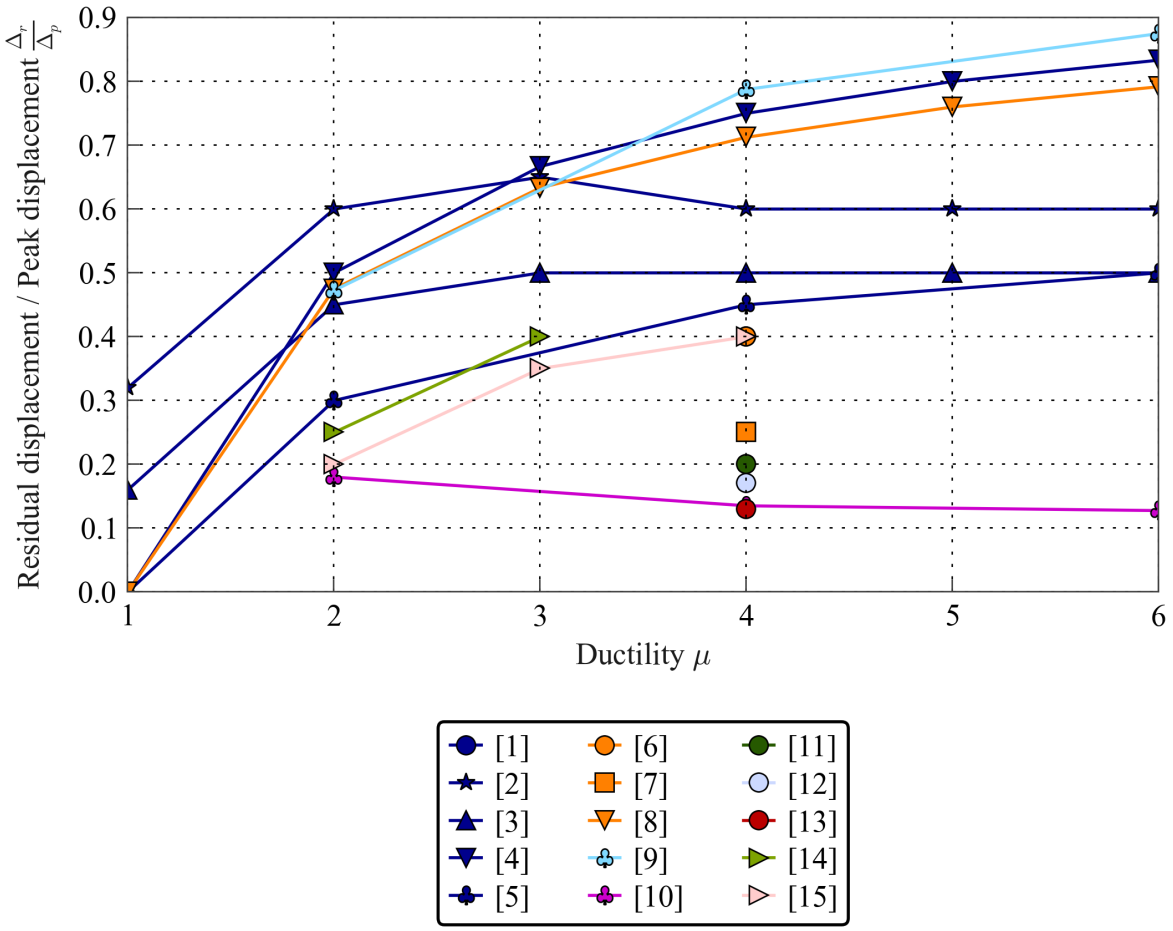

Figure 8.1: Results from previous studies on residual deformations (references in table below)

1	Bi linear (a=0.00)	SDOF	Christopoulos et al. (2003)
2	Bi linear (a=0.00)	Multi-storey frame	Abdolahi Rad (2015): 84th percentile values, Assumed $\mu = R$
3	Bi linear (a=0.00)	Multi-storey	Ruiz-García and Miranda (2006a): Assumed $\mu = \eta$
4	Bi linear (a=0.00)	SDOF	Theoretical maximum:
5	Bi linear (a=0.00)	SDOF	Kawashima et al. (1998)
6	Bi linear (a=0.05)	SDOF	Christopoulos et al. (2003)
7	Bi linear (a=0.05)	SDOF	Christopoulos and Pampanin (2004)
8	Bi linear (a=0.05)	SDOF	Theoretical maximum
9	Bi linear (a=-0.05)	SDOF	Kawashima et al. (1998)
10	Bi linear (a=0.1)	SDOF	Kawashima et al. (1998)
11	Takeda (a=-0.05)	SDOF	Christopoulos et al. (2003)
12	Takeda (a=0.00)	SDOF	Christopoulos et al. (2003)
13	Takeda (a=0.05)	SDOF	Christopoulos et al. (2003)
14	HSS (k3/ky=-0.3)	SDOF	Borzi et al. (2001)
15	HSS (k3/ky=-0.2)	SDOF	Borzi et al. (2001)

It is well recognised that the evaluation of residual displacement is very important in determining the economical feasibility and overall life-time performance of a building, therefore it is paramount to be able to predict the expected level of residual deformations during design.

This chapter first provides an overview of performance levels for superstructures looking at both peak and residual deformations to provide context for the performance-based design procedure developed in this dissertation. The remainder of the chapter is focused on the prediction of residual deformations. The study is not intended to provide a comprehensive study into the topic of predicting residual deformations for all building types but is particularly interested in accurately predicting the residual drift of concrete wall buildings and how deformations at the foundation level can modify the behaviour. The overall aim is to provide a simple design expression that can be included in an integrated performance-based design of building-foundations systems (Chapter 11).

8.2 Superstructure performance levels

The limitations on superstructure peak drift are governed by material strains, non structural elements drift limits, pounding against adjacent structures and toppling. Different design standards specific different requirements on each of these parameters depending on the material and perceived level of risk.

The limits on material strains (Table 8.1) and non-structural drifts (Table 8.2) from (Sullivan

et al., 2012) have been used in this dissertation as they are explicit and are directly linked to the performance levels used in this dissertation:

- Level 1: Immediate occupancy and functionality
- Level 2: Repairable
- Level 3: Collapse prevention

Table 8.1: Material strain limits (Sullivan et al., 2012)

Material	Level 1	Level 2	Level 3
Concrete	0.002	Eq. 8.1 < 0.02	Eq. 8.1 < 0.03
Steel rebar	0.015	$0.6\epsilon_{su} < 0.05$	$0.9\epsilon_{su} < 0.08$

Where ϵ_{su} is the ultimate steel strain defined by the manufacturer. Equation 8.1 defines the confined concrete compressive strain limit (ϵ_c) from Mander et al. (1988) (see Mander et al. (1988) for details):

$$\epsilon_c = 0.004 + 1.4\frac{\rho_v f_{yh}\epsilon_{su}}{f'_{cc}} \tag{8.1}$$

Table 8.2: Non-structural elements drift limits (Sullivan et al., 2012)

Type	Level 1	Level 2	Level 3
Brittle non-structural elements	0.4%	2.5%	No limit
Ductile non-structural elements	0.7%	2.5%	No limit
All elements detailed to sustain building displacements	0.010	0.025	No limit

The residual drifts limits stated were also taken from Sullivan et al. (2012) are as stated in Table 8.3.

Table 8.3: Residual drift limits (Sullivan et al., 2012)

Type	Level 1	Level 2	Level 3
Buildings	0.2%	0.5%	No limit

Alternative performance criteria from Uma et al. (2010) based on Pampanin et al. (2002) and the Japanese Guidelines (cite AIJ, 2004) are given in Table 8.4. However, this set of performance criteria were not used in this dissertation as the did not directly correspond to the performance levels specified in Table 3.1.

Table 8.4: Drift limits from Uma et al. (2010)

Type	Fully operational	Operational	Life Safety	Near Collapse
Peak drift (%)	≤ 0.5	≤ 1.0	≤ 2.0	≤ 4.0
Residual drift (%)	≤ 0.2	≤ 0.4	≤ 0.6	≤ 1.0

8.3 Residual drift of fixed base concrete wall SDOF

This section develops predictive equations to quantify the level of residual drift for fixed base concrete wall structures using equivalent non-linear SDOF models. The average residual drift is correlated to the average peak drift to allow the residual drift to be predicted using the design peak drift in a Direct Displacement based Design (DDBD).

8.3.1 Input parameters

The input parameters for the numerical model were based on the equivalent SDOF models developed by designing a series of wall buildings using DDBD (Priestley et al., 2007). The inputs for the design of the series of wall buildings are summarised in Table 8.5. The inputs were chosen to be realistic while still providing a considerable range on height and level of ductility. The walls were designed twice, first with no P-delta considerations and secondly with an adjustment to the base shear to consider P-delta effects as suggested by Priestley et al. (2007) using Equation 8.2.

$$V_{base} = K\Delta + C\frac{P\Delta_d}{H_{eff}} \tag{8.2}$$

Table 8.5: Wall design inputs

Parameter	Range
Number of storeys	$[4, 5, 6, 7, 8, 9, 10]$
Wall width	0.3 m
Storey heights	3.4 m
Wall height to depth ratio	$[3, 4, 6, 8]$
Number of walls	4
Building length	20 m
Building width	12 m
Soil type	C
Design hazard level	0.4
Live load on floors	3 kPa
Dead load on floors	6kPa
Superstructure inter-story drift (θ_{ss})	0.02
Concrete compression strength (f_c)	30 MPa
Rebar strength (f_y)	300 MPa

8.3.2 Numerical model

The numerical model used in this study was the same as in Chapter 6 Section 6.6.2 except that the superstructure element was connected to a fixed base rather than the soil-foundation macro-element. The model is explain again here for completeness. The geometry of the was modelled directly using a lumped horizontal mass (M_{SS}) attached to an elastic zero-shear beam with an inelastic hinge at the base set at 5% of the beam length (Figure 8.2). The hinge hysteretic behaviour was modelled using the Modified Takeda rule with 'Takeda thin' properties ($\alpha = 0.5$, $\beta = 0.0$, NF = 1.0, KKK = 2). The initial stiffness was determined through Equation 8.3 where $K_{ss,eff}$ is the secant superstructure stiffness (Equation 8.4), V the base shear and r is the PYSR of the superstructure. The hinge PYSR was calibrated so that the PYSR for lateral deformation of the structure would match the chosen value of PYSR of the superstructure (Equation 8.6, where LHR is the ratio of hinge length to beam length). The superstructure PYSR is an important parameter in determining residual drifts and as a benchmark was taken as 0.05 as suggested for wall buildings from Priestley et al. (2007), but was also varied to 0.00 and -0.05. The yield displacement was taken from Equation 8.5.

$$K_{ss} = \frac{K_{ss,eff}\mu}{1 + r(\mu - 1)} \qquad \mu \geq 1.0 \tag{8.3}$$

$$K_{ss,eff} = \frac{V}{\Delta_{ss}} \tag{8.4}$$

$$\Delta_y = \frac{\Delta_{ss}}{\mu} \tag{8.5}$$

$$PYSR_{hinge} = \frac{3r(1 - LHR)^2 \times LHR}{1 - r} \tag{8.6}$$

A linear rotational dashpot (C_{SS}) was set at 5% of critical damping between the superstructure and the fixed base to capture the viscous damping of the superstructure. A rotational dashpot was used as opposed to a translational dashpot or a global damping rule to maintain consistency with the numerical model that considered SFSI in Section 8.4, where it was essential to isolate the velocity to only that from the superstructure deformation. The other advantage of a rotational dashpot is that it reduces its effect as the structure behaves inelastically, due to the change in the relationship between displacement and rotation of a cantilever. As the hinge becomes non-linear the relationship between rotation and displacement changes from $\theta = 3\Delta/2H$ for a linear cantilever to close to $\theta = \Delta/H$ post yielding, thus providing a reduction to two-thirds for the effective damping coefficient C. The decrease in the effective damping coefficient is similar to the decrease for Rayleigh tangent stiffness proportional damping, where the damping co-efficient reduces to the square root of the post-yield stiffness so $\sqrt{0.05} = 22\%$.

The consideration of P-delta effects was consistent with the designs, where the designs that ignored P-delta effects were assessed with no P-delta effects and vice versa.

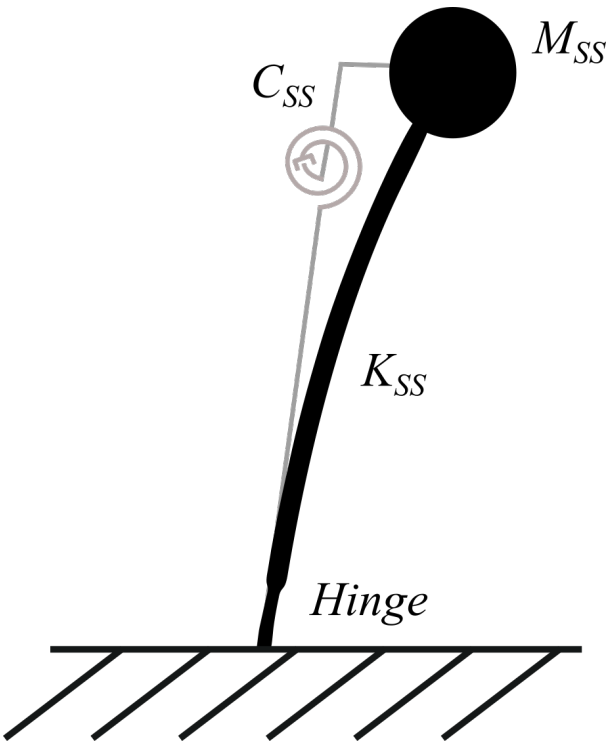

Figure 8.2: Fixed base SDOF numerical model

8.3.3 Ground motions

The ground motion set used for the analyses was identical to that used in Chapter 6 Section 6.6. The records were scaled and selected to give the smallest normalised least squared variation from the design spectrum between periods of 0.4 s and 4.0 s for the NZS 1170.5:2004 (2004) site class C. The motions were scaled to match the spectra for a Z factor of 0.3, equal to that used in the design.

8.3.4 Results

Peak drift

The intention of the relationship between the peak drift and the residual drift was to allow the prediction of residual drifts from the design peak drift, thus the accuracy of the design peak drift was investigated first.

Figure 8.3 shows the average peak drifts from the 40 ground motions over the expected drifts from the design procedure, for all of the fixed base models. Note that the design drifts are a lot lower than the design inter-storey drifts given in Table 8.5 as the design drift here is the SDOF design displacement divided by the effective height.

While only the numerical models with PYSR of 0.05 were consistent with the stiffness as-

sumptions made in the DDBD procedure, the analysis drifts from all of the models were close but consistently less than the design values. There is a clear trend seen with all models where the ductility is over predicted as ductility increases. The trend with ductility is related to the way the viscous damping was implemented in this numerical model setup compared to the model for the development of the displacement reduction factors from Pennucci et al. (2011a). Essentially the difference in damping occurs when the structure behaves inelastically and the original model used Rayleigh tangent stiffness damping which causes a reduction in the damping co-efficient value to 22% of the elastic value, while the current model used a rotational dashpot which only reduces the effective damping coefficient to 67%.

The discrepancy in the displacements is very minor (only 10% at a ductility of six) and is not of any concern given that modelling of viscous damping is still one of the most widely debated topics in the dynamic modelling of non-linear structures.

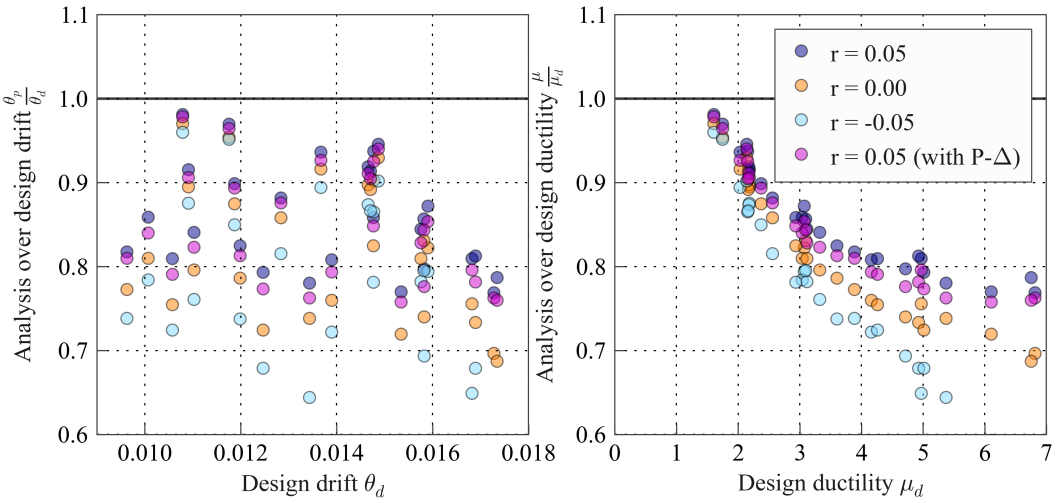

Figure 8.3: Accuracy of the displacement prediction from DDBD

Given that there is a slight bias in the results, especially for the PYSR not equal to 0.05, the average peak drift from the analyses was used as opposed to the design peak drift when determining the residual drift to peak drift ratios.

Residual drift

Given that the residual drift strongly depends on the peak drift, the residual drift ratio (ratio of residual drift to peak drift) (RDR) was determined for all analyses. The RDRs for all four fixed based studies are presented in Figure 8.4, where for the no P-delta cases, there is a clear increase in RDR for a decrease in the PYSR. The dependance on PYSR is similar to what was observed by MacRae and Kawashima (1997) for bi-linear systems, however, the dependance is not as strong for the Takeda-thin hysteretic behaviour.

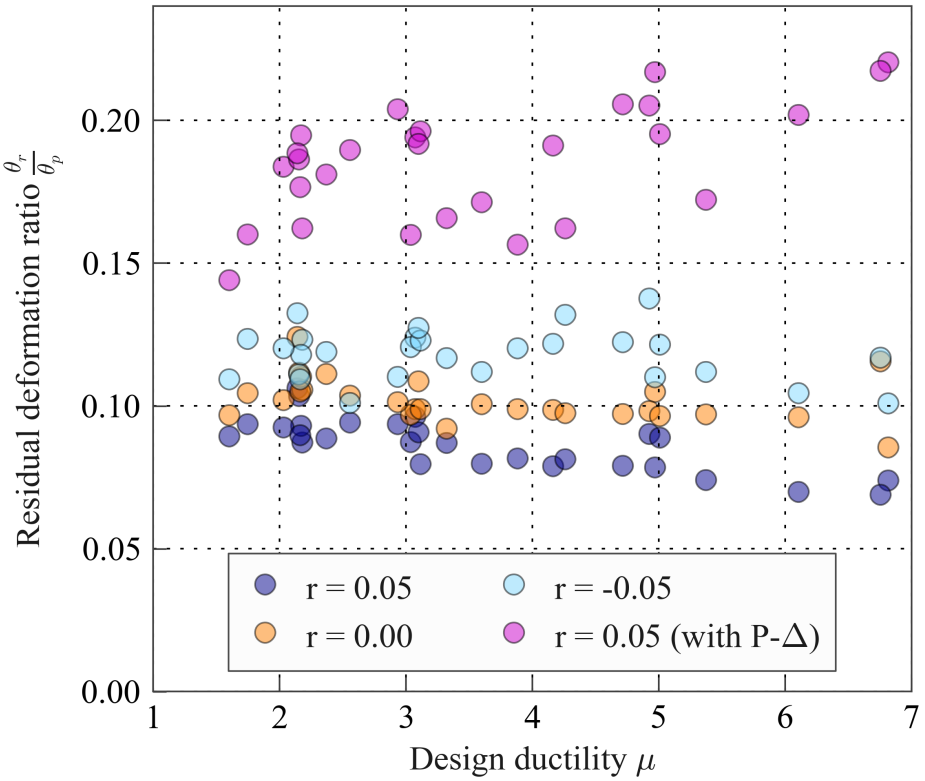

Figure 8.4: Ratio of average residual drift to average peak drift

The results from the case where P-delta effects were included showed some dependence on the ductility and far larger variation in the RDR values. P-delta effects cause two major modifications to the hysteretic behaviour of the structure. The first modification can be considered as a change to the PYSR (Figure 8.5), where the effective PYSR (r_e) can be calculated through Equation 8.7, where P is the axial load applied at height, H.

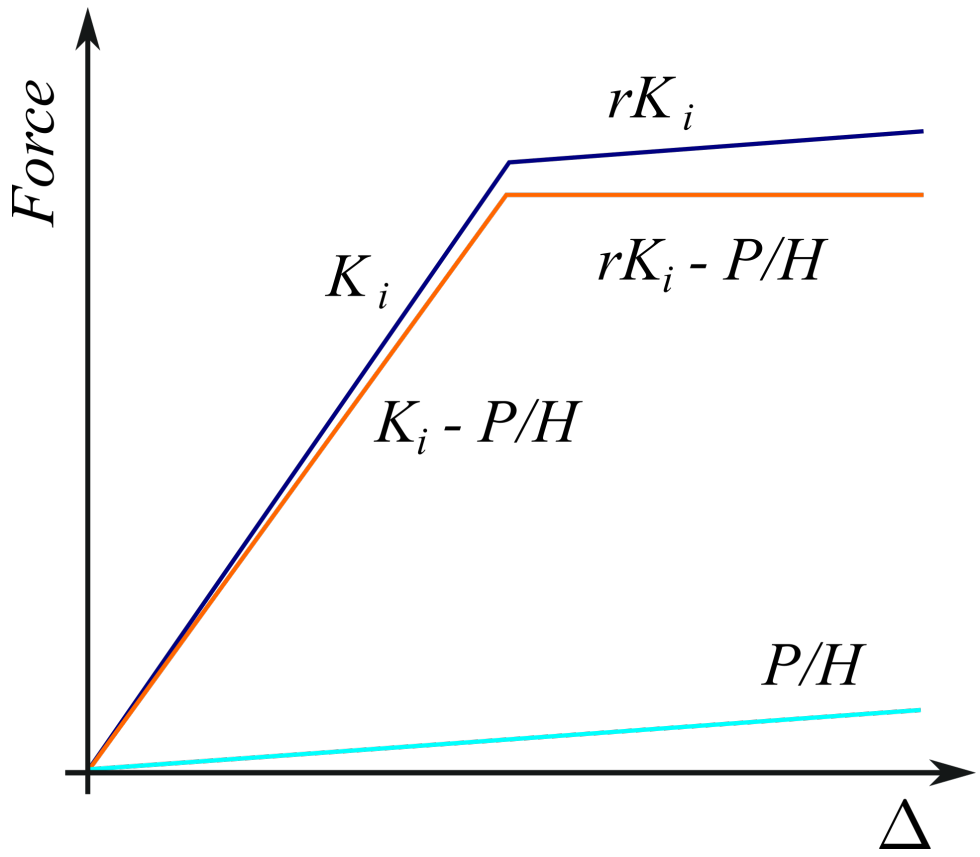

Figure 8.5: The effect of P-delta on the stiffness and post-yield stiffness ratio

$$r_e = \frac{rK_i - P/H}{K_i - P/H} \tag{8.7}$$

Given that the PYSR was independently investigated and did not show a dramatic change to the RDR, it can be expected that this modification was not the major cause of the change in behaviour.

The second modification is due to a change in the unload-reload behaviour of the structure (Figure 8.6). The effect is amplified at small cycles where the structure does not start on its reverse cycle reloading stiffness until after the load has increased to $P\Delta/H$ and starts its forward cycle reloading stiffness when the load drops below this level. The difference in restoring stiffness and the difference in displacement under a single small cycle is clearly seen in Figure 8.6 and it is this effect that accounts for the majority of the increase in the RDR for the P-delta case.

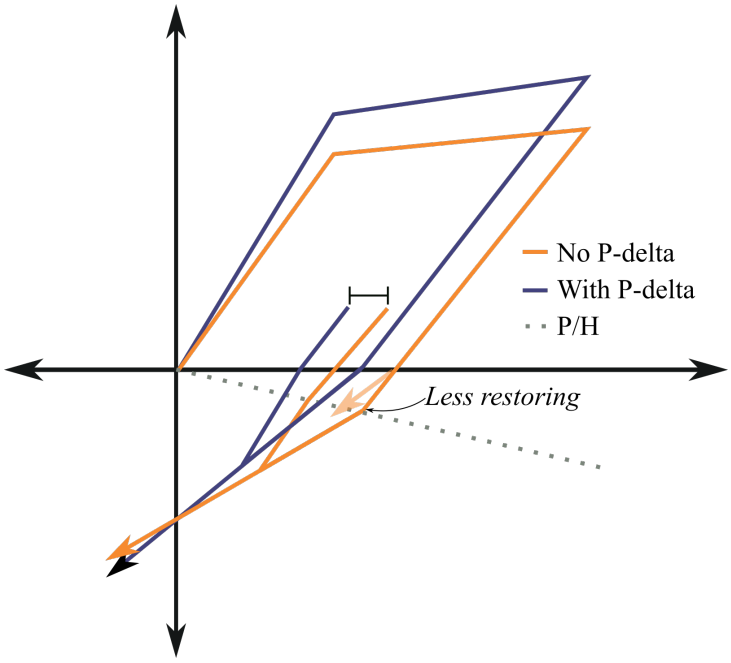

Figure 8.6: The effect of P-delta of the unload-reload behaviour behaviour

Given that the results are from SDOF models using the same hysteretic properties, the two modifications can be accounted for through just two parameters (ductility and pseudo P-delta stiffness divided by the elastic stiffness ($P/(HK_i)$). Multi-linear regression was performed on the results from the P-delta case using the two identified parameters, in which only the results where the design ductility was greater than 2.0 were used.

Figure 8.7 shows the P-delta results along with the expression from the multi-linear regression (Equation 8.8), where the effect of $P/(HK_i)$ has been corrected back to $P/(HK_i) = 0.0$. The expression developed is specific to the Takeda-thin type hysteretic behaviour with PYSR of 0.05, and in fact the modification to the unload-reload behaviour does not exist for a bi-linear type hysteresis.

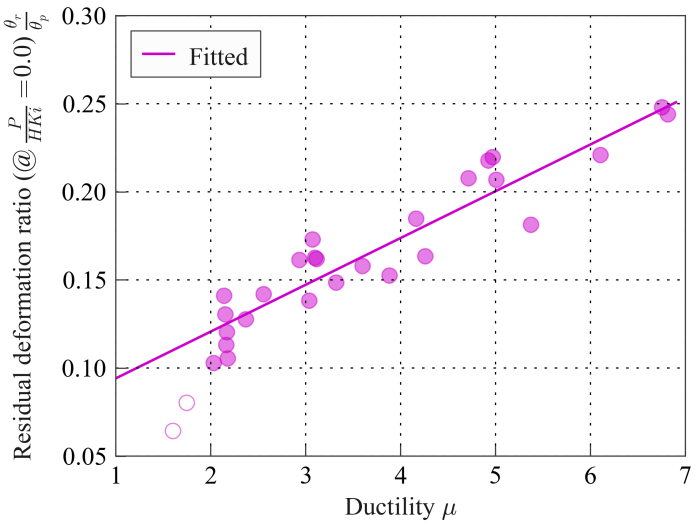

Figure 8.7: The residual deformation ratio considering P-delta effects

$$\frac{\theta_r}{\theta_p} = 0.068 + 0.027\mu + 1.9\frac{P}{HK_i} \tag{8.8}$$

8.4 Effects of SFSI on the residual drift of concrete wall SDOF

This section uses the parametric study results from Chapter 6 Section 6.6 to assess how the effects of deformation at the foundation can modify the ratio of residual to peak drift in concrete wall structures. A full design example can be found in Appendix C. While it is recognised that foundation deformation modifies the superstructure response by extending the vibrational period of the system, typically increasing the overall displacement of the system and potentially causing applied P-delta moments to the superstructure due to permanent foundation rotations, it is unknown whether these modifications would result in a significant change to the expected level of residual deformation.

The building-foundation-soil systems were designed using the Direct Displacement-based Design procedure outlined in Chapter 6 and the inputs and design will not be repeated here. The design and numerical modelling allowed for inclusion of P-delta effects.

8.4.1 Results

Figure 8.8 shows the analysis peak displacement verse the design displacement (a) and the analysis residual displacement divided by the expected residual displacement (b), where the expected residual displacement was determined using the design peak displacement and

Equation 8.8. The peak displacements show reasonably good agreement and their comparison is discussed in depth in Chapter 6 Section 6.6. On inspection of the residual deformations, it appears that the foundation deformations were also well predicted, however, there is considerable scatter in the results at low levels of predicted residual deformation. In fact to understand the influence of SFSI on the residual superstructure deformations we must consider the clear trend between analysis and design for the peak drift, where clearly the slightly over prediction of structural drift at low levels of drift would skew the residual drift as would the under prediction at high levels of drift.

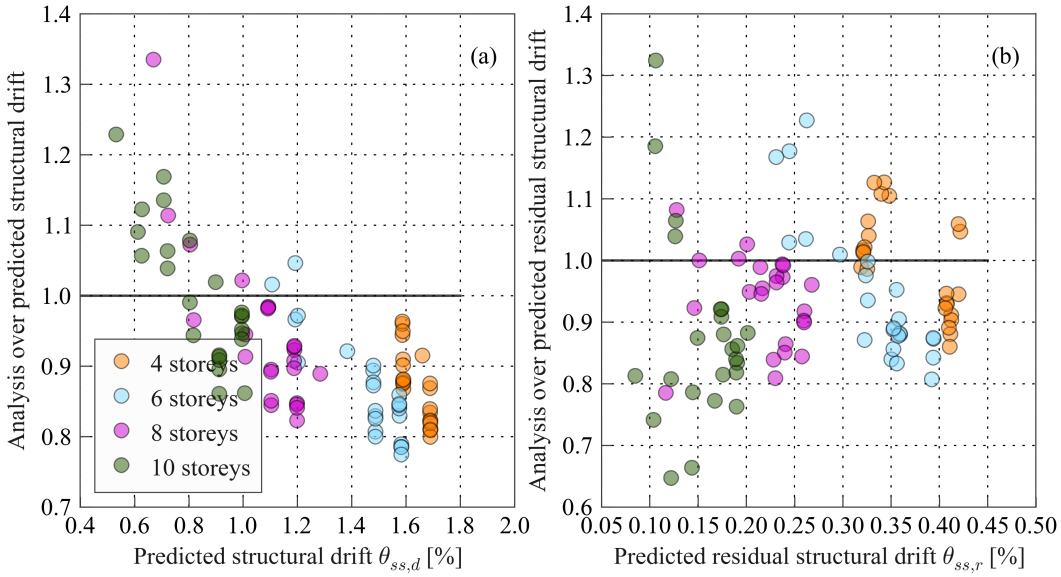

Figure 8.8: Peak and residual superstructure drifts

To remove any bias from the disparity between the design and analysis peak drift, the analysis drift was used to update the residual drift estimates. The results where the design ductility was less than one were also removed as they would be expected to have lower residual drift.

Using the updated set of residual drift predictions the ratio of the predicted to obtained residual drift ratio was plot against against several parameters in Figure 8.9 the influence of the foundation rotation can be seen in plot (a). An increase in foundation rotation leads to an increase in the residual superstructure deformation (approximately $10^{0.08} = 1.20$ @ $\log_{10}(\theta_f) = -2.5$), which may be due to increased foundation residual rotations causing an applied P-delta moment to the superstructure. A simple correction for this effect could be made using a piecewise function, however, the effect is small and therefore it would be a trivial consideration in design. Other small trends were seen with the initial period ($T_{initial}$) in plot (c) and the building effective height to foundation length ratio (H/L) in plot (d), though given that the dispersion was so small the trends did not warrant being considered in the residual drift expression.

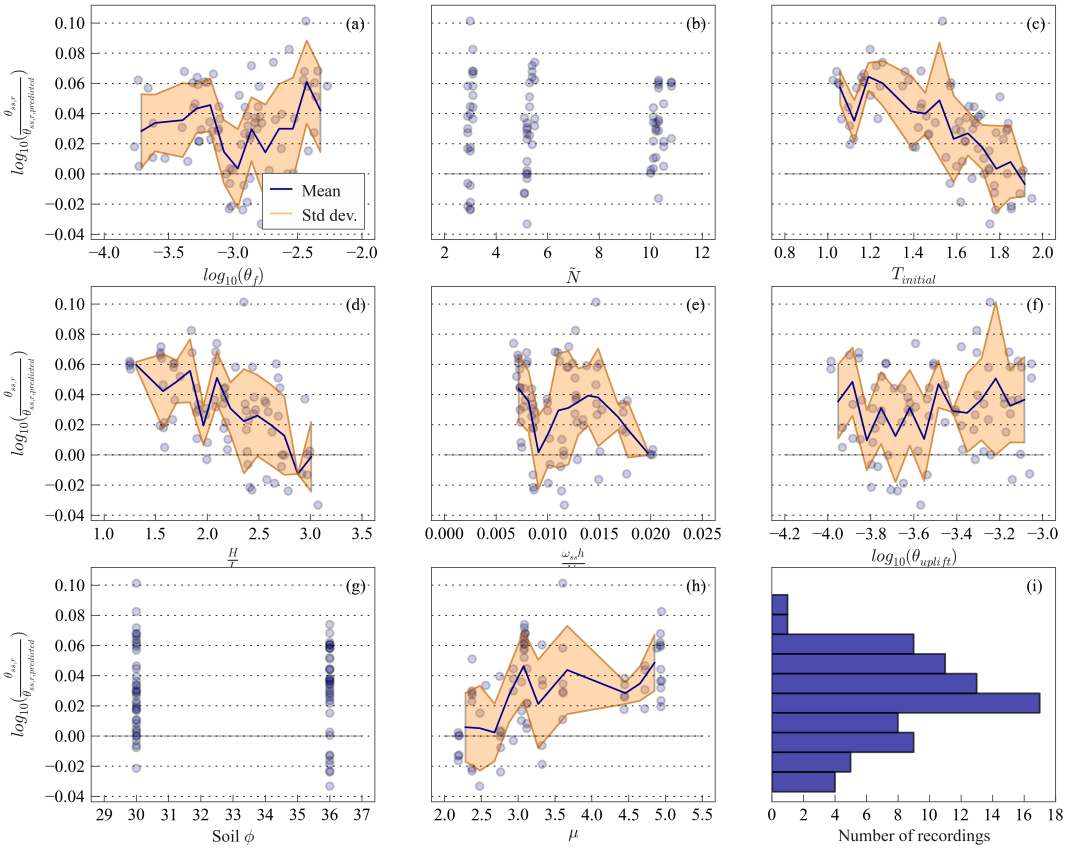

Figure 8.9: Error in the prediction for updated residual superstructure drift

8.4.2 Record-to-record dispersion

Of interest to a designer is the dispersion of the residual drift ratio between different records. Pampanin et al. (2003), Ruiz-García and Miranda (2006b) and Yazgan and Dazio (2011) recognised that the dispersion of residual deformations is greater than that of peak deformations for a given set of earthquake records. It should also be recognised that the dispersion of peak response is usually log-normally distributed (depending on the hysteretic behaviour), while for residual displacements this does not hold true. Figure 8.10 shows that the residual drift for each record from results where the design ductility was greater than or equal to 2.0. The residual drift is normalised by the updated predicted level and it can be seen that points are more dense below the average than above. The 85th percentile is shown on Figure 8.10 as this is equivalent to one standard deviation for normally distributed data and can be taken as twice the predicted value. The dispersion of the residual drift as the residual drift increases also appears to be constant.

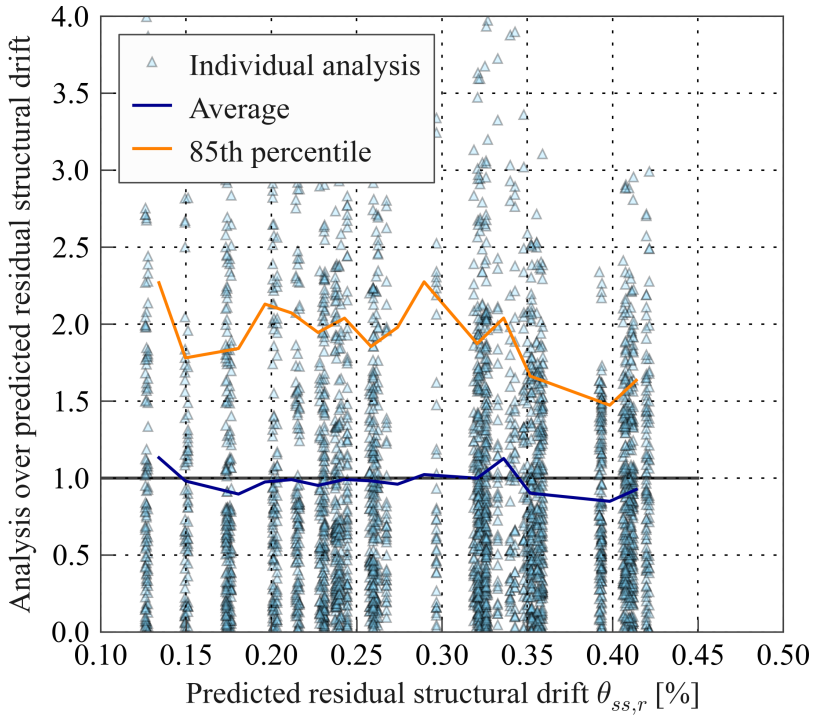

Figure 8.10: The distribution of peak and residual drifts

8.5 Updates to design procedure

This section briefly explains the updates to the design procedure due to the findings in this chapter, the flowchart presented in Chapter 7 Figure 7.18 can be used as a reference to view the updates in Figure 8.11, which are shown in bold.

The major updates include:

- Considerations for superstructure residual performance levels
- Expression to calculate superstructure residual drift

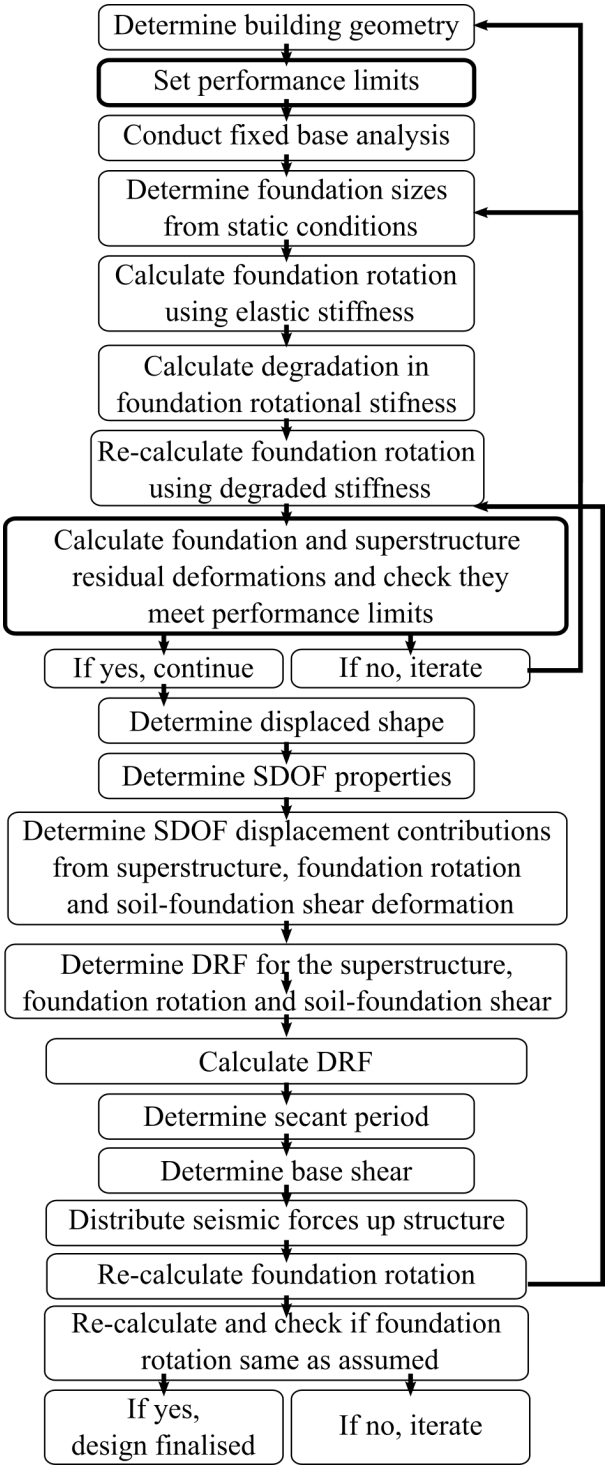

Figure 8.11: Modified direct displacement based design procedure considering non-linear SFSI

8.6 Conclusions

This chapter attempts to quantify the expected level of residual drift in concrete wall buildings using non-linear equivalent single degree-of-freedom systems. The effects of post-yield

stiffness, unload-reload behaviour and P-delta effects were all considered in the development of an expression for fixed based concrete wall buildings. The expression was then used to predicted residual drifts for concrete wall buildings with deformable soil and foundations. The results from the analysis of 96 building-foundation-soil systems subject to 40 ground motions demonstrated at large levels of foundation rotation the ratio of residual to peak drift increases slightly. The increase is expected to be due to permanent foundation rotations causing applied P-delta moments to the superstructure resulting in more residual deformation.

Chapter 9

Influence of SFSI on wall structures

9.1 Introduction

Current research into the effects of soil-foundation-structure interaction (SFSI) has largely been constrained to single degree-of-freedom (SDOF) analysis, mostly to reduce computational effort. The design response spectra for many design codes is also provided as SDOF response spectra, however, it is widely recognised that SDOF models can not model many of the complexities of multiple degree-of-freedom (MDOF) systems (Christopoulos and Pampanin, 2004). In fact, perhaps the most important factors in the design of multi-storey buildings are inter-storey drifts and the distribution of stresses, which by definition, a SDOF model can not capture. The variation in inter-storey drift and stress is highly dependent on the structural type, level of non-linearity and distribution of strength, stiffness and mass, all of which do not exist in a SDOF model. When investigating the effects of SFSI on the performance of structures, a SDOF model can provide useful insights into the level of peak deformations (Chapter 6), residual foundation deformations (Chapters 7 and residual superstructure deformations (Chapter 8), but to quantify the distribution of deformations and stresses in the superstructure the more complex MDOF model must be considered.

Early studies by Jennings and Bielak (1973) into the effects of SFSI on MDOFs showed that the effects of SFSI inertial interaction result in significant decrease in the response of the first mode of a building and a slight decrease in all other modes.

Numerical studies by Bárcena and Esteva (2007) into the effects of SFSI on MDOFs concluded that SFSI effects reduced the ductility in the structure if the structural period (T_s) was shorter than the dominant ground motion period (T_a). SFSI also reduced ductility when T_s exceeded T_a, while an increase in ductility was seen when $T_s \approx T_a$ for structural aspect ratios (building height over building width) of greater than 1.4, and a decrease for aspect ratio less than 1.4. The dependance on aspect ratio was due to radiation damping having a higher contribution for squat structures, resulting in less ductility.

Halabian and Erfani (2010); Halabian and Kabiri (2011) conducted numerical studies con-

sidering two-dimensional frames with generic structural properties, using a sub-structure approach. Their results demonstrated that SFSI had little influence on the reduction factor used to account for a reduction in design loads due to yielding.

Tang and Zhang (2011) conducted a series of time history analyses modelling non-linear shear walls on non-linear foundations. In general the inter-storey drift decreased when the soil-foundation interface was modelled compared to the fixed-based conditions, however, there were cases where an increase was seen.

Ganjavi and Hao (2011, 2012b) highlighted some shortfalls in the SDOF analysis when mapping them to a MDOF response. Studies on shear walls (5 storey, 10 storey, 15 storey) using an equivalent linear soil-foundation macro-element model investigated the difference in response when changing the distribution of strength and stiffness up the structure. These studies showed that the reduction in base shear due to SFSI was influenced by the distribution of strength by about 15%. The reduction in base shear demand from SFSI effects was more prominent in highly inelastic structures and was essentially negligible for low ductility structures. Very uncommon slender structures with a short period of vibration showed an increase in base shear demand for the SFSI case, which was more pronounced at high design ductilities. Ganjavi and Hao (2012a) used the coefficient of variation (COV) of the ductility demand up a shear wall building to determine the effects of SFSI and strength distribution on the building ductility demand. It was shown that SFSI increased the COV across all periods for three different design levels of ductility. Ganjavi and Hao (2012a) also highlighted that slender structures are more influenced by SFSI effects and that the distribution of ductility demand was influenced by SFSI effects. It was noted that no strength distribution method suggested in literature achieved an optimal uniform ductility demand up the structure.

This chapter examines the additional complexities of MDOF systems when considering dynamic SFSI. More specifically this chapter focuses on concrete wall structures on both rigid and soft soil attempting to quantify the additional MDOF mechanisms to allow designers to design wall buildings while considering SFSI.

9.2 Effects of vertically distributed mass

Vertically distributed mass results in additional complexities compared to a lumped-mass SDOF model. A vertically distributed mass model can capture two key parameters that are essential to consider when designing multi-storey buildings, namely the inter-storey drifts and distribution of forces. Both the peak and residual inter-storey drift are of interest as the peak inter-storey drift can provide a proxy for the extent of structural and non-structural damage, while residual drift is important when assessing the repairability and functionality of a structure post event. The distribution of forces is important for the consideration of over-strength design to avoid yielding at unintended places. To understand how SFSI modifies

these two key parameters the additional mechanisms of MDOF systems must be understood.

Examining just the fixed base case, there are many additional considerations compared to a simple SDOF model. All of the considerations highlighted in Figure 9.1 are inter-related and their influence is dependent on the degrees-of-freedom and stiffness distribution (number of storeys and the structural type). Typically, shorter buildings have smaller contributions from higher modes and relatively straight deformation profiles. Frame structures tend to exhibit a shear like deformation profile compared to wall buildings exhibiting a flexural shape. Frame buildings also tend to have non-linear deformation distributed up the structure with the exception of shorter buildings which are sometimes designed to have a single soft storey. Wall buildings tend to have only yielding at the base of the structure and occasionally are designed to allow yielding further up the structure to limit the second mode response in tall buildings.

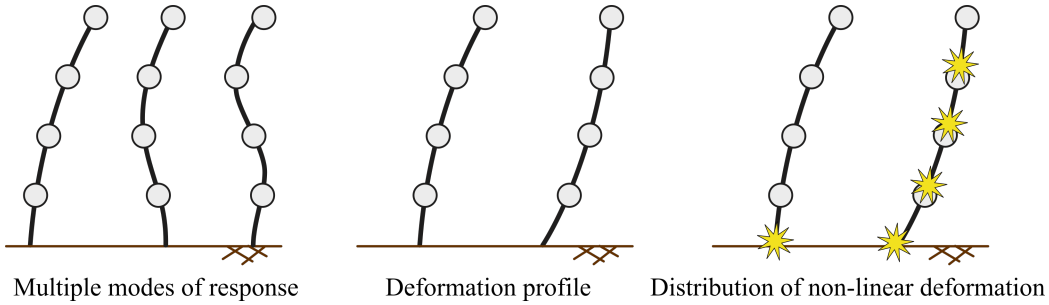

Figure 9.1: Additional considerations for vertically distributed mass

By including SFSI deformation, each of these response features are modified. The deformation at the foundation level immediately shifts the first mode period and can even cap the magnitude of the forces in the first mode by providing a non-linear mechanism at the base of the structure. A mechanism at the base hardly influences higher modes at all, resulting in a greater proportional increase in the influence of higher modes, thus design procedures that are based on the first mode response, such as DDBD should recognise this. To demonstrate this effect a cantilever column with distributed mass along its length is considered in Figure 9.2. The first three modes are all shown for both the full elastic cantilever and for the non-linear case, where the cantilever forms a perfect hinge at the base. Notice how, for the hinge case, the first mode period tends to infinity while the second and third mode periods are only shifted by 33% and 20% respectively.

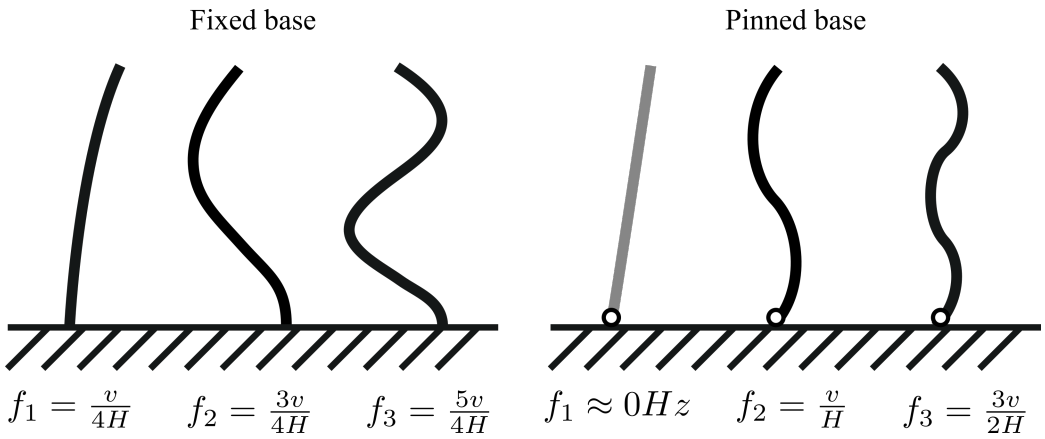

Figure 9.2: Influence on vibration modes due to a nonlinear mechanism at the base for a distributed mass model

The influence of foundation rotation on the deformation profile is somewhat obvious, the rotation at the base causes the deformation profile to straighten. There is greater participating mass in the first mode for wall type buildings, while the first mode participating mass reduces in frame type buildings (Figure 9.3).

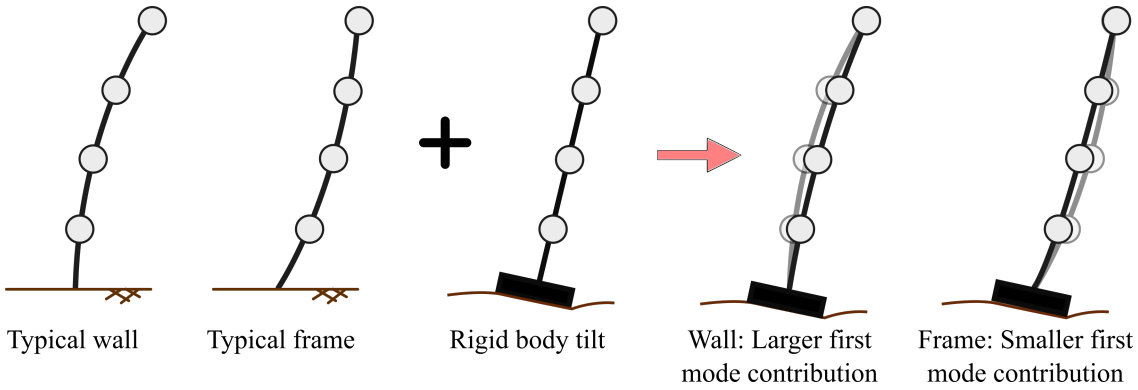

Figure 9.3: Effect of SFSI deformations on first mode participation

The deformation at the foundation level means that the non-linear deformation in the structure tends to be reduced. The foundation deformation can modify the response and limit the forces and deformations in the structure. When looking at the distribution of non-linear deformation, the deformation at the base of the system (soil, foundation and base of wall) increases while the distribution of deformation further up the structure will change due to high mode effects.

9.3 Parametric study on concrete wall structures

In this section the effect of SFSI on the prediction of the peak inter-storey drifts, residual drifts and shear force distribution is quantified. These parameters can not be accurately estimated

through SDOF models and therefore distributed mass and stiffness models must be used. In Section 9.2 it was outlined how SFSI deformations effect many of the deformation characteristics of distributed mass models. In this section concrete wall buildings were designed using DDBD assuming fixed base conditions and then a subset were redesigned considering SFSI deformations for different soil conditions and foundation sizes. The SDOF models for the fixed based walls were assessed in Chapter 8 and the SDOF models considering SFSI were assessed in Chapter 6, whereas here the walls were modelled as MDOF models with lumped masses at each storey.

Both sets of designs were numerically modelled and analysed, with the fixed base cases analysed using fixed base conditions and the designs considering SFSI effects analysed with a macro-element modelling the soil foundation interface. The fixed base model provided a benchmark to assess the ability of DDBD to control the level of inter-storey drift and residual drift, while the SFSI model allowed for the effects of SFSI to be assessed in terms of how they influence the level of inter-storey drift and residual drift.

Inputs for parameteric study

The inputs for the wall buildings and soil properties are given in Table 9.1, resulting in 28 fixed base wall buildings and 96 wall-foundation-soil systems.

Table 9.1: Wall design inputs

Parameter	Fixed base	SFSI included
storeys	$[4, 5, 6, 7, 8, 9, 10]$	$[4, 6, 8, 10]$
Wall width	0.3m	0.3 m
Storey heights	3.4m	3.4 m
Wall height to depth ratio	$[3, 4, 6, 8]$	$[4, 6]$
Number of walls	4	4
Building length	20 m	20 m
Building width	12 m	12 m
Footing height	-	$1.2 + height_{wall}/60$ m
Footing length to width ratio	-	2.5
Footing depth to breadth ratio	-	0.0
Target static bearing capacity factor of safety	-	[2.0, 3.5, 7.0]
Soil type	C	C
Design hazard level	0.4	0.4
Live load on floors	3 kPa	3 kPa
Dead load on floors	6 kPa	6 kPa
Total peak drift limit (θ_t)	0.02	0.025
Superstructure inter-story drift limit (θ_{ss})	0.02	0.02
Soil shear modulus (G)	-	$[50, 120]$ MPa
Soil friction angle (ϕ)	-	$[30, 36]$
Soil unit weight (γ_s)	-	18.0 kN/m^3
Concrete compression strength (f_c)	30 MPa	30 MPa
Rebar strength (f_y)	300 MPa	300 MPa

Numerical model

The numerical analyses were conducted using the non-linear finite element software Ruaumoko3D. The superstructure was a -lumped mass, -lumped plasticity stick model of a single wall and the soil-foundation interface was modelled using a macro soil-foundation interface model in the SFSI analyses (Figure 9.4). Yielding only occurred at the base of the wall, which was consistent with the assumptions made by Amaris (2002), where the DDBD displacement profiles were developed. The horizontal masses at each storey node were equal to the seismic mass at each storey used for the design. The vertical mass was equal to the sum of the horizontal masses and was lumped at the foundation node as the wall vertical stiffness was considered rigid. The wall stiffness was modelled as constant up the structure.

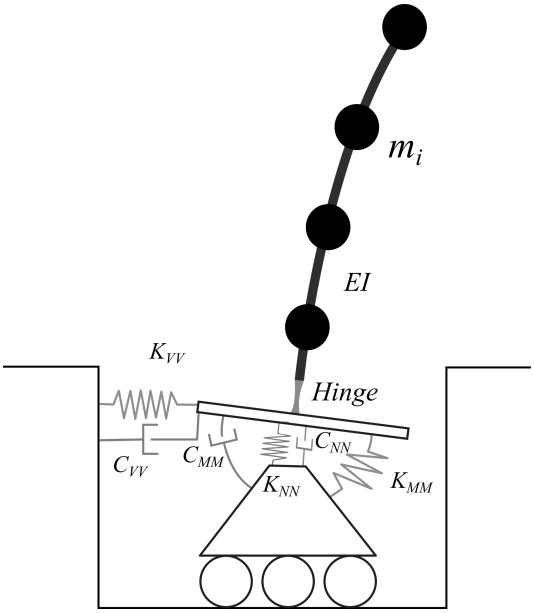

Figure 9.4: Numerical model of wall-foundation-soil system

The numerical model attempted to model the underlying assumptions of the DDBD procedure to highlight the influence of SFSI on the behaviour. However, there were several limitations in the numerical model that meant that not all of the design assumptions could be exactly mapped.

The first issue was due to the DDBD procedure assuming a linear curvature distribution to calculate the yield displacement. The assumption of a linear curvature distribution was justified in the design by the fact that it accounts for various complex mechanisms such as tension shift, and different amounts of cracking up the wall causing a variation to the wall stiffness, which can not be accounted for in the simple lumped plasticity model. Assuming that the curvature profile at yield is similar in shape to that caused by the distribution of design forces, the difference in yield displacement of the adopted model would be approximately 15% smaller than from the assumed linear curvature, profile according to Priestley et al. (2007) .

The second issue also affects the yield displacement, where the DDBD procedure determines the yield displacement as the point when the moment at the wall base reaches the yield moment, while for the lumped plasticity model the moment at the centre of the hinge must reach yield. The yield displacement therefore increases by approximately half of the plastic hinge length divided by the total height.

The third issue was due to the incompatibility between the requirements to match the yield curvature (Equation 9.1), the design yield moment (Equation 9.2) and the SDOF initial period (Equation 9.3). Here ϵ_y is the yield strain of the reinforcement, L_w the wall length, M_D the design moment, r the PYSR, μ the wall ductility and T_s the secant period at design drift.

$$\phi_y = 2.0\frac{\epsilon_y}{L_w} \tag{9.1}$$

$$M_y = \frac{M_D}{1 + r\mu} \tag{9.2}$$

$$T_i = \sqrt{T_s(1 + r\mu)}\mu \tag{9.3}$$

$$\tag{9.4}$$

Work by Pennucci et al. (2011b) demonstrated that the displacement behaviour of a MDOF system at its effective height can be replicated by a SDOF system which has the same initial period and strength reduction factor. To ensure compatibility between the model MDOF and the design assumptions that make use of the SDOF response spectrum, the initial period of the MDOF must match the SDOF period. Given that the loads from the first mode of response provide over 90% of the base moment for tall structures where the mass can be considered distributed and the vibrational period is less than 4.0s (Pennucci et al., 2011b), the yield moments of the SDOF and MDOF should also be similar. However, Equations 9.1 - 9.3 provide an incompatibility, as the initial period is governed by the geometry of the wall, the distribution of mass and the cross-sectional stiffness (EI), where both the geometry and mass distribution are fixed during the design. While Equations 9.1 and Equation 9.2 also provide a required value for EI through Equation 9.5.

$$EI = \frac{M_y}{\phi_y} \tag{9.5}$$

Figure 9.5 demonstrates how the required values of EI differ from satisfying Equations 9.1 and 9.2 compared to Equation 9.2 and 9.3.

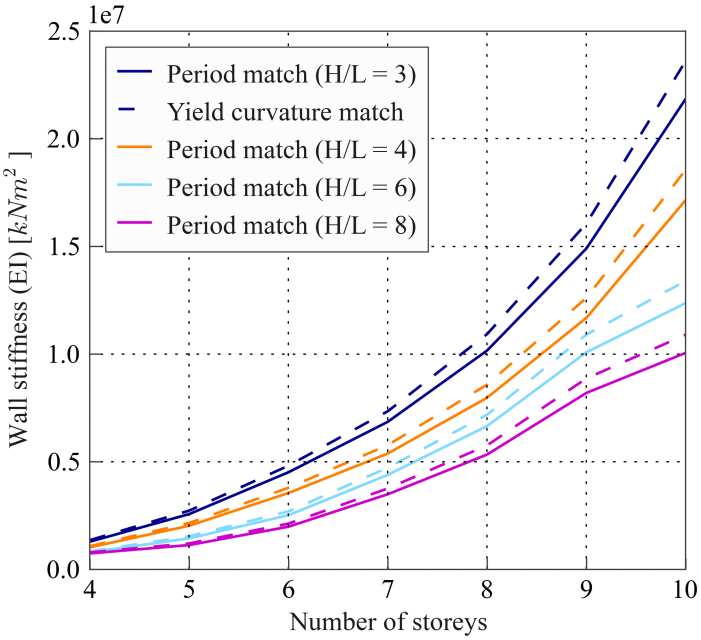

Figure 9.5: Different required values of wall stiffness

The final issue was due to the length of the plastic hinge, where in some cases the length of the plastic hinge from design would exceed the height of the first storey. The Ruaumoko beam element requires a length of non yielding section and therefore the plastic hinge length must be taken as a value less than the storey height.

While all of the issues result in some imperfect mapping, the magnitude of the error is small and parameters were carefully chosen in an attempt to cancel out the errors. The wall stiffness was determined using an ad hoc piece of software that conducted eigenvalue analysis on the wall to match the initial period of the wall to that of Equation 9.3, and the wall was modeled with constant stiffness up the wall height and zero shear deformation (based on the difference in wall stiffness in Figure 9.5 this resulted in approximately a 10% increase in yield displacement).

The plastic hinge was constrained to 5% of the building effective height, which constrained the hinge to well within the first storey. The shift of the yield location from the base of the wall to the middle of the plastic hinge resulted in approximately a 3.5% increase in the yield displacement, while still providing a reasonable approximation to the plastic hinge location necessary to match the displaced shape. These two assumptions, combined with the error due to the difference in yield curvature profiles (approximately 15% decrease), result in expected yield displacements similar to those used in design (see Figure 9.6).

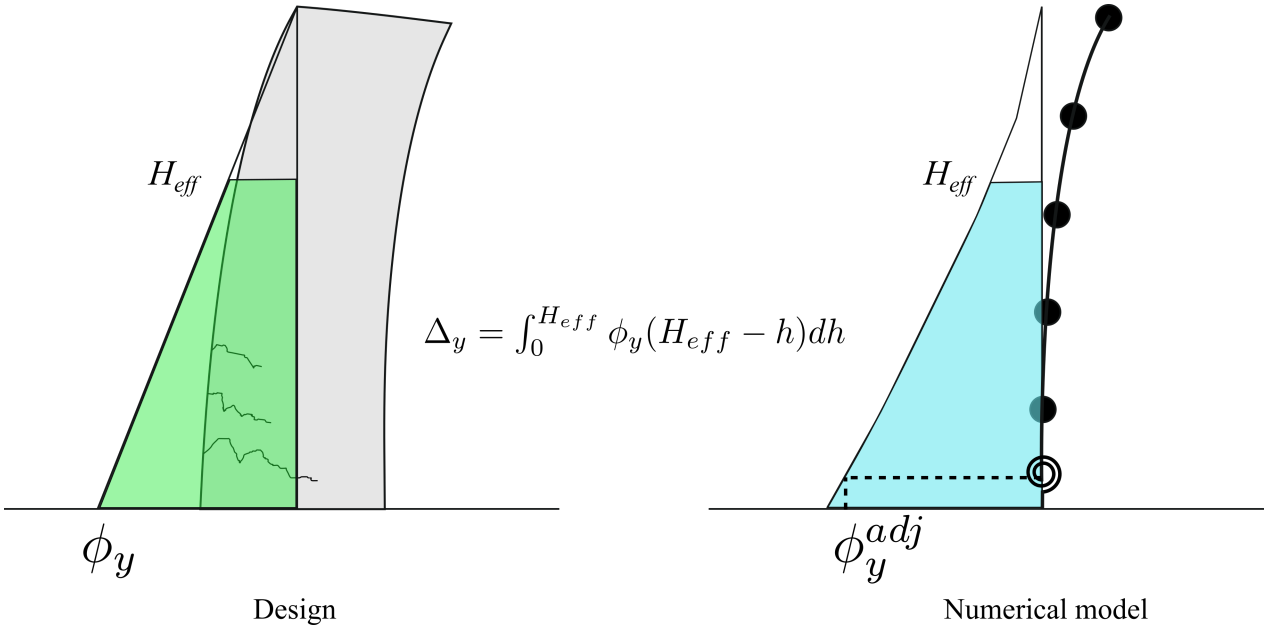

Figure 9.6: Error in the yield displacement

Given that the plastic hinge length (L_p) was set at 5% of the effective height (H_{eff}), the hinge PYSR (r_h) should not be determined from moment curvature analysis as this would result in incompatible assumptions. Instead the hinge PYSR was determined to give a 5% PYSR for the lateral mode of deformation (r_e), assuming the wall behaved identically to the equivalent SDOF model using Equation 9.6 (see full derivation of Equation 9.6 in Chapter 6 Section 6.6.2). The hinge hysteretic behaviour was modelled using the Ruaumoko3D Modified Takeda rule with 'Takeda thin' properties ($\alpha = 0.5$, $\beta = 0.0$, NF = 1.0, KKK = 2).

$$r_h = \frac{3r_e(1 - \frac{L_p}{2H_{eff}})^2 \frac{L_p}{H_{eff}}}{(1 - r_e)} \tag{9.6}$$

The damping was modelled using the global Rayleigh tangent stiffness proportional damping set at 5% of the critical damping for modes one and three, consistent with Amaris (2002). The Rayleigh tangent stiffness proportional damping model provides a reduction in the damping forces when the structure behaves inelastically; however, as pointed out by Grant et al. (2005), the first mode is almost entirely mass proportional, which remains constant and therefore the displacements (which are dominated by the first mode) are over damped compared to a purely tangent stiffness damping model. To account for this inconsistency Priestley et al. (2007) proposed a modification to the first mode damping value, which has been adopted in recent studies on wall buildings (eg. Pennucci et al., 2011b; Fox et al., 2015). The proposed modification was not used here as the focus of this chapter was investigating the modification of the response due to SFSI and therefore applying 5% at modes one and three minimised the complexity.

The consideration of P-delta effects was consistent with the designs, where the fixed base designs ignored P-delta effects and were assessed with no P-delta effects and the SFSI designs included P-delta effects and P-delta effects were considered in the analysis. When P-delta effects were considered the design static load from the wall was evenly apportioned to the storey nodes, with none at the foundation level.

For the numerical models that considered foundation deformations, the vertical load was based on the total mass of the original structure during seismic excitation. The soil-foundation interface was modelled with the macro-element defined in Chapter 4.

9.3.1 Fixed base wall results

The first assessment was the comparison between the predicted inter-storey drift for the fixed base walls and the inter-storey drift obtained from the time history analyses. Figure 9.7 shows the average peak drift divided by the design drift in full circles and individual analyses are shown as small triangles. It can be seen that the average peak drift is over predicted by the design drift and there is a clear dependance on the wall height to length ratio. The wall height to length ratio strongly influences the level of ductility and therefore just like for the SDOF models, the displacement of high ductility structures was consistently over estimated. While a different damping method was used for the MDOF model compared to the SDOF model, the effects of the different methods for the first mode response were almost identical. The Rayleigh tangent stiffness proportional damping model used here resulted in an almost entirely mass proportional first mode and therefore when the structure behaved inelastically the damping forces were larger than the assumed tangent stiffness proportional forces that can be achieved with a SDOF structure (Grant et al., 2005). The results are consistent with research by Pennucci et al. (2011b) where 5% Rayleigh tangent stiffness proportional damping was specified for tall concrete wall buildings.

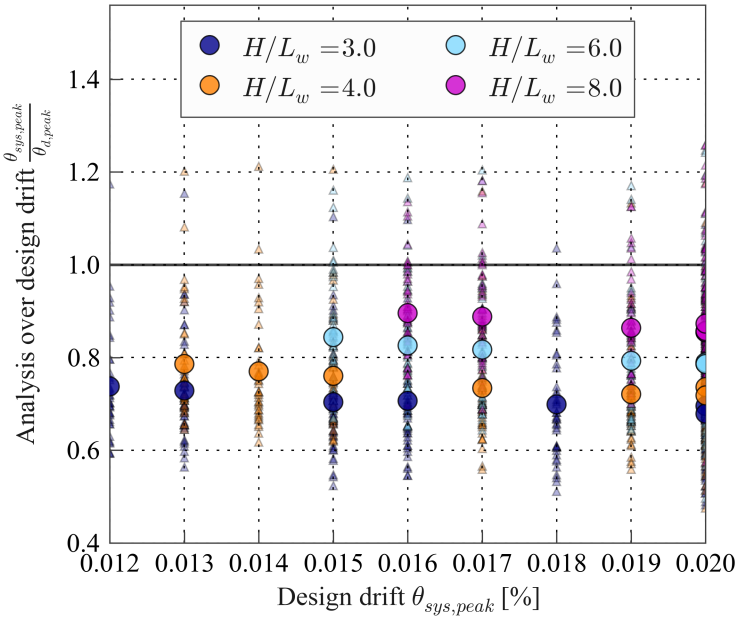

Figure 9.7: Peak interstorey drift from fixed base MDOF model

The displacement profiles for each building in Figure 9.8 also show the same trend as the inter-storey drift, which is not surprising considering that the displacement response for short to medium period buildings is almost entirely driven by the first mode building response. The big discrepancy for shorter building may also be due to the way the shear force was distributed in design, where 90% of the base shear was distributed based on the design displaced shape and the remaining 10% was added to the top storey. This distribution of forces tends to be appropriate for tall buildings were the higher modes can result in significant levels of displacement but may have resulted in an artificially high base moment for shorter buildings.

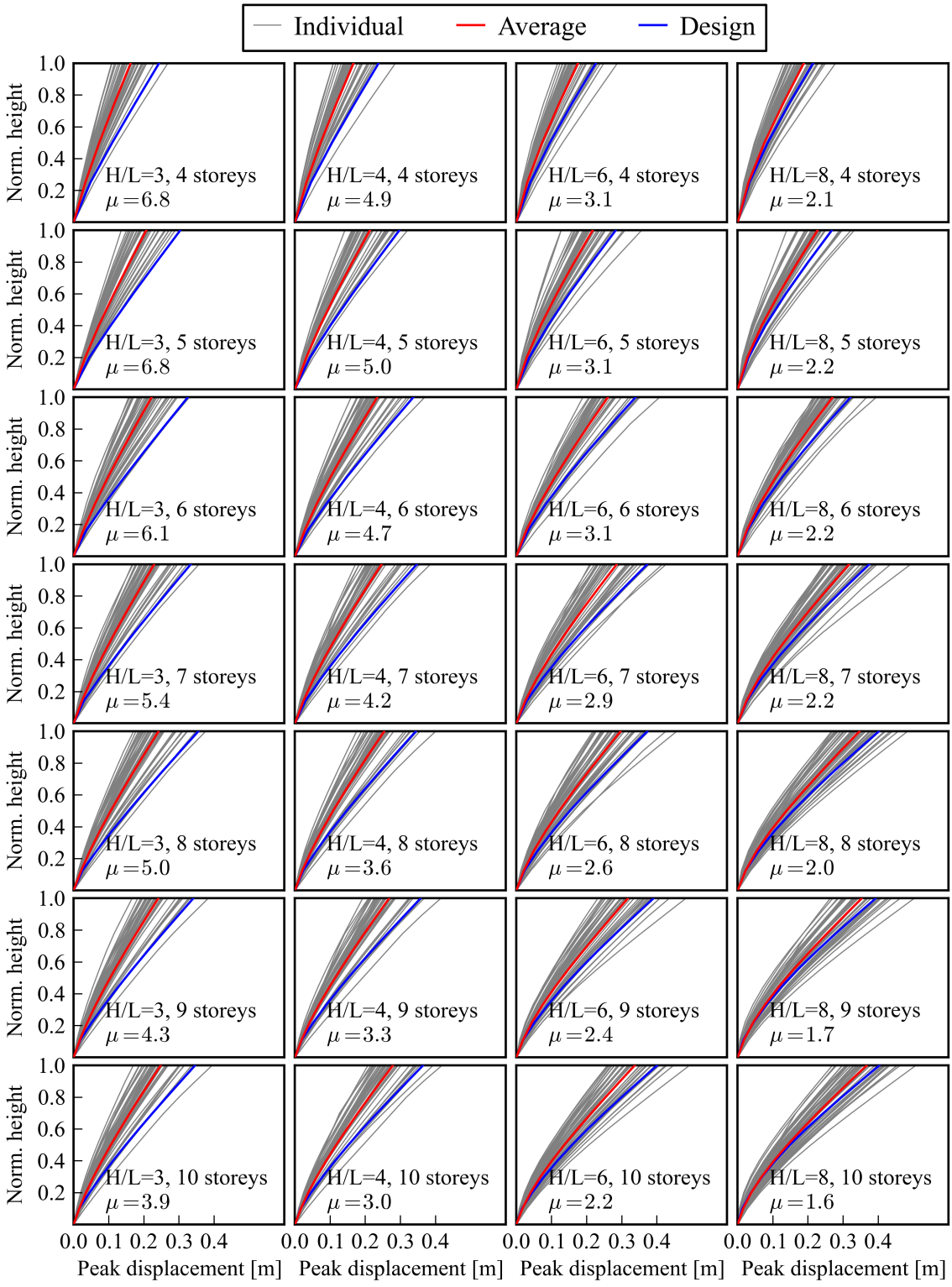

Figure 9.8: Peak interstorey drift from fixed base MDOF model

The peak storey shear force profile was examined in Figure 9.9 against the design over-strength shear profile from (Priestley et al. (2007)) (Equation 9.7), where it can be seen that the equation provides an excellent envelope of the average peak shear forces. For Equation 9.7 and for the over-strength moment (Equation 9.12), the over-strength factor (ϕ^o) was taken

as 1.0 since the wall base moment was set to the nominal moment. The initial period (T_i) was taken as first mode elastic period of the structure and μ the structure displacement ductility from the design.

$$V^o_{Base} = \phi^o \omega_V V_{Base} \tag{9.7}$$

$$\omega_V = 1 + \frac{\mu}{\phi^o} C_{2,T} \tag{9.8}$$

$$C_{2,T} = 0.067 + 0.4(T_i - 0.5) \leq 1.15 \tag{9.9}$$

$$V^o_n = C_3 V^o_{Base} \tag{9.10}$$

$$C_3 = 0.9 - 0.3T_i \geq 0.3 \tag{9.11}$$

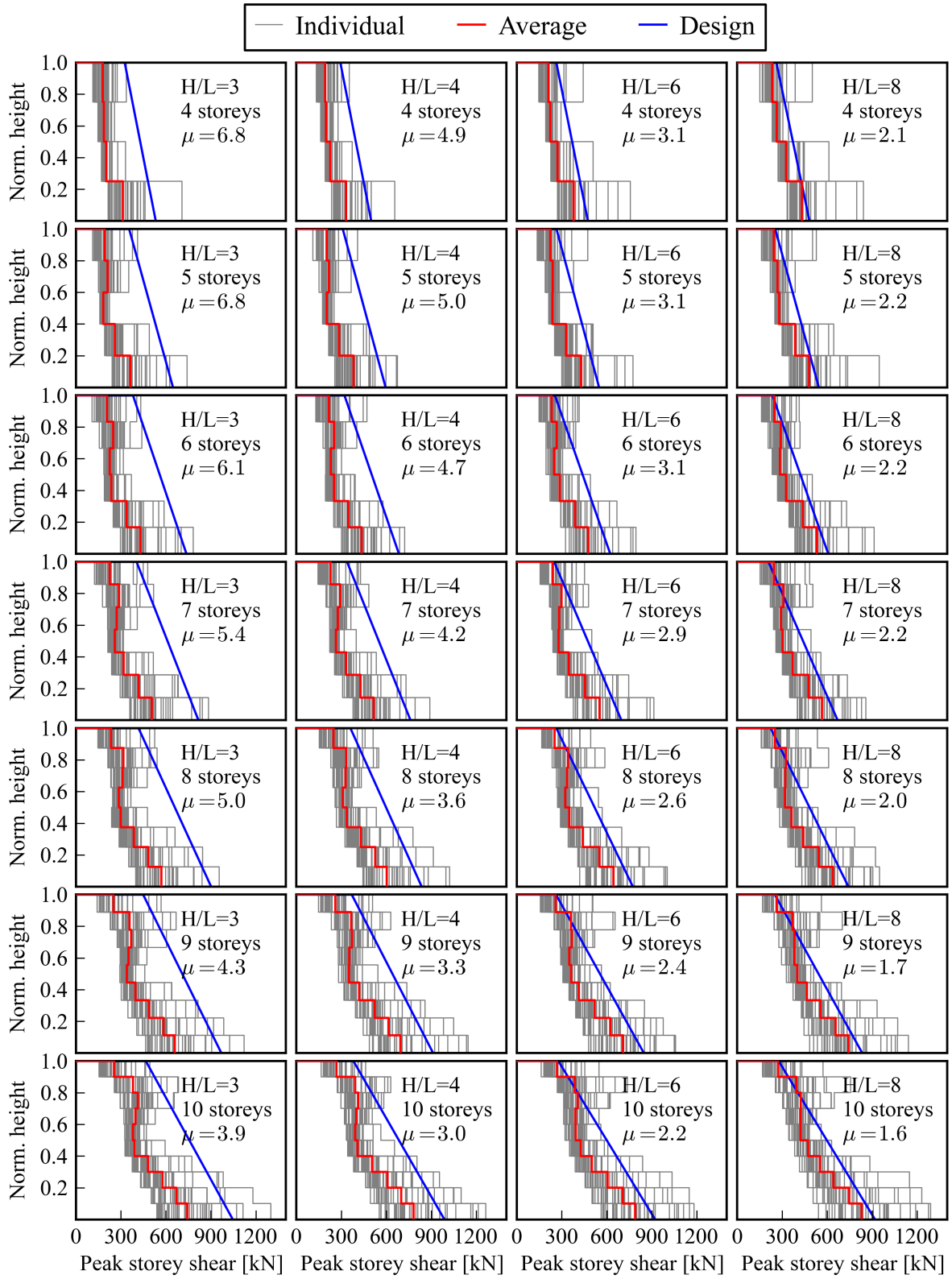

Figure 9.9: Peak shear distribution from fixed base MDOF model

In Figure 9.10 the peak moment profile was examined against the design over-strength moment profile from (Priestley et al. (2007)) (Equation 9.12), where is can be seen that the equa-

tion provides an excellent envelope of the average peak moments.

$$M^{o}_{0.5H} = C_{1,T}\phi^{o}M_{B} \tag{9.12}$$

$$C_{1,T} = 0.4 + 0.075T_{i}(\frac{\mu}{\phi^{o}} - 1) \geq 0.4 \tag{9.13}$$

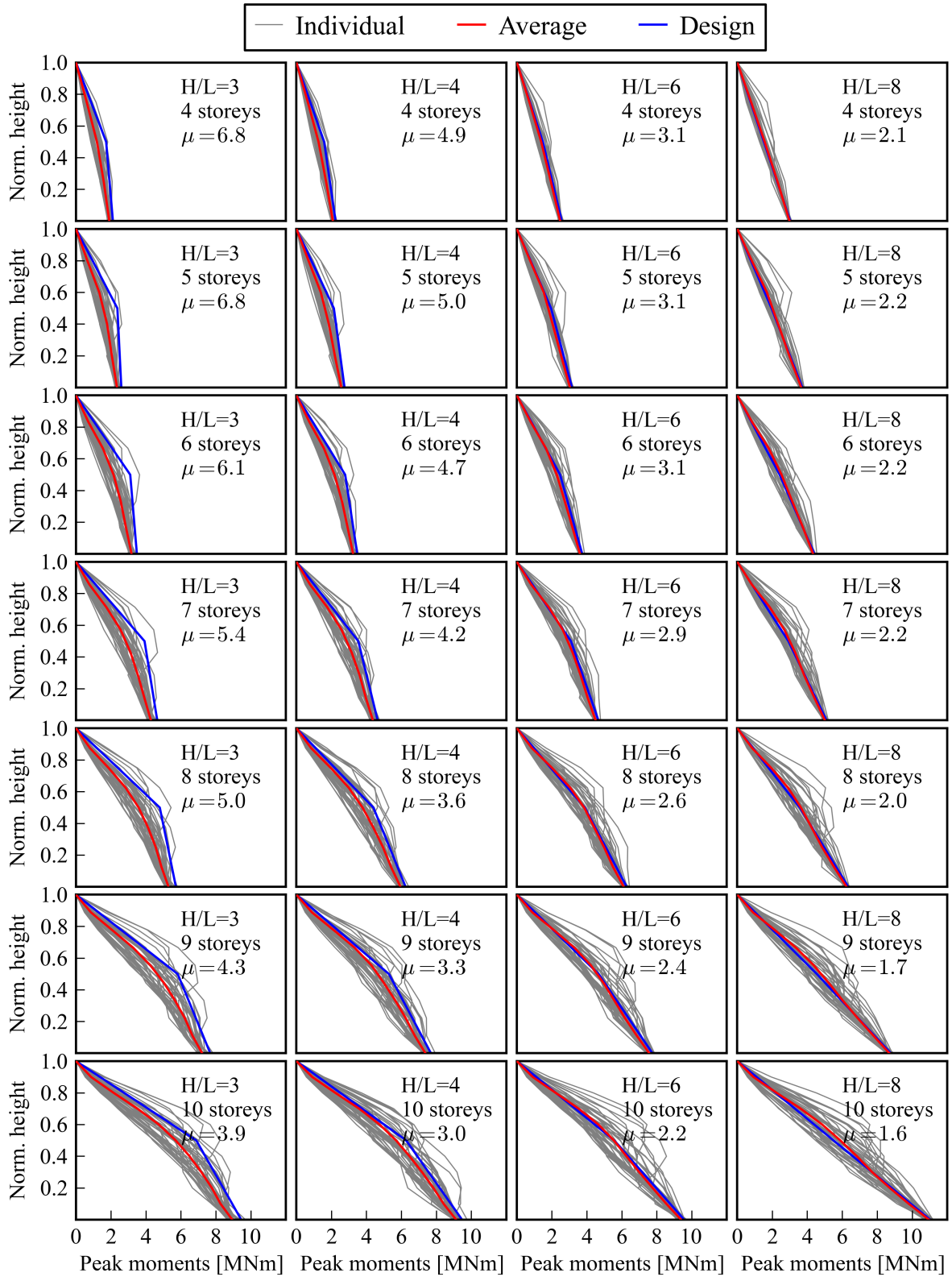

Figure 9.10: Peak moment distribution from fixed base MDOF model

From the SDOF analyses in Chapter 8, the ratio of residual to peak drift was determined as approximately 8.5% for concrete wall buildings when no P-delta effects were considered.

For MDOF systems, unlike SDOF systems, the non-linear deformation occurs at a different location to the peak deformation. In fact the peak inter-storey drift occurs in the top floor while the non-linear behaviour is constrained to the wall base. Moreover, the peak inter-storey drift occurs due to the cumulative flexural deformation up the entire structure, however, the residual inter-storey drift is only influenced by the deformation in the non-linear hinge section, so for multiple storey buildings the peak deformation should increase while the residual drift should stay approximately the same.

Figure 9.11 shows the average residual drift divided by the design peak drift in full circles (individual analyses are shown as small triangles). The average of all the analyses can be seen as 0.057, which compared to the ratio from the SDOF analyses in Chapter 8 which was 0.085, is considerably lower. Although since the peak drift from the analyses was considerably lower than the design drift this does not give a true indication of the residual to peak drift ratio.

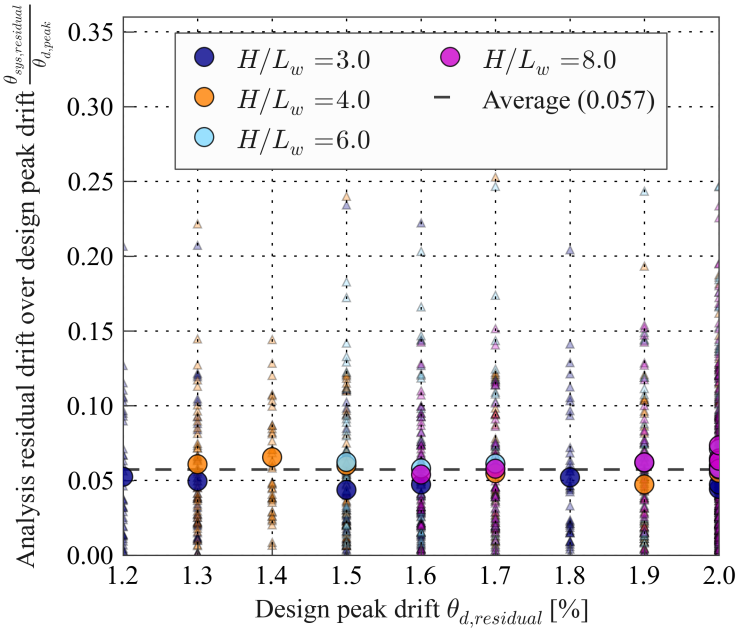

Figure 9.11: Residual interstorey drift from fixed base MDOF model

Figure 9.12 shows the average residual drift divided by the average peak drift from the analyses. The average ratio shifts to 0.073, which is closer to the 0.085 ratio from the SDOF analyses, but still lower as expected. However, it should also be noted that the maximum number of storeys considered here was 10, so the influence of of higher modes and the effect of the peak and residual occurring at different places in the structure would increase with more storeys (see Pennucci et al. (2011b)).

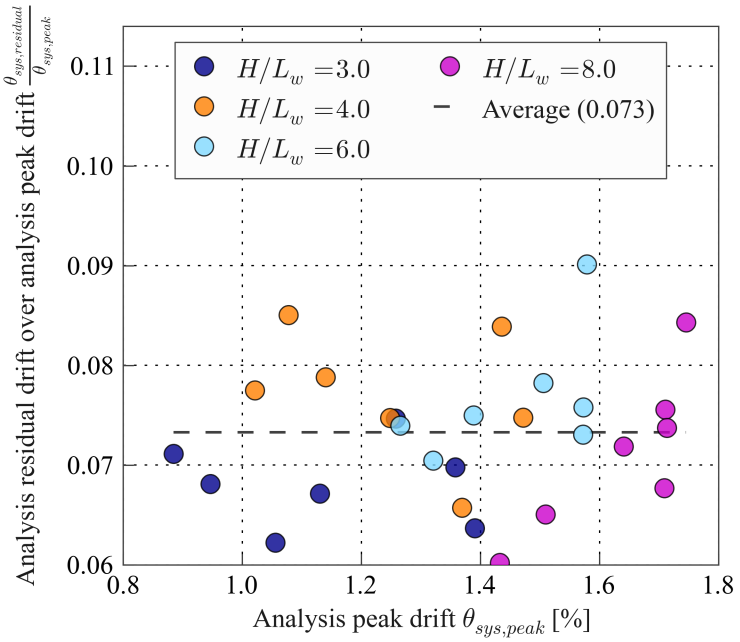

Figure 9.12: Residual interstorey drift from fixed base MDOF model

9.3.2 Wall results considering SFSI and P-delta effects

Figure 9.13 shows the peak displacement profiles compared to the design displacement for all of the buildings where the soil friction angle (ϕ) was equal to 30 (the results for $\phi = 36$ were omitted as they were very similar to $\phi = 30$). The displacements were slightly over estimated due to the issue with damping in the superstructure but demonstrate that the developed design procedure for consider SFSI effects can provide reasonable estimates of the behaviour.

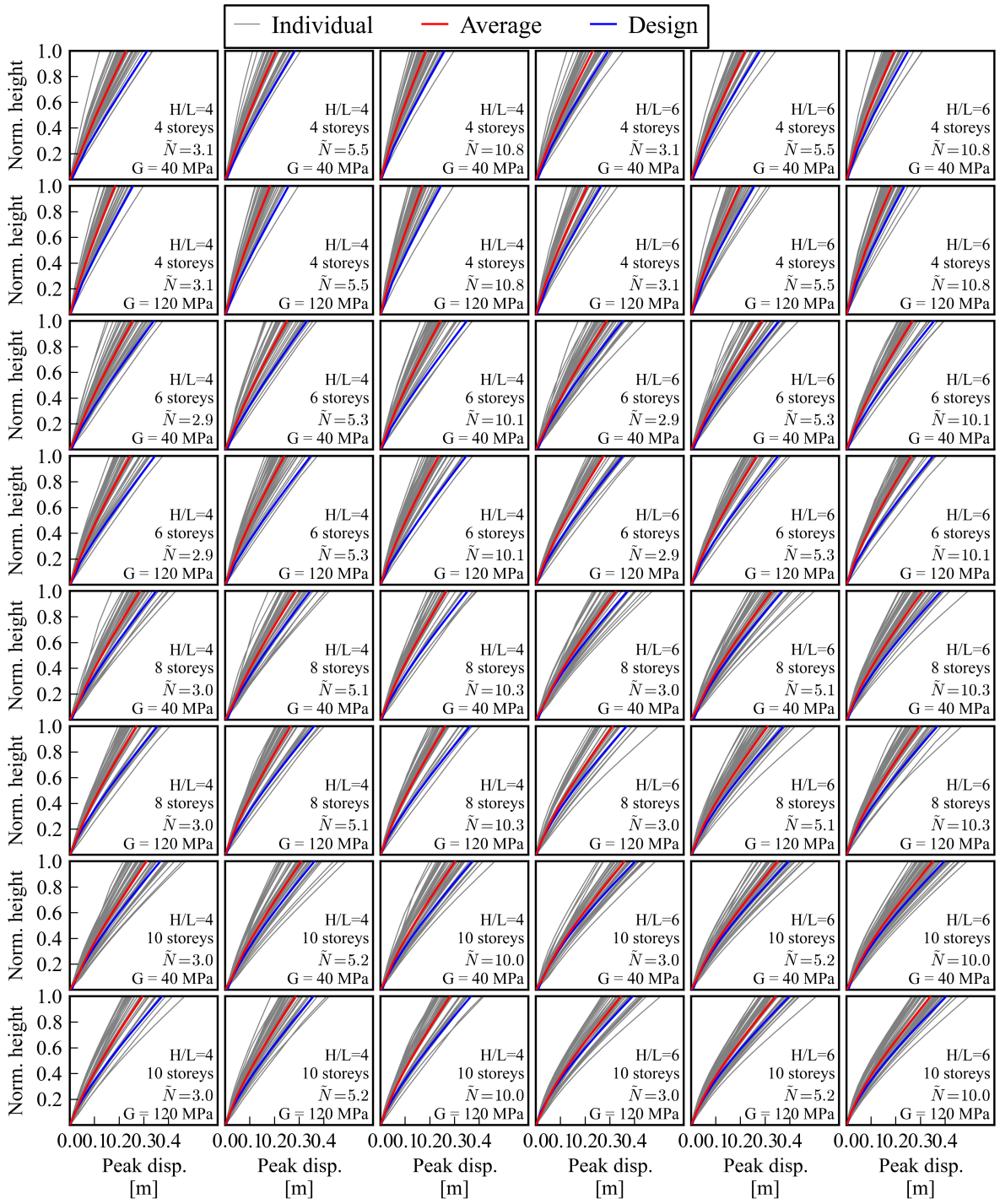

Figure 9.13: Peak displacement versus design displacement profiles from MDOF model with SFSI

Figure 9.14 shows the peak storey shear profiles compared to the design over-strength shear (Equation 9.7). Where the initial period (T_i) was taken as the first mode period of vibration of the entire building-foundation-soil system. The equation provided a suitable envelope to the shear forces.

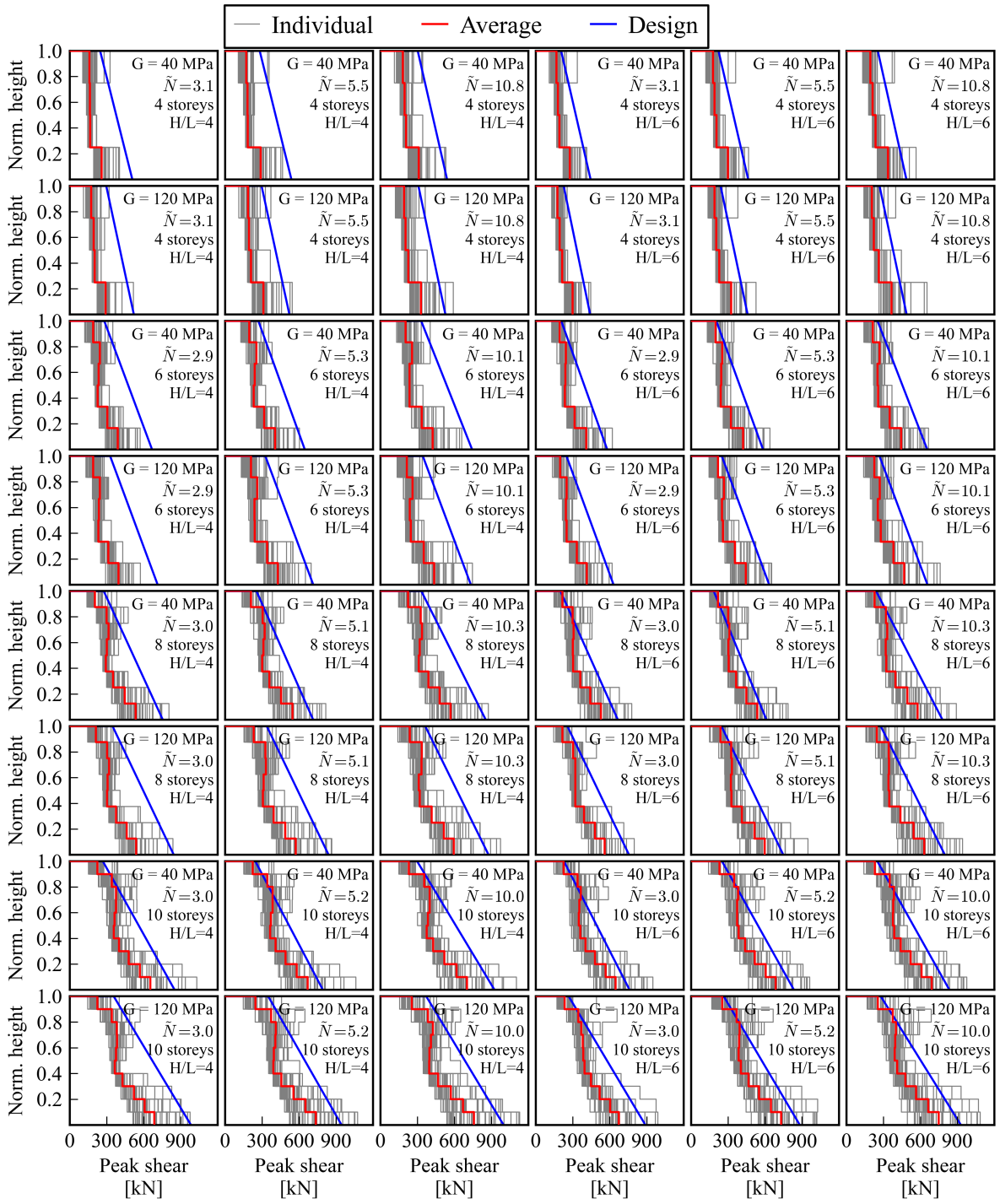

Figure 9.14: Peak shear distribution from MDOF model with SFSI

Figure 9.15 shows the peak moment profiles compared to the design over-strength moment (Equation 9.7). The equation provided suitable estimates in many cases, however, for the taller buildings sited on soil with a shear modulus of only 40 MPa the average analysis values exceeded the estimate. These cases correspond to cases where the foundation contribution is largest and the higher mode effects are largest. To account for the influence of SFSI on the moment demand up the structure a modified over-strength moment equation (Equation

9.14) is proposed using the system ductility (μ_{sys}) instead of the structural ductility. This correction reflects the intention of the original equation where the non-linear deformations of the wall structures (represented by the ductility parameter in the original equation) were all constrained to the base of the wall and now the non-linear deformation includes the deformations of the foundation as well. The extra base flexibility from foundation deformations affects the high mode responses in a similar way to the yielding of the structure. The system ductility can simply be computed as the total design displacement divided by the superstructure yield displacement (based on the equivalent SDOF) using Equation 9.16. The modified over-strength equation (Figure 9.15 - green line) suitably envelopes the average peak moment.

$$M^o_{0.5H} = C_{1,T}\phi^o M_B \tag{9.14}$$

$$C_{1,T} = 0.4 + 0.075T_i(\frac{\mu_{sys}}{\phi^o} - 1) \geq 0.4 \tag{9.15}$$

$$\mu_{sys} = \frac{\Delta_d}{\Delta_y} \tag{9.16}$$

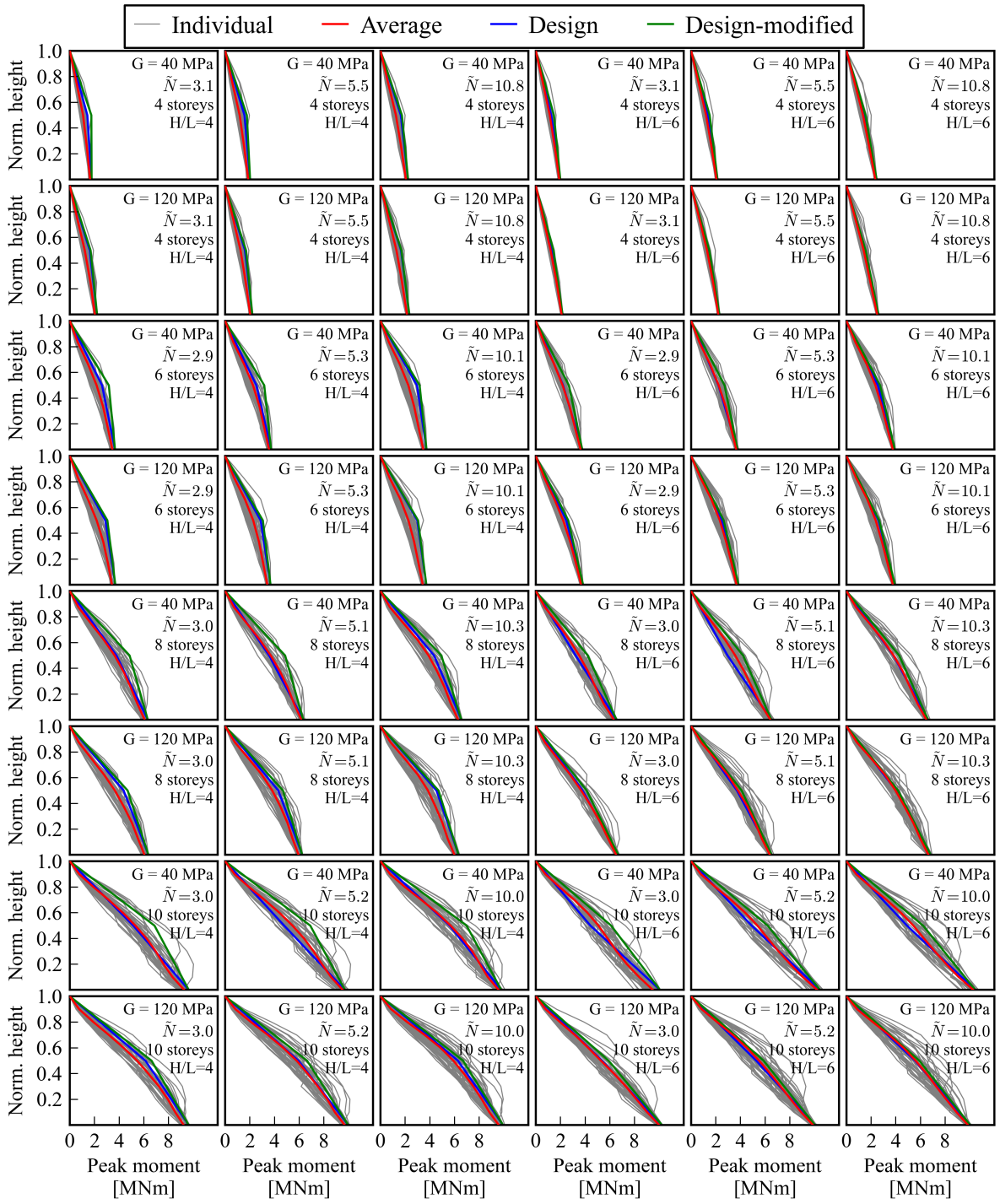

Figure 9.15: Peak moment distribution from MDOF model with SFSI

Figure 9.16 shows the peak inter-storey drift due to structural deformation (ie. the total inter-storey drift minus the deformation due to foundation rotation). As expected the drift from the design was larger than the analysis drift in all cases, due to the discrepancy between the damping model used in the analysis and the behaviour assumed during design. The results showed very little dispersion even for individual records and the running standard deviation from all the individual analysis was approximately 0.15.

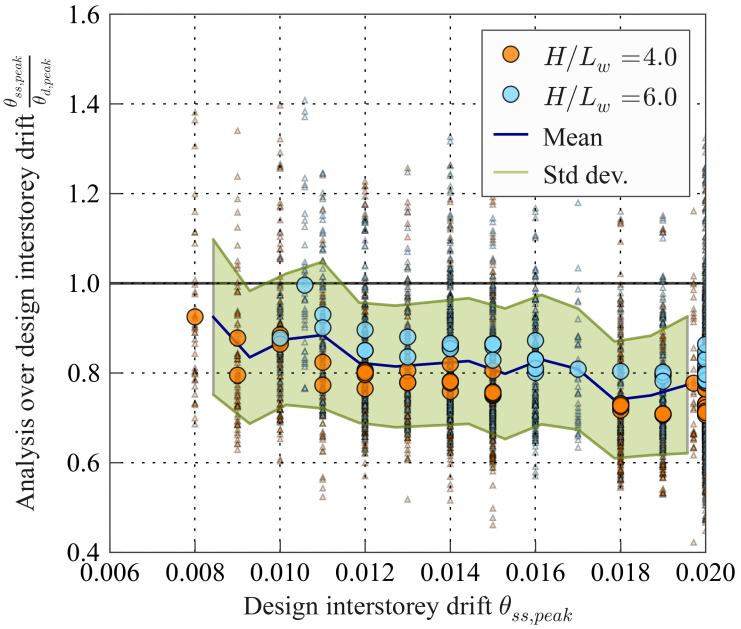

Figure 9.16: Peak interstorey drift from soil-structure MDOF model

The discrepancy with the peak drift was also reflected in the residual drift ratio. The difference between design and average analysis residual drifts seen in Figure 9.17 was very similar to those obtained for the fixed base analyses, although here the residual deformations were estimated using Equation 9.17 developed in Chapter 8 that included P-delta effects.

$$\frac{\theta_r}{\theta_p} = 0.068 + 0.027\mu + 1.9\frac{P}{HK_i} \tag{9.17}$$

Here P is the axial load applied at the effective height which can be taken as the effective mass of the equivalent SDOF multiplied by gravity. The parameter H_{eff} is the effective height and K_i is the initial stiffness of the equivalent SDOF structure.

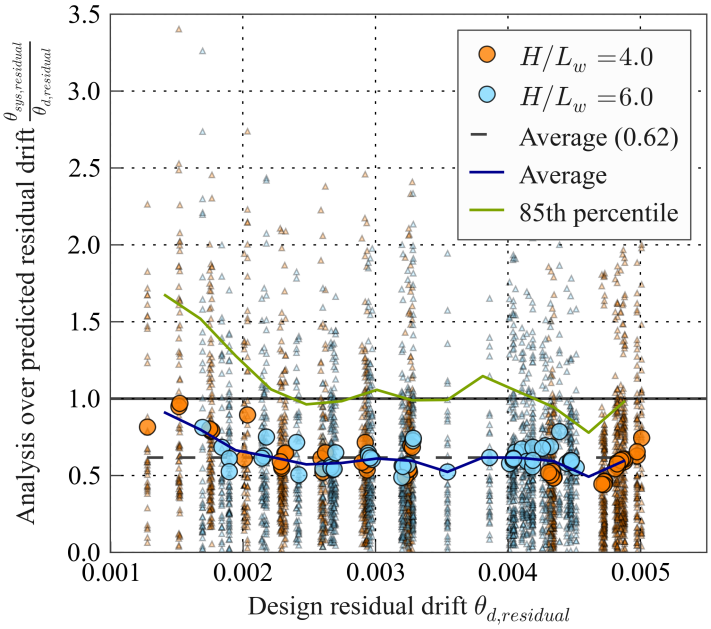

Figure 9.17: Residual interstorey drift from soil-structure MDOF model

The running 85th percentile value of the individual records is shown in Figure 9.17 instead of the standard deviation as the residual deformation was not normally distributed. The average 85th percentile value was approximately 0.4, indicating a considerably larger scatter in the residual deformation than for the peak deformation.

The foundation peak rotation was well predicted as seen in Figure 9.18. Notably there were four average peak rotation values that exceeded 1.5 times the design peak drift, but at higher levels of rotation the design and average peak values were very similar. The average standard deviation can be taken as approximately 0.3 of the design foundation rotation.

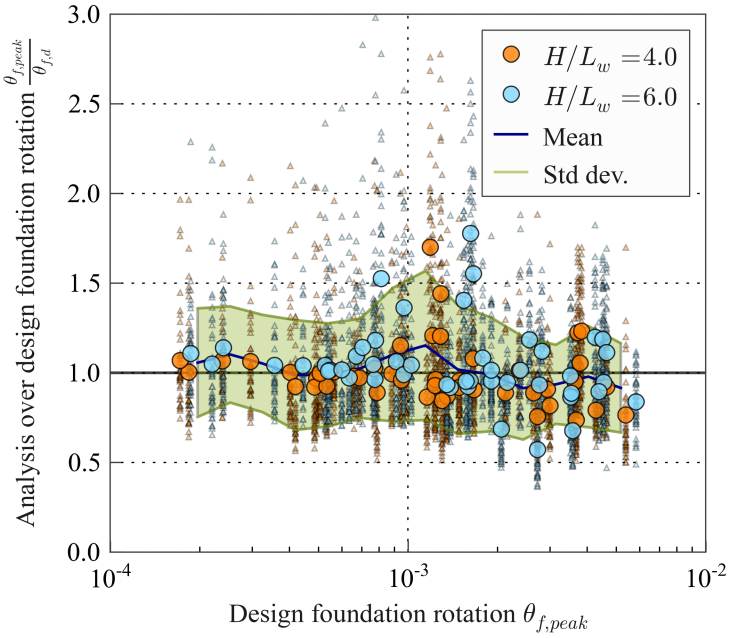

Figure 9.18: Peak foundation rotation from soil-structure MDOF model

Interestingly both the SFSI-induced settlement (Figure 9.19) and the residual rotation showed a clear under estimation of deformation at low levels. The cause for this increased permanent deformation at low levels was due to the difference in behaviour between the MDOF models present here and the SDOF models which were used to calibrate the SFSI-induced settlement and residual rotation. The dispersion was also larger at lower levels of deformation, however, at higher levels where the predicted values were accurate the standard deviation was approximately 0.2 for the settlement and an 85th percentile value of 2 for the residual rotation.

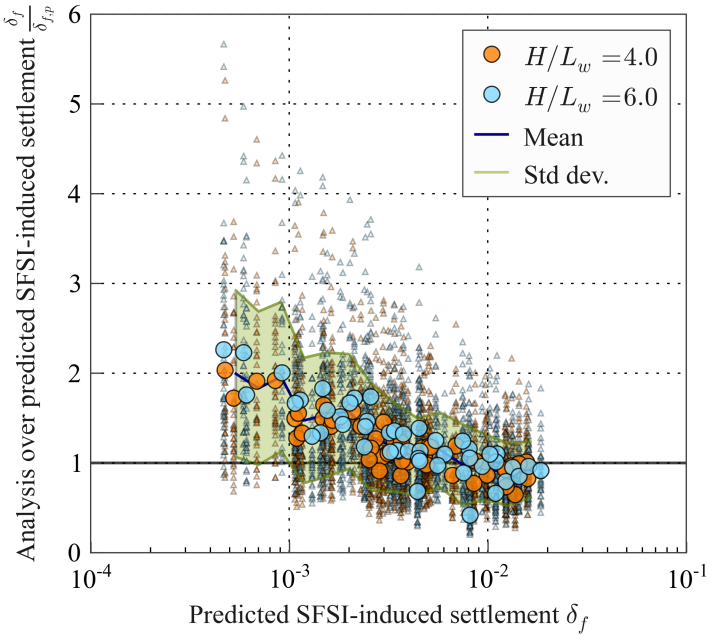

Figure 9.19: SFSI-induced settlement from soil-structure MDOF model

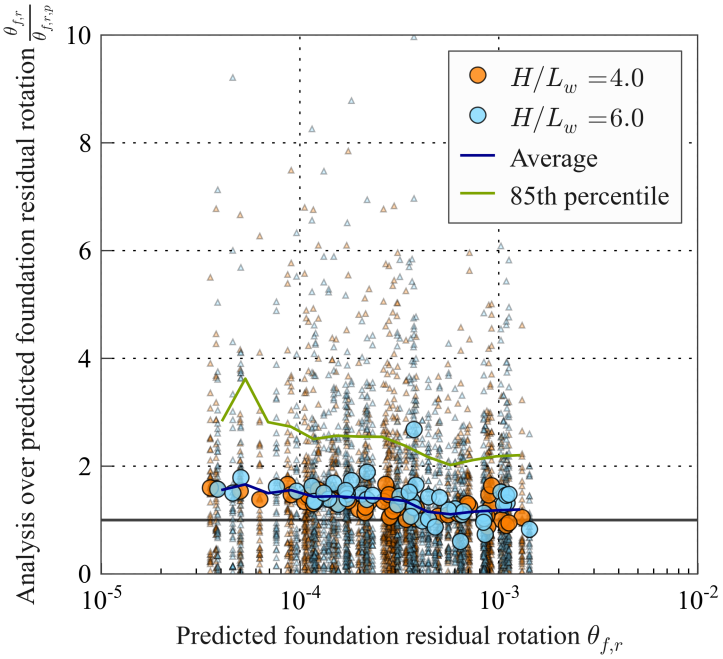

Figure 9.20: Residual foundation rotation from soil-structure MDOF model

9.3.3 Compare MDOF behaviour to SDOF behaviour

There were only three differences between the SDOF and MDOF models, the different damping models, the distribution of vertical load and the distribution of seismic mass. The difference in damping models may provide a small difference in the behaviour especially in the

non-linear range, but the differences were limited as both models had some small reduction in the damping co-efficient when the structure behaved inelastically.

An accurate representation of the vertical load is essential for both the behaviour of the macro-element and for capturing P-delta effects. For the SDOF model the design vertical load was portioned with the lumped mass node having the equivalent amount of vertical load assigned to it, and the remainder was assigned to the foundation node. For the MDOF model the design vertical load was portioned evenly to each storey node and none to the foundation node. Both models attempted to model the design assumptions as accurately as possible and it is unlikely that the difference in behaviour between the two models was due to this discrepancy.

The main cause of the difference in residual to peak drift ratios between the SDOF and MDOF models was the way the SDOF drift versus inter-storey drift from the MDOF model were defined. Another minor contribution may have been due to the converting of the MDOF to an equivalent SDOF, where for the MDOF the first mode participation mass changes when the structure behaves inelastically, which can not be captured by an SDOF model.

The difference in the foundation behaviour is less trivial. In fact the changes in the behaviour come from the additional MDOF mechanisms. Figure 9.21 shows the foundation behaviour in terms of the loads and deformations for a four storey wall building on soil with a shear modulus of 40 MPa subject to the Chi-Chi 1999 earthquake ground motion RSN3317_2 from the NGA-West2 database (Ancheta et al., 2013). It is obvious that the settlement for the MDOF system is greater while the demand moments are almost identical. Interestingly the shear force and the soil-foundation shear deformation are greater for the MDOF model, which is the key cause of the different behaviour. For a SDOF the shear force is limited by the plastic hinge moment, while for an MDOF the higher modes can amplify the shear force at the foundation by more than three times (see Figure 9.14).

The additional high frequency shear forces from higher modes especially at low levels of excitation, as seen by the inset on the shear force plot in Figure 9.21, results in considerable amplification of the settlement. The shear force amplification to the settlement (or shear-induced settlement) is particularly noticeable at the beginning of the rotation versus settlement plot, where the rotation levels are almost identical, however, the settlement of the MDOF is much greater.

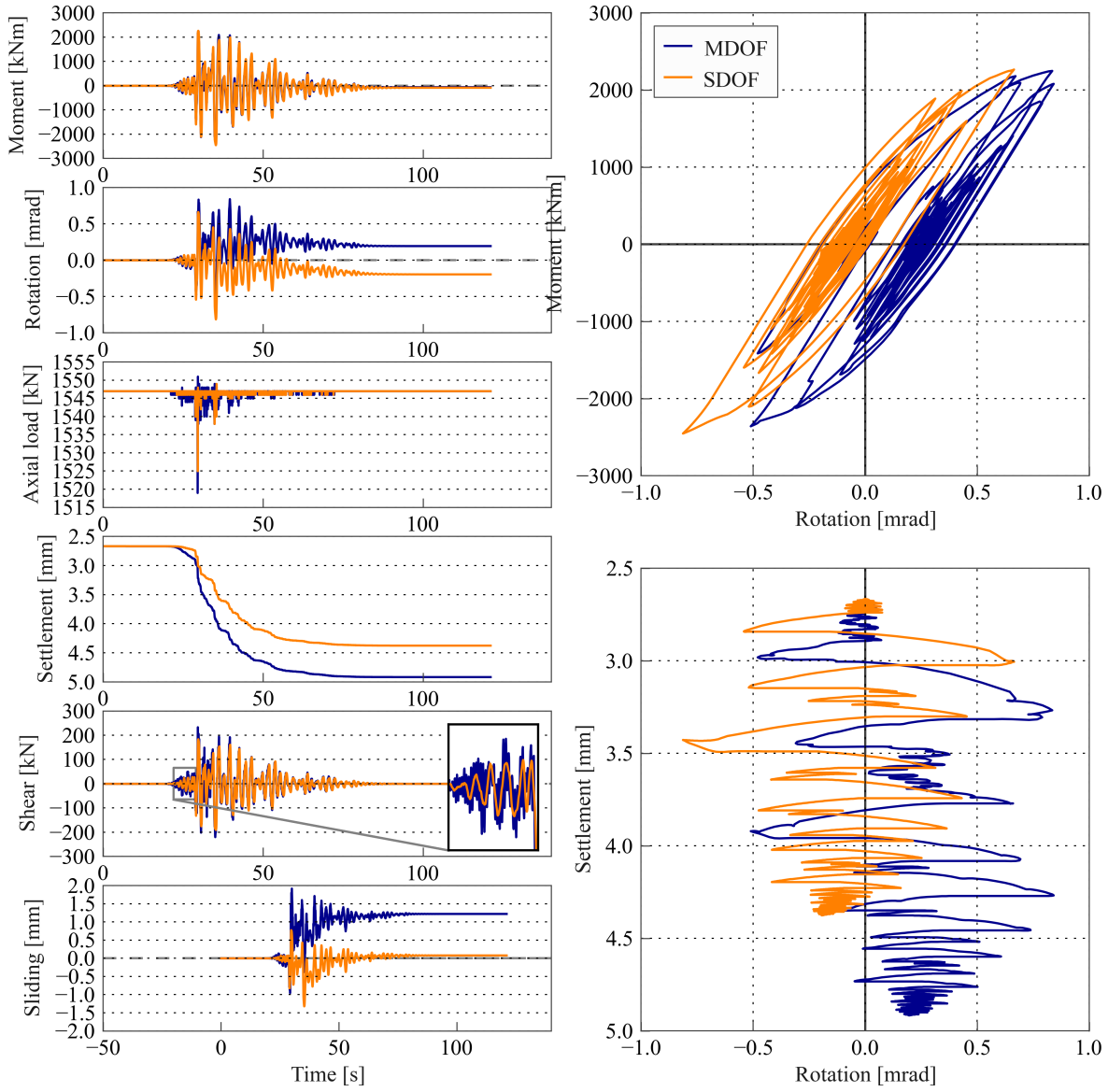

Figure 9.21: Time series

In fact investigating the normalised moment and shear force with reference to the foundation load bounding surface from Nova and Montrasio (1991) in Figure 9.22 the additional shear forces push the foundation closer to failure.

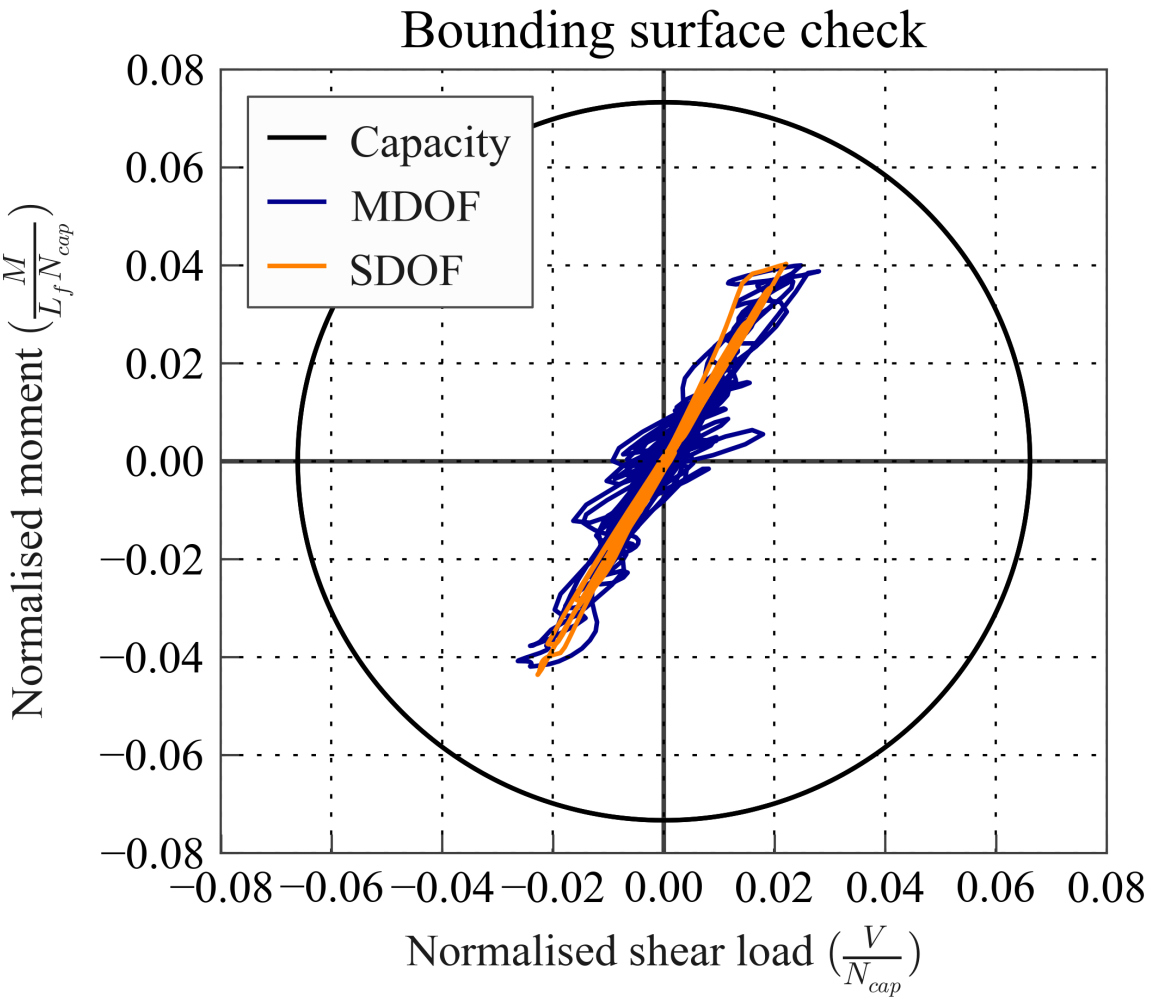

Figure 9.22: Bounding Surface

Just as the ratio of foundation length to structure height was used to account for the influence of the shear force for the foundation rotational stiffness reduction curve and displacement modification factor in Chapter 6, this ratio can be used here for to understand the shear amplification here.

Figure 9.23 plots the ratio of peak foundation rotation of the MDOF over the SDOF in terms of both the amplified shear at the base due to higher modes (V^o_{base}) (Equation 9.7) on the x-axis, and the foundation length to wall effective height (L/H) shown as different coloured points. There was trend for the buildings with a L/H ratio less than 0.4 and to a certain extent less than 0.5, where the larger the shear amplification the larger the ratio of MDOF foundation peak rotation to SDOF, while the trend was less obvious for the large L/H ratio buildings. The other trend was that the MDOF foundation peak rotation increased compared to the equivalent SDOF model, when the L/H was larger.

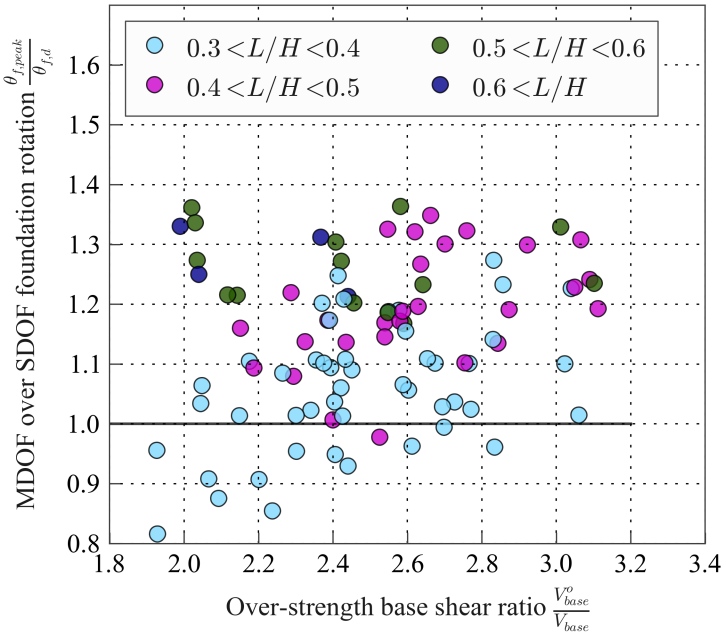

Figure 9.23: Compare peak foundation rotation from MDOF and SDOF models

The same shear amplification trend is starkly obvious for the SFSI-induced settlement in Figure 9.24 and the reason may be two-fold. Not only has the foundation peak rotation increased due to the larger shear force but the shear deformation alone can induce settlement (see Gajan and Kutter (2009)).

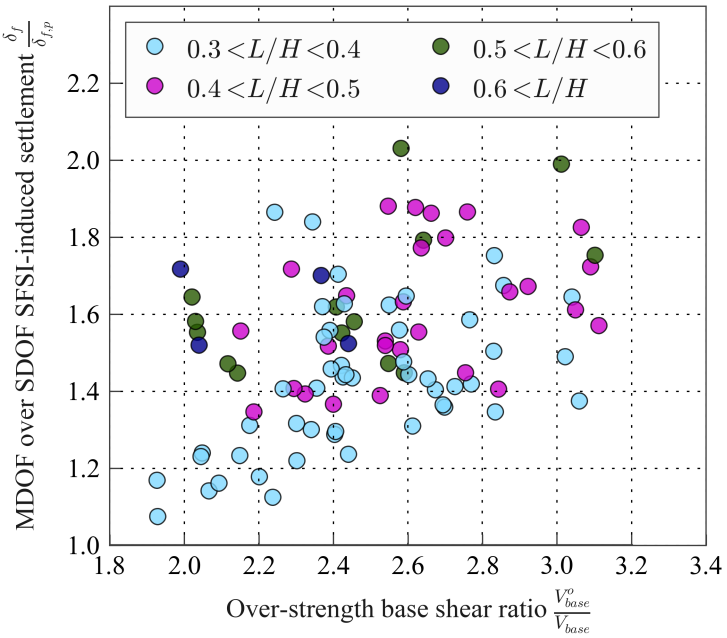

Figure 9.24: Compare SFSI-induced settlement from MDOF and SDOF models

Interestingly there was no observable trend between amplified shear force for the residual

rotation in Figure 9.25.

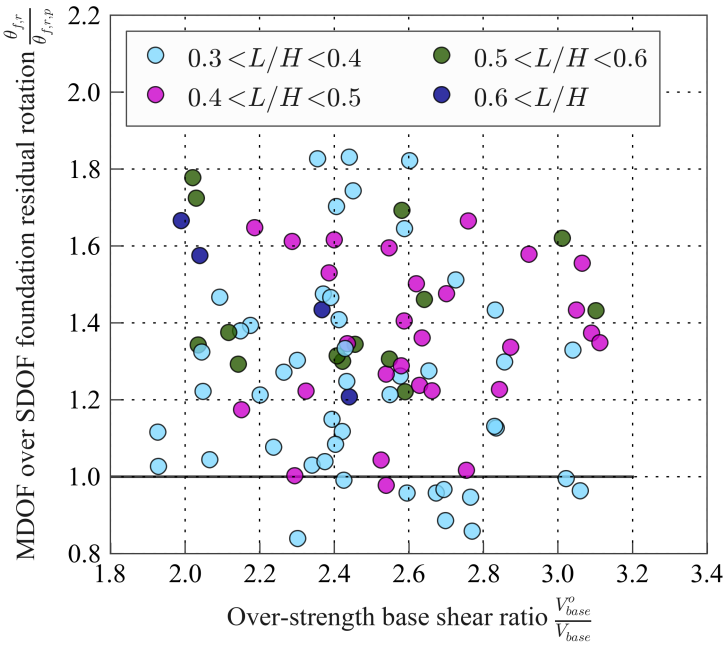

Figure 9.25: Compare residual foundation rotation from MDOF and SDOF models

The amplification of the shear force should be accounted for in the design of foundations for MDOF structures. A simple modification to the effective height parameter can account for these effects on the rotational behaviour. Since the L/H parameter is used as a proxy for the ratio of the shear force to moment for SDOF structures, the parameter can be adjusted to reflect the additional shear for MDOF structures. The amplification of the shear force can be considered as if the effective height H has reduced (eg. for a shear amplification of three the adjusted effective $H^\star$ value would be one-third of the effective height) (See Equation 9.18).

$$\frac{L}{H^\star} = \frac{L}{H} \times \frac{V^o_{base}}{V_{base}} \tag{9.18}$$

This modified foundation length to effective wall height parameter can be used to determine the corrected normalised rotation:

$$\Phi = \left(\frac{\theta_f}{\theta_{uplift}}\right)^{1-0.2(L/H^\star)} 10^{0.25(L/H^\star)} \tag{9.19}$$

The modified $L/H^\star$ parameter provides a suitable correction for the rotational behaviour which would also correct some of the discrepancy with the settlement behaviour; however, as is shown in Figure 9.26 even when the expected settlement is recalculated using the average

peak rotation, the analysis settlement was still larger than the calculated settlement. This amplification of settlement is due to the additional shear induced settlement, which was not seen for the non-linear SDOF models since the shear forces were relatively small, but can be seen for the results of the linear SDOF models that had a high L/H ratio in Figure 7.11 in Chapter 7.

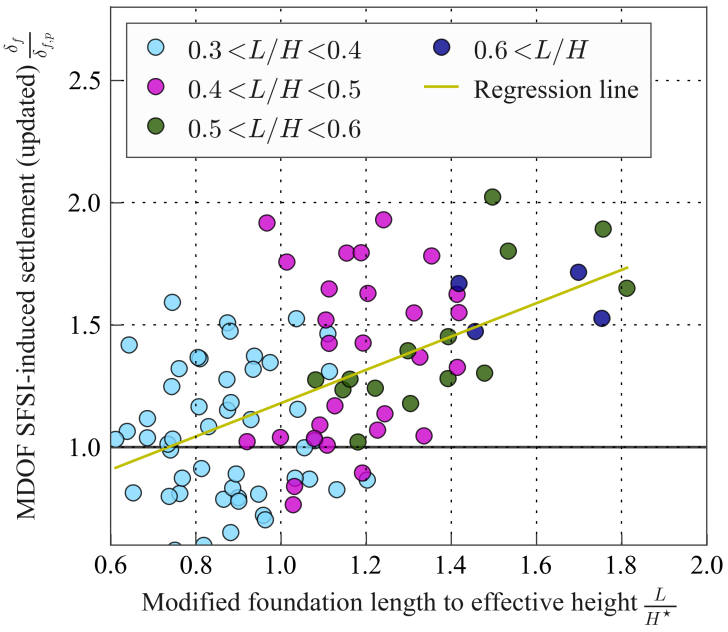

Figure 9.26: SFSI-induced settlement for MDOF model using average peak rotation

To account for the shear induced settlement the SFSI settlement can be multiplied by a shear force factor (s_v) (Equation 11.20), which was determined through simple linear regression through the data in Figure 9.26.

$$s_v = 0.5 + 0.7\frac{L}{H^\star} \geq 1.0 \tag{9.20}$$

Finally the influence of the additional shear force on the shear deformation should be included in design. This can easily be achieved by using the over-strength base shear instead of the design base shear when calculating the shear deformation.

9.4 Conclusion

This chapter discusses the influence of SFSI on MDOF systems. A series of wall buildings that were designed using DDBD assuming a rigid base and a second set that were designed with consideration of SFSI effects were assessed through time history analysis. The numeri-

cal models had lumped masses at each storey and were developed to emulate the underlying assumptions of the design. The fixed base buildings were assessed with fixed base conditions and the buildings design with SFSI considerations were assessed using a macro-element model to simulate the soil-foundation interface.

The assessment showed that for the fixed base buildings the DDBD procedure can accurately predict the peak deformations and peak shear and moment demands. The fixed base results also showed that the residual to peak inter-storey drift of an MDOF is less than the peak to residual drift of a SDOF by about 15%. For the buildings that were designed with SFSI considerations the design displacements were well matched by the average analysis displacements. The maximum storey shear was also accurately enveloped by the design over-strength shear profile from Priestley et al. (2007). The moment distribution up the structure in some cases exceeded the design over-strength moment profile from Priestley et al. (2007) and a simple modification was suggested to include the effects of SFSI.

The foundation behaviour was noticeably modified compared to an equivalent SDOF model and this behaviour was attributed to the amplified base shear due to higher modes. The comparison of behaviour from the MDOF to the equivalent SDOF model allowed the influence of the amplified shear force to be quantified for the rotational behaviour using a simple modification to the corrected normalised rotation parameter. The shear induced settlement was also accounted for through an additional shear force factor to amplify the SFSI-induced settlement. The shear deformation was also larger for the wall model and it was recommended that the designer should use the over-strength shear force for the prediction of shear deformation.

Chapter 10

Influence of SFSI on frame structures

10.1 Introduction

The behaviour of a multiple footing structure is clearly different from one with a single rigid foundation. In fact, the distribution of the soil-foundation contact area affects the deformation behaviour of the foundation, which in turn changes the dynamic response and the way forces are distributed from and into the structure. It is clear that a simple single footing model can not capture the complexities of differential foundation movement, and therefore, to quantify the distribution of deformations and stresses a more complex frame model must be considered. The foundation deformation can be dis-aggregated into rigid body deformations and differential movement; and therefore many of the expressions developed for rigid foundations may still be applicable to the design of foundations that have considerable flexibility. The quantification of the effects of foundation flexibility is no trivial task as there are many additional parameters that must be considered, such as how footings are sized, the stiffness of the foundation relative to both the soil and superstructure, and the distribution of the superstructure loads to the foundation.

Wotherspoon (2009) explored the deformation of frame structures with isolated footings. The footings were sized using three different approaches, based on equal static factor of safety, equal static settlement and equal geometry. The different footing sizing resulted in different distributions of forces and residual deformations throughout the structure and foundation. An examination of the behaviour of internal and external footings showed that internal footings tended to rotate about the footing centre, while external footings rotated about the internal edge and resulted in greater residual deformations. For the investigated three storey structures the differential settlement was relatively minor and well below the cracking threshold of the structure.

Recent numerical studies by Gelagoti et al. (2011) have investigated the behaviour of a two-storey one-bay frame with isolated footings sitting on clay. Two different footings designs were studied, conventional footings and footings that were purposefully designed to allow for rocking at the base. The rocking footings were sized to so that the footing moment ca-

pacity was smaller than that of the corresponding column. The performance of the structure with rocking footings was compared against a structure with conventionally designed footings during pushover analyses and dynamic time-histories. The rocking footings proved to be advantageous, especially during strong shaking well above the design level. The conventional footing structure suffered from extensive damage and collapsed during three out of the 24 ground motions, compared to the rocking footing structure which suffered only minor damage to its columns and survived all of the ground motions. For the particular case study, the SFSI-induced settlement (due to shake-down from subsequent cycles of footing rotation) was very small. Gelagoti et al. (2012) investigated the minimum footing size for frames that would prevent toppling collapse, concluding that the toppling displacement of the system can be taken as half of the footing length when the bearing capacity factor of safety is greater than or equal to four.

This chapter examines the complexities of dynamic SFSI with a focus on concrete frame structures, although all of the findings can be applied to other frame materials. The chapter involves a case study set of structures to highlight some of the major mechanisms, a discussion of potential ways to account for these mechanisms in the integrated design procedure, and finally a limited parametric study investigating the behaviour of buildings designed using the proposed integrated design method.

10.2 Deformable foundation effects

10.2.1 Raft versus pad footings

In all previous analyses in this dissertation the foundation was always considered as a rigid raft foundation. For a rigid raft the distribution of stresses and the moment required for foundation uplift could be approximated using formulations such as those suggested by Cremer et al. (2001, 2002) (Equation 10.1), where N is the axial load on the foundation, N_{ult} the ultimate bearing capacity under purely axial load, B the foundation length, α a factor to account for the distribution of forces under purely elastic conditions, and γ a factor to account for the non-linear behaviour of the soil.

$$M_{uplift} = \frac{NB}{\alpha} e^{-\gamma \frac{N}{N_{ult}}} \tag{10.1}$$

The value of α is based on the stress distribution at uplift and typically for rectangular foundations a value of 4.0 is taken to ensure the centre point of the stress distribution being located at one quarter of the foundation length from the foundation centre (Figure 10.1 - left).

For foundations with individual footings the stress distribution can change considerably. Fig-

ure 10.1 - right, shows the theoretical extreme of this effect, where the pad footings can be considered as point supports and the uplift moment doubles as all of the foundation support comes from the extreme edge.

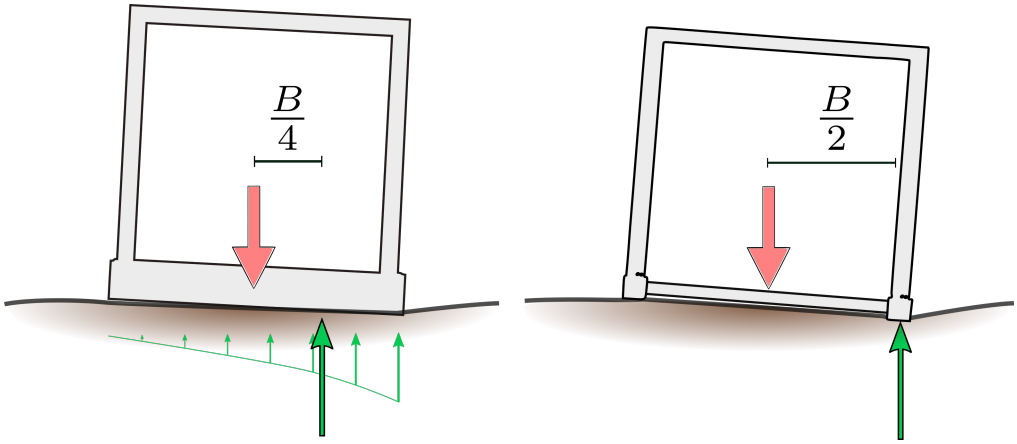

Figure 10.1: Increase in moment arm for isolated footings

The influence of this effect is important and means that the stiffness degradation curve developed in Chapter 6 for raft foundations is no longer valid. For the buildings designed in Section 10.5 the value of alpha was taken as 3.0, as a halfway point between the theoretical possibilities. However, the plastic response also changes due to the loading being more concentrated, as well as the stiffness of the superstructure influencing how the stresses are transferred between footing, thus further research is needed to better estimate a suitable value for α. Advanced finite element modelling may result in improved estimates of the foundation rotational stiffness.

10.2.2 Flexibility in the foundation

The flexibility of the foundation is important to both the overall stiffness and the potential to induce additional stresses in the structure. Figure 10.2 considers the deformations in the foundation as three separate mechanisms and shows the deformations or stresses they cause in the structure.

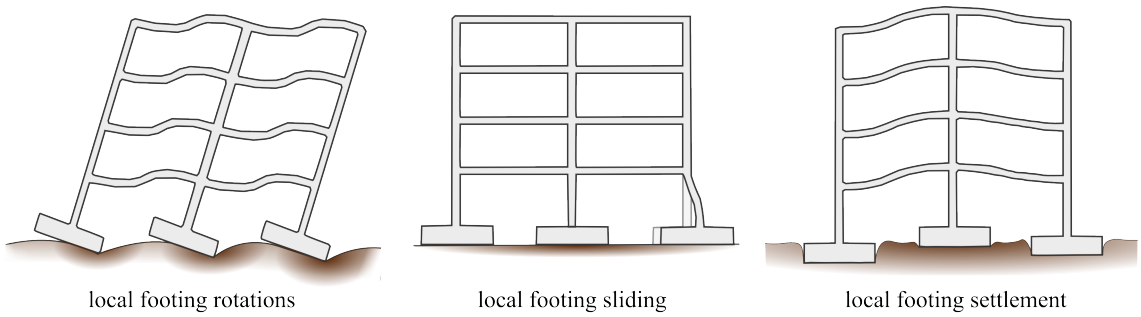

Figure 10.2: Flexible foundation deformations

In reality all deformations, both rigid-body and due to foundation flexibility, can be present, and the induced stresses can compound in some cases. The overall system stiffness can be considerably lower than for rigid foundations due to the additional deformation mechanisms, especially for squat buildings. Figure 10.3 demonstrates the influence on foundation stiffness for a squat five bay building, where the rigid foundation means that the entire foundation contact area is engaged and provides a large rotational stiffness. The flexibility in the foundation results in the superstructure deforming and the full soil-foundation contact area does not engage, thus the system is more flexible.

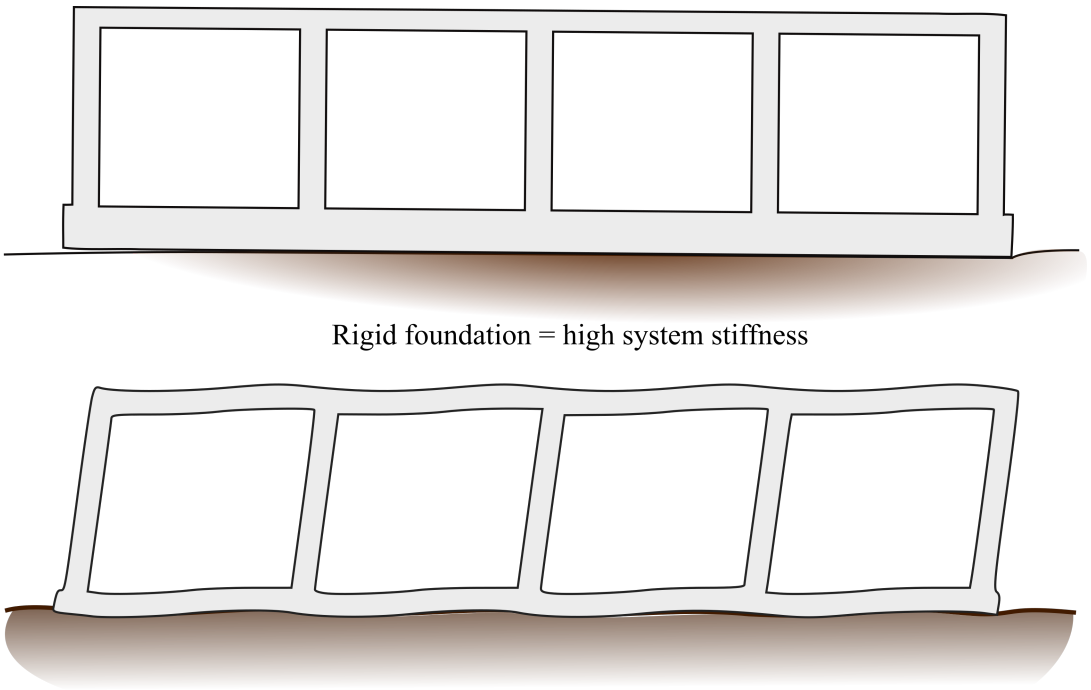

Figure 10.3: Squat buildings with and without foundation flexibility

The level of deformation and stress distribution from each mechanism is strongly influenced by the geometry of the structure and its footings. Figure 10.4 considers two hypothetical frames to demonstrate this. The left frame has short wide footings, which have relatively low rotational stiffness and high vertical stiffness; the right frame has long thin footings, which have high rotational stiffness but a comparatively low vertical stiffness. The two buildings have the same superstructure but under earthquake loading the internal moments that develop are noticeably different. The low rotational stiffness in the left frame means that the moment demand is largely distributed to the beams; while the relatively low vertical stiffness in the right frame limits the shear and moment demand that can be generated in the beams.

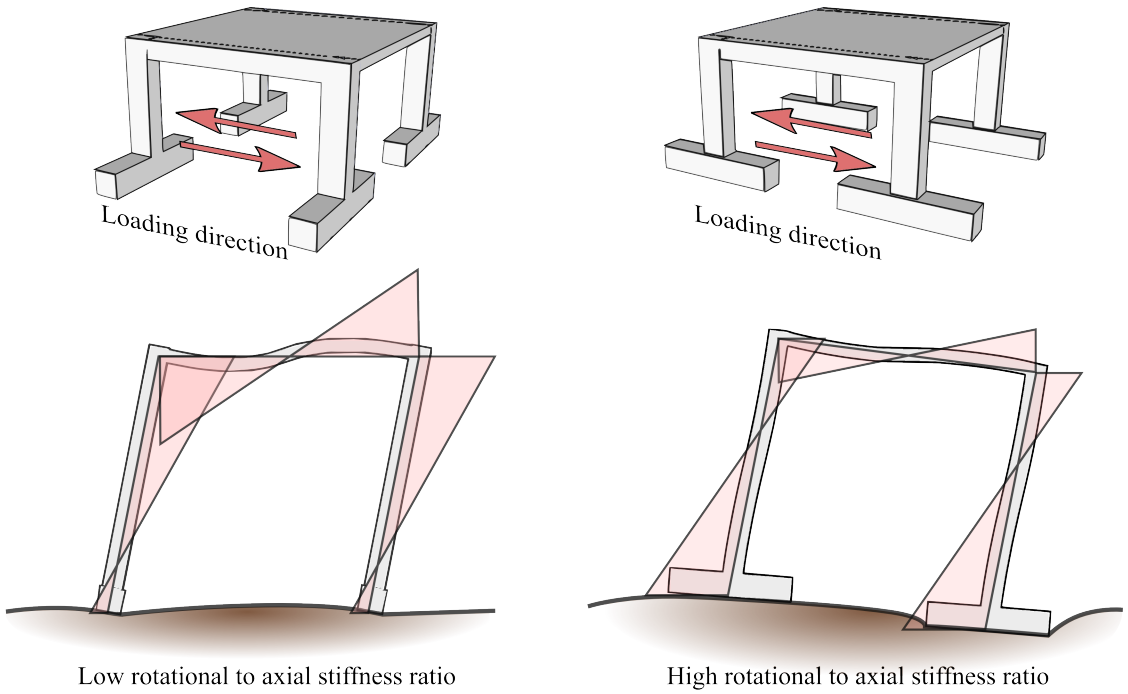

Figure 10.4: Variations in foundation rotational and vertical stiffness and corresponding displaced shape and moment demand

10.3 Case study frame structures

The two theoretical frames were numerically modelled (Figure 10.5 - a) and subjected to the Chi-Chi 1999 (CHY037) ground motion (NGA3276_1 (Chiou et al., 2008)). The influence of the different footings is apparent in the moment demands (Figure 10.5 - b) in the frame. The moments in frame two (low rotational stiffness) were limited at the base due to the increased rotation of the footings. The ratio of the moments between the column base and the beams was noticeably different, with more moment demand distributed to the beams for the footing with low rotational stiffness, as expected. The overall drift and the rigid body rotation of the foundation was approximately the same, thus the increased footing rotation in frame two caused a reduction in the superstructure deformation, reflected in the smaller moments. The rigid body rotation was slightly increased in frame two, this is a reflection of the smaller global rotational stiffness, and the more plastic response.

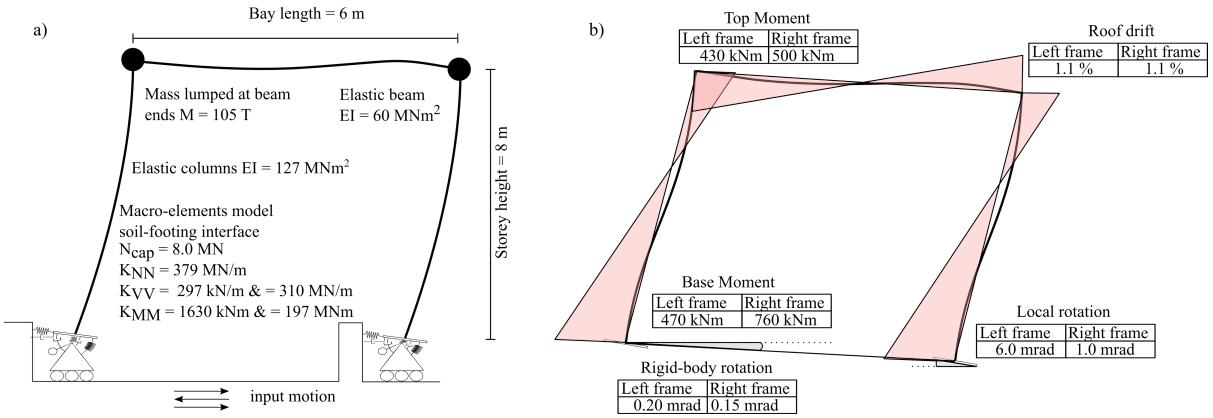

Figure 10.5: Left - Frame numerical model, Right - Frame moment demand and deformations

Another interesting characteristic of isolated footing foundations is the variation in foundation axial load due to frame action. During seismic loading the overturning moment applied to a frame results in alternating tension-compression forces in the outer columns, which get transferred to the foundation and soil. The rotational behaviour and level of settlement is highly dependent on the level of footing axial load (Chapter 7) and therefore the cyclic variation of axial load along with the cyclic applied moment and shear forces on the footing, result in asymmetric behaviour.

Figure 10.6 shows the moment-rotation and settlement rotation behaviour of the left footing from the two frames. The moment-rotation behaviour of the low rotational stiffness footing shows the asymmetric stiffness and moment capacity that occurs due to the changes in the axial load. The negative rotation was accompanied with a reduction in vertical load, thus the moment capacity reduced limiting it to a value close to 400 kNm, in the opposite direction the additional vertical load increased the capacity and stiffness and the moment exceeded 500 kNm. The difference was less apparent for the footings with high rotational stiffness as the capacity was considerably large than demand.

The asymmetric behaviour can also be seen in the rotation-settlement response (Figure 10.6 b), where the changes in axial load result in an up-down motion of the footing. Interestingly the asymmetric settlement behaviour is more prominent in high rotational stiffness, as the shakedown effect is less prominent. The additional frame action mechanism may result in further settlement and increased residual deformation.

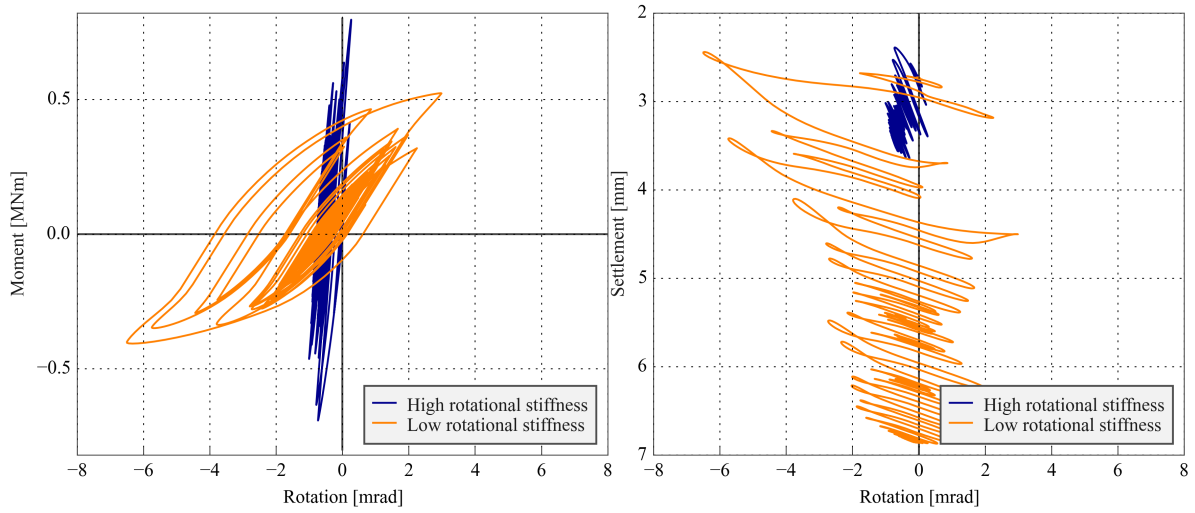

Figure 10.6: Left - Left footing moment-rotation, Right - Left footing settlement-rotation

10.4 Footing deformations

To consider foundation flexibility in design, the engineer needs to be able to estimate the expected level of footing rotation. The first step is to obtain the moments in the footings based on the expected seismic storey forces. Although there are many methods to obtain the footing moments, the moment equilibrium method is suggested here due to the ease in which the building is assessed at its peak response.

Moment equilibrium method

The moment equilibrium method presented here is for regular frame structures (see Figure 10.7); for irregular frames the equations need to be modified to ensure equilibrium is met.

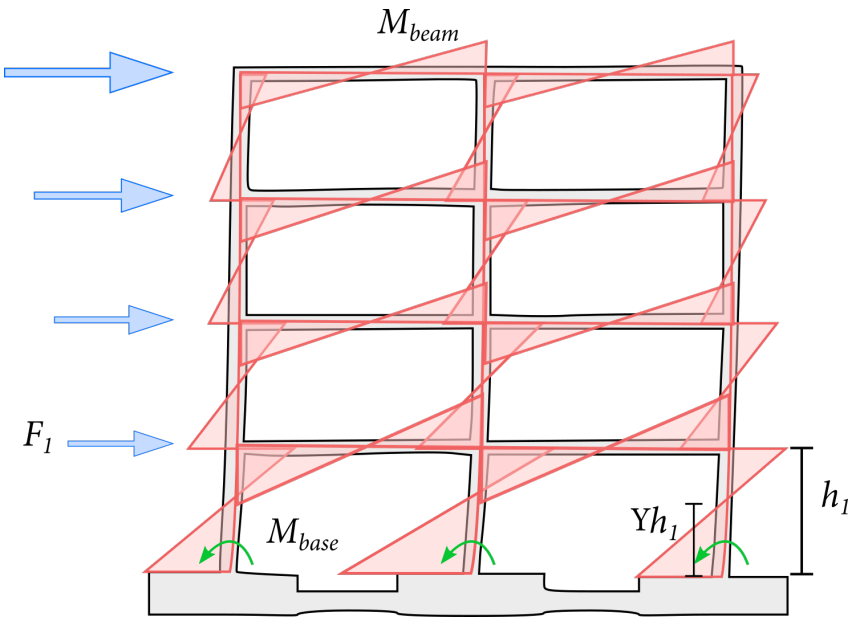

Figure 10.7: Moment equilibrium method

The first step is to determine the total overturning moment of the frame:

$$M_{OT} = \sum_{i=1}^{n_{storeys}} (F_i \times h_i) \tag{10.2}$$

The overturning moment is then portioned between the column base moments (M_{base}) and the moment resisted through frame action (M_{frame}).

$$\sum_{j=1}^{n_{columns}} M_{base} = \mathrm{Y} V_{base} h_1 \tag{10.3}$$

$$M_{frame} = M_{OT} - \sum_{j=1}^{n_{columns}} M_{base} \tag{10.4}$$

Where the coefficient Y corresponds to the point of contraflexural in the ground floor columns and is often taken as 0.6 to prevent soft storey failure.

The necessary tension-compression seismic axial load in the exterior columns is determined from the frame action moment:

$$N_{frame} = \frac{M_{frame}}{L_{building}} \tag{10.5}$$

The seismic axial load must be equal to the sum of the beam shear forces up the structure and can be proportioned in any distribution provided that Equation 10.6 is satisfied:

$$\sum_{i=1}^{n_{storeys}} V_{beam,i} = N_{frame} \tag{10.6}$$

In this dissertation, the beam shear forces were proportioned in the same ratio as the storey shear forces.

$$V_{beam,i} = N_{storey} \frac{V_{storey,i}}{\sum_{i=1}^{n_{storeys}} V_{storey,i}} \tag{10.7}$$

The beam moments are then determined through equilibrium:

$$M_{beam} = 0.5 V_{beam} L_{beam} \tag{10.8}$$

And the column base moments are distributed with the outer columns taking half of the interior columns:

$$M_{base,interior} = \frac{\sum_{j=1}^{n_{columns}} M_{base}}{n_{columns} - 1} \tag{10.9}$$

$$M_{base,exterior} = 0.5 M_{base,interior} \tag{10.10}$$

$$\tag{10.11}$$

10.4.1 Calculating the footing rotation

Provided that the members are designed such that their moment capacities are close to their nominal design moments, the footing moments can be estimated by extrapolating the base moment down to the base of the footing (see Figure 10.8 - where the footing inertia has been ignored but can easily be added through simple equilibrium).

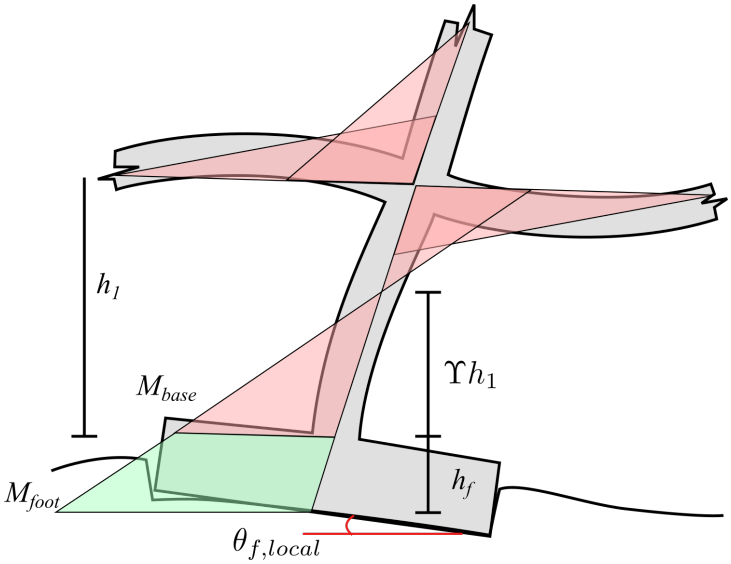

Figure 10.8: Estimate the footing moment

For the case where there are no tie beams the footing rotation can be calculated based on the footing effective rotational stiffness and the design moment:

$$\theta_{footing} = \frac{M_{footing}}{K_{footing,eff}} \tag{10.12}$$

Where the footing effective rotational stiffness ($K_{footing,eff}$) can be determined based on the elastic stiffness ($K_{f,0}$) and the stiffness degradation curve from Chapter 6:

$$\frac{K_f}{K_{f,0}} = 0.8 - 0.04\log(\Phi) - 0.7(1 - \exp^{-0.18\Phi}) \tag{10.13}$$

The additional vertical load in the exterior footing from frame action should be considered as acting in tension when determining the peak rotation as this would provide the lowest rotational stiffness, unless the verical factor of safety is less than two, in which case both tension and compression should be checked. Although the column moment capacities change due to the variation in axial load, it is not necessary to account for such changes unless it is believed that the changes would be very large. The actual rotation of exterior columns is very difficult to estimate due to the asymmetric behaviour resulting in considerable additional residual rotation.

The footing rotation should then be checked against the global rotation to ensure compatibility (Figure 10.9). Footing rotation that is less than the global rotation will increase the curvature in the columns. When the footing rotation is equal to the global rotation then the deformations in the structure are not changed and the rotation is purely a rigid rotation.

When the rotation exceeds the global rotation then the column curvatures are reduced, however, if the calculated rotation is so big that it exceeds the global rotation plus the expected plastic rotation then the design is not possible as the moments at the column base would not develop. The designer must redistribute more of the base moment to the frame action by reducing the value of Y from Equation 10.4, increasing the footing sizes or designing the building to a larger drift.

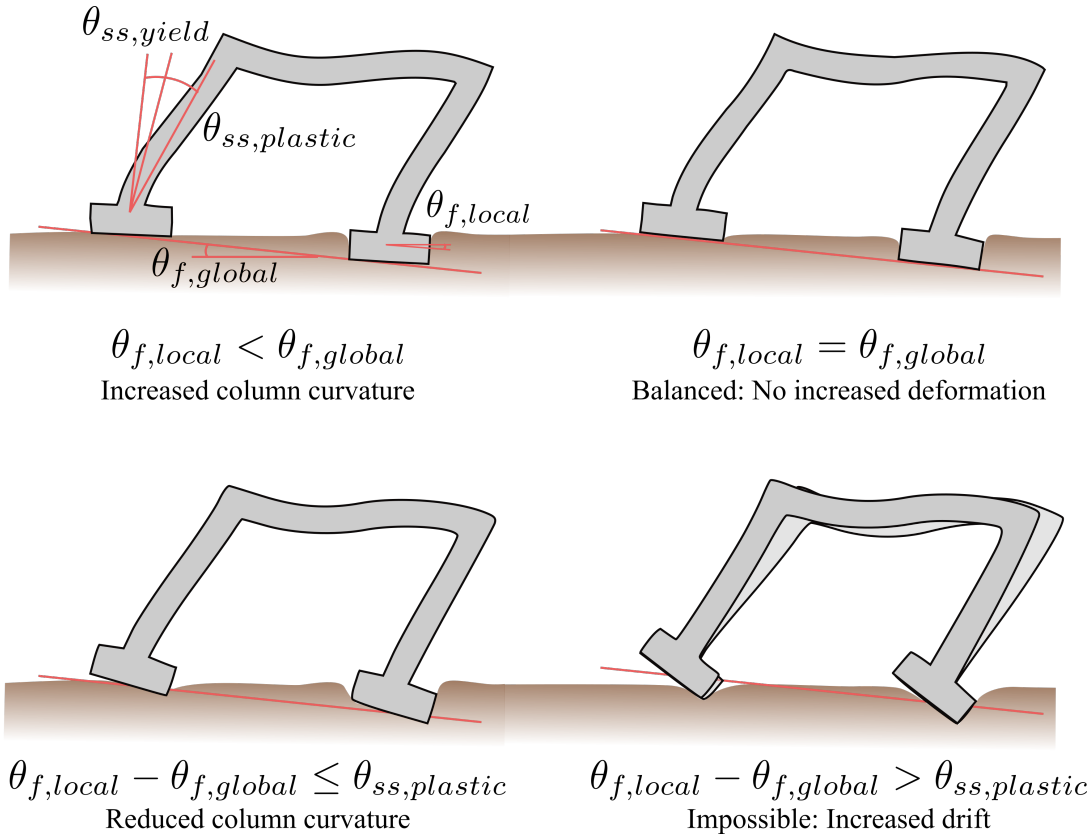

Figure 10.9: Compatibility of footing rotation

When tie beams are used they provide a restoring force towards a purely rigid body rotation. The footing rotation must therefore include the tie beam restoring force through equilibrium analysis, where the deformations in the tie beams must be compatible with the forces they are applying.

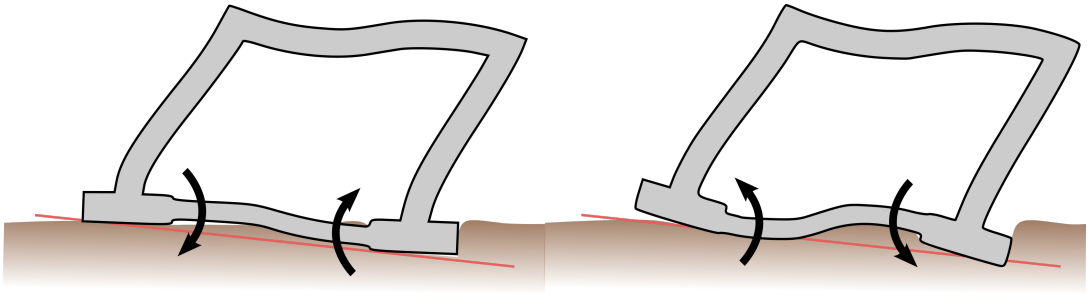

$\theta_{f,local} < \theta_{f,global}$
Tie beams increase rotation

$\theta_{f,local} > \theta_{f,global}$
Tie beams reduce rotation

Figure 10.10: Tie beams

10.4.2 Permanent footing deformations

Permanent deformations of interior footings can be estimated using the same expressions as for walls and other single support structures. The exterior footings may experience additional permanent deformations as the frame action results in asymmetric rotation and additional cyclic vertical displacement as seen in the case study structures in Figure 10.6. For the case where there are no tie beams, the exterior footing permanent deformation can be approximated using single support expressions but with an additional frame action factor to account for the variation in axial. Unfortunately the current formulation of the macro-element model does not provide accurate behaviour when the variation in the axial load is large, which can be the case for tall frame structures. Thus the appropriate frame action factors could not be accurately determined but expressions similar to those provided in Equations 10.14 and 10.15 would be expected.

$$\theta_{f,res,ext.} = \theta_{f,res.pred} \times (1 + q\frac{N_{frame}}{N_{static}}) \tag{10.14}$$

$$\delta_{f,ext.} = \delta_{f,pred.} \times (1 + q\frac{N_{frame}}{N_{static}}) \tag{10.15}$$

When tie beams are used the residual rotations are modified by the forces in the tie beams. The tie beams apply a restoring force towards the footing rotation matching the entire foundation rotation, however, if the tie beams deform inelastically the non-linear behaviour may not be restored and result increased residual deformations.

The differential settlement is also influenced by the stiffness of the beams and tie beams. Differentially settlement results in induced stresses in the beams and ties which also apply a restoring force against differential settlement.

Influence of gravity loads

The orientation of the floors in the building plays an important role in the distribution of gravity forces. For the case where floors are orientated parallel to the frame, the floor loads can be directly transferred into the columns without causing gravity induced moments. For the case where the floors are orientated perpendicular to the frame and are supported by the beams, the floor loads impose additional gravity induced moments on the footings (Figure 10.11). The additional static moment results in asymmetric behaviour of the footing and causes the footings to try to dissipate the moment through rotation.

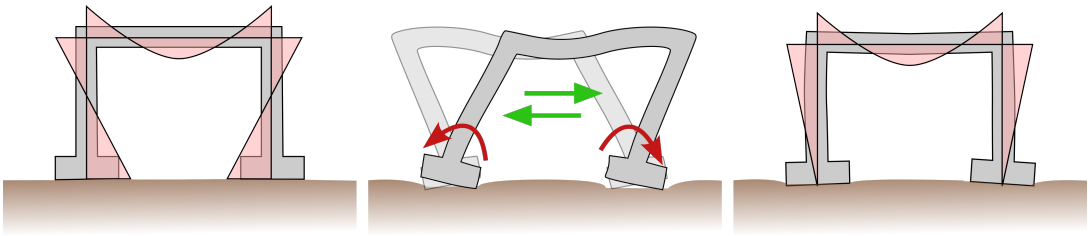

Figure 10.11: Influence of gravity-induced footing moments

10.5 Parametric study on concrete frame structures

To investigate some of the effects discussed in this chapter six frame structures were design and analysed. The inputs for the buildings are shown in Table 10.1 and design procedure followed the proposed design procedure in Section 8.5 in Chapter 8 with a design example provided in Appendix D.

Table 10.1: Frame design inputs

Parameter	Range
Number of storeys (n_s)	$[2, 4, 6]$
Number of bays (n_b)	$[1, 3]$
Bay lengths (l_b)	6.0 m
Storey heights	3.4 m
Beam depth (h_b)	$0.5 + 0.05n_s$ m
Beam width	$0.8h_b$ m
Column depth (h_c)	$0.1n_s + 0.05l_b$ m
Column width	h_c m
Building width $W_{building}$	20 m
Number of frames	2
Footing height	$0.8 + 0.05n_s$ m
Footing length to width ratio	1.0
Footing depth to breadth ratio	0.3
Target static bearing factor of safety	5.0
Soil type	C
Design hazard level	0.4
Live load	3 kPa
Dead load	6 kPa
Total peak drift (θ_t)	0.025
Superstructure inter-story drift (θ_{ss})	0.02
Soil shear modulus (G)	40 MPa
Soil friction angle (ϕ)	34
Soil unit weight (γ_s)	18.0 kN/m^3
Concrete compression strength (f_c)	30 MPa
Rebar strength (f_y)	300 MPa

10.5.1 Numerical model

The numerical analyses were conducted using the non-linear finite element software Ruaumoko3D (Carr, 2015). The superstructure was a -lumped mass, -lumped plasticity stick model of a single frame and each footing was modelled using an independent macro-element soil-foundation interface model (Figure 10.12). The horizontal masses at each storey node were equal to the seismic mass at each storey used for the design and equally portioned at the beam-column joints on that storey. The vertical mass was equal to the sum of the horizontal masses and was lumped at the foundation nodes. The vertical load was based on the total mass of the original structure during seismic excitation. The soil-foundation interface was modelled with the macro-element defined in Chapter 4.

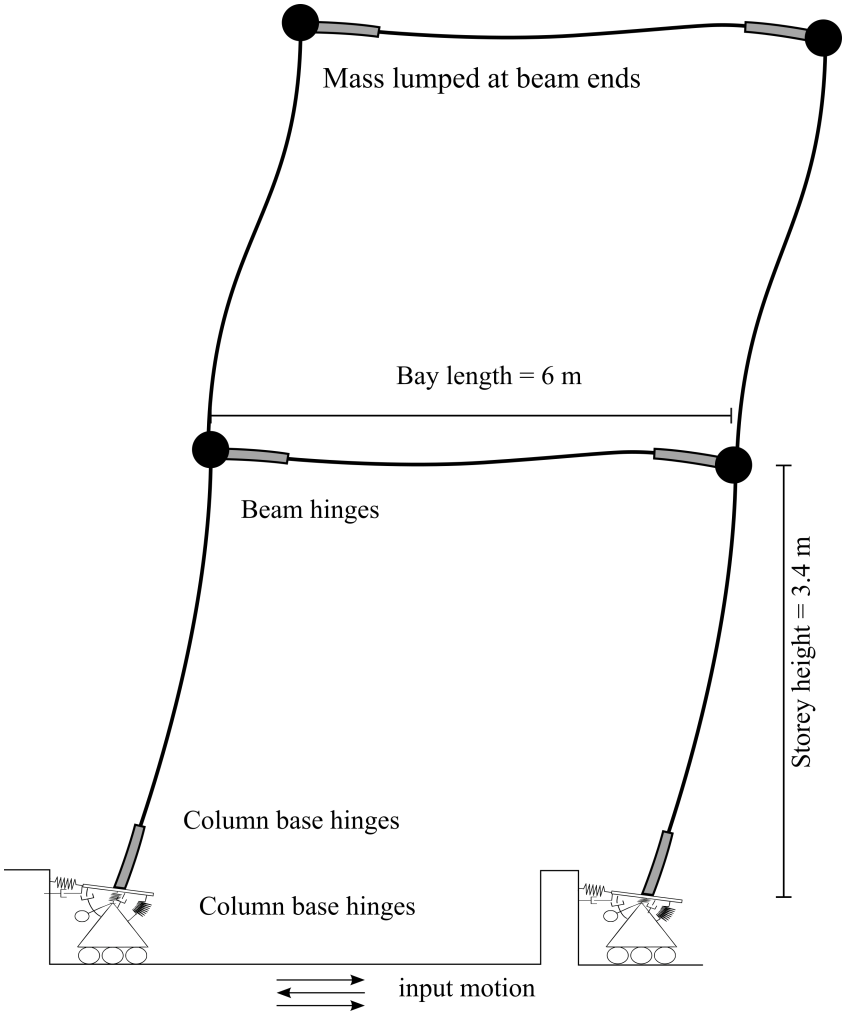

Figure 10.12: Numerical model of frame-foundation-soil system

The BEAM element in Ruaumoko3D was used to model the columns and beams, with non-linear hinge elements at the base of the columns and at the beam ends. The numerical model attempted to model all of the underlying assumptions of the DDBD procedure to highlight the influence of SFSI on the behaviour, therefore all of the hinge moments were set at the nominal column face moments determined through the moment equilibrium method. The hinge post-yield stiffness ratios for the column bases were set to zero and for the beams were set to 0.02. The column hinge lengths were equal to the column depth and the beam hinges were set to half of the beam depth. All of the hinges were modelled with the Ruaumoko3D Modified Takeda rule with 'Takeda fat' properties ($\alpha = 0.4$, $\beta = 0.6$, NF = 1.0, KKK = 2).

Rigid end blocks were assigned to all members except for the column bases on the first storey. The rigid end blocks modelled the beam-column joint and for both the columns and the beams the end block was set at one third of the joint depth. The stiffness of the beam and column elements was determined by matching the fixed base first mode period of the frame to the equivalent SDOF elastic period of the superstructure. The first floor column stiffness was set at 125% of the beam stiffness and the other columns were set at 150% of the beam stiffness;

these ratios represented the different levels of cracking expected in each of the elements. The exact stiffness values were determined by conducting a modal analysis of the superstructure model in Ruaumoko3D.

The damping was modelled using the global Wilson-Penzien linear variation in damping model set at 5% across all modes. Unfortunately the damping coefficients of the Wilson-Penzien model do not decrease when the structure behaves inelastically. The advantage of the Wilson-Penzien model is that unlike the Rayleigh damping model, the constant damping across all modes means that the higher mode vibrations would not be over damped. P-delta effects were not considered in either the design or analysis.

10.5.2 Results

The peak superstructure displacement was well predicted for all the buildings except for the four storey three bay building. This discrepancy may be due to the damping model used as well as issues with the macro element model as discussed later.

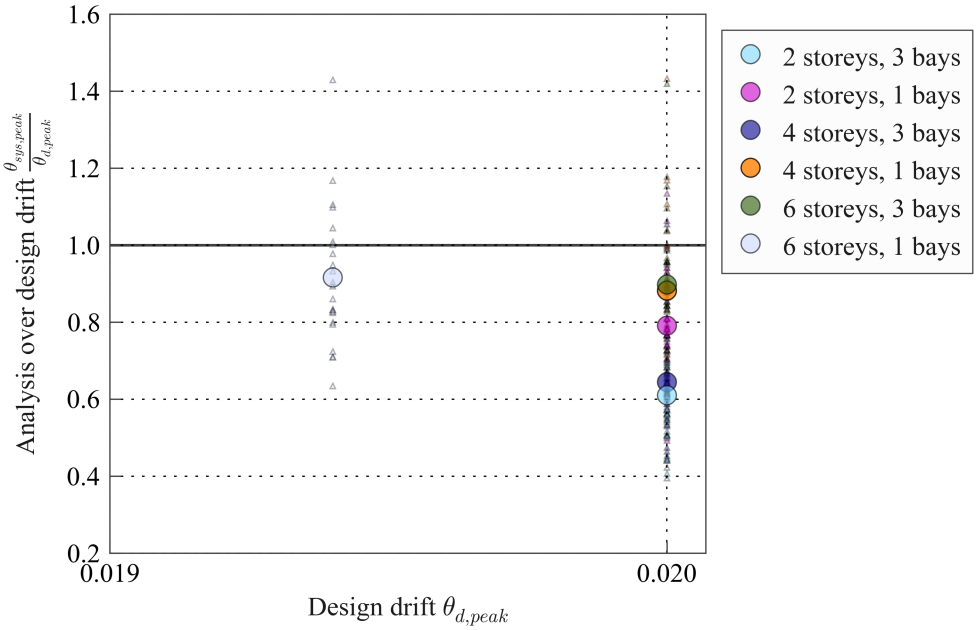

Figure 10.13: Peak interstorey drift from soil-foundation-frame model

The residual drift is compared against the estimate from the SDOF structures of 8.5% of the design inter-storey drift in Figure 10.14. The residual inter-storey drift was higher than for the SDOF, possibly due to the non-linear behaviour having larger hysteretic loops and the large number of non-linear elements in frame. The frame peak drift also occurs in the first floor and this is the location of the majority of the non-linear behaviour.

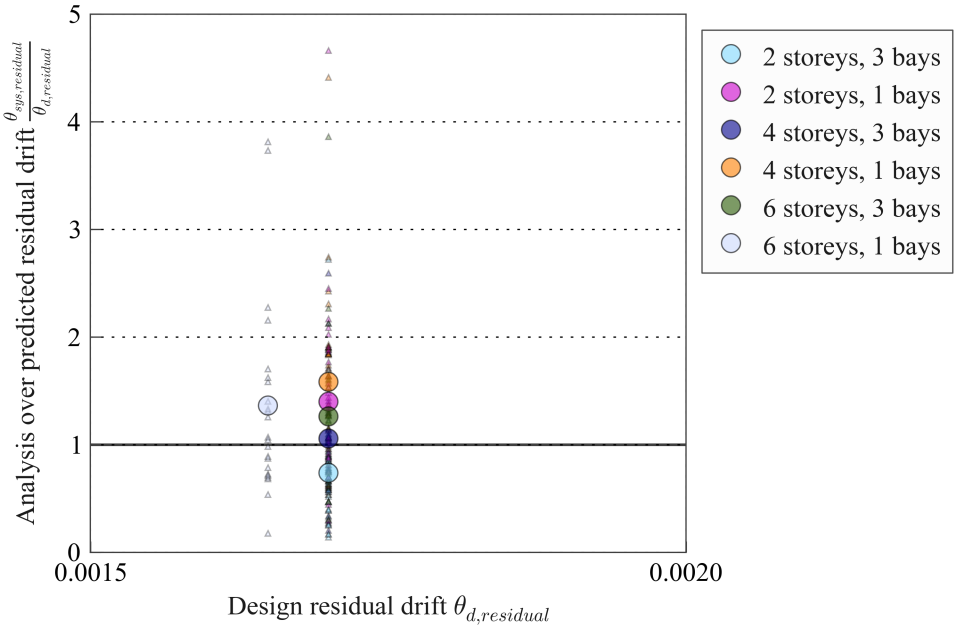

Figure 10.14: Residual interstorey drift from soil-foundation-frame model

The foundation global rotation did not match the design foundation rotation very well. The macro-element is limited in that it uses a 'vertical mapping rule' so the plastic response is governed by rotational and shear loading. In fact, under purely vertical load the behaviour is elastic until it reaches the static bearing capacity. Therefore the foundation behaviour in the global rotation sense was almost elastic and did not show the degradation in stiffness that could be expected if modelled correctly. This led to not only poor estimates of the global rotational behaviour (Figure 10.15) but also the residual global rotational behaviour prediction (Figure 10.16). The two exceptions being the two storey structures where the large deformation occurred due to non-linear footing.

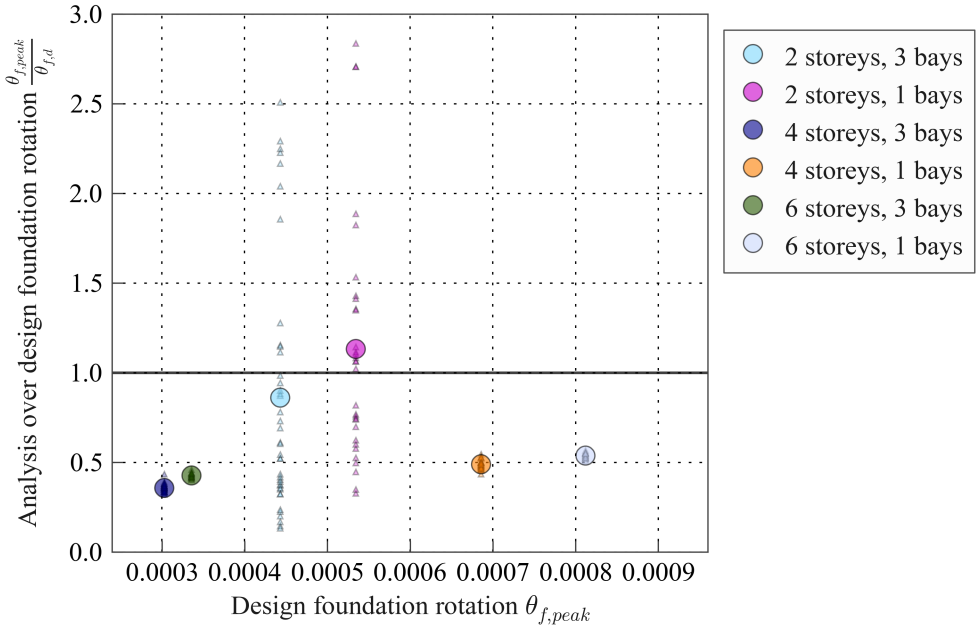

Figure 10.15: Peak foundation rigid rotation from soil-foundation-frame model

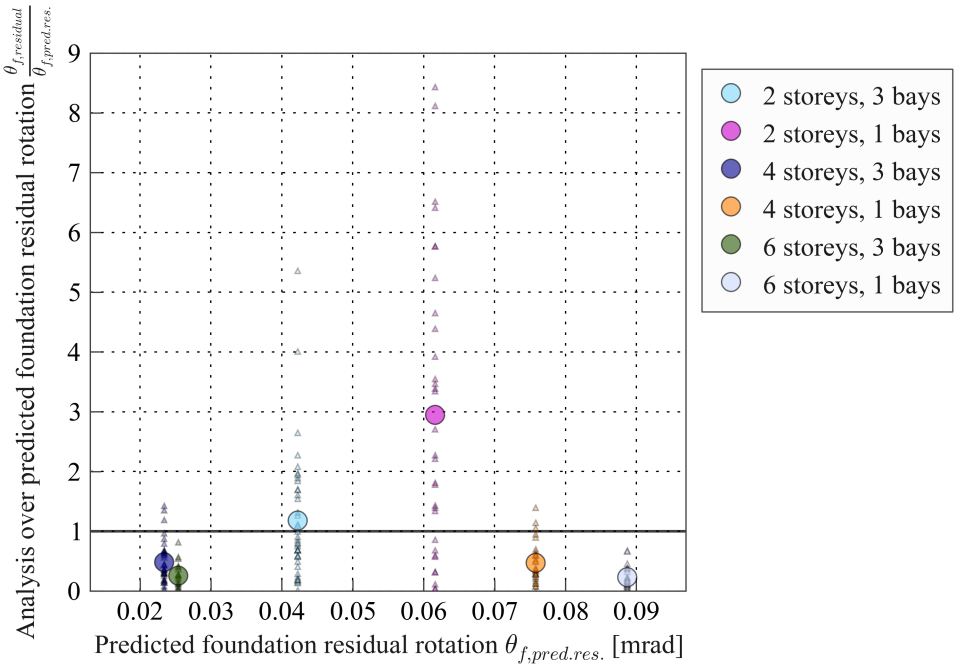

Figure 10.16: Residual foundation rigid rotation from soil-foundation-frame model

The local deformations were far better estimated with the interior frame rotations being very close to the design rotation. The interior rotations were also very consistent, with the two data points for each of the interior footings overlapping for all of the three bay frame buildings (Figure 10.17). The exterior footing rotations were consistently twice as large as the expected design rotation and this was driven by the large level of residual rotation (Figure 10.18) caused

by the asymmetric behaviour.

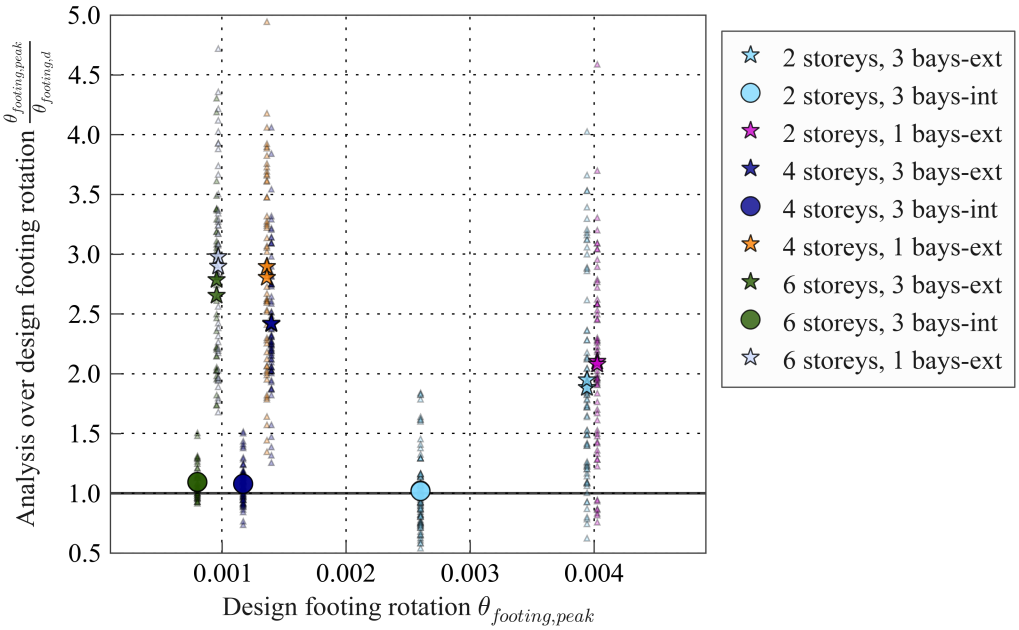

Figure 10.17: Local peak rotations of footings from soil-structure FRAME model

The residual deformations were all bigger than the design values. While the interior footings were reasonably close to the design values the exterior footings were dramatically larger than the predicted values. The worst predicted residual deformations occurred in the taller one bay structures, where the cyclic vertical load due to frame action would be largest. Given that the frame action was not accounted for in the prediction of residual deformation it is no surprise that the residual deformation was under predicted, however, in some cases that residual rotation is larger than the predicted peak rotation which is of some concern. In fact the results for the taller frame structures may be very inaccurate as the numerical model does not correctly simulate large changes in axial load as explained in Section 10.5.3. Looking back at Figure 10.17 it is obvious that the residual rotation of the exterior footings contributed a great deal to the overall peak rotation.

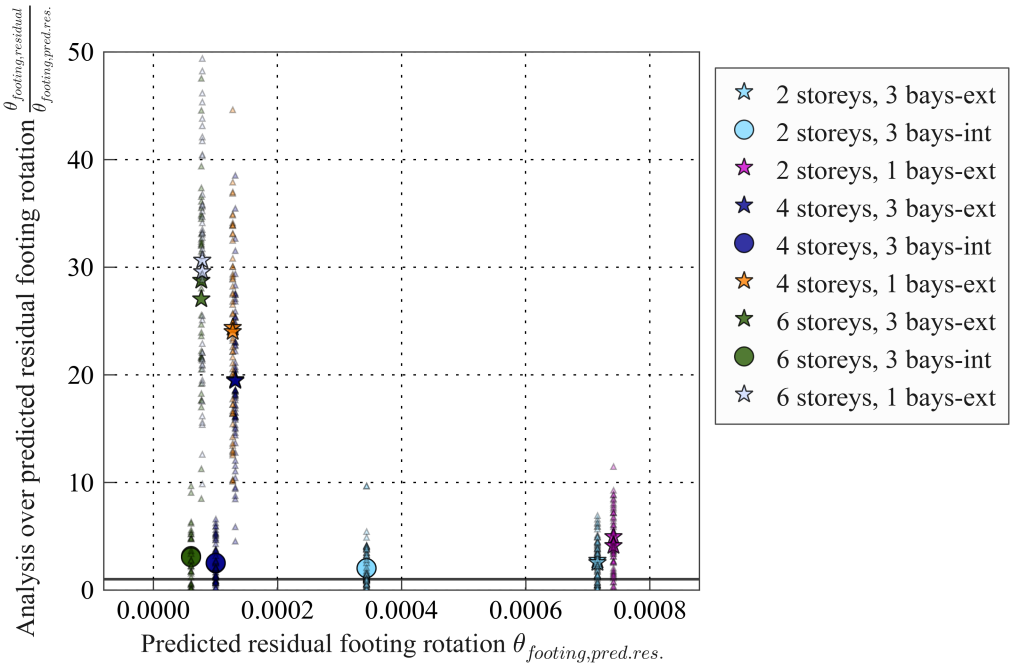

Figure 10.18: Local residual rotations of footings from soil-foundation-frame model

The exterior footing settlements obtained form numerical analyses were all larger than the single support estimates of the proposed method as expected since the frame action mechanism was not accounted for. The interior footings of the taller frame buildings also showed larger than predicted settlements.

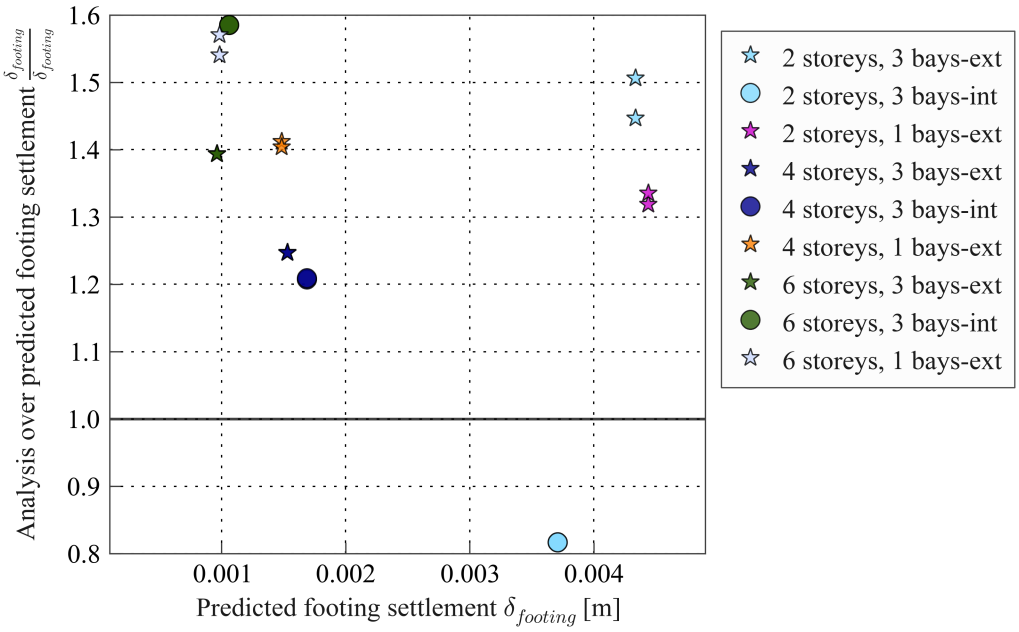

Figure 10.19: Local SFSI-induced settlement of footings from soil-structure FRAME model

10.5.3 Comparison of time history results

Figure 10.20 and Figure 10.21 show the soil-foundation interface behaviour for the two-storey and six-storey three bay frames respectively during the Chi-Chi 1999 earthquake ground motion RSN3317_2 from the NGA-West2 database (Ancheta et al., 2013).

The behaviour for the two storey building looks as expected, the interior footings take more moment and have large axial loads with larger static settlement. The asymmetric behaviour is clearly seen in the rotation plot where the two footings develop cumulative residual rotation and in the moment rotation plot with the footing moment capacity is clearly limited by uplift in one direction. The six storey building demonstrates the same behaviour, however, it is far more extreme. The vertical loading dominates the behaviour and the residual rotations are very large. Since the macro-element has elastic behaviour on unloading it does not restore the plastic deformation and therefore large levels of cumulative deformations occur.

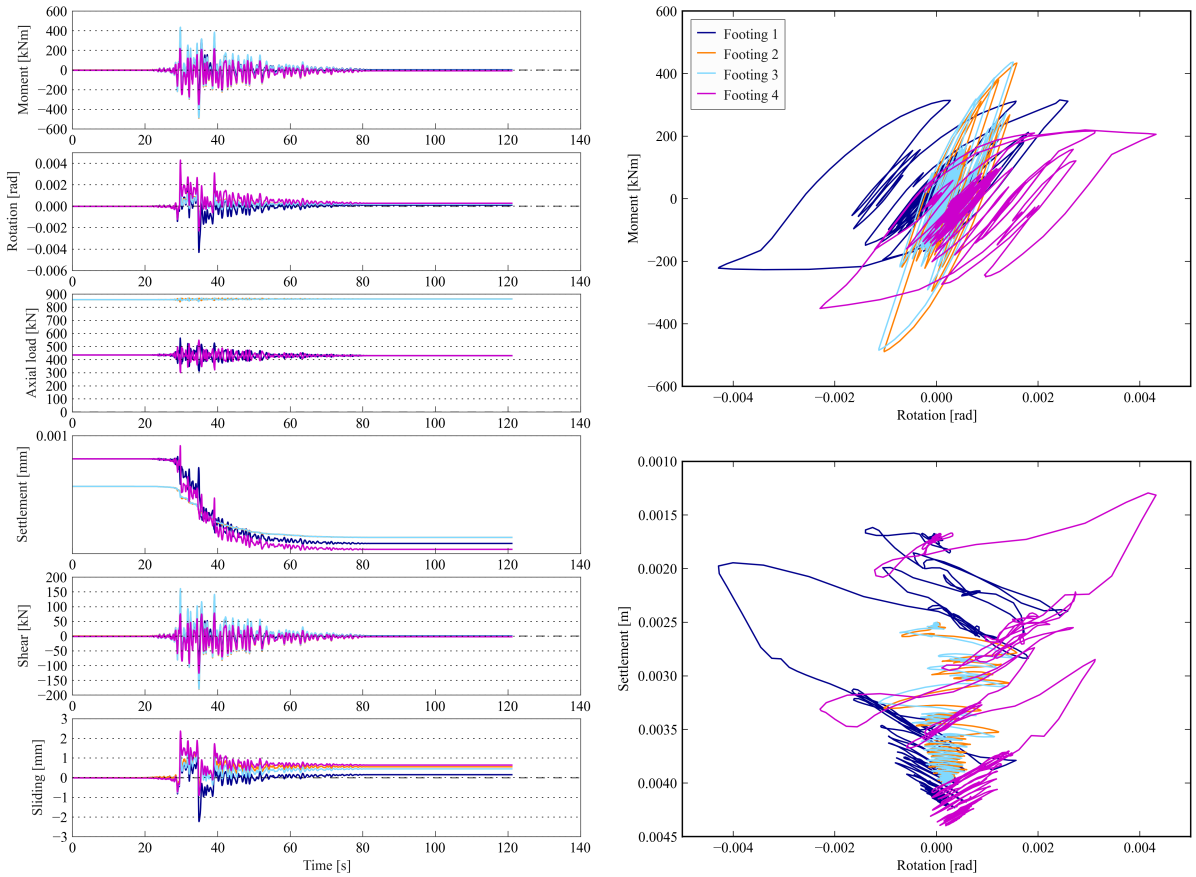

Figure 10.20: Foundation behaviour for two storey three bay model

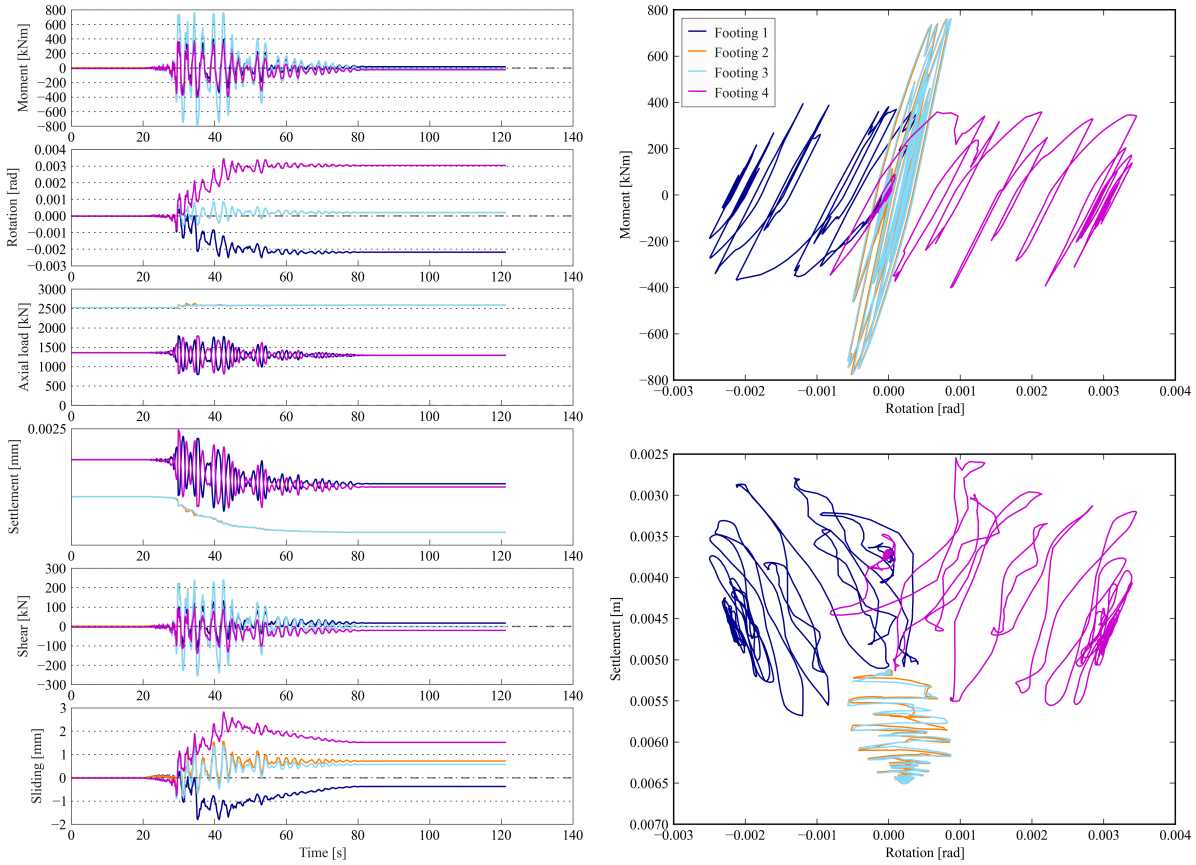

Figure 10.21: Foundation behaviour for six storey three bay model

The variation of the axial loading is clear in Figures 10.22 and 10.23 which show the normalised forces on the foundation for the two storey and six storey buildings respectively. The change in axial load is more prominent for the six storey building and this is the major cause of the cumulative deformation for this model.

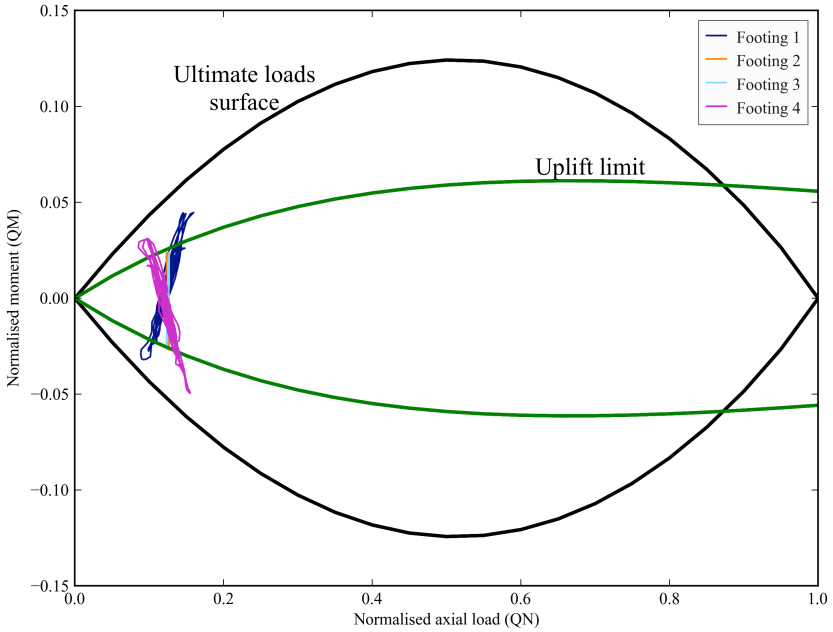

Figure 10.22: Normalised axial and moment plot of two storey three bay model

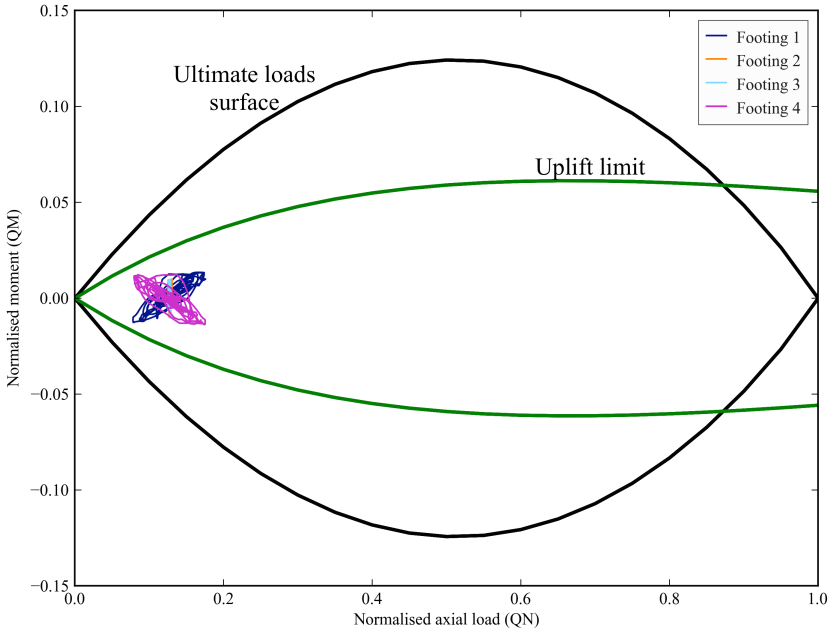

Figure 10.23: Normalised axial and moment plot of two storey three bay model

It is recognised that the macro-element predictive ability may be poor when the variation in axial load becomes significant and this is clearly the case for the six storey building.

Unfortunately the proposed design modifications to account for frame action could not be developed and validated using the current formulation of the macro-element, however, all of the mechanisms that were discussed can clearly be seen in the parametric study shown here.

10.6 Conclusion

This chapter discusses the conceptual SFSI considerations for the design of frame structures or any structure which has several footings. The influence of pad versus raft footings was discussed with reference to the point at which uplift would occur including the overall flexibility of the system. A method was devised to calculate the local deformations and the influence of footing sizes and building geometry was investigated through two case study buildings. The influence of frame action on foundation performance was discussed and how it can be accounted for in the prediction of both transient and permanent foundation deformations. Finally a series of frame buildings were designed and analysed using time-history analysis. The performance of the buildings indicated that the mechanisms discussed in this chapter can be significant, however, the large changes in vertical load due to frame action may have produced unrealistic behaviour.

Chapter 11

An Integrated performance-based building-foundation design framework using a simplified design procedure

11.1 Introduction

The performance-based design procedure presented in this chapter satisfies the main objective of this dissertation, where it attempts to account for the major mechanisms of SFSI. The design expressions developed throughout this dissertation have been summarised within this chapter to provide a comprehensive presentation of the design procedure.

The design procedure has an initial preliminary design considerations phase, where suitable design parameters are selected that should satisfy the performance limits. Following the preliminary phase, a full design is performed where the design loads are determined and performance limits are checked. The design procedure is presented in a step-by-step layout with some discussion on points that were of major interest in this dissertation and references to the relevant chapters for further explanation. Two design examples that make use of this design procedure are provided in Appendix C and Appendix D for a six storey wall building and six storey frame building respectively.

11.2 Preliminary design procedure

The purpose of the preliminary design phase is to provide initial estimates of loads and structural member sizes.

Steps 1 & 2: Building geometry and importance

The first steps in the design procedure are governed by the client requirements and the building use, where the approximate geometry and the building importance level are decided on. The crux of performance-based design is that the design attempts to control the performance of a structure to not exceed set performance levels for particular levels of hazard. Values suggested in Priestley et al. (2007) (Table 11.1) can be adopted for this step or values suggested in other design standards (eg. AS/NZS 1170.0, 2002).

The design levels specified in Table 11.1, correspond to:

- Level 1: Immediate occupancy and functionality
- Level 2: Repairability
- Level 3: Collapse prevention

The importance classes are from EC 8 (2004):

- Importance level 1: Buildings of minor importance for public safety (e.g. agricultural buildings, etc.)

- Importance level 2: Ordinary buildings, not belonging in the other categories.
- Importance level 3: Buildings whose seismic resistance is of importance in view of the consequences associated with a collapse (e.g. schools, assembly halls, cultural institutions etc.)
- Importance level 4: Buildings whose integrity during earthquakes is of vital importance for civil protection (e.g. hospitals, fire stations, power plants, etc.)

Table 11.1: The probability of exceedance for a given performance level in relation to importance of structure (Priestley et al., 2007)

Importance Class	Level 1	Level 2	Level 3
I	Not required	50% in 50 years	10% in 50 years
II	50% in 50 years	10% in 50 years	2% in 50 years
III	20% in 50 years	4% in 50 years	1% in 50 years
IV	10% in 50 years	2% in 50 years	1% in 50 years

11.2.1 Suitable performance limit states

The combination of various foundation and superstructure limit states is a complex task which can be highly dependent on the building materials (Giorgini et al., 2014). While research into this aspect of integrated building-foundation design continues, it is necessary to have some baseline values to work from. The performance limits stated in Table 11.2 are interpreted from several documents, where foundation deformations can be defined as in Figure

11.1.

Table 11.2: Building and foundation performance limits

Type	Level 1 - No damage	Level 2 - Repairable	Level 3 - No Collapse
Concrete strain	0.002§	Eq. 11.1 $<$ 0.02 §	Eq. 11.1 $<$ 0.03 §
Steel rebar strain	0.015§	$0.6\epsilon_{su} < 0.05$§	$0.9\epsilon_{su} < 0.08$ §
Peak inter-story drift ($\theta_{ss,p}$):			
- Brittle non-structural elements	0.004§	0.025§	No limit§
- Ductile non-structural elements	0.007§	0.025§	No limit§
- All elements detailed to sustain building displacements	0.010§	0.025§	No limit§
Residual drift limit ($\theta_{ss,r}$)	0.002	0.005	No limit
Peak (rigid-body) rotation ($\theta_{F,P}$)	0.6%*	1.2%*	2.0%*
Residual (rigid-body) rotation ($\theta_{F,R}$)	0.33%†	0.67%†	P-delta limits
Global (rigid-body) settlement (m) (δ_G)	0.025‡	0.050†	-
Peak angular distortion ($\beta_{F,P}$)	0.6%*	1.2%*	2.0%*
Residual angular distortion ($\beta_{F,R}$)	0.33%†	0.67%†	2.0%*

§ Sullivan et al. (2012)

† Skempton and H (1956)

‡ Eurocode 1 (1994)

$*$ Task Force Report (2007) (Interpreted)

Where ϵ_{su} is the ultimate steel strain defined by the manufacturer. Equation 11.1 defines the confined concrete compressive strain limit (ϵ_c) from Mander et al. (1988) (see Mander et al. (1988) for details):

$$\epsilon_c = 0.004 + 1.4\frac{\rho_v f_{yh}\epsilon_{su}}{f'_{cc}} \tag{11.1}$$

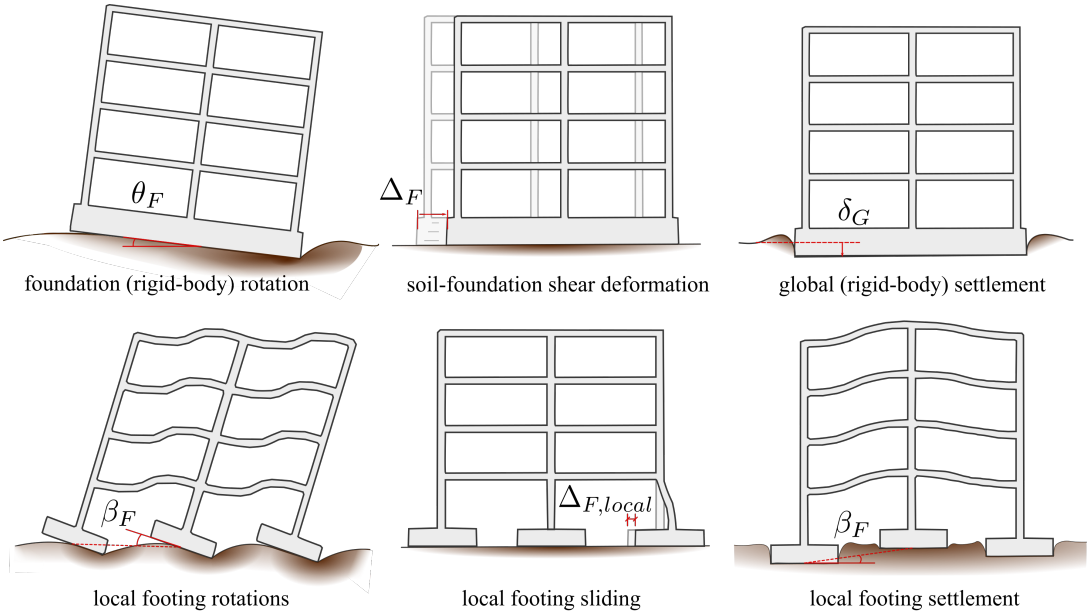

Figure 11.1: Foundation deformation mechanisms

The limits on foundation deformation are debatable and should consider the level of static settlement that has occurred prior to a seismic event. Furthermore, the deformation limits on the foundation and superstructure should reflect their potential to cause irreparable damage and collapse, which is highly dependent on the structural typology. The foundation deformation limits are discussed in many foundation engineering textbooks and articles (eg. Boscardin and Cording, 1989; Burland et al., 1977; Ricceri and Soranzo, 1985), as well as superstructure deformation limits (eg. Pampanin et al., 2002) for various building typologies and uses. The design limits will continue to change as new design methodologies and materials will allow for greater displacements with less damage, while other performance parameters such as floor accelerations may be recognised as more important as designers may look to focus further on protecting the buildings contents.

Step 4: Design hazard levels

For each limit state appropriate hazard levels must be defined based on the importance level of the building, which governs the level of risk that the building can be exposed to. This step is well defined in seismic design codes and the seismic hazard is often given as the single degree-of-freedom response spectrum at 5% of critical damping (see Clause 3.1 in NZS 1170.5:2004 (2004) for the definition of the seismic hazard for New Zealand).

Given that this thesis did not directly consider the kinematic effects of soil-foundation-structure interaction, the hazard may also need to be scaled to account for inclined shear waves and embedded footings (see NEHRP Consultants Joint Venture (2013)).

Step 5: Fixed base analysis

The fixed base analysis gives ballpark estimates of the design loads by considering only the superstructure deformations, thus the dynamic SFSI effects are ignored. This step can be achieved by following the DDBD procedure outlined in Equations 11.2 to 11.8 from Priestley et al. (2007). Where Δ_i is the displaced shape at the design displacement assuming zero foundation deformation, m_i are the storey masses and h_i are the storey heights. Equation 11.2 determines the equivalent SDOF design displacement (Δ_d), Equation 11.3 determines the equivalent SDOF mass (m_e) and Equation 11.4 determines the equivalent SDOF height (h_e).

$$\Delta_d = \frac{\sum_{i=1}^{n} m_i \Delta_i^2}{\sum_{i=1}^{n} m_i \Delta_i} \tag{11.2}$$

$$m_e = \frac{\sum_{i=1}^{n} m_i \Delta_i}{\Delta_d} \tag{11.3}$$

$$h_e = \frac{\sum_{i=1}^{n} m_i \Delta_i h_i}{\sum_{i=1}^{n} m_i \Delta_i} \tag{11.4}$$

The superstructure displacement reduction factor (η_{ss}) is given in Equation 11.5 from Pennucci et al. (2011a) and is specifically for concrete wall buildings, however, others can be found in Pennucci et al. (2011a) or derived from equivalent viscous damping expressions (see Priestley et al. (2007)).

$$\eta_{ss} = \sqrt{\frac{\pi\mu}{8.94\mu - 5.8}} \tag{11.5}$$

Where μ is the displacement ductility of the equivalent SDOF. The expression for the effective period (T_{eff}) (Equation 11.6) is given for a specific design spectrum where the spectrum is defined using a corner period (T_c) and corner displacement (D_c) and the effective period must be shorter than the corner period. For a different design spectrum, Equation 11.6 can be replaced by a function where the displacement reduction factor is applied as a factor to reduce the design spectrum and the effective period corresponds to the intersection between the design displacement and the reduced design spectrum.

$$T_{eff} = T_c \frac{\Delta_d}{\eta_{ss} D_c} \tag{11.6}$$

The effective stiffness (K_{eff}) is determined from the effective period using Equation 11.7 and

represents the secant stiffness to the design displacement of the SDOF.

$$K_{eff} = \frac{4\pi^2 m_{eff}}{T_{eff}^2} \tag{11.7}$$

The base shear is therefore determined using the secant stiffness and the design displacement in Equation 11.8.

$$V_{base} = K_{eff}\Delta_d \tag{11.8}$$

Finally the storey forces (F) are determined by distributing the base shear up the structure according to Equation 11.9, where k is either 0.9 for distributed ductility structures (eg. frames) or 1.0 for lumped ductility at the base of the structure (eg. walls) according to Sullivan et al. (2012).

$$F_i = \begin{cases} kV_{base}\dfrac{(m_i\Delta_i)}{\sum_{i=1}^{n}(m_i\Delta_i)} & \text{Floors 1 to n-1} \\ (1-k)V_{base} + kV_{base}\dfrac{(m_i\Delta_i)}{\sum_{i=1}^{n}(m_i\Delta_i)} & \text{Roof (Floor n)} \end{cases} \tag{11.9}$$

Step 6: Estimate the superstructure residual drift

The superstructure residual drift can be determined using expressions such as that given in Equation 11.10 for concrete wall buildings, developed from SDOF analysis results in Chapter 8 and validated as providing a suitable upper bound for predicting the residual drift of concrete walls in Chapter 9.

$$\frac{\theta_{ss,r}}{\theta_{ss,p}} = 0.068 + 0.027\mu + 1.9\frac{P}{HK_i} \tag{11.10}$$

Where $\theta_{ss,p}$ is the peak inter-storey drift due to superstructure deformation, μ the structural ductility, P the effective mass multiplied by gravity, H the effective height and K_i the initial stiffness for lateral deformation at the effective height.

Step 7: Size the foundation for gravity loads

The foundations are sized to satisfy settlement (see Schmertmann (1999)) and bearing capacity (see Salgado (2008)) requirements under gravity (static) loads. The advantage of sizing the foundations prior to the design of the superstructure is that the level of dynamic SFSI is highly dependent on the size of the foundations and therefore the superstructure can be designed with a consideration of the effects of SFSI.

Step 8: Estimate the peak rigid-body foundation rotation

The peak rigid-body foundation rotation (Figure 11.2) is determined in this step as it is a performance parameter and it is used to estimate other residual deformation parameters.

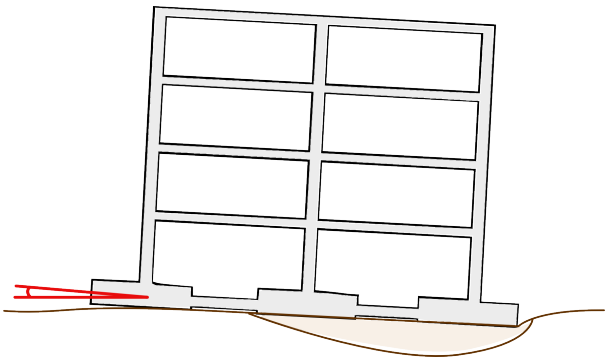

Figure 11.2: Peak rigid-body foundation rotation

The peak rigid-body foundation rotation is estimated using Equation 11.11 based on the applied foundation moment (M_f) and the foundation rotational stiffness (K_f).

$$\theta_{estimate} = \frac{M_f}{K_f} \tag{11.11}$$

Where the foundation moment is determined from the sum of the storey forces (F) multiplied by the storey height (h) and the foundation height (h_f) (Equation 11.12). The foundation rotational stiffness ($K_{f,rot}$) can be determined from the elastic rotational stiffness ($K_{f,rot,0}$) in Equation 11.13 from Gazetas (1991) and the stiffness degradation expression (Equation 11.14) derived in Chapter 6 and shown in Figure 11.3. The expression was developed using a soil-foundation macro-element and was validated against two sets of centrifuge tests using Nevada Sand; it could be expected that the degradation of rotational stiffness may be different for other types of sand.

$$M_f = \sum_{i=1}^{n} F_i(h_i + h_f) \tag{11.12}$$

$$K_{f,rot,0} = \frac{G}{(1-v)} I_{by}^{0.75} \left(3\left(\frac{L_f}{B_f}\right)^{0.15}\right) k_m \tag{11.13}$$

$$\frac{K_{f,rot}}{K_{f,rot,0}} = 0.8 - 0.04\log(\Phi) - 0.7(1 - \exp^{-0.18\Phi}) \tag{11.14}$$

The terms from the elastic rotational stiffness are as follows:

- G: Soil shear stiffness modulus
- v: Soil Poisson's ratio
- I_{by}: The soil-foundation contact area moment of inertia
- L_f: The foundation length
- B_f: The foundation width
- k_m: A frequency dependent amplification factor (see Gazetas (1991))

The stiffness degradation expression requires the corrected normalised rotation (Φ), which can be obtained through Equation 11.15.

$$\Phi = \left(\frac{\theta_f}{\theta_{uplift}}\right)^{1-0.2(L/H^{\star}_{eff})} 10^{0.25(L/H^{\star}_{eff})} \tag{11.15}$$

The corrected normalised rotation is dependent on the psuedo uplift angle (θ_{uplift}), which is the moment required for uplift divided by the elastic rotational stiffness, as defined in Equation 11.16. The other two terms in the corrected normalised rotation are the foundation length (L) and the building adjusted effective height ($H^{\star}_{eff}$). The ratio of $L/H^{\star}_{eff}$ accounts for the influence of shear force on the rotational stiffness. The adjustment to the effective height given in Equation 11.17 and derived in Chapter 9, accounts for the increase in shear force from the design base shear from an SDOF (V_{base}) to the over-strength base shear (V^{o}_{base}) which accounts for higher modes and over-strength design (from Priestley et al. (2007)).

$$\theta_{uplift} = \frac{N \times L}{\alpha K_{MM,elastic}} e^{-\zeta N/N_{cap}} \tag{11.16}$$

$$H^{\star} = H \times \frac{V_{base}}{V^{o}_{base}} \tag{11.17}$$

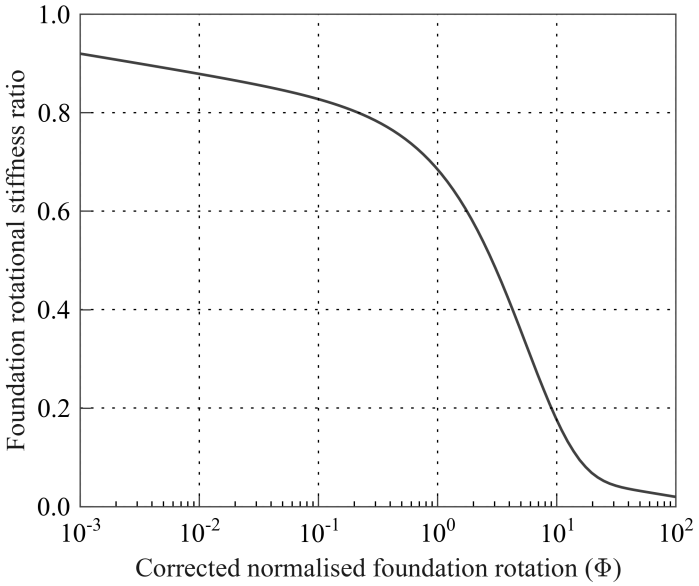

Figure 11.3: Foundation stiffness degradation curve

The pseudo uplift angle (θ_{uplift}) (Equation 11.16) provides a convenient expression to account for the elastic stiffness, the foundation axial capacity (N_{cap}) and the applied axial load (N). The $\alpha = 4$ parameter accounts for the stress distribution at the point of uplift for elastic soil and the $\zeta = 1.5$ parameter provides a correction to the uplift moment for inelastic soil behaviour (see Cremer et al. (2001)).

Step 9: Estimate the foundation residual deformations

The foundation residual rotation and the foundation SFSI-induced settlement can both be determined in this step using simple expressions that were derived in Chapter 7. The residual deformation expressions were developed based on a numerical parameter study using the soil-foundation macro-element from Chapter 4. As with the stiffness reduction factor, improvements and re-calibration of the numerical model for different types of sands may lead to different expressions for the residual foundation deformations.

Foundation residual rotation

The residual rotation occurs due to inelastic soil deformation and is dependant on the level of peak rotation. Equation 11.18 can be used to estimate the residual rotation. Equation 11.18 was developed based on a numerical parametric study of concrete wall buildings in Chapter 7, there was a small trend observed between foundation residual rotation and structural ductility and therefore the equation is only applicably to concrete wall buildings.

$$\frac{\theta_{f,r}}{\theta_{f,d}} = 0.025 log_{10}(\theta_{f,d}) + 0.30 \tag{11.18}$$

It should be noted that higher levels of residual rotation were observed by other researchers from experimental testing (see Deng (2012)) compared to Equation 11.18 and therefore the expression may be not be provide a conservative estimate.

Foundation settlement

The SFSI-induced settlement can be estimated using Equation 11.19. In Chapter 7 the SFSI-induced settlement was quantified using an expression that accounted for the design peak rotation from DDBD as well as the initial period of the system and the axial load ratio. In Chapter 9 when looking at MDOF models of wall buildings the expression was inadequate for predicting settlement when there was a large shear force applied to the footing and therefore the shear amplification factor was added to the settlement expression as given in Equation 11.19.

$$\frac{\delta}{L\theta_f} = \left[(0.0337 + \frac{0.218}{\tilde{N}}) log_{10}(\theta_f) + \frac{1.33}{\tilde{N}} + 0.556 - 0.136 T_{initial}\right] s_v \tag{11.19}$$

Where the shear amplification factor (s_v) is based on the adjusted effective height:

$$s_v = 0.5 + 0.7\frac{L}{H^\star} \geq 1.0 \tag{11.20}$$

The expression can be simplified by using suitable estimates for the $T_{initial}$ and $log_{10}(\theta_f)$ terms, making a simple expression for settlement, dependent only on the foundation length, axial load ratio, peak foundation rotation and adjusted effective height.

Equation 11.21 shows a simplified version of Equation 11.19, using $T_{initial} = 1.0s$ and $log_{10}(\theta_f) = -2.0$.

$$\delta = (0.353 + \frac{0.894}{\tilde{N}}) L\theta_f s_v \tag{11.21}$$

Step 10 & 11: Check that performance meets requirements

Once all of the performance parameters have been estimated they can be checked against the performance requirements summarised in Table 11.2. If the preliminary design does not satisfy the requirements then the SFSI deformations are governing the design and the

foundation or superstructure must be redesigned to reduce deformations. It is important to satisfy the requirements in step 10 as this reduces the amount of iteration required in the full design procedure.

11.2.2 Summary of Preliminary design steps

The preliminary design process is summarised in Figure 11.4 demonstrating each step.

1) 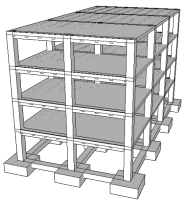

Determine building geometry

2) 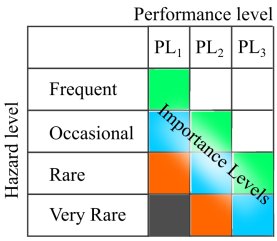

Set building importance

3) 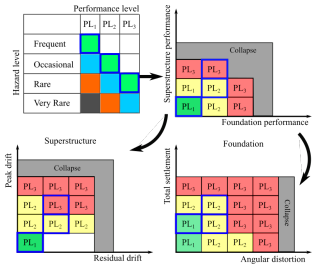

Select suitable combination of several performance criteria

4) 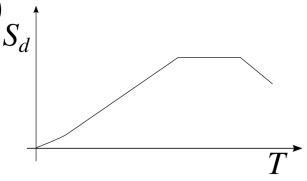

Determine seismic demand for each limit state

5) 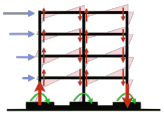

Conduct a fixed base analysis to estimate peak structural drift and loads on foundation

6) 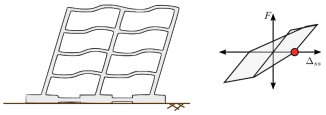

Estimate superstructure residual drift based on peak drift

7) 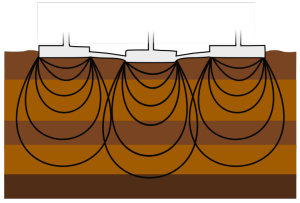

Size foundation to satisy settlement and bearing capacity requirements under gravity (static) loads

8) 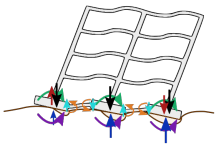

Calculate foundation peak deformations, based on loads and foundation sizes

9) 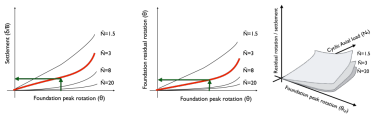

Estimate residual foundation deformations

10) 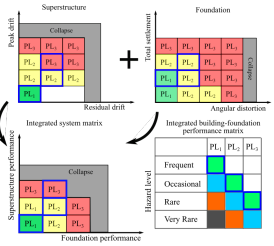

Check combination of peak and residual deformations against limit states criteria

11) 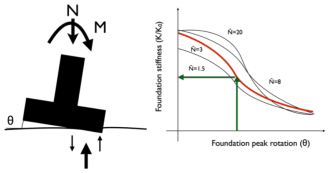

If deformations are not acceptable, resize foundation/structure to reduce drifts and foundation rotations, go back to step 7 and iterate

Figure 11.4: Preliminary design considerations of integrated building-foundation system

11.3 Full design

The full design accounts for the effects of SFSI on the dynamic response of the building and provides more rigorous estimates of the deformations of soil-foundation-structure system as well as final design specifications for all structural members. The procedure uses the estimated peak foundation rotation, the superstructure drift and the foundation geometry from the preliminary design phase.

Step 1: Determine the displacement profile

The displacement profile of the soil-foundation-structure system ($\Delta_{sys,i}$) includes the deformations of the structure ($\Delta_{ss,i}$), as well as the foundation rotation (θ_f) and the shear deformation of the foundation ($\Delta_{f,shear}$) as given in Equation 11.22.

$$\Delta_{sys,i} = \Delta_{ss,i} + \theta_f h + \Delta_{f,shear} \tag{11.22}$$

The super-structure deformation can be estimated using expressions given in Priestley et al. (2007) for different building typologies, whereas the foundation rotation can make use of the initial estimate of the foundation rotation from preliminary design. The foundation shear deformation must be determined from Equation 11.23, where the shear stiffness ($K_{f,shear}$) is defined in Equation 11.24 as the elastic shear shear stiffness ($K_{f,shear,0}$) from Gazetas (1991) given in Equation 11.25 divided by two to account for a reduction in stiffness due to non-linear soil deformation.

$$\Delta_{f,shear} = \frac{V^o_{base}}{K_{f,shear}} \tag{11.23}$$

$$K_{f,shear} = \frac{K_{f,shear,0}}{2} \tag{11.24}$$

$$K_{f,shear,0} = K_y - \frac{0.1GL_f}{0.75 - v}\left(1 - \frac{B_f}{L_f}\right)k_v \tag{11.25}$$

Where:

$$K_y = \frac{GL_f}{(2-v)}\left[2 + 2.5\left(\frac{B_f}{L_f}\right)^{0.85}\right] \tag{11.26}$$

And the frequency dependent coefficient k_v can be taken as 1.0 (see Gazetas (1991)).

Step 2: Determine equivalent SDOF properties

This step makes use of Equations 11.2 - 11.4 from the preliminary design phase, however, the displacement profile now includes the foundation deformations.

Step 3: Estimate the displacement contribution from each mechanism

The displacement contributions from the superstructure, foundation rotation and foundation shear can all be estimated at the effective height using the respective expressions:

$$\Delta_{f,rot} = \theta_f H_e \tag{11.27}$$

$$\Delta_{f,shear} = \Delta_{f,shear} \tag{11.28}$$

$$\Delta_{ss} = \Delta_d - \Delta_{f,rot} - \Delta_{f,shear} \tag{11.29}$$

Step 4: Estimate the displacement reduction factors for each mechanism

The displacement reduction factor from the superstructure can make use of Equation 11.5 or an equivalent expression from Pennucci et al. (2011a) depending on the building typology, where the structural ductility ((Equation 11.30) is the total superstructure displacement divided by the superstructure yield displacement (Δ_y).

$$\mu = \frac{\Delta_{ss}}{\Delta_y} \tag{11.30}$$

The displacement reduction factor for the foundation rotation ($\eta_{f,rot}$) can be determined using Equation 11.31 (plotted in Figure 11.5), which was developed in Chapter 6.

$$\eta_{f,rot} = \sqrt{\frac{1.0}{1.0 + 5.0(1 - e^{-0.15\Phi})}} \tag{11.31}$$

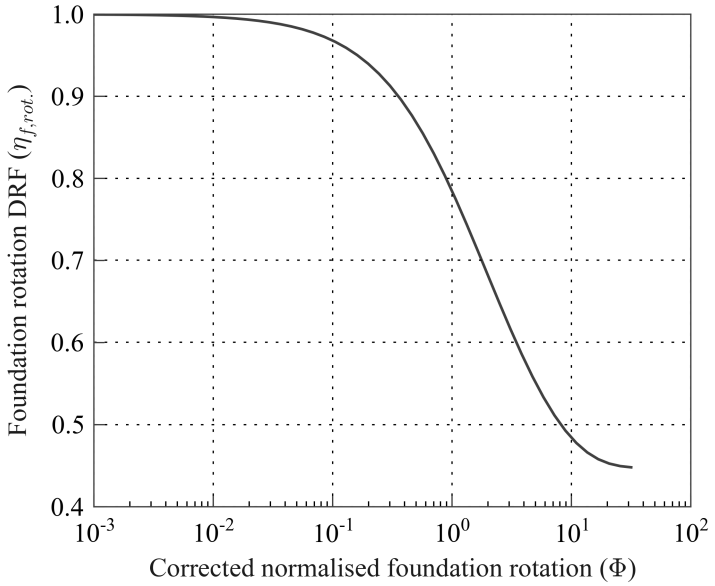

Figure 11.5: Foundation rotation displacement reduction factor

Here Φ is the corrected normalised foundation rotation given in Equation 11.15.

The foundation shear deformation displacement reduction factor ($\eta_{f,shear}$) can simply be taken as 0.76 as determined in Chapter 6, given that foundation shear displacement tends to contribute less than 20% of the displacement for most concrete buildings. If shear displacement is larger than 20% than an improved estimate of the contribution of the shear displacement to the overall dynamic response would be recommended and this procedure would not be appropriate.

Step 5: Determine the system displacement reduction factor

This step makes use of a simple displacement-based weighted average expression (Equation 11.32) to determined the system displacement reduction factor (η_{sys}). The expression was developed and validated in Chapter 6 with a small bias where the displacement was under-predicted when the contributions of the foundation displacement and the superstructure displacement were similar, but in most cases provided suitable estimates (see Figure 6.19 in Chapter 6).

$$\eta_{sys} = \frac{\Delta_{ss}\eta_{ss} + \Delta_{f,rot.}\eta_{f,rot.} + \Delta_{f,shear}\eta_{f,shear}}{\Delta_{sys}} \tag{11.32}$$

Steps 6, 7 & 8: Determine the effective period, base shear and storey forces

These steps make use of Equations 11.6 - 11.9 from the preliminary design stage, however, the system displacement reduction factor is used instead of the superstructure displacement reduction factor and storey forces are distributed using the displacement profile that includes the soil-foundation deformations.

Step 9: Check foundation global deformations against initial deformation estimates

This step recalculates the foundation rotation and shear displacement that are used in Step 1 to check that they are consistent. The foundation rotation is determined in the same manner as in the preliminary design using Equation 11.11, where the foundation moment is updated based on the new storey forces from Step 8. The foundation shear displacement is updated using Equation 11.23 from Step 2 of the full design procedure and using the updated base shear force.

If the deformations are inconsistent then the design is repeated from Step 1 of the full design using the updated deformation values.

Step 10: Determine the internal actions

The internal actions can be determined through structural analysis based on the storey forces, such as in the moment equilibrium method (see Section 10.4 in Chapter 10).

Step 11: Check compatibility of footing deformations with global deformations

This step is necessary for foundation types that may deform during loading, such a foundations consisting of pad footings.

The footing deformations can be estimated based on the footing moments which can be extrapolated from the superstructure internal actions as seen in Figure 11.6, where M_{base} is the design column base moment and γh_1 is the point of inflexion of the moment in the ground floor columns.

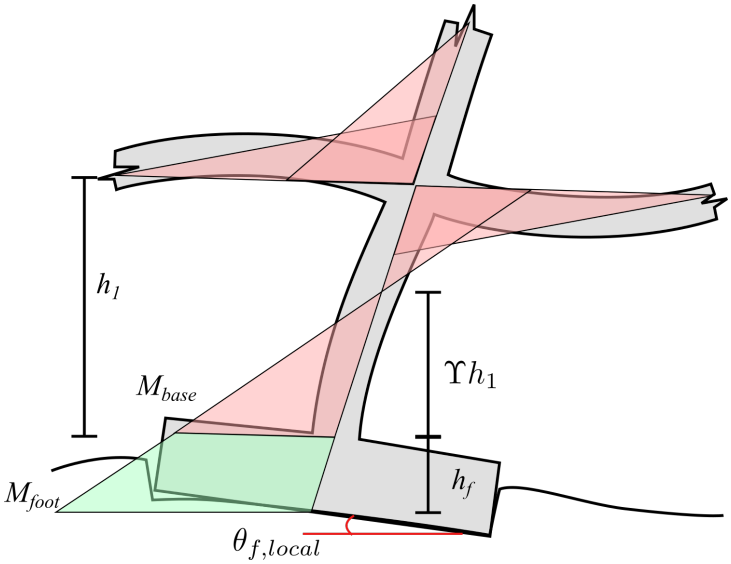

Figure 11.6: Estimate the footing moment

The peak footing rotation ($\theta_{f,local}$) is then determined using Equation 11.33, here $K_{f,local}$ is the footing rotational stiffness determined using Equations 11.13 and 11.14 from the preliminary design, however, the loads and dimensions are for the footing not the whole foundation.

$$\theta_{f,local} = \frac{M_{foot}}{K_{f,local}} \tag{11.33}$$

The footing rotations should be compatible with the global foundation deformation and the superstructure deformation (Figure 11.7). A footing rotation that is less than the global rotation will increase the curvature in the columns. When the footing rotation is equal to the global rotation then the deformations in the structure are not changed and the rotation is purely a rigid rotation. When the rotation exceeds the global rotation then the column curvatures are reduced, however, if the calculated rotation is so big that it exceeds the global rotation plus the expected plastic rotation then the design is not possible as the moments at the column base would not develop. The designer must redistribute some of the over-turning moment away from the columns, increase the footing sizes or design the building to a larger drift.

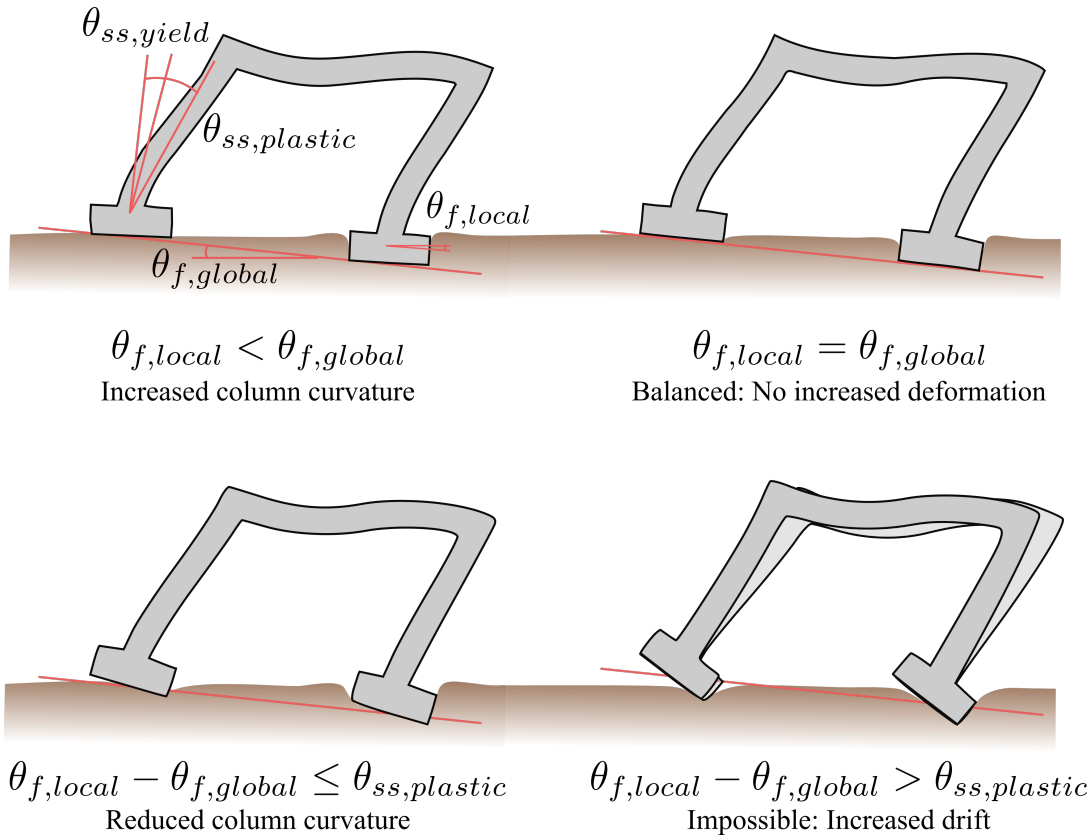

Figure 11.7: Compatibility of footing rotation

The residual footing rotations can also be determined, however, the numerical model used in this dissertation could not accurately model the additional cyclic vertical load from frame-action in the structure and therefore no equations are provided to estimate footing deformations with large changes in vertical load.

Step 12: Check deformations are satisfactory

This step simply checks that the design satisfies the performance requirements for a given limit state (eg. Table 11.2), if the design fails then the superstructure or foundations must be redesigned to ensure the performance requirements are met.

Step 13: Check design for other limit states

The design must satisfy the other limit states and therefore using the foundation sizes the design must be repeated to check that all of the performance requirements are met.

Step 14: Design the structural members

The design of the non-linear structural members must be close to the nominal design values to ensure that excessive strength in the members does not result in extra force being applied to the foundation resulting in additional foundation deformations. The other structural members that are intended to remain elastic should be designed for over-strength forces to prevent unintended yielding up the structure.

The DDBD procedure from Priestley et al. (2007) suggests using higher mode factors to amplify the moment and shear force for over-strength design (Equations 11.34 and 11.36 and respectively). Where $M^o_{0.5H}$ is the over-strength moment at half the height of the structure, V^o_{Base} the over-strength shear force at the base of the structure and V^o_n is the over-strength shear force at the top of the structure, as demonstrated in Figure 11.8.

$$M^o_{0.5H} = C_{1,T}\phi^o M_B \tag{11.34}$$

$$C_{1,T} = 0.4 + 0.075T_i(\frac{\mu}{\phi^o} - 1) \geq 0.4 \tag{11.35}$$

$$V^o_{Base} = \phi^o \omega_V V_{Base} \tag{11.36}$$

$$\omega_V = 1 + \frac{\mu}{\phi^o} C_{2,T} \tag{11.37}$$

$$C_{2,T} = 0.067 + 0.4(T_i - 0.5) \leq 1.15 \tag{11.38}$$

$$V^o_n = C_3 V^o_{Base} \tag{11.39}$$

$$C_3 = 0.9 - 0.3T_i \geq 0.3 \tag{11.40}$$

Where T_i is the initial period of vibration and ϕ^o the over-strength of the non-linear members.

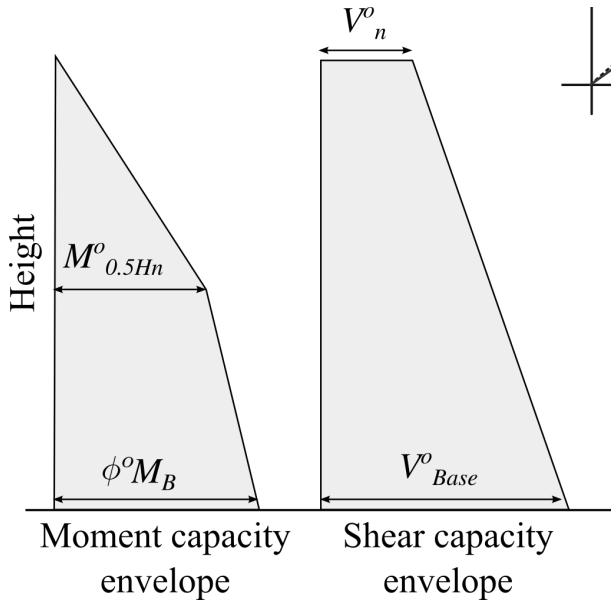

Figure 11.8: Over-strength design envelopes

In Chapter 9 it was noted that Equation 11.34 under predicted the over-strength moment when the soil-foundation displacement contribution was significant. A simple modification to the formula was proposed where the system displacement ductility (μ_{sys}) (Equation 11.41) was used instead of the structural ductility (μ).

$$\mu_{sys} = \frac{\Delta_d}{\Delta_y} \tag{11.41}$$

11.3.1 Summary of full design procedure

1)

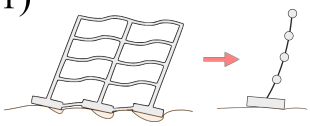

Estimate displaced shape

2)

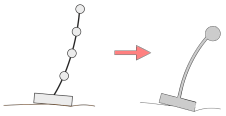

Estimate SDOF properties

3)

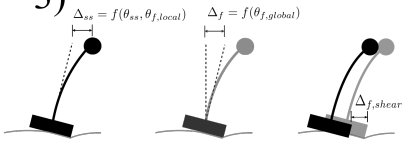

Determine SDOF displacement contribution from each mechanism

4)

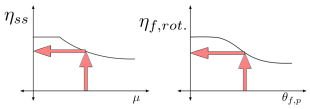

Estimate displacement reduction factor for each mechanism

5)

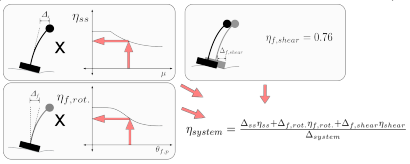

Estimate system displacement reduction factor

6)

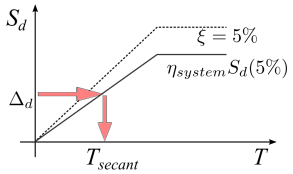

Estimate effective period

7)

$$K_{eff} = \frac{4\pi^2 mass}{T^2_{secant}}$$

$$V_{base} = K_{eff}\Delta_{system}$$

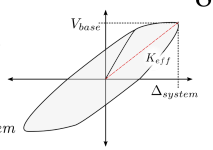

Estimate base shear

8)

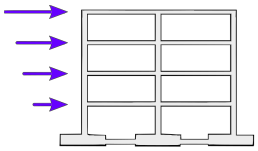

Distribute forces up structure

9)

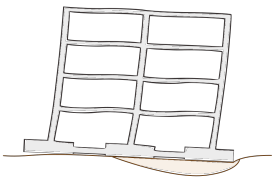

Check foundation global deformations are equal to those assumed, else return to 1)

10)

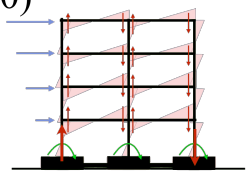

Estimate internal actions

11)

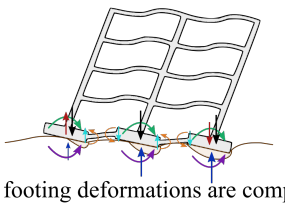

Check footing deformations are compatible with the global deformations, else resize footings

12)

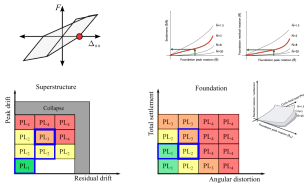

Check residual deformations and performance limits are satisfied, else resize foundations

13)

	Total peak drift	Total residual drift	Structural peak drift	Foundation uniform settlement	Foundation differential settlement
Frequent	0.1%	0.0%	0.1%	0	0
Occasional	0.5%	0.0%	0.5%	0	0
Rare	2.5%	0.5%	2.0%	B/200	1/200
Very Rare	5%	1%	3.5%	B/100	1/75

Check design for other limit states

14)

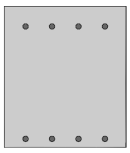

Determine super-structure sections based on internal actions

Figure 11.9: Full design considerations of integrated building-foundation system

11.4 Conclusion

This chapter provides a summary of the performance based building-foundation design procedure that included the major mechanisms of SFSI. The procedure is presented in full, with

explanation of key assumptions and caveats while the remainder of the information regarding each step is referenced to various parts of the dissertation.

Chapter 12

Conclusions and recommendations

The primary goal of this dissertation was to develop a performance based design procedure that includes the major mechanisms of soil-foundation-structure interaction (SFSI). This objective addresses the major short falls of conventional building and foundation design which fail to capture the dynamic aspects of SFSI, as well as the permanent foundation deformations that can occur. The procedure and many of the expressions developed in this dissertation can be extended to the assessment of existing buildings.

The following sections summarises the key findings of this dissertation along with their limitations and recommendations of future works.

12.1 Key contributions

12.1.1 Integrated design procedure

Chapter 11 presented the integrated building-foundation performance based design procedure. A performance framework was developed that explicitly considers foundation deformations and demonstrates how superstructure and foundation limit states can be combined to give a single performance measure for the building-foundation system. The chapter provided explanations for each step in the proposed design, drawing on all of the findings from the dissertation.

The procedure has clear advantages of conventional design solutions where the building is designed first and then the foundation design is based on the over-strength superstructure loads using static force-based analysis. The conventional design approach often results in over designed foundations which attempt to prevent uplift and other deformation in the soil and foundation. These additional deformation mechanisms can be used to dissipate energy and limit accelerations entering the structure if correctly designed for. Not only can foundations deformations be beneficial, but in some cases where buildings are exposed to beyond design level acceleration levels, and cases where a retrofit design results in excess

forces on the foundation, the foundation deformations are unavoidable. The conventional design procedure can not quantify these deformations regardless of whether the forces exceed the design level or not.

The proposed design procedure accounts for the major foundation mechanisms in a rational way through a displacement-based design procedure and a series of empirical equations, so that engineers can not only predict the level of deformation but take advantage of foundation deformation as an energy dissipation mechanism. The proposed design procedure is largely based on the displacement based design procedure presented by Paolucci et al. (2013), however, modifications were made to the procedure to account for shear deformation and for structures with multiple supports. The design procedure is split into two parts, a preliminary phase where the building is analysed as a fixed base structure and the loads are used to estimate the foundation deformations, and a detailed (full) design phase where the foundation deformations are used in the prediction of the seismic loads. Two design examples were presented for concrete walls and frames in Appendices C and D respectively.

12.1.2 Implementation of soil-foundation interface model

Chapters 4 and 5 were focused on the implementation and validation of a soil-foundation macro element in the non-linear finite element software Ruaumoko3D (Carr, 2015). The element makes use of the foundation uplift formulation from Chatzigogos et al. (2011) and the plasticity formulation by Figini et al. (2012) and provides Ruaumoko3D users with an easy tool to model non-linear foundation deformation.

The macro-element was validated against two sets of well documented experiments, using the recommended calibration parameters from the Chatzigogos et al. (2011) and Figini et al. (2012) models to demonstrate that the model provides suitable estimates of the behaviour. The first set of test results were of a pier structure from the fifth experiment (LJD03) from the NEES project: "Innovative Economical Foundations with Improved Performance that is Less Sensitive to Site Conditions" (Deng and Kutter, 2010). The experimental validations showed that the model could accurately capture the transient behaviour of the structure and footing and the resulting level of settlement and foundation residual rotation.

The second set of tests were of a one storey frame structure from the first experiment (HBM02) from the NEES project: "Seismic performance assessments in dense urban environments" (Mason et al., 2010). Similar predictive capabilities were seen for the frame structure where individual macro-elements were used to model separate footings. While the overall response of the frame structure was well predicted there were quite large rotations due to gravity moments and the additional vertical load from frame action may not have been well accounted for in the model. Several issues with foundation damping were also recognised and methods to account for these issues were proposed and implemented.

12.1.3 Development of expressions to quantify the effects of SFSI

Chapter 6 was focused on predicting the transient behaviour of the foundation and superstructure. There are multiple deformation mechanisms involved with the building-foundation-soil system and each is potentially deforming in the non-linear range. The non-linear deformation was accounted for using displacement reduction factors from the direct displacement-based design approach (Pennucci et al., 2011a) and combined together using a displacement weighted average. New displacement reduction factor expressions were proposed for the foundation rotation and shear deformations as well as simple expressions for the effective rotational and shear stiffnesses. The expressions were first developed based on a series of numerical results from SDOF systems with linear structures and the nonlinear soil-foundation macro-element. The expressions were then validated by designing a series of concrete wall buildings and analysing the nonlinear equivalent SDOF of the wall to confirm that displacements were predicted accurately. The ability to combine two nonlinear displacement reduction factors is the cornerstone for the displacement-based design of multiple deformation mechanism structures and allows the designer to control both the deformations in the superstructure and the foundation.

Chapter 7 developed equations to accurately predict the level of SFSI-induced settlement and foundation residual rotation based on the expected level of transient foundation rotation. The strong dependence of both of the residual foundation deformation parameters on peak foundation rotation and foundation axial load was explained through simple concepts. Equations to predict the foundation residual deformations were developed from the statistical regression of data from the two parametric studies on SDOF structures from Chapter 6. The equations form an integral piece of the proposed performance-based design framework and allow the designer to control the expected level of SFSI-induced settlement and residual foundation rotation.

Chapter 8 investigated the prediction of superstructure residual deformations with special consideration for P-delta effects and foundation deformations. A series of fixed base concrete wall structures were designed and their SDOF equivalent structures were assessed through nonlinear time history analysis. The results highlighted the influence of the post yield stiffness ratio and P-delta effects on the ratio of residual to peak drift. A series of concrete wall structures were then designed using the proposed displacement-based design procedure from Chapter 2 and assessed to quantify the effects of foundation deformation on the ratio of residual to peak drift. Multi-linear regression analysis was performed on the two data sets to develop a unique expression to account for the major factors considered in the analyses.

While these expressions provide suitable estimates of behaviour through a rational statistical process, the numerical model was only calibrated on a limited number of experimental tests. All of the proposed expressions use normalised parameters as they are linked to a physical phenomenon, however, different soils may result in different calibration parameters for the

expressions.

12.1.4 SFSI effects on more complex structures

Chapter 9 presented the effects of SFSI on multi-degree-of-freedom (MDOF) systems that have vertically distributed mass. A series of fixed based concrete wall buildings were analysed as MDOF systems to demonstrate the ability of DDBD to predict inter-storey drifts, moment and shear distributions. The wall buildings were redesigned to consider SFSI and were analysed using the implemented macro-element from Chapter 4. The results demonstrated that the amplified base shear due to higher modes results in increased foundation rotation and increased SFSI-settlement. Simple expressions were developed to account for the amplified shear response.

Chapter 10 presents the effects of SFSI on MDOF systems with multiple supports. A set of case study frame buildings were analysed to demonstrate the additional key mechanisms that can not be captured with a simple SDOF model. New expressions were proposed to account for additional cyclic axial load in exterior columns due to frame action, as well as to account for tie beams, gravity loads and deformation of footings. A small parametric study was conducted where a series of frame buildings were designed using the integrated design procedure from Chapter 11 and analysed to demonstrate how the additional mechanisms result in further deformations. Unfortunately the macro-element did not provide accurate results for situations where frame action resulted in large levels of cyclic vertical load in the exterior footings. The macro-element model was not formulated to handle large changes in axial load and therefore an improved formulation may provide greater insight into the performance of frame structures on soft soils.

12.2 Future works

There are many opportunities to improve upon the contributions of this dissertation.

- The soil-foundation macro-element model formulation should be modified to better account for the effects of a varying axial load, radiation damping, and plastic deformations under permanent moment load (see Chapter 4 for an in-depth summary of the proposed improvements/limitations).
- The soil-foundation macro-element model should be validated against more soil types, eg. different types of sands and clayey soils.
- Further experimental tests on different soil types, in particular there are only a limited number of experimental tests of shallow foundations on clayey soils.

- The expressions for dynamic and residual foundation deformations should be re-calibrated for different soil types.
- The expressions for residual superstructure deformation should be developed for other building typologies
- Expressions to quantify the residual deformations in isolated footing that have varying axial load need to be developed and validated
- The acceptable level of foundation deformations need to be decided upon both for transient and residual deformations
- The expressions and design framework should be extended to account for liquefied soil, foundations with piles and structure-soil-structure interaction

12.3 Concluding remarks

All of the findings, summaries and quantification of various phenomenon in this dissertation were presented for use within the proposed integrated building-foundation design and within the framework of performance based design; however, the expressions can provide useful insights to engineering for quantification of SFSI mechanisms outside of these two areas, such as retrofitted design and capacity analysis of existing buildings. The interpretation and implementation of these conclusions should be made with careful consideration to the limitations that the were founded on. Given the potentially large cost saving and greater understanding that the integrated design procedure can provide, further research into the development and refinement of the expressions necessary for implementation in the commercial environment appears warranted.

Bibliography

Abdolahi Rad, A. (2015). Seismic Behaviour of Steel Buildings with Out-of-Plumb. *Earthquake Engineering & Structural Dynamics*, 1–19.

Adamidis, O., G. Gazetas, I. Anastasopoulos, and C. Argyrou (2013, November). Equivalent-linear stiffness and damping in rocking of circular and strip foundations. *Bulletin of Earthquake Engineering*.

Algie, T. B. (2011). *Nonlinear rotational behaviour of shallow foundations on cohesive soil*. Ph. D. thesis, ResearchSpace@ Auckland.

Algie, T. B., M. J. Pender, R. P. Orense, and L. M. Wotherspoon (2010). Dynamic field testing of shallow foundations subject to rocking. *New Zealand Society for Earthquake Engineering Conference, Paper No 15*.

Amaris, A. D. (2002, August). *Dynamic Amplification of Seismic Moments and Shear Forces in Cantilever Walls*. Ph. D. thesis, Rose school.

Anastasopoulos, I. (2009, September). Beyond conventional capacity design : towards a new design philosophy . In *International Workshop on Soil-Foundation-Structure-Interaction*, Auckland, pp. 1–8.

Anastasopoulos, I. (2012). EFFECTIVENESS OF SHALLOW SOIL IMPROVEMENT ON THE PERFORMANCE OF ROCKING-ISOLATED BRIDGE PIERS: MONOTONIC AND CYCLIC PUSHOVER TESTING. In *Second International Conference on Performance-based design in Earthquake Geotechnical Engineering*, Taormina, Italy.

Anastasopoulos, I., F. Gelagoti, A. Spyridaki, J. Sideri, and G. Gazetas (2014, January). Seismic Rocking Isolation of an Asymmetric Frame on Spread Footings. *Journal of Geotechnical and Geoenvironmental Engineering 140*(1), 133–151.

Anastasopoulos, I., M. Loli, T. Georgarakos, and V. Drosos (2013, January). Shaking Table Testing of Rocking—Isolated Bridge Pier on Sand. *Journal of Earthquake Engineering 17*(1), 1–32.

Ancheta, T. D., R. Darragh, J. P. Stewart, S. Emel, W. Silva, B. Chiou, K. E. Wooddell, R. W. Graves, A. R. Kottke, D. M. Boore, T. Kishida, and J. Donahue (2013). PEER NGA-West2 Database. Technical Report 03.

Apostolou, M. and G. Gazetas (2005). Rocking of Foundations under Strong Shaking : Mobilisation of Bearing Capacity and Displacement Demands. In *Proc. 1st Greece–Japan Workshop, Seismic Design, Observation, Retrofit*, Athens, pp. 131–140.

Arulmoli, K., K. K. Muraleetharan, M. M. Hosain, and L. S. Fruth (1992). VELACS laboratory testing program, soil data report. Technical report, Irvine, CA.

AS NZS 1170.1 2002 (2002). Structural design actions.

AS/NZS 1170.0 (2002). Structural design actions .

Avilés, J. and L. E. Pérez-Rocha (2003). Soil-structure interaction in yielding systems. *Earthquake Engineering & Structural Dynamics 32*(11), 1749–1771.

Avilés, J. and L. E. Pérez-Rocha (2011, July). Use of global ductility for design of structure–foundation systems. *Soil Dynamics and Earthquake Engineering 31*(7), 1018–1026.

Bárcena, A. and L. Esteva (2007). Influence of dynamic soil–structure interaction on the nonlinear response and seismic reliability of multistorey systems. *Earthquake Engineering & Structural Dynamics 36*(3), 327–346.

Beck, J. L. and R. I. Skinner (1972). The Seismic Response of a Proposed Reinforced Concrete Railway Viaduct. *DSIR Rept*, 17.

Bienen, B., B. W. Byrne, G. T. Houlsby, and M. J. Cassidy (2006). Investigating six-degree-of-freedom loading of shallow foundations on sand. *Géotechnique 57*(5), 483–484.

Bird, J. F., J. J. Bommer, H. Crowley, and R. Pinho (2006, January). Modelling liquefaction-induced building damage in earthquake loss estimation. *Soil Dynamics and Earthquake Engineering 26*(1), 15–30.

Bird, J. F., H. Crowley, R. Pinho, and J. J. Bommer (2005). Assessment of building response to liquefaction-induced differential ground deformation. *Bulletin of the New Zealand Society for Earthquake Engineering 38*(4), 215–234.

Borowicka, H. (1943). *Uber ausmitting bela- stete starre Platten auf elastschisotropem Untergrung*. *Ingenieur-Archiv*.

Borzi, B., M. G. Calvi, A. S. Elnashai, E. Faccioli, and J. J. Bommer (2001). Inelastic spectra for displacement-based seismic design. *Soil Dynamics and Earthquake Engineering*, 47–61.

Boscardin, M. D. and E. J. Cording (1989). Building Response to Excavation-induced Settlement. *Journal of geotechnical engineering 115*(1), 1–21.

Boussinesq, J. (1883). Application des Potentials a L'Equilibri et due Mouvement des Solides Elastiques. *Gauthier- Villars*, 1–732.

Bozorgnia, Y., M. M. Hachem, and K. W. Campbell (2010, February). Ground Motion Prediction Equation ("Attenuation Relationship") for Inelastic Response Spectra. *Earthquake Spectra 26*(1), 1–23.

Bransby, M. F. and M. F. Randolph (1998). Combined loading of skirted foundations. *Géotechnique 48*(5), 637–655.

Burland, J. B., B. B. B, and V. F. B. De Mello (1977). Behaviour of Foundations and Structures. *Earthquake Engineering Abstracts*, 495–546.

Calvi, M. G. (2012, September). Seismic displacement based design of structures: relevance of soil structure interaction. *Second International Conference on Performance-based design in Earthquake Geotechnical Engineering*, 1–29.

Carr, A. J. (2015). Ruaumoko, Nonlinear FEM Computer Program.

Çelebi, M. and E. Safak (1992). Seismic response of Pacific Park Plaza. I: Data and preliminary analysis. *Journal of Structural Engineering 118*(6), 1547–1565.

Chang, B. J., P. Raychowdhury, T. C. Hutchinson, J. Thomas, S. Gajan, and B. L. Kutter (2006). Centrifuge testing of combined frame-wall-foundation structural systems.

Chang, B. J., P. Raychowdhury, T. C. Hutchinson, J. M. Thomas, S. Gajan, and B. L. Kutter (2007). Evaluation of the seismic performance of combined frame-wall-foundation structural systems through centrifuge testing. In *Proceedings of the 4th International Conference on Earthquake Geotechnical Engineering*.

Chatzigogos, C. T., R. Figini, A. Pecker, and J. Salençon (2011, May). A macroelement formulation for shallow foundations on cohesive and frictional soils. *International Journal for Numerical and Analytical Methods in Geomechanics 35*(8), 902–931.

Chatzigogos, C. T., A. Pecker, and J. Salençon (2007). A macro-element for dynamic soil-structure interaction analyses of shallow foundations. *4th International Conference on Earthquake Geotechnical Engineering*.

Chatzigogos, C. T., A. Pecker, and J. Salençon (2009, July). Macroelement modeling of shallow foundations. *Soil Dynamics and Earthquake Engineering 29*, 765–781.

Chen, Y.-H., W.-H. Liao, C.-L. Lee, and Y.-P. Wang (2006). Seismic isolation of viaduct piers by means of a rocking mechanism. *Earthquake Engineering & Structural Dynamics 35*(6), 713–736.

Chiou, B., R. Darragh, N. Gregor, and W. Silva (2008, February). NGA Project Strong-Motion Database. *Earthquake Spectra 24*(1), 23–44.

Chopra, A. K. and R. K. Goel (2001). Direct Displacement-Based Design: Use of Inelastic vs. Elastic Design Spectra. *Earthquake Spectra 17*, 47–63.

Christopoulos, C. and S. Pampanin (2004). Towards performance-based design of MDOF structures with explicit consideration of residual deformations. *ISET Journal of Earthquake Technology 41*(1), 53–73.

Christopoulos, C., S. Pampanin, and M. J. N. Priestley (2003). Performance-Based Seismic Response of Frame Structures Including Residual Deformations Part I: Single-Degree of Freedom Systems. *Journal of Earthquake Engineering 7*(01), 97–118.

Comartin, C. D., R. W. Niewiarowski, S. A. Freeman, and F. M. Turner (2000). Seismic retrofit and evaluation of concrete buildings: a practical overview of the ATC-40 document. *Earthquake Spectra 16*, 241–261.

Combault, J., P. Morand, and A. Pecker (2000, January). Structural response of the Rion-Antirion Bridge. *Twelfth World Conference of Earthquake Engineering*, 1–7.

Combescure, D. and T. Chaudat (2000). ICONS European program seismic tests on R/C walls with uplift CAMUS 4 specimen. Technical report.

Cremer, C., A. Pecker, and L. Davenne (2001). Cyclic macro-element for soil-structure interaction: material and geometrical non-linearities. *International Journal for Numerical and Analytical Methods in Geomechanics 25*(13), 1257–1284.

Cremer, C., A. Pecker, and L. Davenne (2002). Modelling of nonlinear dynamic behaviour of a shallow strip foundation with macro-element. *Journal of Earthquake Engineering*, 175–211.

Cubrinovski, M., B. A. Bradley, L. M. Wotherspoon, R. Green, J. D. Bray, C. Wood, M. J. Pender, J. Allen, A. Bradshaw, and G. Rix (2011). Geotechnical Aspects of the 22 February 2011 Christchurch Earthquake.

Cubrinovski, M. and I. McCahon (2012, June). Foundations on Deep Alluvial Soils. Technical report.

Deng, L. (2012). *Centrifuge Modeling, Numerical Analyses, and Displacement-Based Design of Rocking Foundations*. Ph. D. thesis, University of California, Davis.

Deng, L. and B. L. Kutter (2010). SEISMIC PERFORMANCE OF BRIDGE SYSTEMS WITH ROCKING FOUNDATIONS: CENTRIFUGE DATA REPORT FOR LJD03. Technical report.

Deng, L. and B. L. Kutter (2012). Characterization of rocking shallow foundations using centrifuge model tests. *Earthquake Engineering & Structural Dynamics 41*(5), 1043–1060.

Deng, L., B. L. Kutter, and S. K. Kunnath (2012, March). Centrifuge Modeling of Bridge Systems Designed for Rocking Foundations. *Journal of Geotechnical and Geoenvironmental Engineering 138*(3), 335–344.

Dep. Building & Housing (2011, July). Compliance Document for New Zealand Building Code Clause B1 Structure. pp. 1–88.

di Prisco, C., R. Nova, and A. Sibilia (2003). Shallow Footings Under Cyclic Loading: Experimental Behaviour and Constitutive Modeling. *Geotechnical Analysis of Seismic Vulnerability of Historical Monuments*.

Drosos, V., T. Georgarakos, M. Loli, I. Anastasopoulos, O. Zarzouras, and G. Gazetas (2012, November). Soil-Foundation-Structure Interaction with Mobilization of Bearing Capacity: Experimental Study on Sand. *Journal of Geotechnical and Geoenvironmental Engineering 138*(11), 1369–1386.

Dwairi, H. M., M. J. Kowalsky, and J. M. Nau (2007, July). Equivalent Damping in Support of Direct Displacement-Based Design. *Journal of Earthquake Engineering 11*(4), 512–530.

EC 8 (2004, January). Eurocode 8: Design of structures for earthquake resistance - Part 1: General rules, seismic actions and rules for buildings.

EC 8 Part 5 (2004, January). Eurocode 8 Part 5: Foundations, retaining structures and geotechnical aspects. *European Standard*, 1–68.

El Ganainy, H. and M. H. El Naggar (2009, August). Efficient 3D nonlinear Winkler model for shallow foundations. *Soil Dynamics and Earthquake Engineering 29*(8), 1236–1248.

Eurocode 1 (1994). Basis of design and actions on structures.

Faccioli, E., R. Paolucci, and M. Vanini (1998). 3D Site effects and soil-foundation interaction in earthquake and vibration risk evaluation. Technical report.

Figini, R. (2010, March). *Non-linear dynamic soil-structure interaction: Application to seismic analysis and design of structures on shallow foundations*. Ph. D. thesis, Politecnico di Milano.

Figini, R., R. Paolucci, and C. T. Chatzigogos (2012, February). A macro-element model for non-linear soil-shallow foundation-structure interaction under seismic loads: theoretical development and experimental validation on large scale tests. *Earthquake Engineering & Structural Dynamics 41*(3), 475–493.

Fox, M. J., T. J. Sullivan, and K. Beyer (2015, July). Evaluation of Seismic Assessment Procedures for Determining Deformation Demands in RC Wall Buildings. *Accepted*, 1–28.

Gajan, S. and B. L. Kutter (2008, August). Capacity, Settlement, and Energy Dissipation of Shallow Footings Subjected to Rocking. *Journal of Geotechnical and Geoenvironmental Engineering*, 1129–1141.

Gajan, S. and B. L. Kutter (2009). Effects of moment-to-shear ratio on combined cyclic load-displacement behavior of shallow foundations from centrifuge experiments. *Journal of Geotechnical and Geoenvironmental Engineering 135*(8), 1044–1055.

Gajan, S., B. L. Kutter, J. D. Phalen, T. C. Hutchinson, and G. R. Martin (2005, August). Centrifuge modeling of load-deformation behavior of rocking shallow foundations. *Soil Dynamics and Earthquake Engineering 25*(7-10), 773–783.

Gajan, S., P. Raychowdhury, T. C. Hutchinson, B. L. Kutter, and J. P. Stewart (2010, February). Application and Validation of Practical Tools for Nonlinear Soil-Foundation Interaction Analysis. *Earthquake Spectra 26*(1), 111–129.

Ganjavi, B. and H. Hao (2011). Elastic and inelastic response of single-and multi-degree-of-freedom systems considering soil structure interaction effects. *Australian Earthquake Engineering Society Conference*.

Ganjavi, B. and H. Hao (2012a, October). A parametric study on the evaluation of ductility demand distribution in multi-degree-of-freedom systems considering soil-structure interaction effects. *Engineering Structures 43*(C), 88–104.

Ganjavi, B. and H. Hao (2012b, July). Effect of structural characteristics distribution on strength demand and ductility reduction factor of MDOF systems considering soil-structure interaction. *Earthquake Engineering and Engineering Vibration 11*(2), 205–220.

Gazetas, G. (1991). Foundation Vibrations. In H.-Y. Fang (Ed.), *Foundation Engineering Handbook*, pp. 553–593. Springer.

Gazetas, G. (2012, November). Should Elastic Response Spectra be the Basis of Seismic Design of Strongly Inelastic and Soft-Soil–Structure Systems ? In *Proceedings of the 3rd International Symposium on Advances in Urban Safety*, Nadjing, pp. 1–12.

Gazetas, G. (2013). Soil–Foundation–Structure Systems Beyond Conventional Seismic Failure Thresholds. In *Proceedings of the 18th International Conference on Soil Mechanics and Geotechnical Engineering*, Paris, pp. 1–16.

Gazetas, G. (2014, October). Soil Dynamics and Earthquake Engineering. *Soil Dynamics and Earthquake Engineering*, 1–17.

Gazetas, G., I. Anastasopoulos, O. Adamidis, and T. Kontoroupi (2013, April). Nonlinear rocking stiffness of foundations. *Soil Dynamics and Earthquake Engineering 47*(C), 83–91.

Gazetas, G., I. Anastasopoulos, and E. Garini (2014, February). Soil Dynamics and Earthquake Engineering. *Soil Dynamics and Earthquake Engineering 57*(C), 37–45.

Gazetas, G. and G. Mylonakis (1998). Seismic soil-structure interaction: new evidence and emerging issues. *Geotechnical earthquake engineering and soil dynamics III*, 1119–1174.

Gelagoti, F., R. Kourkoulis, I. Anastasopoulos, and G. Gazetas (2011, November). Rocking isolation of low-rise frame structures founded on isolated footings. *Earthquake Engineering & Structural Dynamics 41*(7), 1177–1197.

Gelagoti, F., R. Kourkoulis, I. Anastasopoulos, and G. Gazetas (2012, January). Soil Dynamics and Earthquake Engineering. *Soil Dynamics and Earthquake Engineering 32*(1), 87–102.

Georgiadis, M. and R. Butterfield (1988). Displacement of footings on sand under eccentric and inclined loads. *Canadian Geotechnical Journal*, 199–212.

Gerolymos, N., V. Drosos, and G. Gazetas (2009, April). Seismic response of single-column bent on pile: evidence of beneficial role of pile and soil inelasticity. *Bulletin of Earthquake Engineering 7*(2), 547–573.

Ghannad, M. A. and H. Jahankhah (2007, February). Site-dependent strength reduction factors for soil-structure systems. *Soil Dynamics and Earthquake Engineering 27*(2), 99–110.

Giorgini, S., M. Cubrinovski, S. Pampanin, A. J. Carr, and M. Moghaddasi (2012, July). Integrated foundation-structure modelling of a case study from the Christchurch 2011 earthquake. In *Proc. of the 15th World Conference on Earthquake Engineering*, pp. 1–10.

Giorgini, S., S. Pampanin, and M. Cubrinovski (2014). Towards performance-based seismic design ofintegrated foundation-structure systems consideringsoil-foundation interface nonlinearity. In *2014 NZSEE Conference*, pp. 1–10.

Gottardi, G., G. T. Houlsby, and R. Butterfield (1999, July). Plastic response of circular footings on sand under general planar loading. *Géotechnique 49*, 453–469.

Gourvenec, S. (2007, January). Shape effects on the capacity of rectangular footings under general loading. *Géotechnique 57*(8), 637–646.

Grange, S., P. Kotronis, and J. Mazars (2009a, October). A macro-element to simulate 3D soil–structure interaction considering plasticity and uplift. *International Journal of Solids and Structures 46*(20), 3651–3663.

Grange, S., P. Kotronis, and J. Mazars (2009b, December). A macro-element to simulate dynamic Soil-Structure Interaction. *Engineering Structures 31*(12), 3034–3046.

Grant, D. N., C. A. Blandon, and M. J. N. Priestley (2005). Modeling inelastic response in direct displacement-based design. Technical Report 2004/02, Pavia, Italy.

Halabian, A. M. and M. Erfani (2010, December). The effect of foundation flexibility and structural strength on response reduction factor of RC frame structures. *The Structural Design of Tall and Special Buildings*, n/a–n/a.

Halabian, A. M. and S. Kabiri (2011, June). Effect of foundation flexibility on ductility reduction factors for R/C stack-like structures. *Earthquake Engineering and Engineering Vibration 10*(2), 277–290.

Harden, C. W. and T. C. Hutchinson (2009, May). Beam-on-Nonlinear-Winkler-Foundation Modeling of Shallow, Rocking-Dominated Footings. *Earthquake Spectra 25*(2), 277–300.

Hardin, B. O. (1978). The Nature of Stress-Strain Behavior for Soils. In *Earthquake Engineering and Engineering Vibration*, pp. 3–90.

Houlsby, G. and C. Martin (1999). Jackup units on clay: structural analysis with realistic modelling of spudcan behaviour.

Houlsby, G. T. and M. J. Cassidy (2002). A plasticity model for the behaviour of footings on sand under combined loading. *Géotechnique 52*(2), 117–129.

Housner, G. W. (1963). The behaviour of Inverted pendulum structures during earthquakes. *Bulletin of the Seismological Society of America 53*, 403–417.

Jacobsen, L. S. (1960). Damping in composite structures. In *2nd World Conference on Earthquake Engineering*, Tokyo and Kyoto, pp. 1–16.

Jennings, P. C. (1968). Equivalent viscous damping for yielding structures. *ASCE Journal of Engineering Mechanics Division 1*, 103–116.

Jennings, P. C. and J. Bielak (1973). Dynamics of building-soil interaction. *Bulletin of the Seismological Society of America 63*(1), 9–48.

Jeremic, B., S. K. Kunnath, and F. Xiong (2004). Influence of soil–foundation–structure interaction on seismic response of the I-880 viaduct. *Engineering Structures 26*(3), 391–402.

JRA (1996). Design specifications of highway bridges, part I common part, part II steel bridges, part III concrete bridges, part IV foundations and part V seismic design. *Japan Road Association*.

Kausel, E. (2010, May). Early history of soil–structure interaction. *Soil Dynamics and Earthquake Engineering 30*(9), 822–832.

Kawashima, K., G. A. MacRae, J.-i. Hoshikuma, and K. Nagaya (1998). Residual displacement response spectrum. *Journal of Structural Engineering 124*(5), 523–530.

Keino, C. and M. Kohiyama (2012, March). Health disturbance of residents in a house with liquefaction damage in Mihama Ward, Chiba City. *Proceedings of the International Symposium on Engineering Lessons Learned from the 2011 Great East Japan Earthquake*.

Kramer, S. L. (1996, January). *Geotechnical Earthquake Engineering* (1 ed.). Prentice Hall.

Lin, Y.-Y. and E. Miranda (2007, October). Kinematic soil-structure interaction effects on maximum inelastic displacement demands of SDOF systems. *Bulletin of Earthquake Engineering 6*(2), 241–259.

Liu, W., T. C. Hutchinson, B. L. Kutter, M. Hakhamaneshi, M. A. Aschheim, and S. K. Kunnath (2013). Demonstration of Compatible Yielding between Soil -Foundation and Superstructure Components. *Journal of Structural Engineering 139*(8), 1408–1420.

Loli, M., J. A. Knappett, M. J. Brown, I. Anastasopoulos, and G. Gazetas (2014, July). Centrifuge modeling of rocking-isolated inelastic RC bridge piers. *Earthquake Engineering & Structural Dynamics 43*(15), 2341–2359.

MacRae, G. A. and K. Kawashima (1997, June). POST-EARTHQUAKE RESIDUAL DISPLACEMENTS OF BILINEAR OSCILLATORS. *Earthquake Engineering & Structural Dynamics 26*, 701–716.

Mander, J. B., M. J. N. Priestley, and R. Park (1988). Theoretical stress-strain model for confined concrete. *Journal of Structural Engineering 114*(8), 1804–1826.

Mason, H. B., N. W. Trombetta, S. M. Gille, J. N. LunD, H. Puangnak, B. Y. Choy, Z. Chen, C. Bolisetti, J. D. Bray, T. C. Hutchinson, G. L. Fiegel, B. L. Kutter, and A. S. Whittaker (2010). Seismic performance assessment in dense urban environments: Centrifuge data report for HBM02. Technical report.

Massimino, M. R. and M. Maugeri (2013, June). Physical modelling of shaking table tests on dynamic soil–foundation interaction and numerical and analytical simulation. *Soil Dynamics and Earthquake Engineering 49*(C), 1–18.

McHattie, S. A. (2013). SEISMIC RESPONSE OF THE UC PHYSICS BUILDING IN THE CANTERBURY EARTHQUAKES. Master's thesis, University of Canterbury.

McManus, K. (2012, March). Foundation design reliability issues. Technical report.

Millen, M. D. L., M. Cubrinovski, S. Pampanin, and A. J. Carr (2015). Earthquake-induced Rotation and Settlement of Building Foundations. In *ANZGEO conference*, Wellington, pp. 1–9.

Mindlin, R. D. (1949). Compliance of Elastic Bodies in Contact. *ASME Trans J. APpl. Mech. 16*.

Miranda, E. (2000, September). In-elastic displacement ratios for structures on firm sites. *Journal of Structural Engineering* (126), 1150–1159.

Miranda, E. and V. V. Bertero (1994, January). Evaluation of strength reduction factors of earthquake-resistant design. *Earthquake Spectra 10*, 357–379.

Miranda, E. and J. Ruiz-García (2002). Evaluation of approximate methods to estimate maximum inelastic displacement demands. *Earthquake Engineering & Structural Dynamics*, 539–560.

Moghaddasi, M., A. J. Carr, S. Pampanin, J. G. Chase, and A. Pecker (2012, April). The effects of soil-foundation interface nonlinearity on seismic soil-structure interaction analysis. In *2012 NZSEE Conference*, pp. 1–14.

Moghaddasi, M., M. Cubrinovski, J. G. Chase, S. Pampanin, and A. J. Carr (2011a, April). Effects of soil–foundation–structure interaction on seismic structural response via robust Monte Carlo simulation. *Engineering Structures 33*(4), 1338–1347.

Moghaddasi, M., M. Cubrinovski, J. G. Chase, S. Pampanin, and A. J. Carr (2011b, January). Probabilistic evaluation of soil-foundation-structure interaction effects on seismic structural response. *Earthquake Engineering & Structural Dynamics 40*(2), 135–154.

Moghaddasi, M., M. Cubrinovski, S. Pampanin, A. J. Carr, and J. G. Chase (2010, March). Soil-Foundation-Structure Interaction Effects on Nonlinear Seismic Demand of Structures. In *2010 NZSEE Conference*, pp. 1–9.

Mylonakis, G. and G. Gazetas (2000, July). Seismic soil-structure interaction: beneficial or detrimental? *Journal of Earthquake Engineering 4*(3), 277–301.

Mylonakis, G., G. Gazetas, S. Nikolaou, and O. Michaelides (2000, November). The Role of Soil on the Collapse of 18 Piers of the Hanshin Expressway in the Kobe Earthquake. In *Twelfth World Conference of Earthquake Engineering*, pp. 1–7.

Mylonakis, G., S. Nikolaou, and G. Gazetas (2006, September). Footings under seismic loading: Analysis and design issues with emphasis on bridge foundations. *Soil Dynamics and Earthquake Engineering 26*(9), 824–853.

Nakhaei, M. and M. Ali Ghannad (2008, June). The effect of soil–structure interaction on damage index of buildings. *Engineering Structures 30*(6), 1491–1499.

Negro, P., R. Paolucci, S. Pedretti, and E. Faccioli (1999, November). Large scale Soil-structure Interaction Experiments on sand under cyclic loading. *Twelfth World Conference of Earthquake Engineering*, 1–8.

NEHRP Consultants Joint Venture (2013). Soil Structure Interaction for Building Structures.

Newmark, N. M. and W. J. Hall (1969). Seismic design criteria for nuclear reactor facilities. *Building Practices for Disaster Mitigation, National Bureau of Standards, US, Department of Commerce, Reporte* (46).

Nova, R. and L. Montrasio (1991). Settlements of shallow foundations on sand. *Géotechnique 41*(2), 243–256.

NZS 1170.5:2004 (2004, August). Structural Design Actions - Part 5: Earthquake actions- New Zealand.

NZS 1170.5:2004 (2011, June). NZS 1170.5 Supp 1:2004. pp. 1–86.

Pal, S., S. S. Dasaka, and A. K. Jain (1987). Inelastic response spectra. *Computers & Structures 25*(3), 335–344.

Pampanin, S. (2005, June). Emerging Solutions for High Seismic Performance of Precast/Prestressed Concrete Buildings. *Journal of Advanced Concrete Technology 3*, 207–223.

Pampanin, S., C. Christopoulos, and M. J. N. Priestley (2002). *Residual deformations in the performance-based seismic assessment of frame structures*. Research Report ROSE-2002/02.

Pampanin, S., C. Christopoulos, and M. J. N. Priestley (2003). Performance-based seismic response of frame structures including residual deformations Part II: Multi-degree of freedom systems. *Journal of Earthquake Engineering 7*(01), 119–147.

Paolucci, R. (1997, July). Simplified evaluation of earthquake-induced permanent displacements of shallow foundations. *Journal of Earthquake Engineering 1*(3), 563–579.

Paolucci, R., C. di Prisco, R. Figini, L. Petrini, and M. Vecchiotti (2009). Interazione din non lin terreno-struttura nell'ambito della prog sismica agli spostamenti. *Progettazione Sismica, IUSS Press, Pavia*, 1–12.

Paolucci, R., R. Figini, and L. Petrini (2013, May). Introducing Dynamic Nonlinear Soil-Foundation-Structure Interaction Effects in Displacement-Based Seismic Design. *Earthquake Spectra 29*(2), 475–496.

Paolucci, R., M. Shirato, and M. T. Yilmaz (2008). Seismic behaviour of shallow foundations: Shaking table experiments vs numerical modelling. *Earthquake Engineering & Structural Dynamics 37*(4), 577–595.

Pecker, A. (1996, April). Seismic bearing capacity of shallow foundations. In *Eleventh World Conference on Earthquake Engineering*, pp. 1–9.

Pecker, A. (2007, April). Soil Structure Interaction. In *Advanced Earthquake Engineering Analysis*, pp. 1–10. Springer.

Pecker, A. (2011, June). Influence of non linear soil structure interaction on the seismic demand in bridges. In *IBSBI 2011, October 13-15, Athens, Greece*, pp. 1–16.

Pecker, A. and C. T. Chatzigogos (2010, October). Non linear soil structure interaction: impact on the seismic response of structures. In *IX European Conference on Earthquake Engineering*, Ohrid, FYROM, pp. 1–26.

Pecker, A., R. Paolucci, C. T. Chatzigogos, and A. A. Correia (2012, May). The role of nonlinear dynamic soil-foundation interaction on the seismic response of structures . In *Second International Conference on Performance-based design in Earthquake Geotechnical Engineering*, pp. 1–19.

Pecker, A. and M. J. Pender (2000, August). Earthquake Resistant Design of Foundations-New Construction. In *GeoEng2000 conference*, pp. 1–22.

Pender, M. J. (2014, March). Integrated design of structure - foundation systems: the current situation and emerging challenges. In *2014 NZSEE Conference*, Auckland, pp. 1–22.

Pennucci, D., T. J. Sullivan, and M. G. Calvi (2011a, March). Displacement Reduction Factors for the Design of Medium and Long Period Structures. *Journal of Earthquake Engineering 15*(sup1), 1–29.

Pennucci, D., T. J. Sullivan, and M. G. Calvi (2011b). *Performance-Based Seismic Design of Tall RC Wall Buildings*. IUSS Press, Italy.

Perkins, S. W. and C. R. Madson (2000). Bearing capacity of shallow foundations on sand: A relative density approach. *Journal of Geotechnical and Geoenvironmental Engineering 126*(6), 521–530.

Pettinga, D., C. Christopoulos, S. Pampanin, and N. Priestley (2007). Effectiveness of simple approaches in mitigating residual deformations in buildings. *Earthquake Engineering & Structural Dynamics 36*(12), 1763–1783.

Priestley, M. J. N. (2003). Myths and fallacies in earthquake engineering, revisited. In *The Ninth Mallet Milne Lecture*. IUSS press.

Priestley, M. J. N., M. G. Calvi, and M. J. Kowalski (2007). *Displacement Based Seismic Design of Structures*. IUSS Press, Italy.

Priestley, M. J. N., R. J. Evison, and A. J. Carr (1978). Seismic response of structures free to rock on their foundations. *Bulletin of the New Zealand National Society for Earthquake Engineering 11*(3), 141–150.

Priestley, M. J. N. and D. N. Grant (2005). Viscous damping in seismic design and analysis. *Journal of Earthquake Engineering 9*, 229–255.

PWRI (2005). Experimental study on the residual displacements of shallow foundations. Technical report, Tsukuba, Japan.

Ricceri, G. and M. Soranzo (1985). An analysis on allowable settlements of structures. *Rivista Italiana di Geotecnica 4*, 177–188.

Riddell, R., P. Hidalgo, and E. Cruz (1989, January). Response modification factors for earthquake resistant design of short period buildings. *Earthquake Spectra*, 1–20.

Roscoe, K. H. and Schofield (1957). The stability of short pier foundations on sand. *British Welding Journal*.

Ruiz-García, J. and E. Miranda (2003). Inelastic displacement ratios for evaluation of existing structures. *Earthquake Engineering & Structural Dynamics 32*(8), 1237–1258.

Ruiz-García, J. and E. Miranda (2006a). Evaluation of residual drift demands in regular multi-storey frames for performance-based seismic assessment. *Earthquake Engineering & Structural Dynamics 35*(13), 1609–1629.

Ruiz-García, J. and E. Miranda (2006b). Residual displacement ratios for assessment of existing structures. *Earthquake Engineering & Structural Dynamics 35*(3), 315–336.

Sáez, E., F. Lopez-Caballero, and A. Modaressi-Farahmand-Razavi (2013, June). Inelastic dynamic soil-structure interaction effects on moment-resisting frame buildings. *Engineering Structures 51*(C), 166–177.

Safak, E. and M. Çelebi (1992). Recorded Seismic Response of Pacific Park Plaza. II: System Identification. *Journal of Structural Engineering 118*(6), 1566–1589.

Salgado, R. (2008). *The Engineering of Foundations*. McGraw Hill New York.

Schmertmann, J. H. (1999, January). CPT for Predicting Settlement in sands. pp. 1–36.

Sharpe, R. D. and J. R. Binney (1984). Use of Foundation Uplift to Limit Seismic Bridge Pier Forces. *Structures Committee, Road Research Unit, New Zealand National Roads Board*.

Sharpe, R. D. and R. I. Skinner (1983). THE SEISMIC DESIGN OF AN INDUSTRIAL CHIMNEY WITH ROCKING BASE. *Bull. NZ Nat. Soc. Eq. Eng 16*, 1–9.

Shirato, M., T. Kouno, R. Asai, S. Nakatani, J. Fukui, and R. Paolucci (2008). Large-scale experiments on nonlinear behavior of shallow foundations subjected to strong earthquakes. *Soils and foundations 48*(5), 673–692.

Skempton, A. W. and M. D. H (1956). THE ALLOWABLE SETTLEMENTS OF BUILDINGS. *ICE Proceedings: Engineering Divisions 5*(6), 727–768.

Smith, P. C. and J. Devine (2012). Independent assessment of earthquake performance of Inland Revenue Building-224 Cashel Street. Technical report.

Storie, L. B., M. J. Pender, and J. A. Knappett (2015, April). Centrifuge modelling of the rocking response of shallow building foundations on dense sand. In *2015 NZSEE Conference*, Rotorua, pp. 1–8.

Sullivan, T. J., M. J. N. Priestley, and M. G. Calvi (2012). *DBD12: A model code for the displacement-based seismic design of structures*. IUSS Press, Italy.

Sullivan, T. J., S. Salawdeh, A. Pecker, M. Corigliano, and M. G. Calvi (2010, June). Soil-foundation-structure interaction considerations for performance-based design of RC wall structures on shallow foundations . In *The International Workshop on Soil-Foundation-Structure Interaction, SFSI 09*, pp. 1–8.

Tang, Y. and J. Zhang (2011, January). Probabilistic seismic demand analysis of a slender RC shear wall considering soil-structure interaction effects. *Engineering Structures 33*(1), 218–229.

Task Force Report (2007). Geotechnical Design Guidelines for Buildings on Liquefiable Sites in Accordance with NBC 2005 for Greater Vancouver Region. pp. 1–75.

Taylor, P. W. and R. L. Williams (1979). Foundations for capacity designed structures. *Bulletin of the New Zealand Society for Earthquake Engineering 12*.

Terzaghi, K. (1943). Theoretical Soil Mechanics. New York: John Wiley and Sons.

Trombetta, N. W. (2013). *Seismic Soil-Foundation-Structure Interaction in Urban Environments*. Ph. D. thesis, University of California, San Diego, San Diego.

Trombetta, N. W., H. B. Mason, Z. Chen, T. C. Hutchinson, J. D. Bray, and B. L. Kutter (2013, July). Soil Dynamics and Earthquake Engineering. *Soil Dynamics and Earthquake Engineering 50*(C), 117–133.

Trombetta, N. W., H. B. Mason, T. C. Hutchinson, J. D. Zupan, J. D. Bray, and B. L. Kutter (2013, December). Nonlinear Soil–Foundation–Structure and Structure–Soil–Structure Interaction: Centrifuge Test Observations. *Journal of Geotechnical and Geoenvironmental Engineering*, 04013057.

Ugalde, J. A., B. L. Kutter, and B. Jeremic (2010, April). Rocking Response of Bridges on Shallow Foundations. Technical report.

Ugalde, J. A., B. L. Kutter, B. Jeremic, and S. Gajan (2007a). Centrifuge modeling of rocking behavior of bridges on shallow foundations.

Ugalde, J. A., B. L. Kutter, B. Jeremic, and S. Gajan (2007b, February). Centrifuge Modelling of Rocking Behaviour of Bridges on Shallow Foundations. In *4th International Conference on Earthquake Geotechnical Engineering*, pp. 1–12.

Uma, S. R., S. Pampanin, and C. Christopoulos (2010, September). Development of Probabilistic Framework for Performance-Based Seismic Assessment of Structures Considering Residual Deformations. *Journal of Earthquake Engineering 14*(7), 1092–1111.

Veletsos, A. S., A. M. Prasad, and W. H. Wu (1997). Transfer functions for rigid rectangular foundations. *Earthquake Engineering & Structural Dynamics 26*(1), 5–17.

Veletsos, A. S. and B. Verbic (1974, June). Dynamics of elastic and yielding structure-foundation systems. *Proceedings of the 5th world conference on Earthquake Engineering*, 1–4.

Vesic, A. S. (1975). Bearing capacity of shallow foundations. In *Foundations engineering handbook*, pp. 121–147. Winterkorn H.F. and Fang H.Y.

Wolf, J. P. (1988). *Soil-structure interaction analysis in the time domain*. New Jersey: Prentice Hall.

Wolf, J. P. (1994). *Foundation Vibration Analysis Using Simple Physical Model*. Englewood Cliffs, NJ: Prentice-Hall.

Wolf, J. P. and A. J. Deeks (2004, April). *Foundation Vibration Analysis: A Strength of Materials Approach* (1 ed.). Butterworth-Heinemann.

Wolf, J. P. and C. Song (2002). Some cornerstones of dynamic soil–structure interaction. *Engineering Structures 24*(1), 13–28.

Wotherspoon, L. M. (2009, February). *Integrated modelling of structure-foundation systems*. Ph. D. thesis, The University of Auckland.

Yazgan, U. and A. Dazio (2011, November). Simulating Maximum and Residual Displacements of RC Structures: I. Accuracy. *Earthquake Spectra 27*(4), 1187–1202.

Appendix A

Macro-element experimental validation - Pier

A.1 Summary

This appendix presents all the validation of soil-foundation macro-element against the experimental results from the fifth experiment (LJD03) from the NEES project: ”Innovative Economical Foundations with Improved Performance that is Less Sensitive to Site Conditions” (Deng and Kutter, 2010). This appendix is a supplement of Chapter 5 where the experimental test and numerical model setups are explained.

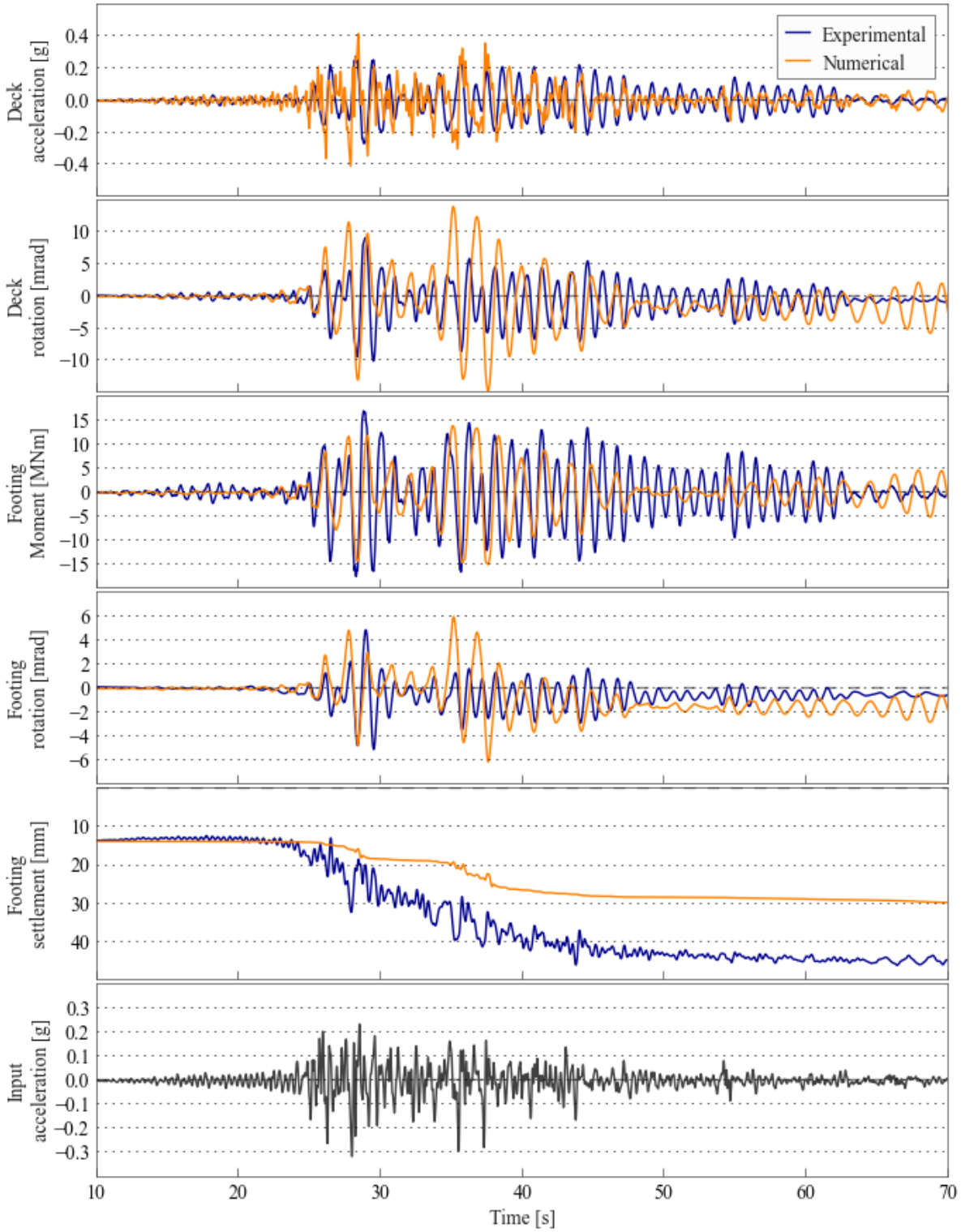

Figure A.1: Comparision of numerical and experimental behaviour - Motion 4

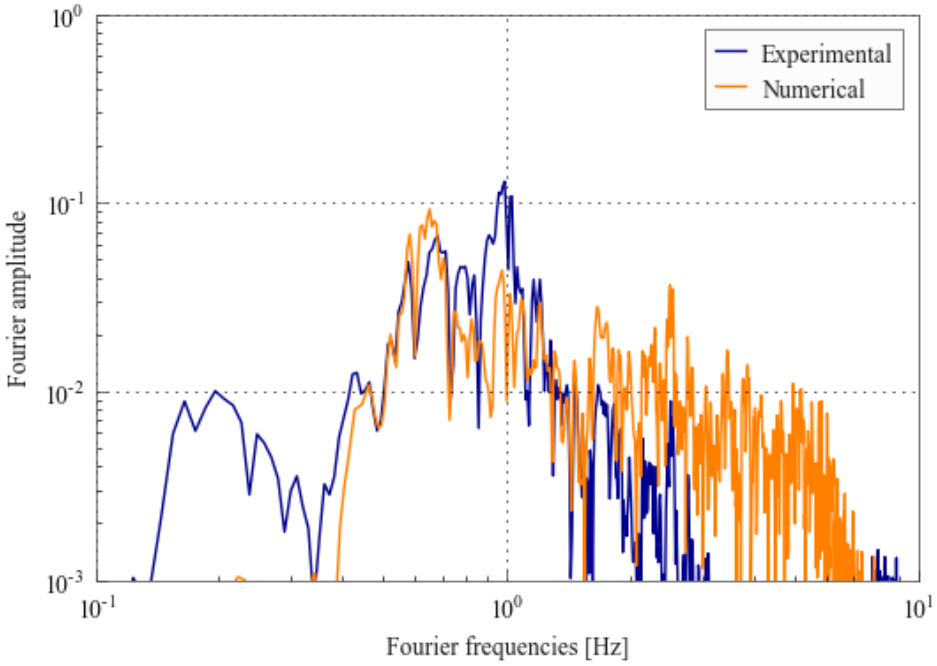

Figure A.2: Roof acceleration Fourier amplitude spectrum - Motion 4

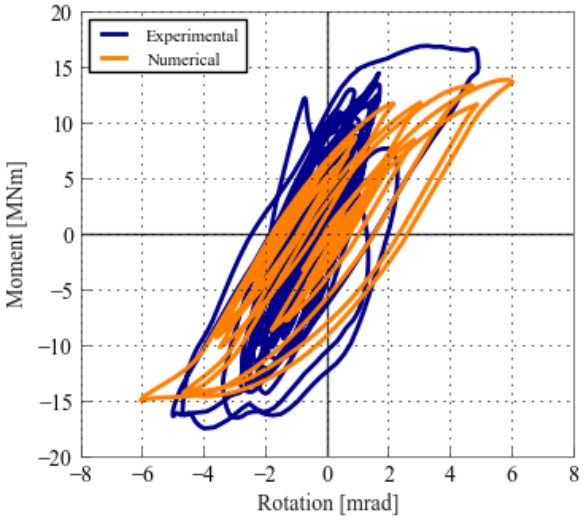

(a) Moment verse rotation of footing - Motion 4

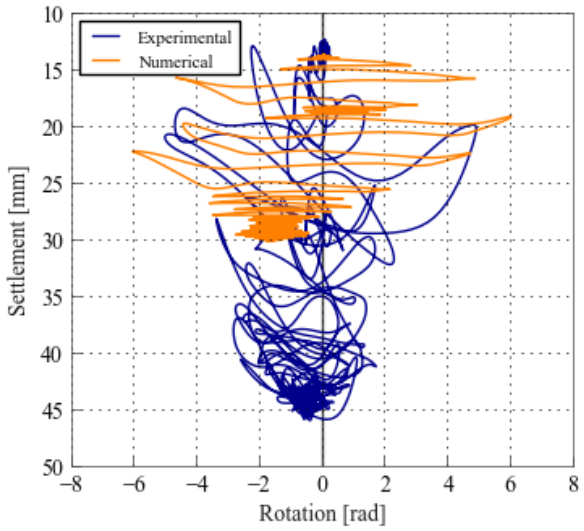

(b) Settlement verse rotation of footing - Motion 4

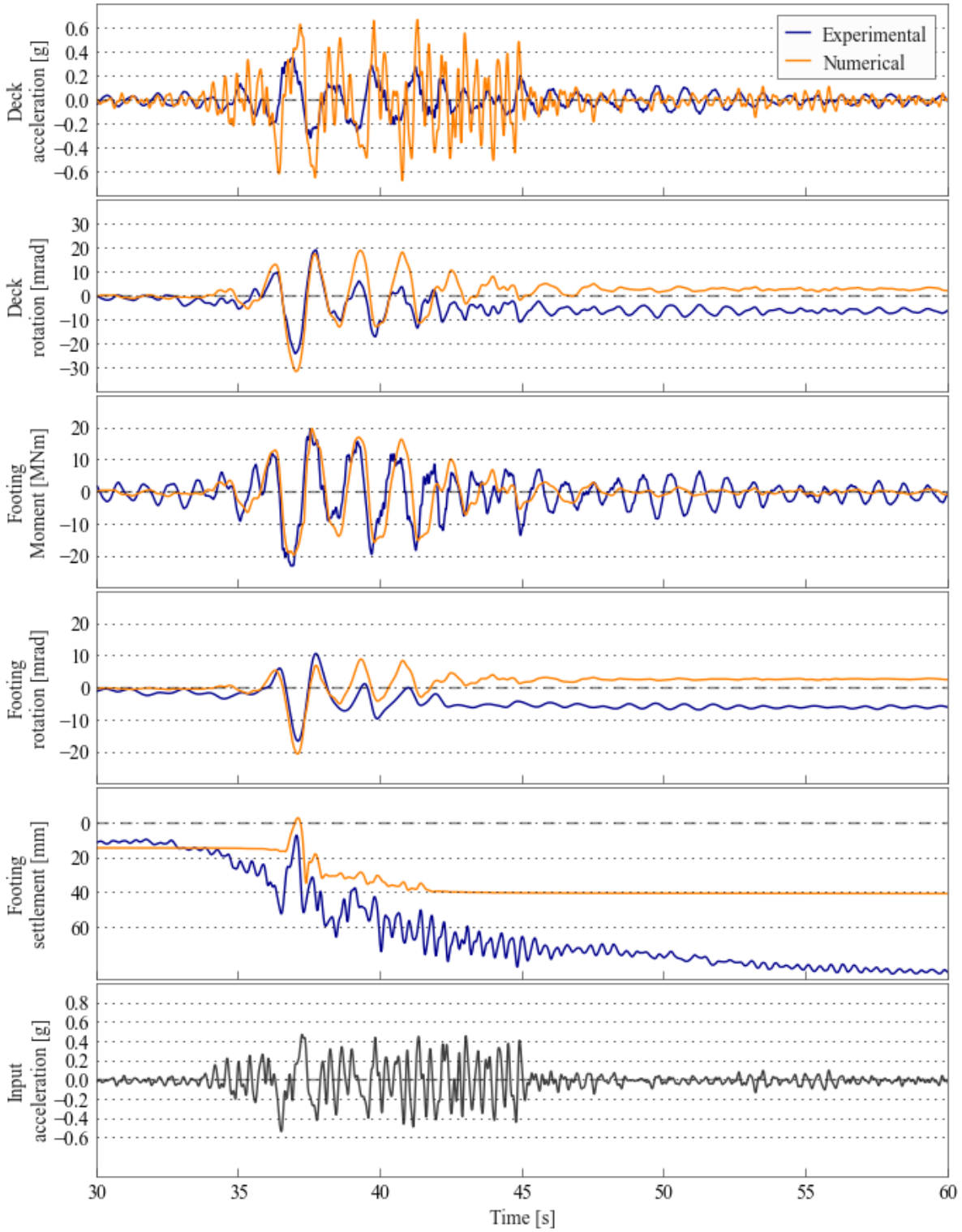

Figure A.3: Comparision of numerical and experimental behaviour - Motion 6

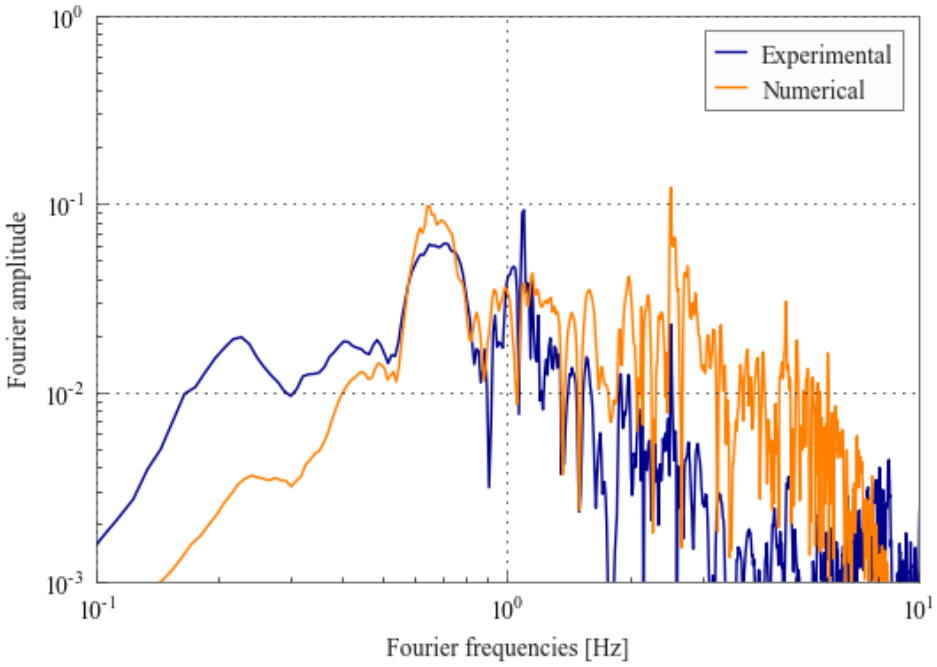

Figure A.4: Roof acceleration Fourier amplitude spectrum - Motion 6

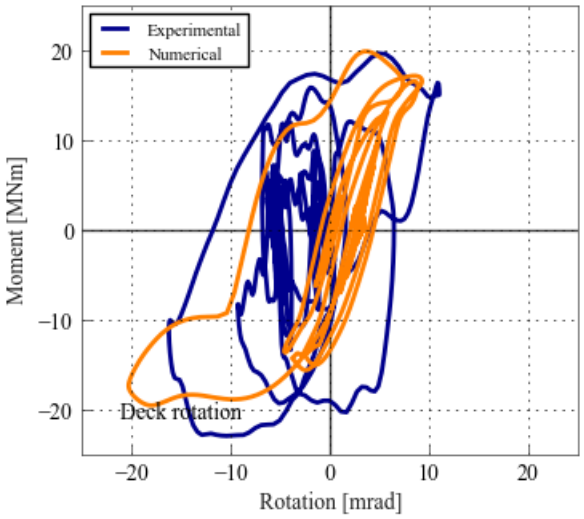

(a) Moment verse rotation of footing - Motion 6

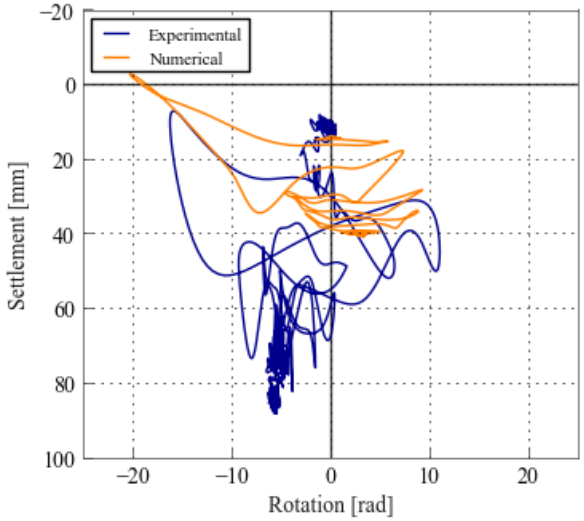

(b) Settlement verse rotation of footing - Motion 6

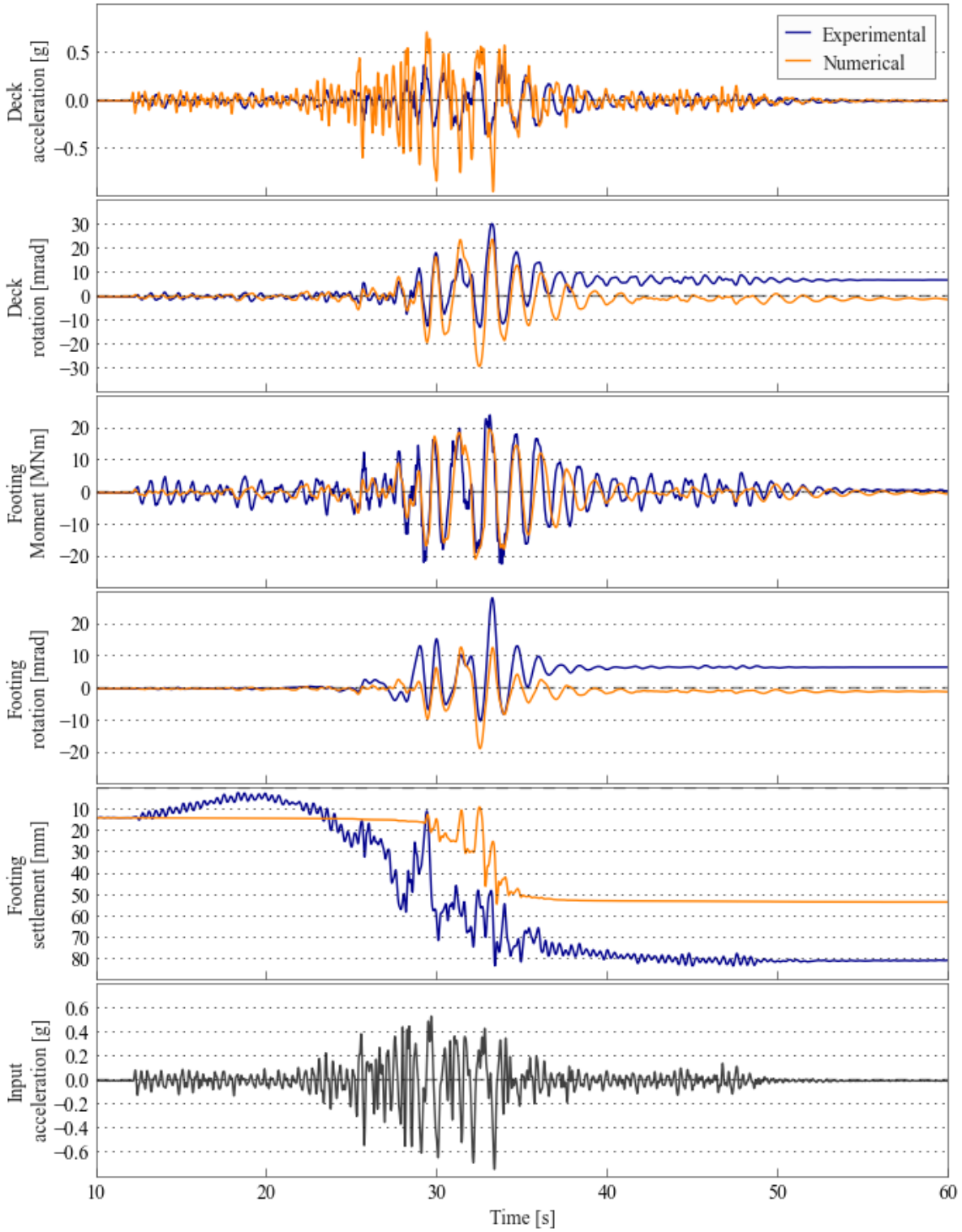

Figure A.5: Comparision of numerical and experimental behaviour - Motion 7

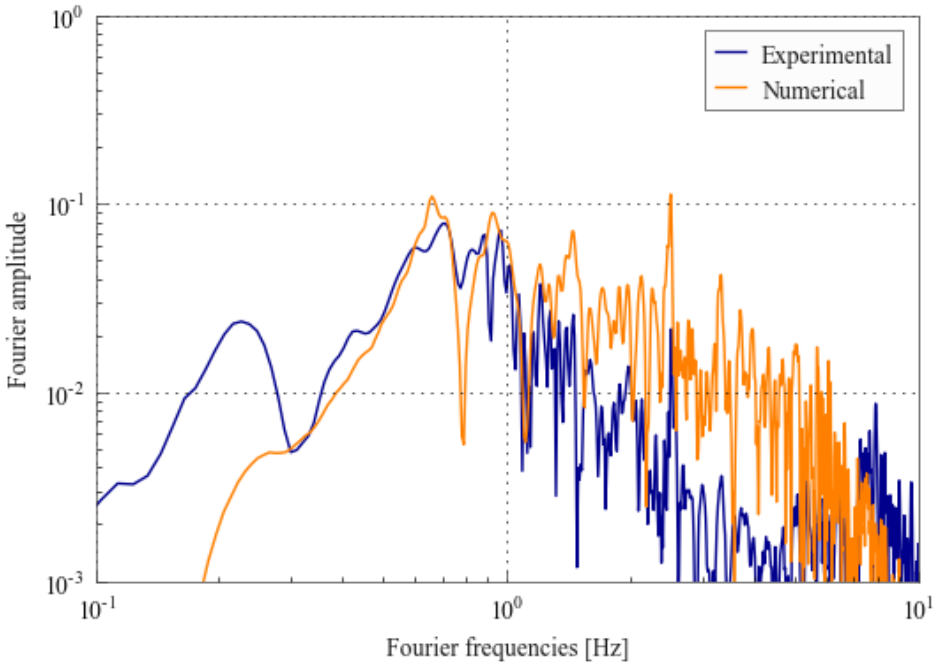

Figure A.6: Roof acceleration Fourier amplitude spectrum - Motion 7

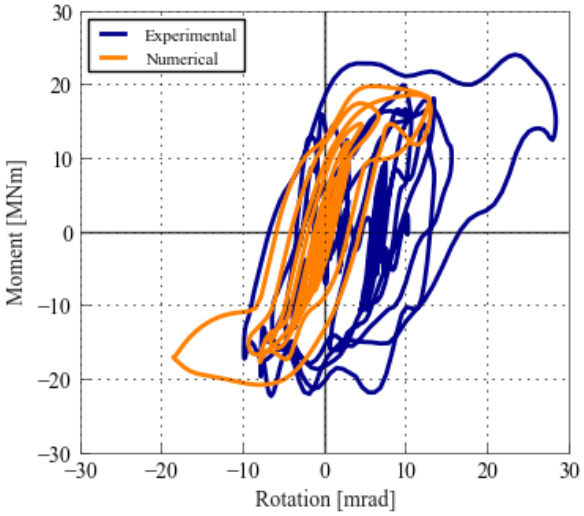

(a) Moment verse rotation of footing - Motion 7

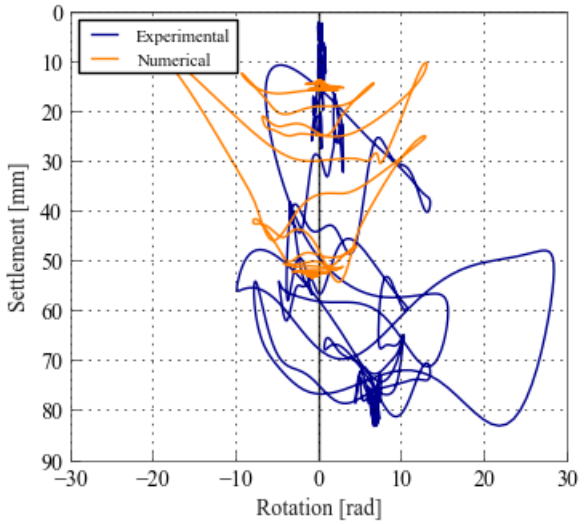

(b) Settlement verse rotation of footing - Motion 7

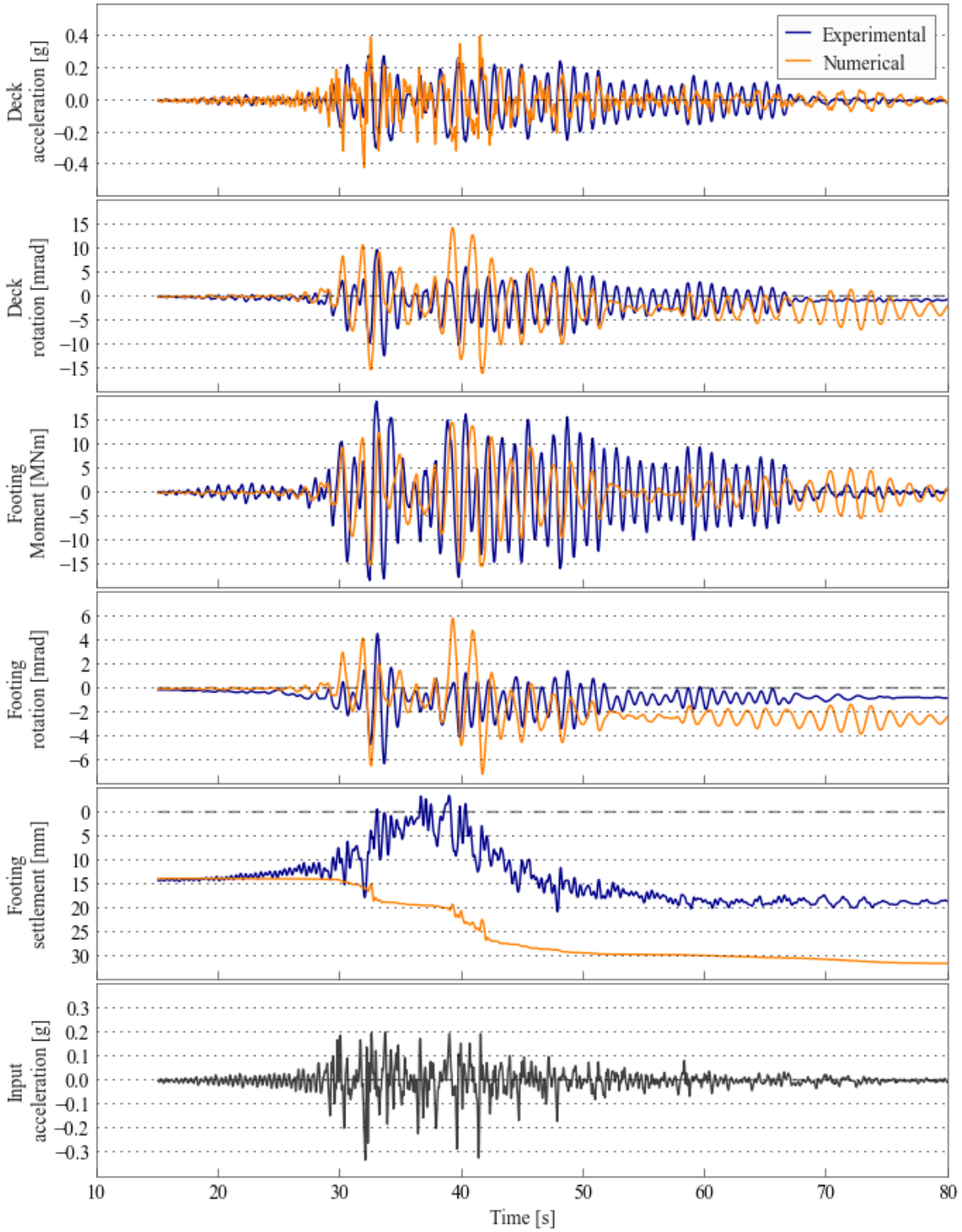

Figure A.7: Comparision of numerical and experimental behaviour - Motion 8

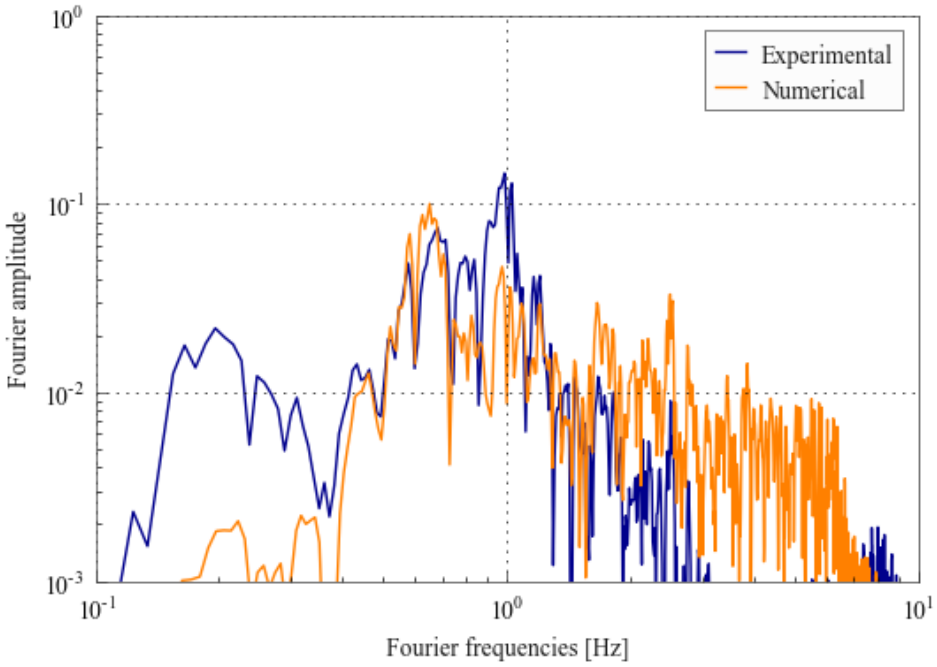

Figure A.8: Roof acceleration Fourier amplitude spectrum - Motion 8

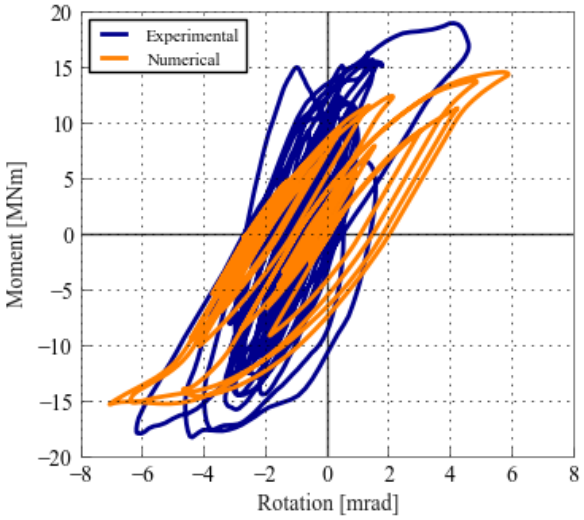

(a) Moment verse rotation of footing - Motion 8

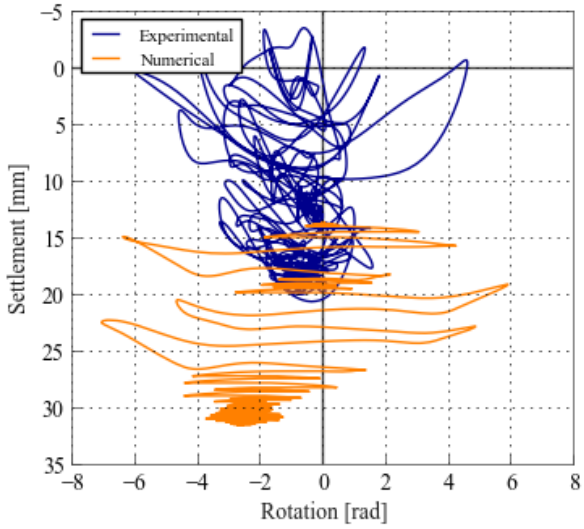

(b) Settlement verse rotation of footing - Motion 8

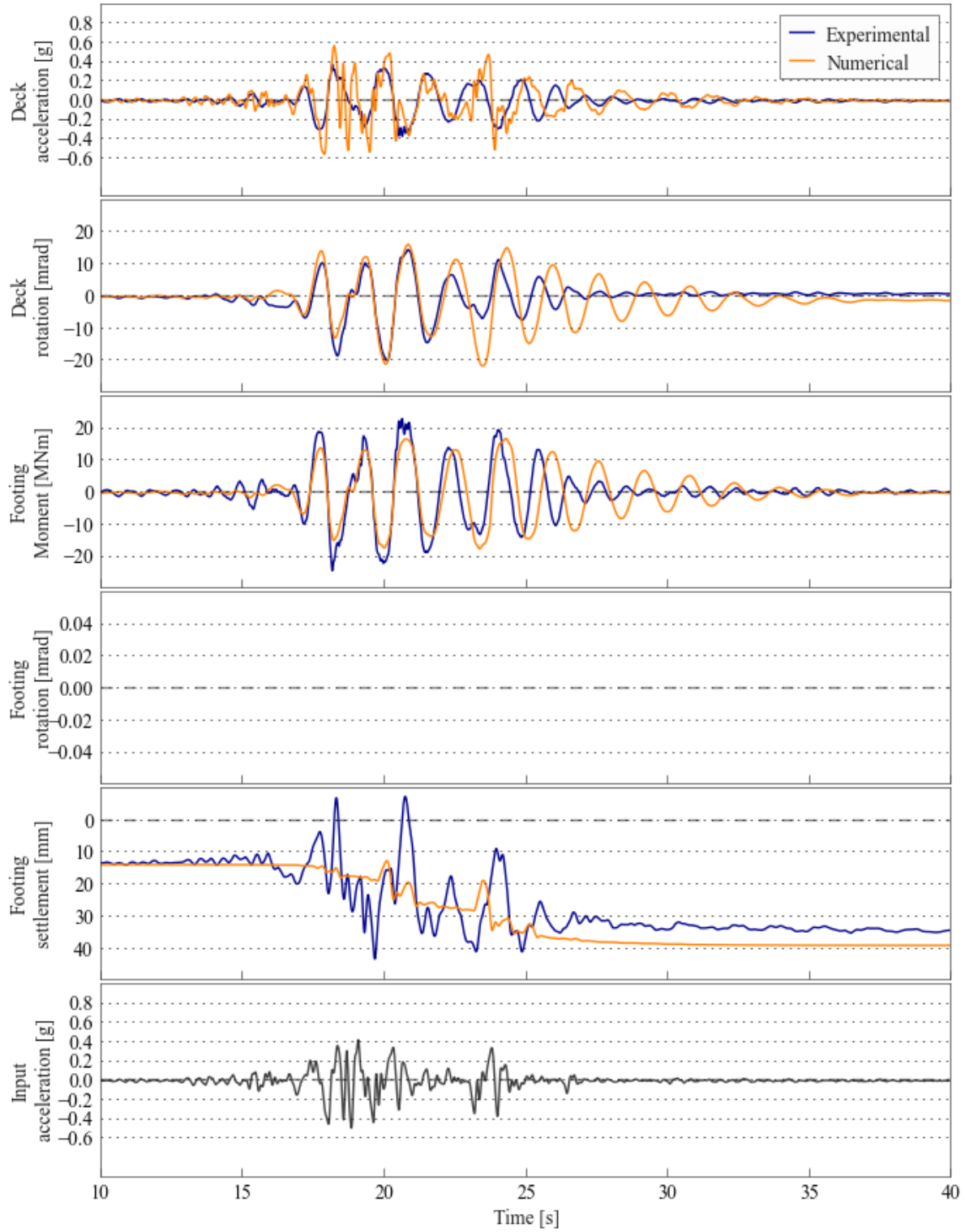

Figure A.9: Comparision of numerical and experimental behaviour - Motion 9

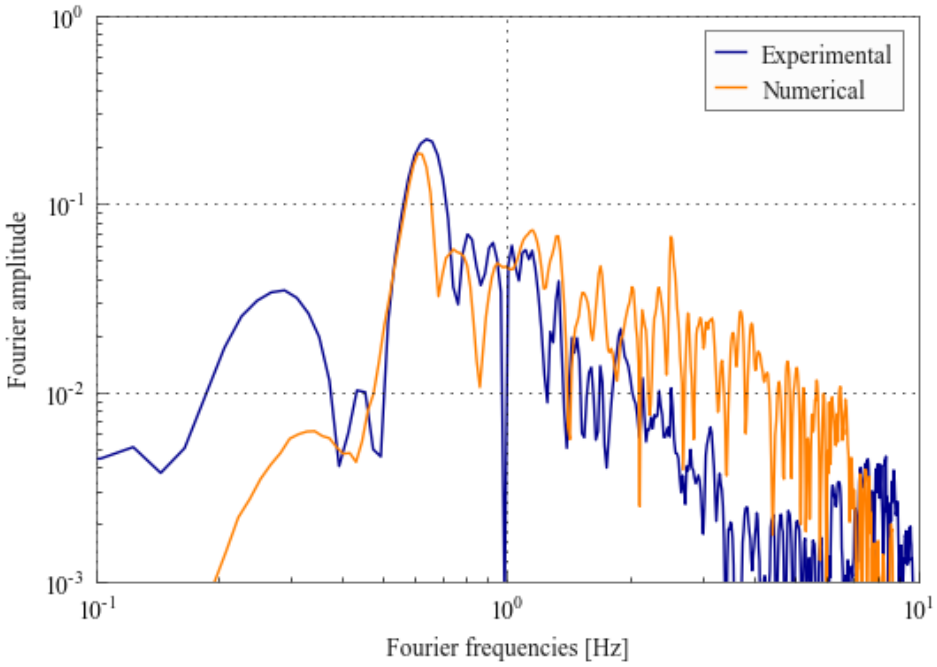

Figure A.10: Roof acceleration Fourier amplitude spectrum - Motion 9

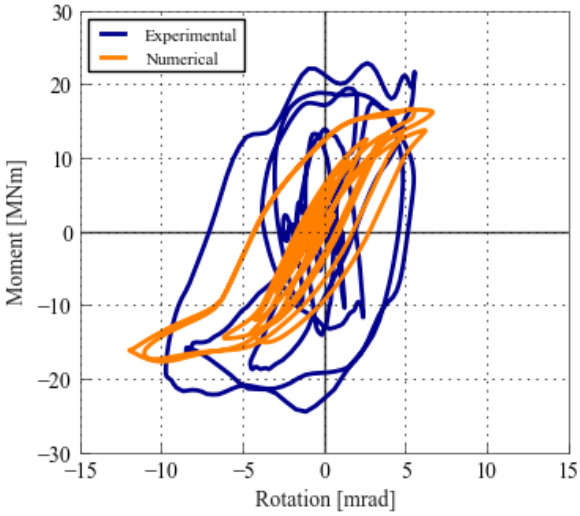

(a) Moment verse rotation of footing - Motion 9

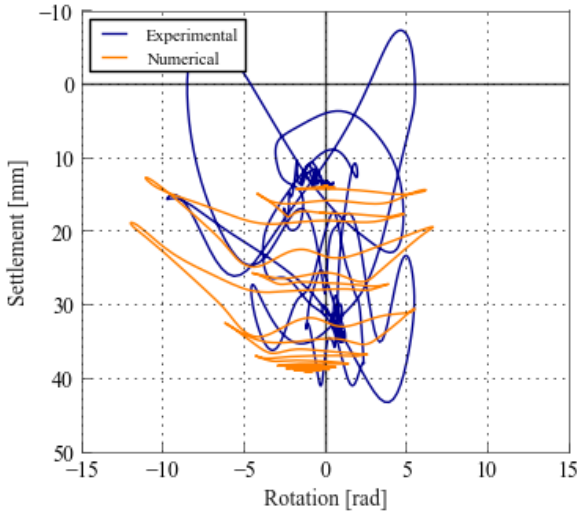

(b) Settlement verse rotation of footing - Motion 9

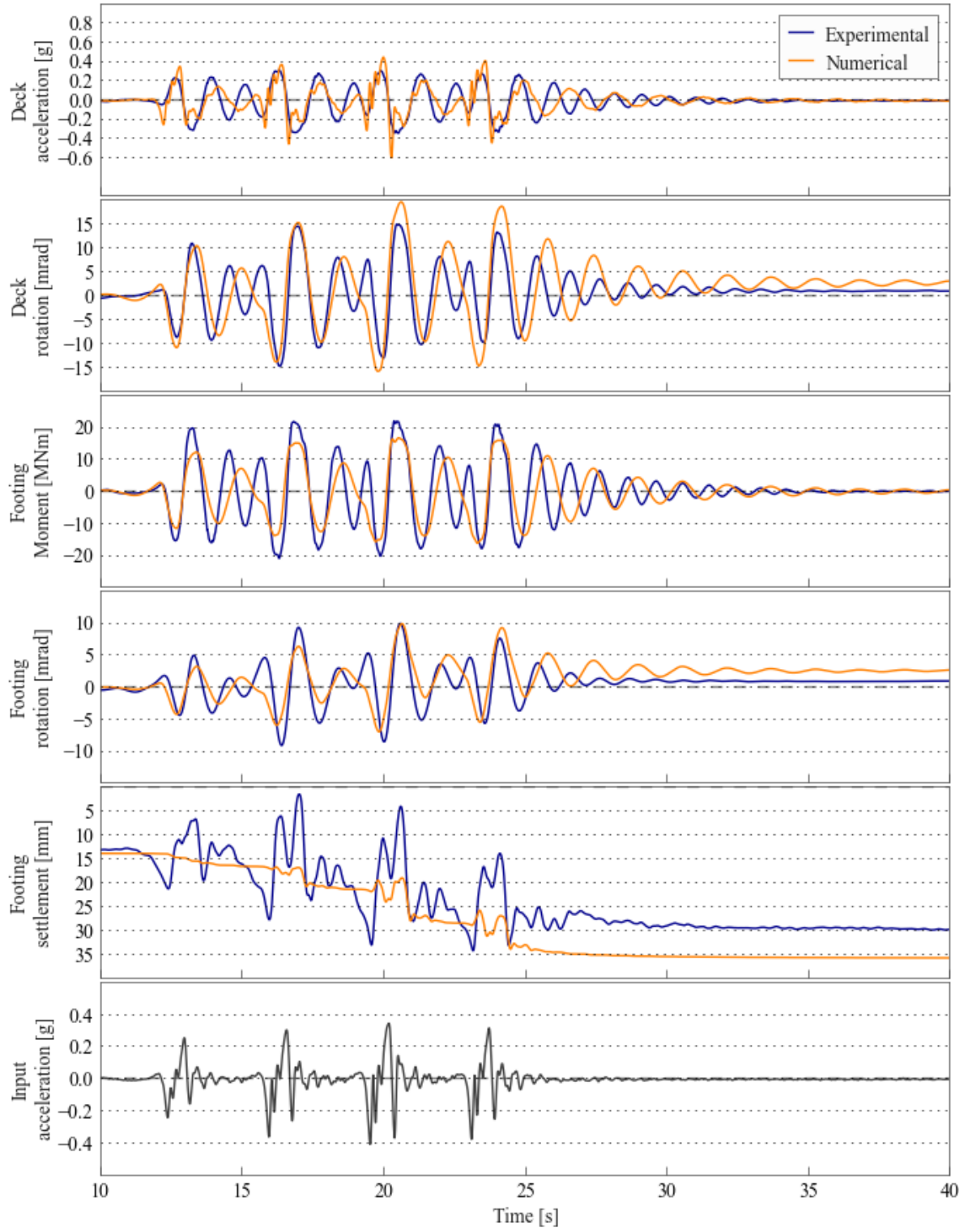

Figure A.11: Comparision of numerical and experimental behaviour - Motion 10

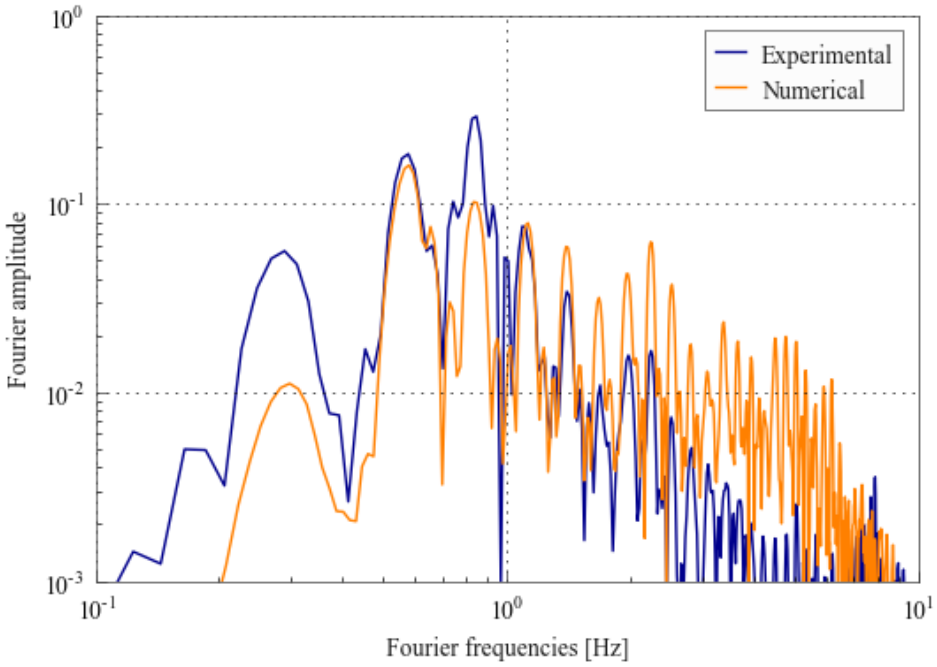

Figure A.12: Roof acceleration Fourier amplitude spectrum - Motion 10

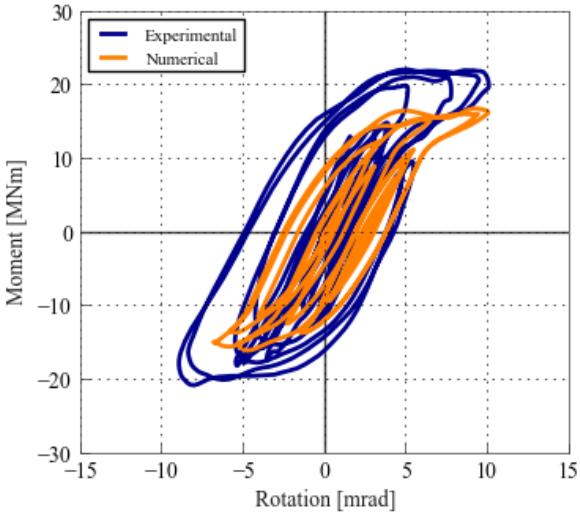

(a) Moment verse rotation of footing - Motion 10

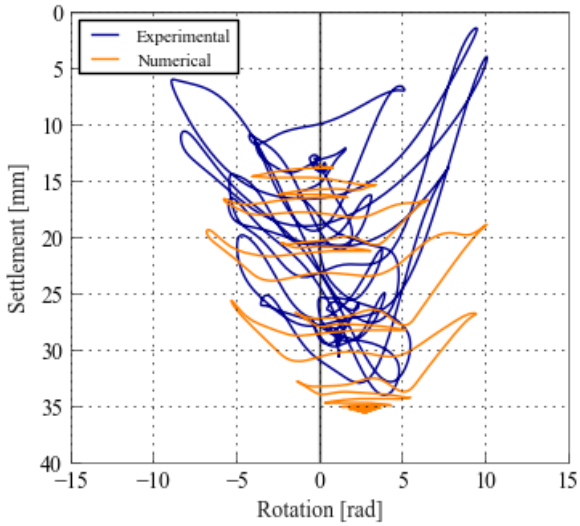

(b) Settlement verse rotation of footing - Motion 10

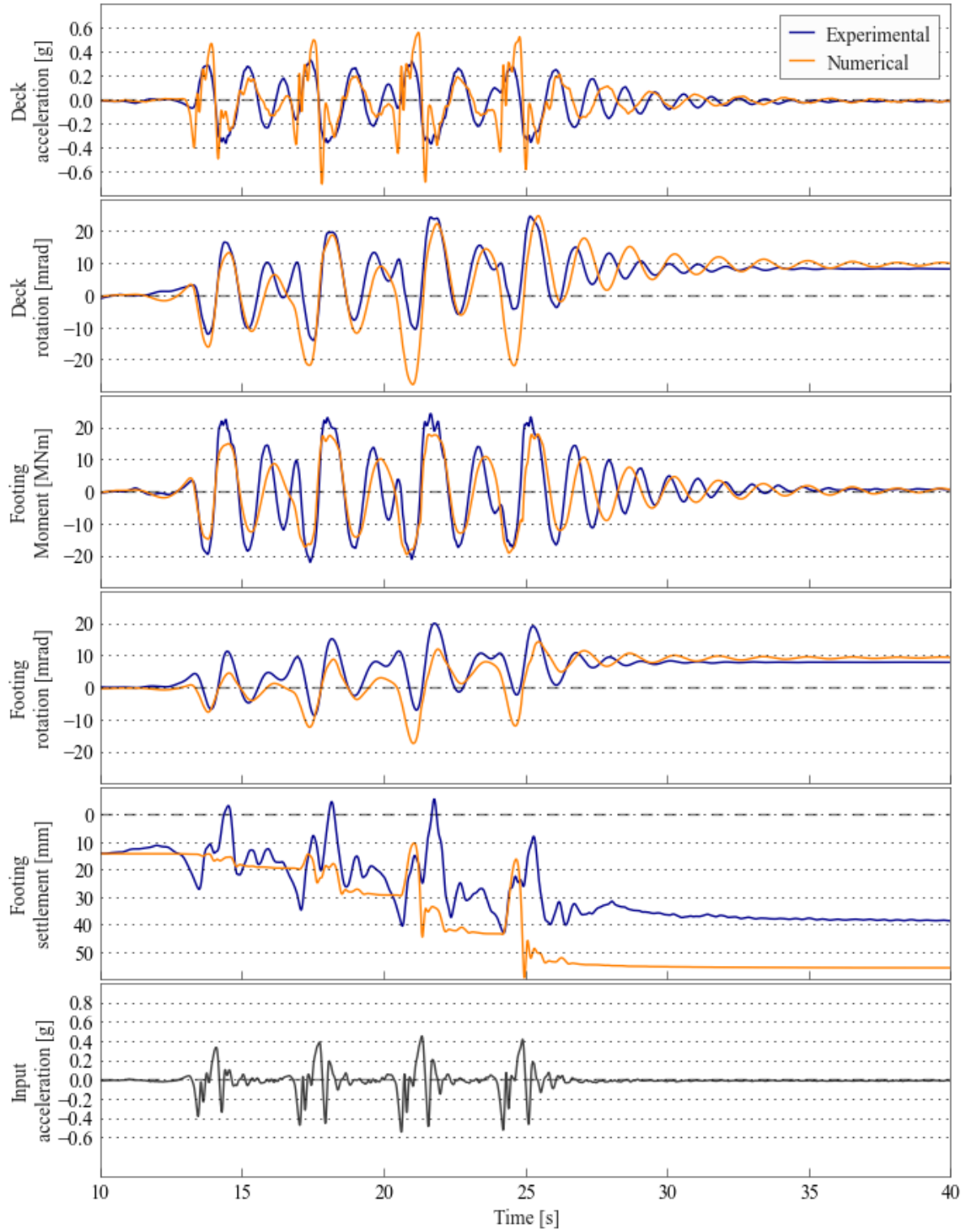

Figure A.13: Comparision of numerical and experimental behaviour - Motion 11

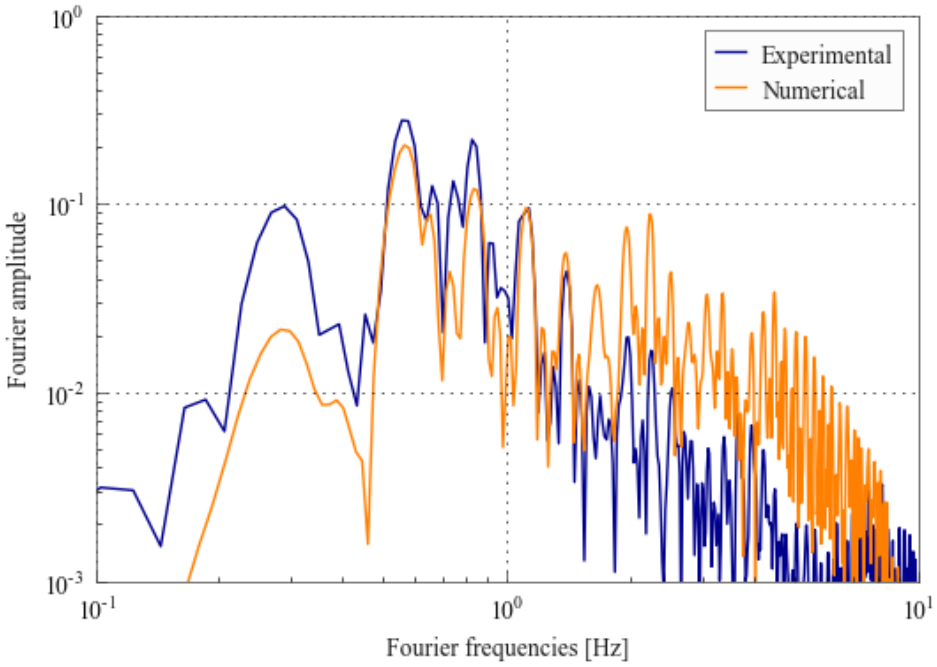

Figure A.14: Roof acceleration Fourier amplitude spectrum - Motion 11

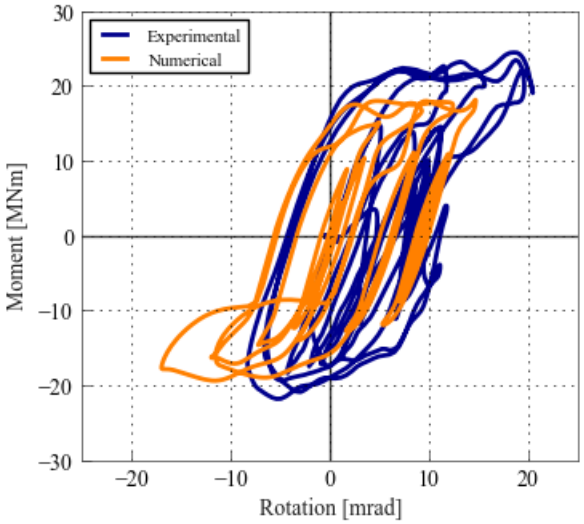

(a) Moment verse rotation of footing - Motion 11

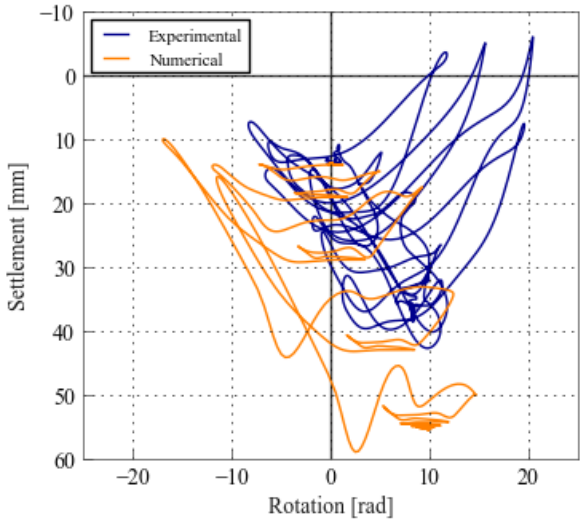

(b) Settlement verse rotation of footing - Motion 11

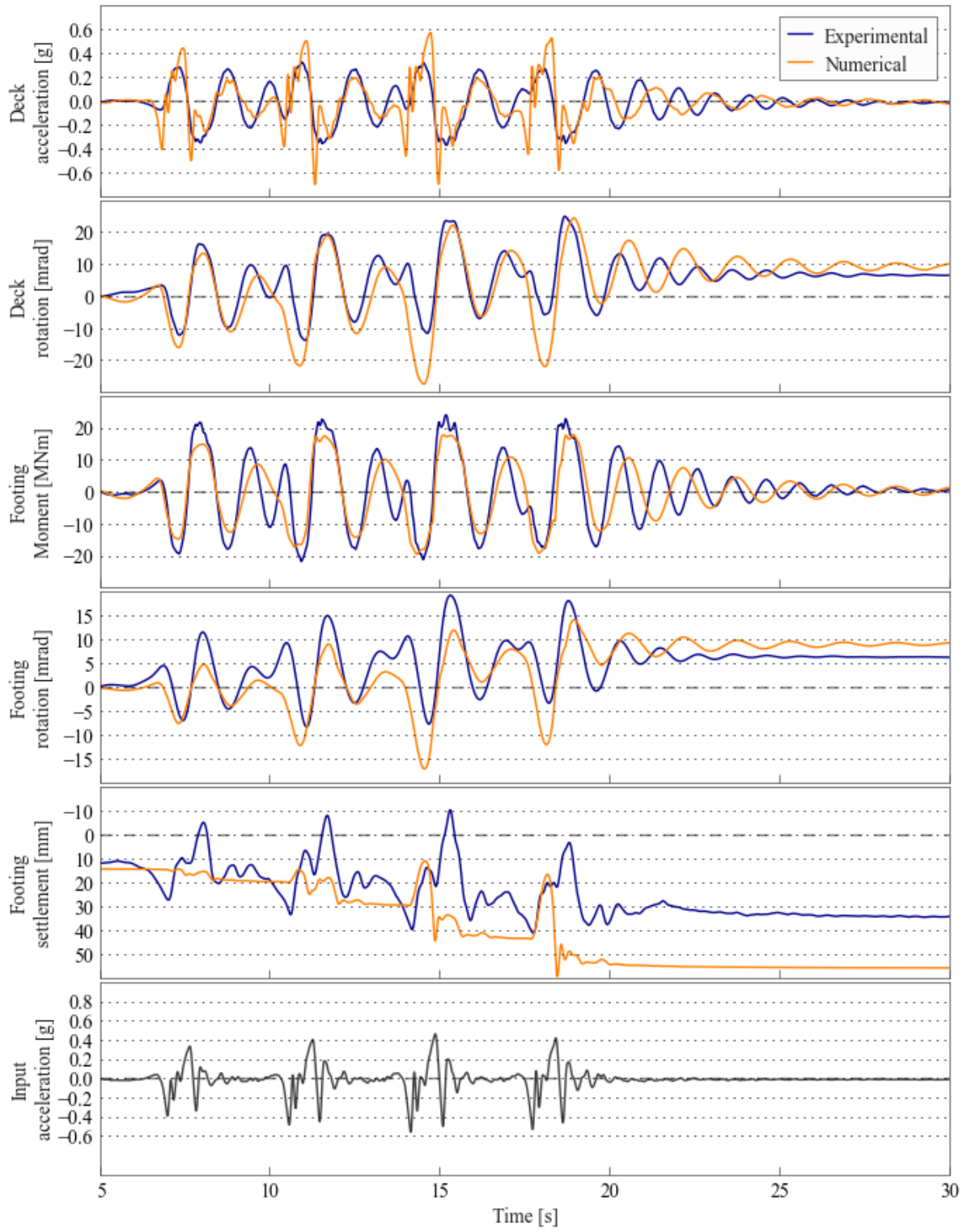

Figure A.15: Comparision of numerical and experimental behaviour - Motion 12

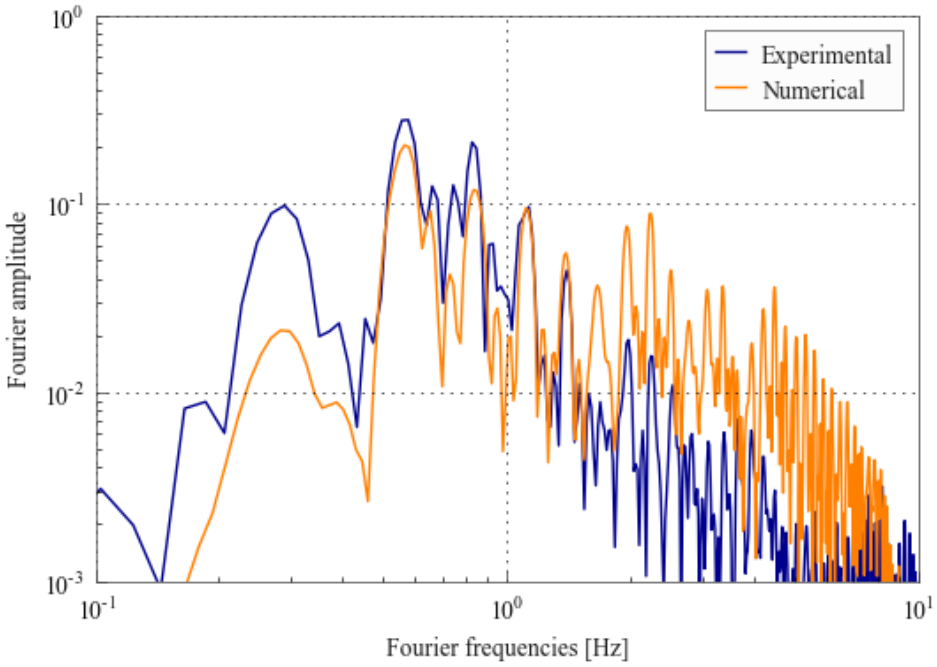

Figure A.16: Roof acceleration Fourier amplitude spectrum - Motion 12

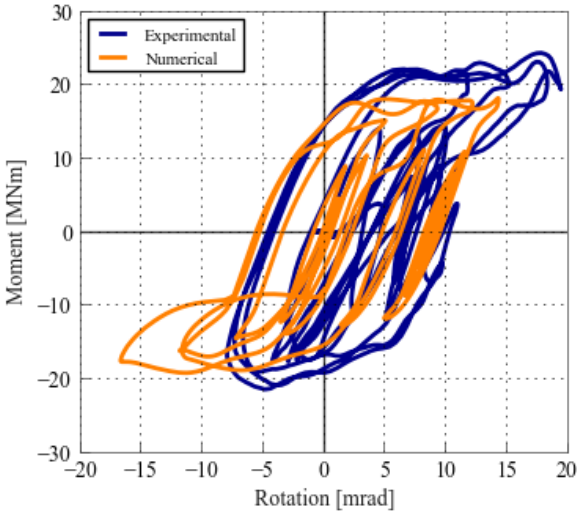

(a) Moment verse rotation of footing - Motion 12

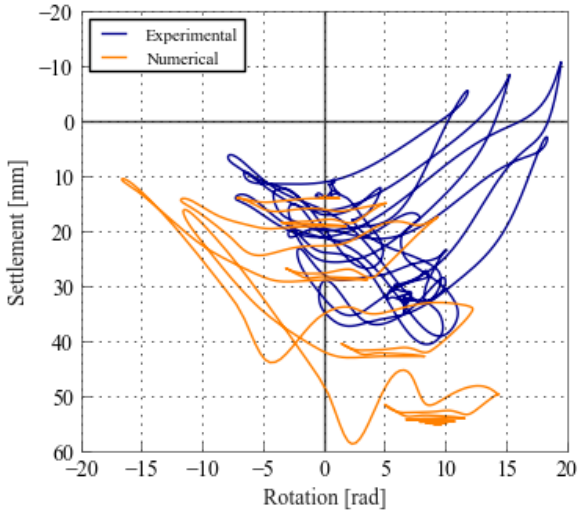

(b) Settlement verse rotation of footing - Motion 12

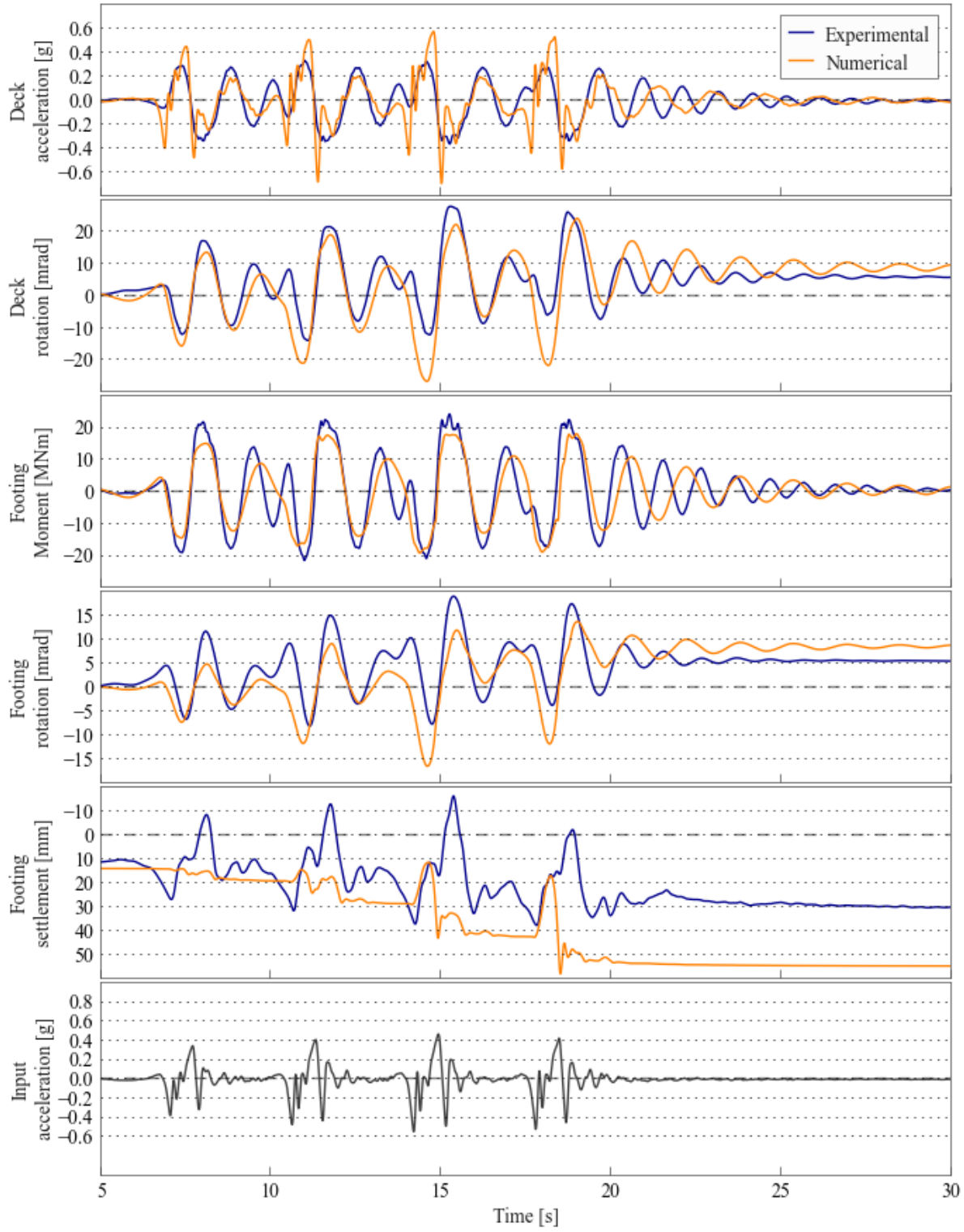

Figure A.17: Comparision of numerical and experimental behaviour - Motion 13

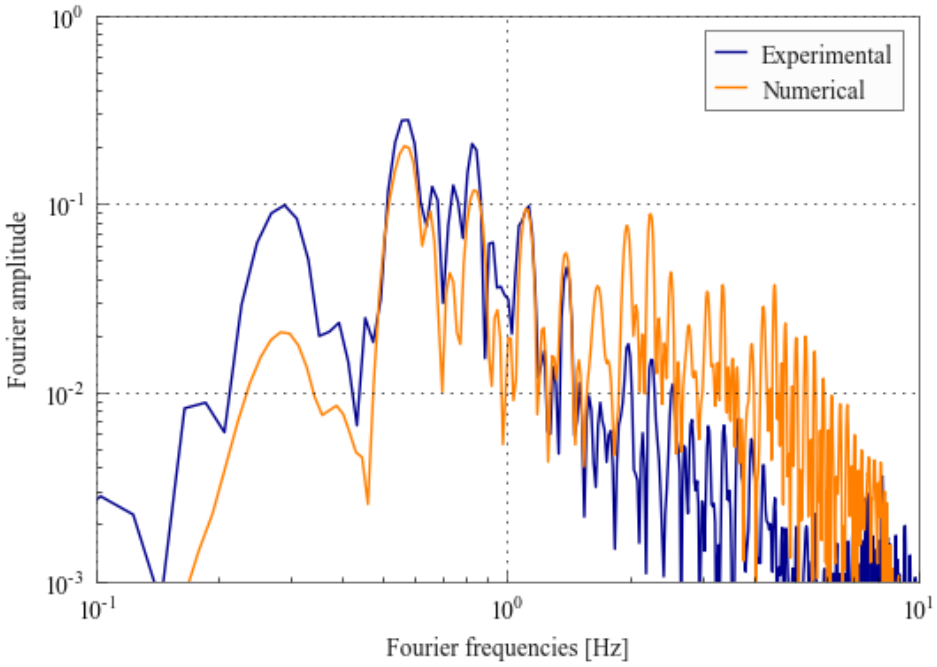

Figure A.18: Roof acceleration Fourier amplitude spectrum - Motion 13

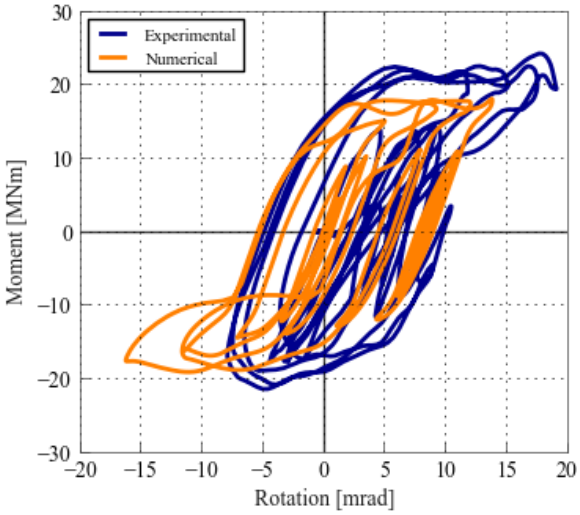

(a) Moment verse rotation of footing - Motion 13

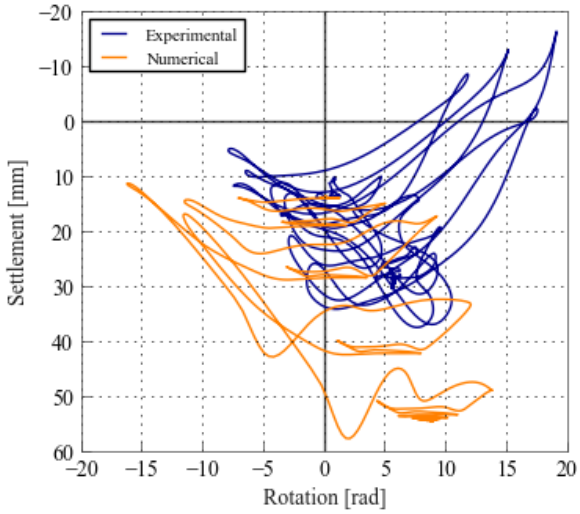

(b) Settlement verse rotation of footing - Motion 13

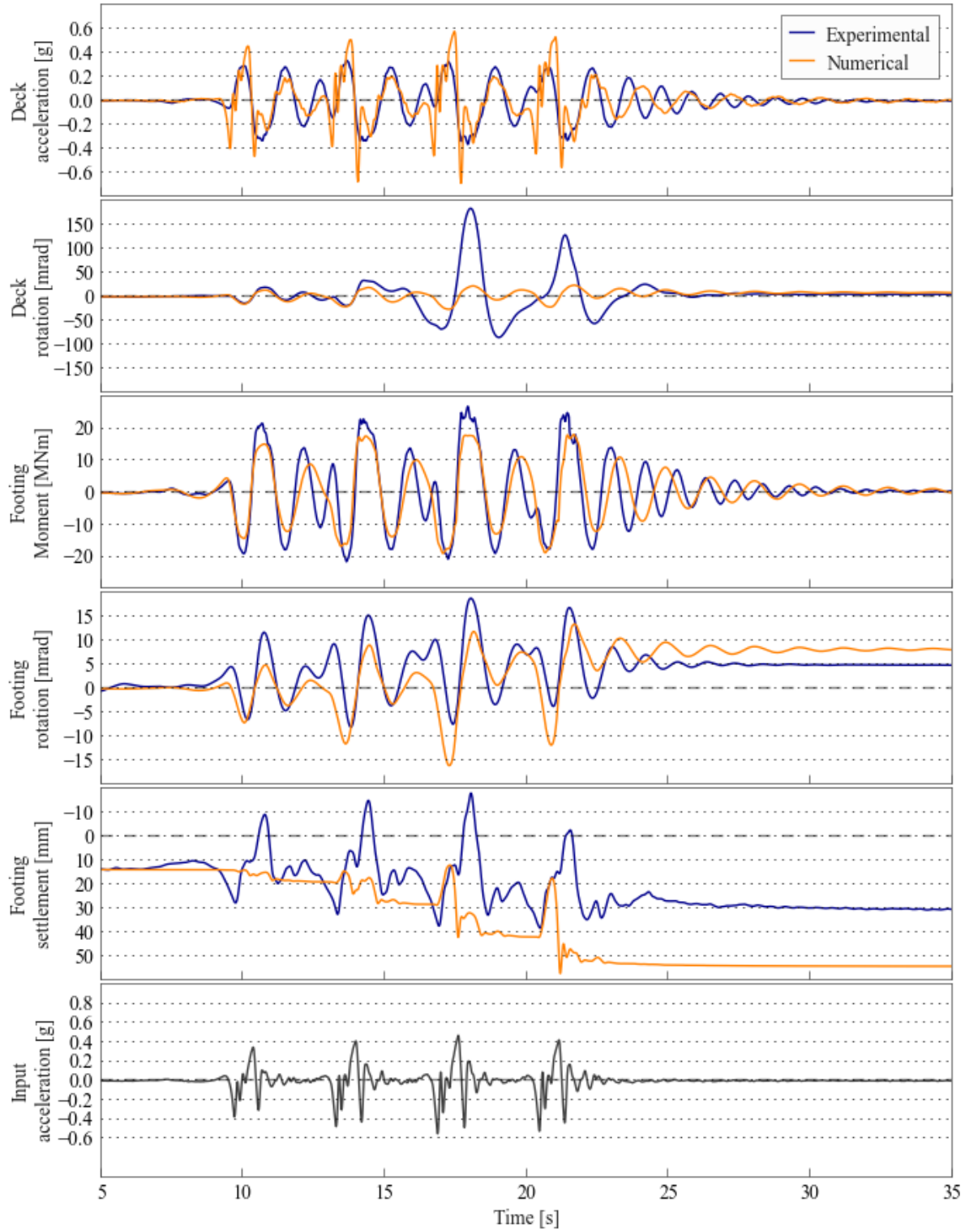

Figure A.19: Comparision of numerical and experimental behaviour - Motion 14

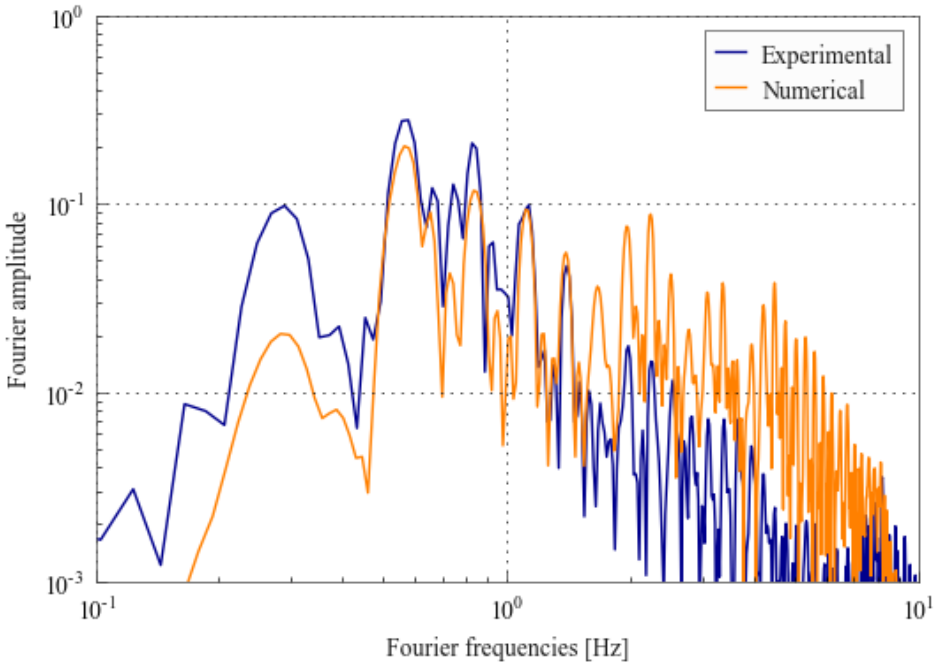

Figure A.20: Roof acceleration Fourier amplitude spectrum - Motion 14

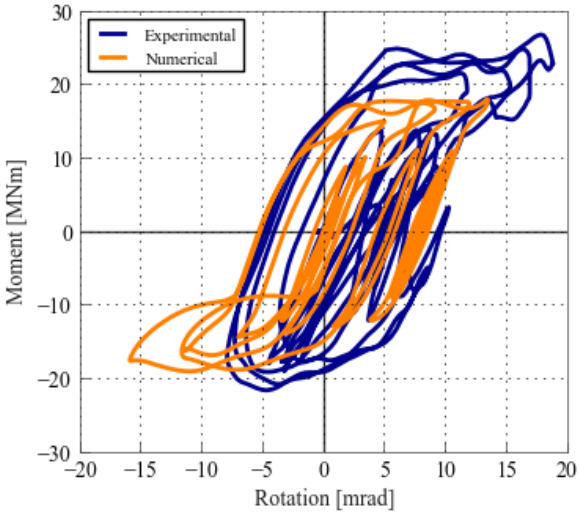

(a) Moment verse rotation of footing - Motion 14

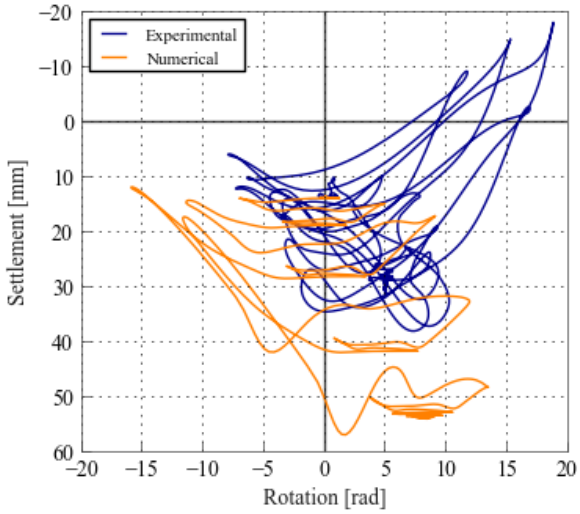

(b) Settlement verse rotation of footing - Motion 14

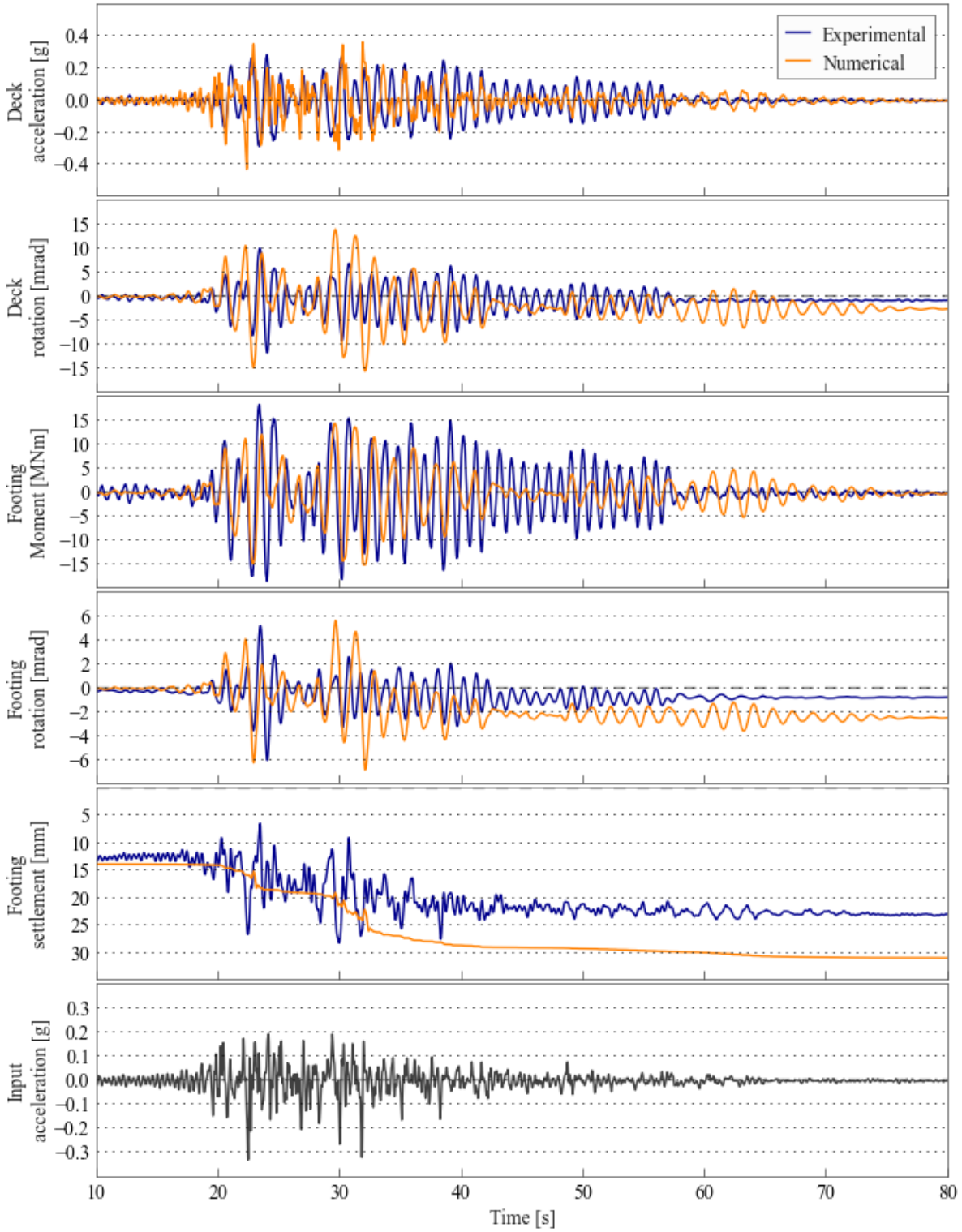

Figure A.21: Comparision of numerical and experimental behaviour - Motion 15

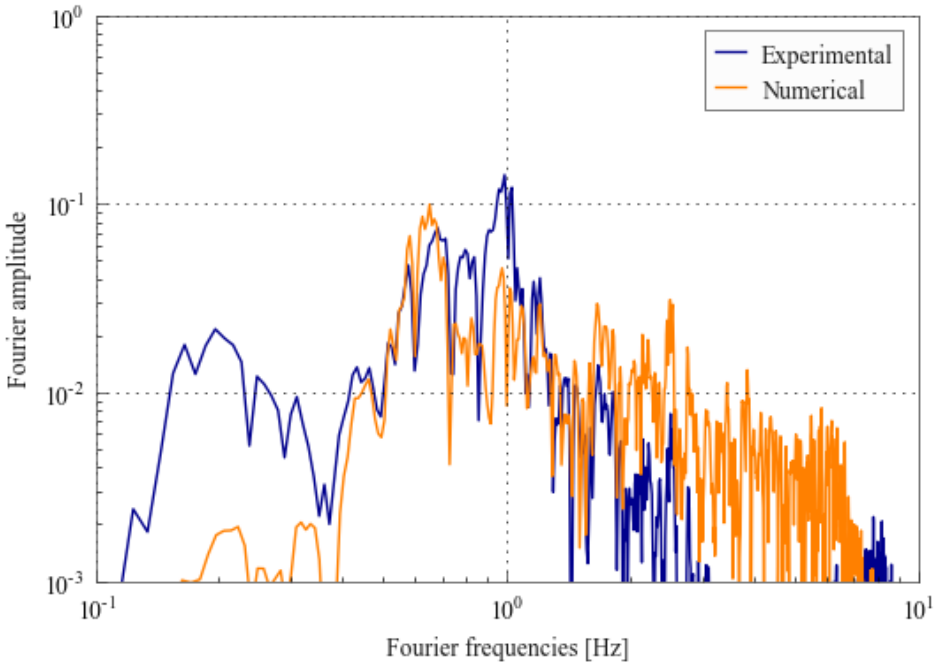

Figure A.22: Roof acceleration Fourier amplitude spectrum - Motion 15

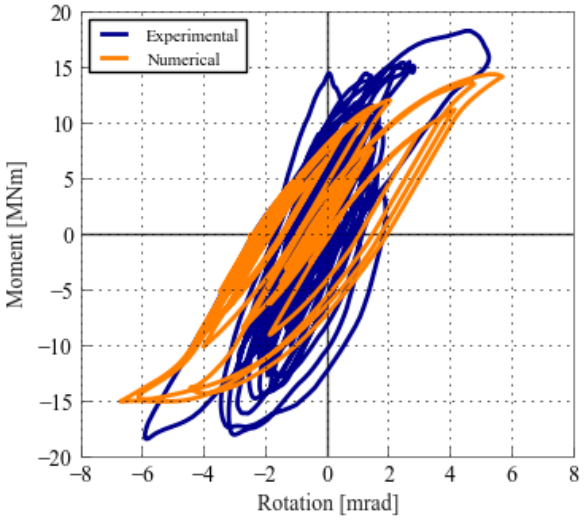

(a) Moment verse rotation of footing - Motion 15

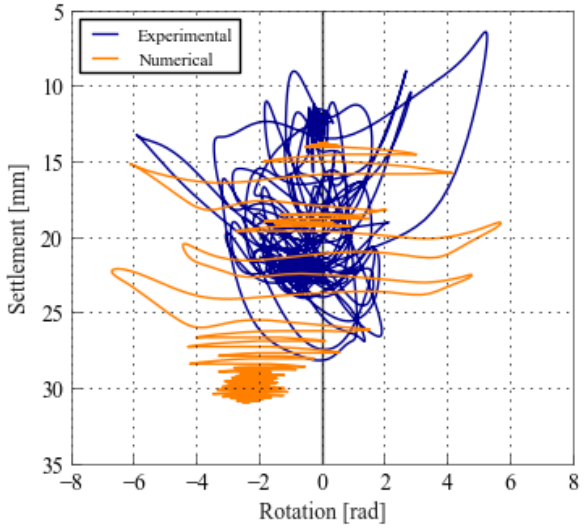

(b) Settlement verse rotation of footing - Motion 15

Appendix B

Macro-element experimental validation - Frame

B.1 Summary

This appendix presents all the validation tests of soil-foundation macro-element against the one storey frame structure from the first experiment (HBM02) from the NEES project: "Seismic performance assessments in dense urban environments" (Mason et al., 2010). This appendix is a supplement of Chapter 5 where the experimental test and numerical model setups are explained.

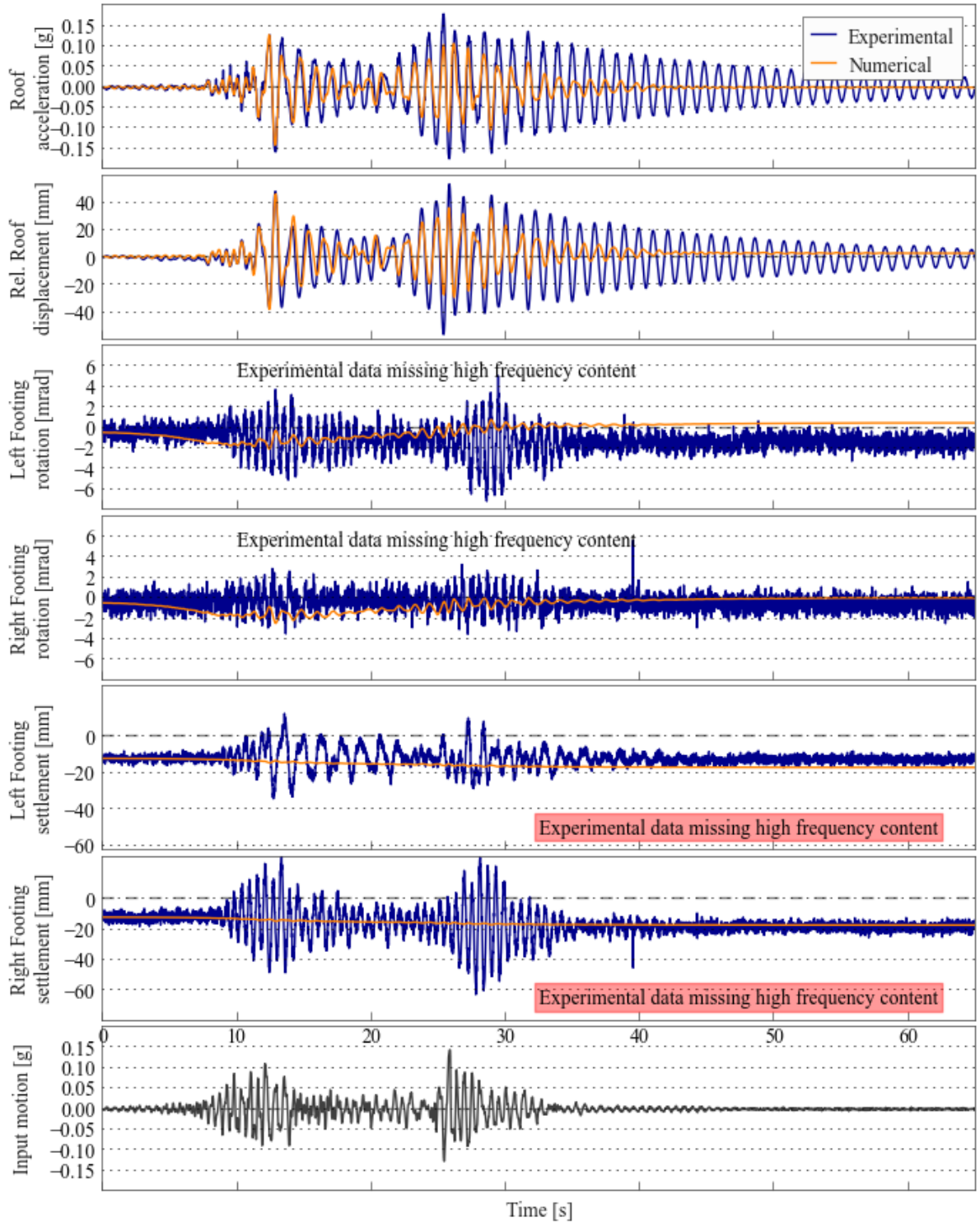

Figure B.1: Comparision of numerical and experimental behaviour - Motion JOS_L_1

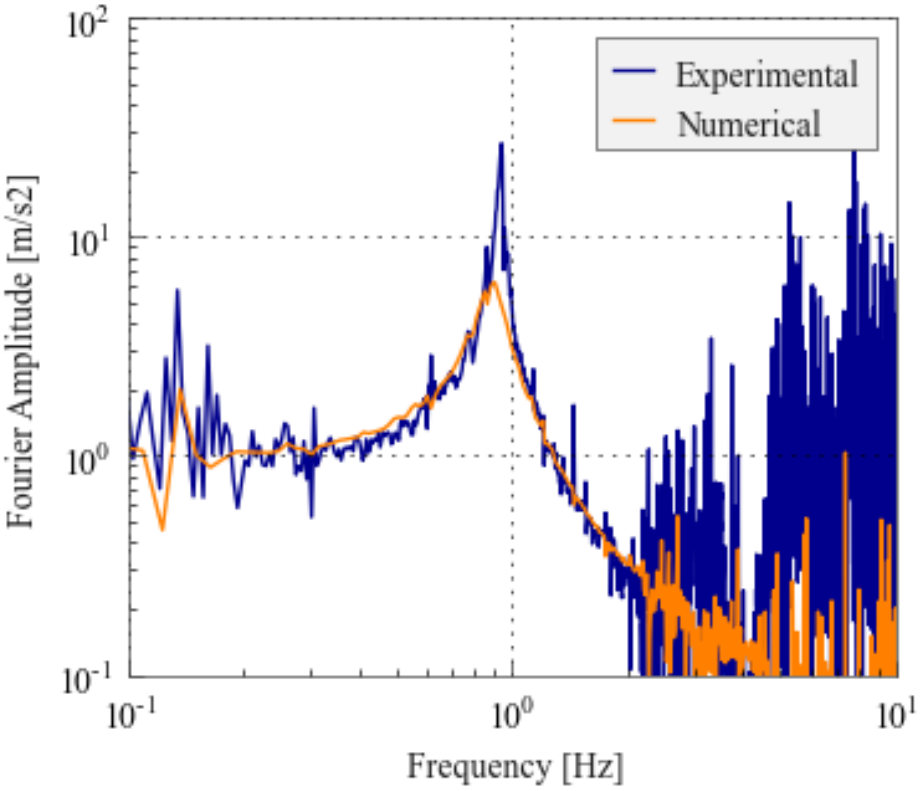

Figure B.2: Roof acceleration Fourier amplitude spectrum - Motion JOS_L_1

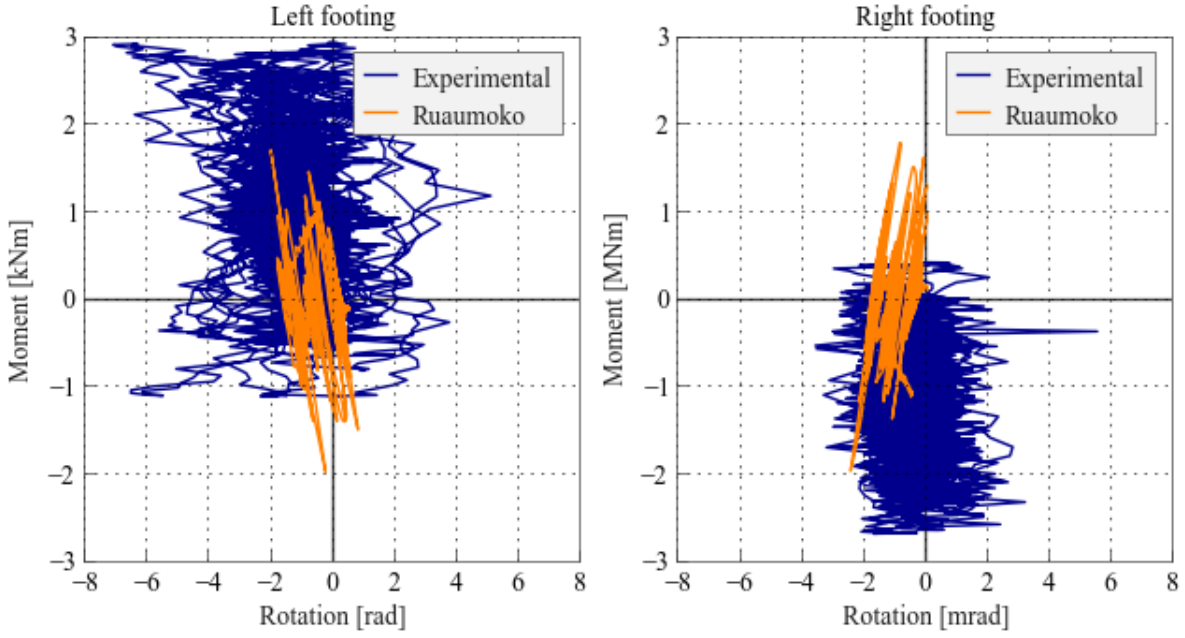

Figure B.3: Moment verse rotation of footing - Motion JOS_L_1

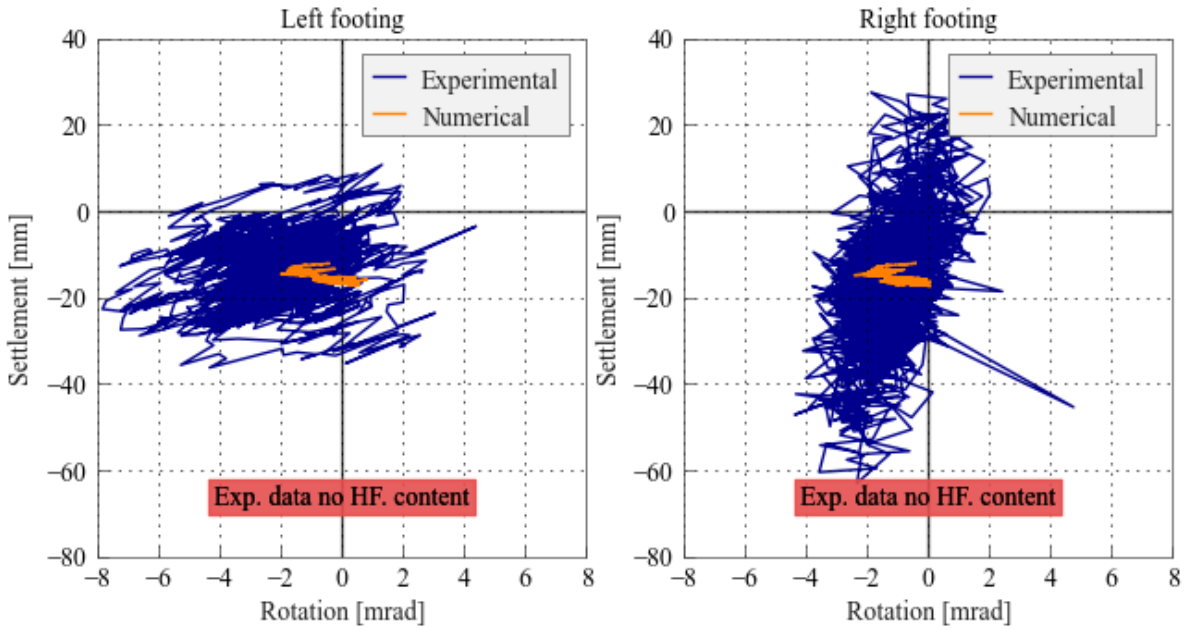

Figure B.4: Settlement verse rotation of footing - Motion JOS_L_1

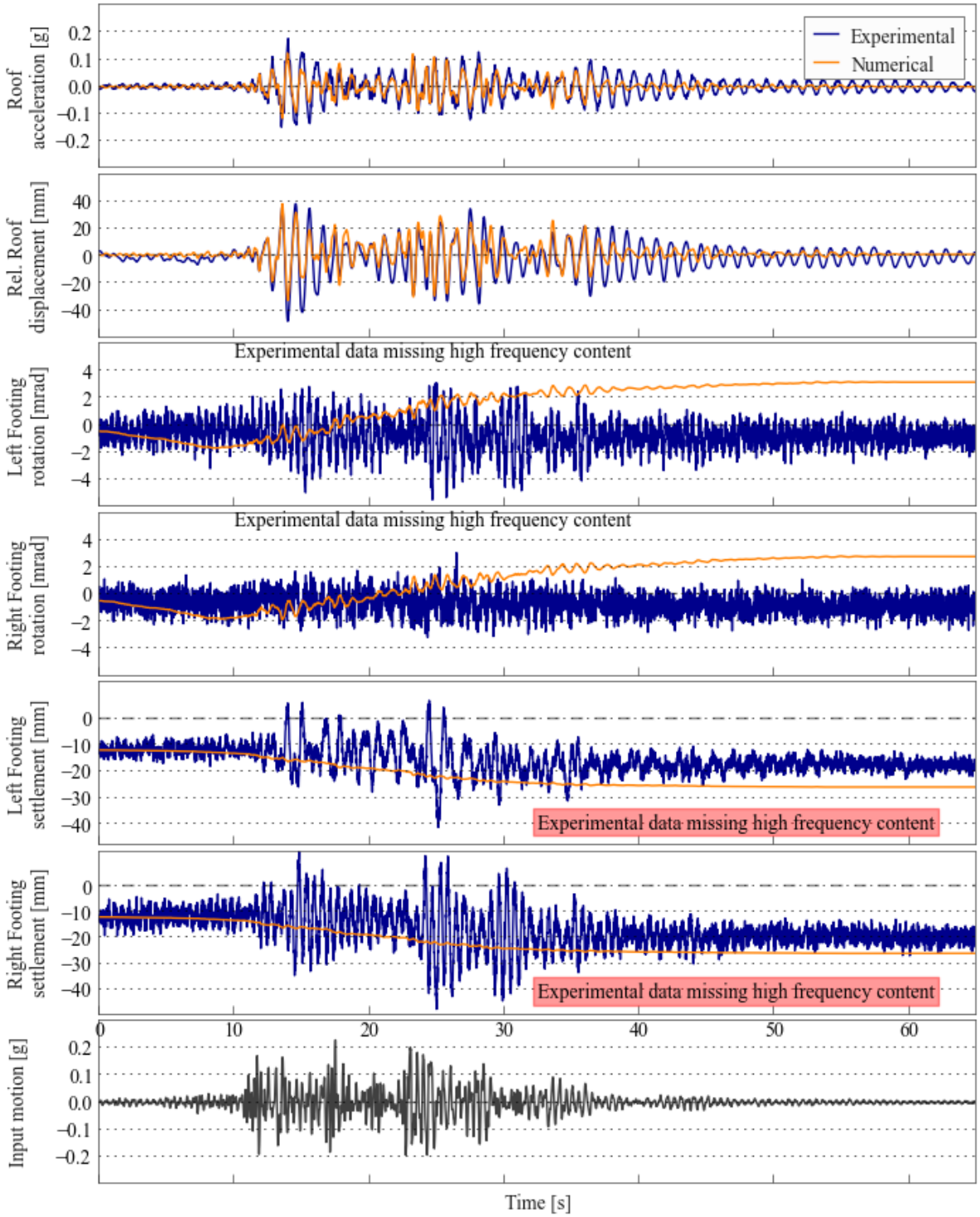

Figure B.5: Comparision of numerical and experimental behaviour - Motion TCU_L

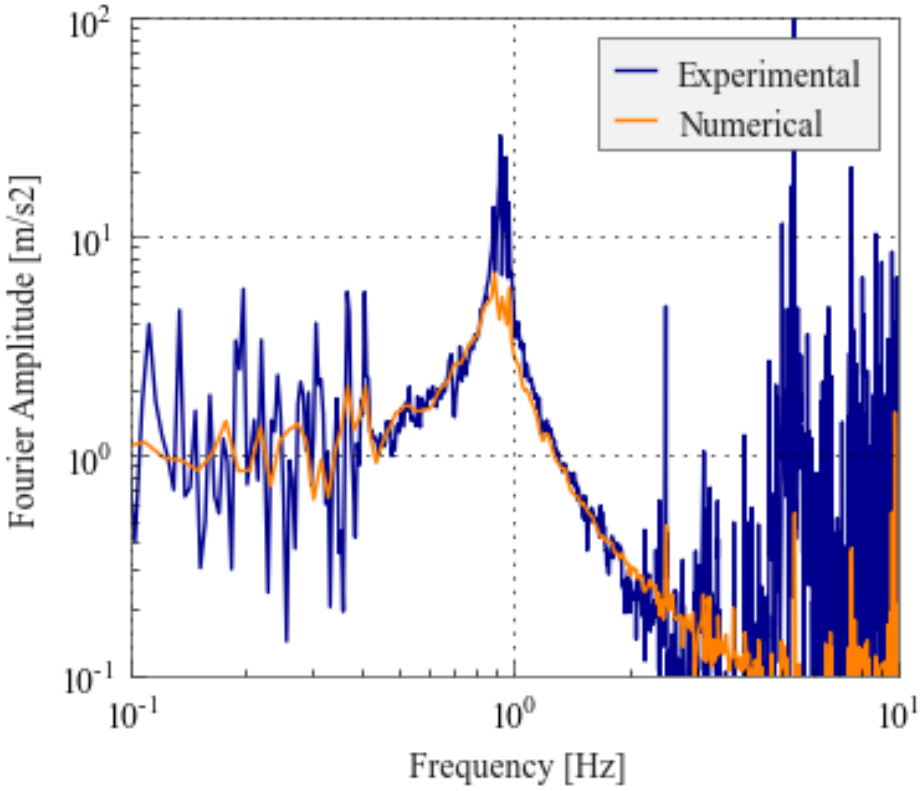

Figure B.6: Roof acceleration Fourier amplitude spectrum - Motion TCU_L

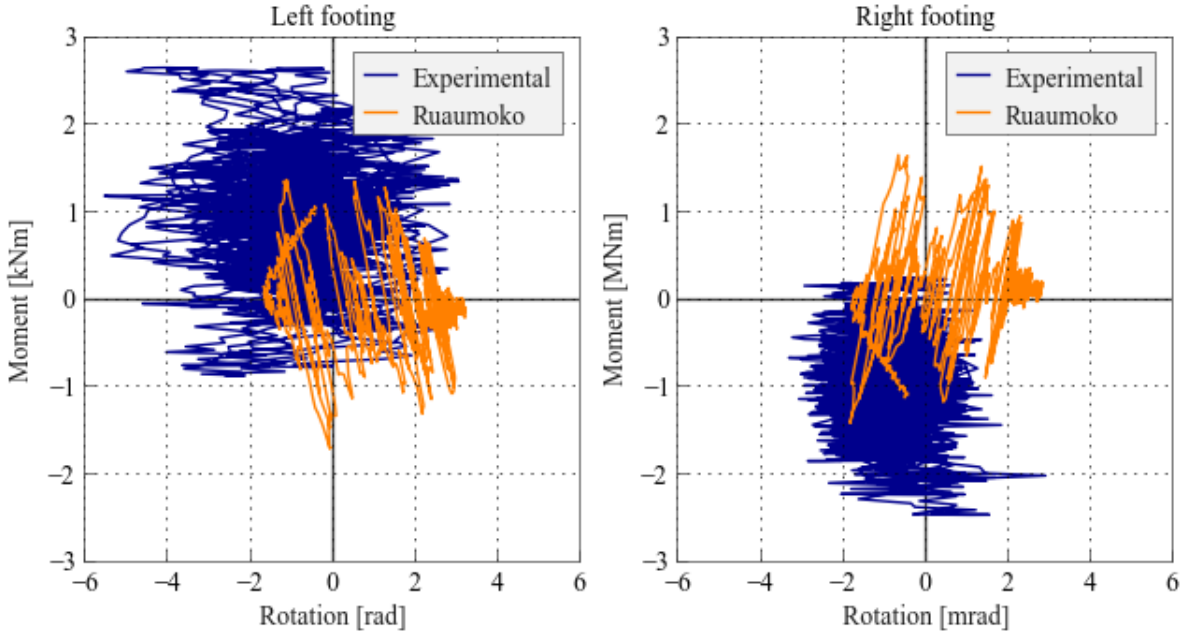

Figure B.7: Moment verse rotation of footing - Motion TCU_L

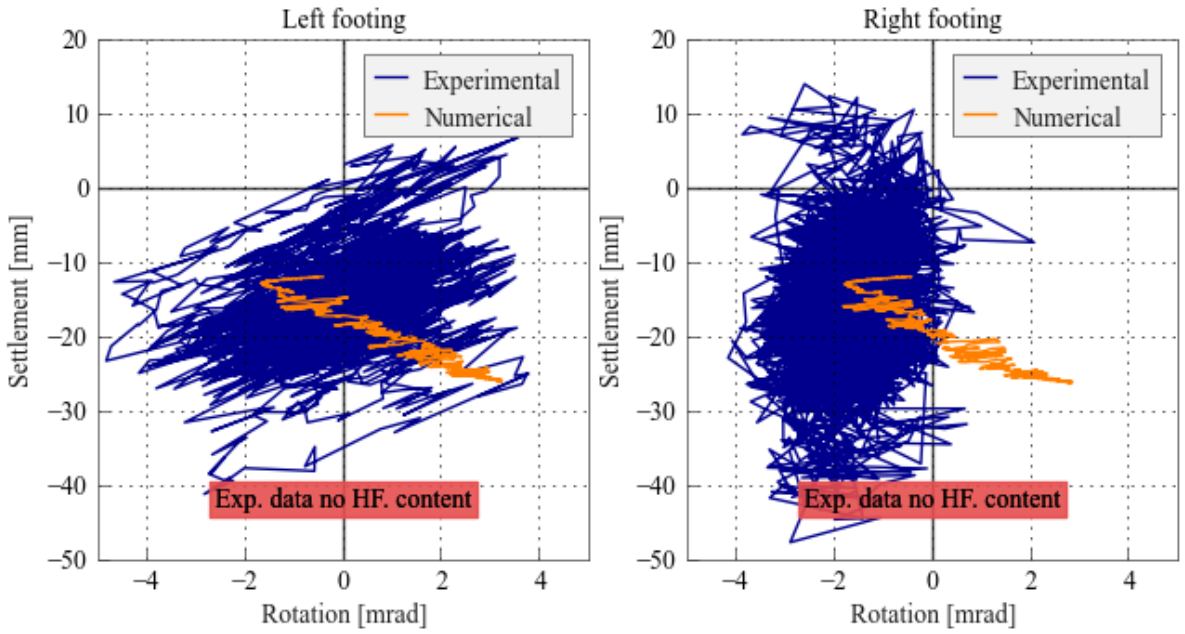

Figure B.8: Settlement verse rotation of footing - Motion TCU_L

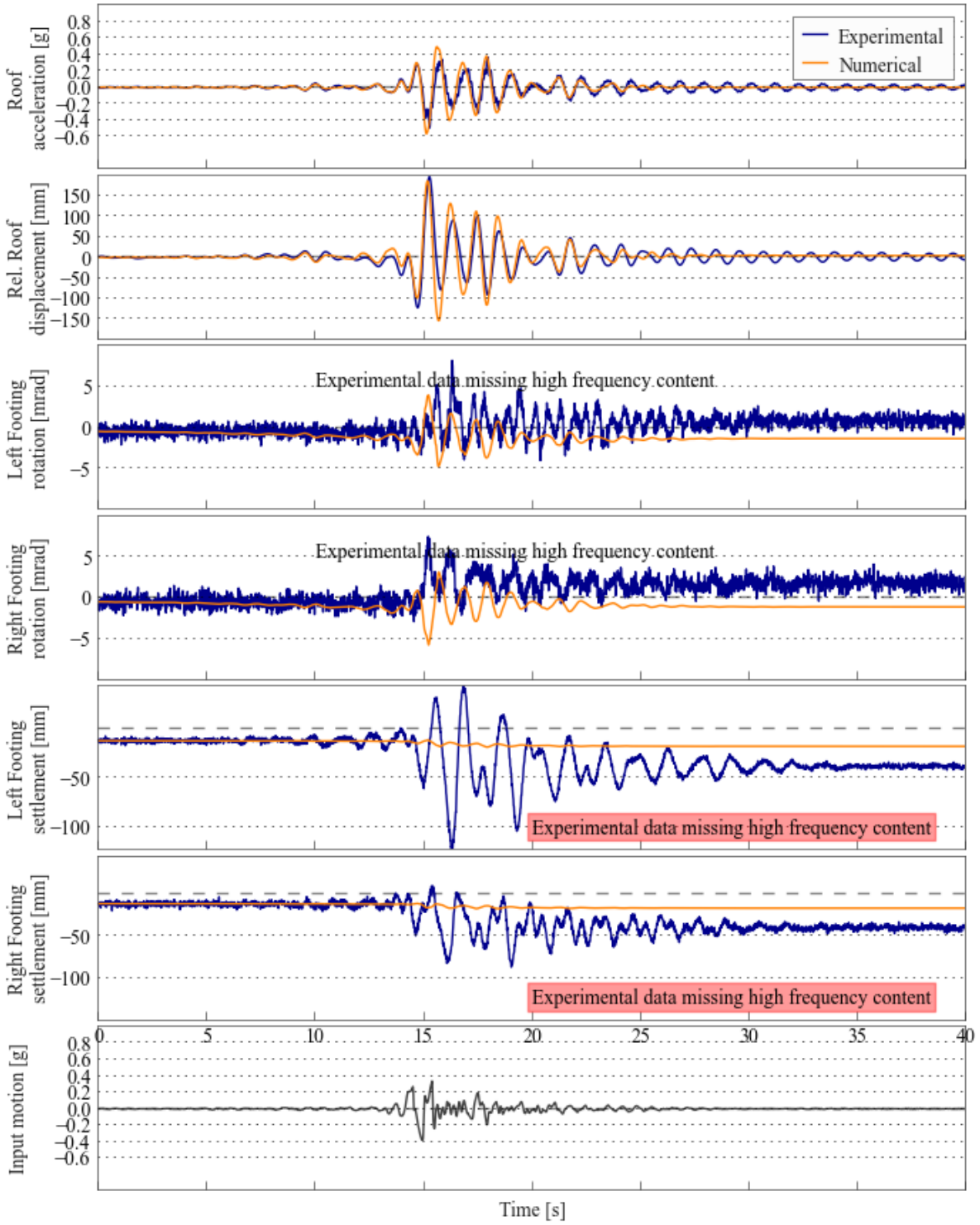

Figure B.9: Comparision of numerical and experimental behaviour - Motion RRS

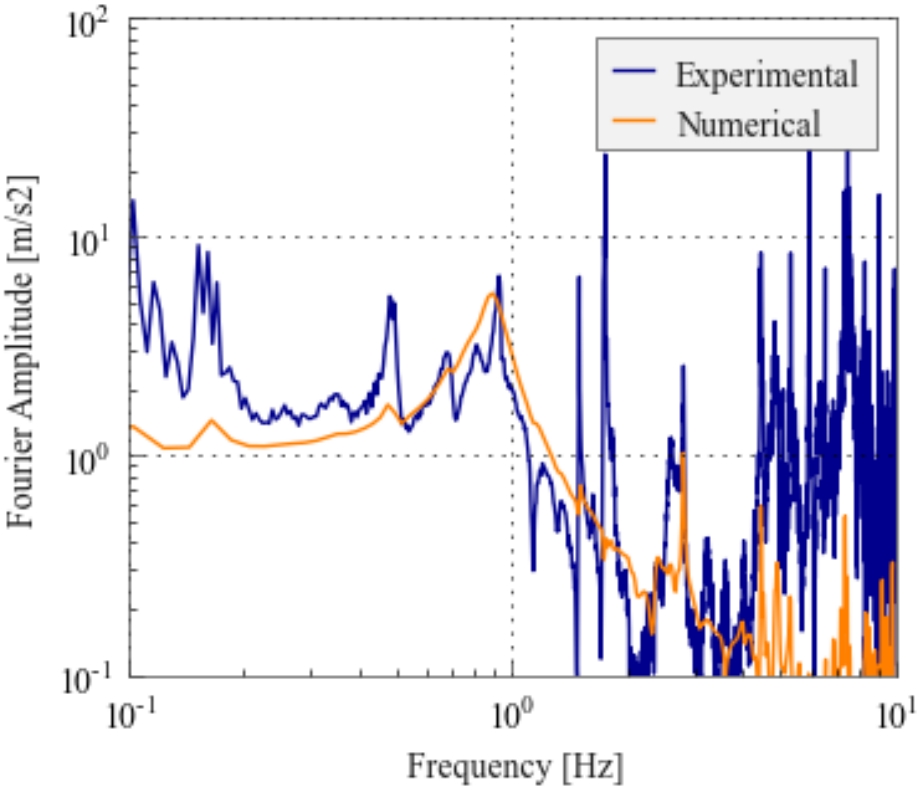

Figure B.10: Roof acceleration Fourier amplitude spectrum - Motion RRS

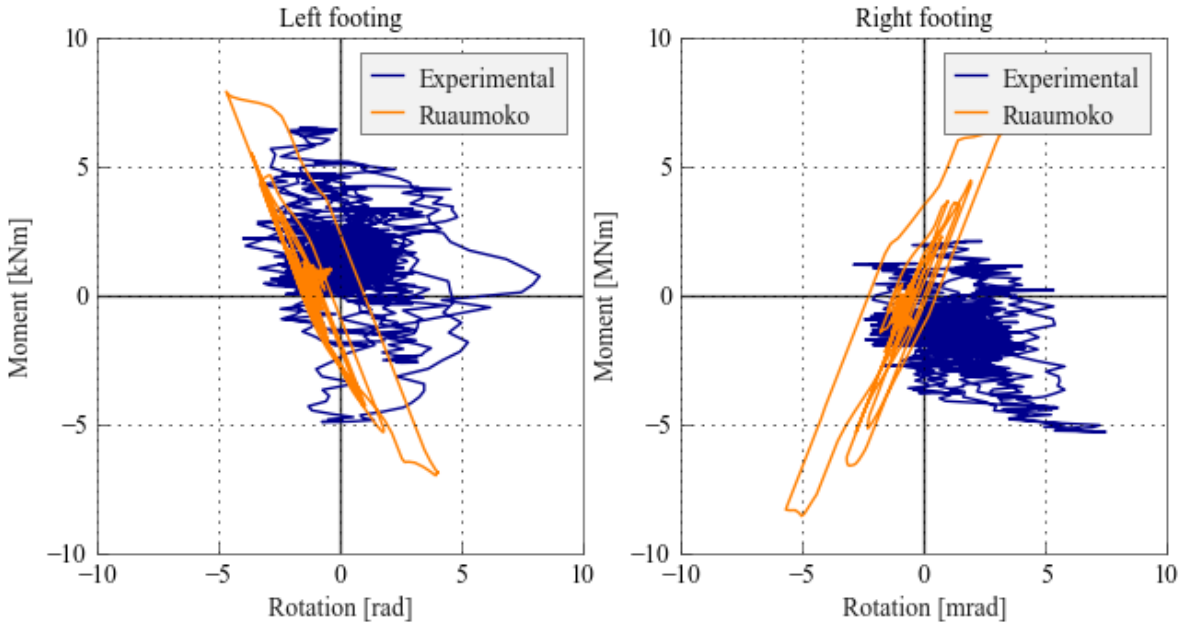

Figure B.11: Moment verse rotation of footing - Motion RRS

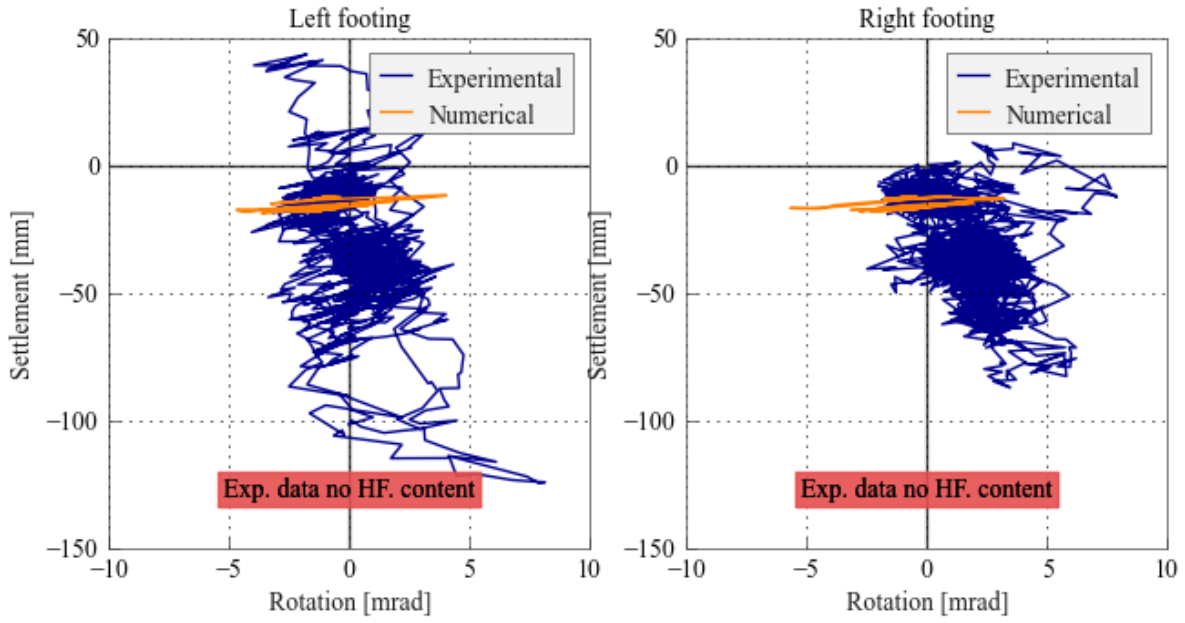

Figure B.12: Settlement verse rotation of footing - Motion RRS

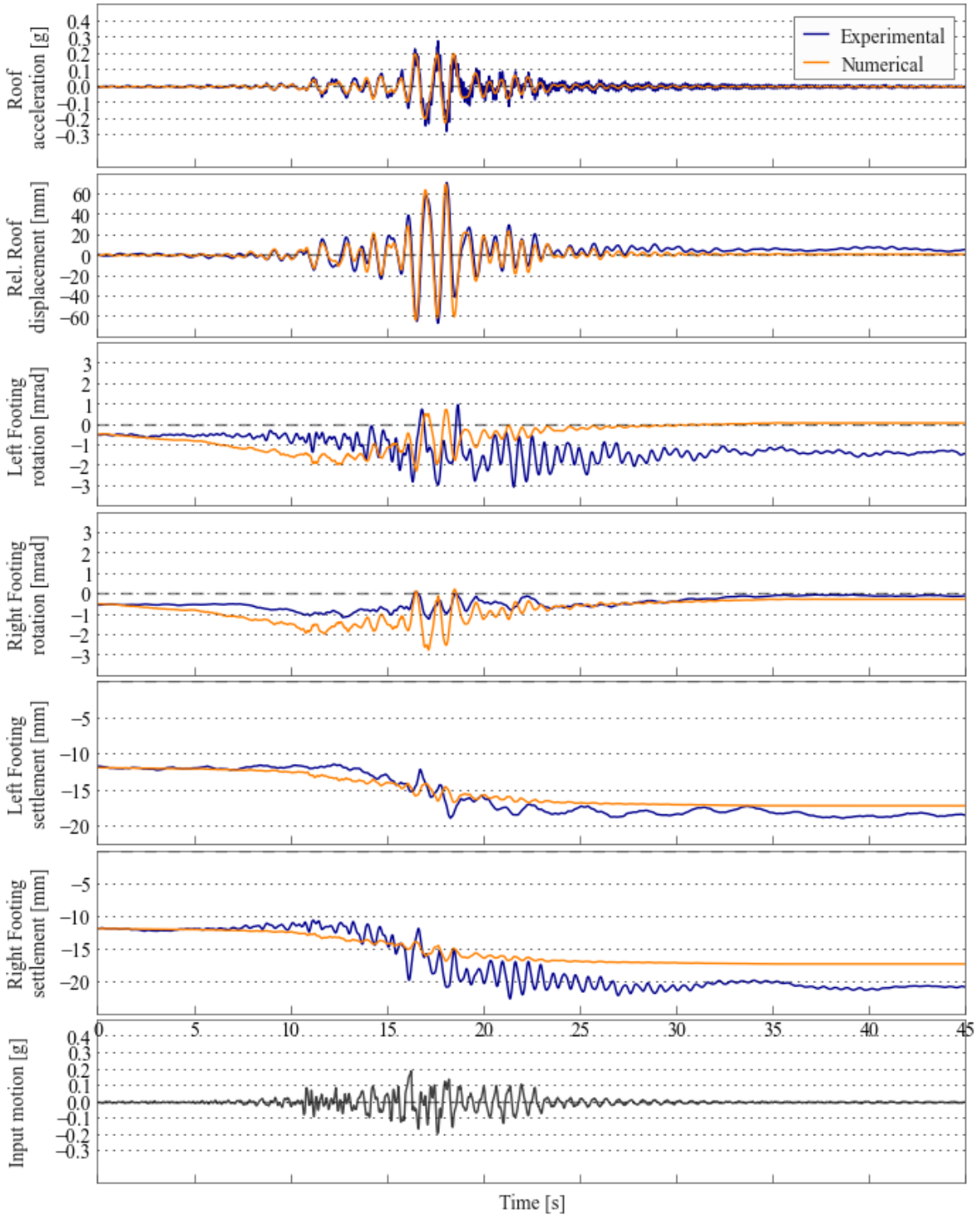

Figure B.13: Comparision of numerical and experimental behaviour - Motion PTS

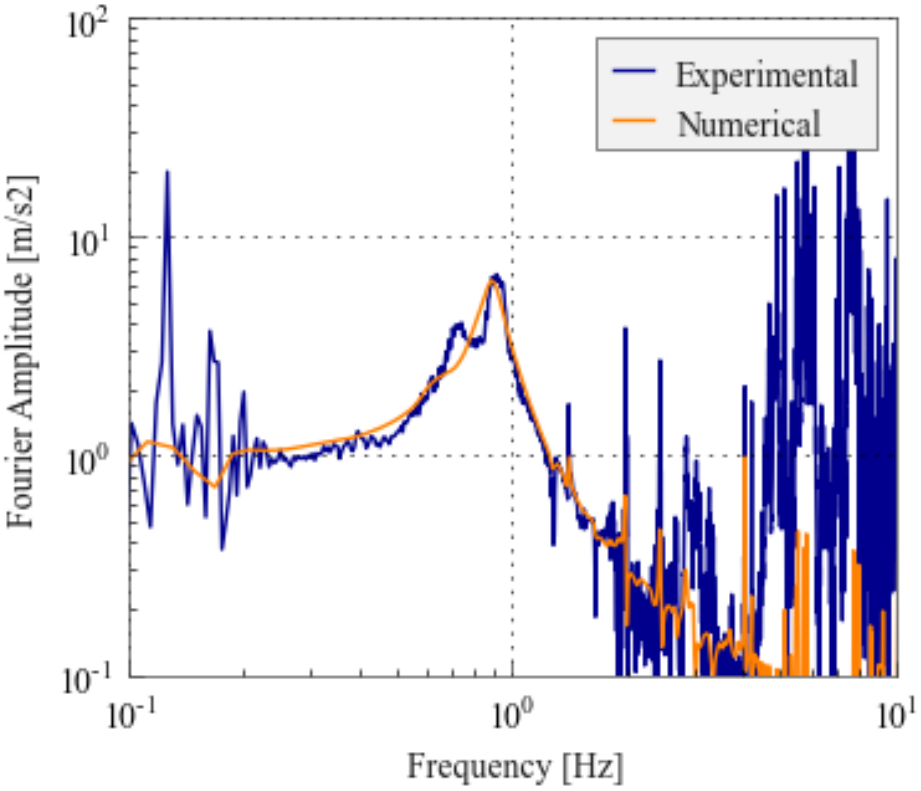

Figure B.14: Roof acceleration Fourier amplitude spectrum - Motion PTS

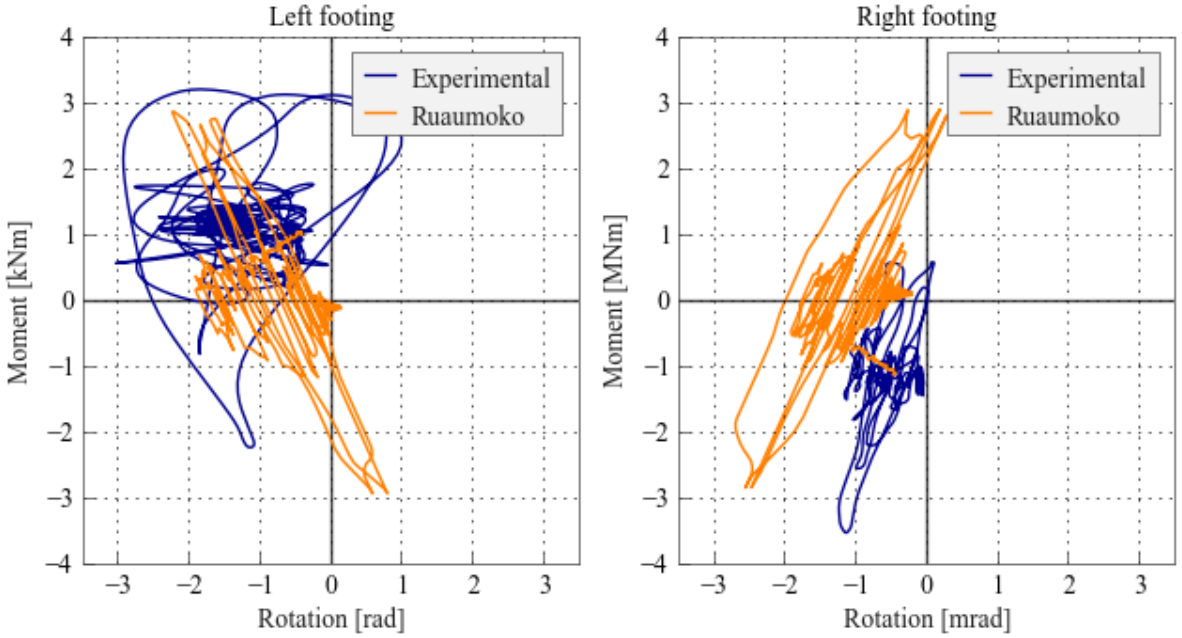

Figure B.15: Moment verse rotation of footing - Motion PTS

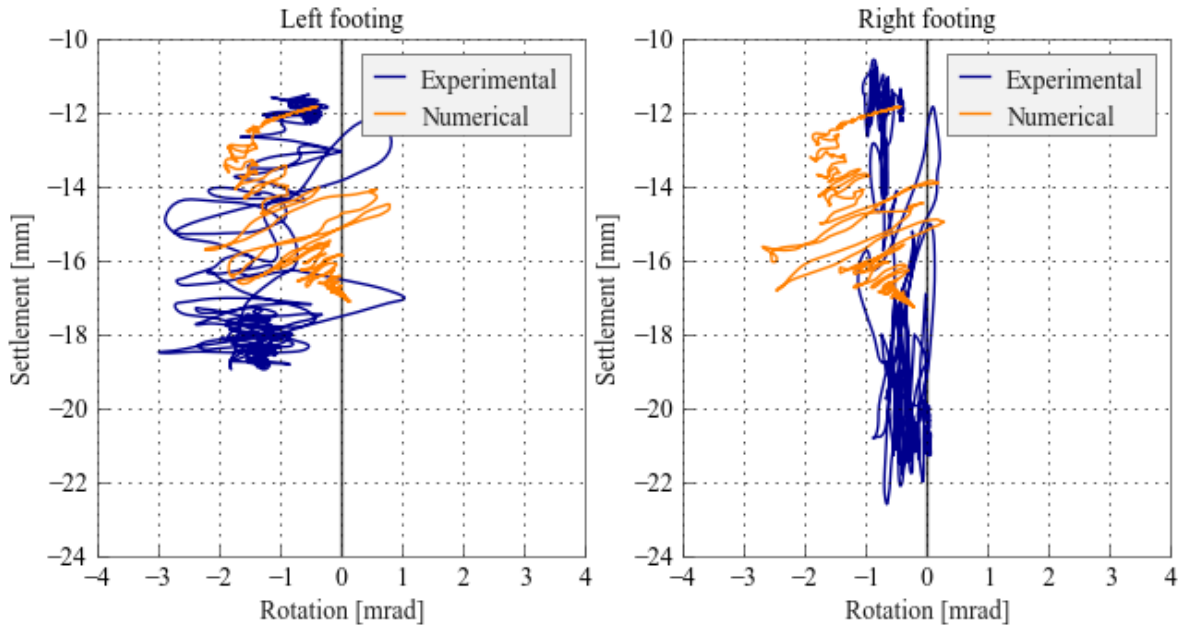

Figure B.16: Settlement verse rotation of footing - Motion PTS

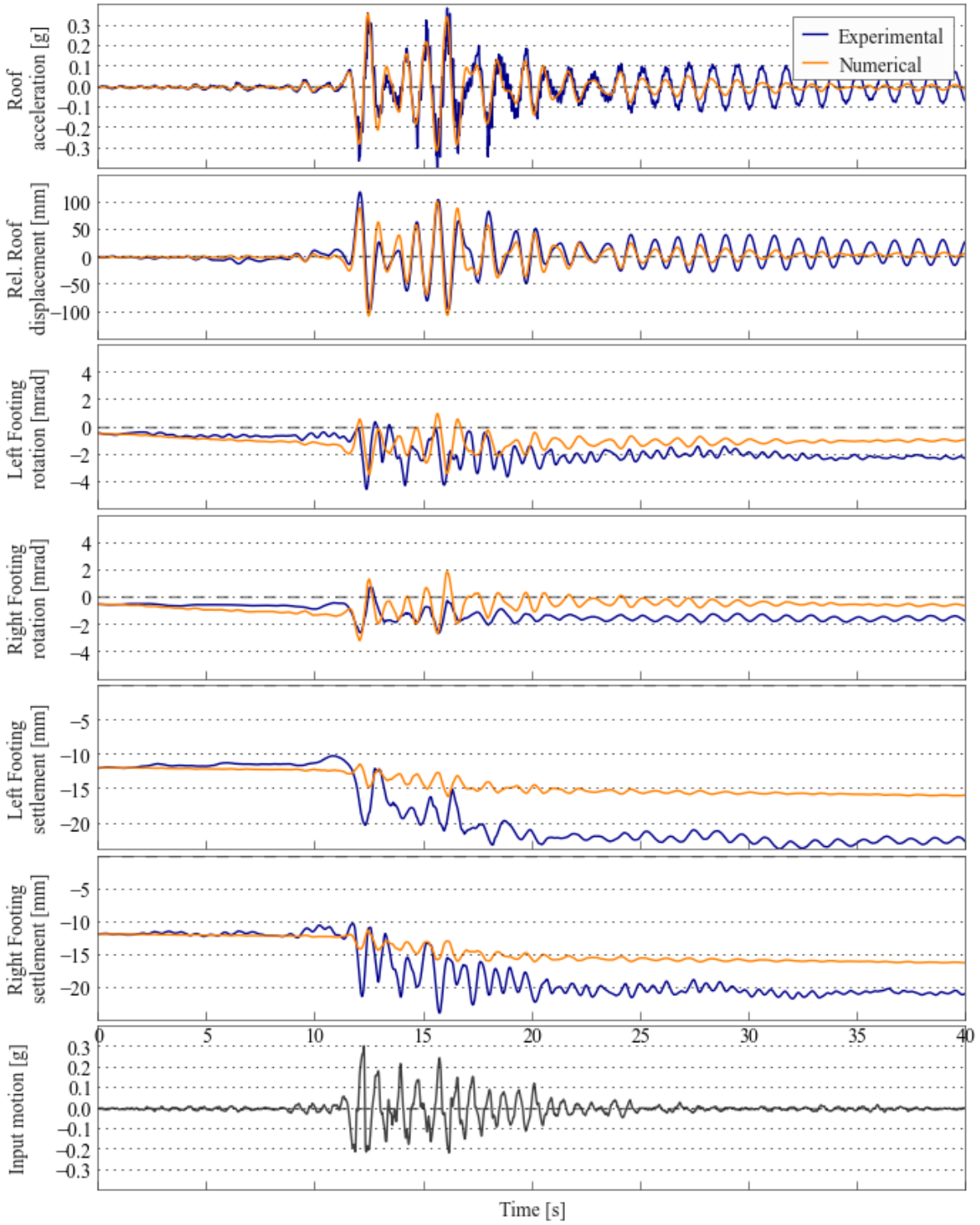

Figure B.17: Comparision of numerical and experimental behaviour - Motion SCS_L_1

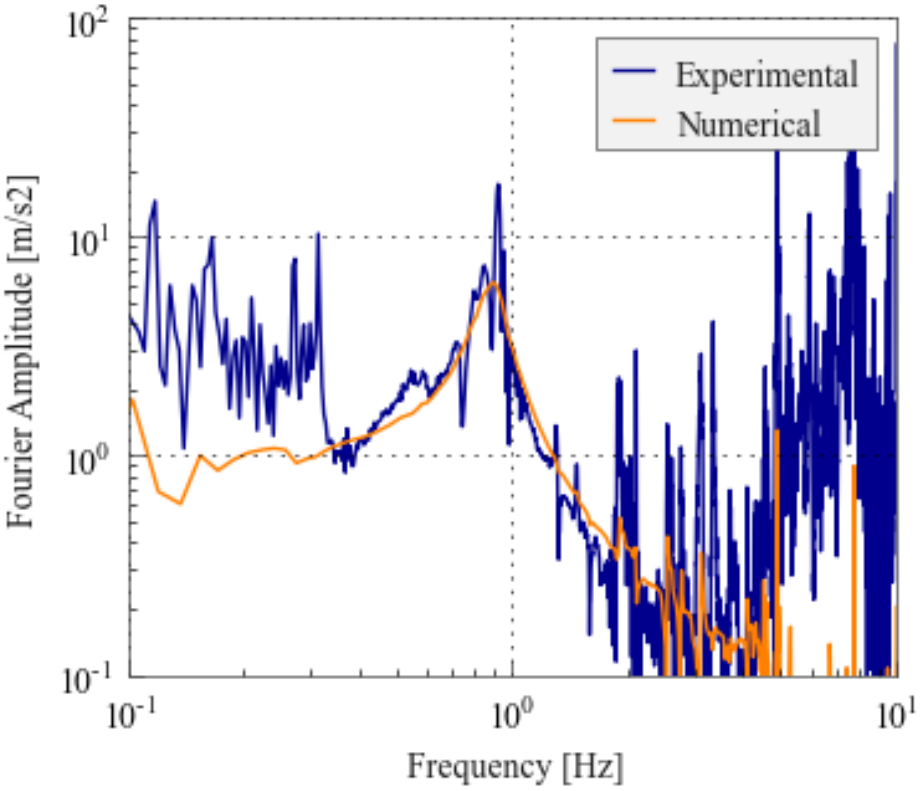

Figure B.18: Roof acceleration Fourier amplitude spectrum - Motion SCS_L_1

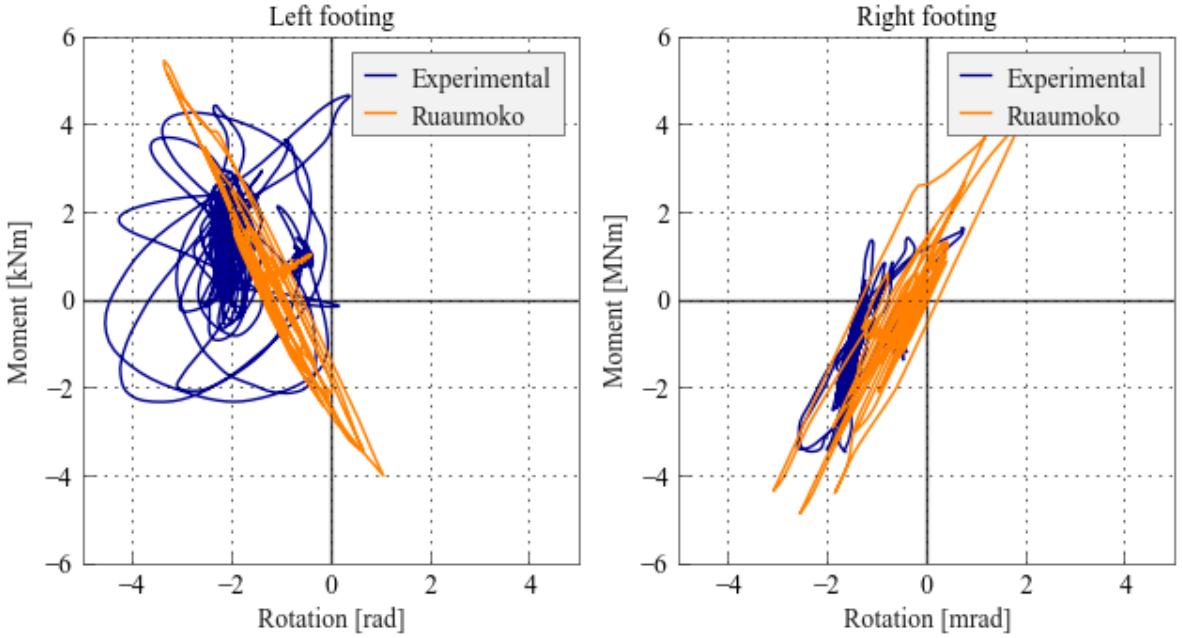

Figure B.19: Moment verse rotation of footing - Motion SCS_L_1

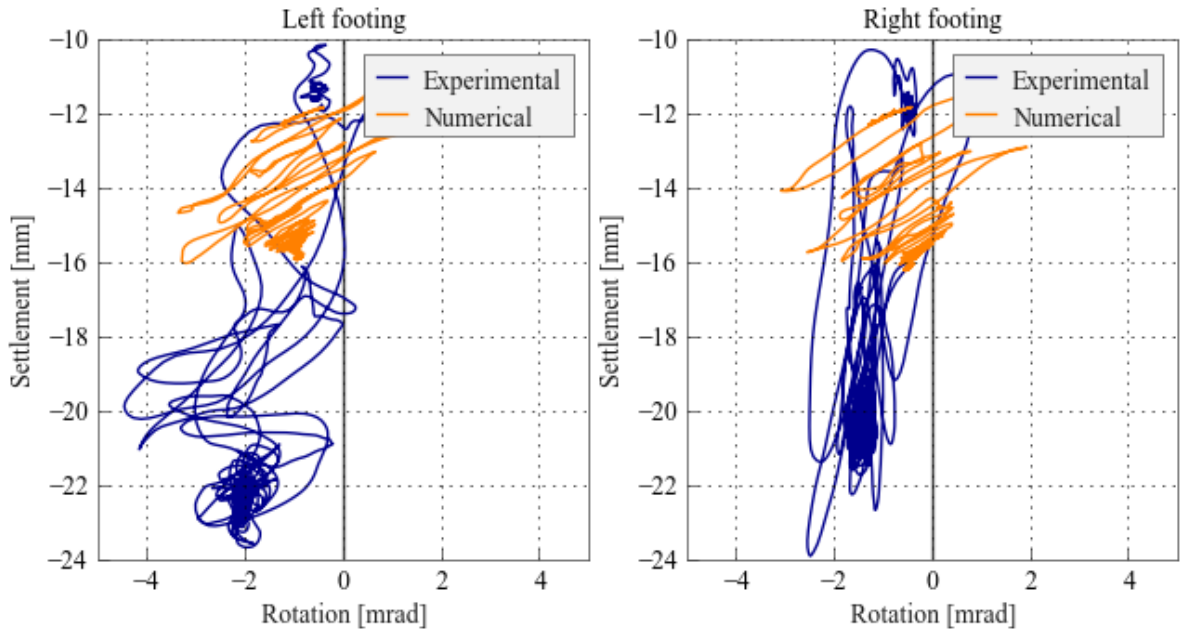

Figure B.20: Settlement verse rotation of footing - Motion SCS_L_1

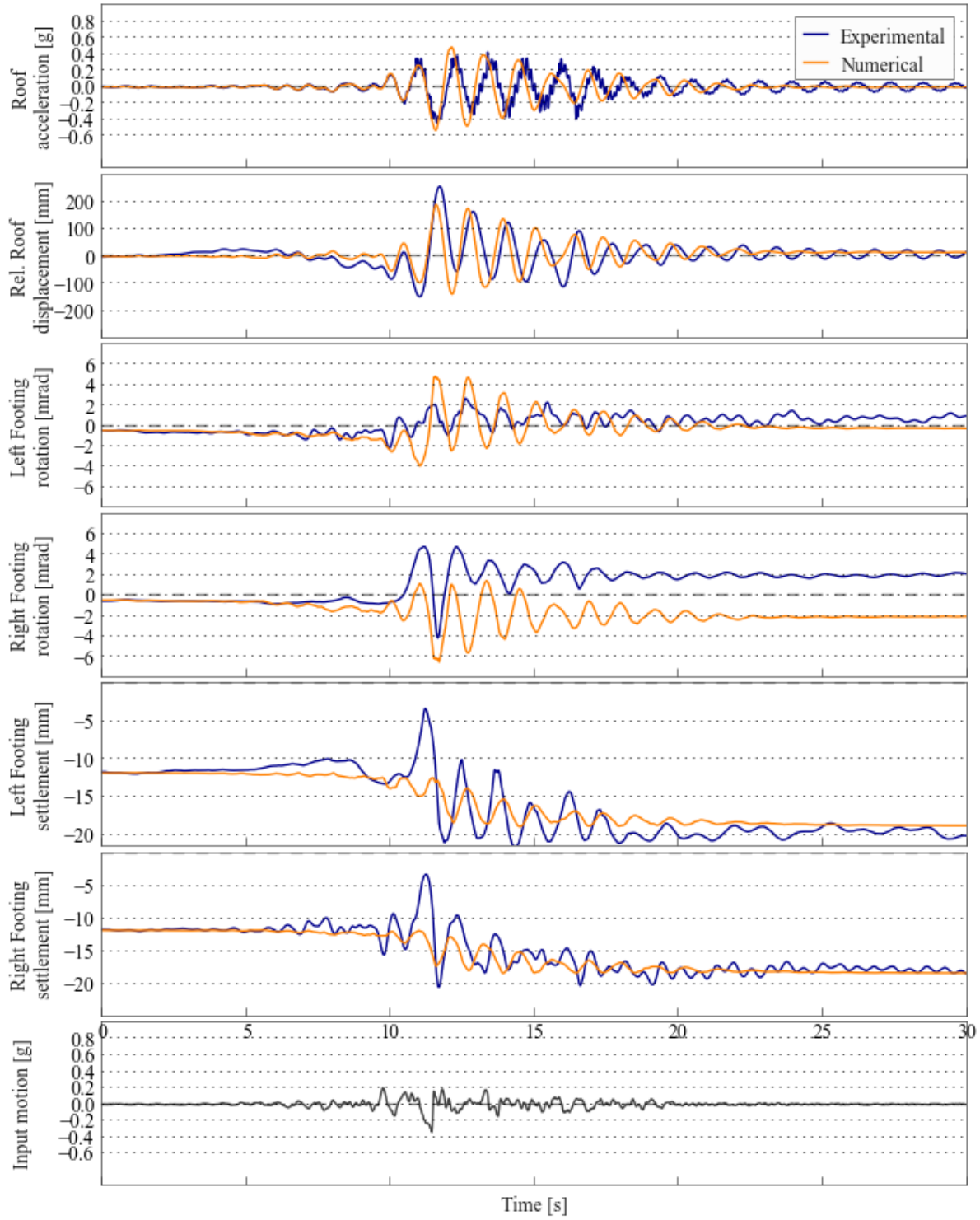

Figure B.21: Comparision of numerical and experimental behaviour - Motion LCN

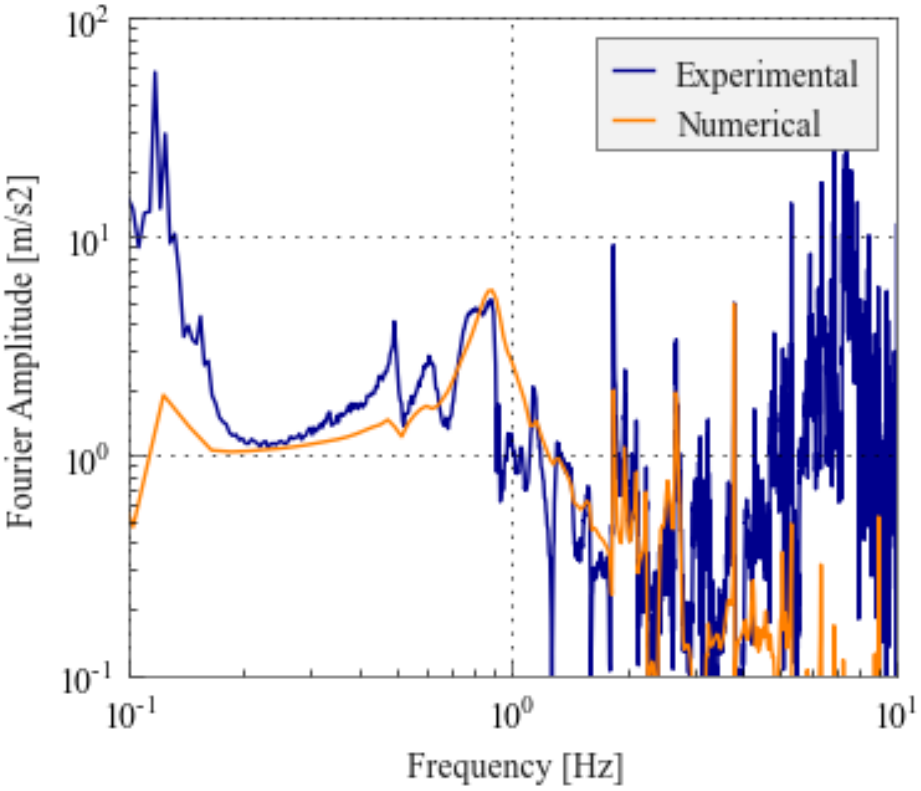

Figure B.22: Roof acceleration Fourier amplitude spectrum - Motion LCN

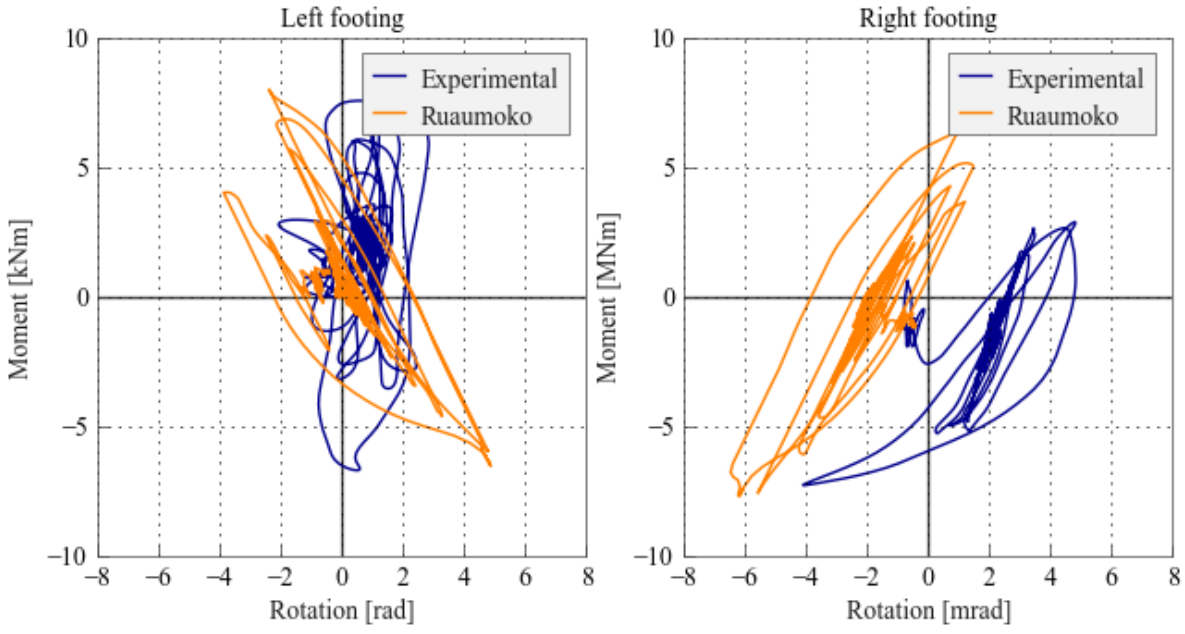

Figure B.23: Moment verse rotation of footing - Motion LCN

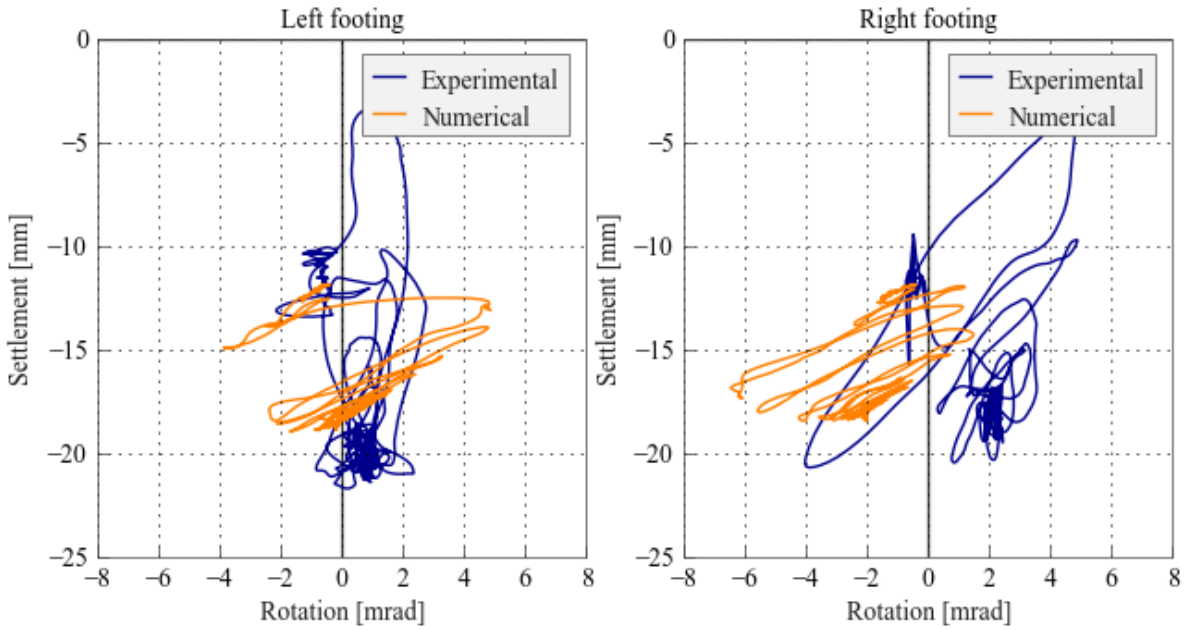

Figure B.24: Settlement verse rotation of footing - Motion LCN

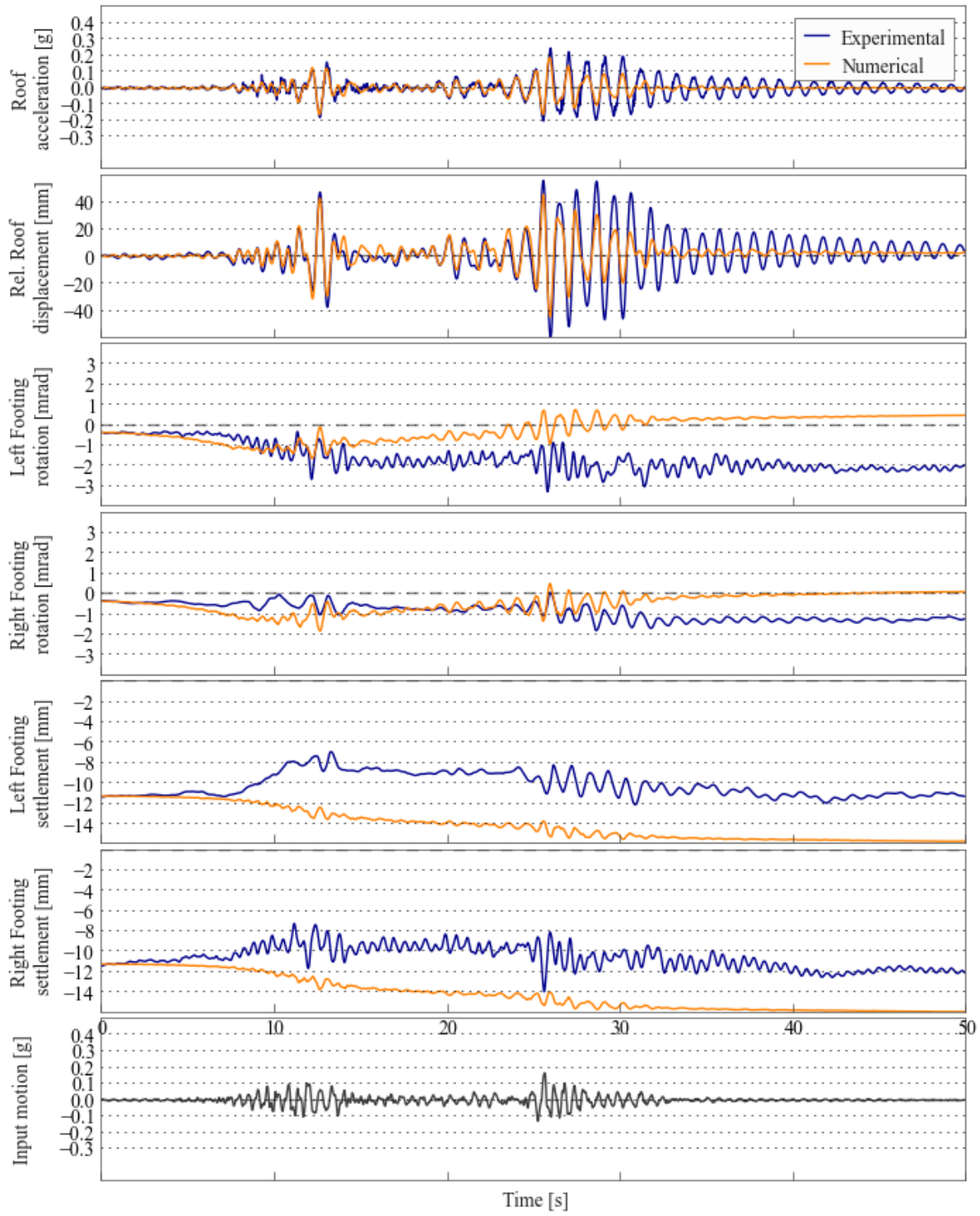

Figure B.25: Comparision of numerical and experimental behaviour - Motion JOS_L_2

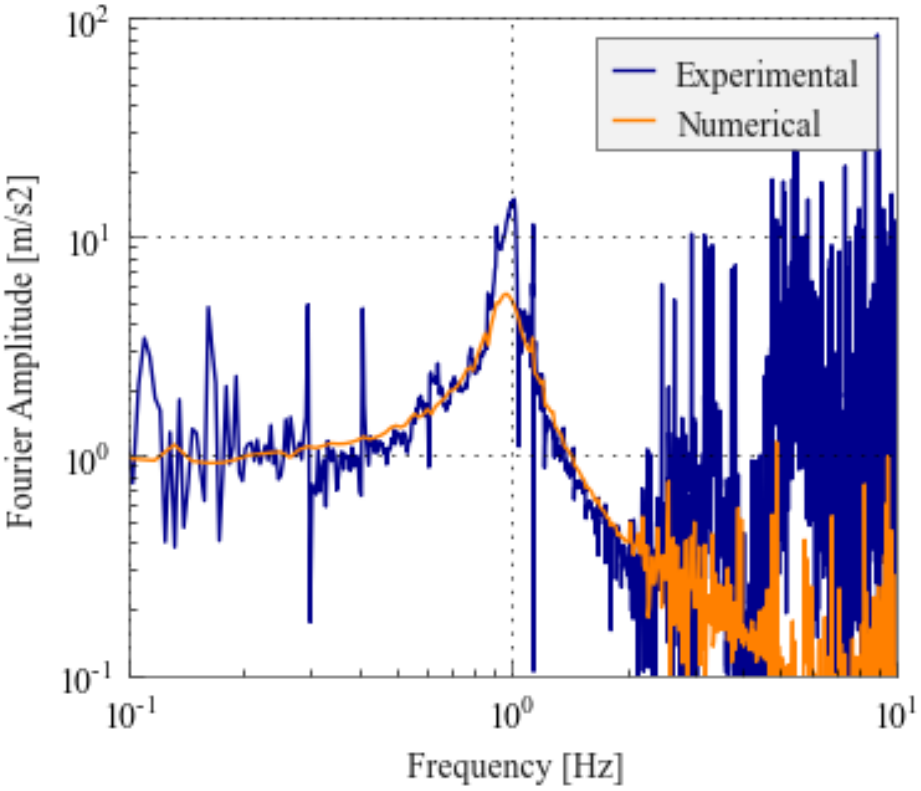

Figure B.26: Roof acceleration Fourier amplitude spectrum - Motion JOS_L_2

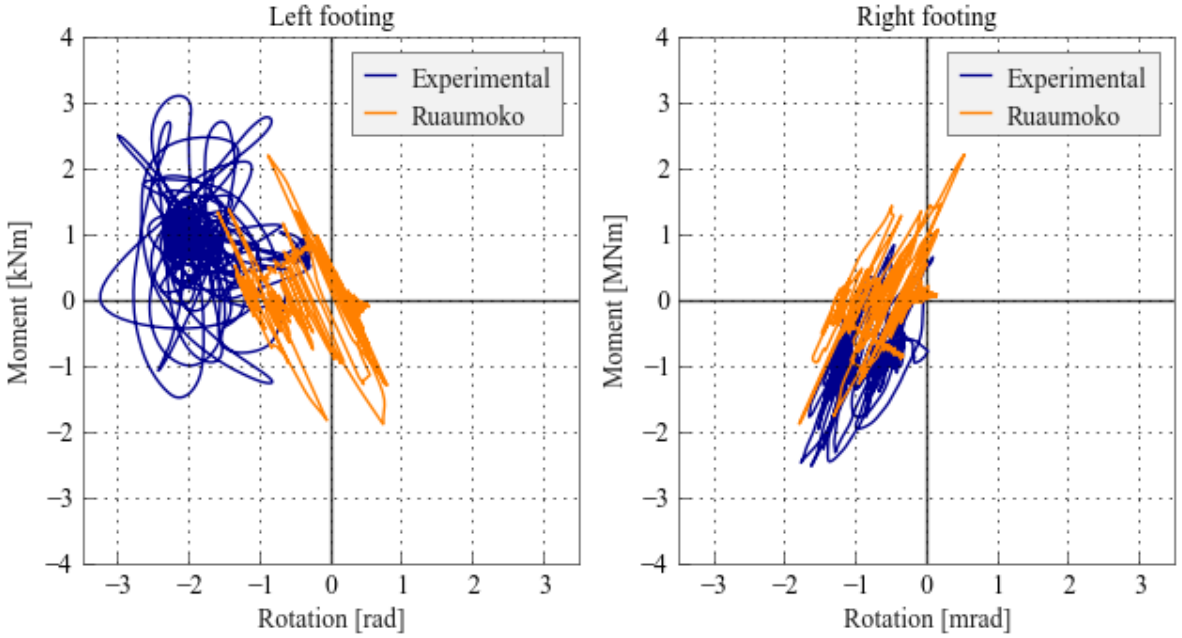

Figure B.27: Moment verse rotation of footing - Motion JOS_L_2

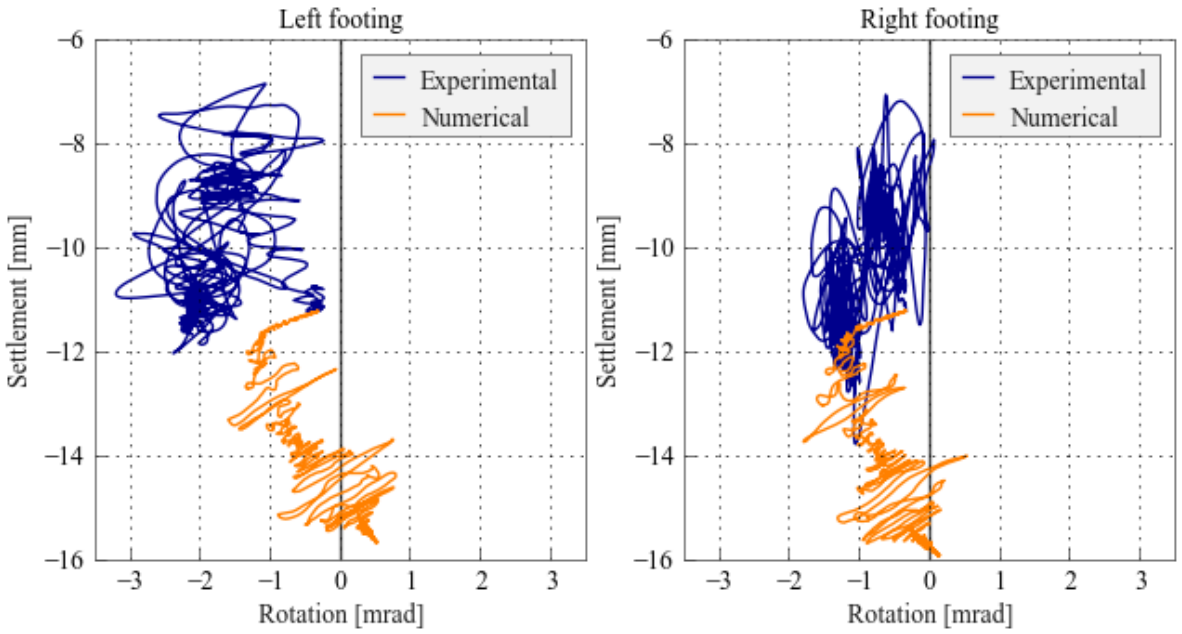

Figure B.28: Settlement verse rotation of footing - Motion JOS_L_2

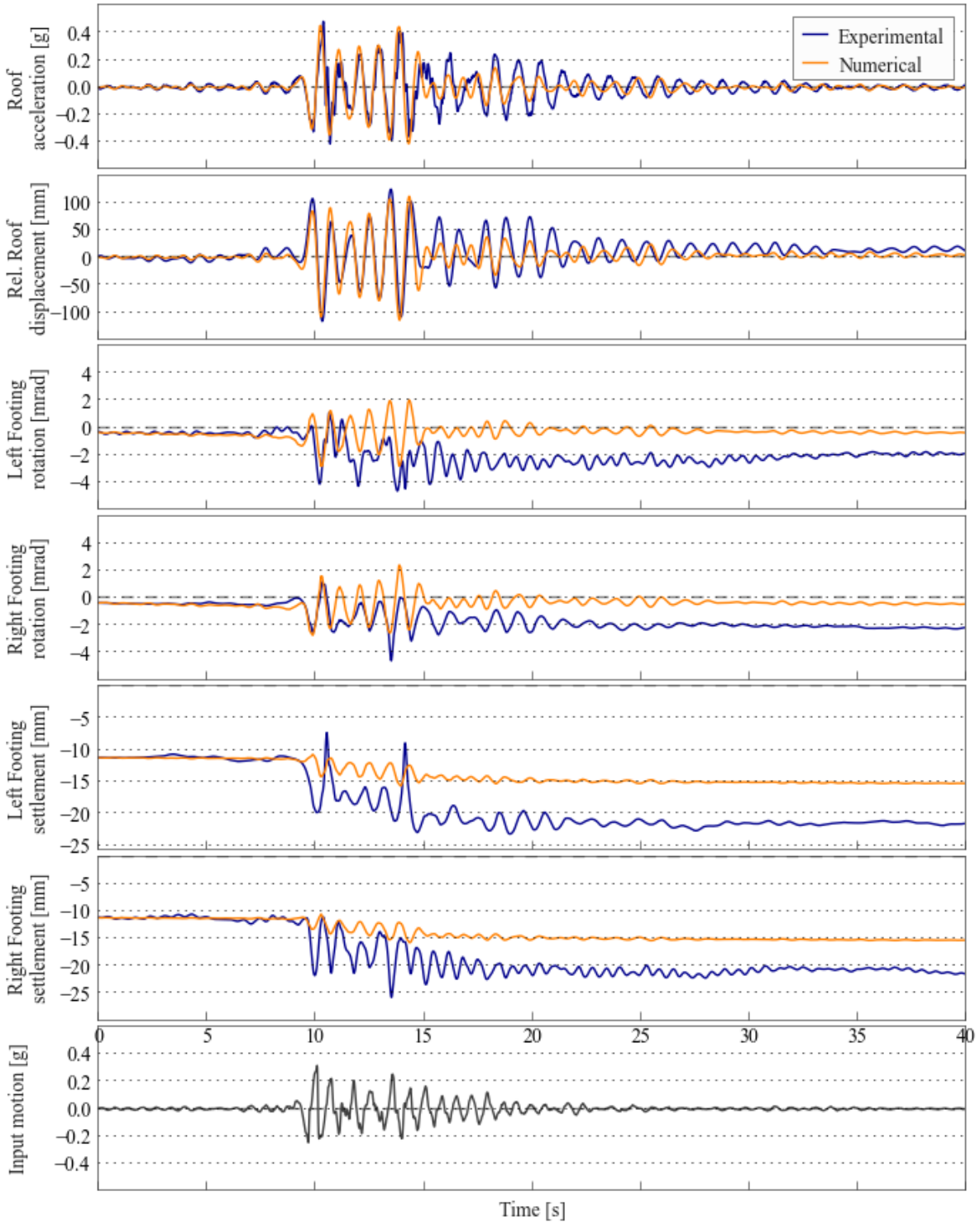

Figure B.29: Comparision of numerical and experimental behaviour - Motion SCS_L_2

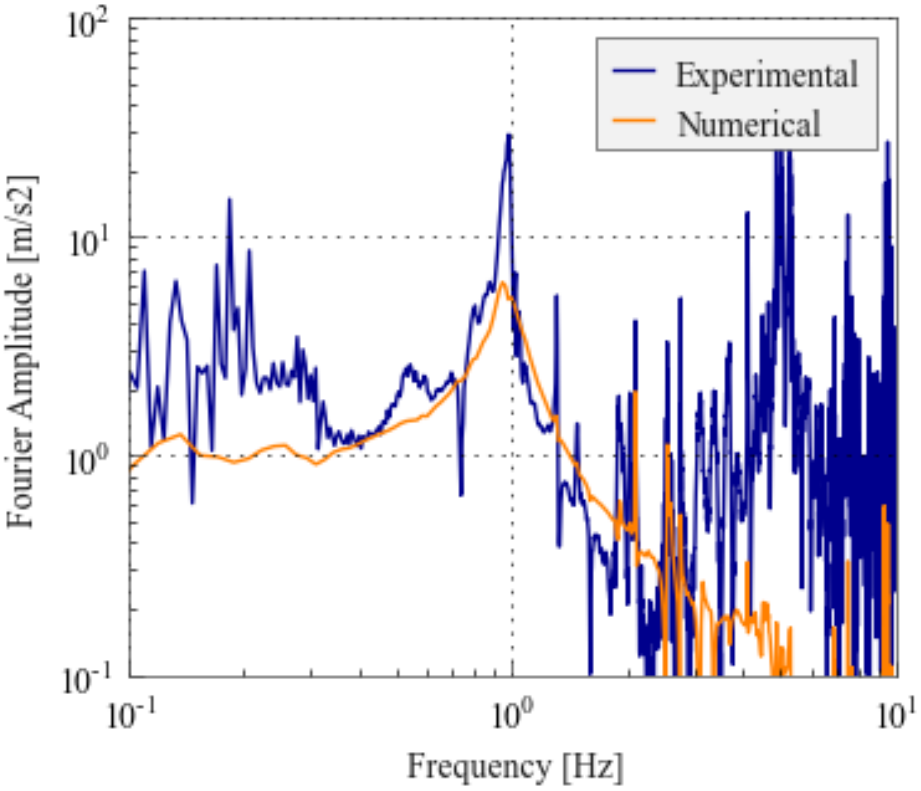

Figure B.30: Roof acceleration Fourier amplitude spectrum - Motion SCS_L_2

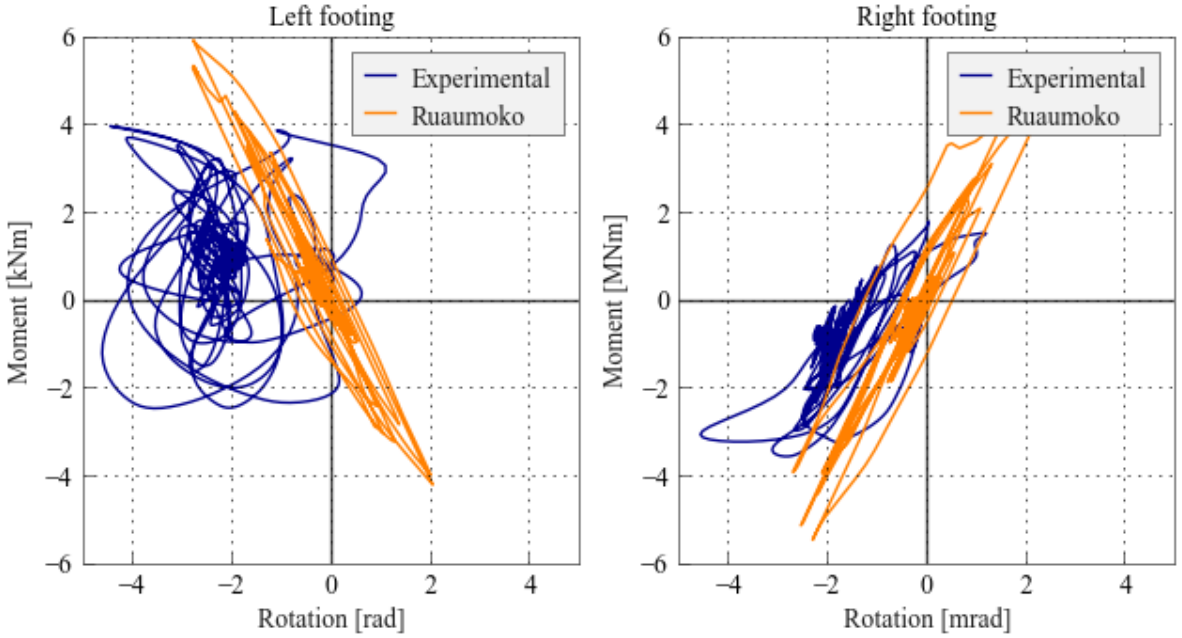

Figure B.31: Moment verse rotation of footing - Motion SCS_L_2

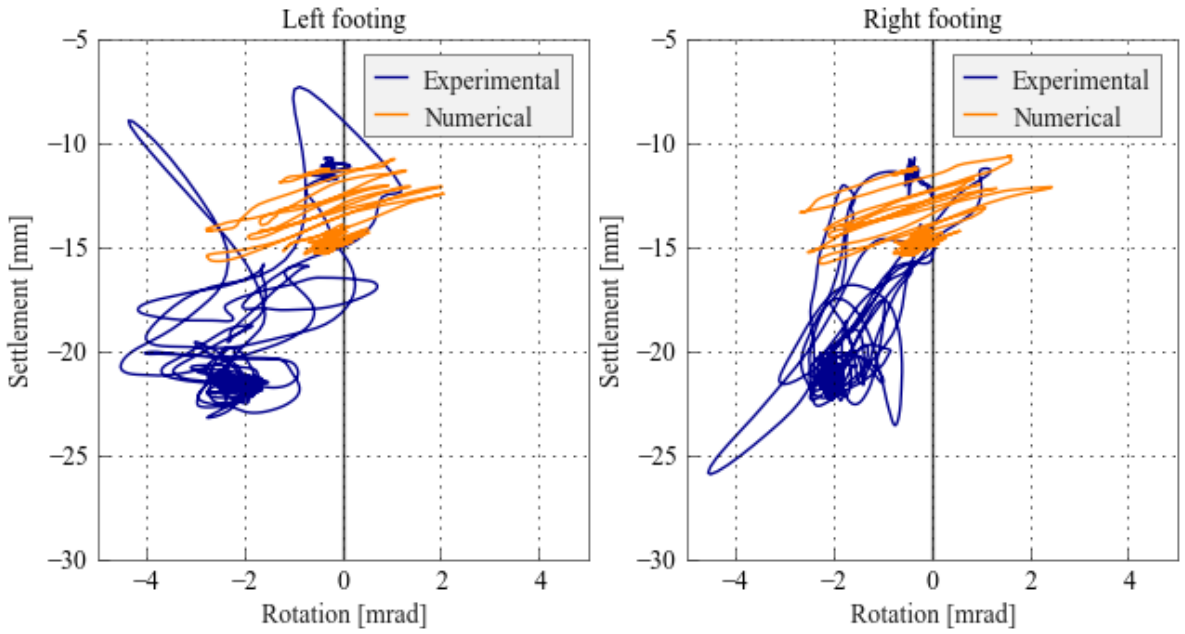

Figure B.32: Settlement verse rotation of footing - Motion SCS_L_2

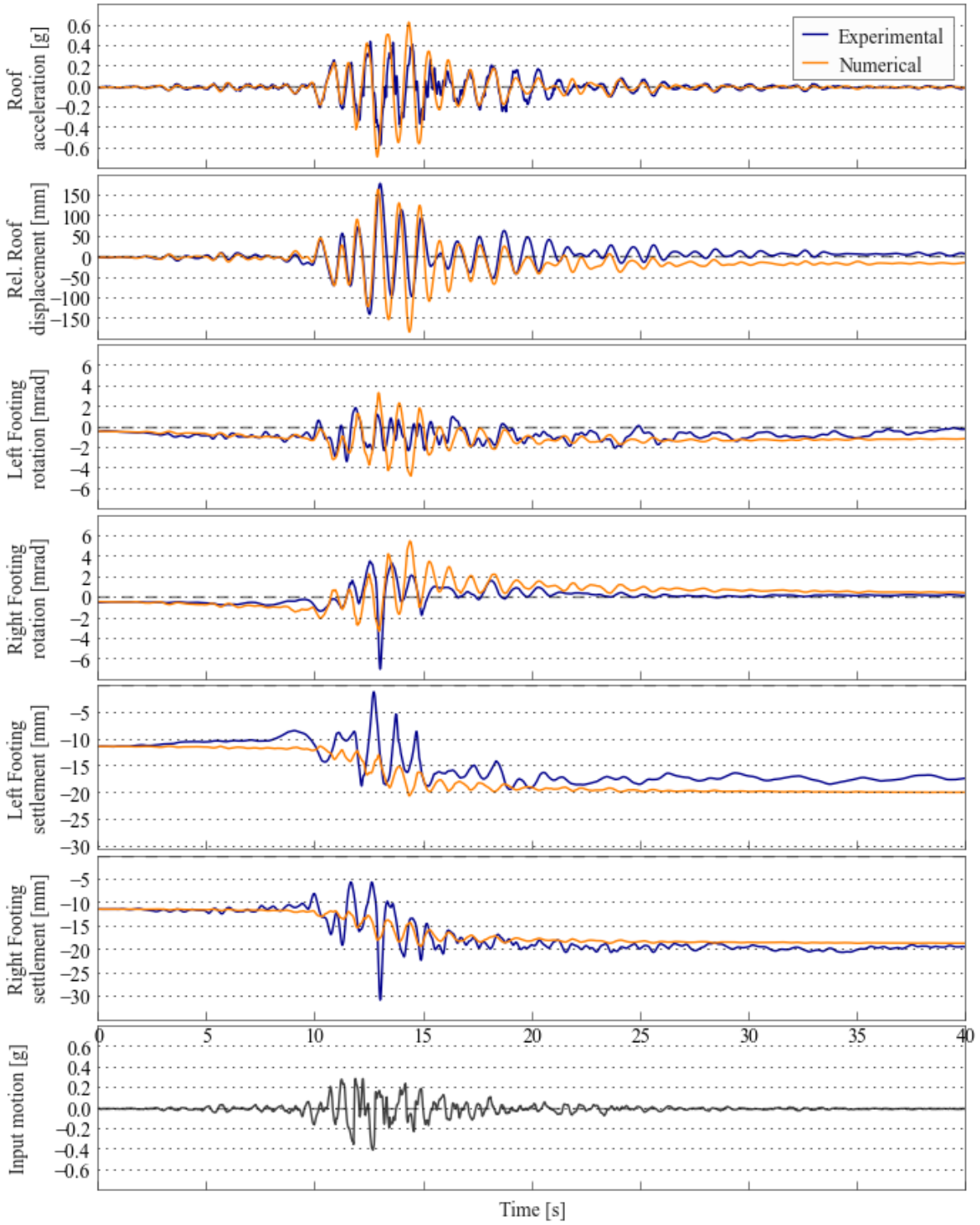

Figure B.33: Comparision of numerical and experimental behaviour - Motion WVC_L

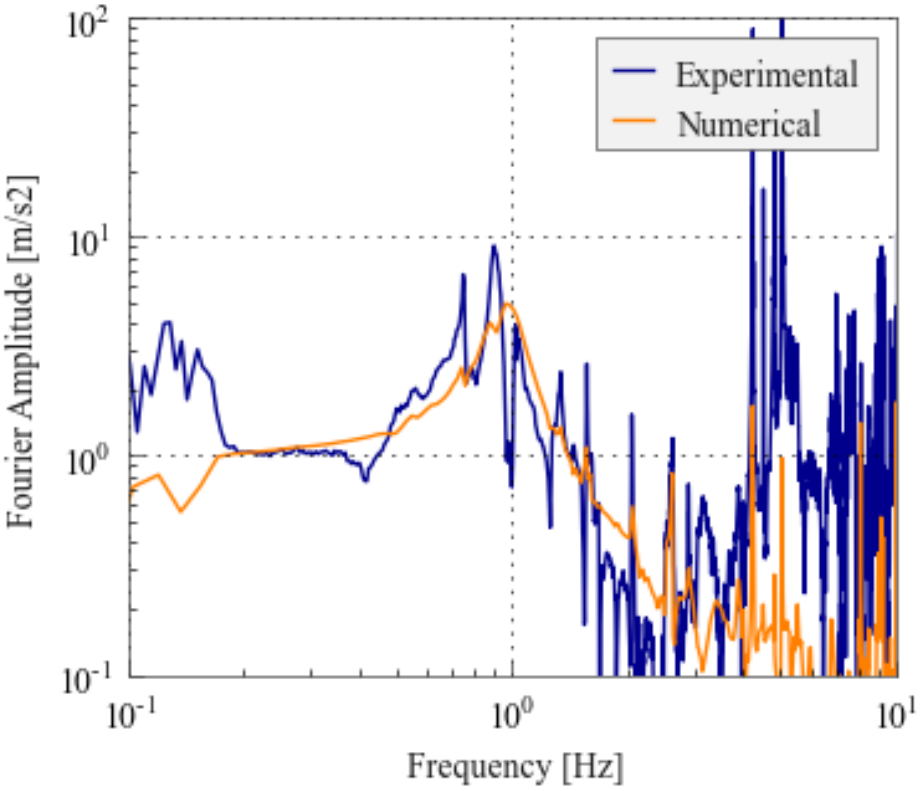

Figure B.34: Roof acceleration Fourier amplitude spectrum - Motion WVC_L

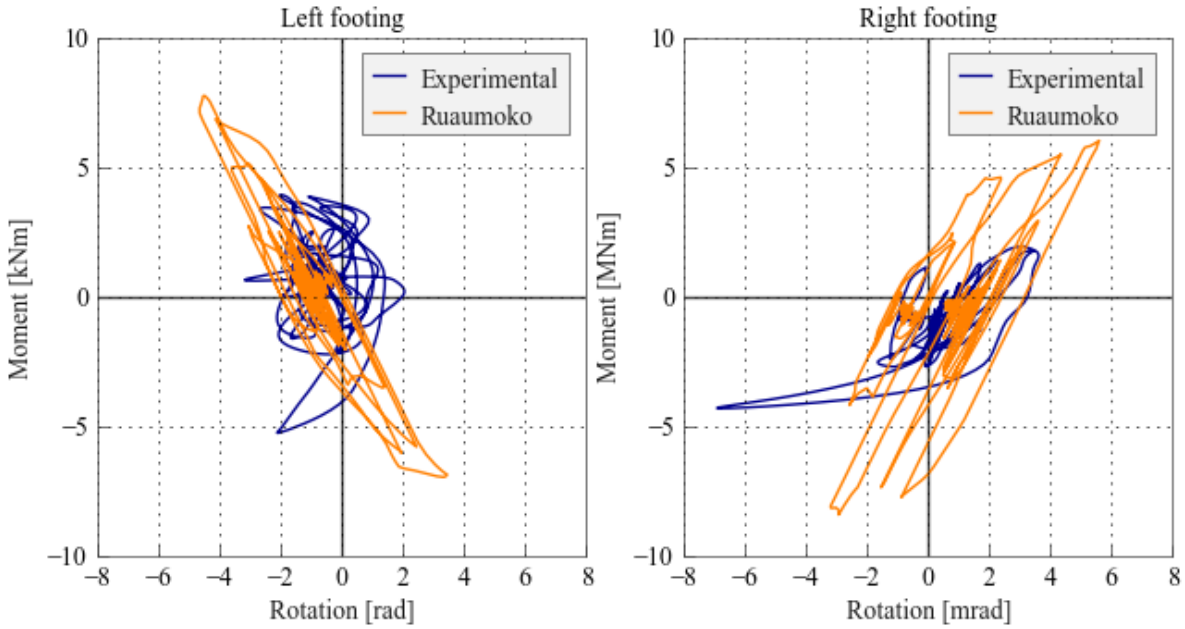

Figure B.35: Moment verse rotation of footing - Motion WVC_L

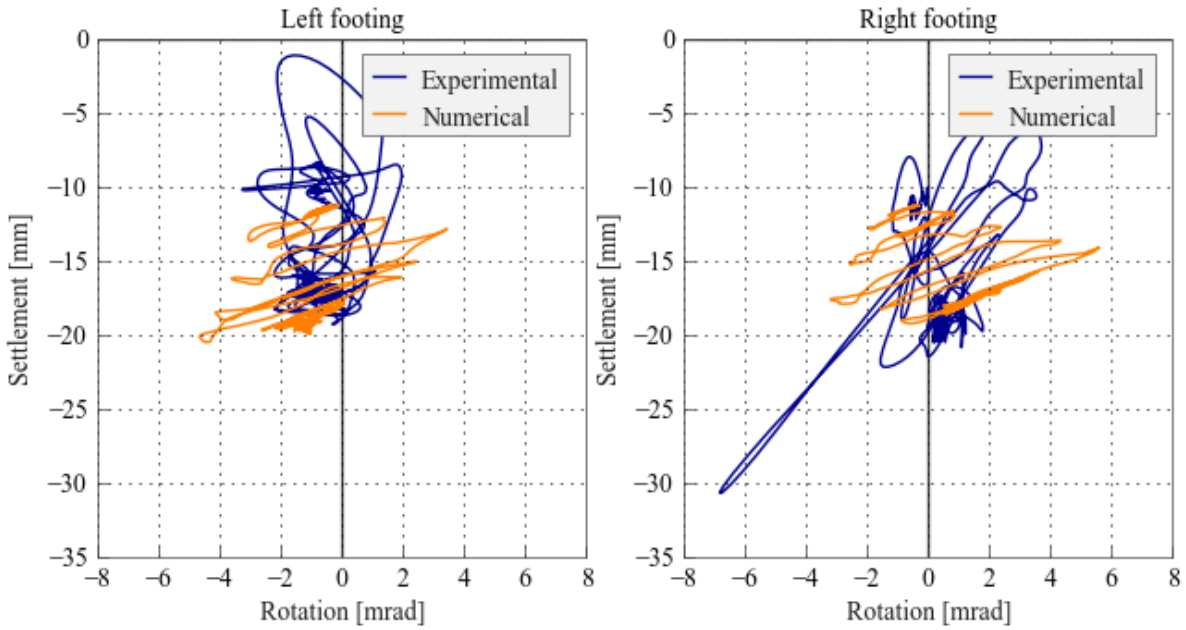

Figure B.36: Settlement verse rotation of footing - Motion WVC_L

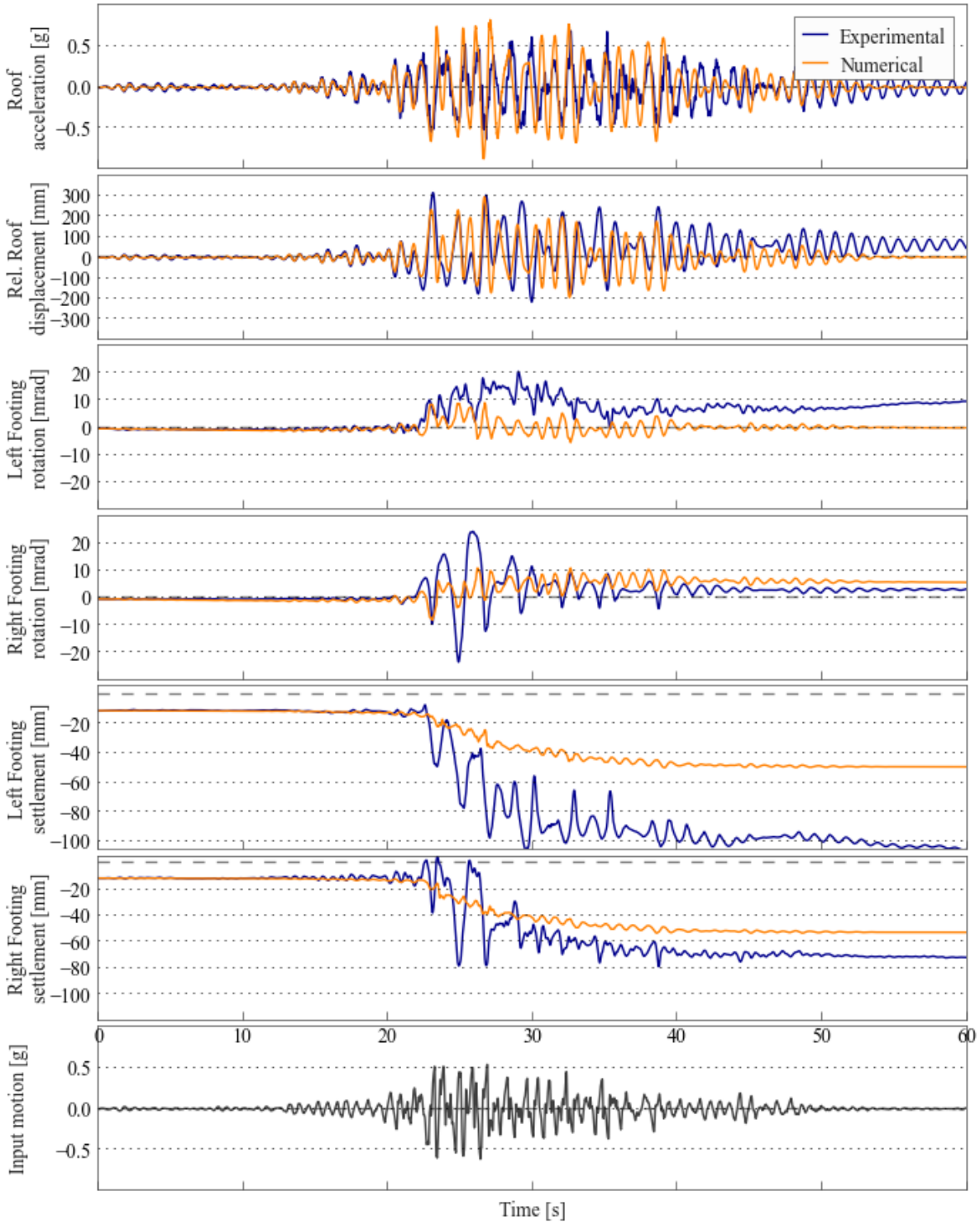

Figure B.37: Comparision of numerical and experimental behaviour - Motion SCS_H

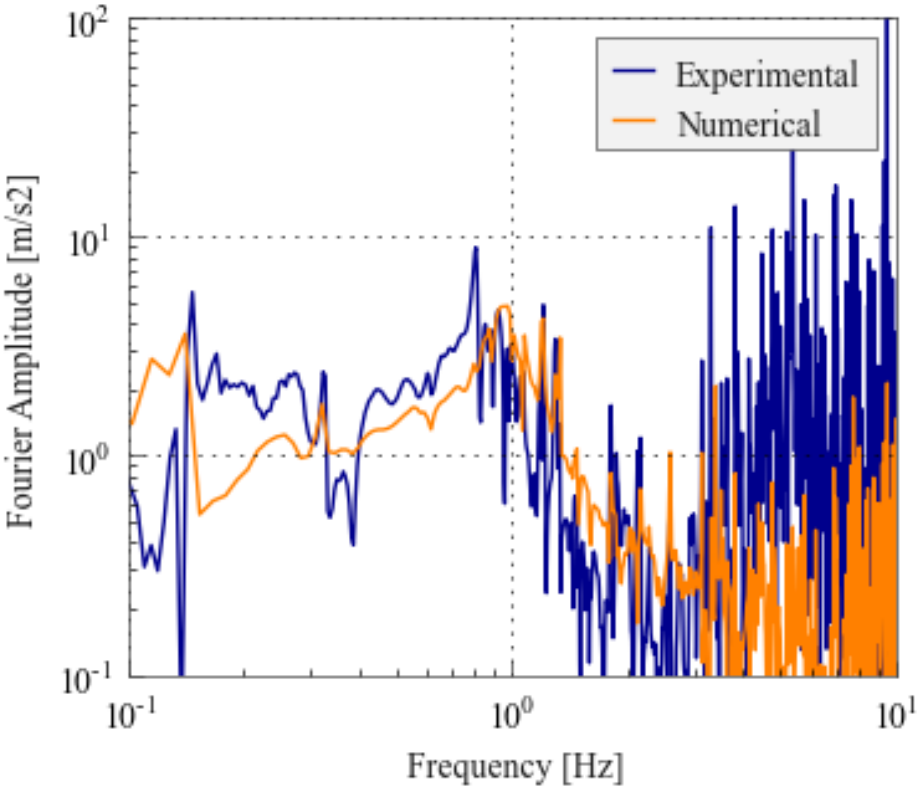

Figure B.38: Roof acceleration Fourier amplitude spectrum - Motion SCS_H

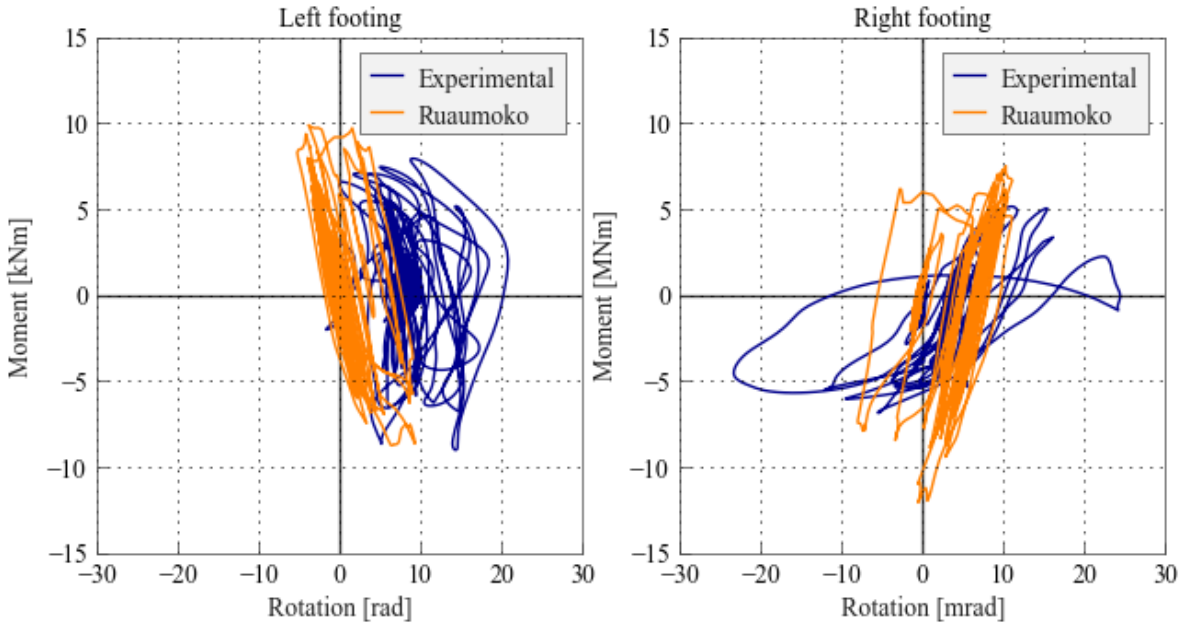

Figure B.39: Moment verse rotation of footing - Motion SCS_H

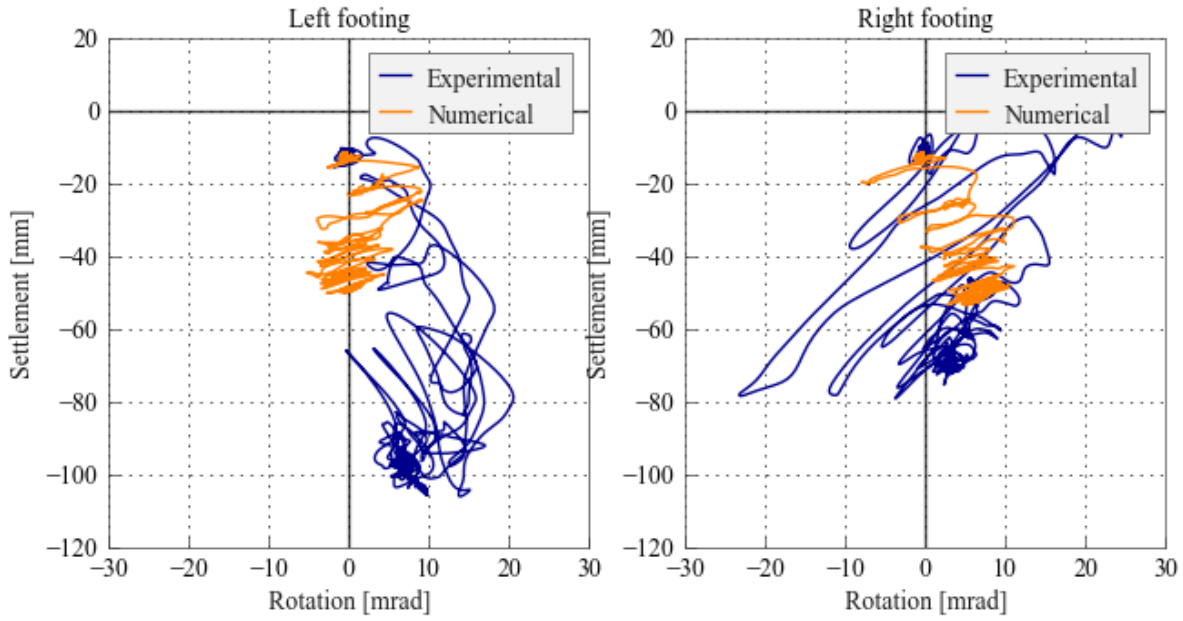

Figure B.40: Settlement verse rotation of footing - Motion SCS_H

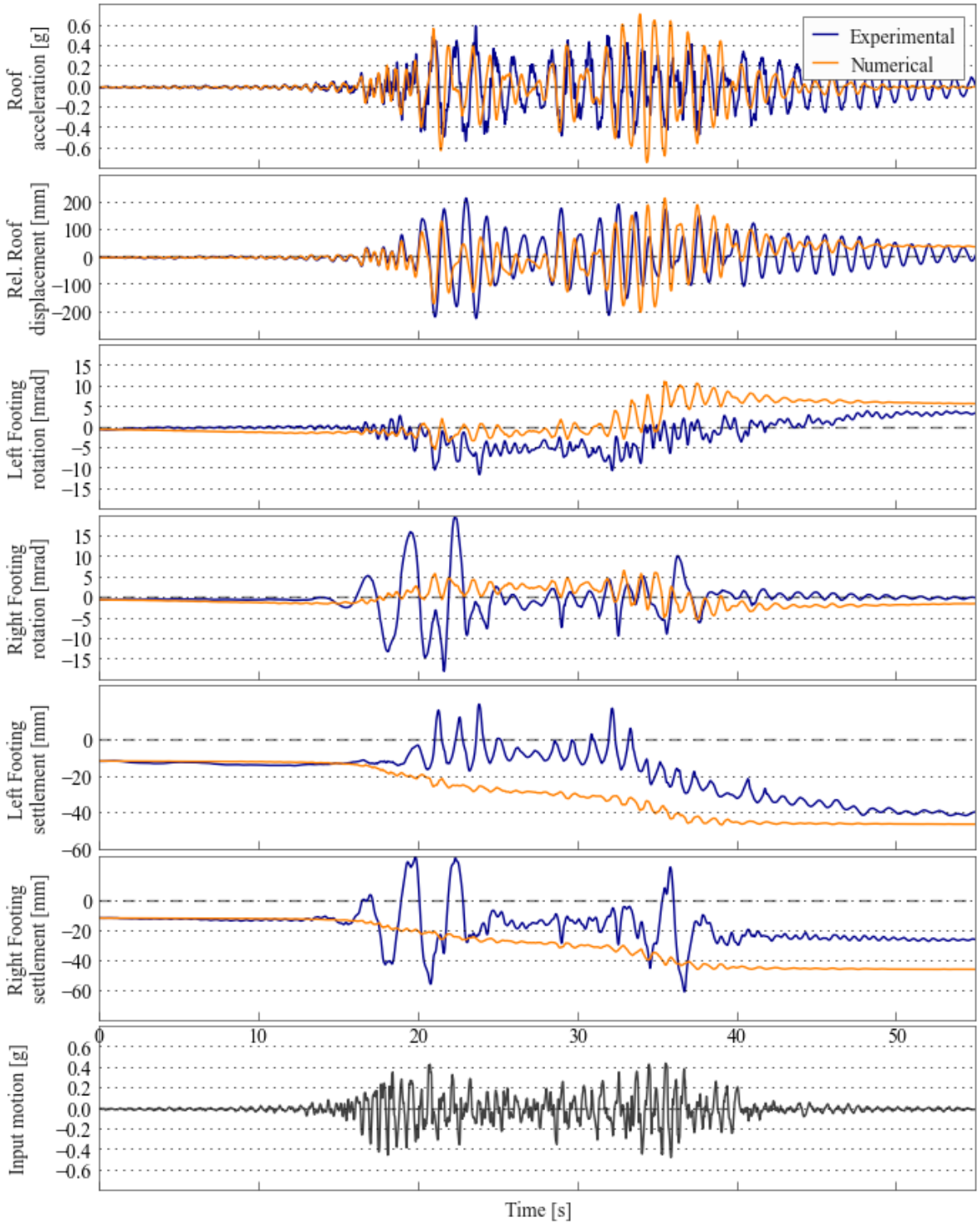

Figure B.41: Comparision of numerical and experimental behaviour - Motion JOS_H

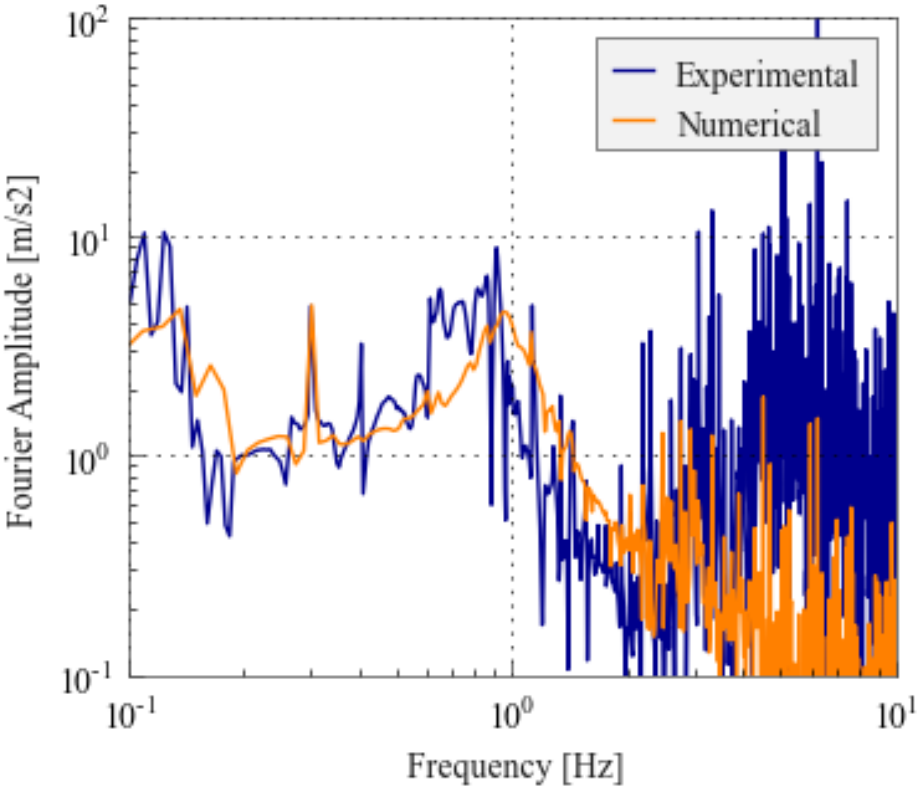

Figure B.42: Roof acceleration Fourier amplitude spectrum - Motion JOS_H

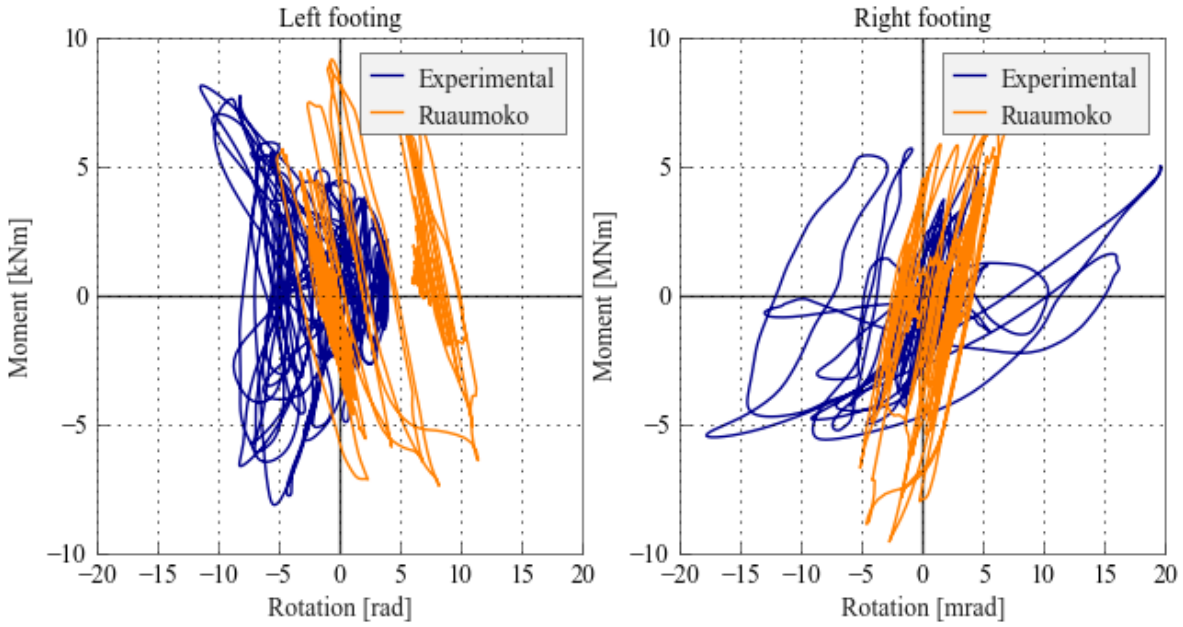

Figure B.43: Moment verse rotation of footing - Motion JOS_H

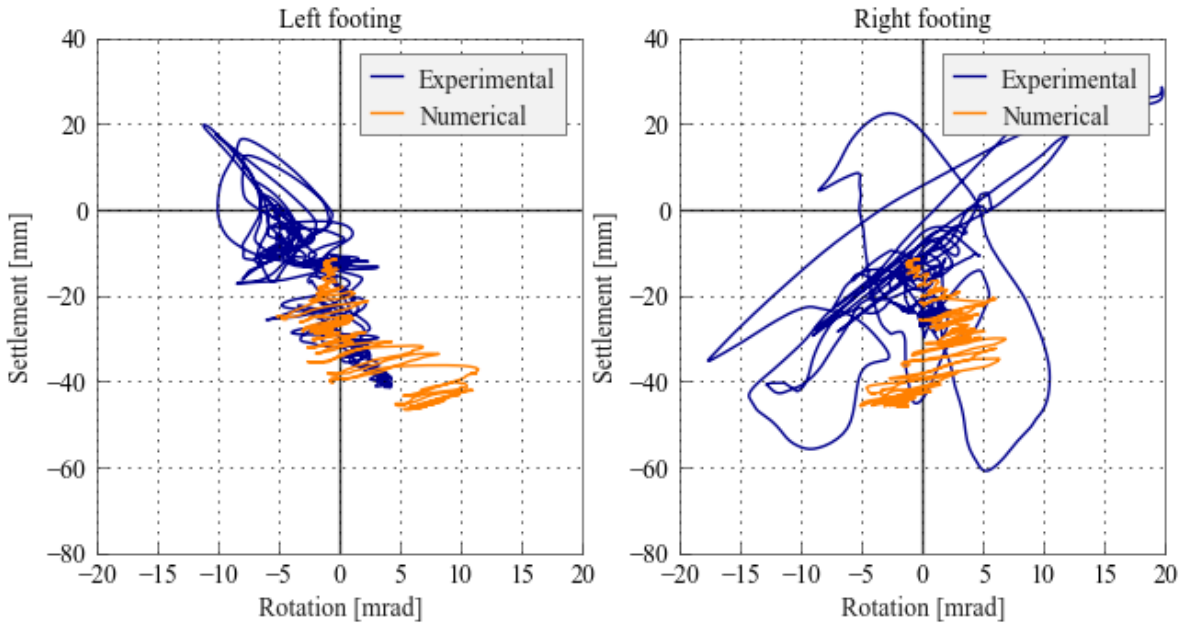

Figure B.44: Settlement verse rotation of footing - Motion JOS_H

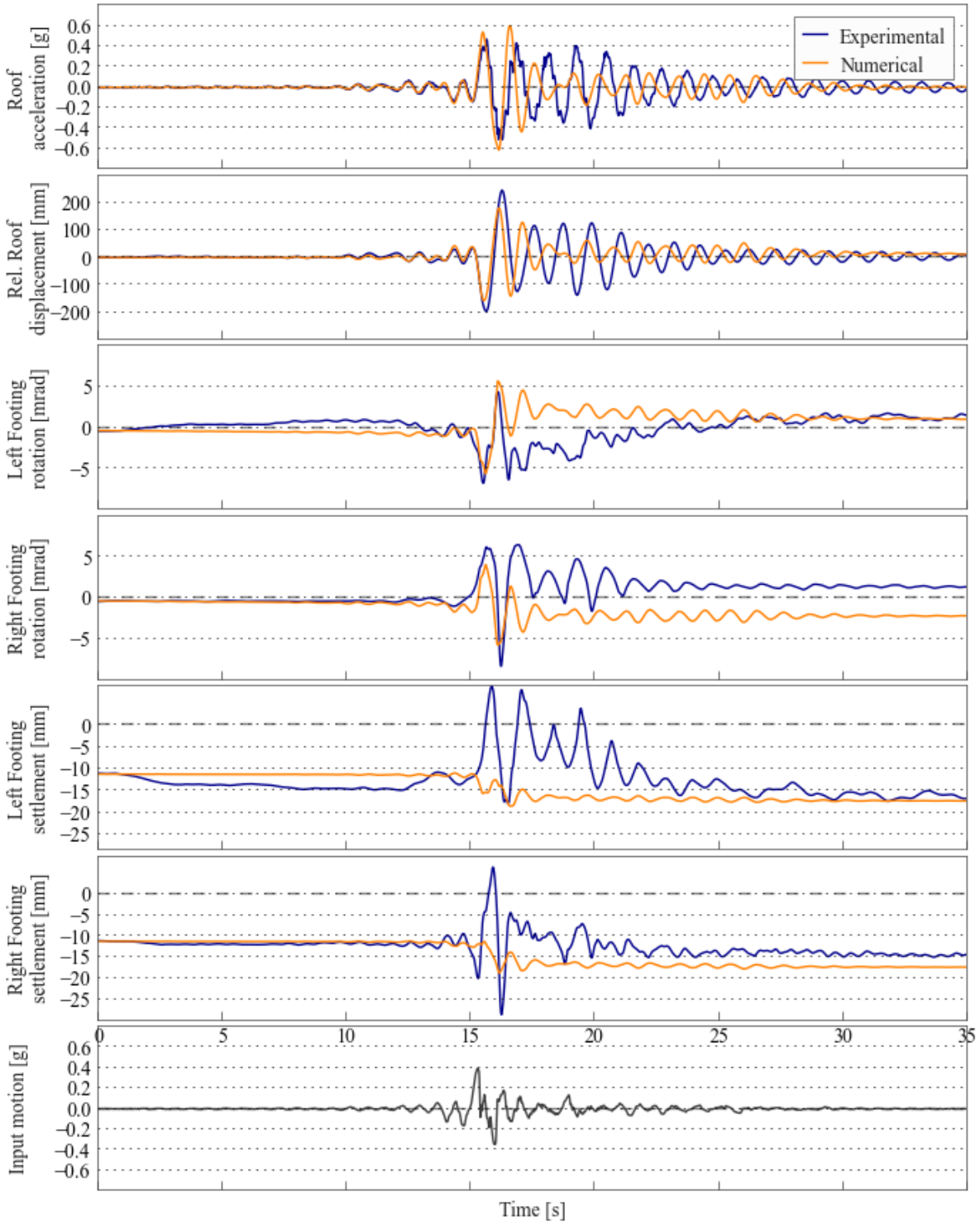

Figure B.45: Comparision of numerical and experimental behaviour - Motion WPI_L

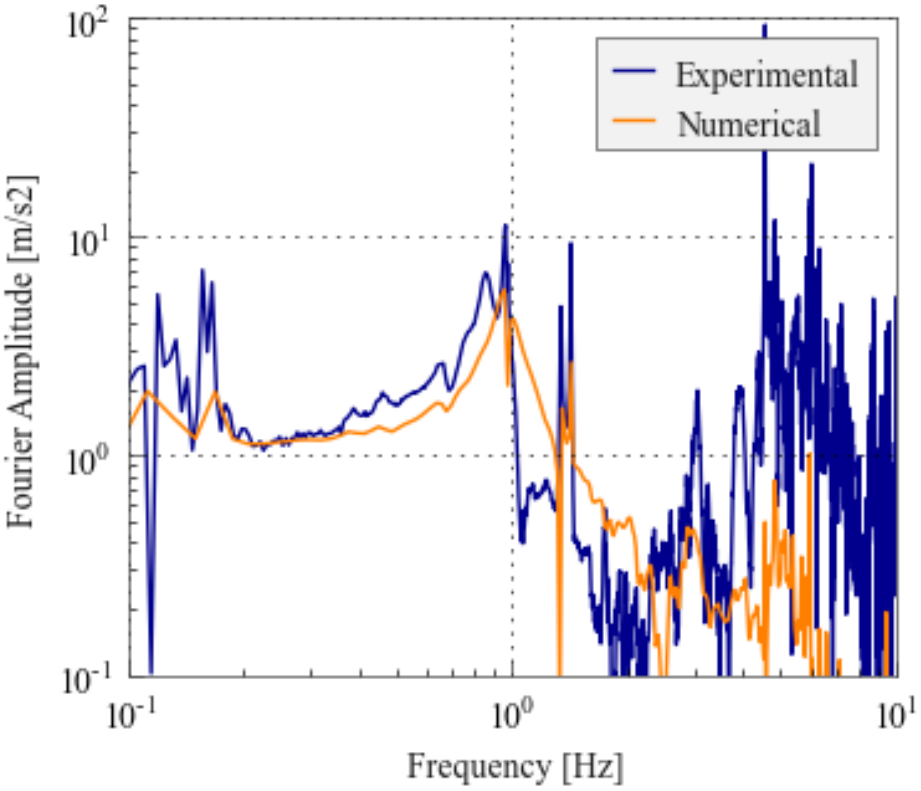

Figure B.46: Roof acceleration Fourier amplitude spectrum - Motion WPI_L

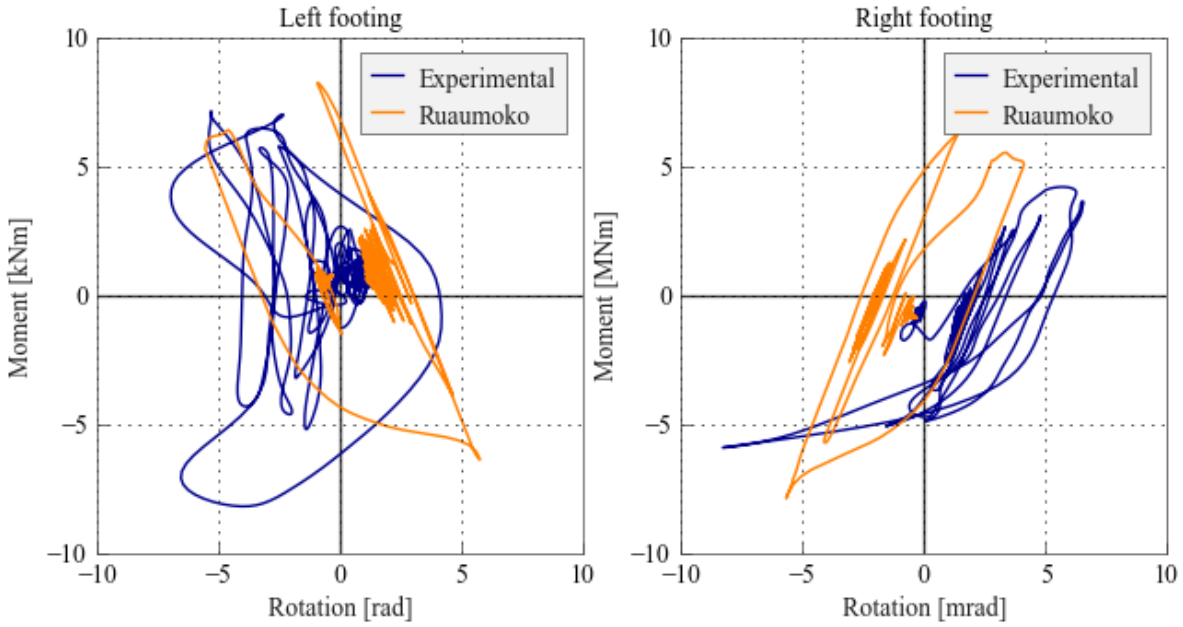

Figure B.47: Moment verse rotation of footing - Motion WPI_L

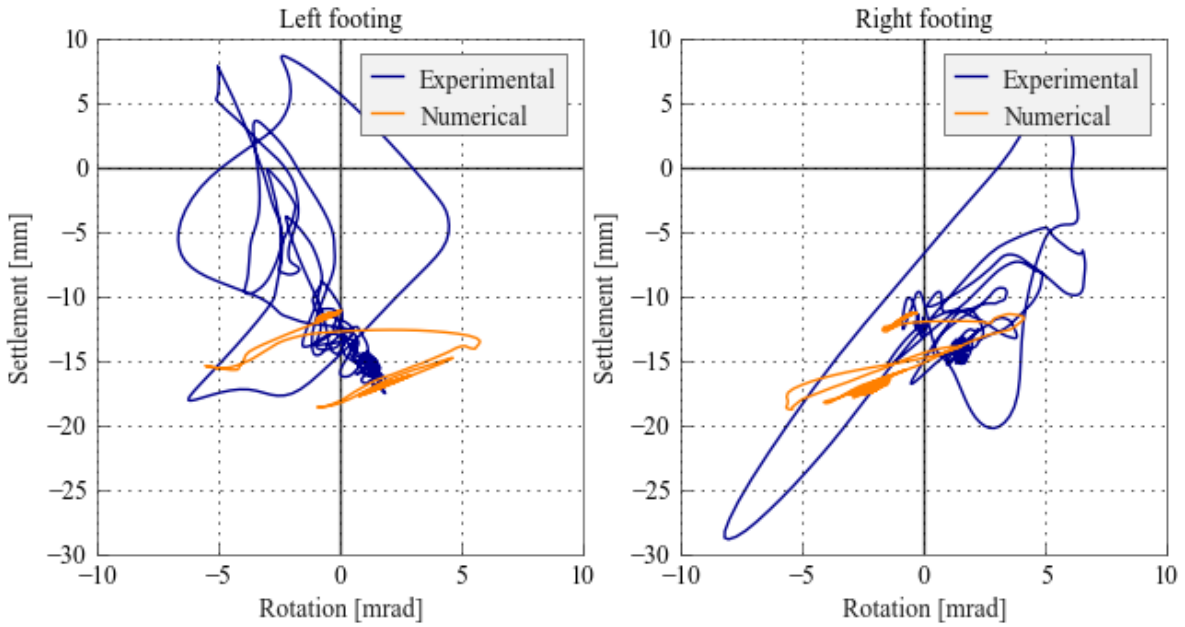

Figure B.48: Settlement verse rotation of footing - Motion WPI_L

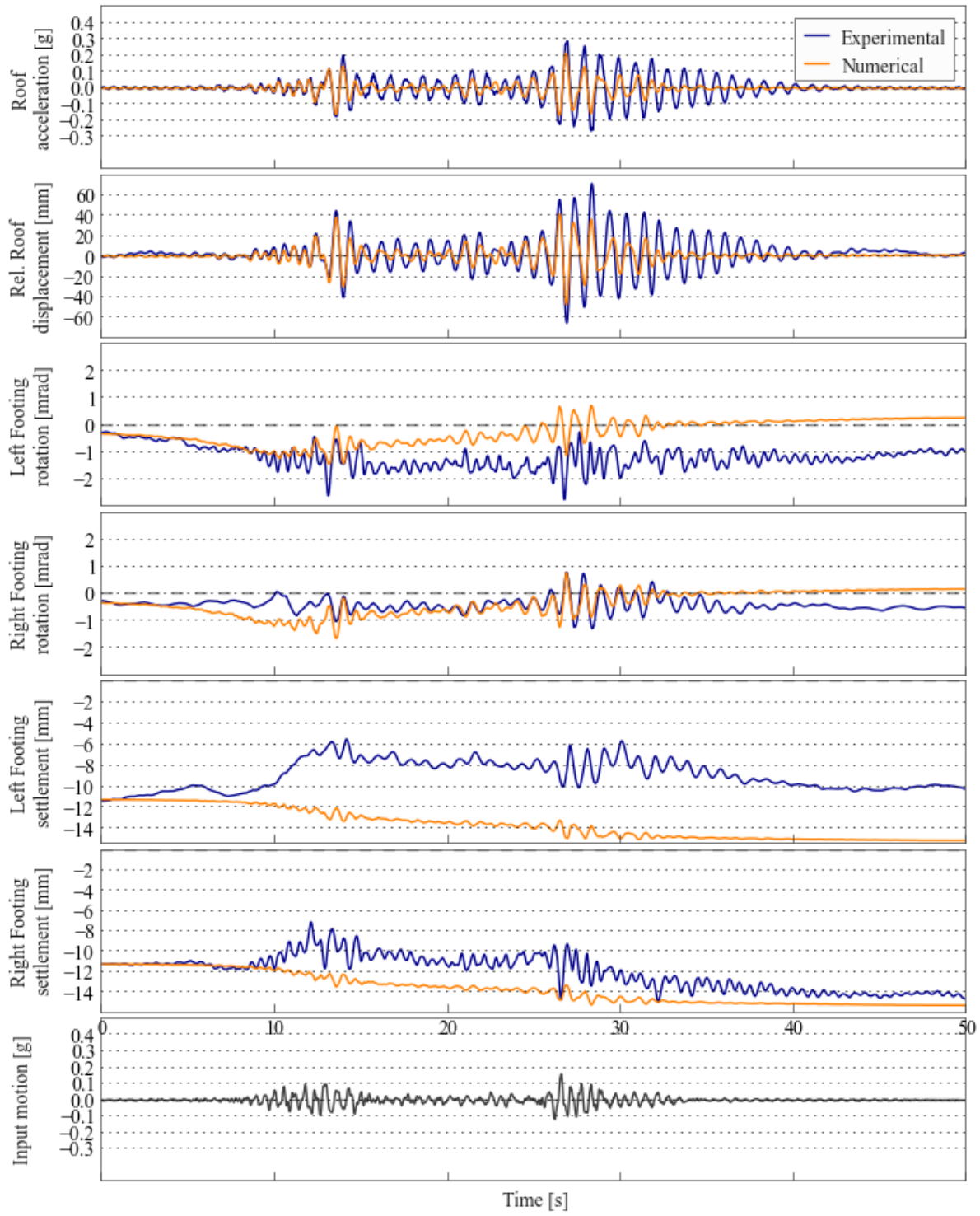

Figure B.49: Comparision of numerical and experimental behaviour - Motion JOS_L_3

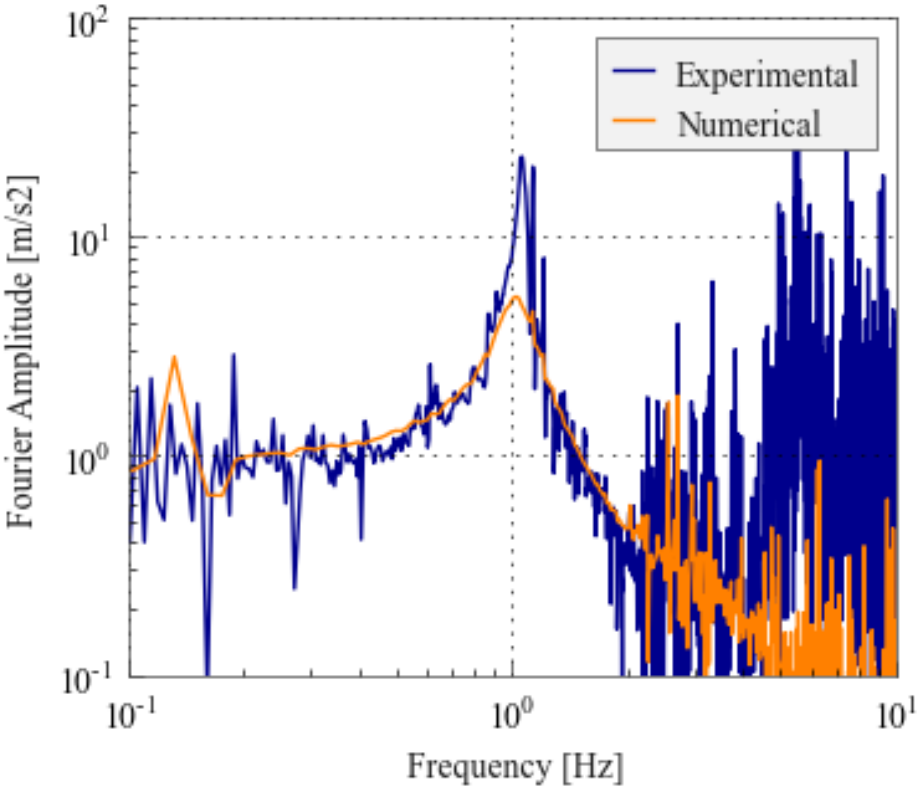

Figure B.50: Roof acceleration Fourier amplitude spectrum - Motion JOS_L_3

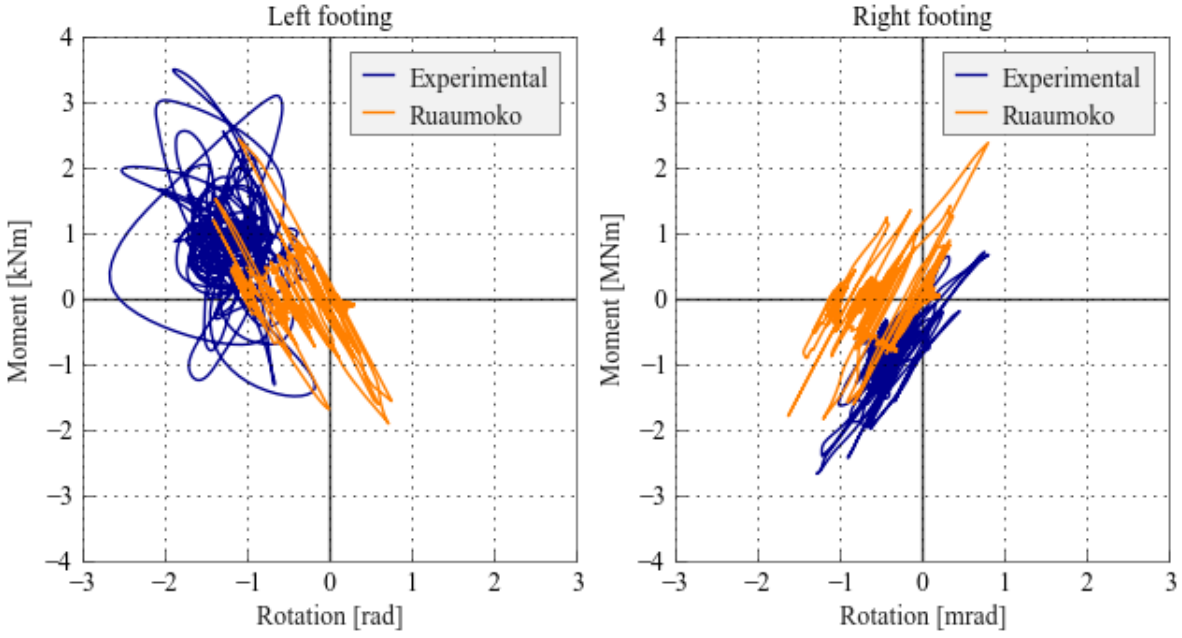

Figure B.51: Moment verse rotation of footing - Motion JOS_L_3

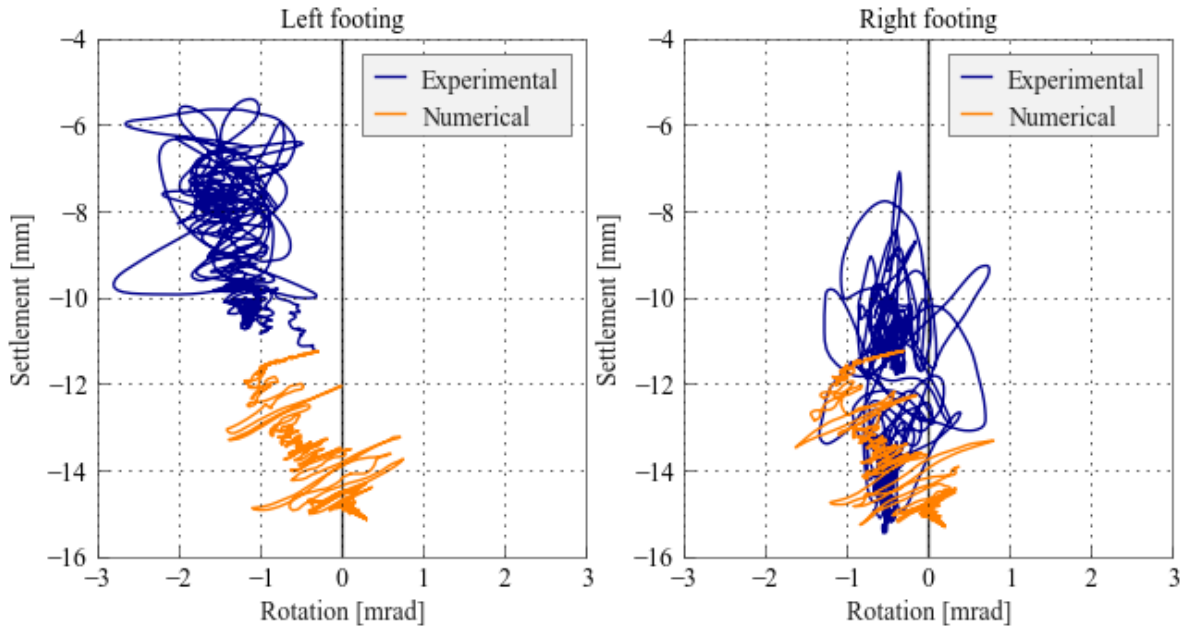

Figure B.52: Settlement verse rotation of footing - Motion JOS_L_3

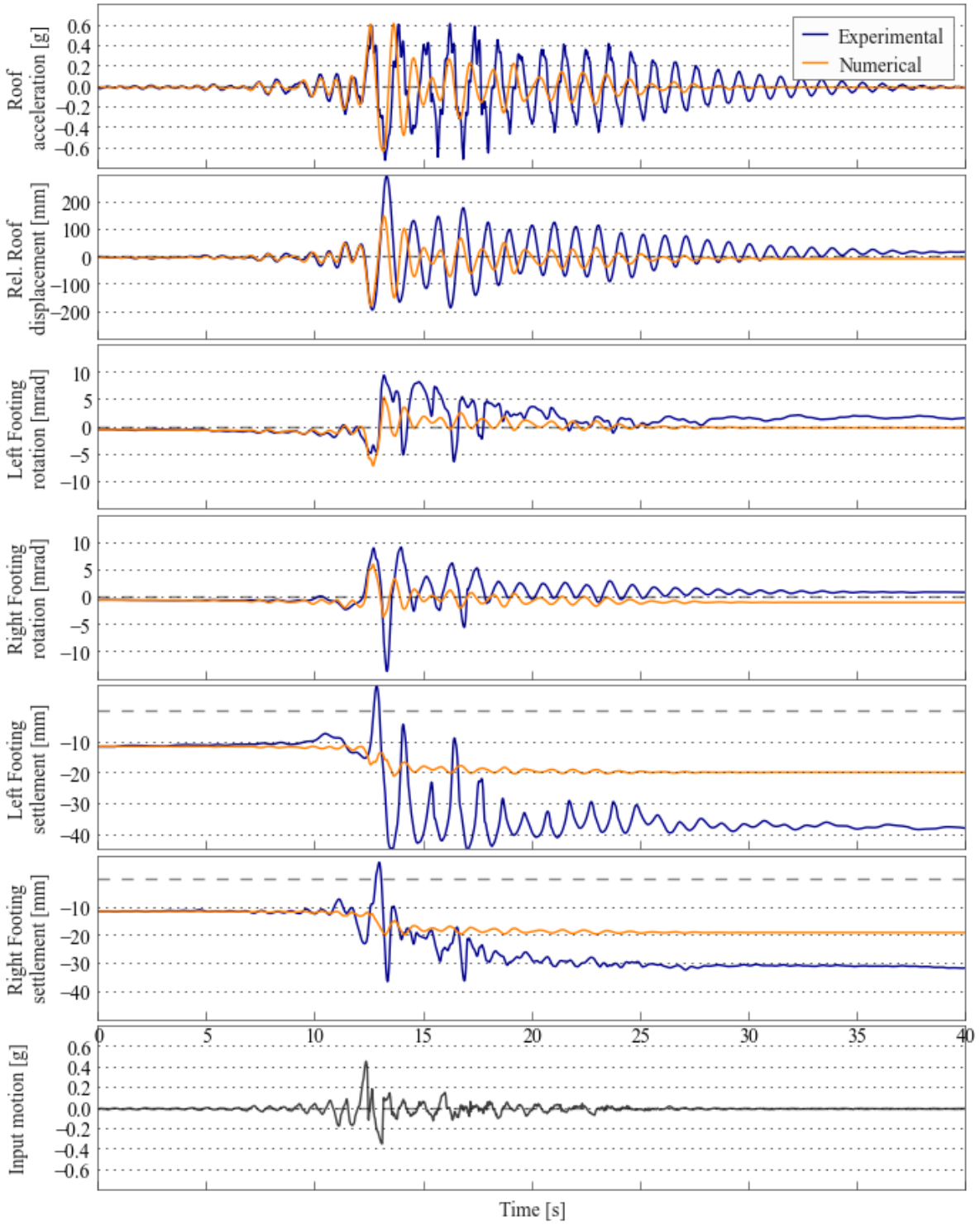

Figure B.53: Comparision of numerical and experimental behaviour - Motion WPI_H

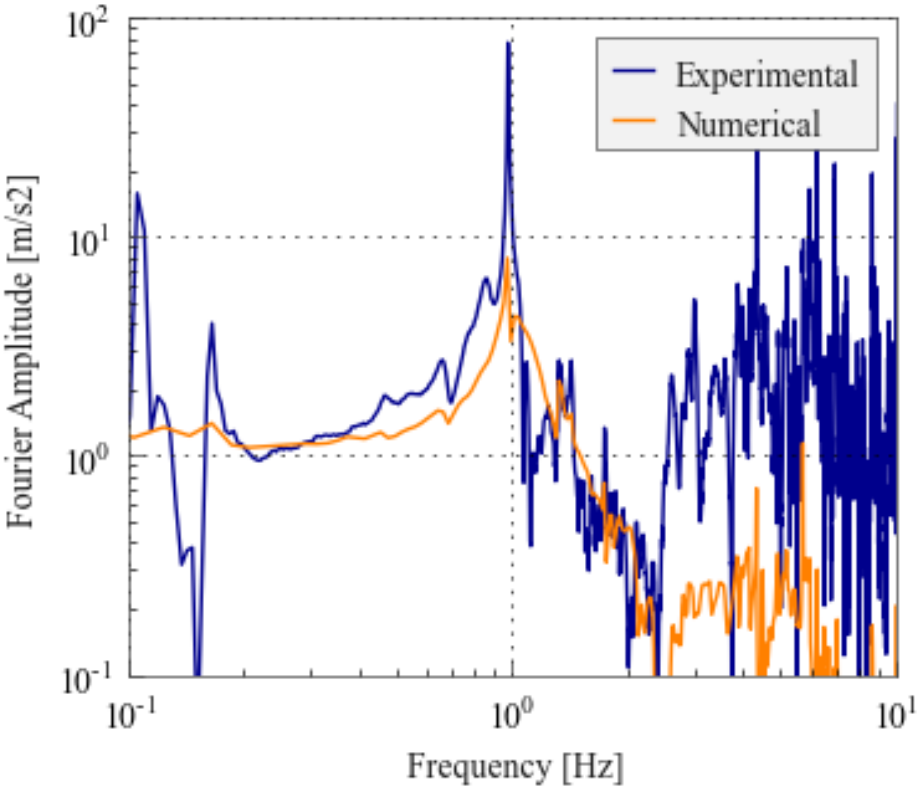

Figure B.54: Roof acceleration Fourier amplitude spectrum - Motion WPI_H

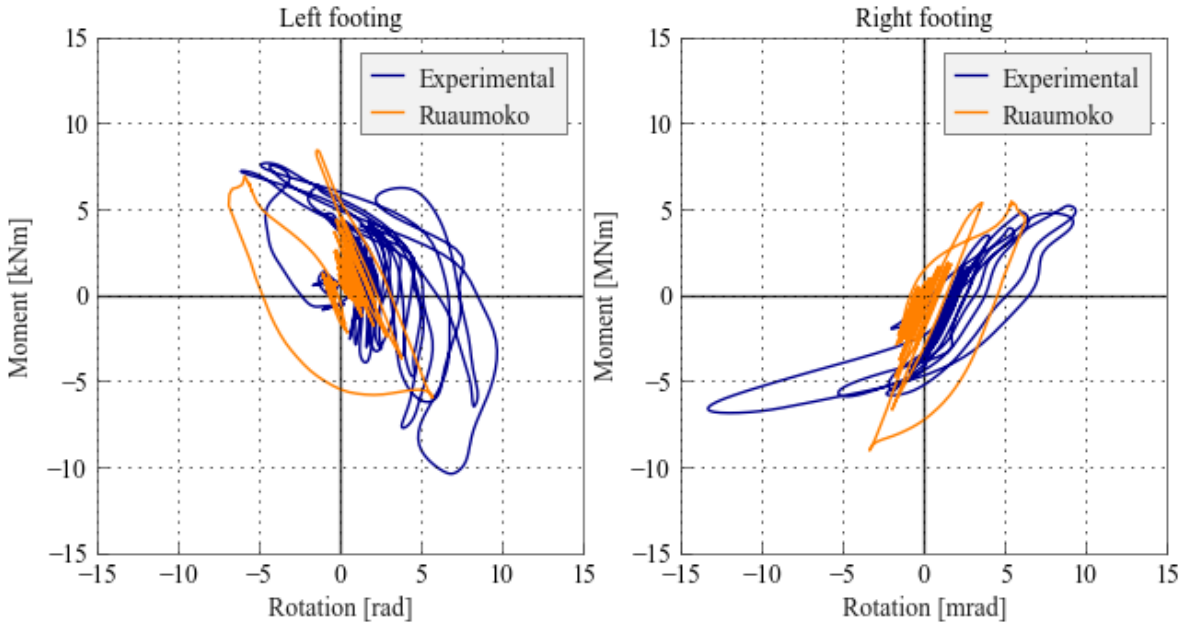

Figure B.55: Moment verse rotation of footing - Motion WPI_H

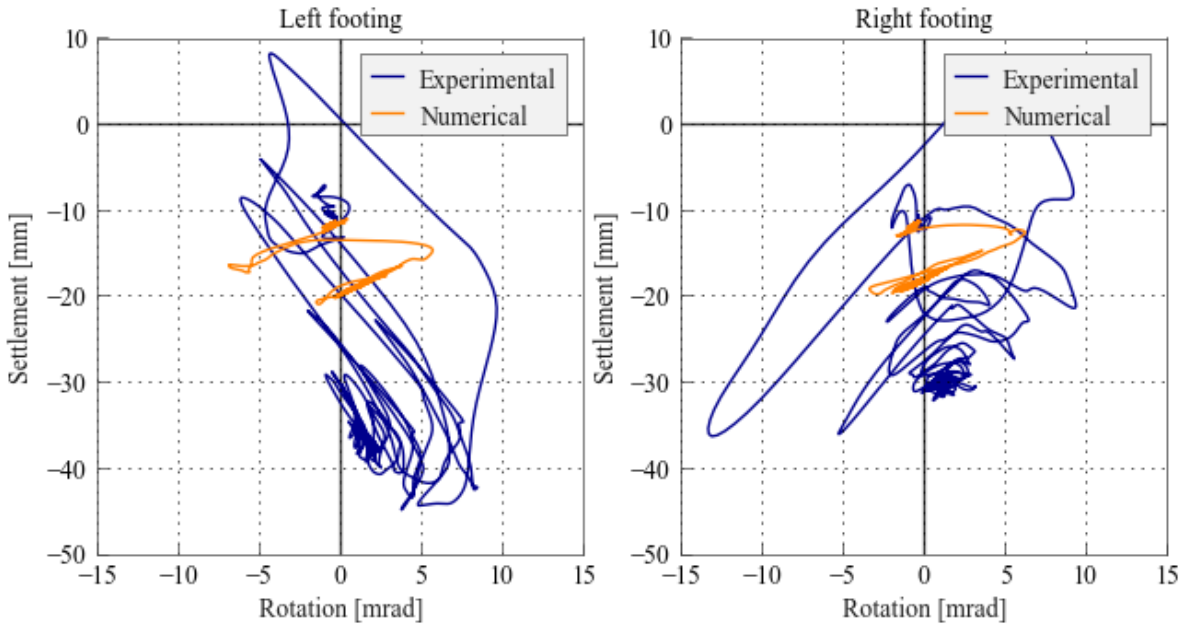

Figure B.56: Settlement verse rotation of footing - Motion WPI_H

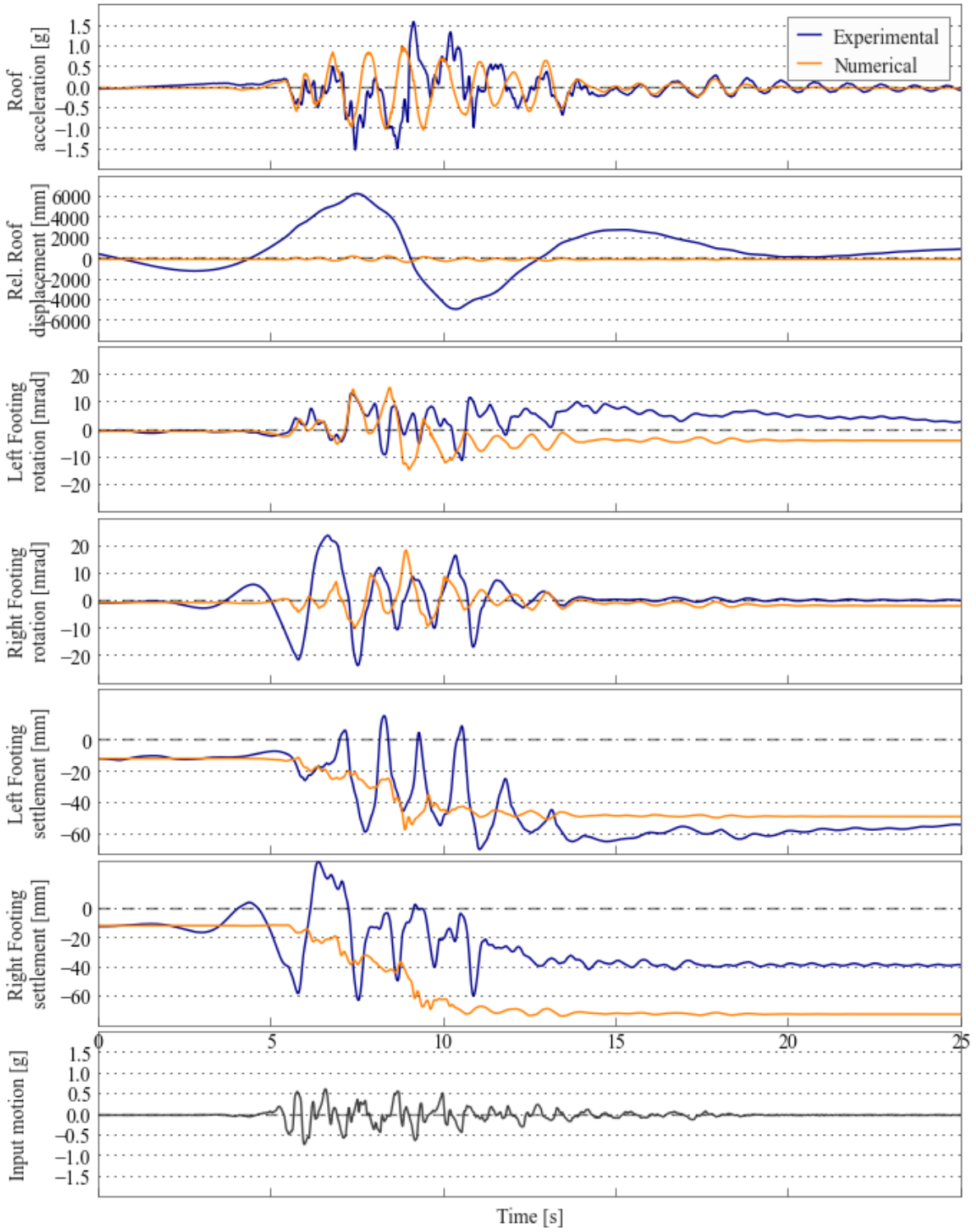

Figure B.57: Comparision of numerical and experimental behaviour - Motion PRI

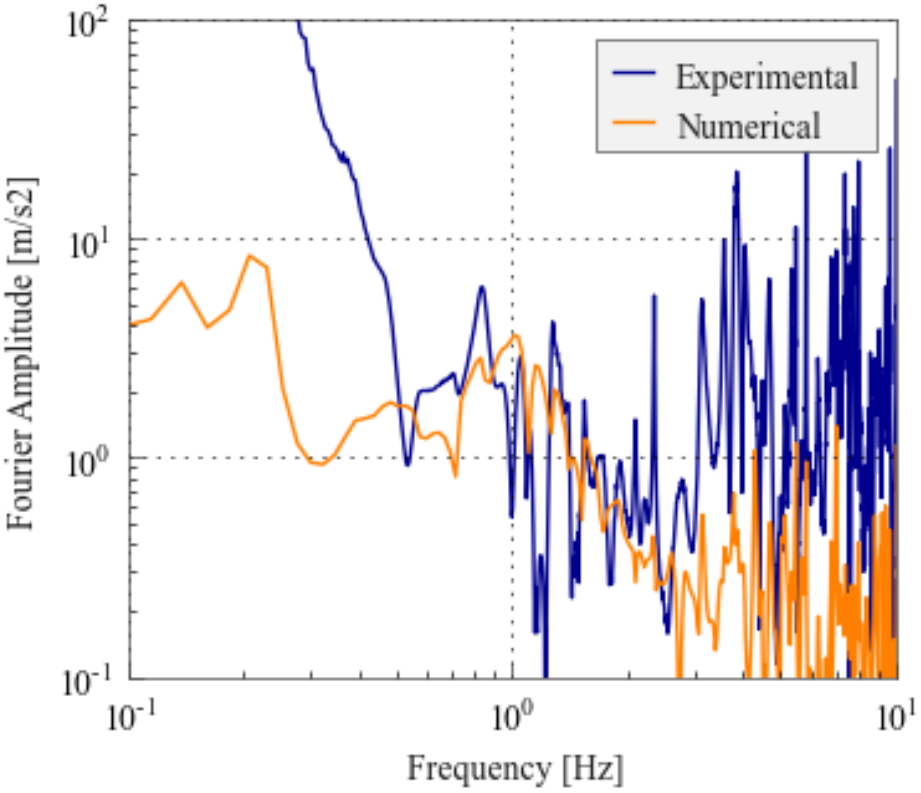

Figure B.58: Roof acceleration Fourier amplitude spectrum - Motion PRI

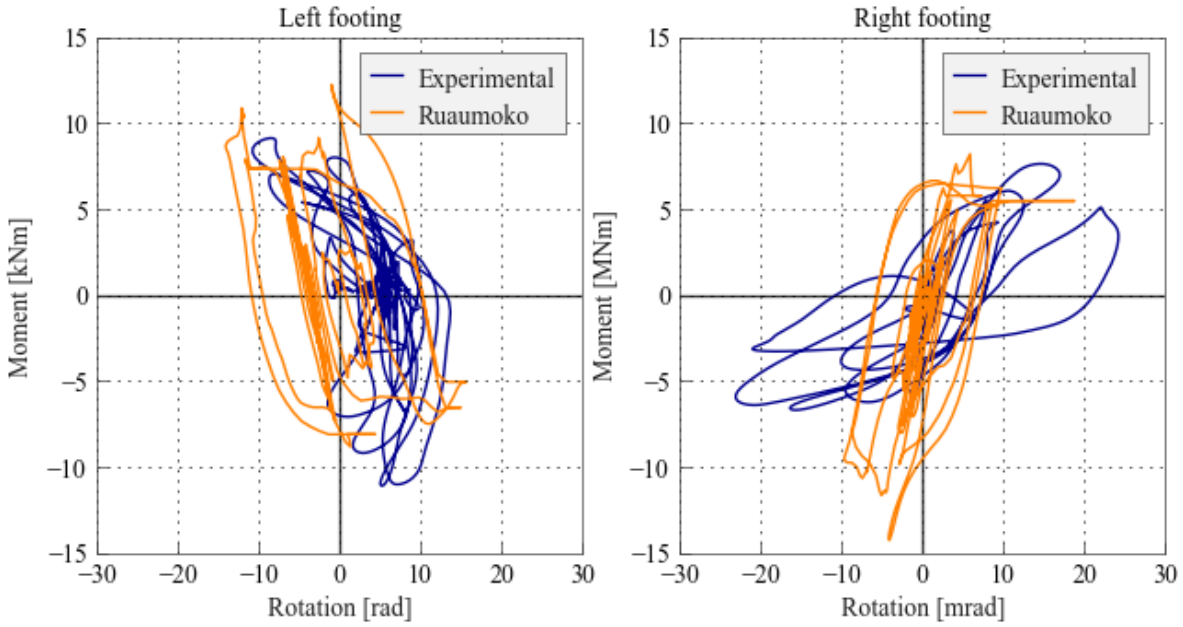

Figure B.59: Moment verse rotation of footing - Motion PRI

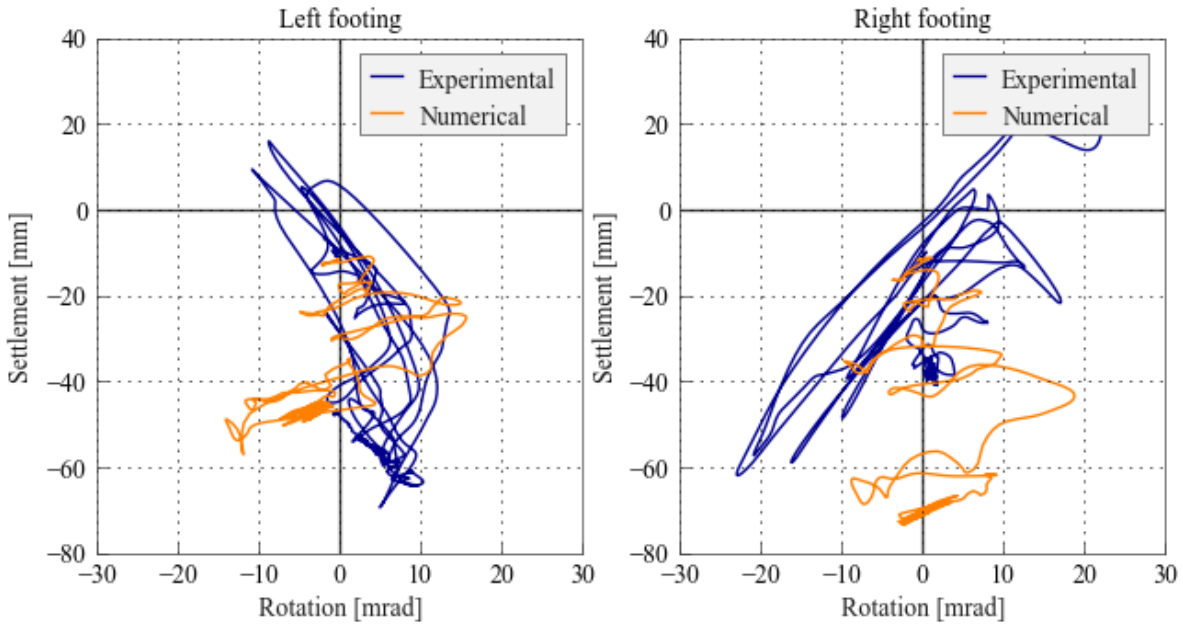

Figure B.60: Settlement verse rotation of footing - Motion PRI

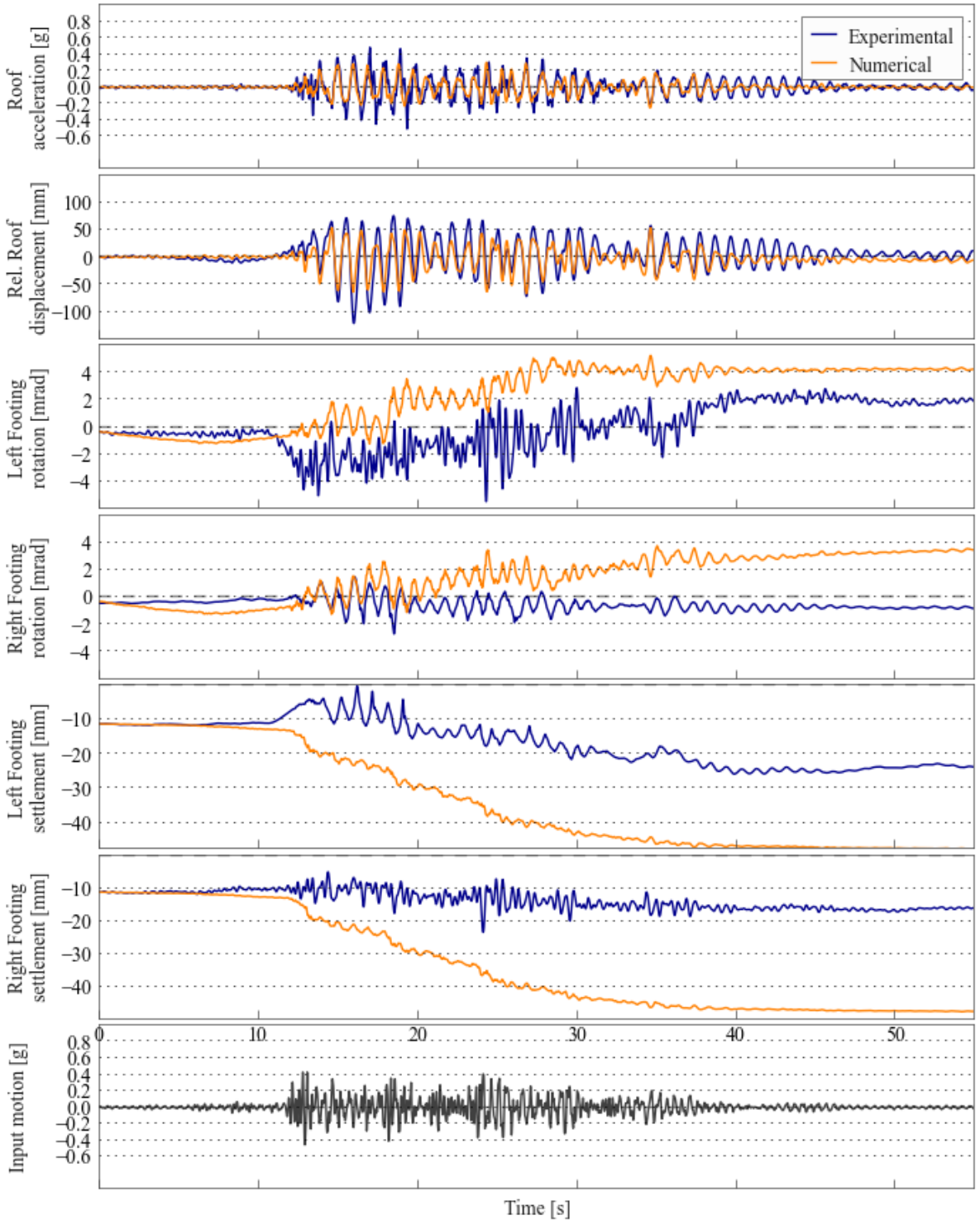

Figure B.61: Comparision of numerical and experimental behaviour - Motion TCU_H

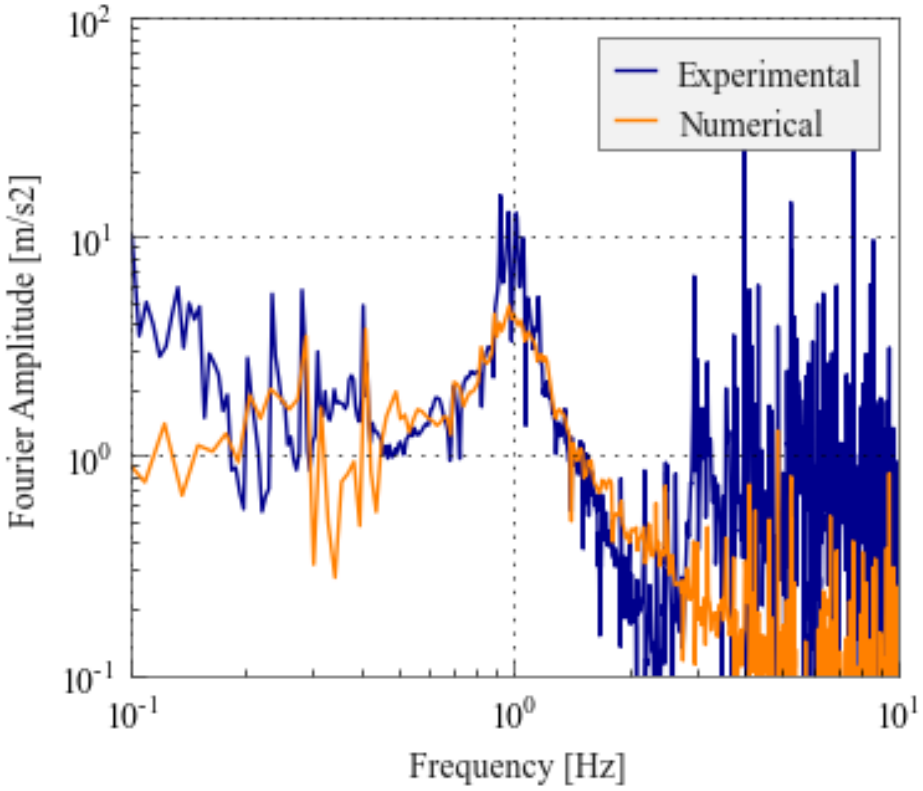

Figure B.62: Roof acceleration Fourier amplitude spectrum - Motion TCU_H

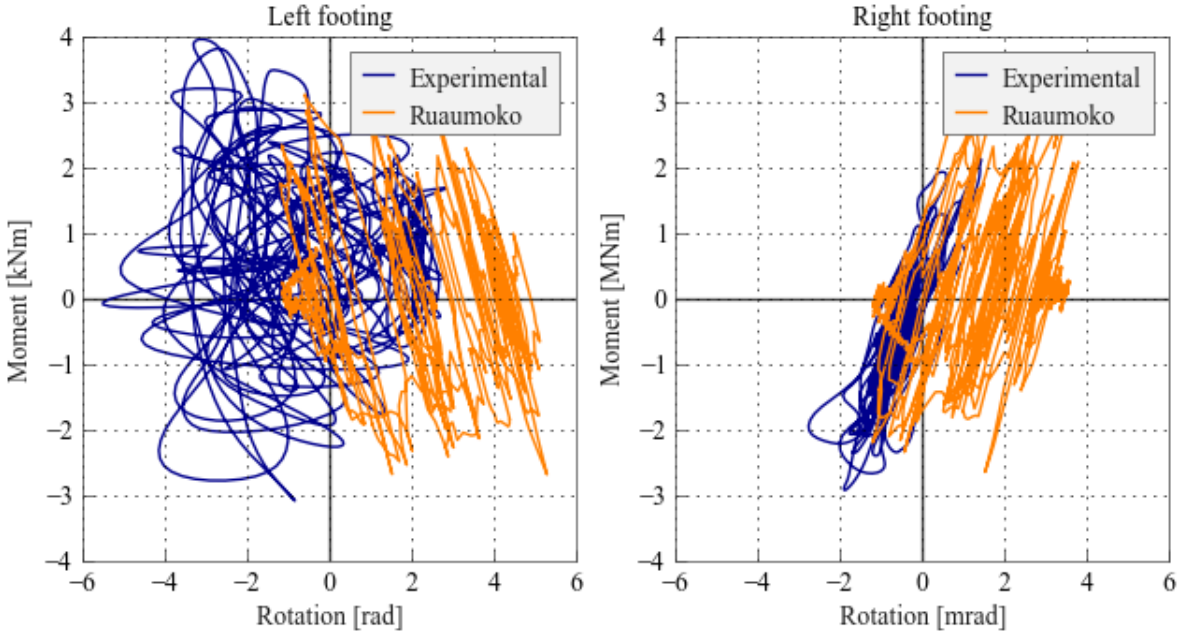

Figure B.63: Moment verse rotation of footing - Motion TCU_H

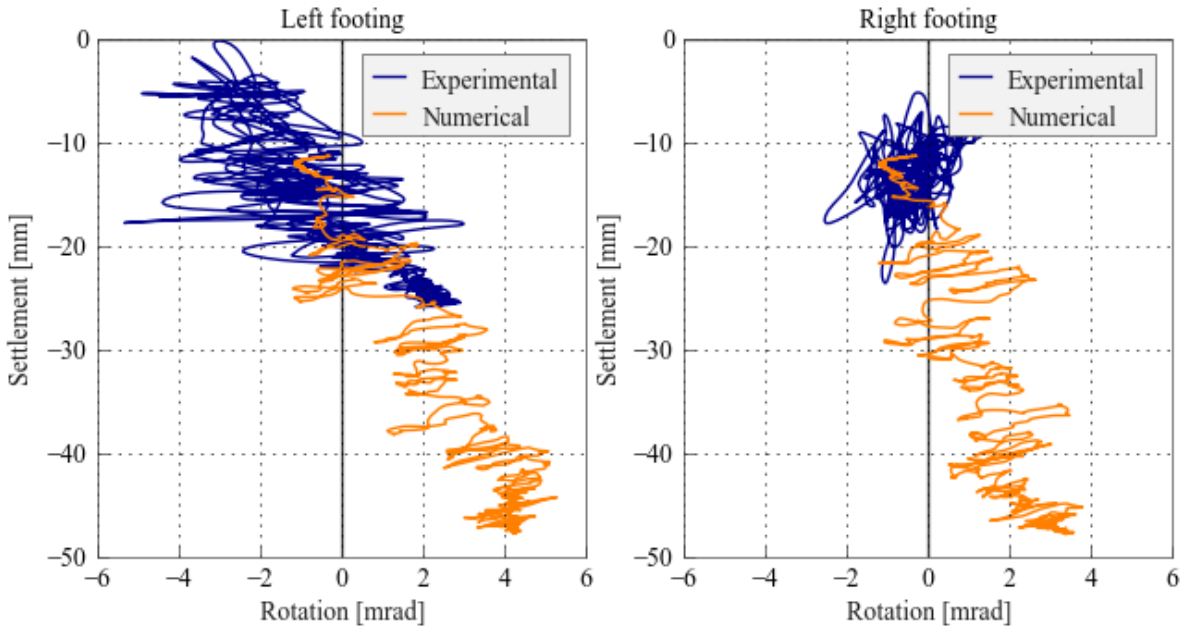

Figure B.64: Settlement verse rotation of footing - Motion TCU_H

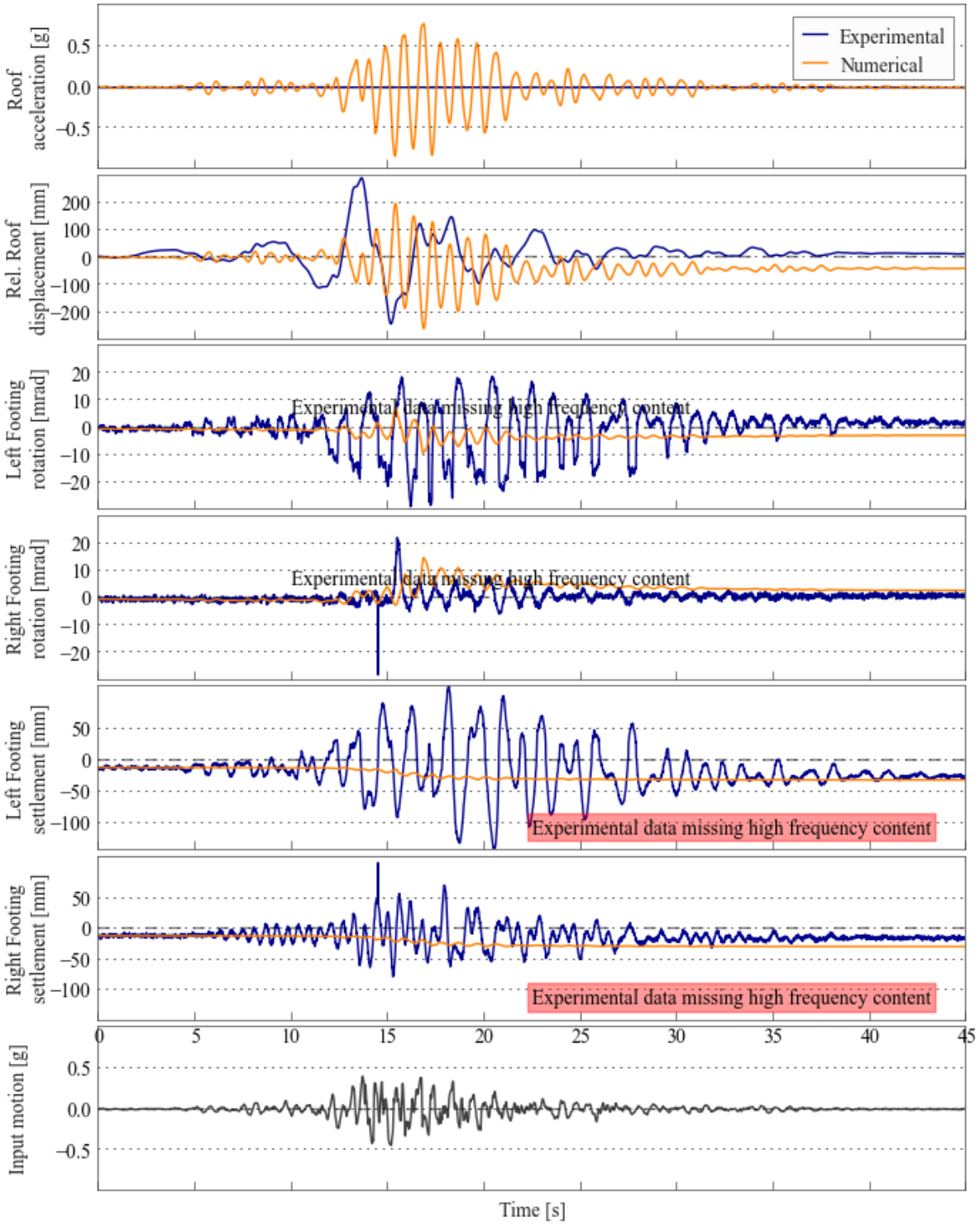

Figure B.65: Comparision of numerical and experimental behaviour - Motion WVC_H

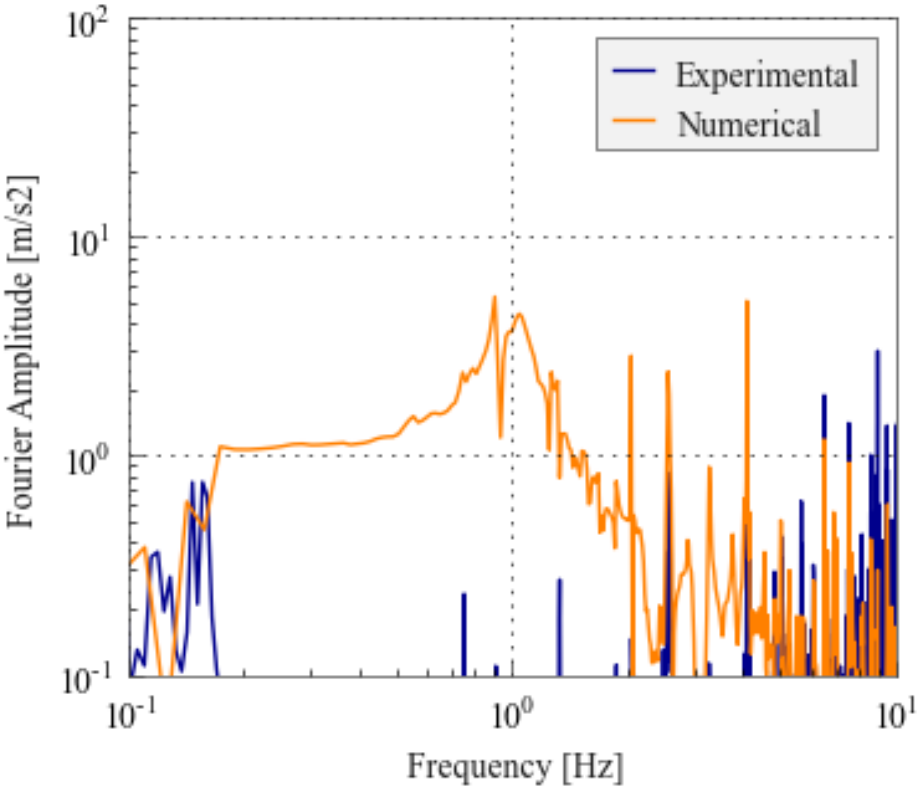

Figure B.66: Roof acceleration Fourier amplitude spectrum - Motion WVC_H

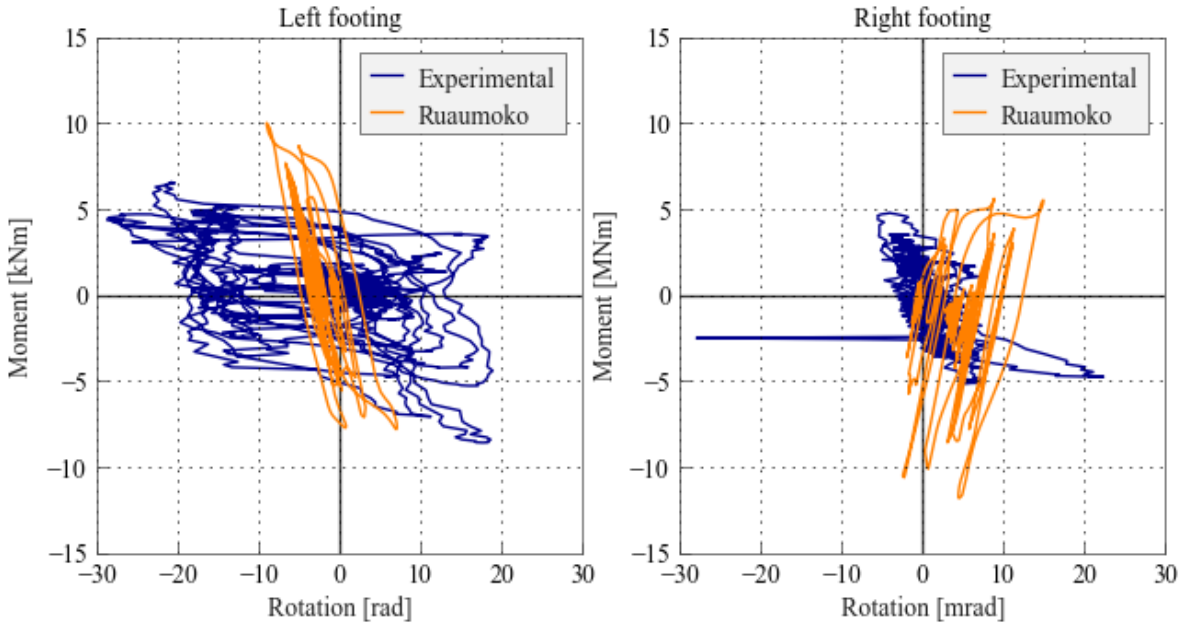

Figure B.67: Moment verse rotation of footing - Motion WVC_H

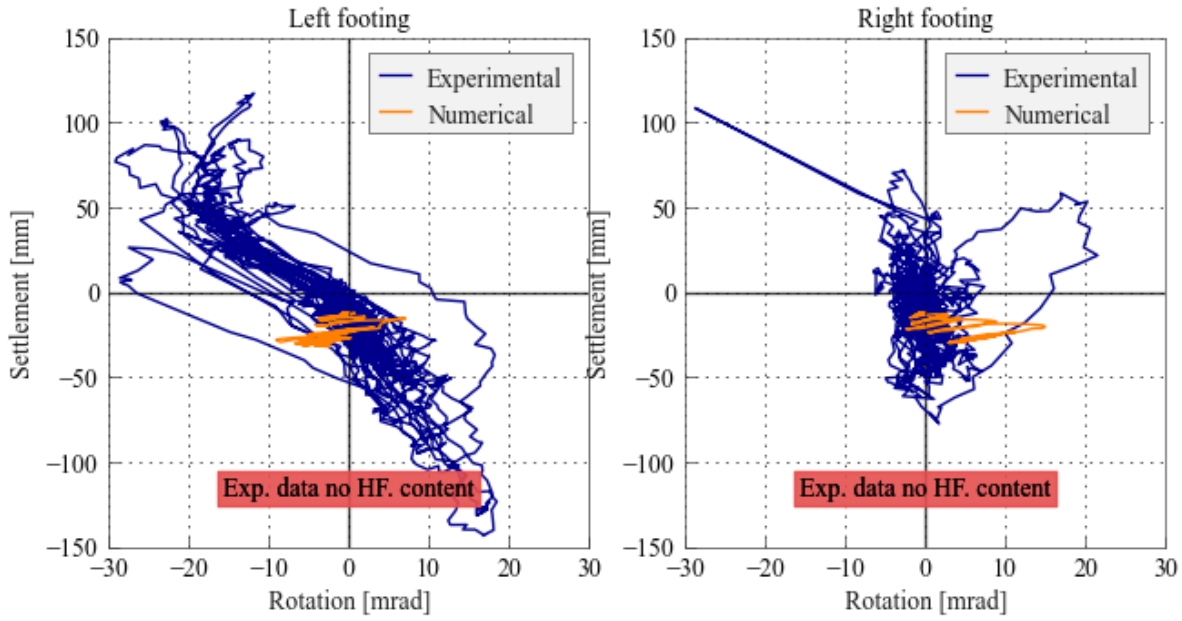

Figure B.68: Settlement verse rotation of footing - Motion WVC_H

B.2 Input file

```
Ruaumoko3D - NEES Frame
! KN,m,secs
! Info
!IPAN    IPLAS   IPCONM   ICTYPE   IPVERT   INLGEO     IPNF    IZERO    ORTHO    IMODE
    2        1        0        2        0        0        0        0        1        0
! NNP     NMEM    NTYPE    NMODE    MODE1    MODE2     GRAV       C1       C2       DT      TIME   FACTOR
   17       18        8        5        1       10     9.80      2.0      2.0 0.013428     74.99     1.00
!KPRNT   KPOST    KPLOT     DFACT     XMAX     YMAX     ZMAX     IFMT   NLEVEL      NUP   IRESID    KDUMP
     0        1        0       1.0      0.0      0.0      1.0        1        2        2        1        0
!     Txx      Txy      Txz      Tyx      Tyy      Tyz
   363.6      0.0      0.0      0.0    363.6      0.0
!MAXIT   MAXCIT    FTEST    WAVEX    WAVEY    WAVEZ    DXMAX    DYMAX    DZMAX        D    OMEGA
    10        5   0.0001      0.0      0.0      0.0      0.0      0.0      0.0      0.0     0.10
NODES
     N        X        Y        Z   FIX_X   FIX_Y   FIX_Z  FIX_RX  FIX_RY  FIX_RZ    KUP1    IOUT    KUP2
     1    0.000   -0.412    0.000       0       0       1       1       1       0       0       0       0   ! Foundation node
     2    0.000    0.770    0.000       0       0       1       1       1       0       0       0       0   ! Base of column hinge
     3    0.000    1.485    0.000       0       0       1       1       1       0       0       0       0   ! Top of column hinge
     4    0.000   11.330    0.000       0       0       1       1       1       0       0       0       0   ! Base of column REB
     5    0.000   12.760    0.000       0       0       1       1       1       0       0       0       0   ! Column-beam connection
     6    1.347   12.760    0.000       0       0       1       1       1       0       0       0       0   ! Outer of beam hinge
     7    2.723   12.760    0.000       0       0       1       1       1       0       0       0       0   ! Inner of beam hinge
     8    4.978   12.760    0.000       0       0       1       1       1       0       0       0       0   ! Central mass node
     9    7.233   12.760    0.000       0       0       1       1       1       0       0       0       0   ! Inner of beam hinge
    10    8.608   12.760    0.000       0       0       1       1       1       0       0       0       0   ! Outer of beam hinge
    11    9.955   12.760    0.000       0       0       1       1       1       0       0       0       0   ! Column-beam connection
    12    9.955   11.330    0.000       0       0       1       1       1       0       0       0       0   ! Base of column REB
    13    9.955    1.485    0.000       0       0       1       1       1       0       0       0       0   ! Top of column hinge
    14    9.955    0.770    0.000       0       0       1       1       1       0       0       0       0   ! Base of column hinge
    15    9.955   -0.412    0.000       0       0       1       1       1       0       0       0       0   ! Foundation node
    16    0.000   -0.825    0.000       1       1       1       1       1       1       0       0       0   ! Left fixed ground
    17    9.955   -0.825    0.000       1       1       1       1       1       1       0       0       0   ! Right fixed ground
DRIFT
     1    5
ELEMENTS
!    N   MTYPE        I        J        K        L        M    IOUT
     1       1        1        2        0        0        Z       0   ! column base to column hinge (full)
     2       2        2        3        0        0        Z       0   ! column hinge
     3       1        3        4        0        0        Z       0   ! column hinge to column REB (full)
     4       3        4        5        0        0        Z       0   ! column EB (EI = 4 x full)
```

```
    5       4       5       6       0       0       Z       0   ! beam EB (full, with rigid section)
    6       5       6       7       0       0       Z       0   ! beam hinge
    7       1       7       8       0       0       Z       0   ! beam hinge to centre (full)
    8       1       8       9       0       0       Z       0   ! centre to beam hinge (full)
    9       5       9      10       0       0       Z       0   ! beam hinge
   10       4      10      11       0       0       Z       0   ! beam EB (full, with rigid section)
   11       3      11      12       0       0       Z       0   ! column EB (EI = 4 x full)
   12       1      12      13       0       0       Z       0   ! column REB to column hinge (full)
   13       2      13      14       0       0       Z       0   ! column hinge
   14       1      14      15       0       0       Z       0   ! column hinge to column base (full)
   15       6      16       1      16       1       Z       0   ! macro soil-foundation element
   16       7      17      15      17      15       Z       0   ! macro soil-foundation element
   17       8      16       1      16       1       Z       0   ! radiation damping dashpot
   18       8      17      15      17      15       Z       0   ! radiation damping dashpot
PROPS
    1          BEAM          Full
!TYPE     IBEAM     IPINZ     IPINY     ICOND     IHYST      ILOS     IDAMG       IGA     IDUCT
    1         1         0         0         0         0         0         0         0         0
!            E             G             A           Jxx           Izz           Iyy     Asz     Asy    Sy    Sz WGT
    0.20000E+09    0.80000E+08   0.2206133E+00    0.16661E+00    0.13884E-01    0.13884E-01 0.22061 0.22061 0.00 0.00 0.0
!     END1z    END2z    END1y    END2y        FJ1z          FJ2z          FJ1y          FJ2y        Y0        Z0
    0.00000   0.0000  0.00000  0.00000 0.00000E+00  0.00000E+00  0.00000E+00  0.00000E+00   0.00000   0.00000

    2         SPRING         H1_col
!TYPE IHYST ILOS IDAMG INCOND ITRUSS  SL  Y0  Z0 ISTOP
    1     2    0     0      0      0 0.0 0.0 0.0     0
!            K1              K2              K3              K4              K5              K6    WGT      RF      RT
   0.5245350E+08   0.2098140E+08   0.2098140E+08   0.3106857E+09   0.3106857E+09   0.1042000E+07    0.0   0.010   0.160
!           FX+             FX-             FY+             FY-             FZ+             FZ-
   0.7683500E+05  -0.7683500E+05   0.1754500E+05  -0.1754500E+05   0.1754500E+05  -0.1754500E+05
!           MX+             MX-             MY+             MY-             MZ+             MZ-
   0.0000000E+00   0.0000000E+00   0.0000000E+00   0.0000000E+00   0.1000000E+05  -0.1000000E+05

    3          BEAM        Top_col
!TYPE     IBEAM     IPINZ     IPINY     ICOND     IHYST      ILOS     IDAMG       IGA     IDUCT
    1         1         0         0         0         0         0         0         0         0
!            E             G             A           Jxx           Izz           Iyy     Asz     Asy    Sy    Sz WGT
    0.20000E+09    0.80000E+08   0.4412265E+00    0.66642E+00  0.55535E-01  0.55535E-01 0.4412 0.44123 0.00 0.00 0.0
!     END1z    END2z    END1y    END2y        FJ1z          FJ2z          FJ1y          FJ2y        Y0        Z0
    0.0000   0.0000   0.0000   0.00000 0.00000E+00  0.00000E+00  0.00000E+00  0.00000E+00   0.00000   0.00000

    4          BEAM       Beam_REB
!TYPE     IBEAM     IPINZ     IPINY     ICOND     IHYST      ILOS     IDAMG       IGA     IDUCT
    1         1         0         0         0         0         0         0         0         0
!            E             G             A           Jxx           Izz           Iyy     Asz     Asy    Sy    Sz WGT
    0.20000E+09    0.80000E+08   0.2206133E+00    0.16661E+00  0.13884E-01  0.13884E-01 0.22061 0.22061 0.00 0.00 0.0
!     END1z    END2z    END1y    END2y        FJ1z          FJ2z          FJ1y          FJ2y        Y0        Z0
    0.35750  0.0000   0.35750  0.00000 0.00000E+00  0.00000E+00  0.00000E+00  0.00000E+00   0.00000   0.00000

    5         SPRING        H2_beam
!TYPE IHYST ILOS IDAMG INCOND ITRUSS  SL  Y0  Z0 ISTOP
    1    2    0      0      0      0 0.0 0.0 0.0     0
!            K1              K2              K3              K4              K5              K6   WGT    RF    RT
   0.1925352E+08   0.7701408E+07   0.7701408E+07   0.7270045E+08   0.7270045E+08   0.4410000E+06   0.0 0.010 0.090
!           FX+             FX-             FY+             FY-             FZ+             FZ-
   0.3448500E+05  -0.3448500E+05   0.3463625E+04  -0.3463625E+04   0.3463625E+04  -0.3463625E+04
!           MX+             MX-             MY+             MY-             MZ+             MZ-
   0.5000000E+05  -0.5000000E+05   0.5000000E+05  -0.5000000E+05   0.5000000E+04  -0.5000000E+04

    6          MACRO   SSI -element
!IPLS  ISL       DIAM       QQMAX         KNN         KVV         KMM       PSI       KSI   PL_P1 PL_P2  WGT IPRNT ITRK
    1    0      4.367   93030.813  617443.891  504003.176 2413644.728     0.629     0.480   0.200 1.000  0.0     0    1
! UP_ALPHA   UP_BETA  UP_GAMMA  UP_DELTA UP_EPSILN   UP_ZETA   NON-ASS   TOPLING        MIN_LAM  TENS FRIC MAPP UPLIFT
       4.00      2.00      1.00      1.00      0.50      1.50     1.000   5000.00     0.1000E+02    No  Yes  Yes     No
!  K_alpha    K_beta     G_Lam     G_Chi      G_Xi
       1.00      1.00      2.50      3.00      0.95

    7          MACRO   SSI -element
!IPLS  ISL       DIAM       QQMAX         KNN         KVV         KMM       PSI       KSI   PL_P1 PL_P2  WGT IPRNT ITRK
    1    0      4.367   93030.813  617443.891  504003.176 2413644.728     0.629     0.480   0.200 1.000  0.0     0    1
! UP_ALPHA   UP_BETA  UP_GAMMA  UP_DELTA UP_EPSILN   UP_ZETA   NON-ASS   TOPLING        MIN_LAM  TENS FRIC MAPP UPLIFT
       4.00      2.00      1.00      1.00      0.50      1.50     1.000   5000.00     0.1000E+02    No  Yes  Yes     No
!  K_alpha    K_beta     G_Lam     G_Chi      G_Xi
       1.00      1.00      2.50      3.00      0.95

    8         DAMPER   SSI -damping
```

```
!TYPE           C1           C2       C3       C4       C5           C6 GAP+ GAP- ALFA LIMIT    SL    KOP   Y0     Z0
    0  0.80343E+04  0.51966E+04  0.0E+00  0.0E+00  0.0E+00  0.44689E+04 0.00 0.00 1.00  1.00 -0.50  0.00  0.00   0.00
!      FXmax        Fxmin        FYmax        FYmin  FZmax  FZmin  MXmax  MXmin  MYmax  MYmin        MZmax        MZmin
  0.2800E+03  0.2800E+03  0.2800E+06  0.2800E+06   0.00   0.00   0.00   0.00   0.00   0.00  0.1000E+07  0.1000E+07

WEIGHTS       0
!   N          Wx          Wy          Wz          Mx          My          Mz
    1   5119.6915   5119.6915      0.0000      0.0000      0.0000   1599.7099   ! foundation
    2      0.0000      0.0000      0.0000      0.0000      0.0000      0.0000
    3      0.0000      0.0000      0.0000      0.0000      0.0000      0.0000
    4      0.0000      0.0000      0.0000      0.0000      0.0000      0.0000
    5    497.2949    497.2949      0.0000      0.0000      0.0000      0.0000   ! Beam end
    6      0.0000      0.0000      0.0000      0.0000      0.0000      0.0000
    7      0.0000      0.0000      0.0000      0.0000      0.0000      0.0000
    8   3350.6261   3350.6261      0.0000      0.0000      0.0000      0.0000   ! Beam centre
    9      0.0000      0.0000      0.0000      0.0000      0.0000      0.0000
   10      0.0000      0.0000      0.0000      0.0000      0.0000      0.0000
   11    497.2949    497.2949      0.0000      0.0000      0.0000      0.0000   ! Beam end
   12      0.0000      0.0000      0.0000      0.0000      0.0000      0.0000
   13      0.0000      0.0000      0.0000      0.0000      0.0000      0.0000
   14      0.0000      0.0000      0.0000      0.0000      0.0000      0.0000
   15   5119.6915   5119.6915      0.0000      0.0000      0.0000   1599.7099   ! foundation
   16      0.0000      0.0000      0.0000      0.0000      0.0000      0.0000
   17      0.0000      0.0000      0.0000      0.0000      0.0000      0.0000
LOADS
!   N          Fx          Fy          Fz          Mx          My          Mz
    1      0.0000   -5119.6915      0.0000      0.0000      0.0000      0.0000   ! foundation
    2      0.0000      0.0000      0.0000      0.0000      0.0000      0.0000
    3      0.0000      0.0000      0.0000      0.0000      0.0000      0.0000
    4      0.0000      0.0000      0.0000      0.0000      0.0000      0.0000
    5      0.0000    -497.2949      0.0000      0.0000      0.0000      0.0000   ! Beam end
    6      0.0000      0.0000      0.0000      0.0000      0.0000      0.0000
    7      0.0000      0.0000      0.0000      0.0000      0.0000      0.0000
    8      0.0000   -3350.6261      0.0000      0.0000      0.0000      0.0000   ! Beam centre
    9      0.0000      0.0000      0.0000      0.0000      0.0000      0.0000
   10      0.0000      0.0000      0.0000      0.0000      0.0000      0.0000
   11      0.0000    -497.2949      0.0000      0.0000      0.0000      0.0000   ! Beam end
   12      0.0000      0.0000      0.0000      0.0000      0.0000      0.0000
   13      0.0000      0.0000      0.0000      0.0000      0.0000      0.0000
   14      0.0000      0.0000      0.0000      0.0000      0.0000      0.0000
   15      0.0000   -5119.6915      0.0000      0.0000      0.0000      0.0000   ! foundation
   16      0.0000      0.0000      0.0000      0.0000      0.0000      0.0000
   17      0.0000      0.0000      0.0000      0.0000      0.0000      0.0000
EQUAKE
!BERG      ISTART          DELTAT      ASCALE         END          VEL          DIS      TSCALE
    6         1.0    0.13428E-01       1.000        -1.0        0.000        0.000       1.000
```

Appendix C

Design example - Concrete wall building

C.1 Introduction

This appendix provides an example of the design process used to design the concrete wall buildings used throughout the dissertation. The example also doubles as an example of the integrated design procedure that was developed in Chapter 11. The buildings used in the dissertation differ slightly from the proposed design procedure in that many of the performance checks were not done since the equations were only developed after the buildings were analysed.

C.2 Preliminary design

Step 1 & 2: Determine building geometry, building use and importance level

All of the buildings used throughout the dissertation were intentionally kept very simple to allow the effects of soil-foundation-structure interaction (SFSI) to be easily identified. The example provided here is the six storey wall building shown in Figure C.1 with plan dimensions of 20 m in the N-S direction and 12 m in the E-W direction. All of the buildings had four walls in the N-S direction and were only assessed in this orientation. The remaining design input parameters are defined in Table C.1.

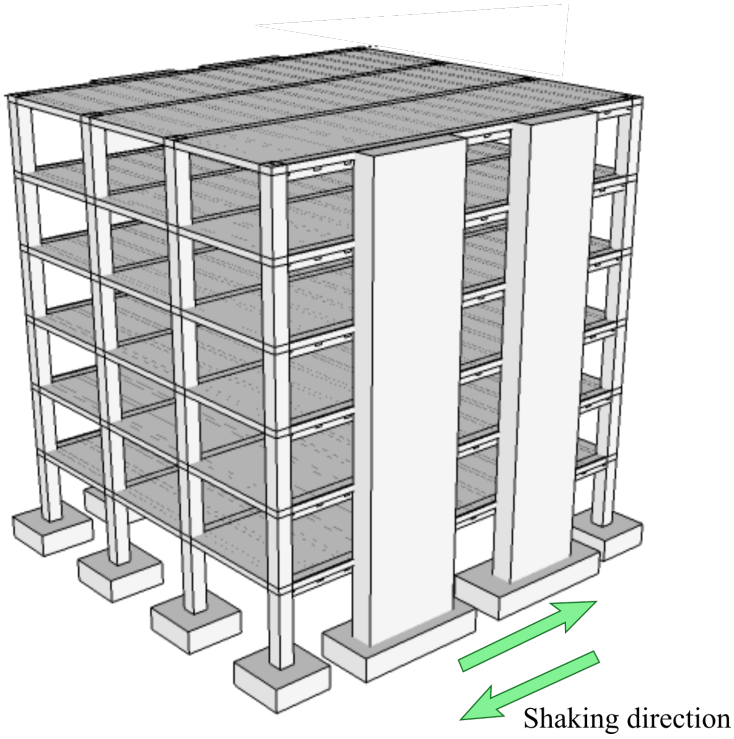

Figure C.1: Design example wall building

Table C.1: Wall design inputs

Parameter	Value
Number of storeys	6
Wall width	0.3 m
Storey heights	3.4 m
Wall height to depth ratio	6
Number of walls (n_{walls})	4
Building length ($L_{building}$)	20 m
Building width ($W_{building}$)	12 m
Footing height	$1.0 + height_{wall}/60$ m
Footing length to width ratio	2.5
Footing depth to breadth ratio	0.0
Target static bearing factor of safety	3.5
Live load (Q)	3 kPa
Dead load (G)	6 kPa
Seismic live load factor (Ψ_E)	0.4
Soil shear modulus (G)	40 MPa
Soil friction angle (ϕ)	30
Soil unit weight (γ_s)	18.0 kN/m^3
Concrete compression strength (f_c)	30 MPa
Rebar strength (f_y)	300 MPa
Rebar ultimate strength (f_u)	420 MPa
Young's modulus of rebar (E_s)	200 GPa

Step 3: Performance limits

The wall buildings used in this dissertation were only designed for the repairability limit state, and foundation permanent deformations checks were not done as the required equations were not available, however, for completeness the limits are provided along with the structural deformation in Table C.2.

The SFSI-induced settlement was set at 0.14m based on the repairability limit for angular distortion of 1.2% and assuming that an internal gravity column located at 6m from the wall would settle only half the amount of the wall.

Table C.2: Wall design inputs

Parameter	Limit
Total peak drift limit ($\theta_{t,lim}$)	2.5%
Superstructure inter-story drift limit ($\theta_{ss,lim}$)	2%
Superstructure residual inter-storey drift limit ($\theta_{ss,r,lim}$)	0.6%
SFSI-induced settlement ($\delta_{f,lim}$)	0.14m
Residual foundation rotation ($\theta_{f,r,lim}$)	0.6%

Notice that no limits are directly imposed on the peak foundation rotation, however, the limit on total peak drift and the limits on settlement and residual rotation put implicit limits on the peak value.

Step 4: Determine seismic hazard

The seismic hazard was defined as an acceleration spectrum using Equation C.1 based on the spectral shape (C_h) from NZS 1170.5:2004 (2004) for soil class C with a design hazard level of 0.4 and return period factor of 1.0, with no near fault amplification (as summarised in Table D.3).

Table C.3: Seismic hazard summary

Parameter	Value
Soil type	C
Design hazard level (Z)	0.4
Return period factor (R)	1.0
Near fault factor (N)	1.0

$$C(T) = C_h(T)ZRN \tag{C.1}$$

Where T is the period of vibration.

Step 5: Fixed base design

The storey masses per wall during seismic excitation were determined from Clause 4.2 from NZS 1170.5:2004 (2004):

$$M_{storey} = (G + Q\Psi_E)L_{building}W_{building}/n_{walls} \tag{C.2}$$

The first step of this design was to estimate the yield displaced shape, where a linear yield curvature profile was assumed and the yield curvature was taken as in Equation C.3, from Priestley et al. (2007).

$$\phi_y = \frac{2\epsilon_y}{L_{wall}} = 0.000882m^{-1} \tag{C.3}$$

The linear profile accounts for tension shift and different amounts of cracking up the wall causing a variation to the wall stiffness (in accordance with Priestley et al. (2007)) and results in the yield displacement defined as:

$$\Delta_{y,i} = \epsilon_y h_i^2 \left(1 - \frac{h_i}{3H_{wall}}\right) \tag{C.4}$$

Where:

$$\epsilon_y = \frac{f_y}{E_s} = 0.0015 \tag{C.5}$$

From the yield curvature and assumed curvature profile the yield drift can be defined as:

$$\theta_y = \frac{\epsilon_y H_{wall}}{L_{wall}} = 0.0090 \tag{C.6}$$

The plastic rotation was limited by both the total drift (Equation C.7) and the curvature limit to prevent excessive material strains (Equation C.8)

$$\theta_p \leq \theta_{ss,lim} - \theta_y \tag{C.7}$$

$$\theta_p \leq (\phi_{material} - \phi_y)L_p \tag{C.8}$$

Where the plastic hinge (L_p) can be defined as:

$$L_p = \max(kH_{wall} + L_{sp} + 0.1L_{wall}, 2L_{sp}) = 1.73m \tag{C.9}$$

Where the coefficient k was taken as:

$$k = \min(0.15(f_u/f_y) - 1), 0.06) \qquad = 0.06 \tag{C.10}$$

and the strain penetration length (L_{sp}) as:

$$L_{sp} = 0.022 f_y d_b[N, m] \qquad = 0.165m \tag{C.11}$$

From Equations C.7 and C.8 the plastic rotation was taken as:

$$\theta_p \qquad = 0.010 \tag{C.12}$$

And the plastic displacement was assumed to be a rigid rotation around the plastic hinge:

$$\Delta_{p,i} = \theta_p(h_i - (0.5L_p - L_{sp})) \tag{C.13}$$

The displacement at the design drift was taken as the sum of yield and plastic displacements:

$$\Delta_{t,i} = \Delta_{y,i} + \Delta_{p,i} \tag{C.14}$$

The displaced shape and distribution of masses was used to determine an equivalent single degree-of-freedom (SDOF) with an equivalent design displacement (Δ_d), effective mass (M_e) and effective height (H_e) using the following set of equations:

$$\Delta_d = \frac{\sum_{i=1}^{n} m_i^2 \Delta_{t,i}}{\sum_{i=1}^{n} m_i \Delta_{t,i}} \qquad = 0.241m \tag{C.15}$$

$$M_e = \frac{\sum i = 1^n m_i \Delta_{t,i}}{\Delta_d} \qquad = 189T \tag{C.16}$$

$$H_e = \frac{\sum_{i=1}^{n} m_i \Delta_{t,i} h_i}{\sum_{i=1}^{n} m_i \Delta_{t,i}} \qquad = 15.3m \tag{C.17}$$

Where the masses were for an individual wall. The following table summarises the calculations:

Table C.4: Wall conversion to SDOF

Storey	height [m]	mass [T]	Δ_y [m]	Δ_p [m]	Δ[m]	$m\Delta$	$m\Delta^2$	$m\Delta h$
1	3.4	42.2	0.005	0.030	0.035	1.46	0.05	5.0
2	6.8	42.2	0.018	0.067	0.085	3.60	0.31	24.5
3	10.2	42.2	0.038	0.105	0.143	6.03	0.86	61.5
4	13.6	42.2	0.063	0.142	0.205	8.68	1.78	118.0
5	17	42.2	0.092	0.179	0.271	11.46	3.11	194.9
6	20.4	42.2	0.122	0.217	0.339	14.33	4.86	292.2
Sum:						45.55	10.97	696.1

The equivalent SDOF yield displacement (Δ_y) can be defined using Equation D.8.

$$\Delta_y = \frac{\phi_y H_e^2}{2}\left(1 - \frac{H_e}{3H_{wall}}\right) = 0.0773m \tag{C.18}$$

And the system ductility can be determined by:

$$\mu = \frac{\Delta_d}{\Delta_y} = 3.12 \tag{C.19}$$

The displacement reduction factor was determined from Equation C.20 from Pennucci et al. (2011a).

$$\eta_{ss} = \sqrt{\frac{\pi\mu}{8.94\mu - 5.8}} = 0.666 \tag{C.20}$$

Which was used to reduce the design displacement spectra:

$$S_{d,red} = \eta_{ss} S_{d,design} \tag{C.21}$$

Where the design spectra was taken as that from NZS 1170.5:2004 (2004) and the secant period ($T_{secant} = 2.76$) was determined as the point where the design displacement matched the reduced spectrum.The base shear was determined based on the effective stiffness multiplied by the design displacement.

$$V_{base} = K_{secant}\Delta_d = 258kN \tag{C.22}$$

Where:

$$K_{secant} = \frac{4\pi^2 M_e}{T_{secant}^2} = 982kNm^{-1} \quad \text{(C.23)}$$

Finally the base shear was distributed up the structure according to the displacement and mass distribution:

$$F_i = \begin{cases} kV_{base}\dfrac{(m_i\Delta_i)}{\sum_{i=1}^{n}(m_i\Delta_i)} & \text{Floors 1 to n-1} \\ (1-k)V_{base} + kV_{base}\dfrac{(m_i\Delta_i)}{\sum_{i=1}^{n}(m_i\Delta_i)} & \text{Roof (Floor n)} \end{cases} \quad \text{(C.24)}$$

Where $k = 0.9$

The fixed base storey forces are summarised in Table D.5.

Table C.5: Fixed base storey forces

Storey	Force [kN]
1	7.4
2	18.4
3	30.8
4	44.3
5	58.5
6	99.0

Step 6: Estimate the superstructure residual drift The expression developed in Chapter 8 can be used to estimate the residual deformation. The vertical load (P) was taken as the effective mass times gravity and the initial stiffness (K_i) was determined from Equation C.26, with the post-yield stiffness ratio (r) taken as 0.05.

$$\frac{\theta_r}{\theta_p} = \frac{2}{3}(0.082 + 0.026\mu + 1.2\frac{P}{HK_i}) = 0.14 \quad \text{(C.25)}$$

$$K_i = \frac{\mu K_{secant}}{1 + r(\mu - 1)} = 2770kNm^{-1} \quad \text{(C.26)}$$

Step 7: Size foundations for static load conditions

Both the bearing capacity and static settlement should be checked during this step, however, for the parametric study the static settlement was ignored for simplicity and instead a variation on the static bearing capacity factor of safety was used to reflect the variation caused by

satisfying the static settlement.

The static bearing capacity equation from Salgado (2008) was used to determine suitable foundation dimensions where an ad-hoc piece of software was written to find the optimal foundation sizes to satisfy the bearing capacity. The static axial load was taken as the factored gravity loads using Equation C.27 from AS NZS 1170.1 2002 (2002).

$$N_G = (1.2G + 1.5\psi_a Q) \times Area_{tributary} = 3334kN \tag{C.27}$$

Where ψ_a is the area factor which was calculated as 0.46 and the tributary area was taken as the plan floor area multiplied by the total number of storeys divided by the number of walls (Equation C.28). Although in most cases this would be a considerably overestimation of the wall axial load, given that static settlement was not directly accounted for the assumption is consistently crude and provides a suitably simple way to size the foundations for the parametric study.

$$Area_{tributary} = \frac{L_{building} W_{building} n_{storeys}}{n_{walls}} \tag{C.28}$$

For the wall building in this example the satisfactory foundation sizes were determined as follows:

Foundation length (L_f): 5.6 m
Foundation width (W_f): 2.25 m
Foundation depth (D_f): 0.0 m

The soil ultimate bearing pressure was determined as 958kPa, resulting in an ultimate bearing capacity of 12,070kN.

The axial load during excitation was determined using the seismic factored gravity loads using Equation D.19 from AS NZS 1170.1 2002 (2002).

$$N_E = (G + \psi_a \psi_E Q) \times Area_{tributary} = 2308kN \tag{C.29}$$

The axial load ratio ($\tilde{N}$) was therefore taken as 5.25.

Step 8: Estimate the foundation peak rotation

The applied moment on the foundation can be estimated based on the fixed base storey forces:

$$M_f = \sum_{i=1}^{n} F_i(h_i + h_f) \qquad = 4428kNm \tag{C.30}$$

Where the footing height ($h_f = 3.4m$) from Table C.1. The elastic foundation rotational stiffness was found using Equation C.31 from Gazetas (1991).

$$K_{f,0} = \frac{G}{(1-v)} I_{by}^{0.75} \left(3(\frac{L}{B})^{0.15}\right).k_m \qquad = 2730MNm \tag{C.31}$$

Where v is the soil Piosson ratio taken as 0.3, I_{by} is the soil-foundation contact area moment of inertia and the k_m factor is a frequency dependent amplification factor, which was taken as 1.0. An initial estimate of the foundation rotation was made using the elastic stiffness:

$$\theta_{estimate} = \frac{M_f}{K_{f,0}} \qquad = 1.6mrad \tag{C.32}$$

The estimated foundation rotation was then used to estimate the secant rotational stiffness of the foundation using Equation C.33 developed in Chapter 6. Note that the walls were designed using the effective height, however, the MDOF studies in Chapter 9 revealed that the adjusted effective height (Equation C.36) should be used to account for the amplified base shear due to higher modes.

$$\frac{K_f}{K_{f,0}} = 0.8 - 0.04\log(\Phi) - 0.7(1 - \exp^{-0.18\Phi}) \qquad = 0.59 \tag{C.33}$$

$$\Phi = \left(\frac{\theta_f}{\theta_{uplift}}\right)^{1-0.2(L/H_{eff})} 10^{0.25(L/H_{eff})} \qquad = 1.81 \tag{C.34}$$

$$\theta_{uplift} = \frac{N \times L}{\alpha K_{MM,elastic}} e^{-\zeta N/N_{cap}} \qquad = 0.893 \tag{C.35}$$

$$H^{\star}_{eff} = H_{eff} \times \frac{V_{base}}{V^{o}_{base}} \tag{C.36}$$

An improved estimate of the foundation rotation was then obtained using the secant stiffness:

$$\theta_{estimate} = \frac{M_f}{K_f} \qquad = 2.7mrad \tag{C.37}$$

Step 9: Estimate the foundation residual deformations

The residual rotation and SFSI-induced settlement can be estimated using Equations C.38 and C.39 respectively developed in Chapter 7 and Chapter 9 and refined in Chapter 11. The adjusted effective height in Equation C.40 can be taken as one third of the effective height for the preliminary phase.

$$\theta_{f,r} = (0.025log_{10}(\theta_{f,global}) + 0.30)\theta_{f,global} = 0.63mrad \tag{C.38}$$

$$\delta = (0.353 + \frac{0.894}{\tilde{N}})L\theta_f s_v \qquad = 0.01m \tag{C.39}$$

$$s_v = \max(0.5 + 0.7\frac{L}{H^\star}, 1.0) \qquad = 1.3 \tag{C.40}$$

Step 10: Check that performance limits are satisfied

The performance limits were not check for the wall buildings used in the parametric study since many of the equations required to estimate the deformations had not been developed, however, in this example they are checked in Table C.6.

Table C.6: Preliminary performance checks

Parameter	Limit	Preliminary
Total peak drift limit (θ_t)	2.5%	2.2%
Superstructure inter-story drift limit (θ_{ss})	2%	1.9%
Superstructure residual inter-storey drift limit ($\theta_{ss,r}$)	0.6%	0.3%
SFSI-induced settlement (δ_f)	0.14m	0.1m
Residual foundation rotation ($\theta_{f,r}$)	0.6%	0.06%

Step 11: Resize the foundation if the performance limits are not meet

In this case the performance limits were satisfied so no changes were made to the foundation dimensions.

C.3 Full design

The full design procedure follows the design procedure outlined in Chapter 11.

Estimate the displacement profile

The estimated foundation rotation from the preliminary design was used to estimate the displacement from the foundation rotation (Equation D.31).

$$\Delta_{f,rot,i} = \theta_f h_i \tag{C.41}$$

The foundation shear deformation ($\Delta_{f,shear}$) was estimated based on the over strength base shear from the fixed base design and the effective foundation shear stiffness:

$$\Delta_{f,shear} = \frac{V^o_{base}}{K_{f,shear}} \qquad = 3.9mm \tag{C.42}$$

The effective foundation shear stiffness was taken as half of the elastic stiffness define in Equation D.33 from Gazetas (1991).

$$K_{f,shear,elastic} = K_y - \frac{0.2GL_f}{0.75 - v}\left(1 - \frac{W_f}{L_f}\right)k_v \qquad = 387MN \tag{C.43}$$

Where:

$$K_y = \frac{2GL_f}{(2-v)}\left[2 + 2.5\left(\frac{W_f}{L_f}\right)^{0.85}\right] \qquad = 417MN \tag{C.44}$$

and the frequency dependent coefficient k_v was taken as 1.0.

The superstructure deformation was recalculated using the same process as for the fixed base case (Equations C.3 - C.14), however the additional requirement that the total drift does not exceed the total limit ($\theta_{t,lim}$). To accomplish this the plastic rotation (θ_p) must also satisfy the following requirement:

$$\theta_p \leq \theta_{t,lim} - \theta_y - \theta_{r,rot.} \tag{C.45}$$

The system displacement profile was taken as the summation of the displacements from the superstructure, foundation rotation and foundation shear:

$$\Delta_{sys,i} = \Delta_{ss,i} + \Delta_{f,rot,i} + \Delta_{f,shear} \tag{C.46}$$

Determine the equivalent SDOF

The conversion to a SDOF was exactly the same as for the fixed base design above, except that the system displacement profile was used instead of the superstructure displacement profile.

$$\Delta_d = 0.283m \tag{C.47}$$

$$M_{eff} = 193T \tag{C.48}$$

$$H_{eff} = 16.5m \tag{C.49}$$

$$\Delta_y = 0.0761m \tag{C.50}$$

Determine displacement contributions

The displacement contributions from the superstructure, foundation rotation and foundation shear where all estimated at the effective height:

$$\Delta_{f,rot} = \theta_f H_e \qquad = 0.045m \tag{C.51}$$

$$\Delta_{f,shear} = \Delta_{f,shear} \qquad = 0.0013m \tag{C.52}$$

$$\Delta_{ss} = \Delta_d - \Delta_{f,rot} - \Delta_{f,shear} \qquad = 0.237m \tag{C.53}$$

Determine the displacement reduction factors

From Chapter 6 the shear deformation was set at 0.76 provided that the wall height to foundation length ratio exceeded 1.0.

The foundation rotation DRF was determined using Equation D.40 developed in Chapter 6.

$$\eta_{f,rot} = \sqrt{\frac{1.0}{1.0 + 5.0(1 - e^{-0.15\Phi})}} \qquad = 0.576 \tag{C.54}$$

The superstructure DRF can be defined just as for the fixed base design using Equation C.20, where the ductility was defined using the yield displacement from the fixed base design and the superstructure displacement from Equation C.53:

$$\mu = \frac{\Delta_{ss}}{\Delta_y} \qquad = 3.12 \tag{C.55}$$

$$\eta_{ss} \qquad = 0.666 \tag{C.56}$$

Determine system displacement reduction factor

The system DRF was determined using the displacement weighted average of the DRFs of each component:

$$\eta_{sys} = \frac{\eta_{ss}\Delta_{ss} + \eta_{f,rot}\Delta_{f,rot} + \eta_{f,shear}\Delta_{f,shear}}{\Delta_d} = 0.652 \quad \text{(C.57)}$$

Determine the secant period, base shear and storey forces

The secant period, base shear and storey forces were determined in the same was as for the fixed base design, however, this time there was no spectrum compatible value for the displacement, since the design displacement was larger than the plateau displacement. The design ductility was adjusted through iteration until a suitable value was found resulting in the following output values:

Design displacement (Δ_d)	0.25m
Effective mass (M_{eff})	194T
Effective height (H_{eff})	16.4m
Superstructure ductility (μ)	2.37
Superstructure DRF (η_{ss})	0.695
Foundation rotation DRF ($\eta_{f,rot.}$)	0.517
System DRF (η_{sys})	0.645
Foundation rotation (θ_f)	0.0044mrad
Secant period (T_{secant})	2.98 s
Base shear (V_{base})	240kN

The estimated foundation rotation was also checked and iterated to produce these values and since the base hinge moment was assumed to equal to the design moment, the foundation rotation could be calculated using the same expressions as from the preliminary design (Equations C.30 - C.37).

Table C.7: Storey forces

Storey	Force [kN]
0	0
1	8.5
2	18.1
3	29.1
4	40.9
5	53.4
6	90.3

Check the foundation rotation

Since the hinge moment was set to be equal to the nominal moment the foundation moment could be determined by extrapolating the moment down the base of the footing. The foundation rotation was then determined using the effective rotational stiffness and the foundation

moment which resulted in $\theta_f = 0.44\%$.

Calculate the foundation permanent deformations

The permanent foundation deformations were determined in the same manner as for the preliminary design using Equations C.38 and C.39.

$$\theta_{f,res} = 0.11\%$$

$$\delta_f = 0.013m$$

Check that performance limits are satisfied

Only the performance limits for the repairability limit state are checked for this example but all of the limit states should be checked.

Table C.8: Wall performance limits checks

Parameter	Limit	Final
Total peak drift limit (θ_t)	2.5%	2.1%
Superstructure inter-story drift limit (θ_{ss})	2%	1.6%
Superstructure residual inter-storey drift limit ($\theta_{ss,r}$)	0.6%	0.2%
SFSI-induced settlement (δ_f)	0.14m	0.13m
Residual foundation rotation ($\theta_{f,r}$)	0.6%	0.11%

All of the performance limits were satisfied so the design was completed.

Determine internal actions and size superstructure members

The wall base hinge was assumed to be equal to the nominal strength, however, if the wall section was properly detailed then there would be some variation from the nominal strength which should be used for the estimate of the foundation moment.

The rest of the wall was designed to remain elastic using the over-strength expression from DDBD:

$$M^o_{0.5H} = C_{1,T}\phi^o M_B = 2558kNm \quad \text{(C.58)}$$

$$C_{1,T} = 0.4 + 0.075T_i(\frac{\mu_{sys}}{\phi^o} - 1) \geq 0.4 = 0.68 \quad \text{(C.59)}$$

$$\mu_{sys} = \frac{\Delta_{sys}}{\Delta_y} = 3.3 \quad \text{(C.60)}$$

$$V^o_{Base} = \phi^o \omega_V V_{Base} = 257kN \quad \text{(C.61)}$$

$$\omega_V = 1 + \frac{\mu}{\phi^o} C_{2,T} = 2.2 \quad \text{(C.62)}$$

$$C_{2,T} = 0.067 + 0.4(T_i - 0.5) \leq 1.15 = 0.51 \quad \text{(C.63)}$$

$$V^o_n = C_3 V^o_{Base} = 100kN \quad \text{(C.64)}$$

$$C_3 = 0.9 - 0.3T_i \geq 0.3 = 0.42 \quad \text{(C.65)}$$

The initial period (T_i) was taken as the elastic first mode period of the system defined as follows:

$$K_{ss,eff} = \frac{V_{base}}{\Delta_{ss}} = 1336kNm^{-1} \quad \text{(C.66)}$$

$$K_{ss} = \frac{\mu K_{ss,eff}}{1 + r(\mu - 1)} = 2970kNm^{-1} \quad \text{(C.67)}$$

$$T_i = 2\pi\sqrt{M\left(\frac{1}{K_{f,rot.}} + \frac{1}{K_{f,rot.}} + \frac{1}{K_{f,rot.}}\right)} = 1.6s \quad \text{(C.68)}$$

C.4 Ruaumoko input file

```
Ruaumoko3D - 6 storey wall
! Author: Maxim Millen
! kN,m,s
    ! Info
    2       1       0       2       0       2       0       0       1       0       0       0
    8       8       8       5       1       3    9.80     5.0     5.0   0.00100 150.000  1.00
    0      20       0     1.0    10.0    10.0    10.0       1       2       1       0       0
   200.0     0.0     0.0     0.0   200.0     0.0
   10      10  0.0001     0.0     0.0     0.0     0.0     0.0     0.0     0.0    0.10
NODES
! No.    X-co    Y-co    Z-co  X-dsip  Y-disp  Z-disp  X-rot.  Y-rot.  Z-rot.  slaved  output  slave2
    1   0.000   0.000   0.000       0       0       1       1       1       0       0       0       0
    2   0.000   3.400   0.000       0       0       1       1       1       0       0       0       0
    3   0.000   6.800   0.000       0       0       1       1       1       0       0       0       0
    4   0.000  10.200   0.000       0       0       1       1       1       0       0       0       0
    5   0.000  13.600   0.000       0       0       1       1       1       0       0       0       0
    6   0.000  17.000   0.000       0       0       1       1       1       0       0       0       0
    7   0.000  20.400   0.000       0       0       1       1       1       0       0       0       0
    8   0.000  -1.340   0.000       1       1       1       1       1       1       0       0       0
DRIFT
```

```
    4    1    3
ELEMENTS
! No.  Member       I       J       K       L       M    IOUT
    1       1       1       2       0       0       Z       0
    2       2       2       3       0       0       Z       0
    3       3       3       4       0       0       Z       0
    4       4       4       5       0       0       Z       0
    5       5       5       6       0       0       Z       0
    6       6       6       7       0       0       Z       0
    7       7       8       1       8       1       Z       0
    8       8       8       1       8       1       Z       0
PROPS
    1      BEAM                    Structure
!       ITYPE       IBEAM       IPINZ       IPINY       ICOND       IHYST        ILOS       IDAMG         IGA       IDUCT
           1           1           0           0           0           4           0           0           0
0
!
!           E           G           A         Jxx         Izz         Iyy     Asz     Asy      Sy      Sz     WGT
   2.0000E+08  1.0000E+09  1.5096E-03  1.0000E+05  1.8115E-02  1.8115E-02   0.000   0.000   0.000   0.000   0.000
!
!       END1z       END2z       END1y       END2y        FJ1z        FJ2z        FJ1y        FJ2y          Y0
Z0
      0.0000      0.0000      0.0000      0.0000      0.0000      0.0000      0.0000      0.0000      0.0000      0.0000
!
!          RA          RT         RFz         RFy
      0.0100      0.0100    0.007125    0.007125
!
!          wH          nH          wH          nH
      0.8218      0.0000      0.8218      0.0000
!
!         PYT         PYC         TYp         TYn       alpha        IEND
   0.0000E+00  0.0000E+00       0.000       0.000       0.000       1.000
!
!          MYp          MYn          MZp          MZn          beta
    3.51531E+03  -3.51531E+03   0.00000E+00   0.00000E+00   0.00000E+00
!
!          MYp          MYn          MZp          MZn          beta
    0.00000E+00   0.00000E+00   0.00000E+00   0.00000E+00   0.00000E+00
!
!          ALFA          BETA            NF           KKK
         0.500         0.000          1.00            2
!

    2      BEAM                    Structure
!       ITYPE       IBEAM       IPINZ       IPINY       ICOND       IHYST        ILOS       IDAMG         IGA       IDUCT
           1           1           0           0           0           0           0           0           0
0
!
!           E           G           A         Jxx         Izz         Iyy     Asz     Asy      Sy      Sz     WGT
   2.0000E+08  1.0000E+09  1.5096E-03  1.0000E+05  1.8115E-02  1.8115E-02   0.000   0.000   0.000   0.000   0.000
!
!       END1z       END2z       END1y       END2y        FJ1z        FJ2z        FJ1y        FJ2y          Y0
Z0
      0.0000      0.0000      0.0000      0.0000      0.0000      0.0000      0.0000      0.0000      0.0000      0.0000
!

    3      BEAM                    Structure
!       ITYPE       IBEAM       IPINZ       IPINY       ICOND       IHYST        ILOS       IDAMG         IGA       IDUCT
           1           1           0           0           0           0           0           0           0
0
!
!           E           G           A         Jxx         Izz         Iyy     Asz     Asy      Sy      Sz     WGT
   2.0000E+08  1.0000E+09  1.5096E-03  1.0000E+05  1.8115E-02  1.8115E-02   0.000   0.000   0.000   0.000   0.000
!
!       END1z       END2z       END1y       END2y        FJ1z        FJ2z        FJ1y        FJ2y          Y0
Z0
      0.0000      0.0000      0.0000      0.0000      0.0000      0.0000      0.0000      0.0000      0.0000      0.0000
!

    4      BEAM                    Structure
!       ITYPE       IBEAM       IPINZ       IPINY       ICOND       IHYST        ILOS       IDAMG         IGA       IDUCT
           1           1           0           0           0           0           0           0           0
0
!
!           E           G           A         Jxx         Izz         Iyy     Asz     Asy      Sy      Sz     WGT
   2.0000E+08  1.0000E+09  1.5096E-03  1.0000E+05  1.8115E-02  1.8115E-02   0.000   0.000   0.000   0.000   0.000
```

```
!
!       END1z       END2z       END1y       END2y        FJ1z        FJ2z        FJ1y        FJ2y          Y0
Z0
      0.0000      0.0000      0.0000      0.0000      0.0000      0.0000      0.0000      0.0000      0.0000      0.0000
!

    5      BEAM                    Structure
!       ITYPE       IBEAM       IPINZ       IPINY       ICOND       IHYST        ILOS       IDAMG         IGA       IDUCT
           1           1           0           0           0           0           0           0           0
0
!
!           E           G           A         Jxx         Izz         Iyy     Asz     Asy      Sy      Sz     WGT
   2.0000E+08  1.0000E+09  1.5096E-03  1.0000E+05  1.8115E-02  1.8115E-02   0.000   0.000   0.000   0.000   0.000
!
!       END1z       END2z       END1y       END2y        FJ1z        FJ2z        FJ1y        FJ2y          Y0
Z0
      0.0000      0.0000      0.0000      0.0000      0.0000      0.0000      0.0000      0.0000      0.0000      0.0000
!

    6      BEAM                    Structure
!       ITYPE       IBEAM       IPINZ       IPINY       ICOND       IHYST        ILOS       IDAMG         IGA       IDUCT
           1           1           0           0           0           0           0           0           0
0
!
!           E           G           A         Jxx         Izz         Iyy     Asz     Asy      Sy      Sz     WGT
   2.0000E+08  1.0000E+09  1.5096E-03  1.0000E+05  1.8115E-02  1.8115E-02   0.000   0.000   0.000   0.000   0.000
!
!       END1z       END2z       END1y       END2y        FJ1z        FJ2z        FJ1y        FJ2y          Y0
Z0
      0.0000      0.0000      0.0000      0.0000      0.0000      0.0000      0.0000      0.0000      0.0000      0.0000
!

    7     MACRO                 SSI -element
! JPLA SL        DIAM        QQMAX         KNN         KVV         KMM     PSI     KSI   PL_P1   PL_P2     WGT  IPRNT  ITRAK
     1  0  5.6250E+00  1.2123E+04  4.8361E+05  3.8656E+05  2.7309E+06   0.545   0.480   0.200   1.000   0.000      0
1
!
!   ALPHA    BETA   GAMMA   DELTA   EPSIL    ZETA NON_ASS    TOPL     min_lam    TENS    FRIC    MAPP  UPLIFT
     4.00    2.00    1.00    1.00    0.50    1.50   1.000  100.00  1.0000E+04      No     Yes     Yes      No
!
!    K_Alfa    K_Beta     G_Lam     G_Chi      G_Xi
       1.00      1.00      2.50      3.00      0.95
!

    8    DAMPER                 SSI -damping
! ITYP          C1          C2     C3     C4     C5          C6 GAP_P GAP_N  ALFA LIMIT    SL   KOP    Y0    Z0
     0  5.3038E+03  3.4305E+03   0.00   0.00   0.00  6.9923E+03   0.0   0.0   0.0   1.0  -0.5   0.0   0.0   0.0
!
  4.6169E+02  4.6169E+02  1.0000E+08  1.0000E+08   0.00   0.00   0.00   0.00   0.00   0.00  1.0000E+08  1.0000E+08

WEIGHTS
    1   0.000000E+00   2.308429E+03   0.000000E+00   0.000000E+00   0.000000E+00   0.000000E+00
    2   4.140000E+02   0.000000E+00   0.000000E+00   0.000000E+00   0.000000E+00   0.000000E+00
    3   4.140000E+02   0.000000E+00   0.000000E+00   0.000000E+00   0.000000E+00   0.000000E+00
    4   4.140000E+02   0.000000E+00   0.000000E+00   0.000000E+00   0.000000E+00   0.000000E+00
    5   4.140000E+02   0.000000E+00   0.000000E+00   0.000000E+00   0.000000E+00   0.000000E+00
    6   4.140000E+02   0.000000E+00   0.000000E+00   0.000000E+00   0.000000E+00   0.000000E+00
    7   4.140000E+02   0.000000E+00   0.000000E+00   0.000000E+00   0.000000E+00   0.000000E+00
    8   0.000000E+00   0.000000E+00   0.000000E+00   0.000000E+00   0.000000E+00   0.000000E+00
LOADS
    1   0.000000E+00  -2.308429E+03   0.000000E+00   0.000000E+00   0.000000E+00   0.000000E+00
    2   0.000000E+00  -0.000000E+00   0.000000E+00   0.000000E+00   0.000000E+00   0.000000E+00
    3   0.000000E+00  -0.000000E+00   0.000000E+00   0.000000E+00   0.000000E+00   0.000000E+00
    4   0.000000E+00  -0.000000E+00   0.000000E+00   0.000000E+00   0.000000E+00   0.000000E+00
    5   0.000000E+00  -0.000000E+00   0.000000E+00   0.000000E+00   0.000000E+00   0.000000E+00
    6   0.000000E+00  -0.000000E+00   0.000000E+00   0.000000E+00   0.000000E+00   0.000000E+00
    7   0.000000E+00  -0.000000E+00   0.000000E+00   0.000000E+00   0.000000E+00   0.000000E+00
    8   0.000000E+00   0.000000E+00   0.000000E+00   0.000000E+00   0.000000E+00   0.000000E+00
EQUAKE
        6       1        0.00100        0.29904        -1    0.0000    0.0000    1.0000
```

Appendix D

Design example - Concrete frame building

D.1 Introduction

This appendix provides an example of the design process used to design the frame buildings used throughout this dissertation. The design process follows the integrated design procedure outlined in Chapter 11 with a couple of minor simplifications.

D.2 Preliminary design

Step 1 & 2: Determine building geometry, building use and importance level

All of the buildings used throughout the dissertation were intentionally kept very simple to allow the effects of soil-foundation-structure interaction (SFSI) to be easily identified. The example provided here is the six storey frame building shown in Figure D.1 with plan dimensions of 20 m in the N-S direction and 12 m in the E-W direction. All of the buildings had two frames in the N-S direction and were only assessed in this orientation. The remaining design input parameters are defined in Table D.1.

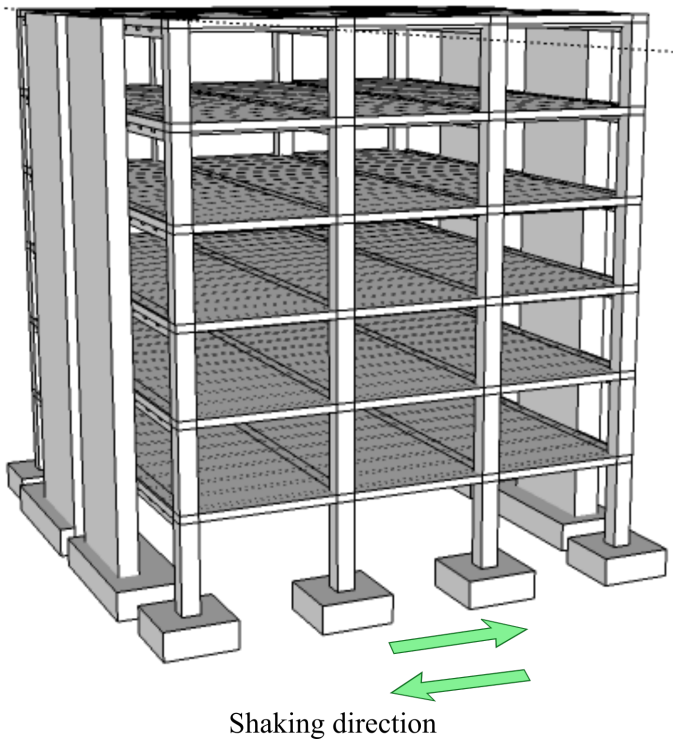

Figure D.1: Design example building

Table D.1: Frame design inputs

Parameter	Range
Number of storeys (n_s)	6
Number of bays (n_b)	3
Bay lengths (l_b)	6.0 m
Storey heights	3.4 m
Beam depth (h_b)	0.7
Beam width	$0.8h_b$
Column depth (h_c)	0.86
Column width	h_c
Building width $W_{building}$	20 m
Number of frames	2
Footing height	1.0 m
Footing length to width ratio	1.0
Footing depth to breadth ratio	0.3
Target static bearing factor of safety	5.0
Soil type	C
Design hazard level	0.3
Live load	3 kPa
Dead load	6 kPa
Total peak drift (θ_t)	0.025
Superstructure inter-story drift (θ_{ss})	0.02
Soil shear modulus (G)	40 MPa
Soil friction angle (ϕ)	38
Soil unit weight (γ_s)	18.0 kN/m^3
Concrete compression strength (f_c)	30 MPa
Rebar strength (f_y)	300 MPa

Step 3: Performance limits

The frame buildings used in this dissertation were only designed for the repairability limit state, and only this step is shown here, however, the designer should check all of the limit states. Although the foundation deformation limits were not used for the design of the frame buildings in Chapter 10 because the predictions equations did not exist, the deformation limits are provided in Table D.2 to demonstrate how they are used in the integrated design procedure. The SFSI-induced settlement was set at 0.14m based on the repairability limit for angular distortion of 1.2% and assuming that some internal gravity column located at 6m from the footing would settle only half the amount of the footing.

Table D.2: frame design inputs

Parameter	Limit
Total peak drift limit ($\theta_{t,lim}$)	2.5%
Superstructure inter-story drift limit ($\theta_{ss,lim}$)	2%
Superstructure residual inter-storey drift limit ($\theta_{ss,r,lim}$)	0.6%
SFSI-induced settlement (δ_f)	0.14m
Residual foundation rotation ($\theta_{f,r}$)	0.6%

Notice that no limits are directly imposed on the peak foundation rotation, however, the limit on total peak drift and the limits on settlement and residual rotation put implicit limits on the peak value.

Step 4: Determine seismic hazard

The seismic hazard was defined as an acceleration spectrum using Equation C.1 based on the spectral shape (C_h) from NZS 1170.5:2004 (2004) for soil class C with a design hazard level of 0.4 and return period factor of 1.0, with no near fault amplification (as summarised in Table D.3).

Table D.3: Seismic hazard summary

Parameter	Value
Soil type	C
Design hazard level (Z)	0.4
Return period factor (R)	1.0
Near fault factor (N)	1.0

$$C(T) = C_h(T)ZRN \tag{D.1}$$

Where T is the period of vibration.

(D.2)

Step 5: Fixed base design

The storey masses per frame during seismic excitation were determined from Clause 4.2 from NZS 1170.5:2004 (2004):

$$M_{storey} = (G + Q\Psi_E)L_{building}W_{building}/n_{frames} \tag{D.3}$$

The first step of this design was to estimate the design displaced shape using Equation D.4 from Sullivan et al. (2012):

$$\Delta_{t,i} = \theta_c h_i \frac{4H_n - h_i}{4H_n - h_1} \tag{D.4}$$

The displaced shape and distribution of masses was used to determine an equivalent single degree-of-freedom (SDOF) with an equivalent design displacement (Δ_d), yield displacement (Δ_y), effective mass (M_e) and effective height (H_e) using the following set of equations:

$$\Delta_d = \frac{\sum_{i=1}^{n} m_i^2 \Delta_{t,i}}{\sum_{i=1}^{n} m_i \Delta_{t,i}} \tag{D.5}$$

$$M_e = \frac{\sum i = 1^n m_i \Delta_{t,i}}{\Delta_d} \tag{D.6}$$

$$H_e = \frac{\sum_{i=1}^{n} m_i \Delta_{t,i} h_i}{\sum_{i=1}^{n} m_i \Delta_{t,i}} \tag{D.7}$$

Where the masses were for an individual frame. The following table summarises the calculations:

Table D.4: Frame conversion to SDOF

Storey	height [m]	mass [T]	Δ[m]	$m\Delta$	$m\Delta^2$	$m\Delta h$
1	3.4	126.7	0.068	8.62	0.59	29.3
2	6.8	126.7	0.130	16.49	2.14	112.1
3	10.2	126.7	0.186	23.61	4.40	240.8
4	13.6	126.7	0.237	29.98	7.09	407.7
5	17.0	126.7	0.281	35.60	10.00	605.1
6	20.4	126.7	0.319	40.47	12.92	825.5
			Sum:	154.75	37.14	2220.5

The equivalent SDOF yield displacement (Δ_y) can be defined based on the effective height and the yield rotation (θ_y):

$$\Delta_y = \theta_y H_{eff} \qquad = 0.081m \tag{D.8}$$

Where the expression from Priestley et al. (2007) can be used to approximate the yield rotation based on the rebar yield strain, bay length and beam depth:

$$\theta_y = 0.5\epsilon_y L_{bay}/h_b \qquad = 0.56\% \tag{D.9}$$

And the system ductility can be determined by:

$$\mu = \frac{\Delta_d}{\Delta_y} \qquad = 3.0 \tag{D.10}$$

The displacement reduction factor was determined from Equation C.20 from Pennucci et al. (2011a).

$$\eta_{ss} = \sqrt{\frac{\pi\mu}{11.04\mu - 7.9}} \qquad = 0.61 \tag{D.11}$$

Which was used to reduce the design displacement spectra:

$$S_{d,red} = \eta_{ss} S_{d,design} \tag{D.12}$$

Where the design spectra was taken as that from NZS 1170.5:2004 (2004) and the secant period was determined as the point where the design displacement matched the reduced spectrum. The base shear was determined based on the effective stiffness multiplied by the design displacement.

$$V_{base} = K_{secant}\Delta_d \qquad = 683kN \tag{D.13}$$

Where:

$$K_{secant} = \frac{4\pi^2 M_e}{T_{secant}^2} \qquad = 2846kNm^{-1} \tag{D.14}$$

Finally the base shear was distributed up the structure according to the displacement and mass distribution:

$$F_i = V_{base}\frac{(m_i\Delta_i)}{\sum_{i=1}^{n}(m_i\Delta_i)} \tag{D.15}$$

The fixed base storey forces are summarised in Table D.5.

Table D.5: Fixed base storey forces

Storey	Force [kN]
1	38.0
2	72.8
3	104
4	132
5	157
6	179

Step 6: Estimate the superstructure residual drift

The residual deformation for frame structures was not quantified accurately in this dissertation. The parametric study structures led to a residual drift of approximately 15% of the peak drift but this was for a very small sample set, where there were issues with the macro-element model and P-delta effects were not included in the analysis.

Step 7: Size foundations for static load conditions

Both the bearing capacity and static settlement should be checked during this step, however, the static settlement was ignored for simplicity and the static bearing capacity factor of safety was set at 3.0.

The static bearing capacity equation from Salgado (2008) was used to determine suitable foundation dimensions where an ad-hoc piece of software was written to find the optimal foundation sizes to satisfy the bearing capacity. The footing depth to breadth ratio only applied to the exterior footings, while the interior footings were set to have the same depth as the interior footings. The static axial load was taken as the factored gravity loads using Equation C.27 from AS NZS 1170.1 2002 (2002).

$$N_G = (1.2G + 1.5\psi_a Q) \times Area_{tributary} \tag{D.16}$$

Where the tributary area was taken as the floor area closest to that column. Although in most cases this would be a considerably overestimation of the frame axial load, given that static settlement was not directly accounted for the assumption is consistently crude and provides a suitable simple way to size the foundations for the parametric study.

$$Area_{tributary,int.} = \frac{L_{building} W_{building} n_{storeys}}{n_{frames} n_{bays}} \tag{D.17}$$

$$Area_{tributary,ext.} = 0.5 Area_{tributary,int.} \tag{D.18}$$

For the frame building in this example the suitable foundation sizes were determined as follows:

	Interior	Exterior
Gravity load (N_G)	6518 kN	3334 kN
Foundation length (L_f)	3.8 m	2.85 m
Foundation width (W_f)	3.8 m	2.85 m
Foundation depth (D_f)	0.85 m	0.85m
Soil ultimate bearing pressure (q_{ult})	1390 kPa	1260 kPa

The axial load during excitation was determined using the seismic factored gravity loads using Equation D.19 from AS NZS 1170.1 2002 (2002).

$$N_{E,int.} = (G + \psi_a \psi_E Q) \times Area_{tributary} \quad = 4590kN N_{E,ext.} \quad = 2310kN \tag{D.19}$$

The global axial load ratio ($\tilde{N}$) was therefore taken as the sum of the bearing capacities divided by the sum of the axial loads ($N = 13790kN$) resulting $\tilde{N} = 4.4$.

Step 8: Estimate the foundation peak rotation

The applied moment on the foundation can be estimated based on the fixed base storey forces:

$$M_f = \sum_{i=1}^{n} F_i(h_i + h_f) \quad = 9800kNm \tag{D.20}$$

The expected level of foundation rotation was determined based on elastic foundation rotational stiffness ((K_f) and the overturning moment:

$$\theta_{f,global} = \frac{M_{OT}}{K_{f,0}} \quad = 0.27mrad \tag{D.21}$$

The elastic rotation stiffness was defined based on the expression from Gazetas (1991):

$$K_{f,0} = \frac{G}{(1-v)} I_{by}^{0.75} \left(3(\frac{L}{B})^{0.15}\right).k_m \quad = 36,258,000kNm^{-1} \tag{D.22}$$

Where G is the soil shear modulus, v is the Soil Piossons ratio, k_m the frequency dependant stiffness coefficient which was taken as 1.0 and I_y was the rotational area moment of inertia:

$$I_y = \sum_{i=1}^{n_footings} \frac{L_{f,i}^3 B_{f,i}}{12} + Area_{f,i} d_i^2 \tag{D.23}$$

The rotational stiffness can be updated using the stiffness degradation expression derived in Chapter 6, although this is not really correct as isolated footing have a different plastic response compared to a rigid raft.

$$\frac{K_f}{K_{f,0}} = 0.8 - 0.04\log(\Phi) - 0.7(1 - \exp^{-0.18\Phi}) \qquad = 0.75 \tag{D.24}$$

The corrected normalised rotation can be determined based on the ratio of building length to effective height (L/H) and the foundation rotation ($\theta_{f,global}$) and the pseudo uplift angle (θ_{uplift}):

$$\Phi = \left(\frac{\theta_{f,global}}{\theta_{uplift}}\right)^{1-0.2(L/H)} 10^{0.25(L/H)} \qquad = 0.54 \tag{D.25}$$

The pseudo uplift angle can be calculated using the following expression, where $\zeta = 1.5$ and α was taken as 3.0 to account for the distributed supports as discussed in Chapter 10 Section 10.2.1.

$$\theta_{uplift} = \frac{N \times L}{\alpha K_{f_0}} e^{-\zeta N/N_{cap}} \qquad = 0.0016rad \tag{D.26}$$

The updated rotational stiffness was then used to recalculate the foundation rotation.

$$\theta_{f,global} = \frac{M_{OT}}{K_f} \qquad = 0.36mrad \tag{D.27}$$

Step 9: Estimate the foundation residual deformations

The residual global rotation and global SFSI-induced settlement can be estimated using Equations D.28 and D.29 respectively developed in Chapter 7. Although the settlement of the foundation largely comes from the local footing deformations.

$$\theta_{f,r} = (0.025log_{10}(\theta_{f,global}) + 0.30)\theta_{f,global} = 0.077mrad \tag{D.28}$$

$$\delta = (0.353 + \frac{0.894}{\tilde{N}})L\theta_f \qquad = 3mm \tag{D.29}$$

$$\tag{D.30}$$

Step 10: Check that performance limits are satisfied

The performance limits were not check for the frame buildings used in the parametric study

since many of the equations required to estimate the deformations had not been developed, however, in this example they are checked in Table D.6.

Table D.6: frame design inputs

Parameter	Limit	Preliminary
Total peak drift limit ($\theta_{t,lim}$)	2.5%	2.0%
Superstructure inter-story drift limit ($\theta_{ss,lim}$)	2%	2.0%
Superstructure residual inter-storey drift limit ($\theta_{ss,r,lim}$)	0.6%	NA
SFSI-induced settlement (δ_f)	0.12m	0.003m
Residual foundation rotation ($\theta_{f,r}$)	0.6%	0.0%

Step 11: Resize the foundation if the performance limits are not meet

In this case the performance limits were satisfied so no changes were made to the foundation dimensions.

D.3 Full design

The full design procedure follows the design procedure outlined in Chapter 11.

Estimate the displacement profile

The estimated foundation rotation from the preliminary design was used to estimate the displacement from the foundation rotation (Equation D.31).

$$\Delta_{f,rot,i} = \theta_f h_i \tag{D.31}$$

The foundation shear deformation ($\Delta_{f,shear}$) was estimated based on the base shear from the fixed base and the effective foundation shear stiffness:

$$\Delta_{f,shear} = \frac{V_{base}}{K_{f,shear}} \tag{D.32}$$

The effective foundation shear stiffness was taken as half of the elastic stiffness define in Equation D.33 from Gazetas (1991).

$$K_{f,shear,elastic} = K_y - \frac{0.2GL_f}{0.75 - v}\left(1 - \frac{W_f}{L_f}\right) \tag{D.33}$$

Where:

$$K_y = \frac{2GL_f}{(2-v)}\left[2 + 2.5\left(\frac{W_f}{L_f}\right)^{0.85}\right] \tag{D.34}$$

and the frequency dependent coefficient k_v was taken as 1.0.

The system displacement profile was taken as the summation of the displacements from the superstructure, foundation rotation and foundation shear:

$$\Delta_{sys,i} = \Delta_{ss,i} + \Delta_{f,rot,i} + \Delta_{f,shear} \tag{D.35}$$

Determine the equivalent SDOF

The conversion to a SDOF was exactly the same as for the fixed base design above, except that the system displacement profile was used instead of the superstructure displacement profile. The results are summarised as follows

Δ_d = 0.26 m
H_{eff} = 15.2 m
M_{eff} = 663 T
Δ_y = 0.086 m

Determine displacement contributions

The displacement contributions from the superstructure, foundation rotation and foundation shear where all estimated at the effective height. It can clearly be seen that the foundation deformations are very small.

$$\Delta_{f,rot} = \theta_f H_e = 0.0045m \tag{D.36}$$

$$\Delta_{f,shear} = \Delta_{f,shear} = 0.0m \tag{D.37}$$

$$\Delta_{ss} = \Delta_d - \Delta_{f,rot} - \Delta_{f,shear} = 0.26m \tag{D.38}$$

$$\tag{D.39}$$

Determine the displacement reduction factors

From Chapter 6 the shear deformation was set at 0.76 provided that the frame height to foundation length ratio exceeded 1.0.

The foundation rotation DRF was determined using Equation D.40 developed in Chapter 6.

$$\eta_{f,rot} = \sqrt{\frac{1.0}{1.0 + 5.0(1 - e^{-0.15\Phi})}} \qquad = 0.85 \qquad \text{(D.40)}$$

The superstructure DRF can be defined just as for the fixed base design using Equation D.11, where the ductility was defined using the yield displacement from the fixed base design and the superstructure displacement from Equation C.53:

$$\mu = \frac{\Delta_{ss}}{\Delta_y} \qquad = 3.0 \qquad \text{(D.41)}$$

$$\eta_{ss} = 0.61 \qquad \text{(D.42)}$$

Determine system displacement reduction factor

The system DRF was determined using the displacement weighted average of the DRFs of each component. Since the foundation deformations were so small the system DRF was essentially equal to the superstructure DRF.

$$\eta_{sys} = \frac{\eta_{ss}\Delta_{ss} + \eta_{f,rot}\Delta_{f,rot} + \eta_{f,shear}\Delta_{f,shear}}{\Delta_d} \qquad = 0.62 \qquad \text{(D.43)}$$

Determine the secant period, base shear and storey forces

The secant period, base shear and storey forces were determined in the same was as for the fixed base design, however, this time there was no spectrum compatible value for the displacement, since the design displacement was larger than the plateau displacement. The design ductility was adjusted through iteration until a suitable value was found and the predicted foundation rotation was consistent, resulting in the following output values:

Design displacement (Δ_d)	0.24m
Effective mass (M_{eff})	663T
Effective height (H_{eff})	15.2m
Superstructure ductility (μ)	2.77
Superstructure DRF (η_{ss})	0.62
Foundation rotation DRF ($\eta_{f,rot.}$)	0.82
System DRF (η_{sys})	0.62
Foundation rotation (θ_f)	0.0004mrad
Secant period (T_{secant})	2.98 s
Base shear (V_{base})	720kN

Determine internal actions and size superstructure members

The storey forces were distributed up the structure in the same manner as for the preliminary design and the moment equilibrium method was used to determine the internal actions. Table D.7 summarises the storey forces and the column moments for the beam, which were then interpolated to determine the column face moments.

Table D.7: Storey forces

Storey	Force [kN]	Beam moment [kNm]
1	48.1	349
2	80.8	325
3	111	287
4	137	233
5	161	167
6	182	88.4

The column base moments were 490 kNm and 245 kNm for the interior and exterior columns respectively.

Calculate the footing deformations

Since the hinge values were assumed to equal to the design moment, the footing moment could be calculated by extrapolating the column base moment down to the footings and the footing rotation could be determined using the effective rotational stiffness. The residual deformations we determined based on the single support formulas with no correction to account for the additional vertical load due to frame action. The results are summarised below:

	Interior	Exterior
M_{foot}	968 kNm	484 kNm
K_f^0	1.46 $\times 10^6$ kNm	0.62 $\times 10^6$ kNm
θ_f	0.9mrad	1.2mrad
δ_f	3 mm	2 mm
$\theta_{f,res}$	0.1mrad	0.1mrad

Since the footing deformations were so small the performance limits were all satisfied, which concludes the design.

D.4 Ruaumoko input file

```
Ruaumoko3D - 6 storey, 3 bay
! Author: Maxim Millen
! kN,m,s
! Info
    2       1       0       2       0       0       0       0       1       0
   32      50      50       5       1       3    9.80     5.0     5.0   2.000E-03 135.000    1.00
    0      20       0     1.0     2.0     2.0     2.0       1       6       1       1       0
     1.0     0.0     0.0     0.0     1.0     0.0
```

```
   10        5  0.0010      0.0      0.0      0.0      0.0      0.0      0.0      0.0     0.10
NODES
    1   0.000    0.000    0.000        0        0        1        1        1        0        0        0        0
    2   6.000    0.000    0.000        0        0        1        1        1        0        0        0        0
    3  12.000    0.000    0.000        0        0        1        1        1        0        0        0        0
    4  18.000    0.000    0.000        0        0        1        1        1        0        0        0        0
    5   0.000    3.400    0.000        0        0        1        1        1        0        0        0        0
    6   6.000    3.400    0.000        0        0        1        1        1        0        0        0        0
    7  12.000    3.400    0.000        0        0        1        1        1        0        0        0        0
    8  18.000    3.400    0.000        0        0        1        1        1        0        0        0        0
    9   0.000    6.800    0.000        0        0        1        1        1        0        0        0        0
   10   6.000    6.800    0.000        0        0        1        1        1        0        0        0        0
   11  12.000    6.800    0.000        0        0        1        1        1        0        0        0        0
   12  18.000    6.800    0.000        0        0        1        1        1        0        0        0        0
   13   0.000   10.200    0.000        0        0        1        1        1        0        0        0        0
   14   6.000   10.200    0.000        0        0        1        1        1        0        0        0        0
   15  12.000   10.200    0.000        0        0        1        1        1        0        0        0        0
   16  18.000   10.200    0.000        0        0        1        1        1        0        0        0        0
   17   0.000   13.600    0.000        0        0        1        1        1        0        0        0        0
   18   6.000   13.600    0.000        0        0        1        1        1        0        0        0        0
   19  12.000   13.600    0.000        0        0        1        1        1        0        0        0        0
   20  18.000   13.600    0.000        0        0        1        1        1        0        0        0        0
   21   0.000   17.000    0.000        0        0        1        1        1        0        0        0        0
   22   6.000   17.000    0.000        0        0        1        1        1        0        0        0        0
   23  12.000   17.000    0.000        0        0        1        1        1        0        0        0        0
   24  18.000   17.000    0.000        0        0        1        1        1        0        0        0        0
   25   0.000   20.400    0.000        0        0        1        1        1        0        0        0        0
   26   6.000   20.400    0.000        0        0        1        1        1        0        0        0        0
   27  12.000   20.400    0.000        0        0        1        1        1        0        0        0        0
   28  18.000   20.400    0.000        0        0        1        1        1        0        0        0        0
   29   0.000   -1.100    0.000        1        1        1        1        1        1        0        0        0
   30   6.000   -1.100    0.000        1        1        1        1        1        1        0        0        0
   31  12.000   -1.100    0.000        1        1        1        1        1        1        0        0        0
   32  18.000   -1.100    0.000        1        1        1        1        1        1        0        0        0
DRIFT
    1    5    9   13   17   21   25
ELEMENTS
    1       1       1       5       0       0       Z       0
    2       2       2       6       0       0       Z       0
    3       3       3       7       0       0       Z       0
    4       4       4       8       0       0       Z       0
    5       5       5       9       0       0       Z       0
    6       6       6      10       0       0       Z       0
    7       7       7      11       0       0       Z       0
    8       8       8      12       0       0       Z       0
    9       9       9      13       0       0       Z       0
   10      10      10      14       0       0       Z       0
   11      11      11      15       0       0       Z       0
   12      12      12      16       0       0       Z       0
   13      13      13      17       0       0       Z       0
   14      14      14      18       0       0       Z       0
   15      15      15      19       0       0       Z       0
   16      16      16      20       0       0       Z       0
   17      17      17      21       0       0       Z       0
   18      18      18      22       0       0       Z       0
   19      19      19      23       0       0       Z       0
   20      20      20      24       0       0       Z       0
   21      21      21      25       0       0       Z       0
   22      22      22      26       0       0       Z       0
   23      23      23      27       0       0       Z       0
   24      24      24      28       0       0       Z       0
   25      25       5       6       0       0       Z       0
   26      26       6       7       0       0       Z       0
   27      27       7       8       0       0       Z       0
   28      28       9      10       0       0       Z       0
   29      29      10      11       0       0       Z       0
   30      30      11      12       0       0       Z       0
   31      31      13      14       0       0       Z       0
   32      32      14      15       0       0       Z       0
   33      33      15      16       0       0       Z       0
   34      34      17      18       0       0       Z       0
   35      35      18      19       0       0       Z       0
   36      36      19      20       0       0       Z       0
   37      37      21      22       0       0       Z       0
   38      38      22      23       0       0       Z       0
   39      39      23      24       0       0       Z       0
```

```
   40      40      25      26       0       0       Z       0
   41      41      26      27       0       0       Z       0
   42      42      27      28       0       0       Z       0
   43      43      29       1      29       1       Z       0
   44      44      30       2      30       2       Z       0
   45      45      31       3      31       3       Z       0
   46      46      32       4      32       4       Z       0
   47      47      29       1      29       1       Z       0
   48      48      30       2      30       2       Z       0
   49      49      31       3      31       3       Z       0
   50      50      32       4      32       4       Z       0
PROPS
  1      BEAM                    Col-Storey: 0 Col: 0
!       ITYPE       IBEAM       IPINZ       IPINY       ICOND       IHYST    ILOS   IDAMG     IGA   IDUCT
           1           1           0           0           0           4       0       0       0       0
!
!           E           G           A         Jxx         Izz         Iyy      Asz     Asy      Sy      Sz     WGT
   3.0151E+06  1.1800E+07  8.1000E-01  8.1000E+01  2.7337E-02  2.7337E-02   0.000   0.000   0.000   0.000   0.000
!
!       END1z       END2z       END1y       END2y        FJ1z        FJ2z    FJ1y    FJ2y      Y0      Z0
       0.0000      0.2667      0.0000      0.0000      0.0000      0.0000  0.0000  0.0000  0.0000  0.0000
!
!          RA          RT          RFz         RFy
       0.0500      0.0500      0.0000      0.0500
!
!          H1          H2          H3          H4
       0.9000      0.9000      0.9000      0.9000
!
!            PYT            PYC            TYp            TYn           ALFA      IEND
     0.0000E+00     0.0000E+00     0.0000E+00     0.0000E+00     0.0000E+00         1
!
!            MyP            MyN            MyP            MyN
     2.4810E+02    -2.4810E+02     2.4810E+02    -2.4810E+02
!
!             M1             M1             M1             M1
     0.0000E+00     0.0000E+00     0.0000E+00     0.0000E+00
!
!         TAK_AL       TAK_BETA         TAK_NF        TAK_KKK
          0.4000         0.6000         1.0000         2.0000
!

  2      BEAM                    Col-Storey: 0 Col: 1
!       ITYPE       IBEAM       IPINZ       IPINY       ICOND       IHYST    ILOS   IDAMG     IGA   IDUCT
           1           1           0           0           0           4       0       0       0       0
!
!           E           G           A         Jxx         Izz         Iyy      Asz     Asy      Sy      Sz     WGT
   3.0151E+06  1.1800E+07  8.1000E-01  8.1000E+01  2.7337E-02  2.7337E-02   0.000   0.000   0.000   0.000   0.000
!
!       END1z       END2z       END1y       END2y        FJ1z        FJ2z    FJ1y    FJ2y      Y0      Z0
       0.0000      0.2667      0.0000      0.0000      0.0000      0.0000  0.0000  0.0000  0.0000  0.0000
!
!          RA          RT          RFz         RFy
       0.0500      0.0500      0.0000      0.0500
!
!          H1          H2          H3          H4
       0.9000      0.9000      0.9000      0.9000
!
!            PYT            PYC            TYp            TYn           ALFA      IEND
     0.0000E+00     0.0000E+00     0.0000E+00     0.0000E+00     0.0000E+00         1
!
!            MyP            MyN            MyP            MyN
     4.9620E+02    -4.9620E+02     4.9620E+02    -4.9620E+02
!
!             M1             M1             M1             M1
     0.0000E+00     0.0000E+00     0.0000E+00     0.0000E+00
!
!         TAK_AL       TAK_BETA         TAK_NF        TAK_KKK
          0.4000         0.6000         1.0000         2.0000
!

  3      BEAM                    Col-Storey: 0 Col: 2
!       ITYPE       IBEAM       IPINZ       IPINY       ICOND       IHYST    ILOS   IDAMG     IGA   IDUCT
           1           1           0           0           0           4       0       0       0       0
!
!           E           G           A         Jxx         Izz         Iyy      Asz     Asy      Sy      Sz     WGT
   3.0151E+06  1.1800E+07  8.1000E-01  8.1000E+01  2.7337E-02  2.7337E-02   0.000   0.000   0.000   0.000   0.000
```

```
!
!       END1z       END2z       END1y       END2y        FJ1z        FJ2z    FJ1y    FJ2y      YO      ZO
       0.0000      0.2667      0.0000      0.0000      0.0000      0.0000  0.0000  0.0000  0.0000  0.0000
!
!          RA          RT          RFz         RFy
       0.0500      0.0500      0.0000      0.0500
!
!          H1          H2          H3          H4
       0.9000      0.9000      0.9000      0.9000
!
!           PYT           PYC           TYp           TYn           ALFA      IEND
     0.0000E+00    0.0000E+00    0.0000E+00    0.0000E+00    0.0000E+00         1
!
!           MyP           MyN           MyP           MyN
     4.9620E+02   -4.9620E+02    4.9620E+02   -4.9620E+02
!
!            M1            M1            M1            M1
     0.0000E+00    0.0000E+00    0.0000E+00    0.0000E+00
!
!         TAK_AL       TAK_BETA         TAK_NF       TAK_KKK
          0.4000         0.6000         1.0000        2.0000
!

  4      BEAM                    Col-Storey: 0 Col: 3
!       ITYPE       IBEAM       IPINZ       IPINY       ICOND       IHYST    ILOS   IDAMG     IGA   IDUCT
           1           1           0           0           0           4       0       0       0       0
!
!           E           G           A         Jxx         Izz         Iyy     Asz     Asy      Sy      Sz     WGT
   3.0151E+06  1.1800E+07  8.1000E-01  8.1000E+01  2.7337E-02  2.7337E-02   0.000   0.000   0.000   0.000   0.000
!
!       END1z       END2z       END1y       END2y        FJ1z        FJ2z    FJ1y    FJ2y      YO      ZO
       0.0000      0.2667      0.0000      0.0000      0.0000      0.0000  0.0000  0.0000  0.0000  0.0000
!
!          RA          RT          RFz         RFy
       0.0500      0.0500      0.0000      0.0500
!
!          H1          H2          H3          H4
       0.9000      0.9000      0.9000      0.9000
!
!           PYT           PYC           TYp           TYn           ALFA      IEND
     0.0000E+00    0.0000E+00    0.0000E+00    0.0000E+00    0.0000E+00         1
!
!           MyP           MyN           MyP           MyN
     2.4810E+02   -2.4810E+02    2.4810E+02   -2.4810E+02
!
!            M1            M1            M1            M1
     0.0000E+00    0.0000E+00    0.0000E+00    0.0000E+00
!
!         TAK_AL       TAK_BETA         TAK_NF       TAK_KKK
          0.4000         0.6000         1.0000        2.0000
!

  5      BEAM                    Col-Storey: 1 Col: 0
!       ITYPE       IBEAM       IPINZ       IPINY       ICOND       IHYST    ILOS   IDAMG     IGA   IDUCT
           1           1           0           0           0           0       0       0       0       0
!
!           E           G           A         Jxx         Izz         Iyy     Asz     Asy      Sy      Sz     WGT
   3.0151E+06  1.0629E+10  8.1000E-01  8.1000E+01  3.2805E-02  3.2805E-02   0.000   0.000   0.000   0.000   0.000
!
!       END1z       END2z       END1y       END2y        FJ1z        FJ2z    FJ1y    FJ2y      YO      ZO
       0.2667      0.2667      0.0000      0.0000      0.0000      0.0000  0.0000  0.0000  0.0000  0.0000
!

  6      BEAM                    Col-Storey: 1 Col: 1
!       ITYPE       IBEAM       IPINZ       IPINY       ICOND       IHYST    ILOS   IDAMG     IGA   IDUCT
           1           1           0           0           0           0       0       0       0       0
!
!           E           G           A         Jxx         Izz         Iyy     Asz     Asy      Sy      Sz     WGT
   3.0151E+06  1.0629E+10  8.1000E-01  8.1000E+01  3.2805E-02  3.2805E-02   0.000   0.000   0.000   0.000   0.000
!
!       END1z       END2z       END1y       END2y        FJ1z        FJ2z    FJ1y    FJ2y      YO      ZO
       0.2667      0.2667      0.0000      0.0000      0.0000      0.0000  0.0000  0.0000  0.0000  0.0000
!

  7      BEAM                    Col-Storey: 1 Col: 2
!       ITYPE       IBEAM       IPINZ       IPINY       ICOND       IHYST    ILOS   IDAMG     IGA   IDUCT
```

```
           1           1           0           0           0           0       0       0       0       0
!
!           E           G           A         Jxx         Izz         Iyy     Asz     Asy      Sy      Sz     WGT
   3.0151E+06  1.0629E+10  8.1000E-01  8.1000E+01  3.2805E-02  3.2805E-02   0.000   0.000   0.000   0.000   0.000
!
!       END1z       END2z       END1y       END2y        FJ1z        FJ2z    FJ1y    FJ2y      YO      ZO
      0.2667      0.2667      0.0000      0.0000      0.0000      0.0000  0.0000  0.0000  0.0000  0.0000
!

  8      BEAM                    Col-Storey: 1 Col: 3
!       ITYPE       IBEAM       IPINZ       IPINY       ICOND       IHYST    ILOS   IDAMG     IGA   IDUCT
           1           1           0           0           0           0       0       0       0       0
!
!           E           G           A         Jxx         Izz         Iyy     Asz     Asy      Sy      Sz     WGT
   3.0151E+06  1.0629E+10  8.1000E-01  8.1000E+01  3.2805E-02  3.2805E-02   0.000   0.000   0.000   0.000   0.000
!
!       END1z       END2z       END1y       END2y        FJ1z        FJ2z    FJ1y    FJ2y      YO      ZO
      0.2667      0.2667      0.0000      0.0000      0.0000      0.0000  0.0000  0.0000  0.0000  0.0000
!

  9      BEAM                    Col-Storey: 2 Col: 0
!       ITYPE       IBEAM       IPINZ       IPINY       ICOND       IHYST    ILOS   IDAMG     IGA   IDUCT
           1           1           0           0           0           0       0       0       0       0
!
!           E           G           A         Jxx         Izz         Iyy     Asz     Asy      Sy      Sz     WGT
   3.0151E+06  1.0629E+10  8.1000E-01  8.1000E+01  3.2805E-02  3.2805E-02   0.000   0.000   0.000   0.000   0.000
!
!       END1z       END2z       END1y       END2y        FJ1z        FJ2z    FJ1y    FJ2y      YO      ZO
      0.2667      0.2667      0.0000      0.0000      0.0000      0.0000  0.0000  0.0000  0.0000  0.0000
!

 10      BEAM                    Col-Storey: 2 Col: 1
!       ITYPE       IBEAM       IPINZ       IPINY       ICOND       IHYST    ILOS   IDAMG     IGA   IDUCT
           1           1           0           0           0           0       0       0       0       0
!
!           E           G           A         Jxx         Izz         Iyy     Asz     Asy      Sy      Sz     WGT
   3.0151E+06  1.0629E+10  8.1000E-01  8.1000E+01  3.2805E-02  3.2805E-02   0.000   0.000   0.000   0.000   0.000
!
!       END1z       END2z       END1y       END2y        FJ1z        FJ2z    FJ1y    FJ2y      YO      ZO
      0.2667      0.2667      0.0000      0.0000      0.0000      0.0000  0.0000  0.0000  0.0000  0.0000
!

 11      BEAM                    Col-Storey: 2 Col: 2
!       ITYPE       IBEAM       IPINZ       IPINY       ICOND       IHYST    ILOS   IDAMG     IGA   IDUCT
           1           1           0           0           0           0       0       0       0       0
!
!           E           G           A         Jxx         Izz         Iyy     Asz     Asy      Sy      Sz     WGT
   3.0151E+06  1.0629E+10  8.1000E-01  8.1000E+01  3.2805E-02  3.2805E-02   0.000   0.000   0.000   0.000   0.000
!
!       END1z       END2z       END1y       END2y        FJ1z        FJ2z    FJ1y    FJ2y      YO      ZO
      0.2667      0.2667      0.0000      0.0000      0.0000      0.0000  0.0000  0.0000  0.0000  0.0000
!

 12      BEAM                    Col-Storey: 2 Col: 3
!       ITYPE       IBEAM       IPINZ       IPINY       ICOND       IHYST    ILOS   IDAMG     IGA   IDUCT
           1           1           0           0           0           0       0       0       0       0
!
!           E           G           A         Jxx         Izz         Iyy     Asz     Asy      Sy      Sz     WGT
   3.0151E+06  1.0629E+10  8.1000E-01  8.1000E+01  3.2805E-02  3.2805E-02   0.000   0.000   0.000   0.000   0.000
!
!       END1z       END2z       END1y       END2y        FJ1z        FJ2z    FJ1y    FJ2y      YO      ZO
      0.2667      0.2667      0.0000      0.0000      0.0000      0.0000  0.0000  0.0000  0.0000  0.0000
!

 13      BEAM                    Col-Storey: 3 Col: 0
!       ITYPE       IBEAM       IPINZ       IPINY       ICOND       IHYST    ILOS   IDAMG     IGA   IDUCT
           1           1           0           0           0           0       0       0       0       0
!
!           E           G           A         Jxx         Izz         Iyy     Asz     Asy      Sy      Sz     WGT
   3.0151E+06  1.0629E+10  8.1000E-01  8.1000E+01  3.2805E-02  3.2805E-02   0.000   0.000   0.000   0.000   0.000
!
!       END1z       END2z       END1y       END2y        FJ1z        FJ2z    FJ1y    FJ2y      YO      ZO
      0.2667      0.2667      0.0000      0.0000      0.0000      0.0000  0.0000  0.0000  0.0000  0.0000
!

 14      BEAM                    Col-Storey: 3 Col: 1
```

```
!       ITYPE       IBEAM       IPINZ       IPINY       ICOND       IHYST    ILOS   IDAMG     IGA   IDUCT
            1           1           0           0           0           0       0       0       0       0
!
!           E           G           A         Jxx         Izz         Iyy     Asz     Asy      Sy      Sz     WGT
   3.0151E+06  1.0629E+10  8.1000E-01  8.1000E+01  3.2805E-02  3.2805E-02   0.000   0.000   0.000   0.000   0.000
!
!       END1z       END2z       END1y       END2y        FJ1z        FJ2z    FJ1y    FJ2y      Y0      Z0
      0.2667      0.2667      0.0000      0.0000      0.0000      0.0000  0.0000  0.0000  0.0000  0.0000
!

 15      BEAM                    Col-Storey: 3 Col: 2
!       ITYPE       IBEAM       IPINZ       IPINY       ICOND       IHYST    ILOS   IDAMG     IGA   IDUCT
            1           1           0           0           0           0       0       0       0       0
!
!           E           G           A         Jxx         Izz         Iyy     Asz     Asy      Sy      Sz     WGT
   3.0151E+06  1.0629E+10  8.1000E-01  8.1000E+01  3.2805E-02  3.2805E-02   0.000   0.000   0.000   0.000   0.000
!
!       END1z       END2z       END1y       END2y        FJ1z        FJ2z    FJ1y    FJ2y      Y0      Z0
      0.2667      0.2667      0.0000      0.0000      0.0000      0.0000  0.0000  0.0000  0.0000  0.0000
!

 16      BEAM                    Col-Storey: 3 Col: 3
!       ITYPE       IBEAM       IPINZ       IPINY       ICOND       IHYST    ILOS   IDAMG     IGA   IDUCT
            1           1           0           0           0           0       0       0       0       0
!
!           E           G           A         Jxx         Izz         Iyy     Asz     Asy      Sy      Sz     WGT
   3.0151E+06  1.0629E+10  8.1000E-01  8.1000E+01  3.2805E-02  3.2805E-02   0.000   0.000   0.000   0.000   0.000
!
!       END1z       END2z       END1y       END2y        FJ1z        FJ2z    FJ1y    FJ2y      Y0      Z0
      0.2667      0.2667      0.0000      0.0000      0.0000      0.0000  0.0000  0.0000  0.0000  0.0000
!

 17      BEAM                    Col-Storey: 4 Col: 0
!       ITYPE       IBEAM       IPINZ       IPINY       ICOND       IHYST    ILOS   IDAMG     IGA   IDUCT
            1           1           0           0           0           0       0       0       0       0
!
!           E           G           A         Jxx         Izz         Iyy     Asz     Asy      Sy      Sz     WGT
   3.0151E+06  1.0629E+10  8.1000E-01  8.1000E+01  3.2805E-02  3.2805E-02   0.000   0.000   0.000   0.000   0.000
!
!       END1z       END2z       END1y       END2y        FJ1z        FJ2z    FJ1y    FJ2y      Y0      Z0
      0.2667      0.2667      0.0000      0.0000      0.0000      0.0000  0.0000  0.0000  0.0000  0.0000
!

 18      BEAM                    Col-Storey: 4 Col: 1
!       ITYPE       IBEAM       IPINZ       IPINY       ICOND       IHYST    ILOS   IDAMG     IGA   IDUCT
            1           1           0           0           0           0       0       0       0       0
!
!           E           G           A         Jxx         Izz         Iyy     Asz     Asy      Sy      Sz     WGT
   3.0151E+06  1.0629E+10  8.1000E-01  8.1000E+01  3.2805E-02  3.2805E-02   0.000   0.000   0.000   0.000   0.000
!
!       END1z       END2z       END1y       END2y        FJ1z        FJ2z    FJ1y    FJ2y      Y0      Z0
      0.2667      0.2667      0.0000      0.0000      0.0000      0.0000  0.0000  0.0000  0.0000  0.0000
!

 19      BEAM                    Col-Storey: 4 Col: 2
!       ITYPE       IBEAM       IPINZ       IPINY       ICOND       IHYST    ILOS   IDAMG     IGA   IDUCT
            1           1           0           0           0           0       0       0       0       0
!
!           E           G           A         Jxx         Izz         Iyy     Asz     Asy      Sy      Sz     WGT
   3.0151E+06  1.0629E+10  8.1000E-01  8.1000E+01  3.2805E-02  3.2805E-02   0.000   0.000   0.000   0.000   0.000
!
!       END1z       END2z       END1y       END2y        FJ1z        FJ2z    FJ1y    FJ2y      Y0      Z0
      0.2667      0.2667      0.0000      0.0000      0.0000      0.0000  0.0000  0.0000  0.0000  0.0000
!

 20      BEAM                    Col-Storey: 4 Col: 3
!       ITYPE       IBEAM       IPINZ       IPINY       ICOND       IHYST    ILOS   IDAMG     IGA   IDUCT
            1           1           0           0           0           0       0       0       0       0
!
!           E           G           A         Jxx         Izz         Iyy     Asz     Asy      Sy      Sz     WGT
   3.0151E+06  1.0629E+10  8.1000E-01  8.1000E+01  3.2805E-02  3.2805E-02   0.000   0.000   0.000   0.000   0.000
!
!       END1z       END2z       END1y       END2y        FJ1z        FJ2z    FJ1y    FJ2y      Y0      Z0
      0.2667      0.2667      0.0000      0.0000      0.0000      0.0000  0.0000  0.0000  0.0000  0.0000
!
```

```
 21      BEAM                    Col-Storey: 5 Col: 0
!       ITYPE       IBEAM       IPINZ       IPINY       ICOND       IHYST    ILOS   IDAMG     IGA   IDUCT
           1           1           0           0           0           0       0       0       0       0
!
!           E           G           A         Jxx         Izz         Iyy     Asz     Asy      Sy      Sz     WGT
   3.0151E+06  1.0629E+10  8.1000E-01  8.1000E+01  3.2805E-02  3.2805E-02   0.000   0.000   0.000   0.000   0.000
!
!       END1z       END2z       END1y       END2y        FJ1z        FJ2z    FJ1y    FJ2y      Y0      Z0
      0.2667      0.2667      0.0000      0.0000      0.0000      0.0000  0.0000  0.0000  0.0000  0.0000
!

 22      BEAM                    Col-Storey: 5 Col: 1
!       ITYPE       IBEAM       IPINZ       IPINY       ICOND       IHYST    ILOS   IDAMG     IGA   IDUCT
           1           1           0           0           0           0       0       0       0       0
!
!           E           G           A         Jxx         Izz         Iyy     Asz     Asy      Sy      Sz     WGT
   3.0151E+06  1.0629E+10  8.1000E-01  8.1000E+01  3.2805E-02  3.2805E-02   0.000   0.000   0.000   0.000   0.000
!
!       END1z       END2z       END1y       END2y        FJ1z        FJ2z    FJ1y    FJ2y      Y0      Z0
      0.2667      0.2667      0.0000      0.0000      0.0000      0.0000  0.0000  0.0000  0.0000  0.0000
!

 23      BEAM                    Col-Storey: 5 Col: 2
!       ITYPE       IBEAM       IPINZ       IPINY       ICOND       IHYST    ILOS   IDAMG     IGA   IDUCT
           1           1           0           0           0           0       0       0       0       0
!
!           E           G           A         Jxx         Izz         Iyy     Asz     Asy      Sy      Sz     WGT
   3.0151E+06  1.0629E+10  8.1000E-01  8.1000E+01  3.2805E-02  3.2805E-02   0.000   0.000   0.000   0.000   0.000
!
!       END1z       END2z       END1y       END2y        FJ1z        FJ2z    FJ1y    FJ2y      Y0      Z0
      0.2667      0.2667      0.0000      0.0000      0.0000      0.0000  0.0000  0.0000  0.0000  0.0000
!

 24      BEAM                    Col-Storey: 5 Col: 3
!       ITYPE       IBEAM       IPINZ       IPINY       ICOND       IHYST    ILOS   IDAMG     IGA   IDUCT
           1           1           0           0           0           0       0       0       0       0
!
!           E           G           A         Jxx         Izz         Iyy     Asz     Asy      Sy      Sz     WGT
   3.0151E+06  1.0629E+10  8.1000E-01  8.1000E+01  3.2805E-02  3.2805E-02   0.000   0.000   0.000   0.000   0.000
!
!       END1z       END2z       END1y       END2y        FJ1z        FJ2z    FJ1y    FJ2y      Y0      Z0
      0.2667      0.2667      0.0000      0.0000      0.0000      0.0000  0.0000  0.0000  0.0000  0.0000
!

 25      BEAM                    Beam-Storey: 1 Bay: 1
!       ITYPE       IBEAM       IPINZ       IPINY       ICOND       IHYST    ILOS   IDAMG     IGA   IDUCT
           1           1           0           0           0           4       0       0       0       0
!
!           E           G           A         Jxx         Izz         Iyy     Asz     Asy      Sy      Sz     WGT
   3.0151E+06  1.1800E+07  5.1200E+01  5.1200E+01  1.0923E-02  1.0923E-02   0.000   0.000   0.000   0.000   0.000
!
!       END1z       END2z       END1y       END2y        FJ1z        FJ2z    FJ1y    FJ2y      Y0      Z0
      0.3000      0.3000      0.3000      0.3000      0.0000      0.0000  0.0000  0.0000  0.0000  0.0000
!
!          RA          RT          RFz         RFy
      0.0100      0.0100      0.0100      0.0200
!
!          H1          H2          H3          H4
      0.4000      0.4000      0.4000      0.4000
!
!           PYT           PYC           TYp           TYn          ALFA      IEND
     0.0000E+00    0.0000E+00    0.0000E+00    0.0000E+00    0.0000E+00         0
!
!           MyP           MyN            M2            M2
     3.0152E+02   -3.0152E+02    0.0000E+00    0.0000E+00
!
!        TAK_AL      TAK_BETA       TAK_NF      TAK_KKK
         0.4000        0.6000        1.0000        2.0000
!

 26      BEAM                    Beam-Storey: 1 Bay: 2
!       ITYPE       IBEAM       IPINZ       IPINY       ICOND       IHYST    ILOS   IDAMG     IGA   IDUCT
           1           1           0           0           0           4       0       0       0       0
!
!           E           G           A         Jxx         Izz         Iyy     Asz     Asy      Sy      Sz     WGT
   3.0151E+06  1.1800E+07  5.1200E+01  5.1200E+01  1.0923E-02  1.0923E-02   0.000   0.000   0.000   0.000   0.000
```

```
!
!       END1z       END2z       END1y       END2y        FJ1z        FJ2z    FJ1y    FJ2y       Y0       Z0
       0.3000      0.3000      0.3000      0.3000      0.0000      0.0000  0.0000  0.0000  0.0000  0.0000
!
!          RA          RT         RFz         RFy
       0.0100      0.0100      0.0100      0.0200
!
!          H1          H2          H3          H4
       0.4000      0.4000      0.4000      0.4000
!
!           PYT            PYC            TYp            TYn           ALFA      IEND
     0.0000E+00     0.0000E+00     0.0000E+00     0.0000E+00     0.0000E+00         0
!
!           MyP            MyN             M2             M2
     3.0152E+02    -3.0152E+02     0.0000E+00     0.0000E+00
!
!         TAK_AL       TAK_BETA         TAK_NF        TAK_KKK
          0.4000          0.6000          1.0000          2.0000
!

 27      BEAM                    Beam-Storey: 1 Bay: 3
!       ITYPE       IBEAM       IPINZ       IPINY       ICOND       IHYST    ILOS   IDAMG     IGA   IDUCT
           1           1           0           0           0           4       0       0       0       0
!
!           E           G           A         Jxx         Izz         Iyy     Asz     Asy      Sy      Sz     WGT
   3.0151E+06  1.1800E+07  5.1200E+01  5.1200E+01  1.0923E-02  1.0923E-02   0.000   0.000   0.000   0.000   0.000
!
!       END1z       END2z       END1y       END2y        FJ1z        FJ2z    FJ1y    FJ2y       Y0       Z0
       0.3000      0.3000      0.3000      0.3000      0.0000      0.0000  0.0000  0.0000  0.0000  0.0000
!
!          RA          RT         RFz         RFy
       0.0100      0.0100      0.0100      0.0200
!
!          H1          H2          H3          H4
       0.4000      0.4000      0.4000      0.4000
!
!           PYT            PYC            TYp            TYn           ALFA      IEND
     0.0000E+00     0.0000E+00     0.0000E+00     0.0000E+00     0.0000E+00         0
!
!           MyP            MyN             M2             M2
     3.0152E+02    -3.0152E+02     0.0000E+00     0.0000E+00
!
!         TAK_AL       TAK_BETA         TAK_NF        TAK_KKK
          0.4000          0.6000          1.0000          2.0000
!

 28      BEAM                    Beam-Storey: 2 Bay: 1
!       ITYPE       IBEAM       IPINZ       IPINY       ICOND       IHYST    ILOS   IDAMG     IGA   IDUCT
           1           1           0           0           0           4       0       0       0       0
!
!           E           G           A         Jxx         Izz         Iyy     Asz     Asy      Sy      Sz     WGT
   3.0151E+06  1.1800E+07  5.1200E+01  5.1200E+01  1.0923E-02  1.0923E-02   0.000   0.000   0.000   0.000   0.000
!
!       END1z       END2z       END1y       END2y        FJ1z        FJ2z    FJ1y    FJ2y       Y0       Z0
       0.3000      0.3000      0.3000      0.3000      0.0000      0.0000  0.0000  0.0000  0.0000  0.0000
!
!          RA          RT         RFz         RFy
       0.0100      0.0100      0.0100      0.0200
!
!          H1          H2          H3          H4
       0.4000      0.4000      0.4000      0.4000
!
!           PYT            PYC            TYp            TYn           ALFA      IEND
     0.0000E+00     0.0000E+00     0.0000E+00     0.0000E+00     0.0000E+00         0
!
!           MyP            MyN             M2             M2
     2.8473E+02    -2.8473E+02     0.0000E+00     0.0000E+00
!
!         TAK_AL       TAK_BETA         TAK_NF        TAK_KKK
          0.4000          0.6000          1.0000          2.0000
!

 29      BEAM                    Beam-Storey: 2 Bay: 2
!       ITYPE       IBEAM       IPINZ       IPINY       ICOND       IHYST    ILOS   IDAMG     IGA   IDUCT
           1           1           0           0           0           4       0       0       0       0
!
```

```
!           E           G           A         Jxx         Izz         Iyy      Asz      Asy       Sy       Sz      WGT
   3.0151E+06  1.1800E+07  5.1200E+01  5.1200E+01  1.0923E-02  1.0923E-02   0.000    0.000    0.000    0.000    0.000
!
!       END1z       END2z       END1y       END2y       FJ1z        FJ2z    FJ1y    FJ2y       Y0       Z0
       0.3000      0.3000      0.3000      0.3000      0.0000      0.0000  0.0000  0.0000   0.0000   0.0000
!
!          RA          RT          RFz         RFy
       0.0100      0.0100      0.0100      0.0200
!
!          H1          H2          H3          H4
       0.4000      0.4000      0.4000      0.4000
!
!           PYT           PYC           TYp           TYn           ALFA      IEND
     0.0000E+00    0.0000E+00    0.0000E+00    0.0000E+00    0.0000E+00         0
!
!           MyP           MyN           M2            M2
     2.8473E+02   -2.8473E+02    0.0000E+00    0.0000E+00
!
!         TAK_AL       TAK_BETA         TAK_NF        TAK_KKK
          0.4000         0.6000         1.0000         2.0000
!

 30      BEAM                  Beam-Storey: 2 Bay: 3
!       ITYPE       IBEAM       IPINZ       IPINY       ICOND       IHYST    ILOS   IDAMG     IGA   IDUCT
           1           1           0           0           0           4       0       0       0       0
!
!           E           G           A         Jxx         Izz         Iyy      Asz      Asy       Sy       Sz      WGT
   3.0151E+06  1.1800E+07  5.1200E+01  5.1200E+01  1.0923E-02  1.0923E-02   0.000    0.000    0.000    0.000    0.000
!
!       END1z       END2z       END1y       END2y       FJ1z        FJ2z    FJ1y    FJ2y       Y0       Z0
       0.3000      0.3000      0.3000      0.3000      0.0000      0.0000  0.0000  0.0000   0.0000   0.0000
!
!          RA          RT          RFz         RFy
       0.0100      0.0100      0.0100      0.0200
!
!          H1          H2          H3          H4
       0.4000      0.4000      0.4000      0.4000
!
!           PYT           PYC           TYp           TYn           ALFA      IEND
     0.0000E+00    0.0000E+00    0.0000E+00    0.0000E+00    0.0000E+00         0
!
!           MyP           MyN           M2            M2
     2.8473E+02   -2.8473E+02    0.0000E+00    0.0000E+00
!
!         TAK_AL       TAK_BETA         TAK_NF        TAK_KKK
          0.4000         0.6000         1.0000         2.0000
!

 31      BEAM                  Beam-Storey: 3 Bay: 1
!       ITYPE       IBEAM       IPINZ       IPINY       ICOND       IHYST    ILOS   IDAMG     IGA   IDUCT
           1           1           0           0           0           4       0       0       0       0
!
!           E           G           A         Jxx         Izz         Iyy      Asz      Asy       Sy       Sz      WGT
   3.0151E+06  1.1800E+07  5.1200E+01  5.1200E+01  1.0923E-02  1.0923E-02   0.000    0.000    0.000    0.000    0.000
!
!       END1z       END2z       END1y       END2y       FJ1z        FJ2z    FJ1y    FJ2y       Y0       Z0
       0.3000      0.3000      0.3000      0.3000      0.0000      0.0000  0.0000  0.0000   0.0000   0.0000
!
!          RA          RT          RFz         RFy
       0.0100      0.0100      0.0100      0.0200
!
!          H1          H2          H3          H4
       0.4000      0.4000      0.4000      0.4000
!
!           PYT           PYC           TYp           TYn           ALFA      IEND
     0.0000E+00    0.0000E+00    0.0000E+00    0.0000E+00    0.0000E+00         0
!
!           MyP           MyN           M2            M2
     2.5265E+02   -2.5265E+02    0.0000E+00    0.0000E+00
!
!         TAK_AL       TAK_BETA         TAK_NF        TAK_KKK
          0.4000         0.6000         1.0000         2.0000
!

 32      BEAM                  Beam-Storey: 3 Bay: 2
!       ITYPE       IBEAM       IPINZ       IPINY       ICOND       IHYST    ILOS   IDAMG     IGA   IDUCT
```

```
           1           1           0           0           0           4       0       0       0       0
!
!           E           G           A         Jxx         Izz         Iyy     Asz     Asy      Sy      Sz     WGT
   3.0151E+06  1.1800E+07  5.1200E+01  5.1200E+01  1.0923E-02  1.0923E-02   0.000   0.000   0.000   0.000   0.000
!
!       END1z       END2z       END1y       END2y        FJ1z        FJ2z    FJ1y    FJ2y      Y0      Z0
      0.3000      0.3000      0.3000      0.3000      0.0000      0.0000  0.0000  0.0000  0.0000  0.0000
!
!          RA          RT         RFz         RFy
      0.0100      0.0100      0.0100      0.0200
!
!          H1          H2          H3          H4
      0.4000      0.4000      0.4000      0.4000
!
!           PYT           PYC           TYp           TYn          ALFA      IEND
     0.0000E+00    0.0000E+00    0.0000E+00    0.0000E+00    0.0000E+00         0
!
!           MyP           MyN            M2            M2
     2.5265E+02   -2.5265E+02    0.0000E+00    0.0000E+00
!
!        TAK_AL      TAK_BETA       TAK_NF      TAK_KKK
         0.4000        0.6000        1.0000        2.0000
!

 33      BEAM                  Beam-Storey: 3 Bay: 3
!       ITYPE       IBEAM       IPINZ       IPINY       ICOND       IHYST    ILOS   IDAMG     IGA   IDUCT
           1           1           0           0           0           4       0       0       0       0
!
!           E           G           A         Jxx         Izz         Iyy     Asz     Asy      Sy      Sz     WGT
   3.0151E+06  1.1800E+07  5.1200E+01  5.1200E+01  1.0923E-02  1.0923E-02   0.000   0.000   0.000   0.000   0.000
!
!       END1z       END2z       END1y       END2y        FJ1z        FJ2z    FJ1y    FJ2y      Y0      Z0
      0.3000      0.3000      0.3000      0.3000      0.0000      0.0000  0.0000  0.0000  0.0000  0.0000
!
!          RA          RT         RFz         RFy
      0.0100      0.0100      0.0100      0.0200
!
!          H1          H2          H3          H4
      0.4000      0.4000      0.4000      0.4000
!
!           PYT           PYC           TYp           TYn          ALFA      IEND
     0.0000E+00    0.0000E+00    0.0000E+00    0.0000E+00    0.0000E+00         0
!
!           MyP           MyN            M2            M2
     2.5265E+02   -2.5265E+02    0.0000E+00    0.0000E+00
!
!        TAK_AL      TAK_BETA       TAK_NF      TAK_KKK
         0.4000        0.6000        1.0000        2.0000
!

 34      BEAM                  Beam-Storey: 4 Bay: 1
!       ITYPE       IBEAM       IPINZ       IPINY       ICOND       IHYST    ILOS   IDAMG     IGA   IDUCT
           1           1           0           0           0           4       0       0       0       0
!
!           E           G           A         Jxx         Izz         Iyy     Asz     Asy      Sy      Sz     WGT
   3.0151E+06  1.1800E+07  5.1200E+01  5.1200E+01  1.0923E-02  1.0923E-02   0.000   0.000   0.000   0.000   0.000
!
!       END1z       END2z       END1y       END2y        FJ1z        FJ2z    FJ1y    FJ2y      Y0      Z0
      0.3000      0.3000      0.3000      0.3000      0.0000      0.0000  0.0000  0.0000  0.0000  0.0000
!
!          RA          RT         RFz         RFy
      0.0100      0.0100      0.0100      0.0200
!
!          H1          H2          H3          H4
      0.4000      0.4000      0.4000      0.4000
!
!           PYT           PYC           TYp           TYn          ALFA      IEND
     0.0000E+00    0.0000E+00    0.0000E+00    0.0000E+00    0.0000E+00         0
!
!           MyP           MyN            M2            M2
     2.0670E+02   -2.0670E+02    0.0000E+00    0.0000E+00
!
!        TAK_AL      TAK_BETA       TAK_NF      TAK_KKK
         0.4000        0.6000        1.0000        2.0000
!
```

```
 35      BEAM                    Beam-Storey: 4 Bay: 2
!       ITYPE       IBEAM       IPINZ       IPINY       ICOND       IHYST    ILOS   IDAMG     IGA   IDUCT
           1           1           0           0           0           4       0       0       0       0
!
!           E           G           A         Jxx         Izz         Iyy     Asz     Asy      Sy      Sz     WGT
   3.0151E+06  1.1800E+07  5.1200E+01  5.1200E+01  1.0923E-02  1.0923E-02   0.000   0.000   0.000   0.000   0.000
!
!       END1z       END2z       END1y       END2y        FJ1z        FJ2z    FJ1y    FJ2y      Y0      Z0
      0.3000      0.3000      0.3000      0.3000      0.0000      0.0000  0.0000  0.0000  0.0000  0.0000
!
!          RA          RT          RFz         RFy
      0.0100      0.0100      0.0100      0.0200
!
!          H1          H2          H3          H4
      0.4000      0.4000      0.4000      0.4000
!
!           PYT           PYC           TYp           TYn          ALFA      IEND
     0.0000E+00    0.0000E+00    0.0000E+00    0.0000E+00    0.0000E+00         0
!
!           MyP           MyN            M2            M2
     2.0670E+02   -2.0670E+02    0.0000E+00    0.0000E+00
!
!         TAK_AL       TAK_BETA         TAK_NF        TAK_KKK
          0.4000         0.6000         1.0000         2.0000
!

 36      BEAM                    Beam-Storey: 4 Bay: 3
!       ITYPE       IBEAM       IPINZ       IPINY       ICOND       IHYST    ILOS   IDAMG     IGA   IDUCT
           1           1           0           0           0           4       0       0       0       0
!
!           E           G           A         Jxx         Izz         Iyy     Asz     Asy      Sy      Sz     WGT
   3.0151E+06  1.1800E+07  5.1200E+01  5.1200E+01  1.0923E-02  1.0923E-02   0.000   0.000   0.000   0.000   0.000
!
!       END1z       END2z       END1y       END2y        FJ1z        FJ2z    FJ1y    FJ2y      Y0      Z0
      0.3000      0.3000      0.3000      0.3000      0.0000      0.0000  0.0000  0.0000  0.0000  0.0000
!
!          RA          RT          RFz         RFy
      0.0100      0.0100      0.0100      0.0200
!
!          H1          H2          H3          H4
      0.4000      0.4000      0.4000      0.4000
!
!           PYT           PYC           TYp           TYn          ALFA      IEND
     0.0000E+00    0.0000E+00    0.0000E+00    0.0000E+00    0.0000E+00         0
!
!           MyP           MyN            M2            M2
     2.0670E+02   -2.0670E+02    0.0000E+00    0.0000E+00
!
!         TAK_AL       TAK_BETA         TAK_NF        TAK_KKK
          0.4000         0.6000         1.0000         2.0000
!

 37      BEAM                    Beam-Storey: 5 Bay: 1
!       ITYPE       IBEAM       IPINZ       IPINY       ICOND       IHYST    ILOS   IDAMG     IGA   IDUCT
           1           1           0           0           0           4       0       0       0       0
!
!           E           G           A         Jxx         Izz         Iyy     Asz     Asy      Sy      Sz     WGT
   3.0151E+06  1.1800E+07  5.1200E+01  5.1200E+01  1.0923E-02  1.0923E-02   0.000   0.000   0.000   0.000   0.000
!
!       END1z       END2z       END1y       END2y        FJ1z        FJ2z    FJ1y    FJ2y      Y0      Z0
      0.3000      0.3000      0.3000      0.3000      0.0000      0.0000  0.0000  0.0000  0.0000  0.0000
!
!          RA          RT          RFz         RFy
      0.0100      0.0100      0.0100      0.0200
!
!          H1          H2          H3          H4
      0.4000      0.4000      0.4000      0.4000
!
!           PYT           PYC           TYp           TYn          ALFA      IEND
     0.0000E+00    0.0000E+00    0.0000E+00    0.0000E+00    0.0000E+00         0
!
!           MyP           MyN            M2            M2
     1.4833E+02   -1.4833E+02    0.0000E+00    0.0000E+00
!
!         TAK_AL       TAK_BETA         TAK_NF        TAK_KKK
          0.4000         0.6000         1.0000         2.0000
```

```
!

 38      BEAM                    Beam-Storey: 5 Bay: 2
!       ITYPE       IBEAM       IPINZ       IPINY       ICOND       IHYST    ILOS   IDAMG     IGA   IDUCT
            1           1           0           0           0           4       0       0       0       0
!
!           E           G           A         Jxx         Izz         Iyy     Asz     Asy      Sy      Sz     WGT
   3.0151E+06  1.1800E+07  5.1200E+01  5.1200E+01  1.0923E-02  1.0923E-02   0.000   0.000   0.000   0.000   0.000
!
!       END1z       END2z       END1y       END2y        FJ1z        FJ2z    FJ1y    FJ2y      Y0      Z0
       0.3000      0.3000      0.3000      0.3000      0.0000      0.0000  0.0000  0.0000  0.0000  0.0000
!
!          RA          RT          RFz         RFy
       0.0100      0.0100      0.0100      0.0200
!
!          H1          H2          H3          H4
       0.4000      0.4000      0.4000      0.4000
!
!           PYT           PYC           TYp           TYn           ALFA      IEND
     0.0000E+00    0.0000E+00    0.0000E+00    0.0000E+00    0.0000E+00         0
!
!           MyP           MyN            M2            M2
     1.4833E+02   -1.4833E+02    0.0000E+00    0.0000E+00
!
!         TAK_AL       TAK_BETA         TAK_NF        TAK_KKK
          0.4000         0.6000         1.0000         2.0000
!

 39      BEAM                    Beam-Storey: 5 Bay: 3
!       ITYPE       IBEAM       IPINZ       IPINY       ICOND       IHYST    ILOS   IDAMG     IGA   IDUCT
            1           1           0           0           0           4       0       0       0       0
!
!           E           G           A         Jxx         Izz         Iyy     Asz     Asy      Sy      Sz     WGT
   3.0151E+06  1.1800E+07  5.1200E+01  5.1200E+01  1.0923E-02  1.0923E-02   0.000   0.000   0.000   0.000   0.000
!
!       END1z       END2z       END1y       END2y        FJ1z        FJ2z    FJ1y    FJ2y      Y0      Z0
       0.3000      0.3000      0.3000      0.3000      0.0000      0.0000  0.0000  0.0000  0.0000  0.0000
!
!          RA          RT          RFz         RFy
       0.0100      0.0100      0.0100      0.0200
!
!          H1          H2          H3          H4
       0.4000      0.4000      0.4000      0.4000
!
!           PYT           PYC           TYp           TYn           ALFA      IEND
     0.0000E+00    0.0000E+00    0.0000E+00    0.0000E+00    0.0000E+00         0
!
!           MyP           MyN            M2            M2
     1.4833E+02   -1.4833E+02    0.0000E+00    0.0000E+00
!
!         TAK_AL       TAK_BETA         TAK_NF        TAK_KKK
          0.4000         0.6000         1.0000         2.0000
!

 40      BEAM                    Beam-Storey: 6 Bay: 1
!       ITYPE       IBEAM       IPINZ       IPINY       ICOND       IHYST    ILOS   IDAMG     IGA   IDUCT
            1           1           0           0           0           4       0       0       0       0
!
!           E           G           A         Jxx         Izz         Iyy     Asz     Asy      Sy      Sz     WGT
   3.0151E+06  1.1800E+07  5.1200E+01  5.1200E+01  1.0923E-02  1.0923E-02   0.000   0.000   0.000   0.000   0.000
!
!       END1z       END2z       END1y       END2y        FJ1z        FJ2z    FJ1y    FJ2y      Y0      Z0
       0.3000      0.3000      0.3000      0.3000      0.0000      0.0000  0.0000  0.0000  0.0000  0.0000
!
!          RA          RT          RFz         RFy
       0.0100      0.0100      0.0100      0.0200
!
!          H1          H2          H3          H4
       0.4000      0.4000      0.4000      0.4000
!
!           PYT           PYC           TYp           TYn           ALFA      IEND
     0.0000E+00    0.0000E+00    0.0000E+00    0.0000E+00    0.0000E+00         0
!
!           MyP           MyN            M2            M2
     7.8949E+01   -7.8949E+01    0.0000E+00    0.0000E+00
!
```

```
!         TAK_AL       TAK_BETA         TAK_NF        TAK_KKK
          0.4000         0.6000         1.0000         2.0000
!

 41      BEAM                    Beam-Storey: 6 Bay: 2
!       ITYPE       IBEAM       IPINZ       IPINY       ICOND       IHYST    ILOS   IDAMG     IGA   IDUCT
           1           1           0           0           0           4       0       0       0       0
!
!           E           G           A         Jxx         Izz         Iyy     Asz     Asy      Sy      Sz     WGT
   3.0151E+06  1.1800E+07  5.1200E+01  5.1200E+01  1.0923E-02  1.0923E-02   0.000   0.000   0.000   0.000   0.000
!
!       END1z       END2z       END1y       END2y        FJ1z        FJ2z    FJ1y    FJ2y      Y0      Z0
       0.3000      0.3000      0.3000      0.3000      0.0000      0.0000  0.0000  0.0000  0.0000  0.0000
!
!          RA          RT          RFz         RFy
       0.0100      0.0100      0.0100      0.0200
!
!          H1          H2          H3          H4
       0.4000      0.4000      0.4000      0.4000
!
!           PYT           PYC           TYp           TYn           ALFA      IEND
     0.0000E+00    0.0000E+00    0.0000E+00    0.0000E+00    0.0000E+00         0
!
!           MyP           MyN            M2            M2
     7.8949E+01   -7.8949E+01    0.0000E+00    0.0000E+00
!
!         TAK_AL       TAK_BETA         TAK_NF        TAK_KKK
          0.4000         0.6000         1.0000         2.0000
!

 42      BEAM                    Beam-Storey: 6 Bay: 3
!       ITYPE       IBEAM       IPINZ       IPINY       ICOND       IHYST    ILOS   IDAMG     IGA   IDUCT
           1           1           0           0           0           4       0       0       0       0
!
!           E           G           A         Jxx         Izz         Iyy     Asz     Asy      Sy      Sz     WGT
   3.0151E+06  1.1800E+07  5.1200E+01  5.1200E+01  1.0923E-02  1.0923E-02   0.000   0.000   0.000   0.000   0.000
!
!       END1z       END2z       END1y       END2y        FJ1z        FJ2z    FJ1y    FJ2y      Y0      Z0
       0.3000      0.3000      0.3000      0.3000      0.0000      0.0000  0.0000  0.0000  0.0000  0.0000
!
!          RA          RT          RFz         RFy
       0.0100      0.0100      0.0100      0.0200
!
!          H1          H2          H3          H4
       0.4000      0.4000      0.4000      0.4000
!
!           PYT           PYC           TYp           TYn           ALFA      IEND
     0.0000E+00    0.0000E+00    0.0000E+00    0.0000E+00    0.0000E+00         0
!
!           MyP           MyN            M2            M2
     7.8949E+01   -7.8949E+01    0.0000E+00    0.0000E+00
!
!         TAK_AL       TAK_BETA         TAK_NF        TAK_KKK
          0.4000         0.6000         1.0000         2.0000
!

   43          MACRO   SSI -element
!   JPLA SL         DIAM        QQMAX          KNN          KVV          KMM     PSI     KSI   PL_P1   PL_P2     WGT  IPRNT
ITRAK
       1  0  2.8500E+00  1.0244E+04  3.6969E+05  2.9421E+05  6.1551E+05   0.506   0.480   0.200   1.000   0.000       0
1
!
!   ALPHA    BETA   GAMMA   DELTA   EPSIL    ZETA NON_ASS    TOPL       min_lam    TENS    FRIC    MAPP  UPLIFT
     4.00    2.00    2.00    0.50    0.75    1.50   1.000 1000.00    1.0000E+04      No     Yes     Yes      No
!
!    K_Alfa    K_Beta     G_Lam     G_Chi      G_Xi
       1.00      1.00      2.50      3.00      0.95
!

   44          MACRO   SSI -element
!   JPLA SL         DIAM        QQMAX          KNN          KVV          KMM     PSI     KSI   PL_P1   PL_P2     WGT  IPRNT
ITRAK
       1  0  3.8000E+00  2.0128E+04  4.9291E+05  3.8635E+05  1.4590E+06   0.506   0.480   0.200   1.000   0.000       0
1
!
!   ALPHA    BETA   GAMMA   DELTA   EPSIL    ZETA NON_ASS    TOPL       min_lam    TENS    FRIC    MAPP  UPLIFT
```

```
     4.00    2.00    2.00    0.50    0.75    1.50   1.000 1000.00    1.0000E+04      No      Yes      Yes       No
!
!    K_Alfa    K_Beta     G_Lam     G_Chi      G_Xi
       1.00      1.00      2.50      3.00      0.95
!

   45          MACRO   SSI -element
!   JPLA SL         DIAM        QQMAX          KNN          KVV          KMM     PSI     KSI   PL_P1   PL_P2     WGT  IPRNT
ITRAK
       1  0  3.8000E+00  2.0128E+04  4.9291E+05  3.8635E+05  1.4590E+06   0.506   0.480   0.200   1.000   0.000       0
1
!
!   ALPHA    BETA   GAMMA   DELTA   EPSIL    ZETA NON_ASS    TOPL       min_lam    TENS    FRIC    MAPP  UPLIFT
     4.00    2.00    2.00    0.50    0.75    1.50   1.000 1000.00    1.0000E+04      No      Yes      Yes       No
!
!    K_Alfa    K_Beta     G_Lam     G_Chi      G_Xi
       1.00      1.00      2.50      3.00      0.95
!

   46          MACRO   SSI -element
!   JPLA SL         DIAM        QQMAX          KNN          KVV          KMM     PSI     KSI   PL_P1   PL_P2     WGT  IPRNT
ITRAK
       1  0  2.8500E+00  1.0244E+04  3.6969E+05  2.9421E+05  6.1551E+05   0.506   0.480   0.200   1.000   0.000       0
1
!
!   ALPHA    BETA   GAMMA   DELTA   EPSIL    ZETA NON_ASS    TOPL       min_lam    TENS    FRIC    MAPP  UPLIFT
     4.00    2.00    2.00    0.50    0.75    1.50   1.000 1000.00    1.0000E+04      No      Yes      Yes       No
!
!    K_Alfa    K_Beta     G_Lam     G_Chi      G_Xi
       1.00      1.00      2.50      3.00      0.95
!

   47         DAMPER   SSI -damping
! ITYP          C1          C2     C3     C4     C5          C6 GAP_P GAP_N  ALFA LIMIT    SL   KOP    Y0    Z0
     0  3.3866E+03  2.1905E+03   0.00   0.00   0.00  8.0232E+02   0.0   0.0   0.2   0.0  -0.5   0.0   0.0   0.0
!

   48         DAMPER   SSI -damping
! ITYP          C1          C2     C3     C4     C5          C6 GAP_P GAP_N  ALFA LIMIT    SL   KOP    Y0    Z0
     0  6.0207E+03  3.8942E+03   0.00   0.00   0.00  2.5357E+03   0.0   0.0   0.2   0.0  -0.5   0.0   0.0   0.0
!

   49         DAMPER   SSI -damping
! ITYP          C1          C2     C3     C4     C5          C6 GAP_P GAP_N  ALFA LIMIT    SL   KOP    Y0    Z0
     0  6.0207E+03  3.8942E+03   0.00   0.00   0.00  2.5357E+03   0.0   0.0   0.2   0.0  -0.5   0.0   0.0   0.0
!

   50         DAMPER   SSI -damping
! ITYP          C1          C2     C3     C4     C5          C6 GAP_P GAP_N  ALFA LIMIT    SL   KOP    Y0    Z0
     0  3.3866E+03  2.1905E+03   0.00   0.00   0.00  8.0232E+02   0.0   0.0   0.2   0.0  -0.5   0.0   0.0   0.0
!

WEIGHTS
    1   0.000000E+00   1.944000E+03   0.000000E+00   0.000000E+00   0.000000E+00   0.000000E+00
    2   0.000000E+00   1.944000E+03   0.000000E+00   0.000000E+00   0.000000E+00   0.000000E+00
    3   0.000000E+00   1.944000E+03   0.000000E+00   0.000000E+00   0.000000E+00   0.000000E+00
    4   0.000000E+00   1.944000E+03   0.000000E+00   0.000000E+00   0.000000E+00   0.000000E+00
    5   3.240000E+02   0.000000E+00   0.000000E+00   0.000000E+00   0.000000E+00   0.000000E+00
    6   3.240000E+02   0.000000E+00   0.000000E+00   0.000000E+00   0.000000E+00   0.000000E+00
    7   3.240000E+02   0.000000E+00   0.000000E+00   0.000000E+00   0.000000E+00   0.000000E+00
    8   3.240000E+02   0.000000E+00   0.000000E+00   0.000000E+00   0.000000E+00   0.000000E+00
    9   3.240000E+02   0.000000E+00   0.000000E+00   0.000000E+00   0.000000E+00   0.000000E+00
   10   3.240000E+02   0.000000E+00   0.000000E+00   0.000000E+00   0.000000E+00   0.000000E+00
   11   3.240000E+02   0.000000E+00   0.000000E+00   0.000000E+00   0.000000E+00   0.000000E+00
   12   3.240000E+02   0.000000E+00   0.000000E+00   0.000000E+00   0.000000E+00   0.000000E+00
   13   3.240000E+02   0.000000E+00   0.000000E+00   0.000000E+00   0.000000E+00   0.000000E+00
   14   3.240000E+02   0.000000E+00   0.000000E+00   0.000000E+00   0.000000E+00   0.000000E+00
   15   3.240000E+02   0.000000E+00   0.000000E+00   0.000000E+00   0.000000E+00   0.000000E+00
   16   3.240000E+02   0.000000E+00   0.000000E+00   0.000000E+00   0.000000E+00   0.000000E+00
   17   3.240000E+02   0.000000E+00   0.000000E+00   0.000000E+00   0.000000E+00   0.000000E+00
   18   3.240000E+02   0.000000E+00   0.000000E+00   0.000000E+00   0.000000E+00   0.000000E+00
   19   3.240000E+02   0.000000E+00   0.000000E+00   0.000000E+00   0.000000E+00   0.000000E+00
   20   3.240000E+02   0.000000E+00   0.000000E+00   0.000000E+00   0.000000E+00   0.000000E+00
   21   3.240000E+02   0.000000E+00   0.000000E+00   0.000000E+00   0.000000E+00   0.000000E+00
   22   3.240000E+02   0.000000E+00   0.000000E+00   0.000000E+00   0.000000E+00   0.000000E+00
   23   3.240000E+02   0.000000E+00   0.000000E+00   0.000000E+00   0.000000E+00   0.000000E+00
```

```
   24   3.240000E+02   0.000000E+00   0.000000E+00   0.000000E+00   0.000000E+00   0.000000E+00
   25   3.240000E+02   0.000000E+00   0.000000E+00   0.000000E+00   0.000000E+00   0.000000E+00
   26   3.240000E+02   0.000000E+00   0.000000E+00   0.000000E+00   0.000000E+00   0.000000E+00
   27   3.240000E+02   0.000000E+00   0.000000E+00   0.000000E+00   0.000000E+00   0.000000E+00
   28   3.240000E+02   0.000000E+00   0.000000E+00   0.000000E+00   0.000000E+00   0.000000E+00
   29   0.000000E+00   0.000000E+00   0.000000E+00   0.000000E+00   0.000000E+00   0.000000E+00
   30   0.000000E+00   0.000000E+00   0.000000E+00   0.000000E+00   0.000000E+00   0.000000E+00
   31   0.000000E+00   0.000000E+00   0.000000E+00   0.000000E+00   0.000000E+00   0.000000E+00
   32   0.000000E+00   0.000000E+00   0.000000E+00   0.000000E+00   0.000000E+00   0.000000E+00
LOADS
    1   0.000000E+00   0.000000E+00   0.000000E+00   0.000000E+00   0.000000E+00   0.000000E+00
    2   0.000000E+00   0.000000E+00   0.000000E+00   0.000000E+00   0.000000E+00   0.000000E+00
    3   0.000000E+00   0.000000E+00   0.000000E+00   0.000000E+00   0.000000E+00   0.000000E+00
    4   0.000000E+00   0.000000E+00   0.000000E+00   0.000000E+00   0.000000E+00   0.000000E+00
    5   0.000000E+00  -2.160000E+02   0.000000E+00   0.000000E+00   0.000000E+00   0.000000E+00
    6   0.000000E+00  -4.320000E+02   0.000000E+00   0.000000E+00   0.000000E+00   0.000000E+00
    7   0.000000E+00  -4.320000E+02   0.000000E+00   0.000000E+00   0.000000E+00   0.000000E+00
    8   0.000000E+00  -2.160000E+02   0.000000E+00   0.000000E+00   0.000000E+00   0.000000E+00
    9   0.000000E+00  -2.160000E+02   0.000000E+00   0.000000E+00   0.000000E+00   0.000000E+00
   10   0.000000E+00  -4.320000E+02   0.000000E+00   0.000000E+00   0.000000E+00   0.000000E+00
   11   0.000000E+00  -4.320000E+02   0.000000E+00   0.000000E+00   0.000000E+00   0.000000E+00
   12   0.000000E+00  -2.160000E+02   0.000000E+00   0.000000E+00   0.000000E+00   0.000000E+00
   13   0.000000E+00  -2.160000E+02   0.000000E+00   0.000000E+00   0.000000E+00   0.000000E+00
   14   0.000000E+00  -4.320000E+02   0.000000E+00   0.000000E+00   0.000000E+00   0.000000E+00
   15   0.000000E+00  -4.320000E+02   0.000000E+00   0.000000E+00   0.000000E+00   0.000000E+00
   16   0.000000E+00  -2.160000E+02   0.000000E+00   0.000000E+00   0.000000E+00   0.000000E+00
   17   0.000000E+00  -2.160000E+02   0.000000E+00   0.000000E+00   0.000000E+00   0.000000E+00
   18   0.000000E+00  -4.320000E+02   0.000000E+00   0.000000E+00   0.000000E+00   0.000000E+00
   19   0.000000E+00  -4.320000E+02   0.000000E+00   0.000000E+00   0.000000E+00   0.000000E+00
   20   0.000000E+00  -2.160000E+02   0.000000E+00   0.000000E+00   0.000000E+00   0.000000E+00
   21   0.000000E+00  -2.160000E+02   0.000000E+00   0.000000E+00   0.000000E+00   0.000000E+00
   22   0.000000E+00  -4.320000E+02   0.000000E+00   0.000000E+00   0.000000E+00   0.000000E+00
   23   0.000000E+00  -4.320000E+02   0.000000E+00   0.000000E+00   0.000000E+00   0.000000E+00
   24   0.000000E+00  -2.160000E+02   0.000000E+00   0.000000E+00   0.000000E+00   0.000000E+00
   25   0.000000E+00  -2.160000E+02   0.000000E+00   0.000000E+00   0.000000E+00   0.000000E+00
   26   0.000000E+00  -4.320000E+02   0.000000E+00   0.000000E+00   0.000000E+00   0.000000E+00
   27   0.000000E+00  -4.320000E+02   0.000000E+00   0.000000E+00   0.000000E+00   0.000000E+00
   28   0.000000E+00  -2.160000E+02   0.000000E+00   0.000000E+00   0.000000E+00   0.000000E+00
   29   0.000000E+00   0.000000E+00   0.000000E+00   0.000000E+00   0.000000E+00   0.000000E+00
   30   0.000000E+00   0.000000E+00   0.000000E+00   0.000000E+00   0.000000E+00   0.000000E+00
   31   0.000000E+00   0.000000E+00   0.000000E+00   0.000000E+00   0.000000E+00   0.000000E+00
   32   0.000000E+00   0.000000E+00   0.000000E+00   0.000000E+00   0.000000E+00   0.000000E+00
EQUAKE
    6         1    5.00000E-03 2.990E-01        -1 0.000E+00 0.000E+00     1.000
```